SIM AUD 2017

Toronto Canada

2017 Proceedings of the
Symposium on Simulation for Architecture and Urban Design

Edited by
Michela Turrin
Brady Peters
William O'Brien
Rudi Stouffs
Timur Dogan

2017 Proceedings of the

Symposium on Simulation for Architecture and Urban Design

Edited by

Michela Turrin
Brady Peters
William O'Brien
Rudi Stouffs
Timur Dogan

Cover & Layout by

John Yee

2017 Proceedings of the Symposium for Architecture and Urban Design
Michela Turrin, Brady Peters, William O'Brien, Rudi Stouffs, Timur Dogan, editors

978-1-365-88878-6

Contents

Preface

The built environment is a complex system, contradictory, and constantly changing. It embodies the complex, historical evolution of human knowledge, desires and technology. Computer simulations enable designers to better respond to the increasing complexity of cities, buildings, and the lives of the occupants within them. Simulations support specific disciplinary expertise and enable interdisciplinary collaboration. They can address many scales from the urban to the building component. Innovation in computer simulation questions disciplinary boundaries and derives knowledge from the convergence of different fields. The 8th annual Symposium on Simulation for Architecture and Urban Design (SimAUD) tackles the interdisciplinary aspects of the development and use of simulations to measure, predict, assess, comprehend and manage the performances of buildings and cities, in regard to their technical and non-technical requirements.

It has been a pleasure to chair this edition of SimAUD. We have been happy to see that submissions came from a broad spectrum of fields, operated at a wide range of scales and that many crossed the boundaries of several disciplines. To understand and design the built environment converging competencies are essential. The papers included in these proceedings witness the liveliness of this joint effort and the high quality of the interdisciplinary contributions brought together at SimAUD. We wish to highlight also the crucial interaction between outstanding academicians and cutting-edge practitioners, which is one of the remarkable traits of SimAUD. This edition has comprised participants from highly-ranked Universities from across the globe (such as Harvard, Stanford, UCL, and NUS) and from renowned architectural firms and engineering practices (such as ZHA, RWDI, Front Inc, and The Living). We also highlight the participation of both design schools (such as AA, CITA, and IAAC) and engineering institutes (such as EPFL, ETHZ, SUTD, and TU Delft). Finally, we have been extremely impressed by the growing community of excellent young authors who are opening up promising perspectives.

The contributions in this book present new knowledge and innovations in: simulations for occupants' behavior and human centered comfort; energy in buildings and cities; urban mobility and urban microclimates; simulation-based processes from design conception to materialization and fabrication; and, computational processes for design exploration by means of simulations. In the program, we had the pleasure to include the keynote lectures by Robert Woodbury, William Braham and David Benjamin. Respectively, the lectures tackle the topics of simulations free in cost, time and intellectual access; of intelligible models corresponding to meaningful design issues; and of automatic generation, evaluation on measurable goals, and development of

numerous design options as design workflow. We had the pleasure to include also two panel discussions with invited panelists, among which experts from Arup (Erin Morrow), ESTECO (Enrico Nobile) and Autodesk (Azam Khan). One panel has been shaped on the interdisciplinarity and simulations in the early design phases; the second one on energy-simulations for buildings and cities. The topic of simulations toward fabrication has been featured in a special evening event. Finally, SimAUD 2017 has marked the first edition of the pre-conference workshops, which have been organized in collaboration with Timur Dogan, Siobhan Rockcastle, María Lovísa Ámundadóttir, Umberto Berardi and ESTECO Academy.

The success of this edition derives from countless work hours from a dedicated team. We would like to thank and acknowledge the Scientific Chairs: William O'Brien, Rudi Stouffs, and Timur Dogan for managing the peer-reviewed process, the papers' selection and revisions. Their committed work and rigorous procedures have been essential to meet the high standards of this conference. We would also thank the members of the Scientific Committee for reviewing the papers. Our extreme gratitude goes to Ramtin Attar at Autodesk for his essential support and guidance, and to his colleagues: Rhys Goldstein for his continuous contributions and John Yee for the handling of the proceedings. SimAUD is run in partnership with Society for Modeling & Simulation International (SCS). Many thanks to Oletha Darensburg and all the SCS officers who helped us organizing and managing the conference. Thanks to the faculty, staff, and students at the John H. Daniels Faculty of Architecture, Landscape, and Design. We have been honored to work with the University of Toronto as our academic and venue partner for the event.

And most of all, we wish to thank all the authors for their high quality contributions, which are the main ground for SimAUD's high quality standards in research and interdisciplinary ties across domains. We look forward to the involvement of current and future authors and participants. We are confident that future editions will build upon the current success and will continue strengthening our community.

Michela Turrin
General Chair, SimAUD 2017
Assistant Professor, Delft University of Technology

Brady Peters
Program Chair, SimAUD 2017
Assistant Professor, University of Toronto

All accepted papers will be published in the ACM Digital Library at the SpringSim Archive.
Sponsored by The Society for Modeling and Simulation International.

Keynote Speakers

Robert Woodbury

University Professor, Simon Fraser University
Director of Smartgeomety

Robert Woodbury is a University Professor at Simon Fraser University. His research is in computational design, visual analytics, and human-centered systems for sustainable living. He holds a PhD and MSc from Carnegie Mellon, and a BArch from Carleton. He has over 150 publications, including his book Elements of Parametric Design. In 2009 he chaired Team North, a Canadian entry to the 2009 Solar Decathlon. In 2008 he was awarded the Innovative Research Award from the Association for Computer Aided Design in Architecture and the Tee Sasada Award from the Association for Computer-Aided Architectural Design Research in Asia. He is a Director of Smartgeometry.

For over 30 years, Woodbury has focused on new design media and how design work changes through its use. He has made contributions to solids modeling, generative design, parametric modeling, end-user programming in design, sustainability and, especially, design alternatives. Design work universally proceeds through creation, critique and refinement of alternatives, yet a near-universal feature of computational design interfaces is a limitation to seeing and interacting with a single-state of a design at a time. This limit flies in the face of observed practice in manual media, in which the sketchbook supports rapidly generating multiple alternatives. It also fails to employ much of the human cognitive system, in which people rely on visual scanning and comparison as an integral part of work. Design alternatives are foundational: all design, analysis and simulation systems could benefit from a design alternatives capability. Woodbury's current work is focused on direct designer interactions with large collections of alternatives in parametric modeling systems.

William W. Braham

Professor, University of Pennsylvania

William W. Braham, PhD, FAIA is a Professor of Architecture at the University of Pennsylvania, where he previously served as Chair, and is currently Director of the Master of Environmental Building Design and of the Center for Environmental Building + Design. He has worked on energy and architecture for over 30 years as a designer, consultant, researcher, and author of numerous articles and books. He recently published Architecture and Systems Ecology: Thermodynamic Principles for Environmental Building Design, in three parts (2015). He also co-edited Energy Accounts: Architectural Representations of Energy, Climate, and the Future (2016), Architecture and Energy: Performance and Style (2013), and Rethinking Technology: A Reader in Architectural Theory (2007). He is currently working on a project called, The City Always Writes in the Plural: Narratives of Urban Self-Organization.

Recent work has operated at three scales: looking at building products and components, such as responsive building skins and advanced glass products developed with material scientists; building performance & design, including energy and daylighting focusing recently on management strategies for large collections of buildings; and urban and Regional assessment, land use strategies, resource allocation, and decision making for resilient development.

David Benjamin

Founding Principal, The Living, an Autodesk Studio
Assistant Professor, Columbia GSAPP

David Benjamin is Founding Principal of The Living, an Autodesk Studio. He and the studio have won design awards from the Architectural League, the American Institute of Architects, Architizer, the Museum of Modern Art, Ars Electronica, the German Federal Government, and Holcim. Recently the firm was ranked third on Fast Company's list of World's Ten Most Innovative Companies in Architecture. David has lectured about his work in many parts of the world, and he currently teaches at Columbia University Graduate School of Architecture, Planning and Preservation. Before receiving a Master of Architecture from Columbia, he received a Bachelor of Arts from Harvard.

The Living combines research and practice, exploring new ideas and technologies through prototyping. The studio welcomes rapid change, embraces design with uncertainty, develops rules rather than forms, and designs with unknowable forces. The work embraces the complexity at the intersection of ideas, technologies, materials, culture, humans, non-humans, and the environment. It also explores generative design, feedback-based robotics, machine learning, and new materials. The studio's research is developed through applied projects for real-world problems. Clients include City of New York, Seoul Municipal Government, Nike, Prada, Google, 3M, Airbus, BMW, Quantified Self, Miami Science Museum, and Björk. Recent projects include Project Discover (generative design for architecture), the Airbus Bionic Partition (biological algorithms and generative design for manufacturing), the Princeton Embodied Computation Lab (an open source building), and Hy-Fi (new bio materials for architecture).

Investigating the Effects of the Geometry on Speech Privacy of Semi-Enclosed Meeting Spaces

Pantea Alambeigi, Jane Burry, Eva Cheng

Royal Melbourne Institute of Technology (RMIT)
Melbourne, Australia
{Pantea.Alambeigi, Jane.Burry, Eva.Cheng}@rmit.edu.au

ABSTRACT
This paper investigates the effect of the room geometry on speech privacy of small meeting areas. The aim is to explore different semi-enclosed room shapes within an open plan office and study their influence on speech privacy and the significant parameter and performance metric, Speech Transmission Index (STI). This is a simulation study in the room acoustic modeling software (ODEON).

The impact of the geometry on the sound of the large spaces such as concert halls has been widely reported, however, at the scale of the small, particularly semi-enclosed, meeting room the role of geometry in tuning the acoustic performance needs to be studied further.

This research investigates the potential impact of room shape on speech privacy by exploring whether this impact lies above or below the Just Noticeable Difference (JND). Matrices of studies have been developed to study diverse variables individually and the results demonstrate how speech privacy might be affected by modifying room shape.

Author Keywords
Room geometry; speech privacy; speech transmission index; acoustic simulation.

ACM Classification Keywords
I.6 SIMULATION AND MODELING

1 INTRODUCTION

Since the emergence of open plan layouts in the last decades, a large body of literature is devoted to the advantages and disadvantages of the transition from private offices to reconfigurable open plan offices. After decades of developing open plan interiors, there is a little architectural approach to fulfilling acoustic requirements. In response to the occupants' need for more privacy and less disruption, fully enclosed quiet rooms or small booths are integrated into the design of open plan offices. However, this type of space is in contrast with the inherent open flow characteristic of the landscaped interiors and therefore imposes a regression to conventional design and requires particular arrangements such as air conditioning and separate sprinklers. While the value of a proper size meeting area in the newly introduced office layouts is emphasized [9], the concept of semi-enclosed meeting rooms which fit within the open plan interior is still an area hardly considered in architectural studies. This paper presents form exploration on these types of meeting room.

Most of the acoustic solutions in practical design are based on material modification [16]. To resolve acoustic problems, in particular speech privacy in open plan interiors, a typical approach is to apply technical engineering solutions including the adoption of uniform ceilings and high absorbent acoustic materials [26]. In this research, we investigate the probability of improving the speech privacy through altering room global shape.

Inadequate acoustic knowledge and terminology compel architects to take acousticians' advice with no architectural design interference and this commonly happens in the late stages of the design. Architects, barely consider acoustics as a design driver. However, they should admit the consequences of their geometric design decisions and be able to measure the influences of geometry alteration on the sound perception in space [16]. They would then be able to be actively involved in the process of acoustic design and modify the aural experience of space through a wise choice of geometry. This paper briefly demonstrates that regardless of acoustic materials, how a trivial design modification in semi-enclosed meeting rooms might affect the speech privacy in open plan offices.

The concept of shaping the sound in space through altering the geometry in large spaces like concert halls is well investigated and documented in the literature [2,8,15]. However, there are only a few studies for small scale spaces mainly by acoustic engineers rather than architects. In the project distortion II, Peters [17] thoroughly demonstrated a parametric design of an "S" shape space divider with trihedral folded plate which provides two different acoustic subspaces on [27] each side. Another instance is origami-based partitions developed by Vyzoviti and Remi [26]. FabPod project is also an architectural design which investigates the effects of hyperboloid modules in tuning the acoustic performance of a semi-enclosed meeting space [5]. While these projects investigate the effects of surface geometry on the auditory experience of the space, there is limited research on the relative importance of overall room shape as well. All above-mentioned studies question the probable influence of geometry variation on the sonic

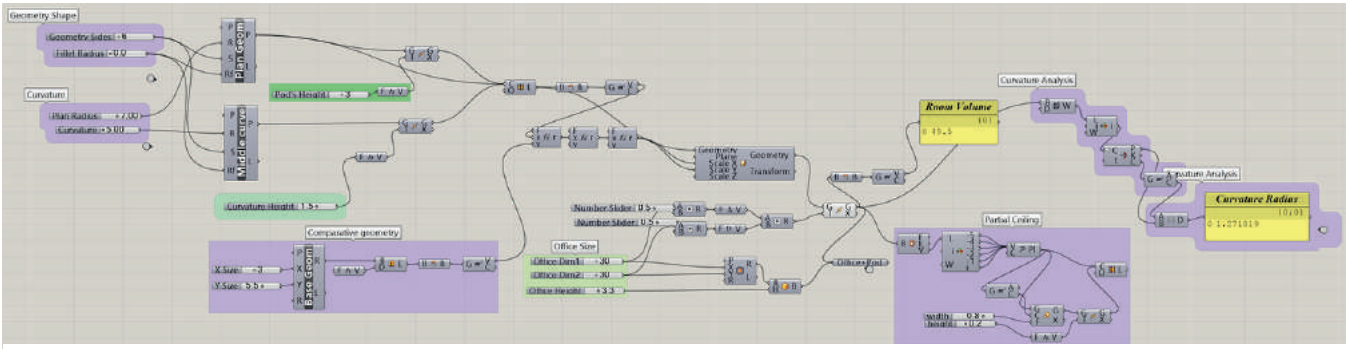

Figure 1. A parametric grasshopper script including set of geometrical parameters for rapid form generation

experience and speech intelligibility inside the space. However, this paper explores the potential impact of the room global shape on the speech privacy of the open plan working and learning space, where the semi-enclosed room is placed.

2 METHODOLOGY

2.1 Simulation Technique

Recently, developed acoustical software provides an opportunity to quickly simulate and analyze various design iterations with an acceptable level of reliability [19]. Since there are still limitations in integrating acoustic performance analysis in parametric design tools [18], digital sound simulation is considered a relatively a time-consuming and recurring process from 3D CAD modeling to acoustic software and vice versa [25].

Simulation methods have developed remarkably from solo image source or ray tracing approach to the combination of both in hybrid models with adopting the effects of the sound scattering characteristic in space. Ray tracing, based on geometric acoustics, is a method of simplifying sound propagation by replacing sound waves with rays [13]. Therefore, it fails to take into account the diffraction and interference wave-related phenomena [25]. Yet, it is an effective time-saving tool for sound simulation particularly of enclosed spaces [14].

There are different views regarding the reliability of computer modeling techniques. However, it is undeniable that many valuable results can only be achieved from digital simulation rather than scaled modeling or prototyping [21]. For instance, in this study, parametric geometry modification and design iterative design cycle are only practical through applying digital modeling simulation. Moreover, it would be really difficult, if not impossible, to get an acoustic performance overview of each and every point in a space for various acoustical parameters with scaled models or 1:1 prototypes. But this becomes viable in a reasonable time with digital sound modeling by offering a graphical grid response map in all commonly applied software.

Acknowledging the limitations of all the geometrical acoustic based programs, they can still offer an acceptable level of accuracy by predicting approximately 80 percent of the sound performance in space [7]. Considering the impossibility of achieving 100% accurate prediction and the amount of effort that wave based programs require to obtain 90 to 95% of the answer [7], acoustical geometric software is an accepted method of providing valid results at present [3].

In this research, a commercial acoustic analysis software, Odeon version 13.02, which adopts a hybrid calculation method, was applied in the analysis cycle.

Authors had access to data for a built project, which provides a reference to compare the simulation reliability to measured data. The results of the Odeon software in predicting speech privacy of semi-enclosed meeting spaces had been fully studied and compared with two other methods of evaluation that are an objective measurement of 1:1 prototype and subjective experimental analysis of human auditory perception. The relative consistency between the evaluative methods suggests that human perception of the privacy in a semi-enclosed pod can be predictable with Odeon software with an acceptable level of agreement to privacy perception in a real and natural environment of an open plan office [1].

2.2 Speech Privacy Evaluative Parameter

Analysing the data obtained from simulation requires some level of acoustic knowledge. Most of the acoustic analysis software, regardless of the calculation methods, provides a wide range of acoustical measures. Selecting the appropriate parameter to interpret acoustic performance accordingly becomes very crucial in achieving meaningful results. For many years Reverberation Time (RT) was considered the primary indicator of room acoustics [4], yet it only demonstrates the latter part of the decay curve that is less significant for the human auditory perception [24]. Today, better descriptors have been developed to define the quality of speech [4].

Since speech privacy is attributed to the speech intelligibility and clarity rather than speech level [6], the two effective measures defining the speech privacy of an environment are the speech intelligibility and speech clarity of the space. Speech Transmission Index (STI) is an indicator of speech intelligibility. It is “the quality of the speech transferred from the speaker to the receiver” [24], and considered one of the best parameters for describing

Frequency (Hz)	*63*	*125*	*250*	*500*	*1000*	*2000*	*4000*	*8000*
Ceiling	0.30	0.30	1.00	1.00	1.00	1.00	0.97	0.97
Floor	0.00	0.00	0.05	0.05	0.10	0.05	0.00	0.00
Walls	0.11	0.110	0.08	0.07	0.06	0.05	0.05	0.05
Pod	0.02	0.02	0.05	0.10	0.25	0.55	0.80	0.80

Table 1. Absorption coefficient (α) of the open interior and pod surfaces

and measuring speech intelligibility and consequently speech privacy of the space. STI is a variable between 0 and 1. Odeon calculates STI applying the indirect method in compliance with the international standards ISO 9921 and IEC 60268 [20].

Speech Clarity (C50) is also another efficient descriptor in assessing privacy of the space. Unlike RT, the ratio of early arrival reflections in 50 milliseconds to late arrival reflections is the determinant of the clarity of speech in the space [4].

Obviously, speech clarity and speech intelligibility have an adverse relationship with privacy. That is to say, less C50 and STI signifies more speech privacy in open plan office.

2.3 3D Architectural CAD Modeling

Developing various matrices to map the acoustic effects of combining changes in two different shape variables required rapid modification of the geometry. A parametric script was created in Grasshopper, a parametric plugin for McNeel Rhinoceros 5.0 (Figure 1). The script includes a set of geometrical parameters such as number of sides, curvature type and magnitude, distance, and length. These parametric components have been altered separately to produce each matrix and to analyze various aspects of geometry alteration. Since the volume of the room is one of the influential factors in shaping the sound in space [13], it had been kept constant in outlining the parametric script. All the semi-enclosed pods in this study have 49.5 cubic meters' volume with the height of 300 cm and 30 cm below the finished ceiling of the simulated open plan office. In the parametric model different aspects of the overall geometry and its relationship to the office could be addressed individually.

Since the pod and open layout interior interactively influence each other in terms of acoustic performance, the open space dimensions were kept constant and symmetrical in all matrices. The dimensions were specified 30x30 meters in width and length and 30.3 meters high.

2.4 Acoustical Specifications

To eliminate the impact of the material on the sound performance of the pods and open plan space, all surfaces were assigned with the absorption coefficient as provided in Table 1. To further evaluate the effects of the absorption coefficient and its reciprocal impact on the speech privacy and overall geometry, a different matrix is developed to analyze a selected pod in three different situations of anechoic, fully reverberant and a commonly used open plan interior.

3 ACOUSTIC SIMULATIONS

The most important advantage of acoustic simulation is the broad range of information quickly provided which cannot be accessible through other methods of evaluation. Rindel [22] categorized the benefits in 4 sections: reflectogram as a tool, display of reflection paths, grid response displays, and auralization. Among all, grid response display might be the most beneficial tool for architects to fully visualize the sound performance in their architectural design workflow and to obtain pragmatic statistical data readily. In this study, the matrices demonstrate the auditory performance of the pods in terms of STI and C50 with a grid colored map in each square meter of the space. Also, the reflection path is employed to analyze the output data from the Odeon and to interpret the results.

3.1 Room Acoustic Parameters

Two acoustic parameters had been selected to inspect privacy according to the standard 3382-3:2012 [11]. STI which is an indicator of speech intelligibility and C50 which demonstrates the speech clarity in space. The more speech clarity and intelligibility bring less speech privacy.

It is important to notice that approaching the open layout in design will deliver some degrees of compromise regarding speech intelligibility and privacy constitutionally [23]. That is to say, a well-understood conversation with minimum vocal effort is desired to provide an excellent environment for communication, while at the same time there is an intention to offer at least an acceptable level of speech privacy where the discussion cannot be overheard. It is, therefore, crucial to understanding the priority of the space before starting to design. Since in a very small meeting rooms the distance between the speaker and the listener is relatively short, the direct sound is the most determinant source of facilitating the intelligibility in a face to face conversation. Thus, the privacy of the conversation is the problem which needs to be given primacy.

For having a private zone in which the discussion cannot be overheard, the standard 3382-3:2012 specifies an STI of 0.2 or below. Also, according to the same standard, the distraction distance starts where the STI falls below 0.5. That means occupants would be distracted easily in any locations with the STI more than 0.5.

Speech Transmission Index (STI)	*Speech Privacy*
0.00 - 0.05	Confidential
0.005 – 0.20	Good
0.20 – 0.40	Reasonable
0.40 – 0.60	Poor
0.60 – 0.75	Very Poor
0.75 – 1.00	No privacy

Table 2. Privacy definition according to the STI range [10]

More recent subjective research offered an STI of 0.6 for the distraction distance [1]. Further experimental studies divided these numbers to provide more details. Table 2 shows the suggested STI specified by Hongisto [10] in 6 categories. This table was beneficial in analyzing the results of the simulation.

C50 has been specified to range between -3 and +9 dB in most spaces designed for speech [4]. The negative and positive sign stand for the acoustic characteristic of the space. Space acoustic characteristics turn from a more reverberant to a less reverberant sound environment from negative to positive values.

The Just Noticeable Difference (JND) is a minimum change in a value of a parameter which can be readily perceived by human ears. If any acoustical treatment provides less than JND difference in the sound parameter, the practice would probably not be beneficial regarding improving the human auditory experience. It is suggested that for an easily detectable improvement in everyday environments, 3 dB and 0.1 might be considered for JND of C50 and STI in practice [4].

In this research the effects of the geometry on increasing speech privacy would be studied in terms of STI and C50 and the investigation is carried out to find whether the speech privacy improvement meets the minimum value of JND or above.

3.2 Simulation Setup

The 3D models exported from Rhinoceros and then imported in Odeon, the commercial room acoustic software. The absorption coefficient was assigned to each surface as described in Table 1. The 0.05 scattering coefficient was also assigned to all surfaces

The predefined sound source, ISO3382-3_OMNI.SO8 was selected and located in the center of the pod and open plan interior 1.2 meters above the floor.

4 MATRICES OF STUDY

There are many variables which might affect the speech privacy in designing a semi-enclosed meeting space. It has not been the aim to address all aspects, but rather to think of some as fundamental patterns and variables. In this study, the influence of geometry alteration in both plan and section is presented in 4 matrices.

4.1 Matrix I

In the first matrix, the impact of the number of the sides which modifies the plan of the geometry symmetrically is being investigated in the X axis. In the Y axis, the corners of geometry were rounded with ascending radius. (Figure. 2). The results of this matrix indicate that with adding geometry sides and moving from triangle to octagon geometry in the X axis, the STI is reduced. Also, it is well observable that by increasing the radius of rounding corners the speech privacy is dramatically improved. Both the X

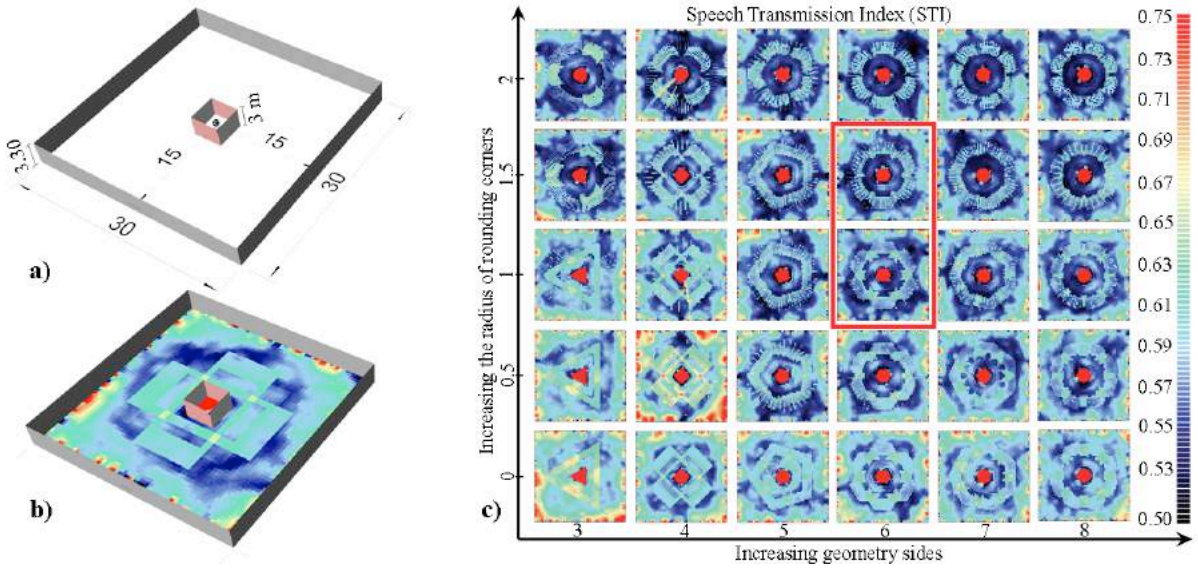

Figure 2. a) Outline of the space and dimensions, b) STI simulation of a conventional square pod as a benchmark, c) Matrix I: Investigating the effects of increasing geometry sides and radius of rounding corners

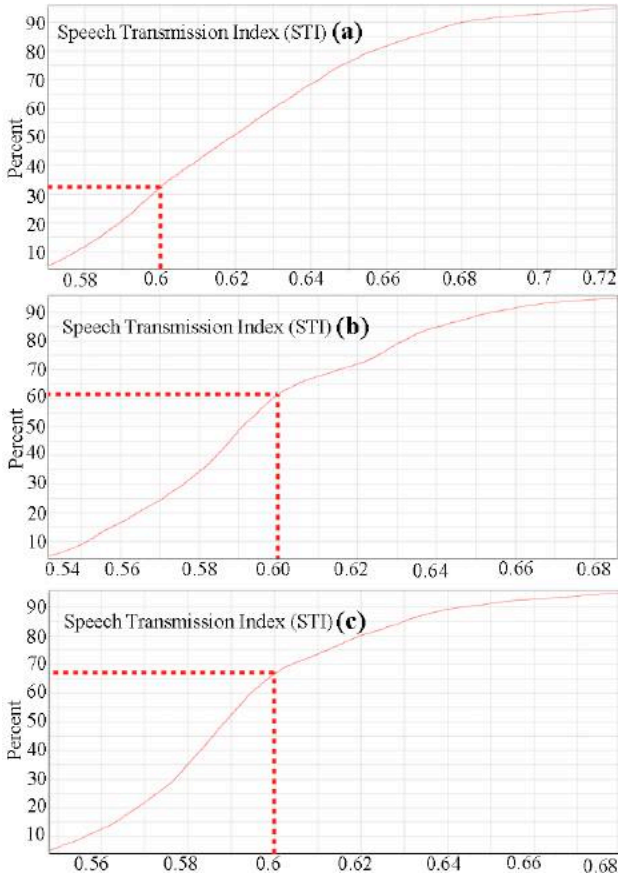

Figure 3. STI cumulative distribution graph for a) 3-sided, b) 6-sided and c) 8-sided

and Y axis are heading forward to getting close to the circle shape. Therefore, it can be concluded that approaching to the cylindrical shape might have the best effect on improving speech privacy.

By looking closer into the reflection path, the reason was clearly understood. The geometries which have the most similar shape to the cylinder are actually capturing the sound energy inside the pod by continuously reflecting the sound from their boundaries. The sound rays are not allowed to easily spread into the open plan office and they would reach the pod's top edge after several reflections from the boundaries which reduce the sound energy before propagating it into the open interior. Repetitive reflections may increase the sound pressure level, but on the other hand, decrease the speech clarity which helps to improve the security of speech.

In the overview of the visualized map, it can be seen that the STI reduction from hexagon to the octagon is below the JND and inspecting several points confirms that from triangle to hexagon there is 0.15 decrease in STI which is above the JND, while from hexagon to octagon the difference is only 0.02. The more accurate analysis of the supplementary cumulative distribution graph (Figure. 3)

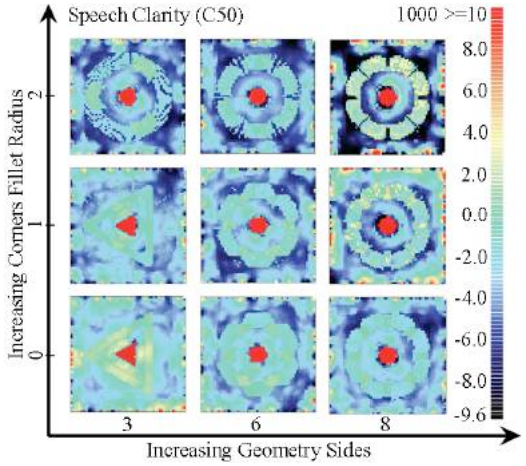

Figure 4. Effects of geometry on speech clarity

shows that in 3-sided geometry only 33% of the area has the STI below 0.6, whereas this percentage is doubled in 6-sided (62%) and just raised to 67% in the octagon shape.

A matrix is also developed for speech clarity for only three selected geometries and it is in agreement with the STI matrix and demonstrates a decrease in clarity by increasing geometry side which brings more speech privacy in space. (Figure. 6) The difference from hexagon to the octagon is 2 dB which is below JND, while from the triangle to hexagon is 3.5 dB which is above the JND for C50.

4.2 Matrix II

According to the results from the first matrix, in designing the second matrix which is investigating the effects of form alteration in the section, only the 6-sided geometry has been taken into account for further analysis.

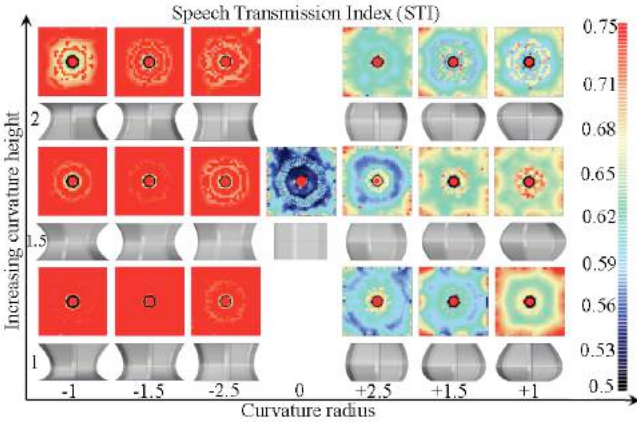

Figure 5. Matrix II: Convex and concave curvature analysis

In this matrix, the influence of curvature in the section is examined. Convex and concave shapes are compared with a cylindrical shape in the center of the matrix. (Figure. 5)

In the X axis, the degree of the curvature is increasing positively at the right side and negatively at the left side of the cylindrical shape. And in the Y axis, the derivative point is relocated from the bottom of the pod to the top edge.

The figure 5 presents that the lowest STI is associated with the cylindrical shape. The probable reason again can be explained through repetitive reflections occurring inside the pod which do not release and scatter the sound quickly inside the space. This can be well observed from 3D animated ray investigation in Odeon.

The convex shape, in contrast, accelerates the sound transmission from the pod to the open interior due to the nature of the funnel form. It is clear from the grid map that the speech source in the pod is fully understandable in all convex forms throughout the space. Although concave pods have superior performance regarding speech privacy, they do not follow a regular pattern when changing the curvature degree and position. For better understanding the reason behind the change of the STI in the nine different concave forms, the reflection paths should be analyzed for each individually, which is beyond the scope of this paper.

4.3 Matrix III

The third matrix aims to explore the effect of the variation in pod's section created by combining different types of curvature in an exterior and interior layer of the pods. Nine pod frames had been studied in this matrix which is illustrated in Figure 6. The pods are identical in plan and material. Both 5 and 6-sided geometries have been investigated in this matrix and for eliminating the effect of the pods' orientation relative to the open plan interior, pentagon and hexagon plan have been rotated 15 degrees (Figure 6). It can be seen from the results that by rotating

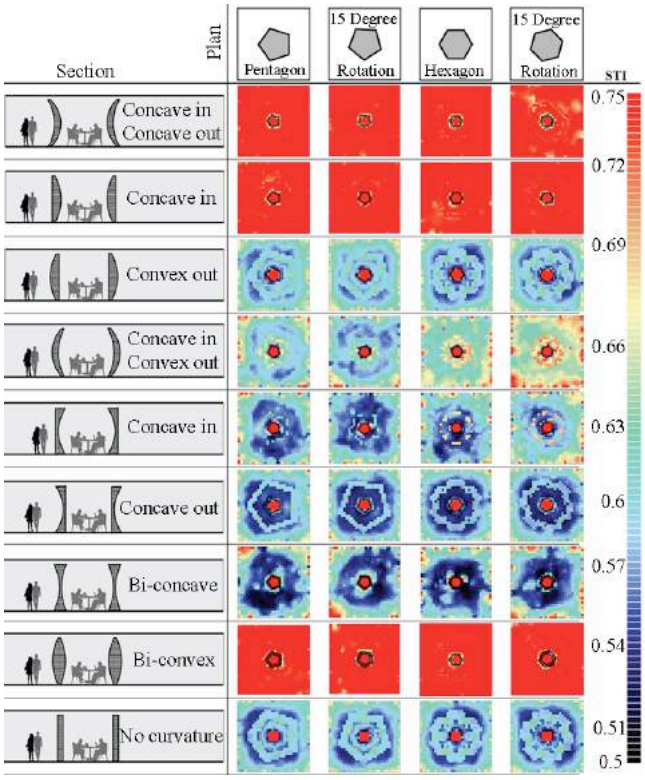

Figure 6. Matrix III: STI matrix of variation in pod's section

the pods no consequential changes above the JND could be captured.

The outcome of the acoustic simulations implies that with a bi-concave geometry the minimum of STI and the highest level of speech privacy could be achieved. Also, regardless of the type of the curvature in the external face of the semi-enclosure, designing a convex shape for the interior surface would dramatically increase the speech intelligibility and therefore speech privacy is dropped.

The red color in the grid map indicates the spots with STI more than 0.75 which is considered as a no privacy zone. The change in the speech intelligibility index is virtually above the JND range for the STI. From the best case scenario which is a bi-concave to the lowest level of speech privacy which is produced by the diverging meniscus, plano-convex and bi-convex geometries there is a minimum of 0.25 increase in the STI which is well above the JND range and it can be greatly perceivable by human ears. Cumulative distribution function provides supplementary information that in interior funnel shape pods 80% of the area have STI above 0.80, while the rest hardly goes below 0.7. This means that the speech in the convex shape pod is fully comprehensible in the open interior space. The trend is reversed in bi-concave geometry where almost 99% of the area has the STI below 0.7. The outcome can be justified through the same reasoning mentioned in the previous sections.

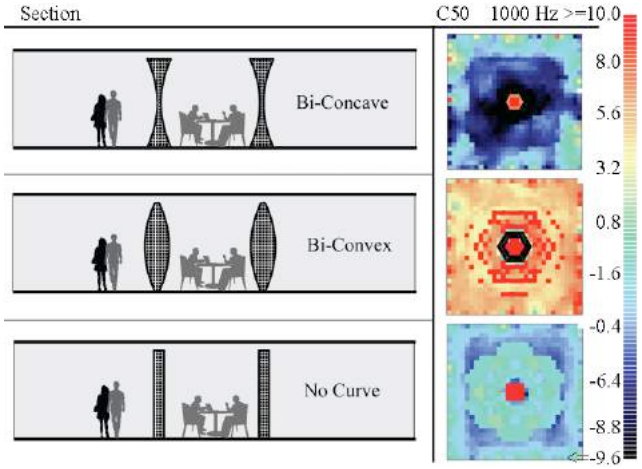

Figure 7. C50 matrix of variation in three geometry combinations

Three combinations were selected for analyzing the C50 and it is well graphed in Figure 7 that there is a dramatic change well over the JND. A minimum of 5 and 10 dB increase in the speech clarity from bi-concave to the pod with no curvature and bi-convex is detected respectively.

4.4 Matrix IV: Examining The Effect of Interactive Relationship Between Geometry and Material

The complex interaction of the room acoustic variables, make the accurate prediction of sound performance very complicated, if not impossible [12]. Although analyzing the material is not the target of this study, it is significant to not

overlook the interaction between the pod's performance and open plan interior's surfaces. Figure 8 clarifies this interaction graphically. It can be observable from the matrix that in changing the absorption coefficient of the office's surfaces from 100% absorbent to 100% reflective there is a substantial downward trend in STI. This conveys that by providing more reverberant space the intelligibility of the speech will be dropped. It is notable that for producing coherent and comparable grid maps a change in the STI range from 0.5-0.75 in previous matrices to 0-1 was required to include a wide range of STI for covering all three conditions.

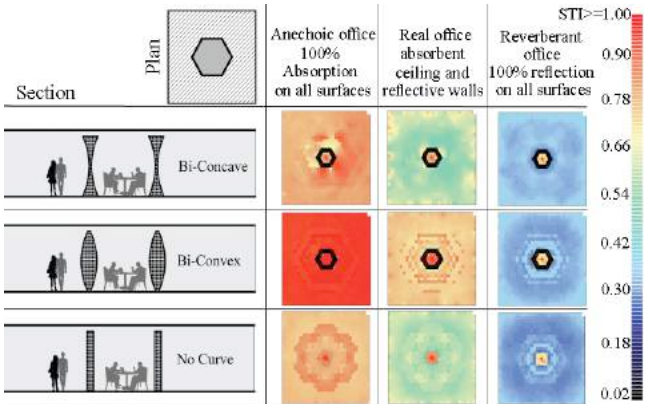

Figure 8. Matrix IV: investigating the interaction of the open interior's surfaces and pod's geometry in three conditions

Obviously, the effect of the reflective environment on STI is so strong that can dominate the geometry influence, yet still, interact with it. Figure 9 shows the reflection path which justifies how the interaction between geometry and reflective surfaces can make the bi-concave form the worst concept in providing the speech privacy.

For eliminating the effect of the surfaces of the open plan office and solely evaluating the pod's geometry a fully absorbent condition is also investigated. There is a remarkable consistency between the first and second column of the matrix in classifying the pod's shape in terms of providing speech privacy. This consistency can validate the reliability of the results in the previous matrices. While the first column shows a totally absorbent office, the second column represents a regular open plan office which commonly has ceiling acoustic treatment. The everyday office situation benefits from the absorptive ceiling, meanwhile, take advantage of reflective walls and possibly floor to increase sound scattering.

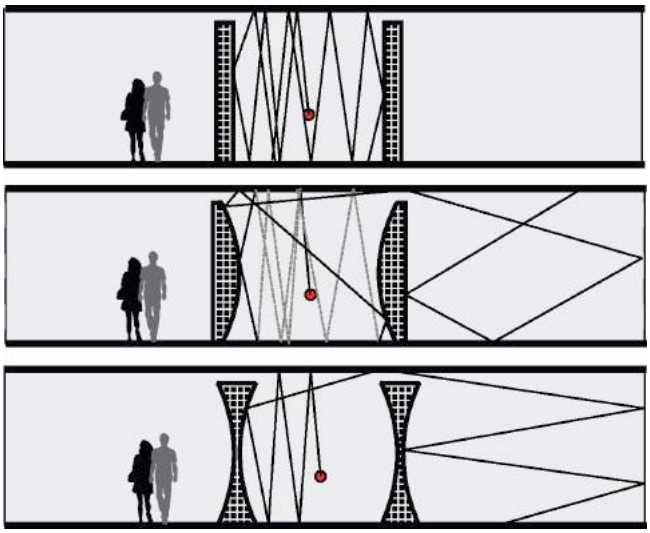

Figure 9. Reflection path of sound propagation in open plan office

5 CONCLUSION

This study aimed to investigate the impact of the overall shape of a semi-enclosed meeting space on the speech privacy of an open plan interior.

Various matrices have been developed to inspect different aspects of geometry alteration both in plan and section that might affect the speech privacy. Many simulations had been carried out with Odeon room acoustic software and two main parameters, Speech Transmission Index (STI) and Speech Clarity (C50), were selected for speech privacy analysis. Also, the Just Noticeable Difference (JND) for each parameter had been taken into account to study whether the influence of geometry on speech privacy of the open interiors are above or below the JND.

The result indicates that modification in both plan and section provides a considerable effect on STI and C50 which is well above the JND. This follows a more regular pattern in the plan variation than in section, however, modifying section captures the impression more extensively in comparison to room plan. Geometry alteration in *section* shows a minimum decrease of 0.25 in STI, while the STI improvement caused by *plan* modification is 0.15. The same trend can be seen in C50 in plan and section variations. 10 dB decrease in the speech clarity in the open interior can be achieved by modifying the section, whereas, the improvement is only 3.5 dB reduction when changing the overall plan.

Any geometry close to the cylinder that provides continuous and prolonged reflections inside the pod, hardly allows the sound rays to quickly spread into the open layout office and therefore increases the speech privacy outside the pod. Since the acoustic treatment in open plan designs is a compromise between speech intelligibility and speech privacy, it is recommended to consider adding reflectors in appropriate places in semi-enclosed meeting spaces to create some repetitive reflections inside the pod.

It is also found that bi-concave geometry would increase the speech privacy of the space by 40% compared to the convex shape and the reason might be due to the converging and non-scattering effect of this type of the shape that can hold the sound inside the pod and provide reflections between the exterior surface of the pod and walls of the open interior.

6 FUTURE WORK

Future works include further analysis of the matrices with different acoustic simulation techniques such as Finite Element Methods (FEM) and to develop more matrices to evaluate a greater range of variables.

ACKNOWLEDGMENTS

The authors would like to acknowledge the feedback of Professor Xiaojun Qiu and Dr. Brady Peters. We would also like to acknowledge the support of the Australian Research Council through the ARC Linkage Project: The Sound of Space with Prof Mark Burry and Partner Organisations Haworth and Sagrada Família Basílica.

REFERENCES

1. Alambeigi, P., et al., Complex human auditory perception and simulated sound performance prediction, *Proc. CAADRIA,* 2016. University of Melbourne. p. 631-640.
2. Barron, M., *Auditorium acoustics and architectural design*. 2009, Routledge.
3. Bork, I., Report on the 3rd round robin on room acoustical computer simulation–Part II: Calculations. *Acta Acustica united with Acustica*, 2005. 91(4): p. 753-763.
4. Bradley, J.S., R. Reich, and S. Norcross, A just noticeable difference in C 50 for speech. *Applied Acoustics*, 1999. 58(2): p. 99-108.
5. Burry, J., Davis, D., Peters, B., Ayres, P., Klein, J., Pena de Leon, A., Burry, M., Modelling Hyperboloid Sound Scattering The Challenge of Simulating, Fabricating and Measuring, *Computational Design Modelling*. 2012, Springer. p. 89-96.
6. Cavanaugh, W. J., Farrell, W. R., Hirtle, P. W., Watters, B. G., Speech privacy in buildings. *The Journal of the Acoustical Society of America*, 1962. 34(4): p. 475-492.
7. Dalenbäck, B.-I. Engineering principles and techniques in room acoustics prediction. *Baltic-Nordic Acoustics Meeting*, Bergen, Norway. 2010.
8. Gade, A.C., The influence of architectural design on the acoustics of concert halls. *Applied Acoustics*, 1990. 31(1-3): p. 207-214.
9. Harrison, A. and A. Cairns, The changing academic workplace. *DEGW on behalf of the University of Strathclyde*. Available for download from www. exploreacademicworkspace. com, 2008.
10. Hongisto, V., A model predicting the effect of speech of varying intelligibility on work performance. *Indoor air*, 2005. 15(6): p. 458-468.
11. ISO 3382-3: 2012, Acoustics – Measurement of room acoustic parameters- Part 3: Open plan offices, *International Organization for Standardization*, Geneva, Switzerland.
12. Keränen, J. and V. Hongisto, Prediction of the spatial decay of speech in open-plan offices. *Applied Acoustics*, 2013. 74(12): p. 1315-1325.
13. Kuttruff, H., *Room acoustics*. 2009: Crc Press.
14. Lehnert, H., Systematic errors of the ray-tracing algorithm. *Applied Acoustics*, 1993. 38(2): p. 207-221.
15. Marshall, A., Acoustical determinants for the architectural design of concert halls.1968, Architectural Science Review, 11(3), 81-87.
16. Peters, B., Parametric acoustic surfaces. ACADIA 2009, 2009: p. 174-181.
17. Peters, B., Tamke, M., Stig Anton, N., Søren Vestbjerg, A., Mathias, H., Responsive acoustic surfaces: Computing sonic effects. *Proc. eCAADe*, 2011.
18. Peters, B. and T. Olesen. Integrating Sound Scattering Measurements in the Design of Complex Architectural Surfaces. *Proc. 28th eCAADe*, Zurich. 2010.
19. Rindel, J.H., Modelling in auditorium acoustics. From ripple tank and scale models to computer simulations. *Revista de Acústica*, 2002. 33(3-4): p. 31-35.
20. Rindel, J.H., Odeon application note. *http://www.odeon.dk*, 2014.
21. Rindel, J.H., Room acoustic modelling techniques: A comparison of a scale model and a computer model for a new opera theatre. *Building Acoustics*, 2011. 18(3-4): p. 259-280.
22. Rindel, J.H., The use of computer modeling in room acoustics. *Journal of vibroengineering*, 2000. 3(4): p. 41-72.
23. Rychtarikova, M., et al. Architectural guidelines for living rooms, classrooms, offices, sports facilities and restaurants. *33rd International Congress and Exposition on Noise Control Engineering*, Prague, Czech Republic. 2004.
24. Svensson, C. and E. Nilsson, Optimum Room Acoustic ComfortTM (RACTM) can be achieved by using a selection of appropriate acoustic descriptors. *Proc. of Euronoise,* 2008.
25. Vlaun, N., Sound working environments: Optimizing the acoustic properties of open plan workspaces using parametric models. 2015, Delft University of Technology.
26. Vyzoviti, S. and N. Remy, Acoustically Efficient Origami Based Partitions for Open Plan Spaces. *Proc. eCAADe*, 2014.
27. Zhao, S., et al., Sound quality inside small meeting rooms with different room shape and fine structures. *Applied Acoustics*, 2015. 93: p. 65-74

Requirements for BIM-based Thermal Comfort Analysis

Fawaz Alshehri[1], Paul Kenny[2] and James O'Donnell[1]

[1]School of Mechanical and Materials Engineering, UCD Energy Institute, University College Dublin, Ireland
fawaz.alshehri@ucdconnect.ie
james.odonnell@ucd.ie

[2]School of Architecture, Planning and Environmental Policy, University College Dublin, Ireland
paul.kenny@ucd.ie

ABSTRACT

When designing and creating a working or living space, the provision of thermal comfort for a building's occupants remains a key objective. However, energy consumption associated with the delivery of indoor environmental conditioning in the commercial building stock is not necessarily translated into improved thermal comfort conditions. When collaborative design utilises Building Information Models (BIMs), much of the data required for thermal comfort analysis is already defined by other project stakeholders. Furthermore, mechanical equipment such as HVAC and lighting fixtures, play a major role in functional performance, resultant thermal comfort and energy consumption. Monitoring building performance and thermal comfort requires additional representative data about indoor environmental conditions and energy consumption.

This paper presents a holistic review of the data and information needed for the integration of BIM with thermal comfort modelling for commercial office spaces. Thermal comfort is dependent on multiple factors such as indoor environmental conditions, user behaviour, properties of building materials, etc. For inclusion in the design process this data must first be categorised in a standardised manner. The outputs of this work contribute to a Model View Definition (MVD) for thermal comfort using the IFC standard.

Author Keywords

Building Information Modelling (BIM); Model View Definition (MVD); HVAC; Industry Foundation Classes (IFC) ; BEPS; AECOO; Thermal Comfort; Thermal Environment; Predicted Mean Vote (PMV).

1 INTRODUCTION

Reducing energy consumption and emissions of greenhouse gases is an important 21st century objective. The benefits of which contribute to the arrest of global warming and compensate for over reliance on fossil fuels. The Intergovernmental Panel on Climate Change reported that in 2010 buildings accounted for 32% of global energy use and 19% of greenhouse gas emissions [18]. However, the amount of energy used by buildings varies between countries. For example, buildings in European countries accounted for 40% of total energy use and 36% of total CO_2 emissions [12]. There are many reasons for energy inefficient buildings: poor design, poor operation, lack of legislation, and strong economic, social and environmental factors just to name a few [13]. The energy performance of a building is only one aspect used to assess the overall performance level. In addition, many important factors related to the indoor environment also contribute to improving building performance. These factors relate to sustainability or may affect people directly and these include: air quality, lighting quality, acoustic performance and thermal comfort.

Providing thermal comfort for a building's occupants and decreasing energy consumption remain a key design challenge. The American Society of Heating, Refrigerating and Air-Conditioning Engineers (ASHRAE) [1] and BS EN ISO 7730:2005 [19] define thermal comfort as "the condition of the mind in which satisfaction is expressed with the thermal environment". The purpose of these global standards is to identify a method for predicting thermal satisfaction level and the degree of comfort /discomfort of people exposed to reasonable thermal environments [24]. Brager [4] suggested that "If building designers and operators can find efficient ways to allow building temperatures to float over a wider range, while affording occupants comfort, the potential for energy savings is enormous". In this context, energy modeling and simulation tools are increasingly used to optimise and predict likely energy consumption and associated thermal comfort levels.

Most Building Energy Performance Simulation (BEPS) software can estimate thermal comfort but use concepts of traditional thermal comfort measurement [29]. BEPS defines the comfort level based on Predicted Mean Vote (PMV) which is based on a heat balance model. However, PMV can be described as a "static" model of human thermal comfort and works on input for environmental and personal factors. These kind of models fail to take personal preferences of individual users into account. Most thermal comfort simulation programs refer to ASHRAE-55-2010 or 2013 standards to determine comfort levels within each space [17]. Typically, simulation software defines the comfort zone by inputting information for the six main environmental factors indicative of thermal comfort in which the PMV is within the required limits, (-0.5 and +0.5).

Computational Fluid Dynamics (CFD) is a more detailed approach to comfort analysis where airflow patterns and temperature distributions are determined for individual zones or a group of zones. However, even with a more rigorous CFD model, many reasons could account for variations between simulation model results and site measure data, these include:

SimAUD 2017 May 22-24 Toronto, Canada

incorrect modeling input, lack of relationships between building objects and data from the model, loss during data exchange and a structure to measure and organize data points [23]. Various applications may also produce different simulation results. When combined, these issues are a challenge for researchers and the Architecture, Engineering, Construction, Owner Operator (AECOO) industry as stakeholders require reliable results for predicted energy use in order to achieve an acceptable comfort level. Accurate thermal comfort models must be updated as the building evolves, from design through to operation, to reflect any relevant changes.

Building Information Modeling (BIM) is a life-cycle collaborative technology that is gaining rapid adoption within the AECOO industry. BIM can link the information used in early design stage through to operation through a common data model. In the context of this paper, BIM is a universal user interface for architectural design and building performance simulations [28]. When coupled, BIM and sustainable building design can not only reduce energy consumption and environmental effects but can also decrease costs and create a comfortable and pleasant living environment [21].

Of the available BIM formats, Industry Foundation Classes (IFC) is the only open life-cycle data model for buildings that is an international standard [16]. As the IFC data model is so large, only carefully defined subsets of the model are required to support specific business processes. These subsets are called Model View Definitions (MVD) where the primary objective of MVDs is to ensure standardised import and export of specific requirements for IFC compliant software [26]. Presently there is an absence of an MVD to support thermal comfort analysis in commercial buildings. Future integration of BIM with simulation tools is very promising [6]. From the early design stage, BIMs contain useful information for different project elements which can be reused to establish BEPS and thermal comfort models. With BIM in place, monitoring of thermal comfort can continue through to and include building operation.

This paper presents a holistic review of the data and information needed for integration of BIM with thermal comfort modelling for commercial office spaces. The first step in this work defines a set of necessary exchange requirements in the form of data and information for life-cycle thermal comfort analysis. This information, provided by the BIM compliant stakeholders, can be used to establish thermal comfort models during design, update during the life-cycle and evaluate against measured results during operation of commercial office spaces. These data and information requirements must be represented in a standardised manner in order to develop a Model View Definition (MVD) for thermal comfort. The outputs of this work will contribute to a MVD for thermal comfort in adherence with the IFC standard.

2 INDOOR ENVIRONMENTAL CONDITIONS

Recent changes in peoples lifestyles have contributed to a perceived improved in their quality of life. However, this advance has been accompanied by a reduction in outdoor activities and reflected in issues of human health and well-being [30]. Today, on average, "people spend 80- 90% of their time indoors, and indoor environment has important effects on human health and work efficiency" [30]. Creating a suitable indoor thermal environment makes an important contribution to employee productivity in commercial office spaces. Furthermore, with increasing global energy costs and CO_2 levels, finding methods that reduce energy use while providing individual thermal comfort are important goals for many industries and researchers in this field. Failing to make employees comfortable is not a minor consideration. About 2 % of employee working hours in the UK are spent in securing environment control, costing more than 13 billion each year [14].

Poorly controlled buildings not only make people unproductive, unhappy and uncomfortable, but also can cause health issues, even leading to death. For example, the excessive heatwave during the summer of 2003 killed more than 70,000 people in European countries. It also killed more than 1200 people in south India, most of them old and many in their own homes [27].

A large number of studies have focused on various aspects of thermal comfort, well-being, and health within workplaces. The Center for the Built Environment suggests that buildings are generally inefficient spaces, especially during their operational phase [7]. Mechanical equipment such as HVAC, lighting fixtures, small power loads, etc. play a major role in associated energy consumption. The EU Energy Efficiency Directive [11] dictates that technical equipment within a given building must accommodate and be adapted to occupants' desires, which might be done by monitoring related data points.

Maintaining thermal conditions during operation is one of the key tasks facing building managers. Temperature preferences are subjective thus making it difficult to satisfy thermal comfort expectations of all occupants. The history of studies that deal with thermal comfort suggest there are six primary factors that have to be considered when defining conditions for thermal comfort: Air temperature (^{o}C), Radiant temperature (^{o}C), Air speed (m/s), Humidity (%), Metabolic rate (Met) and Clothing insulation (Clo).

2.1 Thermal Comfort Models

In 1970 Fanger introduced the first thermal comfort model. This model is still in use today, with slight modifications, and is defined in ASHRAE Standard 55 [20, 1]. Fangers model was based on heat balance in the human body. Thermal comfort is defined as the balance of body heat gain due to metabolic rate and heat loss of the body to the surrounding environment [20]. Generally, the two main methods used for thermal comfort measurements are the predicted mean vote (PMV) and the predicted percentage dissatisfied (PPD). The PMV means the predictable mean vote of a group of people on the thermal condition, based on the 7-point comfort scale as shown in (Table 1). The PPD defines the percentage of people dissatisfied with the thermal environment.

Fanger's model looks at five input variables: operative temperature (^{o}C), air speed (m/s), relative humidity (%), metabolic rate (Met) and clothing insulation level (Clo). The operative temperature is used in this model rather than simple

air temperature because it combines both air (dry-bulb) and radiant temperature. Operative temperature and relative humidity are typically available, but other variables pose problems. Even within a given room, air speeds vary [10], so localised measurements are required for each individual, a previously costly and impractical undertaking. Metabolism and clothing levels are also variable, making them hard to estimate [25]. Moreover, Fangers model does not account for adaptations by the user such as acclimatisation, modification of heating controls and expectations of temperatures.

Table 1. ASHRAE Thermal Satisfaction Scale

Vote	Thermal Satisfaction
3	Too hot
2	Warm
1	Slightly warm
0	Neutral
-1	Slightly cold
-2	Cold
-3	Too cold

While the PMV model has been employed universally, correctly or otherwise, for the evaluation of thermal comfort over a long period, evaluation since a long time, it cannot accommodate changes to the local indoor environment caused by fluctuating air currents, radiation, or temperature variation. PMV can be described as a (static) model of human thermal comfort and works on input of environmental and personal factors only.

Adaptive models [9] try to account for responsive and behavioural measures, such as opening windows, turning on a fan or adjusting clothing. This is typically accomplished by modelling the users optimal comfort temperature relative to the outside temperature. The colder or warmer it is outside, the more adaptive measures a user will take.

A wide range of research has been carried out on residential and non-residential thermal comfort levels. One such study attempted to validate the accuracy of the PMV model and compare it with non-physical parameters of thermal sensation for naturally ventilated homes and office environments in the UK. It concluded that there is a real "context effect", such as gender, age, cultural and economic conditions, on occupants predicted and observed thermal sensation [2]. Another study observed that there is a direct relationship between job satisfaction and thermal comfort levels in office buildings [9, 15]. These findings indicate that the above-mentioned non-thermal parameters were not accounted for in the heat balance model.

Today, one of the key challenges facing building designers and operators is the maintaining of continuous thermal conditions during building operation. Even slight deviations from static comfort levels may lead to stress and negatively affect an occupants performance and comfort. Interoperability between BIM-based design and thermal simulation tools can improve the workflow between the design stage and analysis applications since the information contained in the BIM models can also be reused for analysis. However, the integration in BIM of recognised comfort and well-being standards is presently absent. As such, the models data as contained in BIM has to be recreated in the simulation software, which is costly and labor intensive as well as a complex and a potentially error-prone process.

Building simulation typically adopts concepts of traditional thermal comfort measurement. However, the information provided in such a model may not be as reliable as it should be. A more accurate and complete model definitions would include detailed information representing the data needed by the building designer and operators to deliver satisfactorily levels of thermal comfort. The scope of the Exchange Requirement is to support thermal comfort modelling of occupants in commercial buildings during early design, update the model during the building life-cycle and monitor thermal comfort during building operation. This paper develops requirements based on a comprehensive understanding of both old and new concepts for thermal comfort and then categorises these requirements in a standardised manner in order to develop a MVD for thermal comfort using the IFC standard.

3 BACKGROUND ON INFORMATION EXCHANGE

Computer-based information exchanges occur in a variety of ways in the AECOO industry. One mechanism is a proprietary data model tied to a particular vendor and associated software products [8]. These models generally rely on internal data to capture and store data and the user is restricted to using the tools provided by the vendor. If the user needs to use another software application, a conversion of one form is needed, which is difficult and can lead to information loss and degradation. However, an open data model, conceptually provides unrestricted data exchange between applications. This approach provides an underlying data model that can retain the relevant building information [22].

3.1 Industry Foundation Classes (IFC)

Industry Foundation Classes (IFC) has been under development by buildingSMART since 1994. The IFC schema is broadly known as the common data exchange format for information exchange between applications within the AECOO industry [5]. It gives stakeholders a comprehensive data model that enables exchange and sharing information of building geometry and building properties elements. IFC has the potential to bridge the links between stakeholders and project phases throughout its life- cycle, from early design stage to construction, operation and refurbishment or demolition [5]. IFC uses an object oriented description to assure consistent information exchange and interoperability between a number of stakeholder applications.

IFC4 is the latest release standard of the ISO 16739:2013, which is the only open international standard for BIM data that is shared and exchanged between software applications used by the members of a building construction or facility management project [16]. IFC4 improves the functionality of the IFC specification in its main architectural, building service and structural elements with new geometric and para-

metric objects along with other advantages. These additions are of significant value in the context of energy performance evaluation, environmental solutions, thermal simulations and sustainability assessments [22]. Other improvements include integration of ifcXML and mvdXML with extensively defined EXPRESS and XML schema specifications, enhanced documentation and links to buildingSMART data dictionary [26].

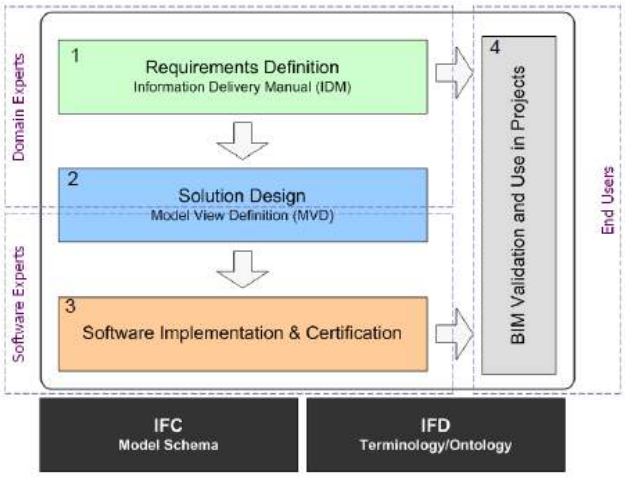

Figure 1. Four Phase Integrated Process

The key objective of this work defines a set of necessary requirements, data and information that needs to be exchanged between processes that evaluate and monitor the thermal comfort level in early design and later during building operation. IFC supports activities at all project stages. However, most of the software applications focus on a specific domain only, depending on the complexity of model [16]. Therefore, the exchange requirements for software applications need to be designed according to domain specific Model View Definitions (MVD).

An integrated MVD process has four phases and involves several participants as shown in Figure 1. The first task is to develop a document use case for the target industry using the IDM process. This document is normally documented in tabular or spread sheet applications for each information exchange identified in the process map. The next phase create the MVD, which is a document subset of the IFC Model Specification that is required for the information exchanges defined in one or more related IDMs. MVDs identify the process for exchange requirements of the AECOO industry from the IFC schema. After requirements have been defined in the form of an IDM, and an implementable solution has been defined in the form of an MVD, the solution cannot be used in projects until it is supported by at least two software applications. This phase requires a software experts. BIM Validation and use in projects is last phase in order to ensure that the exchange meet all requirements defined in the IDM. This is called BIM Validation [3].

At present, it is rare to find programs that can verify if data and information are fulfilling the specifications from the Exchange Requirements in a given IDM. Currently, there is no official mechanism that will allow an automatic translation of an Exchange Requirement into rules within a computer program, as Exchange Requirements are not readable by computer [5]. Therefore, a MVD is needed to satisfy one or many Exchange Requirements between the AECOO industry. The first MVD developed by buildingSMART is known as Coordination View. The main purpose of this view is to allow sharing of building models between different disciplines of the AECOO industry. However, a number of other MVDs are presently under development by groups of developers outside of buildingSMART. They may be submitted to buildingSMART and once accepted, buildingSMART will publish each as an official MVD.

4 REQUIREMENTS FOR BIM-BASED THERMAL COMFORT ANALYSIS

Thermal comfort analysis requires detailed specification of the analysis processes combined with the data and information that needs to be exchanged to support these processes. The target of this research is to describe this data and information in a standardised format. The scope of the Exchange Requirement is to support thermal comfort modelling of occupants in commercial buildings during early design, update the model during the building life-cycle and monitor thermal comfort during building operation.

When used properly, BIM can facilitate an improvement in communication between project stakeholders throughout the building life-cycle. BIM supports early collaboration between stakeholders and can be of particular benefit for participants of the design team. Exchanging building information and models between processes can be challenging within the AECOO industry as most of the applications have interests in a limited area. Currently, there is a lack of common Exchange Requirement for thermal comfort analysis. IFC uses an object-focused description to ensure consistent data exchange and interoperability between several applications. The exchange of information between applications must be made according to a specific MVD. The MVD defines an exchange of IFC data that would meet the end users' needs and implement methods of exchanging data between software applications for specific analysis; in this case CFD simulation for thermal comfort evaluation and monitoring.

Human comfort is a significant consideration when designing a work space and CFD models can be used to provide insight on human comfort levels. Through the use of CFD, decision makers have the ability to evaluate thermal comfort levels, identify opportunities for improvement and control this level with any modification needed during building operation. The AECOO industry requires identification of what data and information is important to include within a BIM, particularly when exporting a selected zone or zones for CFD analysis. Therefor, the main purpose of MVD is to support this exchange process in order to achieve optimum and reliable results of thermal comfort analysis. Once the BIM is complete, the MVD extracts data needed for CFD analysis. For example, if a BIM software has already implemented a MVD to support a CFD model, the output of the IFC file

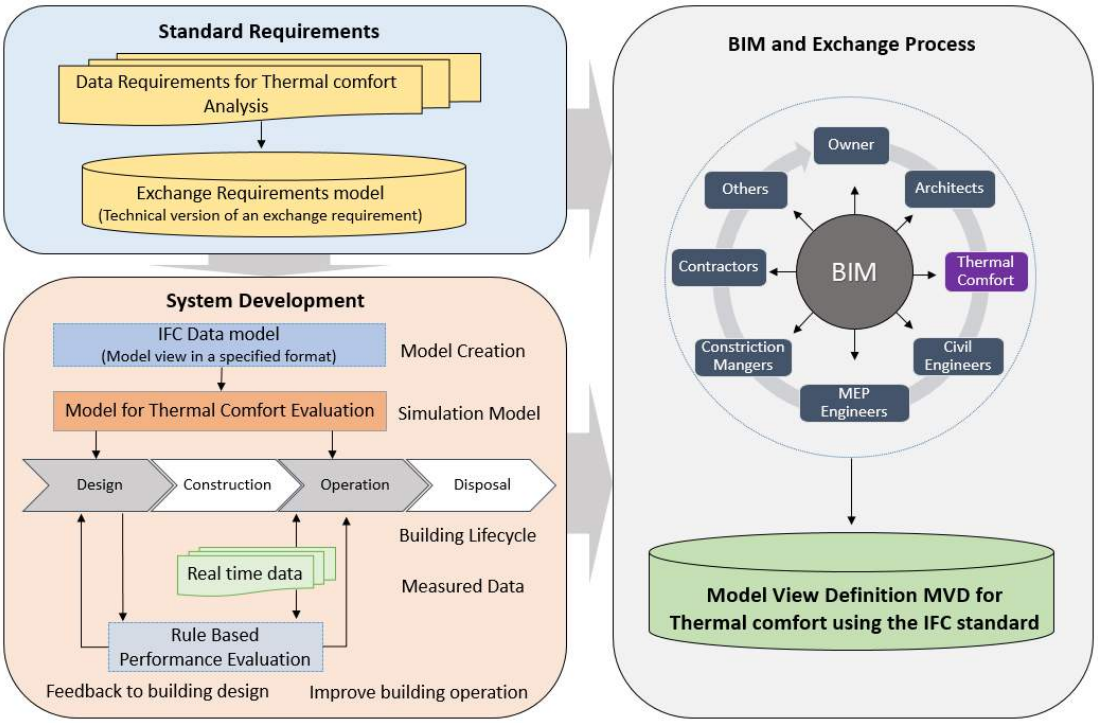

Figure 2. Methodology of integrate MVD for thermal comfort analysis in a building design and operation stages.

will include only the exchange requirements defined for that specific analysis, thus filtering unrelated information. This allows for easier, quicker data transfer and reduces the loss of information when exchanging BIM files between different applications and analysis tools.

As discussed earlier, thermal comfort is dependent on many aspects, not only environmental or personal factors. BEPS tools usually focus on concepts of traditional thermal comfort measurement in order to make decisions but there are multiple factors and variables which can have a major effect on comfort levels. For example, building orientation, window opening strategy, window to wall ratio, shading strategy, lighting fixture, building wall therm-physical properties and thickness, etc. in addition to the psychosocial parameters. To date this work has identified 22 objects with over 800 properties relevant for thermal comfort analysis and the objects include: Actor, Air Terminal, Air Terminal Box, Building, Building Storey, Damper, Door, Element, Element Type, Fan, Material, Opening Element, Project, Slab, Space, Space Heater, Spatial Element, Spatial Zone, Unitary Equipment, Wall, Window and Zone. The importance of each object and property can be denoted by a mandatory or optional tag for each entry.

The thermal comfort model is required to include the mandatory parameters to achieve optimum and reliable results of thermal comfort analysis. It is important to categorise these requirements in a standardised manner first, in order to develop a MVD for thermal comfort using the IFC standard. The proposed MVD defines the exchange requirements required by designers and building managers to assess thermal comfort level. It represents the data and information to be exchanged between two or more stakeholders in support of a specific business process at a particular stage of the building life-cycle, as shown in Figure 2. It is necessary to understand that these requirements come from the end users' needs and the primary role of the IFC model view is to ensure IFC implementation supports these requirements.

4.1 IDM Methodology for Thermal Comfort

The Information Delivery Manual (IDM) is a standardised methodology that has been developed by buildingSMART. This methodology can be used to document and describe the information that has to be exchanged between relevant stakeholders.

The first step in this work is to identify and describe the detailed functions performed by each stakeholder and then associated information requirements. This phase is divided into two part; firstly; detailed specification of the analysis processes for the data and information that needs to be exchanged to support these processes based on a holistic review of past and current thermal comfort models. This provides a description of the information in non-technical terms. They are general statements of requirements and are not specific to a specific IFC release as as illustrated Figure 2. This information is subsequently translated into an exchange requirement for thermal comfort using the IDM and ISO 16739:2013 process as as illustrated in Table 2. The exchange requirement is then mapped to a corresponding BIM format, typically IFC for a detailed MVD definition. The advantage of including IFC in IDMs is that it reduces the risk of error when implementing fine detail. An additional advantage is that IFC makes it pos-

Table 2. Partial Exchange Requirements table for Thermal Comfort analysis

IFC Entities	Property set	Information needed	Property Description	Required	Optional	Property Value	Unit
IFCSpace	**Pset_Space Occupancy Requirements**	**The following property should be included**	**Details description of a property should be included**				
		Occupancy Type	It is defined according to the building code	x		Single	entity
		Occupancy Number	Number of people required for the activity assigned to this space	x		Single	number
		Occupancy Number Peak	Maximal number of people required for the activity assigned to this space in peak time	x		Single	entity
		Occupancy Time Per Day	The amount of time during the day that the activity is required within this space	x		Single	entity
		Area Per Occupant	Design occupancy loading for this type of usage assigned to this space	x		Single	p/m^2
		Is Outlook Desirable	An indication of whether the outlook is desirable		x	Single	entity
		Minimum Head room	Headroom required for the activity assigned to this space		x	Single	mm
	Pset_Space Thermal Load	**The following property should be included**	**Details description of a property should be included**				
		People	Heat gains and losses from people	x		Bounded	Met
		Equipment Sensible	Heat gains and losses from equipment	x		Bounded	kW
		Lighting	Lighting loads	x		Bounded	kW
		Air Exchange Rate	Loads from the air exchange rate	x		Bounded	m^3/s
		Dry Bulb Temperature	Loads from the dry bulb temperature	x		Bounded	°C
		Relative Humidity	Loads from the relative humidity	x		Bounded	%
		Total Sensible Load	Total energy added or removed from air that affects its temperature	x		Bounded	kW
		Infiltration Sensible	Heat gains and losses from infiltration	x		Bounded	W/m^2K

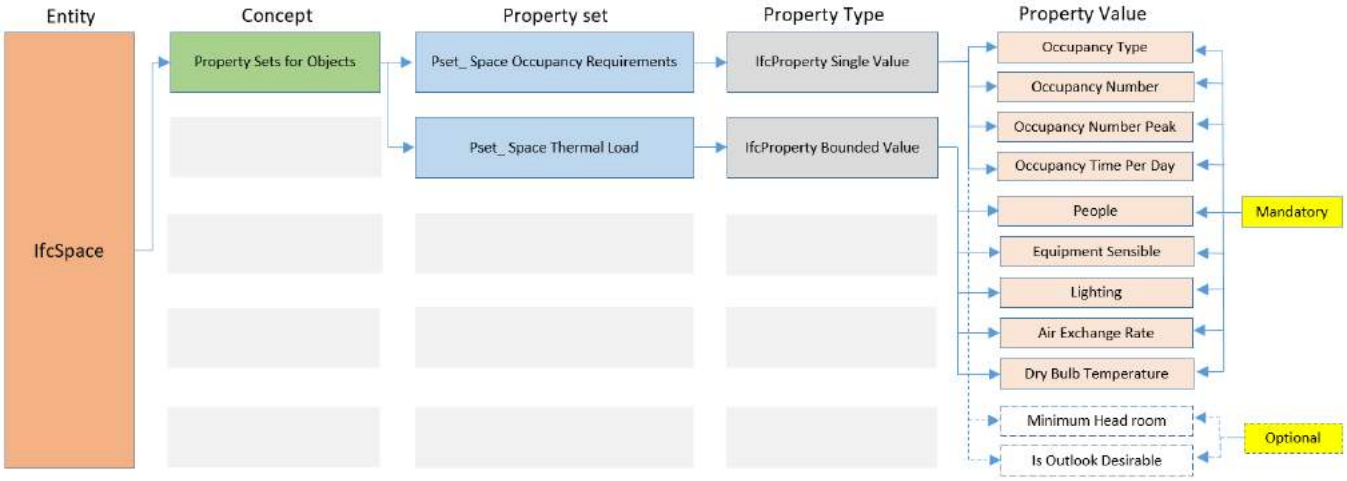

Figure 3. Graphical representation of ifcSpace for a partial Thermal Comfort MVD.

sible to deliver specific business rules and data validation at a detailed level and make the output from the IDM process readable by computers. However, having very detailed and technical specifications in IDM requires that the IDM process will not only need domain expertise and business modelling skills but also require very detailed technical knowledge. To date this phase has identified 22 objects with over 800 properties relevant for thermal comfort analysis. These data represents technical version of an exchange requirement.

Secondly, the development an information exchange system for thermal comfort analysis is the next phase after identifying the exchange requirements. This step includes a novel system for information exchange of thermal comfort analysis data among project stakeholders and for different stages of the building life-cycle, i.e. design and operation. This model integrated BIM, CFD and sensors to predict and measure individual thermal comfort level in a real time data. In doing so, this model supports thermal comfort modelling of occupants in commercial buildings during early design, update of the model during the building life-cycle and monitoring of thermal comfort during building operation (Figure 2). This system allows building designers and managers to make informed decisions to keep occupants within a comfortable range.

The next phase is to create the Model View Definition (MVD) itself and develop appropriate representation of definitions for the exchange requirements capable of supporting indoor thermal comfort performance over the building life-cycle. This information, with the exchange requirements data from the first phase will form the basis of the MVD, which is a specified definition using the IFC data format. A MVD is considered a sub-schema of the overall IFC schema specification and its main purpose is to select and specify the appropriate information entities. The IDM defines the exchange requirements needed for the development of the MVD for thermal comfort and the MVD will bind these requirements in an IFC sub-schema. For example if a BIM software has already implemented a MVD, the output IFC file will contain just the necessary exchange requirements for that particular analysis between BIM and BEPS tools as demonstrated in Figure 2. On completion of a MVD, software vendors can use it to develop IFC export and/or import functions in their software applications. In practice, this means that exported entities and attributes comply with the exchange requirements defined in the MVD. After completion, the MVD will be submitted to a

buildingSMART group for acceptance and publication as an official Model View Definition (MVD) for thermal comfort using the IFC standard.

In order enhance readability and reduce the level of complexity, an illustrated example representative of a part of one subset Exchange Requirements, IfcSpace of the creation of a MVD is presented in the next section.

4.2 Illustrated Example

Overall, this work encapsulates both old and new concepts of thermal comfort and then categorise these requirements in a standardised manner. The example presented in this section details a small subset of zone data requirements for thermal comfort and provides underlying data for only one subset of exchange requirements IfcSpace. The value of internal gains from heat generated by people determines the demand for energy required to keep occupants within a comfortable range. There is a set of properties under space occupancy requirements that needs to be clearly defined before exporting a BIM to thermal comfort analysis tools. For instance, maximum number of people assigned to this space over time, the temporal variation in occupant load during a regular workday, area per occupant for this type of use and the activity type assigned to this space, etc. This information and others must be clearly defined per occupied space instance in order to provide suitable environmental conditions and also directly contributes to the overall energy demands for HVAC equipment. In this case, the exchange requirement space to IFC specification is IfcSpace. The IDM process of exchange requirement is used as shown in Table 2 and then this table is used to create a corresponding graphical representation of the MVD, as shown in Figure 3.

The IFC schema encompasses several hundred entities, including building element-type entities such as IfcRoof and IfcDoor. In this case the entity IfcSpace is defined in the first column (Table 2). Each entity has many property sets which must also be defined. In this case Space Occupancy Requirement and Space Thermal Load as shown in the second column from the left. For each MVD a set of concepts are applied according to the exchange requirement of a particular process as demonstrated in the third column from the left. The fourth column contains a property description field, such as number of people required, maximal number of people and the amount of time during the day that the activity is required within this space. Subsequent columns detail whether a property is mandatory or optional. The final columns indicate the data type, which is either single, Boolean or bounded, and the unit for the property in question.

This example describes only a small part of one IfcSpace entity and the final MVD for thermal comfort analyses will include all the exchange requirements and their relationships. The main purpose of this MVD is to support building designers and managers to assess the thermal comfort level during design stage and monitor this level during building operation. This allows building designers and managers to make informed decisions to keep occupants within a comfortable range.

5 CONCLUSION AND FUTURE WORK

BIM-based Thermal Comfort analysis has been proposed in this paper to improve indoor thermal comfort conditions and building performance. This work presents an overview of the data and information needed for integration of BIM with thermal comfort modelling for commercial office spaces. In this research, a standardised method of information exchange between BIM and BEPS tools was presented. The primary objective of this work is to define a standardised set of information requirements on which software vendors can align their import and export functions. The exchange of information between applications must be designed according to a domain specific MVD. This process is based on the MVD methodology, which defines primarily for implementation of information exchange scenario using IFC, in this case thermal comfort analysis.

BIM enables collaborative working processes and acts as the central data repository for extraction of information. In essence, BIM design models typically have too many architectural and construction details, which are not needed for the performance analysis. Therefore, understanding the level of detail needed for the simulation model is essential for successful integration. Once BIM software has already implemented a MVD to support thermal comfort analysis, the output of IFC file will include only the exchange requirements defined for that specific analysis, thus filtering unrelated information. The deliverable from this paper is a small subset of an IFC compliant MVD to support BIM based thermal comfort evaluation. Some requirements for creating MVD for thermal comfort are not available in the IFC schema. Consequently, necessary additions will be documented within the MVD and requested within future IFC releases.

In subsequent publications a more rigorous extension of the defined model will be presented. Further, in order to examine and validate the proposed BIM exchange requirement, the concept will be applied in a case study, the commercial office space. After completion, the MVD will be submitted to a buildingSMART group for acceptance and publication as an official Model View Definition (MVD) for thermal comfort using the IFC standard.

ACKNOWLEDGMENTS

We thank all colleagues, who provided helpful comments on previous versions of this document. This work was supported by funded by the Department of Education of the Kingdom Saudi Arabia. Grant number IRJN1502/2

REFERENCES

1. ASHARE. ASHRAE Standard 55-2010: Thermal Environmental Conditions for Human Occupancy. *American Society of Heating, Refrigeration and Air conditioning Engineers ASHRAE Sta* (2013), 58.

2. Beizaee, A., and Firth, S. K. A Comparison of Calculated and Subjective Thermal Comfort Sensation in Home and Office Environment. *Prooceedings of Conference: People and Buildings*, September (2011), 1–6.

3. Belsky, M., Sacks, C., and Brilakis, I. A Semantic Enrichment Engine for Building Information Modelling. *Journal of Computer-Aided Civil and Infrastructure Engineering* (2015).
4. Brager, G. S., Zhang, H., and Arens, E. Evolving opportunities for providing thermal comfort. *Building Research & Information 43*, 3 (2015), 274–287.
5. BuildingSmart. IFC Releases, 2016.
6. Cao, J., Wimmer, R., Thorade, M., Maile, T., O'Donnell, J., Rädler, J., Frisch, J., and van Treeck, C. A Flexible Model Transformation to link BIM with different Modelica libraries for Building Energy Performance Simulation. In *14th Conference of International Building Performance Simulation Association*, IBPSA (Hyderabad, India, 2015), 434–441.
7. Center for the Built Environment. Occupant Indoor Environmental Quality (IEQ) Survey, 2016.
8. Corry, E. *A Semantic Web Approach to Enable the Holistic Environmental and Energy Management of Buildings*. PhD thesis, National University of Ireland Galway, 2014.
9. de Dear, R., and Brager, G. S. Developing an Adaptive Model of Thermal Comfort and Preference. Tech. rep., Center for Environmental Design Research, University of California, Berkeley, 1998.
10. Erickson, Varick L., A. E. C. Thermovote: participatory sensing for efficient building hvac conditioning. In *Proceedings of the Fourth ACM Workshop on Embedded Sensing Systems for Energy-Efficiency in Buildings. ACM* (Toronto, Canada, 2012).
11. European Commission. The EU Energy Efficiency Directive, Building and Energy, 2012.
12. European Parliament. European Parliament and Council, 2010a. Directive 2010/31/EU . Tech. Rep. ISSN 1725-2555, European Council, 2010.
13. Gasper, R., Blohm, A., and Ruth, M. Social and economic impacts of climate change on the urban environment, 2011.
14. Gorvett, Z. The never-ending battle over the best office temperature, 2016.
15. Hellwig, R. T., Brasche, S., and Bischof, W. Thermal Comfort in Offices Natural Ventilation vs . Air Conditioning. *Conference Comfort and Energy Use in Buildings. Getting them Right* (2006).
16. International Organization for Standardization. ISO 16739:2013 Industry Foundation Classes (IFC) for data sharing in the construction and facility management industries, 2013.
17. Ioana U., Ilinca N., Ruxandra C., Cristiana C., V. B. Simulation of a Passive House for Thermal Comfort Analysis. In *4th International Conference on Thermal Equipment, Renewable Energy and Rural Development 2015*, Renewable Energy and Rural Development (Posada Vidraru, Romania, 2015).
18. IPCC. Climate Change, Adaptation, and Vulnerability. Tech. Rep. March, Intergovernmental Panel on Climate Change, 2014.
19. ISO. ISO 7730: Ergonomics of the thermal environment Analytical determination and interpretation of thermal comfort using calculation of the PMV and PPD indices and local thermal comfort criteria. *Management 3* (2005), 605–615.
20. Kate E. Charles. Fanger's Thermal Comfort and Draught Models. Tech. rep., Institute for Research in Construction National Research Council of Canada, 2003.
21. Kim, J. B., Jeong, W., Clayton, M. J., Haberl, J. S., and Yan, W. Developing a physical BIM library for building thermal energy simulation. *Automation in Construction 50*, C (2015), 16–28.
22. Liebich, T. IFC4 the new buildingSMART Standard, 2013.
23. Maile, T., Fischer, M., and Bazjanac, V. A method to compare measured and simulated data to assess building energy performance. Tech. Rep. August, Stanford University, Center for Integrated Facility Engineering If, Stanford,USA, 2010.
24. Olesen, B. W. Standards for Ventilation , IAQ , and Thermal EVALUATION OF THE INDOOR ISO EN 7730rev ISO EN 7730rev ISO EN 7730rev PMV-index. Tech. rep., Technical University of Denmark, International Centre for Indoor Environment and Energy,, Lyngby, Denmark, 2013.
25. Peeters, L., de Dear, R., Hensen, J., and D'haeseleer, W. Thermal comfort in residential buildings: Comfort values and scales for building energy simulation. *Applied Energy 86*, 5 (2009), 772–780.
26. Pinheiro, S., Corry, E., Kenny, P., and O'Donnell, J. Development of a Model View Definition for Environmental and Energy Performance Assessment. In *2nd conferenceof the CITA BIM November 12th -13th 2015*, CITA BIM (Dublin, Ireland, 2015).
27. Roaf, S., Nicol, F., and Rijal, H. Designing for comfort at high temperatures. *Architectural Science Review 58*, 1 (2014), 35–38.
28. Volk, R., Stengel, J., and Schultmann, F. Building Information Modeling (BIM) for existing buildings - Literature review and future needs. *Automation in Construction 38* (2014), 109–127.
29. Welle, B., Haymaker, J., and Rogers, Z. ThermalOpt: A methodology for automated BIM-based multidisciplinary thermal simulation for use in optimization environments. *Building Simulation 4*, 4 (2011), 293–313.
30. Yu, B. F., Hu, Z. B., Liu, M., Yang, H. L., Kong, Q. X., and Liu, Y. H. Review of research on air-conditioning systems and indoor air quality control for human health. *International Journal of Refrigeration 32*, 1 (2009), 3–20.

A Simulation-Based Workflow to Assess Human-Centric Daylight Performance

Siobhan Rockcastle, María Lovísa Ámundadóttir, and Marilyne Andersen

LIPID, ENAC, EPFL
Lausanne, Switzerland
Siobhan.rockcastle@epfl.ch

ABSTRACT

This paper will present an annual simulation-based workflow for assessing human perceptual and non-visual responses to daylight across a series of view positions in an architectural case study. Through the integration of mathematical models used to predict visual interest and non-visual health potential, this paper will introduce an automated workflow to assess an array of view positions (located at eye level) under varied sky conditions and across multiple view directions to analyze the predicted impacts of daylight on perception and health in architecture. This approach allows for a spatial and occupant centric analysis of daylight using an integrated simulation-based approach.

Author Keywords
Daylight perception, non-visual health potential, human-centric performance, visual interest, non-visual response, daylight performance, lighting simulation.

1 INTRODUCTION

Daylight is a powerful element in the experience, vitality, and expression of architecture. Its intensity, direction, and color can transform the visual and physiological responses of an occupant, but the inherently variable nature of these elements and their impact on performance can make a holistic assessment particularly challenging. An architect must integrate, control, and re-distribute daylight to meet general illumination requirements, while fulfilling aesthetic design objectives and creating a comfortable and healthy occupant experience. This task is made even more complex by the temporal variability of solar altitude and sky conditions. Most architects and building engineers are familiar with general illumination requirements, but the perceptual and health-related impacts of daylight are less frequently integrated alongside more traditional performance targets in daylight design. A brief overview of research in daylight perception and non-visual effects of light will help position the performance modules in this paper and are further detailed in Section 2.2.

1.1 Impacts of Daylight on Perception

Characteristics of daylight such as composition and contrast can create strong impacts on our perceptual experience in architecture. While many architects openly acknowledge this potential, research into objectifying and/or quantifying these characteristics has been limited [1]. Past studies have revealed a link between daylight and occupant impressions of pleasantness and/or interest using indicators such as average brightness, luminous distribution, and luminance diversity [2-6]. These studies have generally found that some amount of brightness and luminous diversity creates a positive impact on impressions of interest and pleasantness, while excessive brightness and diversity can cause visual discomfort. Although widespread consensus on the measurable impacts of brightness, distribution and diversity has yet to be reached, there are a number of recent studies which have proposed methods of quantifying the compositional characteristics of daylight and their impacts on perception. The Luminance Difference Index [7] is a physically based measure which quantifies the compositional diversity of luminance levels across a range of view directions. The authors of this study found a link between higher luminance diversity and increased ratings of pleasantness, but a dependence on physical measurements limits the use of this index. Integration within the design phase necessitates a simulation-based method capable of assessing unbuilt proposals.

A set of algorithms proposed by Rockcastle et al. [1] were developed to assess rendered images and quantify the compositional and temporal variability of daylight across a fixed view position. Further development of these algorithms by Rockcastle et al. [8] used an online survey to collect subjective ratings for a series of attributes in daylit renderings and fit the distribution of responses for calming - exciting to a modified algorithm called mSC (modified spatial contrast). The model generated from this algorithm and survey will be introduced as a performance module in Section 2.2 to predict instances of visual interest from rendered scenes.

1.2 Impacts of Light on Non-visual Responses

Shifting from visual to non-visual effects of light, there are several factors that have been linked with health-related performance indicators, such as the quantity of light we receive over time and the duration/ timing of that exposure. Increased daytime exposure to bright light (<1000 lx) has been positively associated with sleep quality [9] and shown beneficial effects on alertness and vitality [10-11] Light exposure does not always induce positive effects, however, as night-time exposure of dim light (>100 lx) can shift the

circadian clock and disturb other behavioral/physiological processes such as melatonin production [12]. The concept of 'healthy' lighting is still relatively new in the lighting community, as the existence of novel photoreceptors called ipRGCs was only discovered at the beginning of this century [13-14]. As such, there is a large knowledge gap in understanding how different light properties can influence non-visual responses and how those responses can influence occupant health and wellbeing in buildings.

The estimation of a healthy daily light dose poses many challenges, in part due to the relative novelty of research in this areas, but helping to inform decisions that promote health and wellbeing is beneficial to the lighting design community. Non-visual responses must be evaluated as a dynamic system, which adapt to intensity, wavelength, duration, history, and timing of light received at the eye and ultimately at the retina. Based on recent work by Amundadottir [15], this paper applies a novel model, called non-visual direct-response (nvR_D model). This model evaluates the non-visual health potential of light by integrating its underlying photobiological properties on responses in humans. The function and implementation of the nvR_D model will be further explained in Section 2.2.

1.3 Integrated Approach

Due to the novelty of mathematical models existing in this area of occupant-centric daylight assessment, we have only begun to explore approaches to a computational evaluation. A recent study by Amundadottir et al. simulated a time series of HDR renderings to assess multiple view directions for dynamic impacts of non-visual health potential, visual interest, and gaze behavior [16]. While this approach laid the groundwork for assessing dynamic changes in vertical illuminance and luminance from a human view point, it was limited to a single, fixed view position. As humans generally move through space, a range of view positions would be required to evaluate the diversity of daylight conditions experienced throughout an architectural space.

The workflow presented in this paper will evaluate visual interest and non-visual health potential using a platform which integrates performance modules across an array of view positions and view directions. The results will be shown both spatially (across view positions) and temporally (over time for a select view position) in a select architectural case study. To showcase this approach, the authors have chosen to analyze two floors of the Ryerson Student Learning Center by Snøhetta and Zeidler Partnership in Toronto, Canada.

2 DEVELOPMENT OF AN INTEGRATED PLATFORM

As stated above, the primary motivation for development of this platform is to integrate a performance assessment of daylight *throughout* the building at an occupant scale. The platform provides a simple interface to guide users step-by-step through the simulation setup, resulting in an automated workflow to define inputs and generate the scripts required for the lighting simulation. Using Radiance as the background simulation engine, this platform provides the necessary inputs to the mSC and nvR_D performance modules introduced in Sections 1.1-1.2 (explained further in Section 2.2). After the simulation results have been analyzed, performance is shown spatially and temporally.

2.1 Simulation Workflow

Generalizing the concept of a time-series simulated for a single, centralized position in space [16], this workflow has been implemented to the simulation of multiple viewpoints in space over any number of desired moments and sky conditions. While integrating perceptual and health-based performance modules in a manner that is accessible for less experienced users, the platform remains flexible for more advanced users who want to override defaults. The user is guided through this workflow step-by-step using a simple interface that runs Radiance to generate illuminance and luminance-based outputs.

The simulation workflow is as follows:

1. Load a 3D model (OBJ, DXF, 3DS, SKP) and convert it to RAD material and geometry files. Alternatively, RAD and material files made elsewhere can be loaded directly.
2. Select the site location, weather and moment distribution, and create OCT files (one per moment and sky condition).
3. Define the position of analysis nodes by reading in a text files or export of point locations from a geometry modeling platform (like Rhino).
4. Run the simulation locally (or use the scripts to run simulations on an external server) to generate illuminance and/or luminance outputs.
5. Compute mSC and nvR_D performance modules from the obtained illuminance and luminance data.
6. Visualize the results spatially and temporally.

One of the advantages of using this platform is more efficient data management, where results are stored in an organized data folder system and temporal files are deleted when no longer needed. To speed up simulation times, the location of ambient files is shared, which makes the rendering of many view positions possible without a linear increase in rendering time. Using a method of extracting multiple views from a single 360° image, we store only one rendered scene but from there we can generate as many 180° fisheye images as requested.

Instead of running the simulation locally on a personal computer, the platform can generate shell scripts for running computationally demanding projects on an external server. In the background, the platform creates a project folder, which must be transferred as a whole to ensure that the platform recognizes the project. In this example, the authors used a multi-core server to run individual jobs in parallel. Figure 1 shows an overview of this process from geometry model to the application of performance modules.

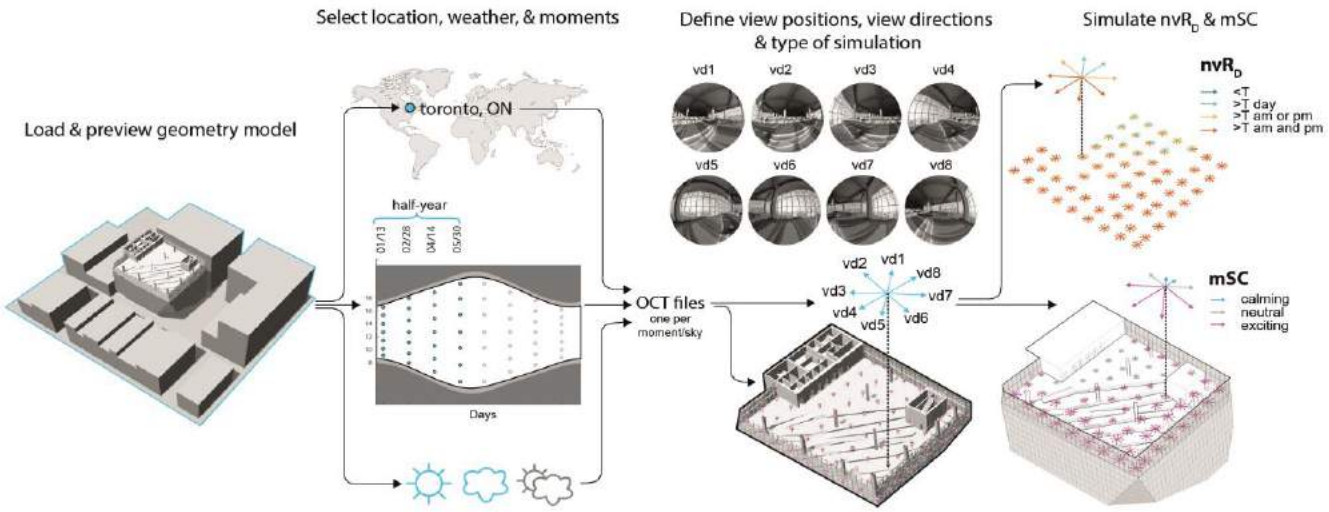

Figure 1. Shows the workflow for our proposed platform; load and preview a geometry models, select location/instances/sky conditions, define location of analysis points/view directions/type of simulation, and run desired performance models (mSC & nvR$_D$).

2.2 Performance Modules

While a detailed mathematical description of the two prediction models described in this paper are introduced elsewhere [8,15,16], the following section will outline the implementation of these models into the proposed simulation platform.

Predicting Visual Interest in Renderings

The study briefly introduced at the end of Section 1.1, proposed an image-based algorithm called mSC to predict attributes of visual interest in daylight renderings. The mSC algorithm was modified from a neighborhood measure called RAMMG which was developed to predict contrast perception in digital images [17]. An online experiment with 167 subjects was used to compare a broad range of image-based algorithms to subject ratings of visual interest using 7-point bi-polar ordinal scales from calming – exciting and subdued – stimulating. The results of this study found that Pearson Correlation Coefficient values between median ratings of mSC [8] and calming- exciting and subdued – stimulating were significantly correlated ($r \geq 0.78$, $p<0.001$). From a population of 167 subjects, logistic regression was used to fit mSC predictions to the distribution of subject responses for each rendering. The fitted logistic function in [8] computes the probability distribution that subjects would rate a rendering in the calming or exciting spectrum based on image composition. The odds of achieving ratings 1-3 on a 7-point scale are significant at $p<0.05$. More detail can be found in [8].

The mSC algorithm is computed on hemispherical images derived from 360° fisheye HDR images obtained using *rpict* > *pinterp* in Radiance. Each Radiance picture is then tonemapped and compressed using *pcond* > *ra_bmp* to provide the appropriate image-based input for computing mSC. Based on the computed mSC value, the fitted model then returns a prediction of visual interest. From the fitted logistic function [8], two thresholds were determined to predict perceptions of calm and excitement (Section 3.4) in a majority percentage of the surveyed population. The application and threshold predictions of calm and excitement mentioned above are described in depth in [16].

Predicting Non-visual Health Potential

Parallel research in non-visual health (introduced in Section 1.2) proposed a novel model called the non-visual direct-response (nvR$_D$) model which predicts the relative non-visual responses to light with the aim of evaluating the dynamic light-response behavior that occurs under real-world settings [16]. The nvR$_D$ takes effective irradiance as an input [18]. Currently, the vertical illuminance is computed using *rtrace* in Radiance and then these values are scaled assuming a constant spectral power distribution of CIE standard indoor illuminant ID65. This assumption limits the material properties in the scene to grey scale. The nvR$_D$ model outputs a smoothed delayed version of the input light signal simulated at the occupant's eye level, accounting for shifts in spectral sensitivity, the effect of intermittent patterns, different exposure durations, and adaptations to prior light history. The application of the nvR$_D$ model thus does not support a point-in-time evaluation, as the current response depends on past inputs.

The outcome of this model is evaluated over a 24-hour day and gives a cumulative response (R$_D$). The cumulative response R$_D$ is mainly sensitive to total light intensity and duration of light exposure, therefore providing a measure of *daily light dose*, which is independent of circadian timing. At any time during the day, it is possible to return an intermediate value if, for example, it is relevant to evaluate a spatial position for shorter periods of time. This is especially relevant in buildings, where our occupation may span anywhere from a couple of minutes to several hours or days. Setting minimum targets or performance goals is

necessary to evaluate non-visual health potential as we would like to know how much daylight we need, within a given space, from a given position and view, to achieve desired health potential. Given a reference profile of an ideal light exposure, the nvR_D model can produce a target for evaluating performance. The nvR_D model is described in detail in [16].

2.3 Visualization of Results

The mSC and nvR_d performance modules take luminance and/or illuminance data as input for a series of view positions within a geometry model and present the results in a format that illustrates whether performance thresholds have been met across each view direction (Section 4.5) over an established time series. The production of simultaneously spatial and temporal data helps to inform designers, engineers, and building operators about *where* and *when* daylight might affect human perceptual and non-visual responses in the built environment. While a preliminary (static) visualization of results for both mSC and nvR_D is provided for a select architectural case study in this paper, future development of this platform will allow users to interact with results across view positions and over time. An overall picture of average daily performance can be just as useful as a detailed assessment of hourly performance or an instantaneous prediction across view directions.

3 SELECTION OF ARCHITECTURAL CASE STUDY

For the demonstration of this simulation-based workflow, we selected an architectural case study that presents a multitude of interior daylight conditions due to its patterned glass façade, varied interior layout, and mix of programmatic uses. The Ryerson Student Learning Center (SLC) in Toronto, designed by Snøhetta and Zeidler Partnership (opened to the public in 2012), is surrounded by a dense urban context, ranging in height from 3 to 9 stories (Figure 2).

Considered as a programmatic expansion to the neighboring library, the SLC houses student work/study spaces and staff offices – both open and enclosed. The daylight design concept harnesses natural illumination using high ceilings and open spaces with translucent frit to minimize direct sunlight and diffuse daylight deep within the interior spaces. The selection of a large fritted pattern on the exterior glass façade produces strong visual effects under direct sunlight.

3.1 Selection of Spaces for Comparative Study

The Ryerson SLC contains 9 floors, but to demonstrate the impacts of architectural form, orientation, and façade patterns on human-centric daylight performance, we decided to simulate a series of points across the 6th and 7th floors, which provide two plan configurations. The 6th floor is composed of informal open study space across a series of ramped floor levels. Using a 5-meter spacing, the floor plan was divided into a grid of 59 points, offset a minimum of 2 meters from the façade and circulation cores.

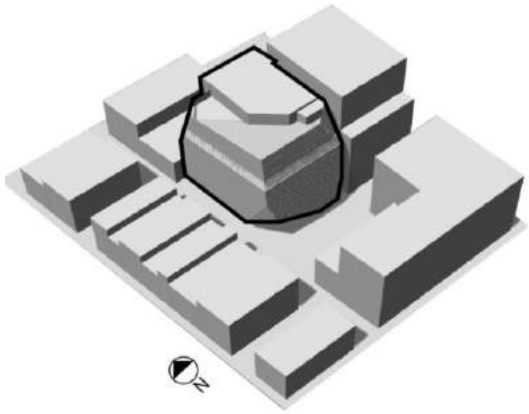

Figure 2. The Ryerson SLC is shown in its surrounding urban context as a digital rhino model.

A 5-meter grid was used to analyze a moderate number of interior view position, while limiting computational expense. Figure 3 shows the layout of space, distribution of sensor points, and a sample of rendered view directions from a select view position. The 7th floor is split into three open study spaces, flanked by two rows of enclosed study rooms, as seen in Figure 3. All enclosed study rooms look out onto the open study spaces through an interior glazed wall. While many of these spaces require electric light at all times of the day due to insufficient natural illumination deep within the floor plate, we decided to simulate only the daylight to evaluate the carbon-neutral potential for interest and health-related lighting performance. Using the same spacing as for the 6th floor, with the addition of points at the center of each enclosed study room, we established a grid of 76 points.

3.2 Translation of Geometry Model into RAD Format

The geometry of our selected case study was received as a DXF and imported into Rhinoceros. After re-grouping layers by material definition, we re-built the glass façade so frit patterns were individual glass objects and could properly read material transmission values. We defined a 5 m grid of points at eye level (1.21 m from the floor while sitting) and exported those point locations as a text file. Depending on the specific nature of a desired analysis, a denser array of view positions could be used, but this would result in higher computational cost and must be considered alongside other input selections.

Using the DIVA toolbar, we exported our model and material definitions in the RAD format and imported them into the platform. We selected 28 semi-annual instances (7 hourly instances on each of January 13, February 28, April 14, and May 30) to give us a comprehensive snap shot of a symmetrical half year. This time series was developed from the Lightsolve method [19], which uses 56 symmetrical instances to interpolate an annual temporal profile of illuminance-based data. We chose 8 view directions per view position (135 points between the 6th and 7th floors) to conduct a series of illuminance and luminance-based simulations as inputs for our mSC and nvR_D models.

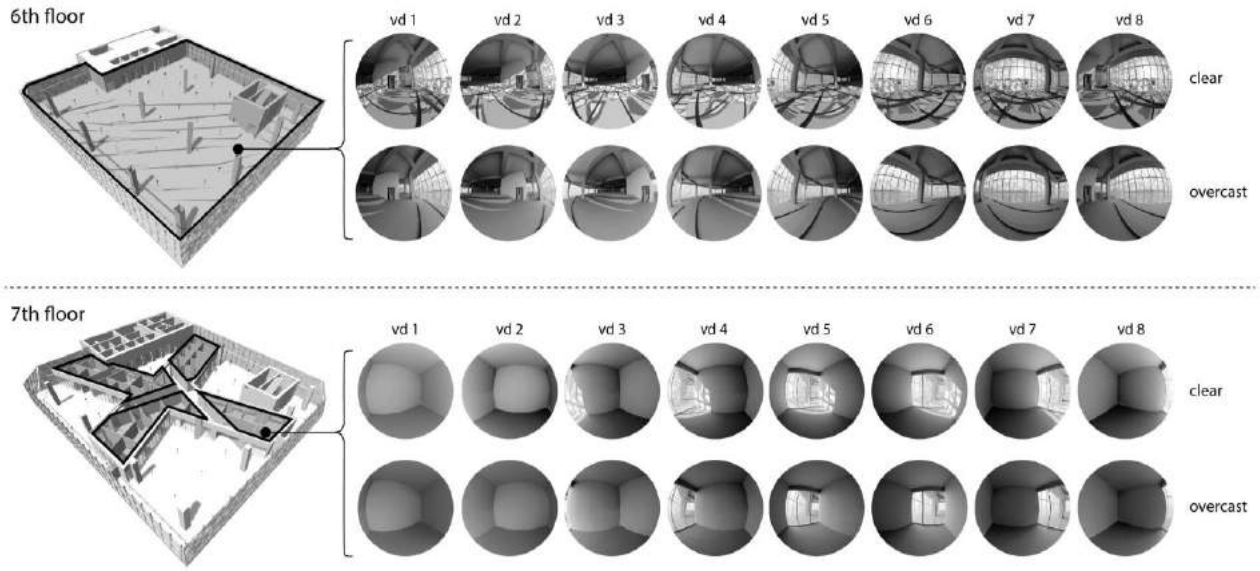

Figure 3. This image shows the two floors (6th above and 7th below) selected for analysis in our case study, alongside a sample of hemispherical renderings produced from each selected view position and view direction (1-8).

3.3 Interpretation of Performance Modules

For each view position and view direction (60,480 in total = 135 view positions x 8 view directions x 28 instances x 2 sky conditions) we applied the mSC algorithm to rendered hemispherical images [8]. For the same view positions and directions, the cumulative response R_D was also calculated using effective irradiance [18].

Visual Interest

Two threshold values were used to categorize results of the mSC algorithm into three categories:

1. Calming, mSC < 6.96
2. Neutral, mSC < 6.96, < 11.75
3. Exciting, mSC > 11.75

Results in this paper are presented as both the average daily mSC achieved across each view direction, but also as instantaneous moments. The average daily mSC allows the user to visualize a compact overview of the perceptual impact on each view direction, while the instantaneous hourly results allow him/her or see how those results vary over time. Results for each view direction are shown using colored arrows, with the length determined by the output of the mSC model and the color (cyan, grey, and magenta) determined by the thresholds listed above.

Non-visual Health Potential

A threshold value T = 4.2 [16] was used to categorize the resulting daily cumulative responses R_D into four categories:

1. Not achieved during the day, $R_D < T$ (poor)
2. Achieved during the day, $R_D > T$ (fair)
3. Achieved am or pm, $R_D > T$ (good)
4. Achieved both am and pm, $R_D > T$ (excellent)

Achieving $R_D > T$ over the period of full day is not necessarily considered sufficient. The goal of T = 4.2 can be achieved during mornings or afternoons only if the duration of the solar day is sufficient, since the nvR_D model depends on duration. By binning the results into am and pm the user can better understand the influence of time of day and how it can affect the accumulation of dose received. The binning of the data should be adjusted to every case study depending on specific program use. Results are shown with colored arrows in each view direction, with length indicating the magnitude of R_D and the color indicating the threshold it falls into (dark green, light green, yellow, or orange). The desired performance is to achieve $R_D > T$ before noon (am) or/and after noon (pm).

4 RESULTS

The results of our exemplary analysis are show at both building scale and occupant scale. Figure 4 shows two axonometric views of the 7th floor with average daily mSC and daily dose predictions for nvR_D on April 14 under clear skies. Figure 5 shows a zoom in on one view position on the 7th floor (in a closed private study room) with daily average and instantaneous predictions of mSC across the day. Figure 6 shows average daily mSC and daily dose predictions for nvR_D on February 28 for both the 6th and 7th floors under clear and overcast sky conditions overlaid in plan. Figure 6 also shows a frequency distribution of model predictions for each floor under clear and overcast sky conditions for each of the 4 days included in our analysis.

4.1 Visual Interest

If we look at the results for February 28, the 6th floor shows mostly exciting predictions for average daily mSC under clear sky conditions (Figure 6a), with a slight shift toward more neutral predictions under overcast skies (Figure 6b).

The 7th floor shows a significant shift towards calming predictions under both sky conditions (Figures 6e & 6f), with the peripheral open-study spaces achieving much more exciting predictions than the closed study rooms on the interior.

While we can draw certain spatial conclusions from the overall daily averages in Figures 4 and 6, some of which are fairly intuitive, Figure 5 shows a more nuanced overview of the dynamic hourly experience within a single view position. In this instance (April 14, clear sky), the prediction for excitement shift dramatically across each view direction depending on the time of day and resulting sun position. The instantaneous predictions in Figure 5 illustrate the variable nature of perceptual performance as shifting sun positions from one moment to the next can change the evaluation of excitement in our visual field. Depending on the intended program use and qualitative ambiance in an architectural space, these hourly performance predictions can be useful for the designer to know when, over the course of the day and year, impacts of daylight are likely to alter an occupant's emotional state.

4.2 Health Potential

Figure 6c-6h shows the daily cumulative response R_D across each viewpoint in plan on February 28. The results for the 6th floor show excellent performance throughout the space under clear sky (Figure 6c). Lower light intensities caused by overcast sky conditions show reduced performance in view directions facing North and East, where viewpoints did not exceed the desired performance (Figure 6d). During solar hours for each of the 4 days the percentage frequency of the 4 performance categories (Section 3.4) is counted for all viewpoints in the scene and displayed using a stacked bar graph.

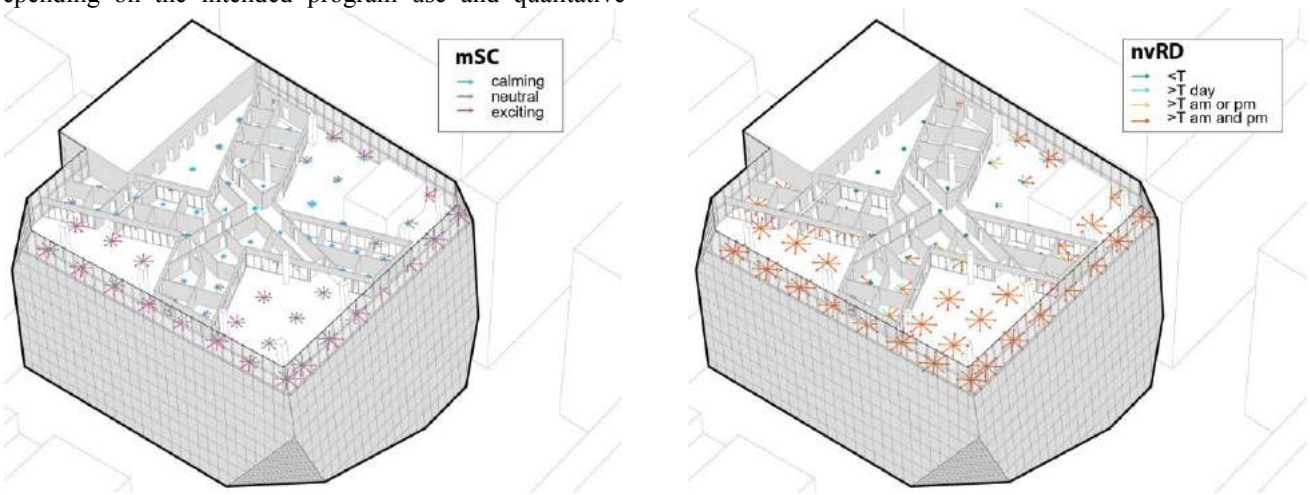

Figure 4. Showing two axonometric views with average daily mSC and cumulative response R_D for each point in the 7th floor on April 14 under clear sky conditions. The length of arrow is determined by the output of each model and colored by threshold (described in Section 3.4).

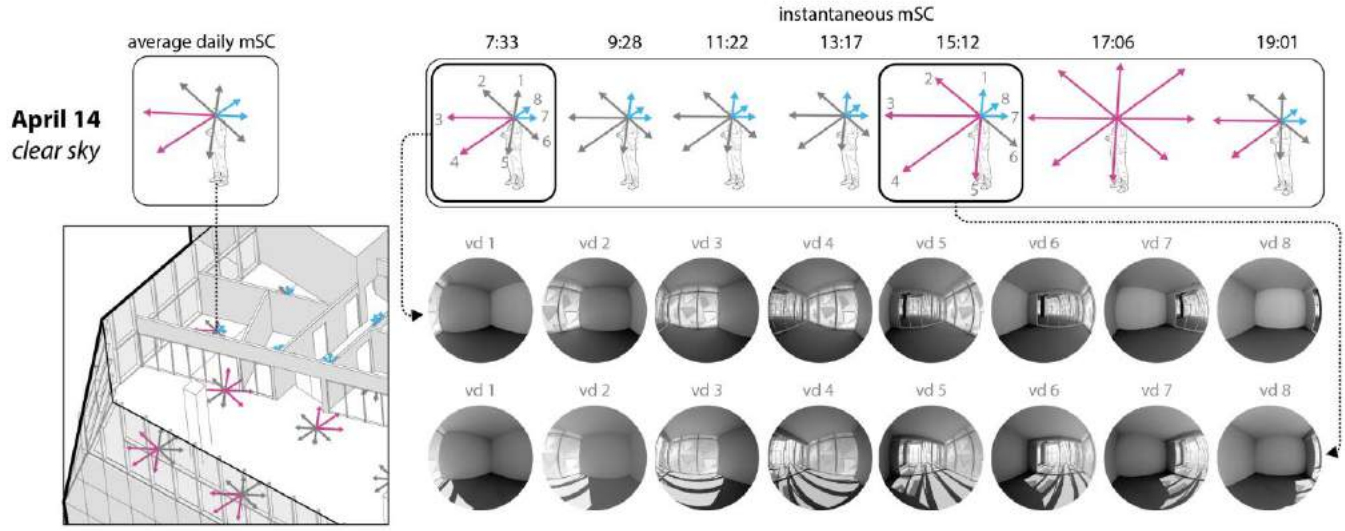

Figure 5. Shows a zoom in on one view position on the 7th floor. Average daily predictions of mSC are shown on the left (April 14 under clear skies), with instantaneous hourly predictions of mSC shown on the right, with associated hemispherical renderings for two instances (7:33 and 15:12) to illustrate relationships between occupant prediction and rendered daylight conditions.

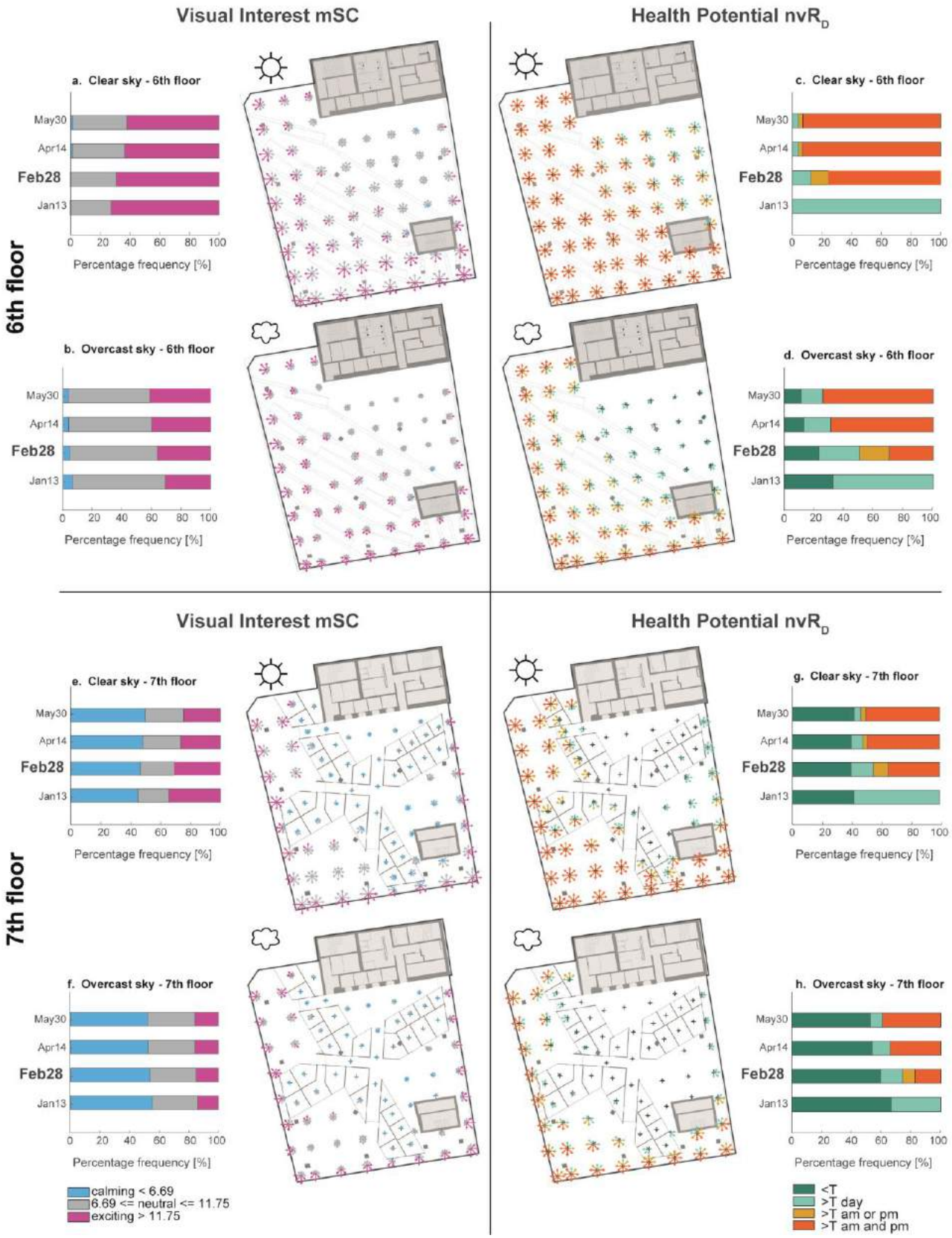

Figure 6. Average daily values for mSC (on the left) and cumulative daily dose predictions for nvR_D (on the right) are overlaid in plan to show the impact of clear vs. overcast skies on each view position and view direction in the 6th and 7th floors.

The results for the 6th floor under clear sky conditions are similar for most days of the year except during the darkest winter months, where the number of solar hours limits the overall health potential. As expected, the performance under overcast skies is reduced. Interestingly, the category of achieving T = 4.2 during am or pm increases on February 28, which means that achieving non-visual health potential is more sensitive to timing of occupation for overcast than clear skies around this time of year. This can be explored in more details by analyzing different time periods of the day.

The results for the 7th floor are less spatially homogeneous as compared to the 6th floor, which is explained by the partition of the 7th floor into open and enclosed study rooms. Less than half of the simulated points belong to open study spaces (30/76) resulting in a lower overall performance for the 7th floor. Under clear sky conditions on February 28 good and excellent performance is achieved for 45% of the viewpoints (Figure 6g), which reduces to 22% under overcast conditions (Figure 6h). As seen in Figures 6g and 6h, enclosed study rooms receive much less light than open study spaces. Under overcast sky conditions almost none of the viewpoints in enclosed spaces (ca. 1%) achieve the desired performance, while it is achieved under clear sky conditions in the enclosed rooms facing South and West.

5 CONCLUSION

This paper has introduced a simulation platform to evaluate in parallel two performance modules in daylight perception and health potential. Developed to automate the process of assessing human-centric performance predictions across a range of view positions and view directions within a given geometry model, the proposed platform creates a user-friendly support for daylight simulation. While past studies have used a similar workflow on a single view position in space, this paper offers a more streamlined protocol, allowing for the analysis of many view positions in a computationally efficient way. The speed of simulations is significantly improved through shared ambient files and data storage is optimized by keeping only the illuminance and luminance data necessary for the analysis of the performance modules. Visualizations of the data presented in this paper, while preliminary, provide insights regarding the daylighting performance of visual interest and non-visual health potential at the scale of the occupant, but also at the scale of the building. An array of view positions allows the user to compare performance predictions across multiple points in the case study and understand the impact of architectural composition on those predictions.

ACKNOWLEDGEMENTS

This work was supported by the Ecole Polytechnique Fédérale de Lausanne (EPFL) and through grants from the Swiss National Science Foundation [grant number 153018] and the Velux Stiftung Foundation [grant number 936].

REFERENCES

1. Rockcastle S, Andersen M. Measuring the dynamics of contrast and daylight variability in architecture: A proof-of-concept methodology. *Building and Environment, 81* (2014).
2. Wymelenberg K, Inanici M. The effect of luminance distribution patterns on occupant preference in a daylit office environment, *Leukos 7(2)* (2010).
3. Veitch J, Newsham G. Preferred luminous conditions in open plan offices: Research amd practice recommendations. *Light. Res. Technol*. 32(4) 2000.
4. Loe D, Mansfield K, Rowlands E. Appearance of lit environment and its relevance in lighting design: Experimental study *Light. Res. Technol.*, *26(3)* (1994).
5. Cetegen D, Veitch J, Newsham G. View size and office illuminance effects on employee satisfaction. *Ljubljana, Slovenia Proceedings of Balkan Light* (2008).
6. Tiller D, Veitch J. Perceived room brightness: Pilot study on the effect of luminance distribution, *Light. Res. Technol., 27(2)* (1995).
7. Parpairi K, Baker N, Steemers K, Compagnon R. The luminance differences index: a new indicator of user preferences in daylit spaces. *Light. Res. Technol., 34(1)* (2002).
8. Rockcastle S, Amundadottir ML, Andersen M. Contrast measures for predicting perceptual effects of daylight in architectural renderings. *Light. Res. Technol., (online first)* (2016).
9. Hubalek S, Brink M, Schierz C. Office workers' daily exposure to light and its influence on sleep quality and mood. *Light. Res. Technol., 42(1)* (2010).
10. Smolders KC, de Kort YA, van den Berg S. Bright light and mental fatigue: Effects on alertness, vitality, performance and physiological arousal. *J. Environ. Psychol., 39* (2014).
11. Smolders KC, de Kort YA, van den Berg SM. Daytime light exposure and feelings of vitality: Results of a field study during regular weekdays. *Environ. Psychol, 36* (2013).
12. Zeitzer JM, Dijk DJ, Kronauer RE, Brown EN, Czeisler CA. Sensitivity of the human circadian pacemaker to nocturnal light: melatonin phase resetting and suppression. *J. Physiol.,* 3 (2000).
13. Berson DM, Dunn FA, Takao M. Phototransduction by Retinal Ganglion Cells That Set the Circadian Clock. *Science, 295(5557)* (2002).
14. Hattar S, Liao HW, Takao M, Berson DM, Yau K. Melanopsin-containing retinal ganglion cells: architecture, projections, and intrinsic photosensitivity. *Science, 295(5557)* (2002).
15. Amundadottir ML. Light-driven model for identifying indicators of non-visual health potential in the built environment. *Ecole Polytechnique Fédérale de Lausanne*, 2016.
16. Amundadottir ML, Rockcastle S, Sarey Khanie M, Anderden M. A human-centric approach to assess daylight in buildings for non-visual health potential, visual interest and gaze behavior. *Building and Environment, (online first)* (2016).
17. Rizzi A, Algeri G, Medeghini D, Marini A. A proposal for contrast measure in digital images. *Aachen, Germany: Second European Conference on Color in Graphics, Imaging and Vision* (2004).
18. Amundadottir,ML, Lockley SW, Andersen M. Unified framework to evaluate non-visual spectral effectiveness of light for human health. *Light. Res. Technol. (online first)*, (2016).
19. Kleindienst S., Bodart M., Andersen M. Graphical Representation of Climate-Based Daylight Performance to Support Architectural Design. *Leukos*, 5(1) (2008).

A computational design exploration platform supporting the formulation of design concepts

Ding Yang [1, 2, 3], Yimin Sun [1, 2], Danilo di Stefano [4], Michela Turrin [2, 3]

[1]School of Architecture,
South China University of Technology
Guangzhou, China
d.yang-2@tudelft.nl,
arymsun@scut.edu.cn

[2]State Key Laboratory of Subtropical Building Science, South China University of Technology
Guangzhou, China
{d.yang-2, m.turrin}@tudelft.nl,
arymsun@scut.edu.cn

[3]Faculty of Architecture and the Built Environment, Delft University of Technology
Delft, The Netherlands
{d.yang-2, m.turrin}@tudelft.nl

[4]ESTECO SpA
Trieste, Italy
distefano@esteco.com

ABSTRACT

The comparison of various competing design concepts during conceptual architectural design is commonly needed for achieving a good final concept. For this, computational design exploration is a key approach. Unfortunately, most of existing research tends to skip this crucial process, and purely focuses on the late-stage design optimization based on a single concept that, they assume, has been good enough or accepted already. This paper focuses on information or knowledge extracted from a multi-objective design exploration for the formulation of a good geometrical building design concept. To better support the exploration process, a new integration plug-in is developed to integrate parametric modelling software and process integration and optimization software. Through a case study that investigates the daylight and energy performances of a large indoor space, this paper 1) tackles the importance of design exploration on the formulation of a good design concept; 2) presents and shows the usability of the new integration plug-in for supporting the exploration process.

Author Keywords

Multi-objective design exploration; Design concepts; Trade-off; Comparison; Top daylighting; Energy; Daylight

ACM Classification Keywords

J.6 COMPUTER-AIDED ENGINEERING

1 INTRODUCTION

There are multiple definitions of conceptual design and design concepts. According to Pahl [1], conceptual design is the phase in which the design requirements defined in the first phase are synthesized into a number of concept variants thus a final concept. O'Sullivan [2] includes into conceptual design the phase in which the designer takes specifications for an item to be designed and constructs a statement (subject to further modification) upon which the generation of many solutions is initiated. In this research, we define a *designňconcept* as a collection of ideas or principles that aim to achieve all the requirements of a design situation. Thus, to describe a design concept (which includes many potential solutions), there are at least two aspects that need to be specified: the design requirements and how to achieve them by applying the design ideas or principles. Moreover, similar to the definition in [1], we consider *conceptualň design* includes the phases of generating multiple potential design concepts, of evaluating and comparing the concepts for the most suitable one.

In computational design, parametric modelling [3, 4] is usually avoided during the conceptual design, especially in the very early phases. This is because the hierarchical structure of parametric models is considered to hinder the freedom of explorative thinking and to prematurely freeze ideation [5-7]. It is more widely applied, after a final design concept has been chosen (i.e. after the conceptual design), in combination with performance simulation for predicting various building performances. In this context, the design requirements are indicated by the performance criteria being considered; and the design ideas are implemented via the definition of parameters of the parametric model corresponding to the final concept. Thus, in some sense, the description of a design concept includes the formulation of an optimization problem, except for added values of design (such as cultural values, beauty, emotions, etc.). As such, a design concept is partially described or formulated by: a set of objective and constraint variables (i.e. output variables that are selected among performance criteria, to form an objective space); and a set of design variables (i.e. input variables that are selected among parameters of a parametric model, to form a design space).

In this paper, we claim that parametric modelling, together with performance simulation and computational design

exploration, are also useful during the conceptual design, but in the relatively late phases. That is, when multiple competing design concepts are generated, they are useful for evaluating and comparing the different concepts, identifying the promising ones, and then re-formulating them or even ideating entirely new concepts. For this, the computational design exploration is a key approach.

Computational design exploration differs from design optimization. In this study, *design exploration* refers to the process of extracting information or knowledge and applying it to formulate or re-formulate a design concept. This process includes two levels of exploratory activities: 1) the exploration of information or knowledge hidden behind obtained data sets; and one step further, 2) the exploration of how to apply the extracted information or knowledge to support the human decision-making on ideation. This is an iterative process during which the definitions of objective variables, constraint objectives and design variables may change towards a better concept formulation. This change occurs in two ways: modification of existing design concept or creation of new design concept, which is similar to Gero's definition of design exploration [8]. In contrast, *design optimization* refers to the process that is only keen on searching for optimal design solution(s) by using various optimization algorithms, when the design concept has been well-defined. Thus, optimization typically occurs in a later stage, during which the definitions of objective variables, constraint objectives and design variables remain fixed.

The design exploration precedes the design optimization and it is more important. If one defined an improper or a bad design concept, he/she might probably get poor results no matter how advanced the optimization algorithm was. Unfortunately, most of existing research tends to skip the process of formulating a good design concept, and rather focuses on the late-stage optimization based on a single given design concept. As response, this paper focuses on the formulation of a good geometrical building design concept based on the information or knowledge extracted from a multi-objective design exploration.

Accordingly, a process integration platform is required that is suitable for multi-objective and multi-disciplinary design exploration and supports the decision-making on ideation. However, most of existing platforms integrating parametric modeling and simulation systems with a design exploration and optimization environment lack important features, like scalability, extensibility [9], ease in using advanced sampling techniques and post-processing tools etc. This largely limits their applications in conceptual architectural design. In our research, to better support the exploration process, a new integration plug-in is developed to integrate parametric modeling software (i.e. McNeel's Grasshopper – GH [10]) and process integration and optimization software (i.e. ESTECO's modeFRONTIER - MF [11]).

In a case study that investigates the daylight and energy performances of a large indoor space, three typical types of top daylighting design are explored; and eventually, an improved design concept comes up based on the design exploration. Through this case, the paper 1) highlights the importance of design exploration on the formulation of a good design concept; 2) shows the usability of the new integration plug-in for supporting the computational design exploration process.

2 METHODOLOGY

2.1 Computational framework

The overall computational framework is shown in Figure 1. It consists of two iterative loops: a design exploration loop (indicated by a large cycle: the outer loop, involving Stage 1, 2 and 3) and a design optimization loop (indicated by a small cycle: the inner loop involving Stage 1 and 4). Different from the traditional focus on design optimization, this paper focuses on design exploration.

Stage 1 - formulation of initial design concepts: it is involved in the process for one time (marked in dash lines in Figure 1). In this stage, multiple initial design concepts are created and ready for the subsequent design exploration. The tasks below are required:

- Formulation of design variables, parametric model(s)
- Formulation of objective variables, simulation model(s)

Stage 2 - computational design exploration: this is the key of the design exploration loop. It generates and collects data; explores the information or knowledge behind the obtained data (i.e. the first level of exploration); and explores how to apply the extracted information or knowledge to support the human decision-making on ideation (i.e. the second level of exploration). The tasks below are required:

- Workflow establishment
- Simulation run & Data storage
- Data analysis & Knowledge extraction
- Promising concept identification & Preference integration

Stage 3 - re-formulation of new design concepts: it is the consequence of the previous stage. In this stage, new design concepts are created and ready for the subsequent design

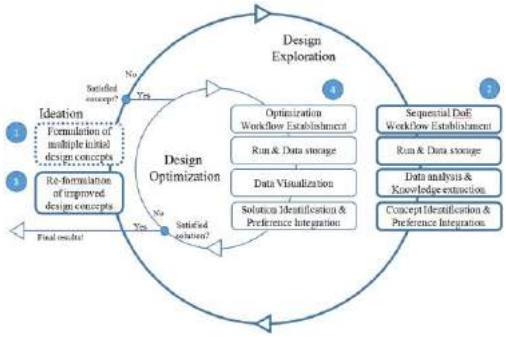

Figure 1. Overall computational framework

optimization (note that the optimization run is not included in this paper). The tasks below are required:

- Re-formulation of design variables, parametric model(s)
- Re-formulation of objective variables, simulation model(s)

2.2 Software Platform

To well support the computational framework, especially the computational design exploration, a process integration platform is required. It should be able to (1) connect with software familiar to architects and engineers; (2) cope with challenges related to computational power; and (3) include data analysis tools to facilitate analytic decision making etc.

Considering all these and other requirements, Grasshopper and modeFRONTIER have been chosen and integrated into one desired platform in this research (more information in Section 3). Grasshopper (integrated with Rhinoceros) is one of the most popular parametric modelling environments among architectural design professionals. It includes plug-ins for integrating various building performance simulations. modeFRONTIER is a process integration and automation platform for multi-objective and multi-disciplinary design exploration and optimization. It allows the integration with a variety of third party CAD and CAE tools; supports parallel computing; and offers a number of easy-to-use post-processing tools for data analysis and visualization.

2.3 Computational Design Exploration

Considering the relative importance of computational design exploration, as mentioned in Section 2.1, this section focuses on the computational process of Stages 2, for which the following four steps are involved.

Workflow Establishment

The parametric models and simulation models are set in GH, based on the formulation of multiple initial design concepts. The preliminary establishment of the workflow is facilitated by GH-MF integration. Through an *introspection* process, the input and output variables being investigated in GH are automatically propagated to MF. Thus, a modeFRONTIER workflow is preliminarily established, as shown in Figure 2. Moreover, some settings still need to be configured before the workflow is fully established. First, the domain and step of each input variable should be set properly; second, Design of Experiments (DoE) sampling strategies should be applied for guiding the choice of computer experiments or test designs; third, the sequential evaluation of previously defined test designs should be set. It is worth noting that DoE is very useful for design exploration. It helps to extract the most relevant qualitative information from a limited number of test designs. It is especially meaningful for the case that has relatively long simulation time. Uniform Latin Hypercube (ULH) [12] is one of the commonly used DoE sampling strategies in MF.

Simulation Run & Data Storage

Via various simulation engines, performances are predicted and the data are stored for later use. The simulation run and data storage is automated by GH-MF integration. During a *run* process, for each test design, MF automatically sends the input values to GH, and then receives the output values from GH when the simulation results are generated. Meanwhile, numerical simulation data are stored in MF database; images and 3D models are saved in the MF working directory. All the results can be browsed through MF user interface (more information in Section 3).

Data Analysis & Knowledge Extraction

Based on the data obtained, useful information (about data) is extracted by using statistical techniques. The information needed to know during design exploration includes *output-output* relationships and *input-output* relationships. The former refers to the inter-correlations between pairs of output variables; the latter refers to the impact of input variables on output variables. Considering the relatively large number of variables being considered, Multivariate Analysis (MVA) techniques are used to identify patterns and relationships among these variables. Self-Organizing Map (SOM) and Hierarchical Clustering (HC) [12] are among the handy MVA tools in MF.

The SOM is an unsupervised neural network for ordering of high-dimensional data in such a way that similar data are grouped spatially close to one another [13]. It represents multi-dimensional data in a two-dimensional space, which is very useful and directly interpretable. It can be used to identify the *output-output* relationships as well as other unexpected multiple variable correlations. The Cluster analysis tries to identify homogeneous subgroups of samples in a data set such that they both minimize within-group variation and maximize between-group variation [14]. The HC classifies large amounts of data into manageable and meaningful subgroups, which provides more abstract views to the inherent structure of the data. It facilitates to identify the *input-output* relationships by using a more refined data set.

Figure 2. modeFRONTIER workflow showing input and output variables

Based on the information obtained, useful knowledge (about building disciplines) is extracted via designers' interpretation. The knowledge to be extracted during design exploration may include reasons: why different criteria are correlated in some patterns and why different groups (or concepts) of designs perform differently? To obtain this knowledge, a good understanding of all input and output variable definitions is crucial, because it helps designers to interpret the information in building disciplinary contexts.

Promising Concept Identification & Preference Integration

Based on the knowledge obtained, the variables describing the most promising concept need to be identified, for the re-formulation of a new design concept. First, based on the correlation patterns between different criteria, the most contradictive criteria and/or the criteria with significantly different correlation patterns are selected as objective variables (not more than three); the remaining criteria can be selected as constraint variables. This ensures obtaining a meaningful set of Pareto trade-off solutions (from DoE test designs). Second, a special design variable that controls the switch among different groups (or concepts) of designs is crucial (see Section 4.3). Based on its effect on the selected objectives, the performance of each initial design concept is observed; and hence the design variables describing the most promising concept are identified.

It is worth noting that design preference integration is also important during the identification of the promising concept. Human designers or clients may have subjective preference on "soft" criteria (e.g. aesthetics) which are hard to evaluate numerically. The incorporation of design preference allows human to balance between visually preferred and high-performing concepts. For instance, one could select visually preferred but mid- or low-performing concepts for further research. In this sense, it is helpful to have a user-friendly interface that allows monitoring the variation of geometry while exploring data and simulation results, such as the interface provided by MF, as shown in Figure 3 (top right).

2.4 Re-formulation of New Concepts

There are two ways to re-formulate new concepts based on the most promising one. According to Gero [15], one option is to change the ranges of values for design variables (i.e. innovative design); while the other option is to introduce new design variables (i.e. creative design). In this paper, we are interested in the latter. Thus, new design variables are inspired via the analysis of the promising concept.

3 GH-MF INTEGRATION

The integration of Grasshopper and modeFRONTIER is useful for supporting computational design exploration. This potential has been shown in existing research [16-18], in which the GH-MF integration is provided by a previous version of customized nodes (both in GH and MF). To overcome some limitations in the last version (like manual operations, unstable process initiation and automation etc.), an improved version of the precedent is developed. The development has been implemented by using the myNODE tool [12] (a tool enabling the creation of custom nodes for the integration of external software in MF), and the Python tool (scriptable components in GH).

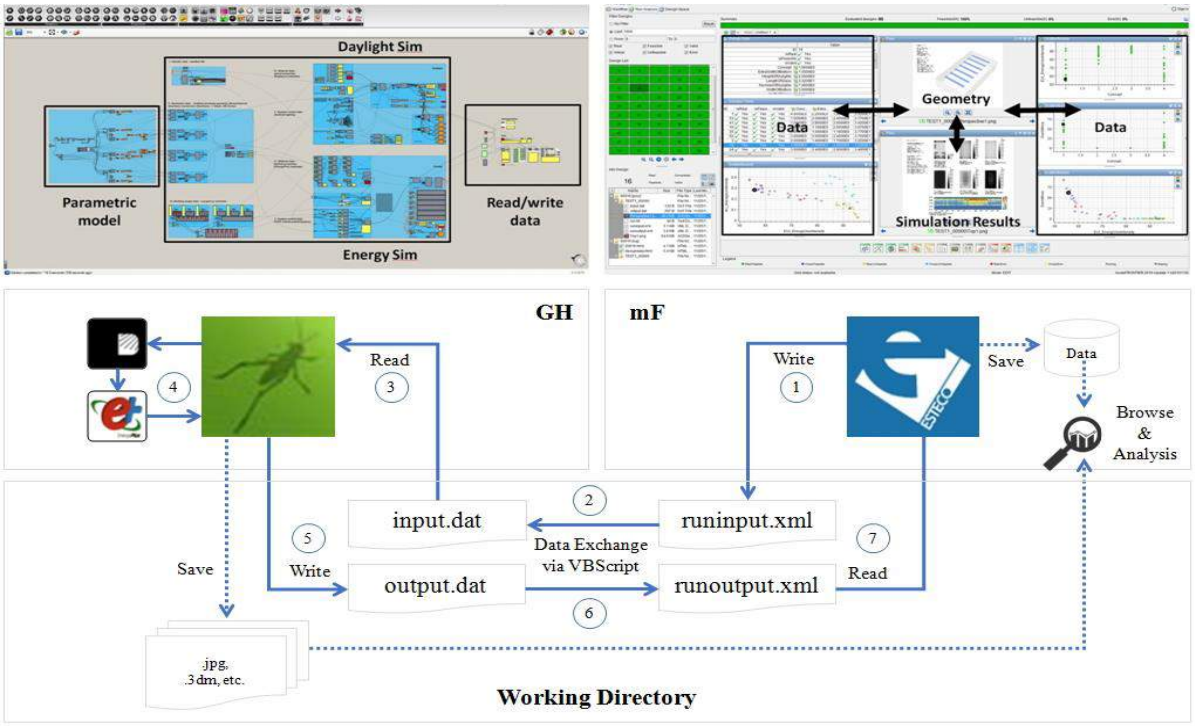

Figure 3. Grasshopper UI (top left); modeFRONTIER UI (top right); diagram of GH-MF integration (bottom)

Compare with the precedent, the new GH-MF integration streamlines the integration process through automatically recognizing input and output variables from GH in the *introspection* phase; facilitates the initiation of the *run* phase by one-click action; and improve the stability of the *run* phase by automatically calling and closing GH and Rhinoceros applications for each simulation run (instead of keeping them always alive which may increase the risk of crashing). Moreover, the new GH-MF integration is also supposed to work on Grid, for which, some bugs still need to be fixed. The communication between GH and MF is achieved via the automatic data exchange between .dat and .xml files, as shown in Figure 3 (bottom).

4 CASE STUDY

The case study investigates how to design the geometry of top-daylighting elements to improve daylight and energy performances of a large indoor space (i.e. 40m*70m*15m). It is structured as following. Three typical types of top-daylighting design are introduced as initial design concepts (Section 4.1). The formulation of the initial concepts is described, including the selection of objective variables (Section 4.2) and design variables (Section 4.3). Then, the computational design exploration process is followed; results about the obtained data, and results of the data analysis, knowledge extraction and design inspiration are showed (Section 4.4). Last, the performances of a new concept obtained are compared with that of the initial concepts (Section 4.4).

4.1 Initial Design Concepts

Top daylighting is a common and effective way of bringing light deep into a building, thus, it is often used in large single level space, such as indoor sports halls. Three typical types of top-daylighting design shown in Figure 4 (in the dash box) are initial design concepts. They are: skylights (Concept 1), roof monitors (Concept 2) and saw-tooth roofs (Concept 3). They perform differently in term of daylight and energy performances, due to different strategies of introducing light into the space. In addition, Concept 4 is the new concept proposed after the design exploration.

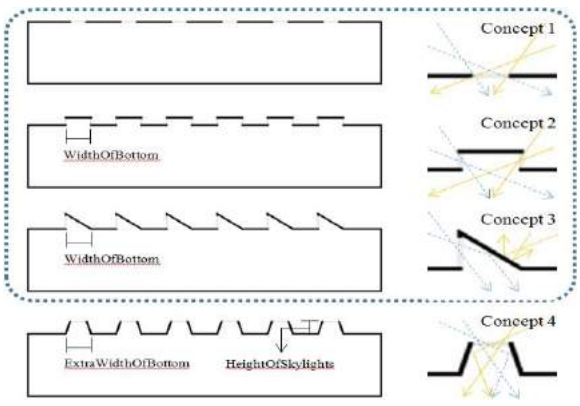

Figure 4. Initial design concepts (1-3); new concept (4)

Although there might be some general understanding of the initial concepts, it is not sufficient to support a good decision on which type we should choose. There are a lot of geometrical variations for each initial concept. The different geometrical variations perform differently though they belong to the same concept. Thus, there is a risk that one may choose a relatively high performing solution, but from a less promising concept. In that case, they may overlook a lot of better solutions or equally good trade-off solutions in a more promising concept. In this sense, it is crucial to have a clear view of the overall performance trend or pattern of each initial concept.

4.2 Objective Variables

Three categories of objective variables are selected for the formulation of the initial concepts, namely, energy, daylight and geometry related objectives. Energy related objectives include: Energy Use Intensity (EUI, energy used per square meter of floor area), Percentages of Cooling, Heating, Lighting, Equipment. Daylight related objectives include: Useful Daylight Illuminance (i.e. UDI(<100), UDI(100-2000) and UDI(>2000)); DaylitArea; OverlitArea; Average Uniformity. Here, UDI represents the percentage of floor area that meets the specified illuminance range at least 50% of the occupied time. DaylitArea represents the percentage of floor area that is above 300 lux for at least 50% of the occupied time (i.e. sDA). OverlitArea represents the percentage of floor area that is above 3000 lux for at least 5% of the occupied time, which indicates potential glare or overheating. Average Uniformity represents the annual average of the minimum-to-average uniformity ratio of illuminance. Geometry related objective is Area of Glass. It calculates the total area of the glass being used, which is often an interesting criterion associate with investment cost.

Moreover, Daysim [19] and EnergyPlus [20], as frequently used daylight and energy simulation engines, are chosen in this research. And the Grasshopper plug-ins Ladybug and Honeybee [21] are used to integrate parametric models with these simulation engines.

4.3 Design Variables

A special design variable called "Concept" is used to facilitate the simultaneous investigation of the multiple concepts. It controls the switch among different groups (or concepts) of designs; and determines the selection of other design variables that formulate the initial concepts. Normally, changing the value of a design variable will not affect the selection of other design variables. That is, the dimensions of the design space will be fixed, as the design variable changes its value. But, in this case, the variable "Concept" is a nominal variable, which is used for labelling the specific group (or concept) of designs without any quantitative meanings. The "values" of this variable include: Concept1, Concept2 and Concept3. When a specific "value" is chosen, different set of design variables will be selected to create the geometry of the corresponding

Type	Design variable	Range	Step
Share by Concept 1-4	NumberOfSkylights	2-10	1
	LengthOfGlass	30-38m	0.1 m
	WidthOfGlass	1-3 m	0.1 m
Share by Concept 2, 3	WidthOfBottom	1-3 m	0.1 m
Only for Concept 4	HeightOfSkylights	1-3 m	0.1 m
	ExtraWidthOfBottom	1-3 m	0.1 m

Table 1. Design variables and their ranges and steps.

initial concept. Thus, the specific "value" determines the dimensions of the design space being investigated. That is, by using the special variable "Concept", the dimensions of the design space are not fixed in this case, which is good for the simultaneous investigation of the multiple concepts.

Moreover, the design variables determined by the variable "Concept" are shown in Table I, together with their ranges and steps. Some of them are shared by multiple concepts; while some are only for a specific concept.

4.4 Results

Following the steps of computational design exploration (Section 2.3) and re-formulation of new concepts (Section 2.4), all the results obtained are reported in this section.

First, results about the obtained data are shown in Figure 5. They include: all the numerical data of design variables and objective variables; images showing daylight and energy simulation outcomes; and images showing geometries. This data are generated by applying ULH sampling strategy and running sequential simulations of the samplings. Second, results of the data analysis, knowledge extraction and promising concept identification are described in two parts: identification of promising objective variables and design variables. Self-Organizing Map and Hierarchical Clustering are used to analyze the data; then useful information and knowledge are extracted, based on which, a promising concept is identified. Last, results of the re-formulation of new concepts are shown. A new concept is formulated in a more informed manner, and its performances are compared with the performances of the initial concepts.

Identification of Promising Objective Variables

Self-Organizing Map is used to identify the *output-output* relationships. It is created by including all initial objective variables, based on the data sets related to initial concepts. As shown in Figure 6 (left), SOM maps of different variables are distributed on a hexagonal grid; and those with similar patterns are placed in adjacent positions. The color represents the values of variables; deep red means highest values and deep blue means lowest values. The level of similarity between patterns indicates the level of their correlation. Moreover, to facilitate observation, the general direction of achieving a desired performance goal of each objective variable is shown by a write arrow. For instance, EUI aims for a minimization goal, thus the direction of achieving this goal is from left bottom (high value) to top right (low value). Similar principles apply to others as well. By comparing the directions and patterns between pairs of initial objective variables, the following information and knowledge are obtained.

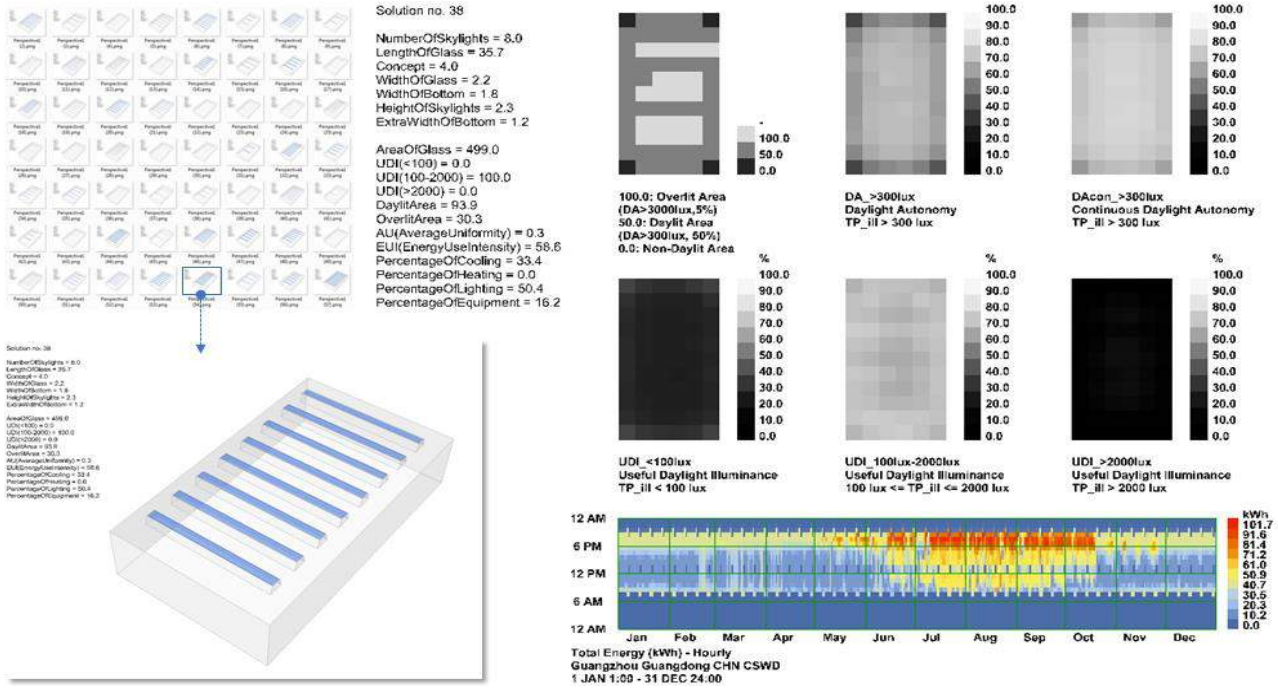

Figure 5. Geometry and simulation results

(1) *EUI* changes in the similar direction as *Percentageňofň Lighting*, but in the opposite direction as *Percentageňofň Lighting/Equipment/Heating*. By further checking the variable values, we notice that the increase of total energy use is mainly due to the increase of lighting energy use.

(2) *EUI* changes in the similar direction as *DaylitArea, UDI(<100),ň UDI(100-2000)*. This indicates that total energy use becomes high when more space has insufficient daylighting level and vice versa.

(3) *EUI* changes in the opposite direction as *OverlitArea*, and their patterns are very similar. This indicates that there might be an obvious trade-off between minimizing both total energy use and the risk of glare.

(4) *EUI* changes in the opposite direction as *Averageň Uniformity*, but their patterns are significant different. This indicates that there might be a less obvious trade-off between minimizing energy use and maximizing daylight uniformity.

(5) *EUI* changes in a different (not exactly opposite) direction as *AreaňofňGlass*, and the similarity level between their patterns is medium. This also indicates an interesting potential trade-off between minimizing both total energy use and investment cost.

Based on the above information and knowledge extracted, EUI, OverlitArea, Average Uniformity and Area of Glass (which may lead to interesting trade-off relations) are identified as promising objective variables.

Identification of Promising Design Variables

Hierarchical Clustering facilitates to identify the *input-output* relationships by using a clustered data set. The clusters are created by including the design variable "Concept" and the four objective variables identified, based on the data sets related to initial concepts. As shown in Figure 6 (right), the clusters are visualized by a clustering parallel coordinate chart which shows their distribution in all selected variables. Each cluster is represented by a colored band. The mean of each cluster is represented as a thick center line, whereas the confidence interval is represented as the band width. The selected variables are represented by parallel vertical lines. Moreover, to facilitate observation, the general direction of achieving a desired performance goal of each selected objective variable is shown by a black arrow. By using the concise visualization, the following information and knowledge are obtained.

(1) *Concept1* (i.e. green band) performs very well in *EUI*; but less well in *Averageň Uniformity*; and very bad in *OverlitArea* and*ňAreaňofňGlass*. This may be associated with the widest angle of receiving daylight from all directions compare with other concepts.

(2) *Concept2* (i.e. blue band) performs very well in *Averageň Uniformity,ňOverlitAreaň*and*ňAreaňofňGlass*; but relatively bad in *EUI*. This relatively balanced overall performance may benefit from the protruding roof elements blocking daylight from certain unwanted directions.

(3) *Concept3* (i.e. red band) performs very well in *OverlitAreaň*and*ňAreaňofňGlass;ň*but very bad in *Averageň Uniformityň* and *EUI*. This may be associated with the asymmetric geometry of the saw-tooth roof which makes the daylight unevenly distributed.

Based on the above information and knowledge extracted, Concept2 is considered as a more promising initial concept out of three, with relatively balanced overall performance. The design variables describing the concept are identified.

Re-formulation of a New Concept

We are interested in getting a new and high-performing concept by adding new design variables, as mentioned in Section 2.4. Based on the concept identified, improving its EUI performance while maintaining its advantages in other performances is the key to improve its overall performance. Triggered by the previous analysis, we notice that good EUI, OverlitArea and Average Uniformity performances may be associated with the use of horizontal windows, protruding elements and symmetrical geometries; and that good Area of Glass performance can be achieved by searching within a certain concept, given its relatively wide band width.

Inspired by the above indications, a new concept (i.e. Concept4 shown in Figure 4) is proposed. It leaves the glazing exposed horizontal to the sun, blocks daylight by

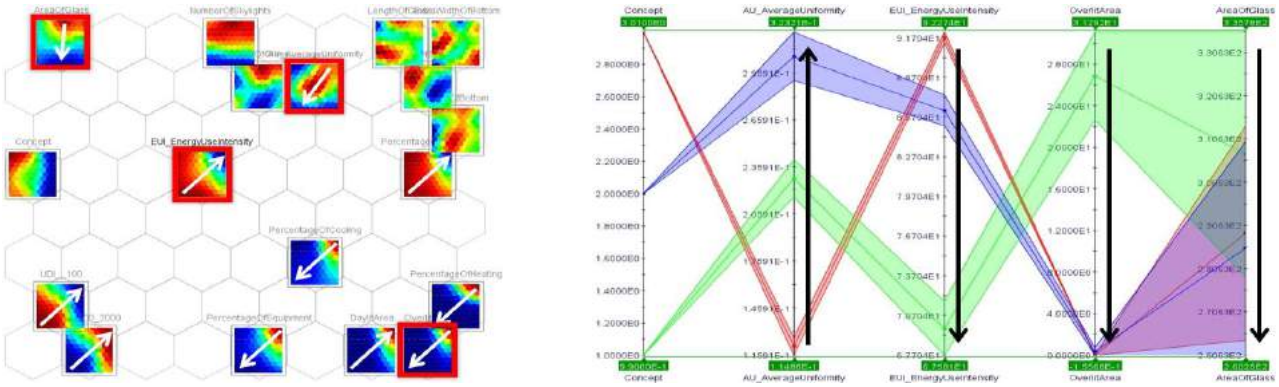

Figure 6. Self-Organizing Map (left); clustering parallel coordinate chart (right)

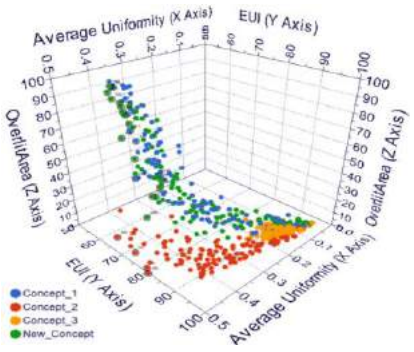

Figure 7. Objective space for new and initial concepts

using inclined protruding elements while remaining the symmetrical geometry. In this concept, the height and angle of the protrusion are important, thus HeightOfSkylights and ExtraWidthOfBottom are added to replace some original design variables in the initial promising concept. To better understand how the new concept performs, it is sampled by using the same sampling strategy and run. Data obtained are plotted in a 3D objective space, together with the data of the three initial concepts, as shown in Figure 7 (the objective Area of Glass is left out for the easy of visualization). The results show that, out of total 25 Pareto solutions, 15 solutions belong to the new concept, while Concept1 and Concept2 account for only 6 and 4 solutions respectively. This confirms the potential of the new concept in achieving better Pareto solutions, compared with the other concepts.

5 CONCLUSION

In conclusion, computational design exploration is crucial for formulating good design concepts in conceptual design stage. During the exploration, information and knowledge extraction plays an important role. To support this process, an integration and automation platform with powerful post-processing capability is highly useful. In this regard, GH-MF integration is a good option with great potential.

ACKNOWLEDGMENTS

We thank ESTECO for supporting the development of the GH-MF integration.

REFERENCES

1. Pahl, G., Beitz, W., Feldhusen, J., & Grote, K.H. (2007). *Engineering design: a systematic approach (3rd ed.)*. Germany: Springer-Verlag London.
2. O'Sullivan, B. (2002). Interactive constraint-aided conceptual design. In *Journal of Artificial Intelligence for Engineering Design, Analysis and Manufacturing*. 16(4), 303–328.
3. Aish, R., & Woodbury, R. (2005, August). Multi-level interaction in parametric design. In *International symposium on smart graphics* (pp. 151-162). Springer Berlin Heidelberg.
4. Hudson, R. (2010). *Strategies for Parametric Design in Architecture: An application of practice led research*
5. Kilian, A. (2006). Design exploration through bidirectional modeling of constraints.
6. Kilian, A. (2006). Design innovation through constraint modeling. *International journal of architectural computing*, *4*(1), 87-105.
7. Burry, J., & Burry, M. (2008, September). The bonds of spatial freedom. In *Proc. of the 26th eCAADe Conference-Architecture in Computro, Antwerpen, Belgium* (pp. 301-308).
8. Gero, J. S. (1994, January). Towards a model of exploration in computer-aided design. In *Formal design methods for CAD* (pp. 315-336).
9. Janssen, P. (2015). Dexen: A scalable and extensible platform for experimenting with population-based design exploration algorithms. *Artificial Intelligence for Engineering Design, Analysis and Manufacturing*, *29*(04), 443-455.
10. Grasshopper. http://www.grasshopper3d.com/
11. modeFRONTIER. http://www.esteco.com/modefrontier
12. ESTECO SpA. modeFRONTIER User Guide
13. di Stefano, D. (2009, November). Technical Report 2009-001: Multivariate Analysis algorithms in modeFRONTIER v4
14. Jain, A. K., Murty, M. N., & Flynn, P. J. (1999). Data clustering: a review. *ACM computing surveys (CSUR)*, *31*(3), 264-323.
15. Gero, J. S. (1990). Design prototypes: a knowledge representation schema for design. *AI magazine*, *11*(4), 26.
16. Yang, D., Sun, Y., Turrin, M., von Buelow, P., & Paul, J. (2015, August). Multi-objective and multidisciplinary design optimization of large sports building envelopes: a case study. In *2015 Proceedings of the International Association for Shell and Spatial Structures (IASS)*.
17. Sileryte, R., D'Aquilio, A., Di Stefano, D., Yang, D., & Turrin, M. (2016, May). Supporting Exploration of Design Alternatives using Multivariate Analysis Algorithms. In *2016 Proceedings of the Symposium on Simulation for Architecture and Urban Design (SimAUD)*. (pp. 215-222).
18. Yang, D., Sun, Y., di Stefano, D., Turrin, M., & Sariyildiz, S. (2016, July). Impacts of problem scale and sampling strategy on surrogate model accuracy: An application of surrogate-based optimization in building design. In *2016 IEEE Congress on Evolutionary Computation (CEC)*, (pp. 4199-4207). IEEE.
19. Daysim. http://daysim.ning.com/
20. EnergyPlus. https://energyplus.net/
21. Ladybug + Honeybee. http://www.grasshopper3d.com/group/ladybug

An Interactive Approach for Evolving Pareto Optimal Architectural Form

Camilo Cruz , Michael Kirley ,and Justyna Karakiewicz

University of Melbourne
Melbourne, Australia
ccruz@student.unimelb.edu.au, {mkirley,justynak}@unimelb.edu.au

ABSTRACT

Architectural design is regarded as a challenging open ended activity aimed to transform an existing reality into a desired one. This transformation takes place via the generation of design alternatives. Digital morphogenesis techniques lend themselves to the task of producing design alternatives quicker and easily. In this paper, we introduce an interactive population-based model for evolving design alternatives. Our model enables designers to steer the trajectory of the evolutionary process. We use a population-based evolutionary approach that allows us to represent, evaluate and evolve design alternatives. We illustrate how the model is capable of generating a diverse space of alternatives, increasing the probability of finding unexpected designs. Finally we examine the results obtained, by defining measures of quality related to design intentions.

Author Keywords

Evolutionary computing; digital morphogenesis; interactive design; genetic algorithm.

ACM Classification Keywords

I.6.1 SIMULATION AND MODELING: Evolutionary computing; genetic algorithms

1 INTRODUCTION

Designing environments for human inhabitation is a challenging, purposeful open ended activity aimed to transform an existing reality into a desired one [29]. This transformation generally takes place via the production of a physical artefact [35, 19]. In general terms, the design process can be described as the iteration between synthesis and evaluation [25, 33], which begins with a set of intentions, that derive from the need and desires to transform the existing reality, and a preconceived shape that provides a notion of what the final artefact could be [30]. Designers then modify the initial shape, generating alternatives to it. These alternatives are then analysed, searching for one that matches the design intentions. The generation of alternatives, as well as the evaluation process, are generally informed by the experience, knowledge and/or intuition of the designer [3]. This constrains the exploration of design space to the boundaries of that knowledge, preventing the development of diversity, hence the appearance of unexpected or novel design alternatives.

Digital technology has been used in the design practice since the 1960s, as computers can offer an improved capacity to perform operations that are either difficult or time-consuming for designers. Automation of repetitive tasks, generation of complex geometries and shapes, or *morphogenesis*, and optimisation of performance, are some of the applications that have been developed using computers, contributing to a more efficient design process.

If designer are to truly exploit the power of computational techniques in the design process, it is necessary to define what *good design* is. From our perspective, this definition can only be determined by addressing the following three questions:

Q1: How are the design alternatives represented?

Q2: How are they evaluated?

Q3: How are they transformed, in order to fulfil the design intentions?

Answering these questions can inform the development of techniques for the systematic generation and evaluation of design alternatives, enabling designers to steer the design process towards the fulfilment of their intentions, and highlighting the potential of using digital morphogenesis for for design.

The aim of this research is to explore ways in which digital morphogenesis tools can contribute to the creative stage of the architectural design process in a meaningful way. In this paper we present an interactive model for digital morphogenesis based on an evolutionary algorithm. The model is capable of generating and evolving design alternatives so decisions can be made understanding the trade-offs between them. For this implementation we define three strategies to address the questions indicated above. Design alternatives are represented as networks of spatial units, where each unit is an inhabitable space, defined by how it is connected to other spatial units. In order to evaluate design alternatives we explore the use of graph theory-based metrics that represent possibly conflicting design intentions. We use an interactive approach to evolve design alternatives, where the user is part of the selection process. This helps to capture and preserve features present in some of the design alternatives, that would otherwise be disregarded by the in silico evaluation methods. Thereby, the user can steer the trajectory of the search through the design alternatives, looking to match the intentions, which contributes to the production of diversity, increasing the probability of producing novel designs.

A series of simulations are proposed to investigate the capabilities of the model in the production of design alternatives

SimAUD 2017 May 22-24 Toronto, Canada

with emergent spatial characteristics. The proof of concept implementation allows us to explore the formal implications of using conflicting design intentions, as well as the possibilities that integrating the designer to an otherwise fully automated process opens.

The remainder of this paper is organised as follows. In section 2 we set the context for what we understand as the architectural design process, followed by the introduction of work related to computational morphogenesis, generative design and the use of evolutionary approaches for the generation of form. In section 3 we present a detailed description of our model and how it uses design intentions to generate and evolve design alternatives. In this section we also describe some of the results obtained in the process of testing the model. Finally, in section 4 we summarise and discuss the results and its implications, before succinctly introducing potential future work.

2 BACKGROUND

In this section we introduce a working definition of the architectural design process and its characteristics. We briefly review some of the relevant computational techniques for design, in order to contextualise the development of the proposed interactive model.

2.1 Design process

In engineering, the process of design is typically understood as the sequence of actions taken in order to solve a particular problem, and it can be summarised in the following steps [5]:

1. Conceptual design: conception of how the problem is going to be solved
2. Detailed design: definition of how the conceptual design will be implemented
3. Evaluation: checking that the performance of the design meets the requirements defined in the problem statement
4. Redesign: iterative process between 2 and 3, while requirements are not met

This definition implies that a problem is clearly defined, that the extent to which the problem is being solved can be measured, and that design is the process through which some artefact capable of solving said problem is devised. However, architecture is regarded as an ill-defined problem [24], where information and goals are ambiguous, thus, solutions are not necessarily true or false, but range between good and bad. As it is stated in section 1, generally speaking, the outcome of an architectural or urban design process is a physical artefact intended to meet a list of requirements of different nature. Some of these are related to function and performance, but ther are others that reflect abstract desires and intentions of the actors involved in the process [19], which makes them difficult to characterise, therefore virtually impossible to accurately measure. Moreover, the formalisation of design intentions differ greatly based on cultural context [14]. So how do designers define that a generated physical artefact allows for the desires and intentions being satisfied?.

According to [3] the architectural design process, in its traditional form, is based on knowledge and experience, to which [31] adds intuition. This process starts with a set of design intentions, some concrete, some abstract, and a vague idea of a shape. Then it uravels as the performance of a series of transformations to the initial form, aimed to find a configuration where the intentions fit best. Therefore, it is possible to say that design is developed as a generative process, where candidates are synthesised [33] and design choices are probed and evaluated to identify what [28] refers to as 'satisficing' alternatives. In other words, as [12] has suggested, the nature of this kind of design can be directly paralleled to the processes of evolution as they happen in nature, in that successful outcomes of the process of generation of form are being further developed -evolved- by means of prototyping, mutation, replication and selection.

Under this perspective, the introduction of computers to the design process seems like a logical step, given the capabilities these tools provide in evaluation and classification of characteristics.

2.2 Digital morphogenesis

The introduction of computers to the design practice, in the 1960s [23, 1], opened the possibility to explore the generation of form beyond human imagination. Generative systems, in use as a methods to investigate novelty in architecture since Aristotle [23, p.30], became more efficient and powerful in their computational incarnations, lending themselves to the exploration of novel, more sophisticated geometries and shapes. Alexander's work with 'patterns' [2] and Stiny's 'shape grammars' [32] are notable examples of said progress.

Computational (or digital) morphogenesis techniques, use digital media for the derivation of and manipulation of 'form' [13, 26], where abstract computer simulations are used to foster the gradual development and adaptation of shapes [34]. Using bottom-up generative methods, they combine a number of concepts including self organization, pattern formation, self-assembly and 'form-finding.' Self-organization is a process that increases the order and statistical complexity of a system as a result of local interactions between lower-level, simple components [8, 27]. Emergence represents the concept of the patterns, often unpredictable ones, which form in large scale systems [15, 20]. Emergent properties arise when a complex system reaches a combined threshold of diversity, organization and connectivity. For example, the self-assembly of geometric primary elements (or 'building blocks') may, in some systems, be an emergent form-finding property guided by strict rules dictating 'bonding' patterns [11, 17].

2.3 Evolutionary approaches in design

The architectural design process can be assimilated to natural evolution (see section 2.1). Evolutionary algorithms represent one of the methods that can be used to investigate the possibilities of digital morphogenesis.

Evolutionary algorithms [9] have been used in architecture and design to solve a range of functional and formal problems with varying degrees of success (see [12] for an introduction). Evolutionary algorithms can be generally described

as guided search heuristics that mimic ideas of natural adaptation and evolution in a computational model. They are frequently employed to find optimal solutions to performance-oriented problems [30]. For example, in the work of [21], evolutionary strategies are used to improve the acoustic performance of a particular space. In a similar manner, [7] proposes the use of a genetic algorithm for the development of buildings with a lower carbon footprint, and [22] propose a method for optimising concrete shells using conflicting criteria.

The nature of designing environments for human inhabitation can be directly paralleled to the processes of natural evolution, in that successful outcomes of the process of generation of form (morphogenesis) can be further developed – evolved – by means of prototyping, mutation, replication and selection [12]. However, for an *in silico* evolutionary model to be useful, the guided stochastic search process must be augmented by multiple objectives to frame that diversity within the limits of what is needed and desired in the design process. The work of [12], [5], and more recently [30], illustrate how evolutionary techniques can be used in the conceptual stage of design, for the generation of innovative, or 'creative' outcomes. We use these studies as the basis for the development of the model used in this study.

Multi-objective optimisation (MOO) techniques are being incorporated to architectural design as a method to explore the way in which conflicting objectives can be combined and integrated. The work of [16] investigates the use of this approach in the early stages of design, looking to produce design alternatives above a certain threshold of performance, on top of which more abstract design decisions can be made. Similarly, [4] use MOO as a method to generate feedback that the designer can use to inform the development of the object being produced. This suggests that establishing instances through which the user can interact and steer the trajectory of the process, as it has been done in arts [18], can represent a contribution to the creative stages of design.

3 MODEL

In this paper, we introduce a multi-stage interactive model that uses design intentions as evaluation criteria to evolve diagrams of architectural form. The model allows users to steer the evolution of design alternatives along a desired trajectory, by relying on both *in silico* and human selection. We use a multi-objective optimisation (MOO) approach, through which a population of design alternatives is evolved using representations of the design intentions as 'objectives'. This model differs from typical MOO implementations used in architectural design, in that measures for the evaluation of non performance-based attributes are introduced, in order to reflect design intentions more accurately. By making the designer part of the evaluation, an intuitive component is added to the evolutionary process. This contributes to the production of a more diverse design search space, which increases the probability of finding unexpected alternatives to address the intentions being sought. The model is implemented using the Python programming language in Grasshopper for Rhinoceros 5.0.

3.1 Representation

In order to represent design alternatives, we use networks of spatial units. These units are arranged in a 3D grid of size (x,y,z), where x, y and z are the number of spatial units in each direction. Design alternatives are defined by the topology of the network, determined by which partitions of the grid are active or inactive.

We use a binary string (genotype) to represent each alternative. The length of the string is determined as $[x \times y \times (z+1)] + [x \times (y+1) \times z] + [(x+1) \times y \times z]$. Each bit of the binary string corresponds to one subdivision of the grid, and its value (*0* or *1*) determines if that subdivision is inactive or active.

The graphic expression (phenotype) for each spatial configuration is generated by mapping the binary string on to a 3D grid, as shown in figure 1 (a), where the position and orientation of a subdivision is determined by its position in the binary string. This produces a 3D diagram of the spatial configuration being represented. Finally, as it is shown in figure 1 (b), we use connectivity graphs, derived from the spatial diagram, as an alternative expression of the phenotype. In the graph, each node corresponds to the centre of one cell of the grid, and the connections to neighbouring nodes are determined by the presence of subdivisions between them. It is important to note that we use a 3D version of the von Neuman neighbourhood, where each node has neighbours to the north, east, south, west, up and down (6 neighbours in total).

3.2 Evaluation criteria

Performance-based attributes, such as structural robustness, exposure to sunlight and ventilation, just to name some, have known methods for measurement associated with them. 'Good' performance refers to the desire of obtaining either a high or a low value when measuring these attributes, which makes the translation into objectives straight forward. However, when dealing with qualitative intentions (e.g. 'conti-

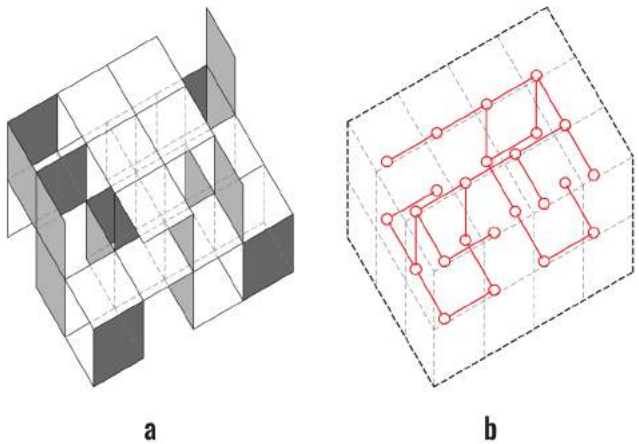

Figure 1. An example of a randomly generated individual of size (4,3,2) represented as spatial diagram (a) and as a graph (b).

nuity of the space', regularity, or other spatial characteristics that can't be measured with a specific number), defining a 'good' result becomes a challenge, and the use of different methods for evaluation will produce different design outcomes.

In a traditional design process, the translation of design intentions into form is done based on the knowledge and/or intuition of the designer. Conversely, when performing fully computerised form generation, the results rely on the criteria being used to evaluate the design alternatives. Therefore, the accuracy with which these criteria represent design intentions becomes a crucial issue to obtain outcomes that satisfy the initial intentions.

Computing the 'quality' of individuals requires of methods to evaluate them. For this purpose, what we call 'design intentions' have to be translated into 'objectives' that the computer can classify and compare. In other words, it is necessary to quantify design intentions. Here, we combine a performance-based measure, with a more abstract one, allowing us to experiment in a scenario where the design is feasible, but it has a certain qualitative spatial character.

We selected *spatial continuity* and *structural feasibility* as evaluation criteria. Considering that continuity is understood as a space with the least possible number of subdivisions, and structural feasibility can only be achieved as result of the presence of vertical elements that carry loads to the ground, these attributes can be considered as conflicting.

It is important to note that the selected objectives are not the primary focus of this study. Spatial continuity and structural feasibility were used because they are easy to implement and understand, which make them suitable examples for the proof of concept for our approach.

Spatial continuity represents the possibility of accessing every single spatial module in a design alternative, from every neighbouring spatial module, by foot, as illustrated in figure 2.

Continuity is measured based on degree distribution –the number of connections for each node in a graph, using equation 1.

$$c = \frac{\sum_{n=1}^{w} d_n}{W} \tag{1}$$

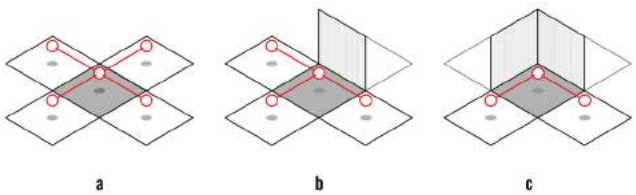

Figure 2. Three examples of spatial continuity: a) the gray horizontal partition has full connectivity, since it can be accessed from all its neighbours, b) the gray horizontal partition has a connectivity of 0.75, since one neighbour can't be directly accessed from it. Finally, in c) the the gray horizontal partition has a connectivity of 0.5.

Where w is the number of horizontal subdivisions that are *active*, d_n is the ratio of the degree distribution of a node n over its maximum possible degree distribution (looking only at horizontal connections), and W is the maximum number of horizontal subdivisions for a configuration. The resulting c is a ratio, where 1 represents full continuity and 0 represents no continuity at all.

As an example, the highest score for *continuity* would be a configuration where all the horizontal subdivisions are active and all the vertical ones (except for the perimeter ones) are inactive.

Structural feasibility is defined as the ratio of 'complete pillars' in a design alternative, over the number of potential pillars. A pillar is defined as continuous vertical line, located on the points where vertical subdivisions meet (as indicated in red on figure 3(a)), that span from the base to the top of the grid, as shown in figure 3(b). This is calculated using an algorithm that iterates through the intersections of the grid, from bottom to top, counting active vertical subdivisions.

3.3 Algorithm

Our model has to be capable of generating design alternatives, as well as evaluating and sorting them based on non-weighted, and often in conflict, design intentions. We use a modeified version of NSGA-II [10]: a population-based, elitist genetic algorithm that uses non-dominated sorting. The sorting process is based on the concept of dominance. An individual dominates another when it performs at least equally well on every evaluation criteria, and outperforms it in at least one. The group of non-dominated individuals is called Pareto front (see figure 5).

In a typical NSGA-II implementation the process starts with the generation of a population. This population is then evaluated and sorted based on performance. The 'best' individuals are kept as an 'elite population', which helps to maintain the quality of individuals in future generations. In parallel, a mating pool is generated, as a method to generate diversity. Subsequently, the mating pool is modified, typically using standard evolutionary operations (e.g. cross-over and mutation), to produce new individuals. This 'offspring' population is

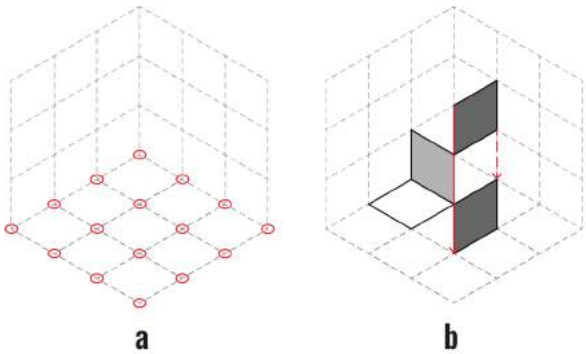

Figure 3. a) In red, all the possible pillars (one on each intersection of the xy plane of the grid) are illustrated for a 3x3x3 grid. b) The configuration of one pillar that bears load from top to bottom is illustrated.

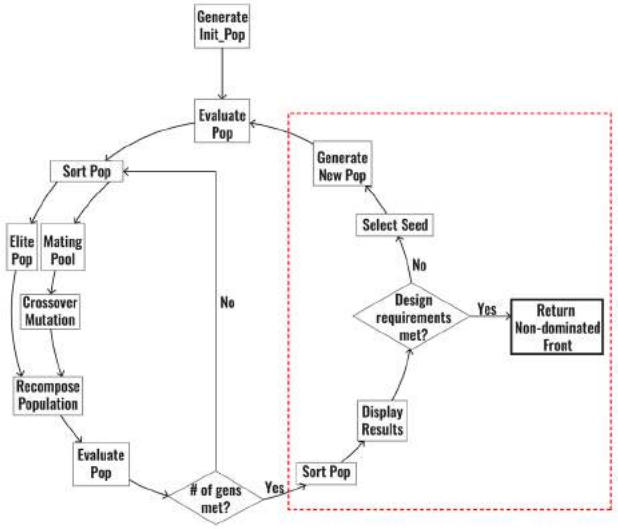

Figure 4. A diagram of the modified NSGA-II algorithm being used.

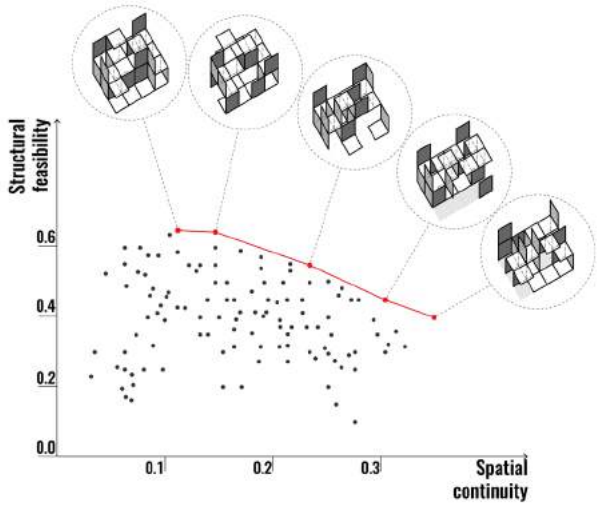

Figure 5. Scatter plot of a population, after being evaluated and sorted. The vertical axis represents structural feasibility and the horizontal axis represents spatial continuity, as defined in section 3.2. Each dot represents one individual. The red line shows the non-dominated front. In the circles, graphic representations of the design alternatives in the non-dominated front are illustrated.

added to the elite group to conform the new population, which is re-evaluated. This represents the completion of one generation. At this point an exit condition check is performed, in order to determine if the process has to stop and show results, or if it has to continue.

In our implementation, each individual in the population represents a design alternative. As it is shown in figure 4, we start by generating a population of size n, where the individuals are randomly produced. This population is then evaluated using the criteria described in section 3.2. As elite population we select $n/4$ individuals. The mating pool, of size $3 \times n/4$ individuals, populated using a dominance-based tournament system: two random individuals are selected from the overall population and are made to compete against each other. The winner is picked based on dominance. For the modification of the mating pool we use standard two-point cross-over, as well as mutation (bit flip), with a rate of 5%. Then, the full population is reassembled and re-evaluated. Up until this point, the implementation of our model works as a typical NSGA-II, which should work well for problems based on straight optimisation.

However, given the 'wicked' nature of architectural design, even if all the non dominated solutions are equally valid from an optimisation perspective –'good' solutions–, it may happen that some alternatives are better suited to accommodate the intentions of the designer, due to features that escape the evaluation criteria. Similarly, it is likely that some of the dominated alternatives present valuable attributes that are not captured by the evaluation criteria. This is why, as shown in the dashed line box in figure 4, we introduce an interactive evaluation stage, which could be considered as an intuitive evolutionary operator. After the model has performed automated optimisation for a number of generations (defined by the user), a set of design alternatives are selected, using a k-means clustering algorithm [6], and displayed in an interactive interface, as illustrated in figure 6: The top row shows individuals from the Pareto front (i.e. the individuals on the red line in figure 5), and the bottom row shows selected dominated individuals. By using k-means clustering, it becomes possible to represent different parts of the design space. The user is then prompted to select individuals from the pool of alternatives. The selection is used to seed the initial population of the following cycle, which is supplemented with randomly generated individuals, in order to reach the required population size. This mechanism ensures that some features that might end up disappearing in a typical optimisation process can be maintained if they appear to be important from a design perspective. The user can repeat the process until satisfied with the generated results.

3.4 Experiments

A series of experiments were conducted in order to test the capabilities of the proposed model. We specifically focused on the generation of diversity and the characteristics of the design alternatives being produced, in relationship to the design intentions being used to drive the evolutionary process.

Methods

The experiments were run using design alternatives (individuals) of size (4,3,2), as shown in figure 1. We use a population of 50 individuals, and the evaluation criteria defined in section 3.2 to run our algorithm for 150 generations.

Two implementations of the algorithm were tested: The first one corresponds to a fully automated NSGA-II algorithm, the second one is the interactive version presented in section 3.3 (see figure 4). The interactive experiments were run in 10 cycles of 15 generations each. At the end of each cycle, the user was prompted to select design alternatives to seed the following generation.

Results and discussion

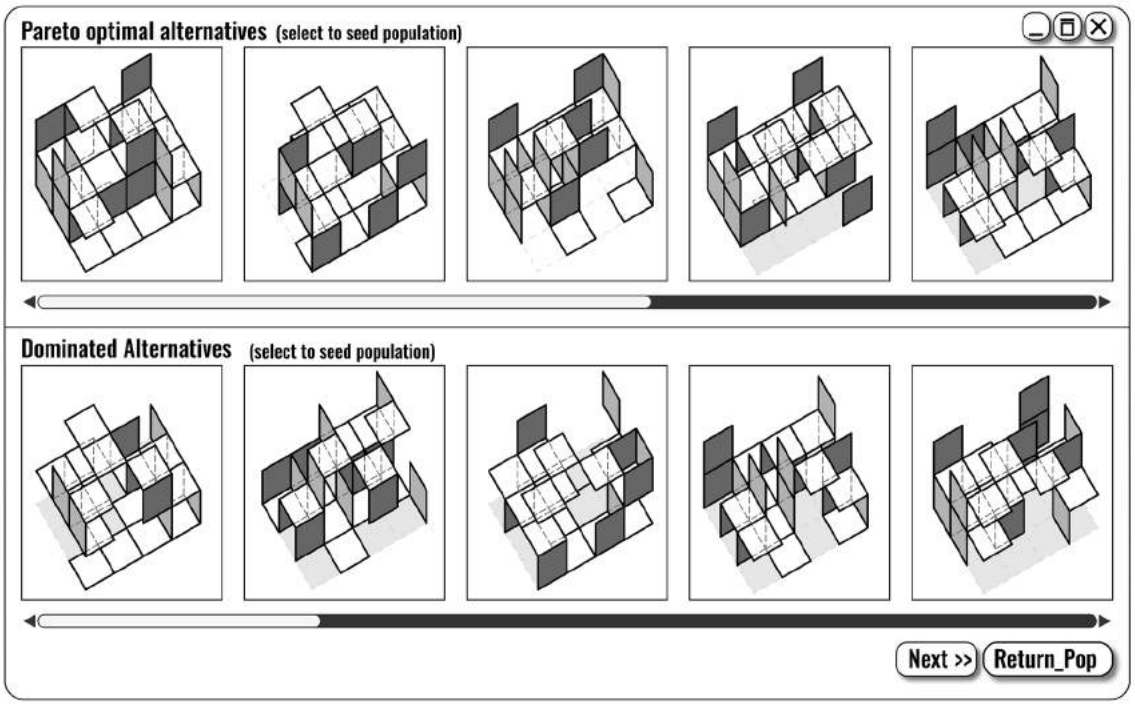

Figure 6. Graphic interface allows designers to interact by selecting alternatives to seed the initial population of the following evolutionary cycle. The top row displays Pareto optimal alternatives. The bottom row displays dominated alternatives, selected using k-means clustering (where k is the number of clusters being represented). The user is prompted to select those alternatives that present features that have to be preserved as the the design process evolves.

Through these experiments we have demonstrated that the implementation of our model is capable of generating and evolving design alternatives, using design intentions, provided by the user, as evaluation criteria. By doing this interactively, designers are enabled to introduce their experience, knowledge and intuition into an otherwise fully automated optimisation-based digital morphogenesis process, which could help to promote features in the design alternatives that may otherwise end up lost or never discovered.

We argue that an interactive digital morphogenesis process could outperform a fully automated morphogenetic model in terms of their capability to generate a diverse design space for designers to search through, increasing the probability of finding unforeseen ways of addressing design intentions through physical artefacts.

In order to measure this improvements, we plot the trajectories of the Pareto fronts for a fully automated process (figure 7(a)) and an an interactive one (figure 7(b)). Every Pareto front corresponds to a cycle of 15 generations.

In figure 7(a) it can be observed that the distance between the fronts is larger than in figure 7(b), and the values seem to be closer to reaching the maximum of the spectrum. This means that the automated process is faster in producing alternatives close to optimal alternatives. However, the interactive process shows more, and better distributed individuals along each front, which illustrates its capacity to produce a more diverse search space. Moreover, the automated process shows that after six cycles of 15 generations, the number of alternatives being produced is low, which could be interpreted as the system finding a good-enough set of solutions, and settling on it.

4 CONCLUSION

In this paper we have introduced a proof of concept for a model capable of evolving diverse spatial configurations by defining abstract design intentions, rather than trying to optimise performance based attributes. The overarching aim was to investigate ways in which digital tools for the generation of form can help designers' creativity. By implementing a platform where design alternatives are generated based on objective and subjective attributes, and displayed side by side, the trade-offs implicit in the design process are made explicit, enabling designers to make better informed decisions.

The approach presented in this paper provides a robust platform for the production of diversity in digital morphogenesis. This is seen as a strength, since it increases the probability of unveiling unexpected, or novel means to take care of particular design intentions. It can be argued that by incorporating the user as a decision maker in the evolutionary process, we are able to extend the capabilities of traditional evolutionary operators (mutation, crossover, etc.), enabling designers to steer the trajectory of the search process, hence opening the possibility for exploration and experimentation.

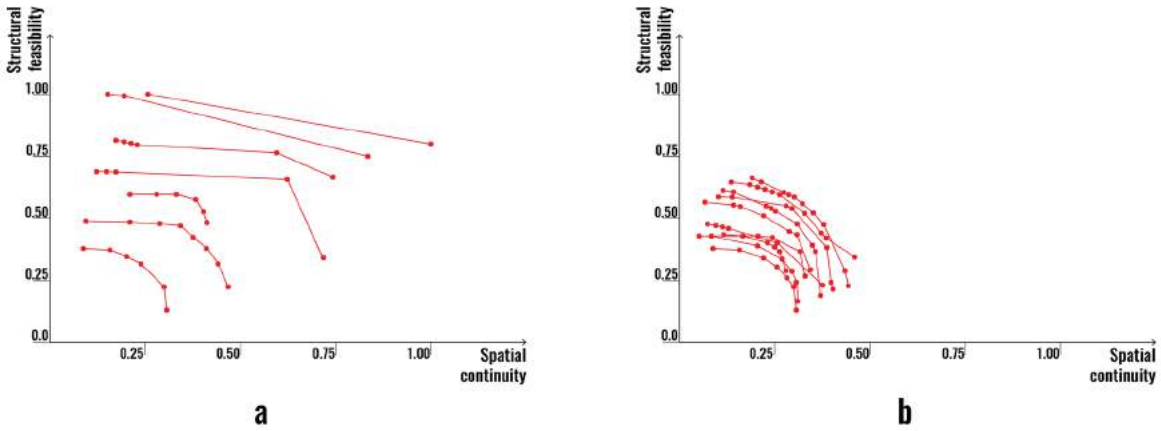

Figure 7. (a) Plot of Pareto fronts generated every 15 generations for a fully automated run of the model. It is interesting to note that, even if the model seems to be very efficient, it tends to converge towards a low number of solutions. (b) Plot of Pareto fronts generated every 15 generations for an interactive run of the model. Each iteration was generated after the user seeded the population. In this case the model seems to be less efficient than in (a). However, the diversity being produced is higher, which increases the probability of finding a relevant solution

It is important to note that the model presented in this paper is not intended as a tool to provide complete design 'solutions'. It is aimed to help designers in the conceptual –creative stage of the design process, by expanding design space. Methods to numerically understand the characteristics of the spaces being produced have been introduced in the form of evaluation functions. However, it is not guaranteed that the results provided using these methods will satisfy the actual intentions. The ambiguous nature of incorporeal design intentions makes capturing their complexity very difficult, which limits the possibility of computing their quality using optimisation techniques.

We foresee many opportunities to build on top of the work presented in this paper. One avenue to explore is the development of methods to translate abstract design intentions into relevant evaluation criteria, in order to improve the quality of the alternatives being produced. A second avenue that could be interesting to explore is to making an implementation of our model, in the form of a plugin for Grasshopper in Rhinoceros 5.0, available for the design community to use in different contexts (currently work in progress).

REFERENCES

1. Alexander, C. *Notes on the Synthesis of Form*, vol. 5. Harvard University Press, 1964.
2. Alexander, C., Ishikawa, S., and Silverstein, M. *A pattern language: towns, buildings, construction*. Oxford University Press, 1977.
3. Arlati, E., Bottelli, V., Fogh, C., and Tirassa, M. Modelling process knowledge in architectural design: A case-based approach. In *Proceedings of the 8th International Conference on Systems Research, Informatics and Cybernetics* (1995), 1–8.
4. Ashour, Y., and Kolarevic, B. Optimizing creatively in multi-objective optimization. In *Proceedings of the Symposium on Simulation for Architecture & Urban Design*, Society for Computer Simulation International (2015), 128–135.
5. Bentley, P. J., and Wakefield, J. P. Conceptual evolutionary design by a genetic algorithm. *Engineering design and automation 3* (1997), 119–132.
6. Bishop, C. M. *Pattern recognition*, vol. 128. Springer, 2006.
7. Caldas, L. *An evolution-based generative design system: using adaptation to shape architectural form*. PhD thesis, Massachusetts Institute of Technology, 2001.
8. Camazine, S. *Self-organization in biological systems*. Princeton University Press, 2003.
9. De Jong, K. A. *Evolutionary computation: a unified approach*. MIT press, 2006.
10. Deb, K., Pratap, A., Agarwal, S., and Meyarivan, T. A fast and elitist multiobjective genetic algorithm: Nsga-ii. *IEEE transactions on evolutionary computation 6*, 2 (2002), 182–197.
11. Dorin, A., and McCormack, J. Self-assembling dynamical hierarchies. *Artificial Life 8* (2003), 423–428.
12. Frazer, J. *An Evolutionary Architecture*. Themes VII. Architectural Association, London, 1995.
13. Hensel, M., Menges, A., and Weinstock, M. *Emergence: morphogenetic design strategies*. Wiley-Academy Chichester, 2004.
14. Hillier, B., and Hanson, J. *The social logic of space*. Cambridge university press, 1989.
15. Holland, J. H. *Adaptation in natural and artificial systems: an introductory analysis with applications to biology, control, and artificial intelligence*. MIT press, 1992.

16. Keough, I., and Benjamin, D. Multi-objective optimization in architectural design. In *Proceedings of the 2010 Spring Simulation Multiconference*, SpringSim '10, Society for Computer Simulation International (San Diego, CA, USA, 2010), 191:1–191:8.

17. Kondacs, A. Biologically-inspired self-assembly of two-dimensional shapes using global-to-local compilation. In *Proceedings of the 18th international joint conference on Artificial intelligence*, Morgan Kaufmann Publishers Inc. (2003), 633–638.

18. Kowaliw, T., Dorin, A., and McCormack, J. Promoting creative design in interactive evolutionary computation. *IEEE transactions on evolutionary computation 16*, 4 (2012), 523.

19. Lawson, B. *How designers think: The design process demystified*, second edition ed. Routledge, 1990.

20. Man, G. M. The quark and the jaguar: Adventures in the simple and the complex.

21. Mendez, T. *Computational Search in Architectural Design*. PhD thesis, Politecnico di Torino, 2014.

22. Mendez, T., Pugnale, A., and Sassone, M. Multi-objective optimization of concrete shells. *Structures and Architecture. Concepts, Application and Challenges, CRC Press/Balkema, Leiden* (2013), 217–218.

23. Mitchell, W. J. *Computer-aided architectural design*. John Wiley & Sons, Inc., New York, 1977.

24. Rittel, H., and Webber, M. M. Planning problems are wicked problems. *Polity 4* (1973), 155–69.

25. Rosenman, M. A. An exploration into evolutionary models for non-routine design. *Artificial Intelligence in Engineering 11*, 3 (1997), 287–293.

26. Roudavski, S. Towards morphogenesis in architecture. *International journal of architectural computing 7*, 3 (2009), 345–374.

27. Shalizi, C. R. Methods and techniques of complex systems science: An overview. In *Complex systems science in biomedicine*. Springer, 2006, 33–114.

28. Simon, H. A. Rational choice and the structure of the environment. *Psychological review 63*, 2 (1956), 129.

29. Simon, H. A. The sciences of the artificial. *Cambridge, MA* (1969).

30. Song, H., Ghaboussi, J., and Kwon, T.-H. Architectural design of apartment buildings using the implicit redundant representation genetic algorithm. *Automation in Construction* (2016).

31. Steadman, P. *The Evolution of Designs: Biological analogy in architecture and the applied arts*. Routledge, 2008.

32. Stiny, G. Introduction to shape and shape grammars. *Environment and planning B 7*, 3 (1980), 343–351.

33. Swann, C. Action research and the practice of design. *Design Issues 18*, 1 (2002), 49–61.

34. Thompson, D. W., et al. On growth and form. *On growth and form.* (1942).

35. Woodbury, R. F. Searching for designs: paradigm and practice. *Building and Environment 26*, 1 (1991), 61–73.

Are Genetic Algorithms Really the Best Choice for Building Energy Optimization?

Thomas Wortmann*[1], Christoph Waibel*[2, 3], Giacomo Nannicini[1], Ralph Evins[2, 5], Thomas Schroepfer[1], Jan Carmeliet[3, 4]

[1] Architecture and Sustainable Design, SUTD, Singapore

[2] Laboratory for Urban Energy Systems, Empa, Duebendorf, Switzerland

[3] Chair of Building Physics, ETH Zurich, Switzerland

[4] Laboratory for Multiscale Studies in Building Physics, Empa, Duebendorf, Switzerland

[5] Energy Systems and Sustainable Cities Group, University of Victoria, Canada

ABSTRACT

This paper considers which black-box optimization methods are most appropriate for building energy optimization by revisiting a seminal work concerned with this question. We benchmark three categories of black-box optimization methods—(1) direct search, (2) metaheuristics and (3) model-based methods—on three building energy optimization problems. Considering speed of convergence and stability, we find well-performing methods from all categories, but the widely popular genetic algorithm performs poorly. We also extensively analyze the fitness landscape of one of the three problems. To understand why algorithms fail or succeed, we relate this analysis to the methods' performance. Our results show that the sweeping generalizations on the appropriateness of metaheuristics, and especially genetic algorithms, for building energy optimization require critical scrutiny, while other types of algorithms deserve increased interest in this field.

Author Keywords

Building Energy Optimization, Genetic Algorithms, Direct Search, Model-based Optimization, Fitness Landscape Analysis

ACM Classification Keywords

I.6.1 Simulation and Modelling, B.5.2 Optimization

1 INTRODUCTION

To find energy-efficient building designs, building energy simulation is increasingly combined with black-box optimization methods. This paper considers which black-box optimization methods are most appropriate for building energy optimization (BEO) by revisiting a seminal work [23] concerned with the same question. Specifically, we ask if genetic algorithms—the most popular algorithm in BEO [5], [15]—should really be the preferred choice.

Black-box (i.e., derivative-free) optimization methods [3, 25] require no knowledge about the mathematical formulation of an optimization problem, but only consider the problem inputs (variables) and output (cost). The relationship between variables and cost defines a cost function whose range is often referred to as a fitness landscape. In BEO, one usually calculates the cost function with a simulation program such as EnergyPlus.

An important criterion for black-box optimization methods is whether they are local or global. While local methods work best on unimodal fitness landscapes with a single optimum, global methods apply to multimodal problems with multiple optima. The local optima of multimodal problems, which are optimal only relative to a region of the fitness landscape, easily trap local methods. Global methods avoid this entrapment by balancing (global) exploration, which surveys the overall form of the fitness landscape, with (local) exploitation, which finds good solution in promising regions of the landscape.

This study evaluates the performance of optimization methods currently available for Grasshopper—a popular parametric modelling software among architects with links to various simulators—for solving BEO problems. We consider three categories of black-box optimization methods: direct Search, metaheuristics and model-based methods.

1.1 Direct Search

Direct search methods are deterministic and sequential. The mathematical optimization community prefers them over metaheuristics due to their proven convergence properties [3] and generally superior performance on (convex, non-convex, smooth and non-smooth) benchmark problems [19]. There are local and global direct search methods.

1.2 Metaheuristics

Metaheuristics [26] often lack proven convergence properties and often draw their motivation from physical and biological phenomena. While many mathematicians view them as methods "of last resort" [3], according to the BEO literature, metaheuristics are preferable to direct

* These two authors contributed equally to this work.

search methods. The BEO literature supposes that fitness landscapes in BEO are non-convex, non-smooth and discontinuous [23], and that, due to their stochastic and population-based characteristics, metaheuristics tackle such discontinuous fitness landscape more easily and without getting trapped by local optima[1], [11].

Such arguments are pervasive [5], [14], [15] and next to ease of implementation and availability explain the popularity of metaheuristics. This popularity also applies to structural design optimization and leads [7] to suggest that "evolutionary algorithms may be overused, specifically for continuous problems". In BEO, the rare comparisons between direct search and metaheuristic methods usually feature dated direct search methods like Hooke-Jeeves or Simplex [15].

1.3 Model-based Methods

Global model-based methods are a younger category of algorithms. They use machine-learning methods such as Neural Networks, Support Vector Machines and Radial Basis Functions (RBF) to approximate the unknown fitness landscape [12]. The surrogate model replaces or supplements time-intensive simulations since, although less accurate, it is much faster to evaluate. To determine a promising solution to simulate next, the algorithm searches the model deterministically, randomly or with a metaheuristic. The model is then updated with information gained from the simulation.

Model-based algorithms are seldom used for sustainable building design, although Wortmann and Nannicini present promising benchmark results for daylight optimization [25].

Local model-based methods—also known as Trust Region methods [3]—also employ a surrogate model. However, they construct only partial and comparatively simple models. Accordingly, trust region methods work best for convex fitness landscapes without multiple optima.

2 METHODOLOGY

This section discusses the considered black-box optimization algorithms, the problems from energy simulation and our benchmarking methodology and criteria.

2.1 Black-Box Optimization Algorithms

We compare the performance of nine black-box algorithms, all of which are available for Grasshopper. For the global model-based algorithm, we test two types of surrogate model. Algorithms where no reference is given are covered in [26].

Direct Search Algorithms

SUBPLEX [20] hybridizes two local direct search algorithms. It aims to improve the performance of the Nelder-Mead Simplex algorithm—one of the algorithms tested in [23]—by decomposing the fitness landscape into smaller regions (i.e., subspaces). It searches individual regions with the Simplex algorithm and moves from one region to a better one with line search. Line search algorithms [3] iteratively select a direction to move to and search for a better solution in that direction.

DIRECT [9] is a global method that considers the whole fitness landscape. It recursively subdivides this landscape into multidimensional hyperrectangles. The algorithm estimates the potential of each rectangle to contain an improved solution and subdivides the most promising one. The result is a grid of solutions that is coarse in unpromising regions and fine in promising ones. DIRECT is rarely applied to building performance optimization, but has shown good performance for structural and daylighting optimization problems [25].

We test the implementations of SUBPLEX and DIRECT from the NLopt library[8], which is linked to Grasshopper via the free Goat plug-in.

Metaheuristic Algorithms

We consider three "classic" metaheuristics algorithms—a genetic algorithm, particle swarm optimization and simulated annealing—and CRS2, a method which falls in-between direct search and metaheuristics.

Genetic algorithms evolve a population of good solutions through genetics-inspired operations. Crossover and recombination of individual solutions allow large jumps across the fitness landscape that help to avoid entrapment by local optima, while mutation facilitates gradual changes. Selection ensures the convergence of the population towards a group of good, often very similar, solutions.

Schooling behaviors exhibited by, for example, birds and fish inspired particle swarm optimization (PSO). The swarm's particles represent a population of solutions. A particle moves towards a direction weighted randomly between the best solution encountered by itself and the best solution overall. In this way, the swarm converges gradually in a good region of the landscape, while a broad initial distribution of particles insures against entrapment by local optima.

Simulated annealing (SA) considers only a single solution. Mimicking the movement of an atom in a cooling metal, the solution initially changes more randomly—there is a chance that the solution will get worse—and becomes more stable—only accepting improved solutions—as the "temperature" drops. In other words, this method gradually shifts from exploration to exploitation.

Controlled random search (CRS2) shares similar features with a Nelder-Mead Simplex and is a metaheuristic algorithm in the sense that it heuristically improves a randomly generated population of solutions [10].

We test implementations of a GA and SA that are included in Galapagos, the PSO implementation in Silvereye [2] and the implementation of CRS2 in NLopt linked to by Goat. Galapagos is distributed with Grasshopper, while Silvereye is a free, third-party plug-ins.

Model-based Algorithms

COBYLA [17] and BOBYQA [18] are local, trust region algorithms. COBYLA uses a linear and BOBYQA a quadratic model.

We test a global model-based method that interpolates the surrogate model with Radial Basis Functions [6] and a GA to search it. These functions allow different interpolations, of which we test thin-plate spline (RBFtps) and cubic (RBFc), the two best-performing interpolations in [4].

We test the implementation in the open-source RBFOpt library [4], which is linked to Grasshopper via Opossum, a free Grasshopper plug-in.

2.2 Building Energy Optimization Problems

We apply the nine optimization algorithms to three building energy design problems using the building energy simulation (BES) program EnergyPlus V8-5-0 linked to Grasshopper via a custom script.

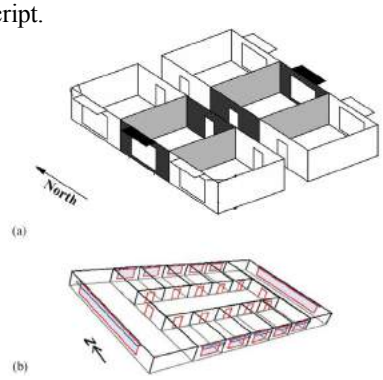

Figure 1. Office buildings used in the numerical experiments: (a) problem 1, (b) problem 2 and 3. Image from: [23]

Problem 1 is a simple office building with four decision variables: building orientation α in [°], window width for the West and East façade w_W and w_E in [m], and the shading device transmittance τ. Problem 2 is a more detailed office building, where the decision variables control the window width and heights for the North, West, East and South façade (w_N, w_W, w_E, w_S), the depth of the window overhangs in West, East and South (o_W, o_S, o_E), the setpoint of the shading devices in [W/m²] at the North, East and South façade (s_W, s_E, s_S), the setpoint for the zone air temperature for night cooling during summer and winter in [°C] (T_u, T_l), and the cooling design supply air temperature used for the HVAC system sizing in [°C] (T_d). Problem 3 is identical to Problem 2 with the only difference being the use of discrete variables.

We test problem 1 with Seattle, problem 2 with Houston and problem 3 with Chicago weather. The building models for all problems are shown in **Figure 1**. Table 1 summarizes the variables, their bounds and their discretization step sizes (form Problem 3). The optimization aims to identify variable values that minimize the annual energy consumption in kWh/m²a for heating, cooling and lighting of the office spaces (i.e., the cost value).

The BEO problems used here originate from a seminal work by Wetter and Wright [23] where a thorough description of the problems including cost functions can be obtained. In our study, we use a different EnergyPlus version than in [23]. We obtained the original files from the authors and used the official EnergyPlus file updater for transitioning to the current version. The weather files are identical to the original study.

In [23], the authors conclude that the hybrid PSO/Hook-Jeeves algorithm finds the best solutions and the simple GA offers faster convergence (i.e. less time-intensive simulations to be run) at a slight decrease in solution quality.

Variable symbols		*lb*	*ub*	*s*
Simple model	α	-180	180	-
	w_W, w_E	0.1	5.9	-
	τ	0.2	0.8	-
Detailed model	w_N, w_W, o_W	0	1	0.05
	w_S, o_S	0	1	0.05
	w_E, o_E	0	1	0.05
	s_W, s_E, s_S	100	600	25
	T_u, T_l	20	25	0.25
	T_d	23	18	0.25

Table 1. Variable symbols, lower bound *lb*, upper bound *ub* and step size *s*

2.3 Benchmarking

Following [23], we run Problem 1 for 300 function evaluations (simulations) and Problems 2 and 3 for 500. On an Intel Core i7 6700K CPU with 4.0 GHz, one simple simulation takes about 3 seconds and one detailed simulation about 5 seconds.

Algorithm Parameters

We use default parameters for all algorithms. Although the performance of optimization algorithms, and especially of metaheuristics, can vary greatly with different parameters, finding the best parameters for a specific problem can require many more function evaluations than the actual optimization process itself.Comparing algorithms in this manner reflects a practical situation where little is known about the optimization problem and time constraints limit the number of function evaluations.

The large performance differences between the optimization algorithms presented here suggest that, rather than spending an evaluation budget on tuning an algorithm to a specific problem, one should try two or three different algorithms. Note that the arguments for applying metaheuristics outlined in section 1.2 do not depend on specific parameters.

Performance Criteria

We assess the algorithms' performance with two criteria: speed of convergence and stability, i.e. quality and reliability. We measure speed of convergence as the best solution found relative to the number of function evaluations—with the computational overhead for the optimization algorithms considered negligible—and stability as the standard deviation of the results from ten optimizations runs per algorithm.

DIRECT is the most stable algorithm since it is fully deterministic. COBYLA and BOBYQA also are deterministic, but require a starting solution that we assigned randomly.

3 BENCHMARK RESULTS

This section presents the benchmarking results for Problems 1, 2 and 3 from section 2.2.

3.1 Problem 1

After 300 evaluations of the continuous Problem 1, DIRECT, RBFtps and PSO find mean solutions at 133.0 kWh/m^{2}a, with SA and RBFc 0.1 and CRS 0.2 kWh/m^{2}a removed (Figure 2). DIRECT, RBFtps and RBFc exhibit early convergence, with PSO and SA catching up at around 150 evaluations. Generally, these better converging algorithms also display high stability; of the six best-performing algorithms PSO exhibited the largest variation (0.3 kWh/m^{2}a) and SA one outlier (Figure 3).

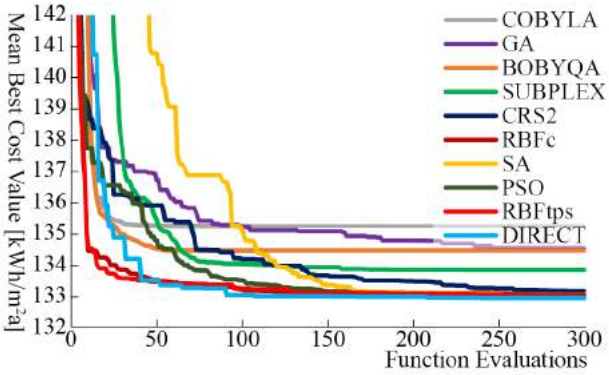

Figure 2. Problem 1: Mean minimum energy consumption from ten runs, as a function of the number of function evaluations.

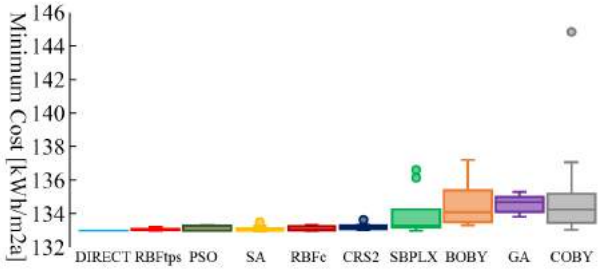

Figure 3. Problem 1: Boxplot of minimum energy consumption after 300 function evaluations from ten runs.

3.2 Problem 2

After 500 evaluations of the continuous Problem 2, Subplex finds the best mean solution at 141.3 kWh/m^{2}a, with DIRECT and SA 0.3, and RBFc and RBDtps 0.5 kWh/m^{2}a removed (Figure 4). For the first 200 evaluation, Subplex exhibits the slowest speed of convergence and RBFc and RBDtps the fastest, after which Subplex rapidly improves. Except one dramatic outlier by SA, the better converging algorithms display high stability (Figure 4).

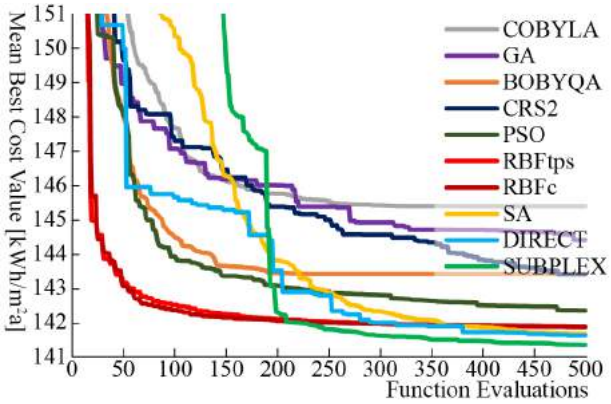

Figure 4. Problem 2: Mean minimum energy consumption from ten runs, as a function of the number of function evaluations.

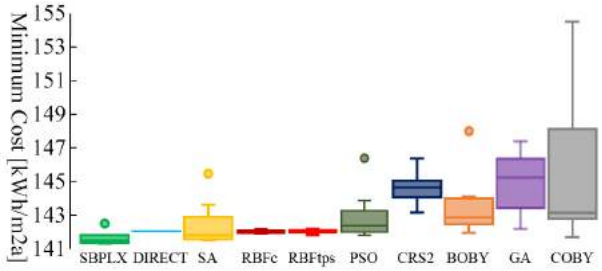

Figure 5. Problem 2: Boxplot of minimum energy consumption after 500 function evaluations from ten runs.

3.3 Problem 3

After 500 evaluations of the discrete problem 3, SA finds a solution at 136.0 kWh/m^{2}a, with DIRECT and RBFc 0.2 and PSO 0.3 kWh/m^{2}a removed (Figure 6). Initially, RBFc displays the fastest convergence; it is overtaken by SA at around evaluation 150. Problem 3 reveals a large (0.8 kWh/m^{2}a) difference between RBFc and RBFtps—probably due to the discretization—which otherwise perform very similarly. Except small outliers by RBFc and PSO, the better converging algorithms display high stability (Figure 7).

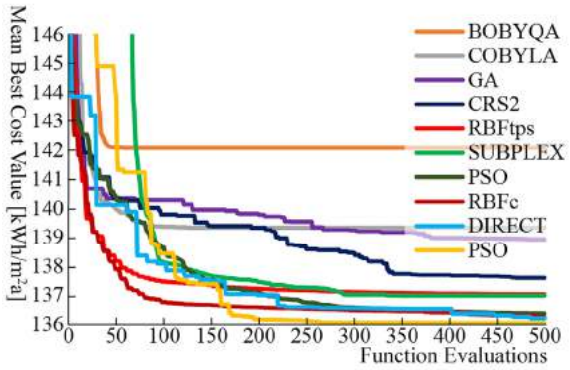

Figure 6. Problem 3: Mean minimum energy consumption from ten runs, as a function of the number of function evaluations.

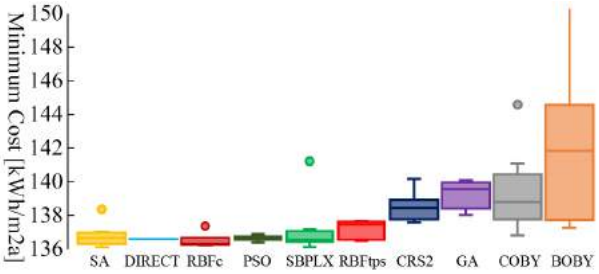

Figure 7. Boxplot of minimum energy consumption after 500 function evaluations from ten runs.

4 FITNESS LANDSCAPE ANALYSIS

Using a variety of methods, this section presents a detailed analysis of the fitness landscape for problem 2.

4.1 Sensitivity Analysis

We apply the Sobol method, a variance-based sensitivity analysis technique, in order to quantify the amount of variance in the cost value *f(x)* that can be attributed to changing variable values *x*. The first first-order effect S_i indicates the variance in *f(x)* caused by varying only a single variable x_i, whereas the total effects S_{Ti} indicate the variance in *f(x)* caused by a variable x_i if all other variables are varied as well. Hence, S_{Ti} shows the higher-order effects of a variable, i.e. if it interacts with other variables [21]. Both indicators give crucial information about the fitness landscape, as it reveals the most sensitive decision variables in the optimization. For computing S_i and S_{Ti} we generate a Sobol (also called LP_T) sequence, which is a pseudo-random sequence to uniformly distribute samples in a multidimensional hypervolume. The Sobol method is an important technique in BES uncertainty research [13], [22].

S_i and S_{Ti} for the n = 13 variables $x_i \in \{w_N, w_W, o_W, w_S, o_S, w_E, o_E, s_W, s_E, s_S, T_u, T_i, T_d\}$ of problem 2 are shown in Figure 8, using a LP_T sequence of $m = (n + 2) * 1000 =$ 15.000 samples. It is striking that only two variables (T_u and T_d) significantly contribute to the cost *f(x)*, while all other variables appear to be negligible. It is worth noting, however, that the total effects S_{Ti} of T_u and T_d are substantially higher than their first-order effects, indicating a strong interaction between other variables.

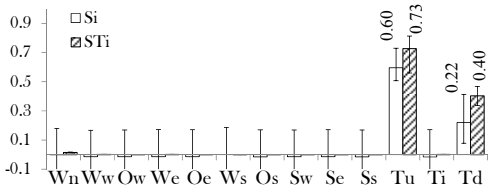

Figure 8. First-order (S_i) and total effects (S_{Ti}) from the Sobol method for problem 2.

4.2 Uni- and Bivariate Correlation

We correlate the m samples from the LP_T sequence of problem 2 to study the relation of each variable x_i to the cost *f(x)*. In the previous section, we identify two major variables, while other variables appear negligible. This impression is confirmed in our correlation plots in Figure 9, where we show the univariate correlation between variables w_N, T_u and T_d over *f(x)* on the right side of the figure. Variable w_N is representative for all other variables (other than T_u and T_d), i.e. they show a similar pattern. From the univariate correlations, clear patterns can be recognized for T_u and T_d, while this is less the case for the remaining variables (represented by w_N).

On the left in Figure 9 we show a bivariate correlation of T_d and T_u over *f(x)*. Each dot is a sample from the LP_T sequence, i.e. *x[m]*. We overlay a thin plate spline interpolation surface using the Matlab curve fitting toolbox. The importance of the two variables T_d and T_u becomes especially clear this way, as it shows their joint relation in affecting *f(x)*. Computing the residuals of the samples in relation to the interpolation surface reveals a range between +20 and -10 kWh/m²a. In other words, by solely controlling T_d and T_u, *f(x)* varies between ~400 and ~150 kWh/m²a; by controlling the remaining variables, *f(x)* can be further varied in the range of +20 and -10 kWh/m²a. These last 10 kWh/m²a reduction form the true challenge to be addressed by the optimization algorithms, as indicated in section 3.

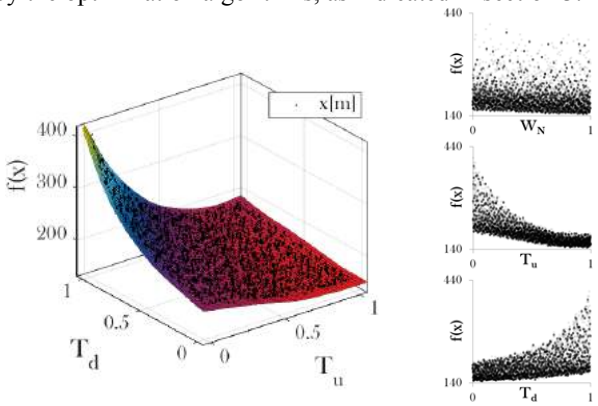

Figure 9. Problem 2. Left: Bivariate correlation between two most sensitive variables T_d and T_u and cost *f(x)*. Right: Correlation between variables w_N, T_u and T_d and cost *f(x)*.

4.3 Fitness Distance Correlation

Fitness Distance Correlation (FDC) aims to correlate the cost value of a solution and its normalized Euclidean distance in terms of variable space to the global optimum [16]. One of the practical challenges is knowledge about the global optimum *x**. As a best possible guess, we assume that our global optimum is the best-found solution of all function evaluations from the LP_T sequence and from all conducted optimization runs. Despite the large sample sizes (15.000 for problem 2) of LP_T sequences, the best solutions found by optimization algorithms—which typically use a far smaller number of function evaluations (here 500)—are almost always better than the best solutions found by sampling. This efficiency is a strong argument for the need for black-box optimization methods to search design spaces.

While the FDC value indicates how consistently an algorithm is searching the variable space towards the global

optimum, plotting the distribution of cost *f(x)* over distance provides insights into the structure of the problem and the behavior of an algorithm.

In Figure 10 we show the FDC plot for problem 2, using the samples generated by the LP_T sequences. The global optimum lies at 0 on the distance axis. The cost value of the optimum is given in the plot as *f(x*)*. Furthermore, the best and worst solutions of the LP_T sequences in terms of cost value ($f(x[m])_{min}$ and $f(x[m])_{max}$) and distance ($d[m]_{min}$ and $d[m]_{max}$) are given in the plot. The pattern of problem 2 is highly scattered and does not show any clear lower and upper bounds. It becomes apparent how rugged and non-smooth the problem landscape is: solutions with similar cost might vary significantly in terms of distance and getting closer to the variables of the best solution might not necessarily improve cost.

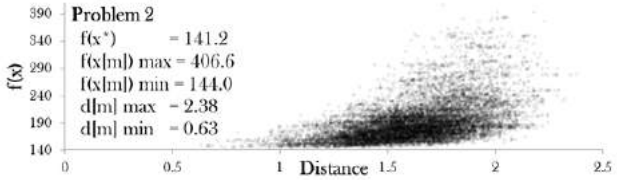

Figure 10. FDC plot of LP_T sequences for problem 2.

Figure 11 shows FDC plots for all algorithms and all runs for problem 2. Similar to the convergence graphs, the axes are clipped at 150 kWh/m²a and distance 1.5, since most of the search is conducted in this region. The plots also indicate the FDC values, lowest cost (f_{min}) and mean lowest cost of all runs ($\bar{f}_{500}$).

The fast convergence of RBFtps and RBFc discussed in section 3 can also be observed here. They invest most of the evaluations to successively reduce the distance towards the best-known value. All runs seem to have a similar search track so that individual runs cannot be identified—proof of the algorithms' stability. PSO shows a similar pattern to RBF, but the search tends to get stuck in local optima. Each run results in discernably different results, indicating a lower stability of this algorithm.

CRS2 shows high randomness of the sample distribution and no consistency in approaching the best-known value. Similarly, GA also shows high randomness, albeit greater convergence to specific regions. But it is unsuccessful in approaching the best-known value and shows very low stability between individual runs.

SA reaches cost values close to the best-known solution, but is unable to approach this solution in terms of variable space: the distance does not fall significantly below 0.5. While individual search tracks can be seen in the distribution of the samples, SA consistently approaches the same cost value. DIRECT comes close to the best-known value. Its division of the search space into hyperrectangles can be recognized in the distribution of the samples.

The local algorithms SUBPLEX, BOBYQA and COBYLA are easily distinguished in the FDC plots. Individual runs can be tracked by their search paths, especially with BOBYQA. For COBYLA and BOBYQA, this characteristic is fatal. Depending on their starting solutions, they get trapped by local optima and can only refine them. On the other hand, the division into sub-spaces by SUBPLEX allows it to break out of local optima. In this case, it even finds the best value, suggesting that local search can be very effective when started in the right region.

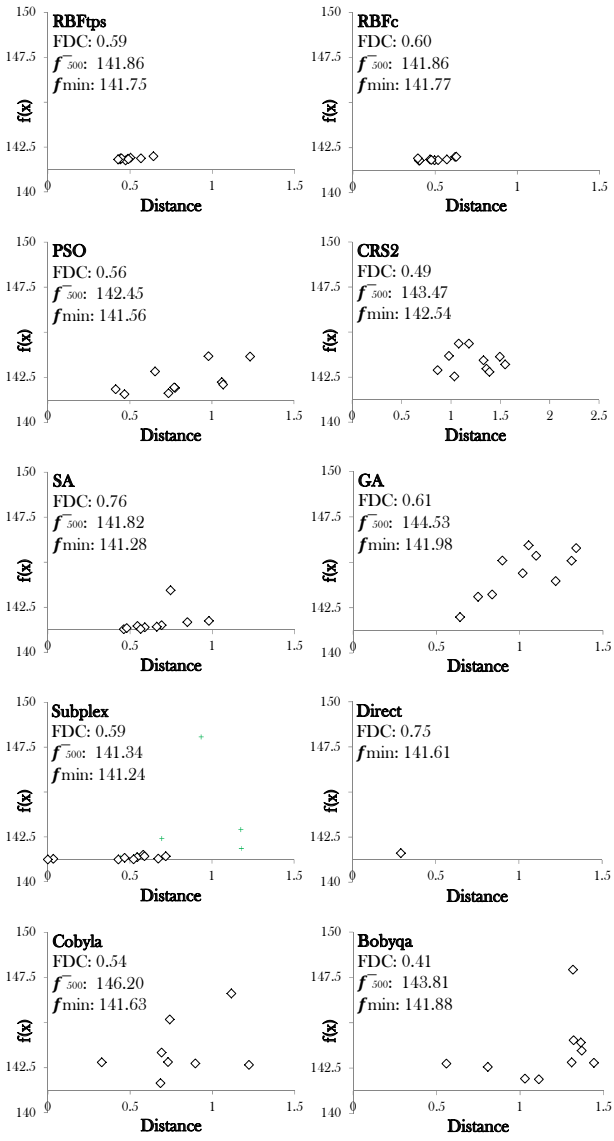

Figure 11. FDC plots of all algorithms for problem 2. The best solution found per run is highlighted as a white diamond shape.

4.4 Performance Map

Figure 12 is a "Performance Map" of Problem 2, that—like the FDC plots in Figure 11—visualizes the relationship between variable values and cost. Here, the 13 variables are

mapped onto the plane by linearly combining variable values with 13 radial coordinate axes: $p = x_1 v_1 + \cdots + x_n v_n$, where p denotes the point location on the plane, x is a variable value, v is its corresponding radial vector, and n is the number of decision variables. Cost is indicated as color with a logarithmic scale. To create the figure, we map all samples (from the optimization runs and the LP_T sequence), triangulate them and interpolate the colors using barycentric coordinates. [24] covers this method in detail.

The map indicates clusters of very good (~141 kWh/m²a) and good (~142 kWh/m²a) solutions. These clusters confirm the problem's multimodality. The location of the clusters in the upper right quadrant of the figure—which is associated with the variables for window size—suggests that better solutions tend to have larger west and east windows and smaller set-points for the shading devices and summer cooling. These better solutions are interspersed with worse ones, which reveals a high degree of discontinuity of the fitness landscape with many local optima.

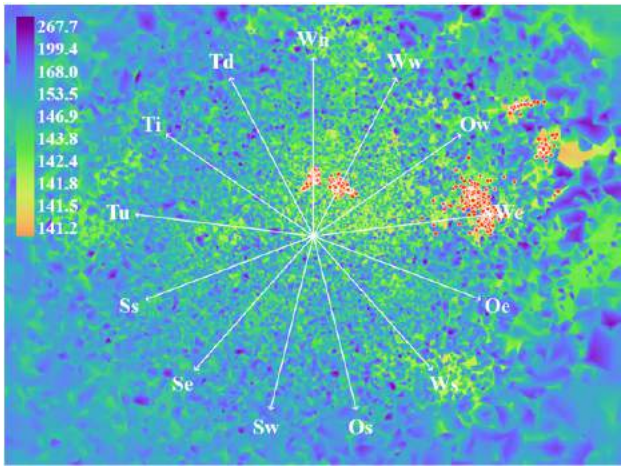

Figure 12. Performance Map of Problem 2. The map visualizes the most relevant portion of the fitness landscape. The red dots indicate solutions within 0.1% of the best solution.

5 CONCLUSIONS

In this benchmark, the best converging algorithms are a global direct search method (DIRECT) on Problem 1, a local global search method (SUBPLEX) on Problem 2 and a metaheuristic (SA) on Problem 3. DIRECT and SA converged fast on other problems as well, although SA is less stable. The RBF algorithms performed slightly less well overall. They excelled in early global exploration, but struggled with exploiting promising local regions. On problems 1 and 3, PSO did well and SUBPLEX struggled, with the reverse being true for problem 2, making these algorithms worth trying. BOBYQA, COBYLA, GA and CRS2 exhibited impractically slow convergence and lower stability than the other algorithms.

Based on the tested implementations, the GA is a poor choice of default algorithm, with DIRECT or SA being better candidates. For problems with a limited number of function evaluations—for example time-intensive daylighting simulations—we recommend RBFc. ([7] and [25] present similar results for structural and daylighting problems.) Since the performance of optimization algorithms is problem-specific, we advise trying several algorithms from different categories when possible.

Sensitivity analysis showed a large impact of two variables for cost reduction and only a small impact by the remaining variables. Nevertheless, their small contributions result in a complex, non-smooth and rugged fitness landscape. This complexity appears in the FDC plots (Figure 11) and performance map (Figure 12). Awareness of a problem's structure helps to understand the performance of optimization algorithms. In this example, algorithms that smooth fitness landscapes (i.e. RBF) or avoid distraction by local optima (i.e. SA, SUBPLEX and DIRECT) successfully balance global exploration and local exploitation.

The authors of [23] assume that local direct search algorithms should perform better on the "rather smooth" Problem 1 and metaheuristics should perform better on Problem 2, because it has "discontinuities (…), which makes optimization with descent algorithms difficult". This hypothesis has not been validated by our results, which do not indicate a clear relationship between the category of algorithm and its performance. Also, only local direct search and no model-based methods were tested in [23].

Compared to [23], we cannot recommend the GA due to its relatively poor performance in our benchmarks. While a direct comparison to [23] cannot be made, mainly since we use different implementations and settings, we can reopen the issue of algorithm choice in the BEO community: The sweeping generalizations one finds in the literature (such as "Evolutionary algorithms are robust in exploring the search space for a wide range of building optimization problems" [1] or "Direct search methods can be very efficient if the objective function doesn't have large discontinuities, otherwise it can fail or get trapped in local minima" [14]) on the appropriateness of metaheuristics for multimodal problems and the limitations of direct search deserve critical scrutiny. In our tests, the GA (a metaheuristic) struggled on all problems, while DIRECT (a direct search method) and RBF (a model-based method) performed well.

One should thus hesitate to generalize the performance of optimization algorithms and not be limited to only one algorithm—or category of algorithm—for a design task, since an algorithm's success depends on the specifics of a problem. The question when to choose which optimization algorithm and with what parameters is of great relevance for designers: There are many algorithms next to the GA and other famous metaheuristics that deserve close attention.

ACKNOWLEDGMENTS

The work is related to the Competence Center – Energy and Mobility "Synergistic Energy and Comfort through Urban Resource Effectiveness" project and the Swiss Competence Centers for Energy Research "Future Energy Efficient Buildings and Districts" project.

We thank Michael Wetter and Jonathan Wright for kindly providing us with the original files and for useful discussions. We also thank Georgios Mavromatidis for his kind support on the sensitivity analysis.

REFERENCES

1. Attia, S., Hamdy, M., O'Brien, W., and Carlucci, S. Assessing gaps and needs for integrating building performance optimization tools in net zero energy buildings design. *Energy and Buildings* 60, (2013), 110–124.
2. Cichocka, J., Browne, W., and Rodriguez, E. Evolutionary Optimization Processes as Design Tools: Implementation of a Revolutionary Swarm Approach. *Proceedings of 31th International PLEA Conference Architecture in (R)Evolution*, 2015.
3. Conn, A., Scheinberg, K., and Vicente, L. *Introduction to Derivative-Free Optimization*. Philadelphia, PA: Society for Industrial and Applied Mathematics, 2009.
4. Costa, A. and Nannicini, G. RBFOpt: an open-source library for black-box optimization with costly function evaluations. *Optimization Online* 4538, (2014).
5. Evins, R. A review of computational optimisation methods applied to sustainable building design. *Renewable and Sustainable Energy Reviews* 22, (2013), 230–245.
6. Gutmann, H.-M. A Radial Basis Function Method for Global Optimization. *Journal of Global Optimization* 19, 3 (2001), 201–227.
7. Hare, W., Nutini, J., and Tesfamariam, S. A survey of non-gradient optimization methods in structural engineering. *Advances in Engineering Software* 59, (2013), 19–28.
8. Johnson, S. G. *The NLopt nonlinear-optimization package*.
9. Jones, D. R., Perttunen, C. D., and Stuckman, B. E. Lipschitzian optimization without the Lipschitz constant. *Journal of Optimization Theory and Applications* 79, 1 (1993), 157–181.
10. Kaelo, P. and Ali, M. M. Some Variants of the Controlled Random Search Algorithm for Global Optimization. *Journal of Optimization Theory and Applications* 130, 2 (2006), 253–264.
11. Kämpf, J. H., Wetter, M., and Robinson, D. A comparison of global optimization algorithms with standard benchmark functions and real-world applications using EnergyPlus. *Journal of Building Performance Simulation* 3, 2 (2010), 103–120.
12. Koziel, S. and Leifsson, L. *Surrogate-Based Modeling and Optimization*. Springer New York, 2013.
13. Kristensen, M. H. and Petersen, S. Choosing the appropriate sensitivity analysis method for building energy model-based investigations. *Energy and Buildings* 130, (2016), 166–176.
14. Machairas, V., Tsangrassoulis, A., and Axarli, K. Algorithms for optimization of building design: A review. *Renewable and Sustainable Energy Reviews* 31, 1364 (2014), 101–112.
15. Nguyen, A.-T., Reiter, S., and Rigo, P. A review on simulation-based optimization methods applied to building performance analysis. *Applied Energy* 113, (2014), 1043–1058.
16. Pitzer, E. and Affenzeller, M. A Comprehensive Survey on Fitness Landscape Analysis. *Recent Advances in Intelligent Engineering Systems* (2012), 161–191.
17. Powell, M. J. A Direct Search Optimization Method that Models the Objective and Constraint Functions by Linear Interpolation. , in *Advances in Optimization and Numerical Analysis*, S. Gomez and J.-P. Hennart, Eds. Dordrecht: Springer Netherlands, 1994, 51–67.
18. Powell, M. J. The BOBYQA algorithm for bound constrained optimization without derivatives. University of Cambridge, Cambridge, UK, NA Report NA2009/06.
19. Rios, L. M. and Sahinidis, N. V. Derivative-free optimization: A review of algorithms and comparison of software implementations. *Journal of Global Optimization* 56, 3 (2013), 1247–1293.
20. Rowan, T. H. Functional Stability Analysis of Numerical Algorithms. Ph.D. Dissertation, The University of Texas, Austin, TX, 1990.
21. Sobol′, I. Global sensitivity indices for nonlinear mathematical models and their Monte Carlo estimates. *Mathematics and Computers in Simulation* 55, 1 (2001), 271–280.
22. Tian, W. A review of sensitivity analysis methods in building energy analysis. *Renewable and Sustainable Energy Reviews* 20, (2013), 411–419.
23. Wetter, M. and Wright, J. A comparison of deterministic and probabilistic optimization algorithms for nonsmooth simulation-based optimization. *Building and Environment* 39, 8 (2004), 989–999.
24. Wortmann, T. Surveying design spaces with performance maps: A multivariate visualization method for parametric design and architectural design optimization. *International Journal of Architectural Computing* 15, 1 (2017).
25. Wortmann, T. and Nannicini, G. Black-box optimization for architectural design: An overview and quantitative comparison of metaheuristic, direct search, and model-based optimization methods. *Living Systems and Micro-Utopias*, (2016), 177–186.
26. Yang, X.-S. *Engineering Optimization: An Introduction with Metaheuristic Applications*. Hoboken, NJ: John Wiley & Sons, 2010.

Project Discover: An Application of Generative Design for Architectural Space Planning

Danil Nagy, Damon Lau, John Locke, Jim Stoddart,

Lorenzo Villaggi, Ray Wang, Dale Zhao and David Benjamin

The Living, an Autodesk Studio
New York, NY USA
life@thelivingnewyork.com

ABSTRACT

This paper describes a flexible workflow for generative design applied to architectural space planning. We describe this workflow through an application for the design of a new office space. First, we describe a computational design model that can create a variety of office layouts including locating all necessary programs and people using a small set of input parameters. We then describe six unique objectives that evaluate each layout based on architectural performance as well as worker-specific preferences. Finally, we show the use of a multi-objective genetic algorithm (MOGA) to search through the high-dimensional space of all possible designs, and describe several visualization tools that can help a designer to navigate through this design space and choose good designs. We conclude by discussing the future of such computational workflows in design and architecture. Our hope is that they go beyond basic automation to create an expanded role for the human designer and a more dynamic and collaborative interaction between computer design software and human designers in the future.

Author Keywords

Parametric modeling, simulation, genetic algorithms, multi-objective optimization, evolutionary design, generative design, architecture

ACM Classification Keywords

I.6.5 SIMULATION AND MODELING - Model Development

1 INTRODUCTION

Computers and computer-aided design (CAD) software have had a dramatic impact on architectural practice since the emergence of computers in academia in the 1950s, and especially since the introduction of personal computing in the 1980s. Although early researchers envisioned a wide-ranging future interaction between computers and human designers [10], the first computer tools to be widely adopted by architectural designers were computerized versions of traditional drafting and rendering tools. While they allowed designers to produce content much faster than with traditional methods, they did not fundamentally change the process of design.

1.1 Parametric design

In the past decade, a new type of design software has emerged which is fundamentally changing the way designers use computers to develop and refine their designs. Known as *parametric design software*, these tools allow the designer to not only define a final geometric solution, but to describe the entire system behind how a design is generated. Within this larger system description, the designer can expose specific parameters, or values that drive different variations of the design.

Although such a model takes more work initially to describe, it offers the designer many advantages. First, the parametric approach makes it easy to create variations and custom adaptations of a design. Instead of manually creating multiple versions for different applications, the designer can expose the critical parameters that drive different variations and automatically generate different versions by changing those parameters. Second, a well-structured parametric model is more adaptable to change in the future. Since it is defined by a series of operations, the design can be easily adapted to changing conditions instead of rebuilding the model from scratch each time.

Most importantly, the parametric approach allows the designer to think through design solutions in a deeper and more dynamic way than possible with traditional methods. In a traditional approach, the designer studies the design problem, internalizes all of its constraints and objectives, and then uses their skill and experience to craft a single design solution, or a handful at most. With the parametric approach, the constraints and goals of the design problem can be directly embedded within the parametric model, which can then be used to automatically generate a variety of solutions. Instead of designing a single solution, the designer can now think of designing a multi-dimensional 'space' of design. Each dimension of this design space represents one of the critical parameters exposed by the parametric model, and each individual design variation can be found somewhere within this hyper-dimensional space.

1.2 Beyond parametric

While the parametric approach has broadened the possibilities of design and pushed the boundaries of human-computer

SimAUD 2017 May 22-24 Toronto, Canada

interaction in the design process, the exploration of the design space is still limited by the abilities of the human designer. Although some parameters may be set by the constraints found explicitly in the design problem, for the most part the human designer must investigate different design options by manually varying individual parameters and evaluating each option using their own criteria and intuition in a way not much different than with traditional design methods.

The concept of *generative design*, as described in this paper, addresses this limitation by tasking a computer with exploring the design space semi-autonomously, and then reporting back to the designer which options it considers promising for further analysis. Because a computer can process information much quicker than a human, such a system allows a much deeper exploration of complex design spaces. Traditionally, such an approach has been used to optimize a given model to achieve maximum possible performance based on concrete objectives [8]. With a model of sufficient complexity, however, a generative design system can also be used to reveal interesting parts of the design space and discover novel design solutions that would otherwise be hidden to the human designer.

To take advantage of the possibilities of generative design, the basic parametric model must be extended in two ways. First, the model must include concrete metrics by which each design option can be evaluated. Since the computer does not have any inherent intuition about design, the human designer must explicitly describe to the computer how to determine which designs perform better than others. Second, the model needs to be connected to a search algorithm that can control the input parameters of the model, get feedback from the metrics, and intelligently tune the parameters to find high performing designs while also exploring the full possibilities of the design space. One of the most promising of these algorithms is the multi-objective genetic algorithm (MOGA), which uses principles of evolution to create sequential generations of designs and evolve them to contain higher performing designs over time [9].

The remainder of this paper describes our development of a custom workflow for generative design specifically geared towards architectural space planning, and our application of this workflow to the design of a new office space.

2 RELATED WORK

The application of multi-objective optimization towards solving complex mechanical design problems is well-known in the field of engineering. Marler and Arora [8] provide a good overview of various applications. However, being constrained to the goals of engineering problems, these applications are limited to using only structural performance as optimization criteria.

Liggett [7] provides a thorough historical overview of automated methods for space planning in architecture, including the use of genetic search algorithms. Derix [2], Keough and Benjamin [6], Chronis et al. [1] and Gerber et al. [3] have applied similar optimization methods to a variety of architectural problems. However, their optimization criteria are similarly constrained to well-known and easily simulated physical objectives such as structural and environmental performance. In contrast, we propose a more flexible workflow that can accommodate a diversity of optimization criteria, including those dealing directly with how space is used and experienced at the occupant level

The quantification of spatial experience has also been explored by a variety of authors. Hillier, et al. [4] proposed a variety of analytical tools for studying spatial configurations which they called ‘space syntax’. Peponis, et al. [11] extend this work by proposing a universal method for understanding plan topology through linear representation. Turner, et al. [12] propose a view-based ray tracing technique for understanding and analyzing spatial configurations. While the proposed methods can help the designer derive quantitative data about their designs, they are only offered as tools to aid a traditional design process. In contrast, we extend these methods and show how they can be used as measures of spatial performance to guide an automated optimization process.

3 METHODOLOGY

Our proposed workflow of generative design for architecture is organized into four steps: (1) the design of a geometric model which can create many design variations, (2) the design of a series of performance metrics which can be used to measure the performance of a single design, (3) the exploration of the model’s design space through a MOGA, and (4) the investigation of the resulting design data through statistical analysis. Furthermore, we propose this method as only one component within a broader design process. Thus, there are several steps that must be taken both ‘before generative design’ in order to establish a design concept to drive the geometric model and collect necessary data for the performance metrics. Similarly, there are a variety of steps that must be taken ‘after generative design’ in order to achieve other criteria and develop the selected design solution to the level of a final constructible design.

3.1 Before generative design

As with any architectural design project, the process begins by studying the design problem, understanding its goals and constraints, and formulating a vision and concept for the design. The vision of the project was to create a dynamic and highly functional new office space for Autodesk in Toronto. Some of the constraints included:

1. The outline of the three floors of an existing new building where the office would be located
2. The programmatic requirements, including specific numbers of shared amenities such as meeting rooms
3. Occupation by up to 300 workers
4. Diversity of different departments, project teams, and workstyles that the office needed to accommodate

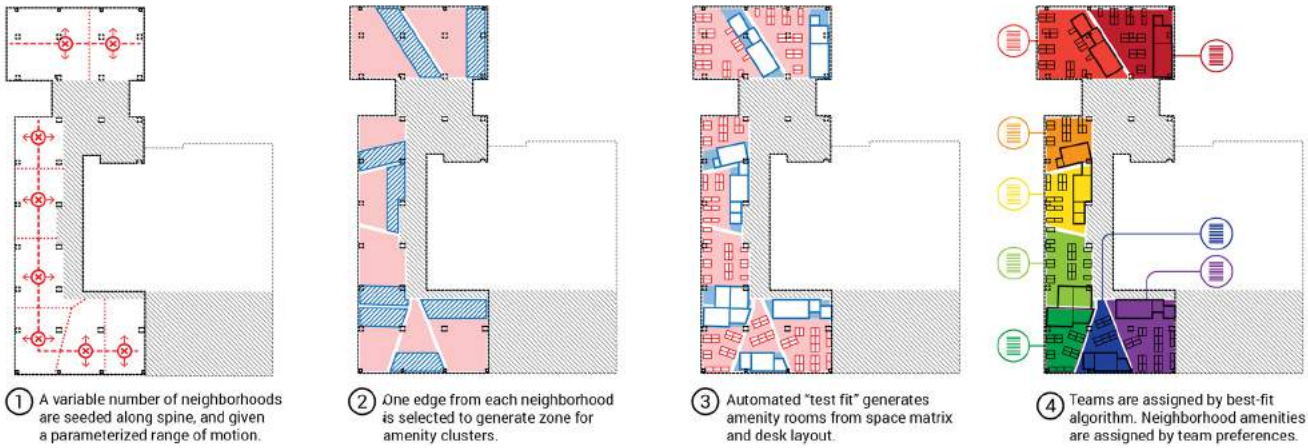

Figure 1. Description of specification of geometric model

Based on the vision of the project and these constraints (the goals of the project were established in a subsequent step), we developed an architectural concept around breaking up the floorplan into a series of individual 'neighborhoods'. In this concept each neighborhood is a work-area for an individual department or project team. The neighborhoods are divided by shared amenity spaces, which are contained within standalone rooms. These rooms create visual variation within the office space as a whole, while providing a degree of privacy and uniqueness to each neighborhood.

Once this basic concept was established, the design problem became the arrangement of neighborhoods within the building floorplan, the location of shared amenity spaces, and the assignment and placement of teams and individual workers in the neighborhoods. In architecture, this type of problem is known as *space planning*, and deals with the optimal arrangement of programs and spaces within a fixed plan. Because there are so many possible variations, this type of problem is traditionally difficult to solve for a human designer, and typically relies heavily on intuition and rules of thumb, along with iterative design and testing of a large variety of solutions before finally choosing the best one. Due to the complexity of this problem, it was actually the subject of one of the first applications of computing to architectural design [5]. For us it was the perfect problem to test the possibilities of the generative design process previously described.

Besides exploring many design options, another advantage of the generative design approach is that we can evaluate designs at a much higher level of detail than possible with traditional approaches, including evaluating some aspects of the design which are often ignored or abstracted in typical space planning projects. In this case we wanted to judge each design not only on global architectural goals such as maximizing the amount of light in the space, but also on local goals having to do with the individual preferences of each of the office's future occupants.

To get information about these preferences we distributed surveys to all individuals and teams in the office, asking their preferences in terms of which amenities they want to be close to, which other teams or individuals they often work with, and the office conditions they prefer. Based on this information, we were ready to construct the generative design model that could generate unique design solutions and evaluate each one based on specific performance metrics.

3.2 Geometric model

The first step was to create a geometric model that could define a set of neighborhoods within the two main floors of the office building, position shared amenity zones between neighborhoods, and then locate specific programs within the amenity zones and individual workers within the neighborhoods. To create each individual design, our geometric model applies the following algorithm (see Figure 1):

1. Locate a seed point for every neighborhood
2. Draw neighborhood boundaries based on edges equidistant from the neighborhood seeds (similar to a voronoi diagram)
3. For each neighborhood, choose one of the edges along which to place a shared amenity zone
4. Place shared programs within amenity zones based on a greedy fill algorithm
5. Assign teams to neighborhoods, also based on a greedy fill algorithm
6. Assign people to specific desks in neighborhood based on list order.

To establish the neighborhood seeds, a linear spine is drawn over the plan and the seeds are distributed evenly along this spine. Then, each seed's exact location is refined by two individual parameters – the first defines the distance to move along the spine from the initial point, and the second defines

the distance to move away from the spine in the perpendicular direction. A third unique parameter chooses the edge along which to place the amenity zone by specifying its normalized distance along the neighborhood boundary. The placement of individual amenity programs, teams, and individuals is not parameterized, but is instead directly determined according to the geometry of the neighborhood boundaries.

With 15 neighborhoods controlled by 3 unique parameters each, the model is completely described by 45 unique parameters. Currently, there are no theories or rules for how many individual parameters a model should contain to ensure that a robust search of the design space is both feasible and complex enough to create a wide variety of design options. In general, the current best practice is to make this number as small as possible, while ensuring that each critical aspect of the design is controlled by a *unique, continuous variable*. The uniqueness of each parameter is important so that the algorithm can directly control each aspect of the design independently while searching for the best combinations. The continuity of each parameter is important because the algorithm should be able to fine-tune the parameter settings by predicting future results based on past experiences. If each setting of a parameter yields completely different results, it will be far more difficult for the algorithm to search through the design space.

Finally, in order to take advantage of learning within the automated search process, the entire model needs to be completely deterministic, relying only on the input parameters exposed to the algorithm to generate each design. No noise or random parameters should be utilized in the geometric model.

3.3 Design metrics

To allow the search algorithm to automatically measure the performance of each design generated, we also defined a set of unique goals, or metrics, which rate the relative performance of each design along a set of criteria. These metrics form the set of output values that the search algorithm can use to evaluate how well each design option performs, and to guide its search of the design space toward discovering higher performing designs.

One apparent limitation of the generative design process is that all performance criteria for a given design system must be exposed to the search algorithm as a numeric quantity. Thus, any performance metric that we want the algorithm to consider must be both quantifiable and computable in a reliable and efficient way for all solutions within the design space.

In engineering applications where similar optimization workflows have been explored for a number of years, the metrics are relatively straight forward. For example, the strength of a structural component is easy to compute using standard finite element analysis (FEA) software. An architectural design problem, however, often has many competing and complex goals, some of which are difficult if not impossible to quantify such as beauty, fairness, quality of space, elegance, and novelty. To deal with this potential difficulty, we divide the set of all possible architectural performance metrics into three groups:

- Those that can be easily quantified and calculated using existing tools (e.g. daylight analysis)
- Those that can theoretically be quantified but cannot be computed using existing tools, for which new computation tools must be developed (e.g. employee work style preference and activity hotspots)
- Those that cannot be quantified and must be addressed through other means outside of generative design (e.g. beauty)

While this classification addresses the current limitations of the generative design workflow, the conclusion of this paper outlines some ideas for future research that suggests machine learning as a way to quantify and evaluate goals that are challenging to compute using direct calculation. In our case, our analysis of the project goals along with discussions with the managers and individual workers yielded six discrete design metrics to evaluate each design (see Figure 2):

1. *Adjacency preference*, which measures the travel distance from each employee to their preferred neighbors and amenities
2. *Work style preference*, which measures the suitability of an assigned neighborhood's daylight and distraction measurements to the assigned team's surveyed preferences
3. *Buzz*, which measures the amount and distribution of high-activity zones
4. *Productivity,* which measures concentration levels at individual desks based on sight lines to other desks and other noise sources
5. *Daylight,* which measures the total amount of natural daylight entering the space throughout the year.
6. *Views to outside,* which measures the ratio of workspaces with an unobstructed view to the exterior glass façade

One of these – daylight – is well understood and can be calculated using existing analysis tools. The other five were either novel or highly specific to our design goals. For these we developed our own custom analysis tools which we built directly into the generative design model.

Each new design project potentially brings with it a unique set of goals and performance requirements, which will never be fully described in any given design software. Thus, part of the responsibility of the designer in the generative design workflow is to be able to use computational tools such as parametric modeling and custom scripting to describe their

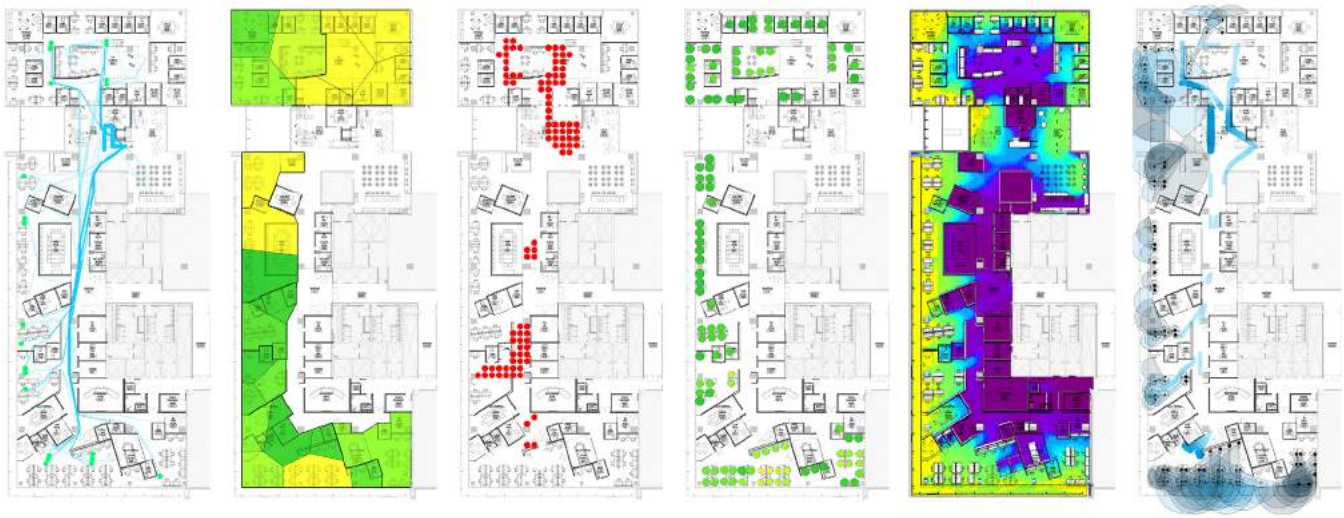

Figure 2. Design metrics (from left to right: adjacency preference, work style preference, buzz, productivity, daylight, and views to outside)

unique design goals to the computer. Although this sometimes makes the design task more difficult, it also has the potential to expand the role of the human designer while opening up new opportunities for design though enhanced human-computer interaction.

Along with the geometric model, the design metrics constitute the second half of the full *generative design model*. This model is a closed system that (1) takes in a discrete set of input parameters, (2) creates a unique design solution based on those parameters, (3) evaluates the design along a set of unique metrics, and (4) outputs those metrics as a set of discrete values. When this system is connected to a search algorithm, it can be automatically explored for good design solutions. However, although the algorithm can explore many more designs than possible through traditional manual means, it can only evaluate them based on the specified metrics output by the model. Thus it is crucial that the chosen metrics sufficiently capture the priorities of the design problem, and accurately describe the relative performance of each design according to those metrics.

3.4 Design evolution

Once we have defined the generative design model, we can use a search algorithm to automatically explore the space of possible designs and discover novel and high performing design options. A search algorithm is a subset of a general optimization algorithm, which is concerned with discovering optimal settings of input parameters of a function which maximizes the value of one or more outputs. Although many search algorithms exist, the one of particular interest to us is the multi-objective genetic algorithm (MOGA).

This algorithm generates designs in groups called generations. The first generation is composed of a set of initial designs either randomly or evenly sampled from the design space. Subsequent generations are then produced by either directly taking high performing designs from the previous generation (a process called *elitism*), or randomly mixing the parameters of two high performing designs to create a single new design (a process called *cross-breeding*). Each new design's input parameters may also be slightly modified before it enters the population (a process called *mutation*). This process is then repeated for multiple generations, either until the target number of generations is reached, or performance fails to improve for a certain number of generations. In this way, a MOGA uses concepts found in natural evolution to generate new designs based on the input parameters (genome) of previous high performing designs, thus gradually promoting the best options (survival of the fittest) and 'evolving' higher performing designs over time.

This type of algorithm has many advantages in the context of generative design. As the name implies, the MOGA can optimize designs along any number of output metrics. Furthermore, the user does not need to prioritize or weight the individual metrics beforehand. This is because the MOGA determines relative performance based on the idea of *dominance* rather than the absolute difference in metric values. A design is considered better performing than another if it dominates or performs better in one or more of the metrics. Thus the algorithm will continue to produce designs that are dominant in as many of the metrics as possible, and the user can later decide how to prioritize the metrics.

Another advantage of the MOGA is that it works stochastically by sampling designs from the design space, and trying to learn optimal configurations of the input parameters through experimentation. Other optimization algorithms such as gradient descent rely on computing gradients for each objective with respect to each input parameter. This is not possible with most parametric design models, which are

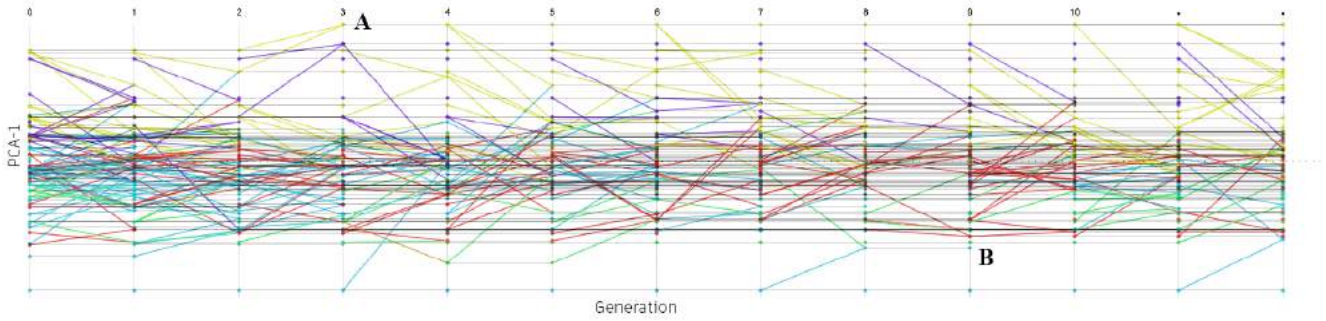

Figure 3. Time plot showing lineages of designs through generations (color indicates design cluster)

defined by a large number of geometric functions, none of which can be easily differentiated. Thus, such model can only by optimized through a stochastic experimental process.

Finally, genetic algorithms have also been shown to be exceptionally good at finding the overall best performing designs within a design space (the global optimum) while avoiding locally high-performing areas that may not be the best overall. By recombining high-performing designs from different areas of the design space, and slightly mutating designs over time, genetic algorithms can avoid local optimums more effectively than simpler, more deterministic algorithms such as gradient descent.

As with any optimization algorithm, the MOGA has hyper-parameters that need to be set before beginning the search process. These hyper-parameters have a significant impact on how the algorithm behaves and thus are an important aspect of generating good results. However, these settings also depend on the nature of the problem, so their tuning is often a product of heuristics and previous experience. The MOGA hyper-parameters include:

- The sampling method or the starting population
- The size of the starting and subsequent populations
- The termination criteria of the process (run for a set number of generations, or continue until no new better designs are found for a number of generations?)
- Cross-over rate, which dictates how many of a generation's designs are created by combining two designs from the previous generations
- Mutation rate, which dictates the rate at which a design's parameters are slightly modified before entering the next generation

In our case, we used generations of 100 designs each and ran the process for 100 generations creating 10,000 designs. The starting population of 100 designs was generated by randomly sampling from the design space. Through experimentation we settled on settings of 95% for cross-over, and 0.2% for mutation. The entire process ran over 5 days on a single MacBook Pro with a 2.60GHz Intel Core i7 processor and 16 GB RAM.

3.5 Data analysis

This process generated a data set containing 10,000 designs, including the input values for each design and its score along the six metrics. One approach at this stage would be to filter the dataset by the metric scores and directly select a few high-performing designs for further analysis. However, depending on the complexity of the design problem such a selection can be challenging for a number of reasons.

First, the various metrics might be directly competing with each other, which means that there is actually no single best design but a range of equally high performing designs along the trade-off between competing metrics. For example, when designing an industrial component there is typically a trade-off between the part's weight and its strength. In this case, unless there is a specific weight or strength target, it would be difficult to select a single 'best' design without first understanding how this trade-off works.

Second, as previously mentioned, the hyper-parameters of the MOGA have a significant effect on how the search works, and proper tuning of these settings depends on the particularities of each generative design model (including how many and what type of input parameters and output metrics are used). Thus, it is rarely enough to run only a single search process, and it is helpful if the results of every search are studied in depth to determine how the hyper-parameters may be tuned for future runs.

Finally, one of the advantages of a learning-based process such as MOGA is that it not only finds high-performing designs but also performs the search in a structured, semi-intelligent manner. By investigating the search process itself, more can be learned about the nature of the problem as a whole. In order to investigate this process and gain a deeper understanding of the design space, we developed a series of data analysis tools to aid the designer in exploring the dataset of designs generated by the MOGA.

Inheritance analysis

In addition to the input and output data for each design, the MOGA also outputs a history of how these designs were generated. Figure 3 shows a plot of this data, with each point

representing a design, and each column of points representing a generation of designs. Two colored lines entering a point from the left indicates that the design was formed through cross-breeding of those two designs. A thin black line indicates that the design was carried over directly into the next generation.

In this plot you can see an instance where a newly formed design is high performing and thus is consistently carried over into future generations (A), as well as a case where a new design gets carried over one generation but then dies out, likely due to the fact that it was not as high-performing as others in its generation (B). Studying such plots helps us understand how the algorithm explored the design space, how dominant design lineages are formed, and helps locate potential blind spots in the design space missed by the algorithm.

Input space analysis and clustering

To analyze how the sampled designs are distributed within the design space, we can use principal component analysis (PCA) to transform the 45-dimensional input space into a new 45-dimensional space where the dimensions are now ordered according to the extent to which they describe the variance in the data. Then we can use the first two PCA components to create the best-possible two-dimensional projection of the high-dimensional design space and see how the sampled designs are organized within that space.

To further study the distribution of designs in the design space we can cluster them based on Euclidean distance in the full 45-dimensional design space using the K-means algorithm (see Figure 4). Intuitively, this gives a representation of different design typologies or strategies that share similar input parameters. Once we have assigned the clusters to each design we can study how these design typologies relate to performance in the output metrics. For example we can see if certain design types perform better in some metrics than others. Such tools can help us understand the design problem in general and reveal potential design strategies, rather than simply picking the single best design.

Metric space analysis

Once we have understood the distribution of designs in the input space, we can study how the designs perform along the six performance metrics. Since there are usually less output metrics than input parameters, the space of outputs is not typically as high-dimensional as the input design space. Nevertheless, if there are more than 3 or 4 metrics it can be difficult to represent the results on a single plot. Our typical approach is to do a pairwise plot of all the output metrics to find combinations of metrics that have an interesting relationship or a clear trade-off. We can then study the tradeoffs in greater detail by plotting them against each other on a scatter plot (see Figure 5).

Once we have studied the performance of the whole set of designs, we can select a subset for further manual analysis. As a baseline the MOGA will provide us with a set of designs which are statistically dominant called the Pareto designs. To narrow it down further we can look for designs that occur at different points along the trade-offs, which can help us to see the effect of those trade-offs on the design solution. We can also use the cluster information generated earlier to identify cases where similar performance was achieved by different typologies of designs.

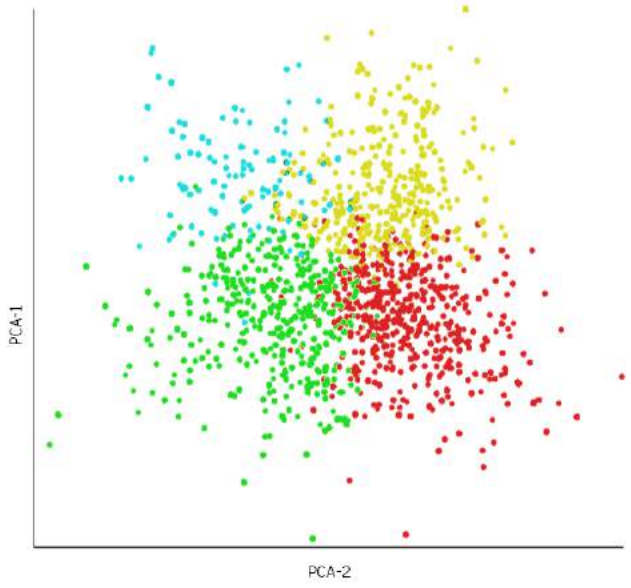

Figure 4. Plot showing clustering in input design space (color indicates design cluster)

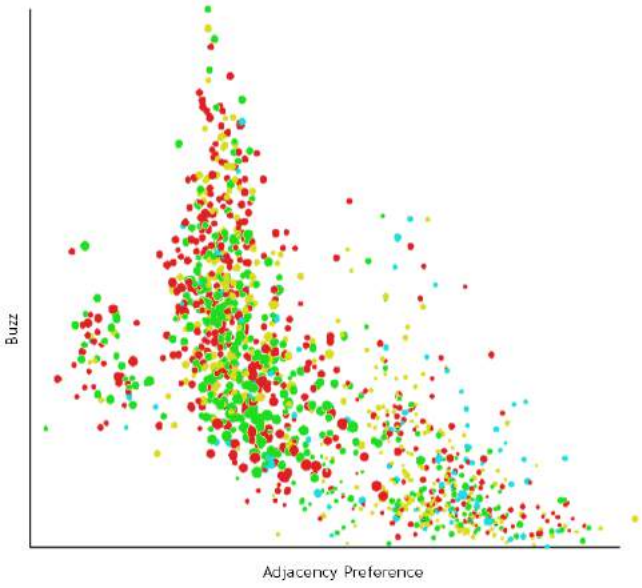

Figure 5. Plot showing tradeoff between two objectives (color indicates design cluster)

3.6 After generative design

Once a set of interesting designs is selected, they can be further analyzed by the human designer, discussed with the stakeholders, and developed into a final design. It is important to note that since the MOGA follows a stochastic process based on sampling a limited number of designs from the design space, the overall optimal design will not necessarily be found through the search process. Furthermore, as discussed previously, not all aspects that are important to an architectural design can necessarily be represented as a metric in the generative design model. Some aspects, such as beauty, cannot be quantified, and thus need to be considered once the generative design process is complete.

Finally, most generative design models including the space-planning model presented in this paper are fairly abstract and oversimplified, providing only rough geometry, boundary, and location information. After a basic space-planning strategy is selected, there is still much refinement and design work to be done, including selecting architectural materials and designing connection details, to get it to the level of a final constructible design.

Therefore, the process does not end with choosing one of the designs found by the algorithm. Instead, a deep analysis of various high performing designs and their trade-offs should suggest potential design strategies that the designer can further explore to achieve a final best design.

4 CONCLUSION

This paper described our development of a generative design workflow for architecture, and our application of it for the design of a new office space for Autodesk in Toronto.

Although the results of this investigation have been very encouraging, the process also has some limitations. Currently, the placement of programs and individual people in the plan depends on the neighborhood geometry, and thus cannot be directly controlled by the MOGA. To get a better and more targeted search we would need to develop methods to directly parameterize this placement and expose those parameters to the algorithm.

Another limitation is that the calculation of each design is still relatively slow – about one minute for each design – which limits the amount of exploration we can do. Automatically analyzing 10,000 designs already dramatically improves the capacity of a human designer, but is relatively small considering it is sampled from a 45-dimensional design space. Distributing the execution of designs within a single generation over several computers in a network would allow many more designs to be evaluated.

Finally, the workflow can be improved by integrating other types of modelling, particularly machine learning, for quantifying aspects of the designs that are difficult or impossible to compute through direct calculation. This is particularly interesting because it might allow the computer to develop knowledge of various design factors such as comfort, beauty, or novelty that are crucial to good design but have traditionally been difficult to relate to a computer.

As these types of workflows continue to develop in the future, it is our hope that they not only allow designers to develop high performing design options, but also help them understand their design problems better through a more collaborative human-machine design interaction. This will allow us to move far beyond the basic automation of tasks evident in early CAD tools, and leverage the full potential of true computer-*aided* design.

REFERENCES

1. Chronis A., Tsigkari M., Giouvanos E., Aish F., Zaki A. A., “Performance driven design and simulation interfaces: A multi-objective parametric optimization process”, *Proc. SimAUD* (2012)
2. Derix, Christian, “In-Between Architecture Computation”. *International Journal of Architectural Computing 7*, 4 (2009), 565-585.
3. Gerber, D., Lin, S., Pan, B., Solmaz, A.S. “Design optioneering: multi-disciplinary design optimization through parameterization, domain integration and automation of a genetic algorithm,” *Proc. SimAUD* (2012)
4. Hillier, Bill, et al. "Space syntax." *Environment and Planning B: Planning and Design 3*, 2 (1976): 147-185.
5. Johnson T., Dietz A. G. H., Weinzapfel G., Drauss R., Morris D., “Space Arrangement,” *AD Architectural Desig*n 9 (1969)
6. Keough I., Benjamin D, “Multi-objective optimization in architectural design,” *Proc. 2010 Spring Sim Multiconference*, Orlando, Florida (2010), 1-8
7. Liggett, Robin S. "Automated facilities layout: past, present and future." *Automation in construction 9*, 2 (2000): 197-215.
8. Marler R.T. and Arora J.S., “Survey of multi-objective optimization methods for engineering,” *Structural Multidisciplinary Optimization 26* (2004), 369–395
9. Murata, T. and Ishibuchi, H., “MOGA: multi-objective genetic algorithms,” in *Evolutionary Computation, IEEE International Conferenc*e on (1995), Vol. 1, p. 289
10. Negroponte N., “Through a Humanism Through Machines,” *AD Architectural Design 9* (1969)
11. Peponis J., Wineman J., Bafna S., Rashid M., Kim S. H., “On the generation of linear representations of spatial configuration,” *Environment and Planning B: Planning and Design 25* (1998), 559-576
12. Turner A., Doxa M., O’Sullivan D., Penn A., “From isovists to visibility graphs: a methodology for the analysis of architectural space”, *Environment and Planning B: Planning and Design 28* (2001), 103-121

Evaluating Architectural Layouts with Neural Networks

Nicole Phelan, Daniel Davis, and Carl Anderson

WeWork
New York, USA
{nicole.phelan, daniel.davis, carl.anderson}@wework.com

ABSTRACT

Determining the mixture of spaces that go into a building (the building's programming) is a difficult decision. Despite decades of research into effective layouts, designers still primarily rely on rules of thumb to determine how to allocate space. In this paper, we describe a new method for predicting meeting room utilization using an artificial neural network trained on empirical data from 56 buildings. This method was able to predict meeting room usage (R^2 = 0.56, $P < 0.0001$), outperforming human designers. We argue that by training machine learning algorithms to recognize usage patterns in built architecture, the algorithm can help the designer make more informed programming decisions.

Author Keywords

Office design; building layouts; machine learning; neural network; building performance; meeting rooms.

ACM Classification Keywords

I.6.1 SIMULATION AND MODELING; I.2.6 CONNECTIONISM AND NEURAL NETS; I.6.3 APPLICATIONS.

1 INTRODUCTION

One of the most important decisions that an architect makes is determining a building's programming. During this process, a designer will define the number of spaces to include within the floor-plate and specify their size, type, and function. By determining the mixture of spaces in a building, the architect sets up most of the logic for how the building will operate. This decision is especially important for office buildings, where there is often a financial incentive to use space effectively and a performance incentive to provide employees with the right amenities, which pressures the designers to find a programming mix that benefits both the employees and the business.

At WeWork, we are constantly considering how best to program our buildings. To date, like most architects, we have programmed our buildings mostly using rules of thumb that have been established through years of practice. But recently, we begun to consider whether algorithms can help us make more informed choices about the mixture of spaces we include in our buildings.

In this paper, we outline a new technique for evaluating programming decisions. In particular, we focus on decisions around the allocation of meeting spaces in office buildings. Using a neural network trained on data gleaned from 690 meeting rooms in 56 office buildings, we demonstrate a method for predicting the utilization of meeting rooms prior to construction. We argue that this technique could be expanded to other aspects of office layout, and perhaps other architectural archetypes, which lays the foundation for machine learning to be used in the evaluation of architecture, potentially allowing us to predict the performance of buildings based on the prior performance of constructed designs.

2 ALLOCATING MEETING ROOMS AT WEWORK

WeWork is a company that provides shared workspace, community, and services for entrepreneurs, freelancers, and businesses. As of December 2016, WeWork has over one hundred offices in 10 countries. Each location has a unique mixture of spaces — private offices, meeting rooms, lounges, phone booths, and other amenities — that are customized for the local market (Figure 1).

Figure 1. Two meeting rooms at WeWork City Hall, New York. The meeting rooms are amenities that WeWork members can reserve.

To program a new location, the designers at WeWork need to determine the right mixture of spaces to build. As they create the plans for a new location, they need to make decisions about how many meeting rooms to create, how many private offices to put on the floor, how many phone booths, etc. The meeting spaces are always a point of doubt. At WeWork, the meeting spaces are special rooms that members can book by the hour and use as a place to come together, to meet, to talk, to pitch potential clients, to hold interviews, to conduct lunch and learns, and to hash out the

details of their next big idea during a brainstorming session. Given the importance of these meetings, WeWork members expect to be able book meeting spaces when needed. If there are too few meeting rooms in a location, members become frustrated that they are constantly booked. On the other hand, if there are too many meeting spaces, then the rooms sit empty and take up space that would have been better allocated to some other function.

Designing meeting spaces isn't a unique problem. A 2012 study by the EIA suggests that there are around 3 million office buildings in the United States [2]. In constructing each of these buildings, the designers have deliberated over how many meeting rooms to build. Given that this decision has already happened 3 million times in the United States, and given that it is a critical decision for effective office buildings, you might expect that there would be standards to guide designers, similar to how there are standards for other important aspects of an office's layout, such as egress standards for life safety. However, no such standards exist. There are surveys of existing buildings done by various real estate groups and furniture manufacturers, but as one such survey by Knoll notes, these surveys are not necessarily effective because there are "many variations of individual, group and social spaces across organizations" [8]. Without any clear standards, designers are left to rely upon rules of thumb or intuition to layout meeting rooms, which often results in buildings with too few or too many rooms.

At WeWork, our designers have historically allocated meeting rooms based on a standard that takes into account the number of people occupying the building. The ratio of rooms per person was based on our experiences designing and operating previous buildings. A major limitation of this technique was that it assumed that all meeting rooms were equal and that everyone would use the meeting rooms in the same way. Analyzing our data, we noticed that people in smaller companies tended to favor different meeting rooms than people from larger companies (for example, large companies are more likely to use large meeting rooms). These nuances weren't captured in our existing standards so we sought to improve our standards to better account for the differences between people inhabiting our buildings and the variation between meeting rooms (both in terms of size and available facilities). Ultimately, we wanted to predict how our meeting rooms would be used before we commenced construction.

3 PREDICTING OFFICE BEHAVIOR

There is a long history of architects using algorithms to help predict the performance of rooms in office buildings. During the 1970s, researchers in Cambridge's Centre for Land Use and Built Form Studies (LUBFS) were using algorithms to calculate walking distances between rooms, which effectively gave each room a walkability score that was then used to optimize the floor plans to reduce walking times (an important consideration when documents had to be physically exchanged rather than emailed) [6]. Around the same time, at The Bartlett in the University College London, early work in the field of space syntax attempted to evaluate urban layouts based on visibility, choice, depth, and other mathematical factors that could be derived from a street network [4]. This work has been subsequently applied to the design of offices to evaluate plans based on qualities such as connectivity and privacy [9, 10, 13]. More recently, there has been a variety of work that attempts to predict the performance of office spaces based upon environmental simulations of architectural phenomena such as lighting, acoustics, and the thermal environment [3].

Our work differs from previous studies in three important ways:

1. Our research focuses exclusively on meeting rooms and does not attempt to develop a tool that evaluates all rooms and all layouts. Our decision to focus on meeting rooms was driven primarily by the business case at WeWork.
2. Our research evaluates rooms based on their programming rather than their layout. In other words, we attempt to predict the success of a meeting room based on its capacity and functionality rather than its position on a floor plan. This will be explained in more detail throughout the paper, but in essence we found that programming was a major factor in determining a meeting room's success.
3. Our research uses machine learning, trained using empirical usage data from 690 rooms in 56 locations. While it is fairly common to identify underutilized rooms using room usage data from individual buildings, it is difficult to apply these findings more generally since the data only pertains to one building. WeWork is in the fairly unique position of designing and managing a number of offices, which means we have data from hundreds of meeting rooms going back at least three years. Given the size of our dataset, we are able to use techniques like machine learning to identify overall patterns in our dataset – techniques that wouldn't be statistically robust on smaller datasets. As we have described in a previous paper, our usage of machine learning is highly original in the context of architectural practice [1].

4 PREDICTING MEETING ROOM USAGE AT WEWORK

Our objective was to predict conference room utilization using data. Since we wanted to make these predictions prior to constructing a new location, we limited ourselves to information that would be accessible prior to construction (the capacity of meeting rooms, the capacity of private offices, the equipment available in meeting rooms) and excluded information that could only be gleaned once a project was completed (the types of companies using the

space, the cultural norms that formed in the building, etc.). Using the construction information as an input variable, we attempted to predict the utilization of meeting rooms, which was measured as the percentage of hours they were occupied (the output variable).

4.1 Data Collection and Preparation

Input Variables

At WeWork, information about the layout of buildings is housed in an Amazon Redshift database. Using the R programming language, we downloaded the data and preprocessed it into a set of inputs. For each location we derived two datasets:

1. A list of meeting rooms, which included their capacity (number of seats) and equipment (whether they had a whiteboard or AV equipment). To remain consistent with internal design tools, the meeting rooms were then grouped into one of four categories based on their size and amenities. These groups were:
    - Large AV Room (capacity ≥ 10 with AV equipment)
    - Medium Rooms (capacity between 4 and 10 with AV)
    - Small AV Rooms (capacity ≤ 4 with AV equipment)
    - Small No AV Rooms (capacity ≤ 4 with no AV equipment).
2. A list of occupied private offices within a building, which included the capacity of each office (number of seats). To remain consistent with internal design tools, the capacity of each office was bucketed into the following groups: 1, 2, 3, 4–5, 6–7, 8–9, 10–11, 12–13, 14–15, 16–24, 25–29, 30–59, and 60 or greater.

With this data, we knew the number of meeting rooms in a building (including the capacity and type of equipment) and the number of people using the building (including the capacity of the private offices they were renting).

Output Variables

Members at WeWork reserve meeting rooms either through the WeWork website or using the WeWork app. Each room costs a certain number of WeWork credits per hour, which are allocated to companies every month based on the size of their office. Additional credits are also available for purchase. The number of credits required to reserve a conference room varies by both room type (with larger rooms requiring additional credits) and time of day (10 A.M. through 4 P.M. are considered peak hours and require an additional credit to reserve). Based on previous internal studies, we know that the reservation data is an accurate proxy for how rooms are actually utilized at WeWork since members are effectively paying to book a room with their credits and therefore have an incentive to show up for their meetings (in other environments where people do not use credits, a large number of no-shows would make this type of analysis ineffective).

A meeting room's utilization was measured as the percentage of hours it was occupied during peak hours (10 A.M. to 4 P.M. on Tuesday through Thursday) over the past six months. Reservations booked on Mondays and Fridays were excluded due to low usage in certain regions on those days. We excluded any locations that were established less than one year prior to the study start date since new buildings take a few months to settle, which left us with 690 meeting rooms in 56 locations. To match the categorization of meeting rooms in the input variables, for every building we calculated the mean utilization of rooms in each category (Large AV, Medium, Small AV, Small No AV).

4.2 Model Training

Given our input variables (meeting rooms and offices), we wanted to predict our output variables (peak utilization). We experimented with a number of techniques, including linear regression and support vector machines, but settled on using a neural network since it proved more accurate on this data set.

How Neural Networks work

Psychologist Frank Rosenblatt first developed the Artificial Neural Network in 1958 [12]. His version was called Perceptron and was designed to loosely mimic the way the human brain processed visual data. Today, artificial neural networks are used to understand complex relationships in a wide variety of applications.

An artificial neural network is organized into layers of nodes (circles in Figure 2) connected by weights (lines). Figure 2 contains one configuration of a neural network. The number of nodes in layer 2, as well as the number of internal layers, are parameters of the neural network that can be adjusted. Over time, these layers of nodes can learn to identify relationships using a training process that involves feeding the network input and output data (this is often called supervised machine learning).

The output is calculated by taking the input variables and multiplying them by the weight (lines connecting each input variable to each node in the second layer, see Figure 3). The initial weights of the model are randomly selected. The product of each input variable and weight are summed at each node in the second layer along with the weight of the bias layer (yellow). This value is then passed through a sigmoid function that transforms and constrains the value to be in range 0–1. The value computed at each node in the second layer is then used as the input value for the following layer. The same computation is computed between the second and third layer of nodes. The third layer (in the configuration shown in Figure 2) is the output layer that is the prediction of the model.

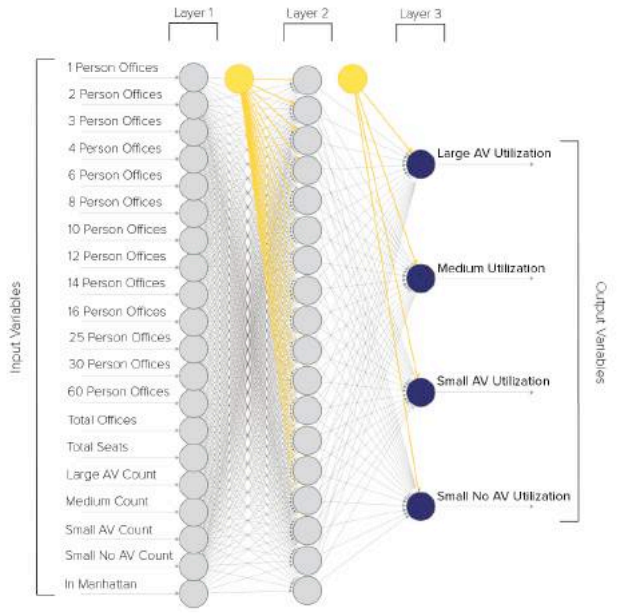

Figure 2. Diagram of artificial neural network trained to predict meeting room usage. Input variables on the left contain information about the office's floor plan. These inputs are fed through the network to generate predictions of utilization, which is shown to the right.

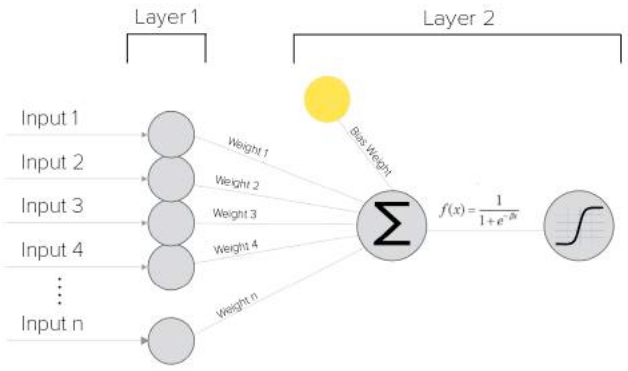

Figure 3. The calculation of a single node in the second layer of a neural network. The input variables are multiplied by their respective weights and summed along with the bias layer weight. This result is then passed through a sigmoid function.

The prediction is then compared the actual value and the error is computed. The neural network uses backward propagation to update the weights based on this error [5]. This process is repeated with the training data until the error falls within an acceptable range. The final product of the training process is a set of weights that can be used to predict the output variable.

Training

The R package *neuralnet* was used to train the neural network [7]. This package contains a function (*neuralnet*) that performs the training described above. This function is fed: a formula, normalized input data, the neural network configuration, an error threshold, and the name of the backward propagation type as parameters. The formula defines the input and output variables from the dataset that is input to the function. The input variables in the dataset were all normalized on a scale of 0 to 1 using the *scale* function in R. This ensures that all input variables are on the same scale so that errors are not dominated by variables with higher scales. The threshold was set to .02 and *rprop+* was used as the backward propagation algorithm.

In order to determine the optimal node configuration, a looping function was created to test multiple variations of the network configuration. This function also performed k-fold cross validation. K-fold cross validation was used to evaluate the ability of the model to generalize to new locations. In this process, the 56 locations were split (80/20) into 66 training locations and 17 testing locations. The six months of training data associated with the 66 training locations was used to train the neural network (feeding the algorithm both the input and output variables). Using the weights derived from the training of the neural network, a prediction was made for the utilization of the meeting rooms for each of the 17 testing locations for the six months of the study. These predictions were then compared to the actual meeting room utilization and the mean squared error (MSE) of the algorithms performance on the testing data was computed and recorded. This process was repeated 20 times for each network configuration, randomly selected training and testing locations each time. The output of this function is a matrix of 20 different errors (one MSE for each training/testing split) for 20 different network configurations. The distribution of errors was evaluated and the configuration with the lowest mean error and variance was selected (Figure 4).

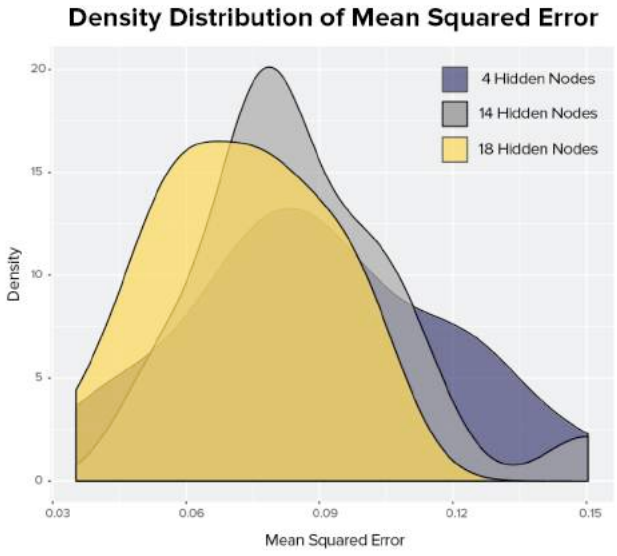

Figure 4. The density distribution for three of the network configurations across the 20 training/testing combinations.

This process was repeated many times testing different variations and combinations of input variables against the accuracy of the model.

4.3 Model Predictions

To test the accuracy of the predictions on real projects, we exported the neural network model to Excel, which was then fed new input data exported directly from Revit. This Excel model would then calculate a predicted utilization of each of the four meeting room types using the finalized weights of the neural network.

In our initial tests, the model performed well when making large changes, but the results were sometimes nonsensical when making small, incremental changes to the floor plan. For example, if one additional medium room was added to a particular floor plan, the utilization of the large AV meeting rooms might increase. This is counterintuitive as adding additional room to a building should result in a redistribution of reservations across more rooms and a lower utilization of other rooms in the building. These unexpected results varied from floor plan to floor plan. Due to the "black box" nature of a neural network, the root of these unexpected results could not be identified.

In order to mitigate these effects, the prediction of the neural network was averaged with the prediction of two additional models. This technique is known as ensemble modeling and is an established method of predictive modeling [11]. The first was a simple average by room type across the meeting rooms in the training dataset. The second was a regression tree (Figure 5). The R package *rpart* was used to create one regression tree for each of the four meeting room types. The result of this algorithm is a series of decision nodes that partition the data to one of various leaf nodes. Each leaf node is related to a prediction.

4.4 Results

The aim of this study was to determine a method to predict meeting room usage prior to building construction. The results of this application of machine learning was a model that could predict 56% of the variation (p-value < .0001) in meeting room usage of different meeting room types when given information about the building (Figure 6).

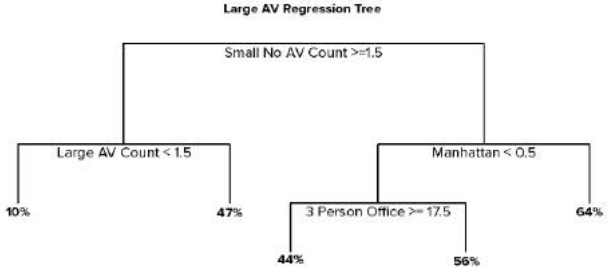

Figure 5. Branches of the regression tree that was combined with the neural network to form an ensemble model, which proved more accurate than the neural network alone.

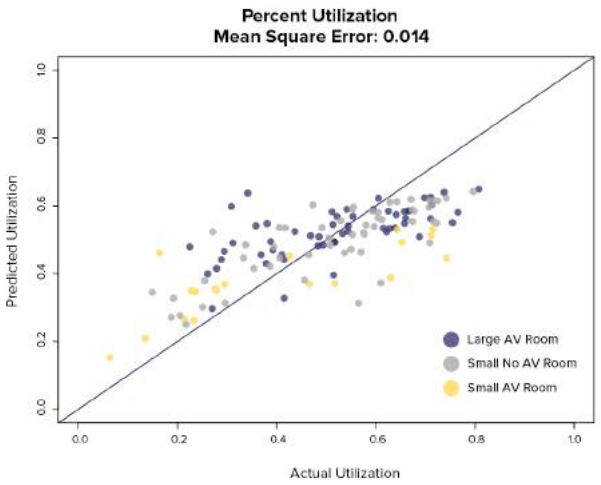

Figure 6. The utilization of the meeting room (x) compared to the prediction (y). If the predictions were totally accurate, the dots would fall on the diagonal line. Although there are a few inaccuracies, for the majority of the rooms the algorithm is fairly accurate and produces better results than a human designer.

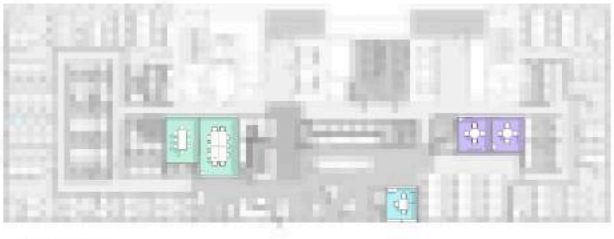

Figure 7. Predictions from the neural network overlaid on a floor plan in Revit. Rooms that are predicted to be underutilized are shown in purple and rooms predicted to be at the right utilization are shown in green. Based on this information the designer can make adjustments to the plan, possibly removing an underutilized meeting room, and see how this affects the predictions.

The most accurate configuration of the neural network consisted of one hidden layer with 18 nodes. The prediction of the neural network was averaged with the mean utilization of each room type and the prediction of the regression tree. This configuration resulted in an average MSE of 0.014. The accuracy of this model was determined using k-fold cross validation to ensure that the model was not overfitted to training data. Given a target utilization of 55%, the MSE of the predictions made by designers across the WeWork portfolio is 0.065, which means the neural network significantly (p-value < .0001, df = 367) outperforms the human designers at this task.

5 DISCUSSION

For WeWork, this research has significantly affected how we program our buildings. Using the neural network in this paper, we have considerably better insight into how frequently people will use our meeting rooms (Figure 7). This means that we can make smarter, more informed decisions about our programming, which has lead to a

better member experience (by increasing the number of meeting rooms in buildings with high predicted utilization) and more efficient layouts (by replacing meeting rooms with low predicted utilization with more popular amenities).

Beyond WeWork, this research has meaningful implications for the architectural profession. We know from past experience that architects often struggle to anticipate how buildings will be used, which has led to decades of research focused on trying to predict inhabitant behavior. This is a complicated subject because there are obviously a range of factors that influence an individual's decision to use something like a meeting room, factors that range from availability, to privacy and prior experiences. Our research suggests that we might be able to sidestep many of these complications by gathering sufficient data on how current buildings perform. With a large enough dataset, it might be possible for a neural network to learn about where people want to sit, which buildings are easiest to navigate, perhaps even which layouts are most energy efficient.

Another way to conceptualize this research is as an enhanced form of post-occupancy evaluation. Rather than evaluating one building at a time, the neural network is studying multiple buildings (in our case hundreds of rooms), identifying common patterns, and using these patterns to evaluate future plans. As more building are documented in a digital format with technologies like BIM, and as more sensors are put on buildings, this type of evaluation is going to become increasingly viable. Our research stands as one example of how this may function in the future.

Our optimism about the future of machine learning in the context of architectural layouts is tempered by our experiences with this project. In particular, we see three primary limitations to the further application of machine learning in the evaluation of architectural layouts:

1. **The amount of data that is required to train an algorithm.** Machine learning generally requires large data sets and a clear metric for success. Neither of these are readily available to many firms or to different components of design. In the case of meeting rooms, WeWork is in a fairly unique position to capture this data across the fleet of meeting rooms in our portfolio.
2. **The potential gaps in training situations.** The neural network is trained to recognize patterns. So, if the network is given a layout that differs substantially from past designs, it might struggle to accurately predict the performance of the new design. Even with the large amount of data we have available within WeWork, it is possible that major changes to our design standards or novel combinations in a building layout may not be within the scope of what the neural network has learned. In order to understand the limitations of the neural network, a Chi-Squared test can be used to compare the input variables (before normalization) the model is attempting to predict to those used to train the neural network. We also implemented warnings to notify designers when they were outside the normal range of previous designs.
3. **The black box nature of the results.** It is difficult to understand precisely what the neural network has learned through its training. When the model predicts low meeting room utilization, the designer has no insight into why that utilization is low or exactly what should be changed to improve the predicted utilization. This also means that there is no way to verify that it has learned something sensical and generalizable. This risk is reduced through thorough testing and the use of k-fold cross validation.

With these limitations in mind, we anticipate that our research is applicable in other architectural settings where there is a large sample set, relatively consistent design patterns, and a clear metric for success. In particular, this research could be immediately applied to hospitals and retail environments.

6 CONCLUSION

In this paper, we've demonstrated how we trained a neural network to predict the usage of meeting rooms at WeWork. We've shown that this network is generally accurate (R^2 = 0.56, $P < 0.0001$, df = 335) and capable of outperforming human designers at anticipating how people will use the meeting rooms. While there are clear benefits for WeWork in terms of a better member experience and more efficient layouts, the real contribution of this research is to suggest that architects can evaluate some aspects of their project's performance by using machine learning to evaluate the performance of past projects. However, we note that any further research is going to be hindered by access to the large amounts of data necessary to train the algorithms, the applicability of the trained algorithm to novel situations, and the black box nature of the results. Assuming these limitations can be overcome, we imagine this technique could be applied to other situations where the architect needs to anticipate how a building will perform, such as energy performance, navigability, and preferences for other types of rooms.

ACKNOWLEDGEMENTS

This research builds upon work done by a number of different teams at WeWork. We'd like to thank our friends and colleagues in the Data, BIM, Research, and Product teams for all the work they've done to make this analysis possible.

REFERENCES

1. Davis, Daniel. Evaluating Buildings with Computation and Machine Learning. *ACADIA 2016*: 116-123.
2. EIA. 2012 CBECS Preliminary Results. https://www.eia.gov/consumption/commercial/reports/2012/preliminary/. As of 7 December 2016.
3. Hensen, Jan, and Roberto Lamberts, eds. *Building Performance Simulation for Design and Operation* (2011). New York: Spoon Press.
4. Hillier, Bill, Adrian Leaman, Paul Stansall, and Michael Bedford. Space Syntax. *Environment and Planning B: Planning and Design* 3, 2 (1976.): 147–85.
5. Hussoun, Mohamad. *The Fundamentals of Neural Networks* (1995). Boston: MIT Press.
6. Keller, Sean. Fenland Tech: Architectural Science in Postwar Cambridge. *Grey Room* 23 (April 2006): 40–65.
7. NeuralNet. https://cran.r-project.org/web/packages/neuralnet/neuralnet.pdf. As of 7 December 2016.
8. O'Neil, Michael and Tracy Wymer. The Metrics of Distributed Work: Financial and performance benefits of an emerging work model. https://www.knoll.com/media/466/356/WP_DistributedWork.pdf. As of 7 December 2016.
9. Peponis, John, and Paul Stansall. "Spatial: An Understanding of the Social Function of Space Is Vital to Insights. *Designers' Journal*, 52–56 (1987).
10. Peponis, John, Sonit Bafna, Ritu Bajaj, Joyce Bromberg, Christine Congdon, Mahbub Rashid, Susan Warmels, Yan Zhang, and Craig Zimring. Designing Space to Support Knowledge Work. *Environment and Behavior* 39, 6 (2007): 815–40.
11. Polikar, Robi. Ensemble Based Systems in Decision Making. *IEEE Circuits and Systems Magazine* 6 (2006): 21-45. http://ieeexplore.ieee.org/document/1688199/
12. Rosenblatt, Frank. Two theorems of statistical separability in the perceptron. United States Department of Commerce, 1958.
13. Wineman, Jean, Yongha Hwang, Felichism Kabo, Jason Owen-Smith, and Gerald F. Davis. Spatial Layout, Social Structure, And Innovation in Organizations. *Environment and Planning B: Planning and Design* 41, 6 (2014): 1100–1112.

Robot-Aided Fabrication of Interwoven Reinforced Concrete Structures

Elif Erdine, Alexandros Kallegias, Angel Fernando Lara Moreira, Pradeep Devadass and Alican Sungur

Architectural Association (AA) School of Architecture
London, United Kingdom

{elif.erdine, alexandros.kallegias, Lara-Moreira}@aaschool.ac.uk

{pappurvsa, sunguralican}@gmail.com

ABSTRACT

This paper describes the outcomes of ongoing research, conducted at the Architectural Association (AA) Summer DLAB Visiting School 2016, to develop an innovative strategy for the construction of three-dimensionally interwoven concrete composite structures. Research methods include the employment of computational design and robotic fabrication techniques that incorporate geometry rationalization and material constraints. Through the analysis of traditional rod bending strategies, this research aims to develop a novel approach by the reduction of mechanical parts for controlling the desired output geometries. This goal is addressed by devising a robotic tool-path, developed in KUKA|prc with Python scripting, where fundamental material considerations, including tolerances and spring-back values, are integrated in the bending motion strategies through a systematic series of mathematical calculations in line with physical tests. Correlations between custom-formed steel reinforcement bars and Polypropylene form-work within the agency of a concrete composite structure are verified through the large-scale prototype. This research serves to test the evolving complexity of embedding parameters related to generative form-finding, geometrical rationalization, material constraints, and robotic toolpath planning within the computational environment and simulation tools, thereby enabling the capacity to implement simple mechanical tools and cost-effective fabrication methods.

Author Keywords

Robotic fabrication; Robotic rod-bending; Concrete composite; Geometry optimization; Polypropylene form-work; Concrete interwoven structure.

ACM Classification Keywords

D.1.5 OBJECT-ORIENTED PROGRAMMING; I.2.9 ROBOTICS (Manipulators); I.3.5 COMPUTATIONAL GEOMETRY AND OBJECT MODELING (Physically based modeling); I.6.5 MODEL DEVELOPMENT (Modeling methodologies); J.2 PHYSICAL SCIENCES AND ENGINEERING (Physics); J.5 ARTS AND HUMANITIES (Architecture) J.6 COMPUTER-AIDED ENGINEERING (Computer-aided manufacturing (CAM))

1 INTRODUCTION

The digital era in architecture has witnessed the production of a vast array of geometrical assemblies through computational form-finding methods in previous decades. With the developments in digital fabrication, the production and assembly of complex forms has been compromised by the constraints of selected fabrication techniques. In recent years, robotic fabrication processes implemented in architecture have begun to incorporate digital and physical paradigms in an unparalleled way due to the multi-axis freedom of an industrial robot arm, its speed, precision, and low tolerances [1]. The development of robotic fabrication processes in architecture within recent years has fuelled the emergence of complexity found in mass-customized assemblies, moving away from previous standardized / sheet-material component fabrication [2].

This paper describes the outcomes of ongoing research to develop an innovative strategy for the construction of three-dimensionally interwoven concrete composite structures. The investigations are conducted as part of the Architectural Association (AA) Summer DLAB Visiting School 2016. Research methods include the employment of computational design and robotic fabrication techniques that incorporate geometry rationalization and material constraints. Research objectives focus on the evaluation and interpretation of a traditional fabrication process, steel rod bending, towards its advancement within the domain of advanced computational and robotic methods. Through the analysis of rod bending strategies in traditional manufacturing industries that are well-documented and established, this research serves to test the evolving complexity of embedding parameters related to generative form-finding, geometrical rationalization, and material constraints within the computational environment and simulation tools, thereby enabling the capacity to implement simple mechanical tools and cost-effective fabrication methods.

SimAUD 2017 May 22-24 Toronto, Canada

In recent years, robotic rod bending workflows have been addressed and developed by research teams. A custom-made, robot-aided CNC bender that is controlled as an additional axis of the generic robotic system has been developed for the "Clouds of Venice" installation at the 2012 Venice Biennale in order to realize mass-customized, robotically bent steel rod elements [3]. Moreover, there is an ongoing research on the integration of robotic fabrication constraints within conceptual architectural design processes through custom-built algorithms [4]. This research aims to expand on the generic properties of a robotic manipulator, whereby attention is kept on the development of custom-made, versatile programming and simulation workflows without the necessity to develop custom-made hardware elements. Through the careful correlation of data pertaining to material properties, including tolerances and spring-back values of steel rods, with fabrication constraints related to robotic toolpath planning, this research presents a methodology for the integration of generative design tools, geometrical optimization, material opportunities and limitations, and fabrication constraints for the robotic bending of steel rods.

The one-to-one scale prototype presented in this research is a case study to test the methodology with the design and construction of a 3-dimensionally interwoven concrete composite structure. The design brief for the prototype entails the design and construction of a one-to-one scale pavilion made from reinforced concrete in a forest located in AA's Hooke Park premises in Dorset, United Kingdom, within a limited time frame, three weeks. There are 3 main constituents of the prototype to test the key research objectives: Steel reinforcement bars, Polypropylene form-work, and a fast setting concrete mix. The dimensions of the structure are 3 meters in width, 3 meters in length, and 2.4 meters in height.

2 COMPUTATIONAL METHODOLOGY

2.1 Computational Form-Finding

Initial computational form-finding techniques explore the generation of a network of interwoven elements via a bundling algorithm developed in Grasshopper. The algorithm enables the user to locally differentiate the amount of connectivity between elements in discrete parts of the global configuration, a condition that can enhance structural performance. The outcomes of this computational process have been organized as a catalogue of variations in order to understand properties of the different options in terms of relationship with context, structural, environmental and spatial qualities (Figure 1).

2.2 Tool and Jig Development

Simultaneously, an automated fabrication process is developed, where custom shaped steel reinforcement bars can be bent using a 6 axis robot (KUKA KR- 150), custom built bending jig made of steel plates, and pneumatic grippers (Figure 2). The bending jig system comprises 3 different bending discs, with radii of 50 mm., 100mm., 150 mm. Gripper, chosen as an appropriate end effector with V metallic channel for holding the rods in position, is made of two pneumatic cylinders separated by an optimal distance of 250mm. Shorter length of the tool can result in kinking the rod during the bending process, while longer length will reduce the length of the rod available for bending. Apart from the pneumatic grippers for the end effector, a stationary third gripper is placed on the bending jig to secure one end of the steel rod inside the jig, controlled through the independent IO of the robot.

In this setup, rod bending process puts forward a set of constraints which have direct feedback on the computational form-finding process. The utilization of 3 different arc radii has been targeted to achieve a smoother transition between 2 consecutive linear members, the absence of which could create extreme angle differentiation between linear members leading to fatigue on steel rods.

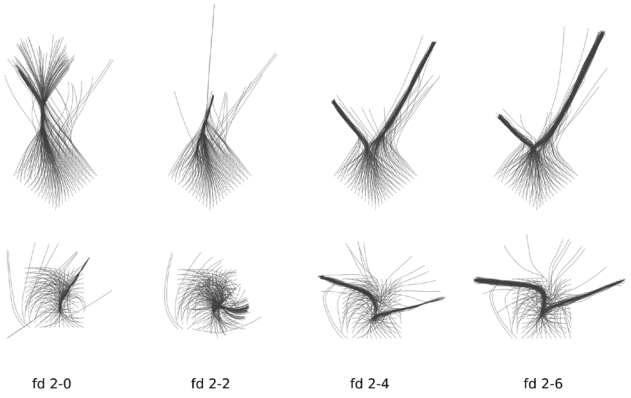

Figure 1. Computational form-finding through custom-built bundling algorithms.

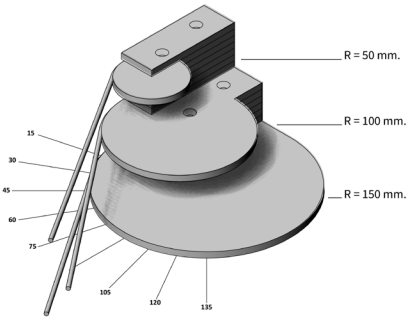

Figure 2. Robotic bending jig system.

2.3 Geometrical Optimization and Integration of Spring-Back

With the aim to establish an analytical relationship between initial form-finding, geometrical optimization, and subsequent manufacturing processes, two main methods have been developed in Grasshopper, the graphical algorithm editor embedded within the three-dimensional modelling software McNeel Rhinoceros. Both methods incorporate custom-built Python scripts that integrate scientific data from mathematical equations or physical experiments. Firstly, geometrical outcomes from initial bundling algorithm experiments, 3-dimensioanlly curved continuous paths, are

optimized via a custom-built Python script inside Grasshopper. With this method, each continuous path is initially divided into domains at specified intervals. The dimension of each interval is determined by taking into consideration the continuity of curvature in the optimized path in comparison to the initial path, steel rod sizes, and rod connection limitations that might occur on site during assembly process. Consequently, each continuous path is divided with an interval of 550 mm. in length, and a polyline model is created according to tangent vector information at each node of the intervals. At this stage, jig radii are assigned to every node according to the angular difference between consecutive beams. For nodes which have an angular difference smaller than 30 degrees, 50 mm. radius is assigned. For nodes which have an angular difference between 30 degrees and 60 degrees, 100 mm. radius is assigned. For nodes which have an angular difference greater than 60 degrees, 150 mm. radius is assigned. In this way, initial continuous paths are rebuilt into a series of lines and arcs with variable bending angles. Lastly, every member is extended by 100 mm. at each end point to provide sufficient overlap between consecutive members during site assembly, thereby creating members of 750 mm in length (Figure 3). The resulting geometry serves as steel reinforcement rods for the concrete structure in the future stages of design and fabrication. This geometrical information is then carried forward to the next pre-manufacturing stage where data pertaining to bending location, bending angle, and jig radius is recorded for each individual rod.

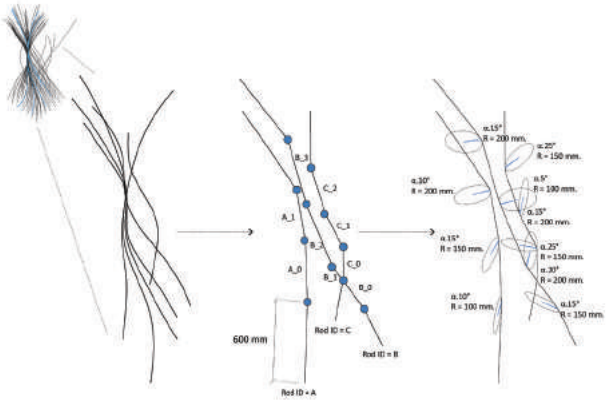

Figure 3. Geometrical optimization process.

The second method formulates a mathematical solution to address spring-back of steel rods in order to prevent undesired results during robotic bending process. Table 1 presents the input parameters for the mathematical equations that are going to be described in this section. Initially, physical experiments have been carried out to test spring back of steel rods with a fixed diameter, 8 mm., fixed length, 1500 mm., and different jig radii. These experiments have been performed manually with the use of a custom-built steel plate bending jig and a base steel plate to score the target and resultant angles. For each jig radius, physical bending tests have been conducted by implementing 4 different bending angles, 30 – 60 – 90 - 120 degrees respectively. These experiments have been carried forward repeatedly for each jig radius and bending angle, totaling 48 individual experiments. For each physical experiment, the jig radius, target bending angle, resultant angle after spring-back, and spring-back values have been documented. Simultaneously, the recorded spring-back values have been tested against a spring-back equation for rods with a circular section (Table 2) [5].

T_y *(Yield stress of the material – N/mm^2)*	200		
Q_s *(Angle of springback from Q_o)*	VAR		
Q_o *(Target angle)*	VAR		
R_o *(Radius of jig in mm)*	50	100	150
E *(Elastic(Young's) modulus – N/mm^2=MPa)*	210000		
d *(rod diameter - mm)*	8		
Coefficent	3.4 (Equation I)	-7.86 (Equation II)	

Table 1. Input parameters for mathematical spring-back equations.

Spring-back equation I	$Q_s = Q_0*[(3.4*T_y*R_0)/(E*d)]$

Table 2. Spring-back equation I.

A series of deviations ranging from 5 degrees to 65 degrees have been observed between the results of physical spring-back tests and the results of spring-back equation I. It has been observed that this undesired result can be related to the material properties of the specific steel rods that have been tested; a slight variation in the rod's elastic modulus and yield stress values can lead to deviations in the equation results. Therefore, the initial spring-back experimentation has resulted with the necessity to devise a refined spring-back equation that can produce results with a highly reduced angular tolerance. As a result, a regression analysis method has been opted to mathematically compute the relationship between the results of the physical spring-back experiments [6]. Comprehensive documentation of physical experiments performed earlier has served as an advantage to implement regression analysis. This analysis sets a new equation with different coefficients for each input to match physical test results, searching for a coefficient that can best estimate the relation between inputs. Regression analysis has been performed in Microsoft Excel where test results of physical

spring-back experiments have been collected on a table to find the best fit ratio for each input to achieve the target angle. After iterative analysis a precise equation has been established (Table 3), and with the use of this equation (spring-back equation II) the angular deviation has decreased below 5 degrees. Table 4 represents a selected series of spring-back results from physical experiments, spring-back equation I, and spring-back equation II.

Spring-back equation II	Qs = [-7.86 + (Q0*0.34*Ty) +(R0*0.12)] / (E*d)

Table 3. Spring-back equation II.

Rod	Target Bending Angle (°)	Physical Bending Result (°)	Physical Spring-back Test (°)	Spring-back (Equation I) (°)	Spring-back (Equation II) (°)	Jig Rad.(mm.)
B_0	30	15	15	1.21	14.34	100
B_1	30	18,4	11.6	1.21	14.34	100
B_2	30	19.1	10.9	1.21	14.34	100
B_3	30	20.2	9.8	1.21	14.34	100
B_4	30	10.2	19.8	0.61	8.34	50
B_5	30	12.2	17.8	0.61	8.34	50
B_6	60	34.2	25.8	3.64	30.54	150
B_7	66.5	37.8	28.7	4.04	32.75	150
B_8	60	38.1	21.9	2.43	24.54	100
B_9	57	39.6	17.4	2.31	23.52	100
B_10	90	49.7	40.3	5.46	40.74	150
B_11	60	32.6	27.4	1.21	18.54	50
B_12	120	65.1	54.9	7.29	50.94	150
B_13	120	66.2	53.8	7.29	50.94	150
B_14	120	66.8	53.2	7.29	50.94	150
B_15	120	68.4	51.6	7.29	50.94	150
B_16	150	75.8	74.2	9.11	61.14	150
B_17	90	65.7	24.3	3.64	34.74	100
B_18	90	65.7	24.3	1.82	28.74	50
B_19	120	81.3	38.7	4.86	44.94	100
B_20	130	88.8	41.2	5.26	48.34	100
B_21	120	88.8	31.2	2.43	38.94	50

Table 4. Comparative analysis of physical experiments, spring-back equation I, and spring-back equation II.

Spring-back equation II is then implemented in a Python script inside Grasshopper so as to convert target bending angle into actual bending angle that integrates spring-back values. As a result, all rods are bent 15 to 60 degrees more to achieve target bending angles. For example, in order to reach 90 degrees bending with a 150 mm. jig, the rod needs to be bent 130.74 degrees to compensate for the 40.74 degree spring-back value (Table 4 – member B_10). This process is finalized by collecting the data relating to rod location in the global geometry, bending location, bending angle, and grip point of robotic arm for each rod, concluding the preparation of rods for robotic bending process (Figure 4).

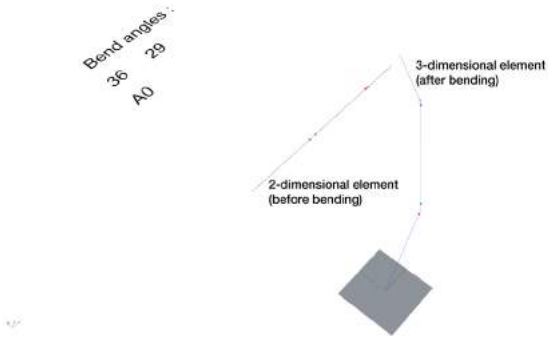

Figure 4. Data collated for each rod member.

3 TOOLPATH DEVELOPMENT FOR ROBOTIC BENDING

3.1 Robotic Toolpath and Programming Development

In the next stage, the custom-built script developed with Python in Grasshopper is incorporated with KUKA|prc, parametric robotic control add-on of Grasshopper [7]. In this way, the information generated for rod-bending, including tolerances and spring-back values, are directly transferred to robotic bending motion. For robotic toolpath planning, steel rod elements of 750 mm. length and 8 mm. diameter have been coupled in pairs, achieving an overall rod size of 1500 mm. This size has been designated as an optimal length in order to avoid collisions during robotic simulation, as both ends of the steel rods are required to be bent. During robotic toolpath planning process, two sets of data have been key parameters, bending angle and jig radius for each end of the steel rod respectively.

Recent developments in architectural programming interfaces for computational design and fabrication, especially in McNeel Rhinoceros and Grasshopper, present users to code and observe real-time results as the robotic simulation is developed. KUKA|prc add-on, developed by Robots in Architecture [8], provides an inverse kinematic (IK) solution within the Rhinoceros-Grasshopper interface, allowing for the prediction and inspection of the problems that can be encountered during robotic simulation. As there has been no ready-made robotic toolpath programming solution for the required task of robotic rod-bending, KUKA|prc's built-in command types for Cartesian Coordinate Programming, namely LIN (Linear Movement), PTP (Point to Point Movement), CIR (Circular Movement), have been employed. The basic input required for these commands is a plane comprised of XYZABC information, XYZ defining the location and ABC defining the orientation of the end-effector. This information can be easily extracted

from planes in Grasshopper, where all geometries and data need to be referenced to the robot base. This process has laid the foundation for the development of an in-house robotic toolpath generation method.

During the development of the robotic toolpath, movement from the initial robot position, defined by steel rod before bending, to the final position, defined by steel rod after bending, has informed the motion of the robot's TCP (Tool Centre Point). This motion is guided by three planes: starting plane, auxiliary plane, and end plane for the bending movement through a CIR (KUKA circular movement command) for smoother bending process. Safe retracts and WAIT commands have been included in the algorithm to avoid any collisions and allow sufficient response time of the pneumatic gripper.

The employment of KUKA|prc's IK solver has presented a challenge due to the fact that predicted robotic simulation errors cannot be automatically rectified. Therefore, industrial software packages—like Mastercam / Robotmater—have been taken into consideration. These packages offer highly competent milling strategies and have the capability to tackle the problem stated; however, they lack custom toolpath generation for custom-made end-effectors, and cause limitations in the transfer, handling, development, and manipulation of irregular geometry. Nevertheless, Robotmaster provides a very powerful optimization interface which not only detects the robotic simulation errors, but also provides an intelligent solution to the problem. Hence, the potential of combining the advanced techniques of Robotmaster for optimising robotic simulations and the power of custom-coding in Grasshopper have been harvested during robotic toolpath planning. A process has been developed in multiple stages: Firstly, on the Grasshopper platform, the custom toolpaths that include handling and manipulation of data have been executed. Then, a post processor has been written on the same platform to generate XYZIJK of the toolpath in Automatically Programmed Tool (APT) code format. In this format, XYZ defines the Cartesian coordinates of Tool Centre Point (TCP) and IJK defines the vector for tool orientation. Thereafter, the code is imported into Robotmaster using the Robotmaster Import Utility Tool in order to perform robotic toolpath optimization. Although this method provides a two-stage process using two different software platforms, it offers a robust and automated output. In this way, more than 80 steel rods, each bearing a unique bending angle and radius, have been robotically bent within a short period of time thanks to the speed, precision, and low tolerances of the custom-made robotic bending protocols (Figure 5).

4 FABRICATION AND ASSEMBLY

The outcome of this phase, a series of interwoven 3-dimensional components made of lines and arcs, is given structural thickness via a built-in meshing algorithm inside Grasshopper that generates a high-resolution mesh around the components. This mesh is then optimized and

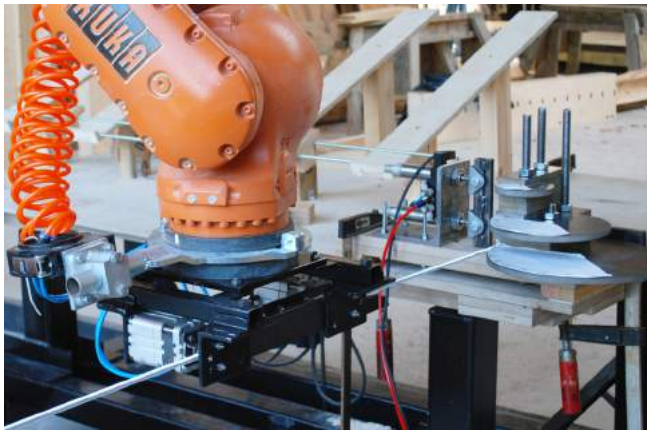

Figure 5. Robotic rod bending process.

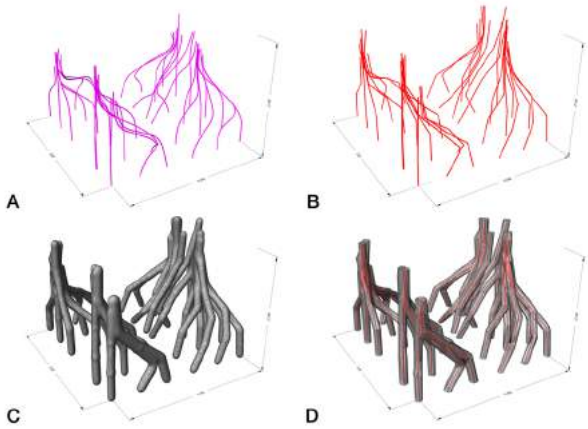

Figure 6. Development of computational model: (A) continuous paths, (B) lines and arcs, (C) high-resolution mesh, (D) triangulated mesh.

triangulated to create developable surfaces that can be unrolled with accuracy in later stages of fabrication (Figure 6). The diameter of each branch in the structure ranges between 100 mm. and 250 mm. according to its location in the global configuration. The global configuration comprises nodes from which multiple linear and arc-formed elements stem out; therefore, it is crucial to address the complexity of the global geometry in relation to appropriate form-work methods.

Methods of designing and fabricating form-work systems for complex reinforced concrete constructions have been researched and documented in the architecture and structural engineering fields. One method, fabric casting, makes use of flexible fabric form-work which allows for the design and production of artefacts that have the potential to yield morphologically interesting and materially efficient assemblies [9]. The process involves the creation of two-dimensional patterns that are stitched together in order to generate a three-dimensional formwork that is then used for concrete casting. This method has been tested previously during AA Summer DLAB 2014, whereby fabric form-work

and earth scaffolding were employed in coordination in order to design and fabricate a reinforced concrete shell structure [10]. During the course of this previous research, the geometric deviation between the digital simulation and the architectural output, coupled with the requirement to provide a stiff scaffolding system led the current research to devise an alternative form-work system that has the potential to construct a complex geometrical configuration, does not need additional scaffolding elements, and can be removed in a short period of time.

The triangulated mesh generated with the geometrical input of steel reinforcement rods acts as the form-work for the structure. At this stage, the fabrication process for the one-to-one scale prototype presents itself with different challenges in regards to the appropriation of complex geometries for digital fabrication methods and the material behaviour of concrete during the pouring process. The form-work necessitates the employment of a material rigid enough to compensate for hydrostatic pressure that acts laterally on the faces of the form-work. Additionally, it has been observed that the material needs to provide a smooth surface finish in order to guarantee an effortless de-moulding process. This set of constraints has driven the choice of form-work material to be Polypropylene sheets of 2440 mm. x 1200 mm. x 3mm.

As the final mesh geometry of the form-work is a developable surface that can be unfolded for a flat sheet fabrication process, the research at this phase has focused on an automated process for unfolding 3-dimensional triangulated mesh geometries. Inspired by traditional mountain and valley paper folding techniques, Pepakura, an origami based software used to translate complex geometries into foldable paper models, has been selected as the preferred software tool for mesh unfolding [11].Initial mesh optimization in Grasshopper has been used to re-triangulate and reduce the number of polygons in order to maintain part specific sizes related to the constraints of the Polypropylene sheet material.

Each branching component of the mesh structure is fed to Pepakura, where a strip based approximation method reinterprets the output mesh as regions or stripes by analysing the triangle's topological distance with respect to its new border. The unfolded piece can be further segmented while maintaining its border cutline. A series of outward facing flaps, which aid in the manufacturing process and ensure overall connectivity between the various pieces, are added. The result is a series of foldable stripes that are unrolled flat on sheet material and are thus suited for CNC milling. A nesting algorithm, Rhino Nest, reduces waste of sheet material and optimizes the scoring patterns of mountain and valley folds [12].

The fabricated sheets are folded back and tied together with zip ties to generate the 3-dimensional components of the interwoven structure. Each component is further wrapped with cloth-backed adhesive tape in order to enhance the structure's performance against hydrostatic pressure during the pouring process. Naturally occurring gaps between joints, a condition due to polypropylene's material thickness, serve a two-fold purpose: Firstly, gaps provide the flexibility required by the overall structure to find its final resting position once the lateral forces of expanding concrete are in effect. Secondly, they offer much needed ventilation in an otherwise airtight form-work, accelerating concrete curing times. As the form-work mesh has been generated directly from the geometry of the steel bent rods, the self-supporting form-work has been guided into position with ease by the robotically bent steel rod reinforcement bars, which has remained at the geometrical centre of the form-work (Figure 7).

During the final stage of assembly, each module has been placed on site, guided by the foundation area that bears a depth of 300 mm (Figure 8). The self-supporting form-work has kept additional scaffolding to a minimum, only requiring temporary supports where needed during concrete pouring process. Furthermore, the elimination of stationary scaffolding has granted an accessible work area that allows for a continuous concrete pouring process, lasting 7 hours in total. Special attention has been paid to the sequence of pouring. The complexity of the geometry has required each branch to be filled simultaneously from ground upwards,

Figure 7. Steel rod reinforcement bars placed inside Polypropylene form-work.

Figure 8. Polypropylene form-work with steel reinforcement bars on site.

contrary to traditional individual casting methods. Coupled with the triangulation of the form-work geometry, the sequence of the pouring process has helped to balance the hydrostatic pressure throughout the structure, thereby preventing ruptures and minimizing overall displacement.

A special mix of aqueous fast setting concrete mixed with fiberglass additives has been poured in one step to homogenize the setting stage, allowing the concrete mix to be cast and cured within several hours. Due to the surface finish of Polypropylene form-work, it has been possible to complete the de-moulding process of the structure in a short period of time (Figure 9). Additionally, the use of Polypropylene has facilitated a reflective surface quality for the prototype (Figure 10). The final configuration is characterized by a continuous network of concrete branches that support each other while creating an amorphous spatial enclosure.

Figure 9. Close-up of one-to-one scale prototype, displaying reflective surface finish.

DISCUSSION

Throughout the design, fabrication, and assembly processes, the strong associations and interfacing between different design, analysis, and simulation protocols have been essential in correlating a multitude of parameters and design drivers. The comparison between the digital simulation of the architectural output and the final output, the prototype itself, provides useful information to be considered and embedded in the future digital simulations. A key challenge during the fabrication process was to have precise control over the sequence of concrete pouring in order to maintain balance of the form-work as well as to resist hydrostatic pressure. This challenge was met by filling each branch simultaneously as to retain a similar height range of fluid concrete in all branches. Nevertheless, future work can incorporate CFD (Computational Fluid Dynamics) simulation of concrete in the digital environment on various selected global configurations in order to test the efficiency of concrete flow. With this method, CFD simulation of

Figure 10. Global configuration of one-to-one scale prototype.

concrete flow can serve as a key driver during design development.

In current research processes, the role of robotic fabrication techniques is moving away from a direct design-to-production approach towards the integration of robots within the design process itself. While the employment of complex hard-ware systems and sensors can be a useful method of enabling this integration, this research presents a methodology to develop custom-made, versatile programming and simulation workflows without the necessity to employ custom-made hardware elements. Hence, this research aims to expand on the generic properties of a robotic manipulator by testing the complexity of embedding parameters related to generative form-finding, geometrical rationalization, material constraints, and robotic toolpath planning within the computational environment and simulation tools, hence enabling the capacity to implement simple mechanical tools and cost-effective fabrication methods.

One of the key aims of this research is to illustrate the architectural possibilities of using concrete in a non-conventional way by creating strong associations between computational design methodologies and robotic fabrication processes. Nevertheless, it is argued that a similar methodology addressing the integration of material properties and robotic fabrication constraints in the early stages of design development can be developed for further material systems and robotic fabrication protocols. Through the utilization of material and fabrication parameters as design drivers from the conceptual design phase onwards, the high level of complexity inherent in design processes can be discovered to serve multiple aspects of performance.

5 ACKNOWLEDGEMENTS

The work presented is part of the research undertaken at Architectural Association (AA) Summer DLAB Visiting School 2016. We would like to thank our tutoring team and students for their great efforts:

- AA Visiting School Director: Dr. Christopher Pierce
- AA Summer DLAB Programme Heads: Dr. Elif Erdine, Alexandros Kallegias
- Tutors: Alexandros Kallegias, Dr. Elif Erdine, Angel Fernando Lara Moreira, Necdet Yagiz Ozkan, Suzan Ucmaklioglu.
- Research Collaborator: Alican Sungur.
- Robotics Collaborator: Pradeep Devadass.
- Students: Artemis Psaltoglou, Anna Rizou, Irini Sapka, Stelios Andreou, Alexandra Marantidou, Melike Culcuoglu, Deniz Ipek Ayasli, Isui Rodriguez, Roger Flores, Reese Lewis, Shang-Fang Yu, Anthony Ip, Mauricio Velarde, Kentaro Fujimoto, Josue Davila, DanielaOrellana, Erik Hoffmann, Zheng Luo, Jeffrey Novak, Veronica Ruiz, Justine Poulin.

REFERENCES

1. Menges, A. ‘Morphospaces of Robotic Fabrication’, in S. Brell-Çokcan, J. Braumann (eds.) *Rob|Arch 2012: Robotic Fabrication in Architecture, Art and Design*, Springer: Vienna (2013), 28 – 47.
2. McGee, W., Feringa, J. and Søndergaard, A. 'Processes for an Architecture of Volume: Robotic Hot-Wire Cutting', in S. Brell-Çokcan, J. Braumann (eds.) *Rob|Arch 2012: Robotic Fabrication in Architecture, Art and Design* (2013), 62-71.
3. Pigram, D. et.al. ‘Protocols, Pathways, and Production’, in S. Brell-Çokcan, J. Braumann (eds.) *Rob|Arch 2012: Robotic Fabrication in Architecture, Art and Design*, Springer: Vienna (2013), 143 – 147.
4. Pigram, D., McGee, W. ‘Formation Embedded Design: a Methodology for the Integration of Fabrication Constraints into Architectural Design’, in Joshua M. Taron (ed.) *Proc. ACADIA 2011: Integration through Computation*, Association for Computer Aided Design in Architecture, (2011), 122 – 131.
5. Pytel, A., Kiusalaas, J., *Mechanics of Materials.* Stamford, CT : Cengage Learning (2012). 465-466.
6. Moore, D.S., McCabe, G., Craig, B.A. *Introduction to the Practice of Statistics.* New York: NY, W.H. Freeman and Company (2017), 10-55.
7. http://www.robotsinarchitecture.org/kuka-prc. Accessed 25 April 2016.
8. Braumann, J., Brell-Cokcan, S. ‘Parametric Robot Control: Integrated CAD/CAM for Architectural Design’, in Joshua M. Taron (ed.) *Proc. ACADIA 2011: Integration through Computation*, Association for Computer Aided Design in Architecture (2011), 241-252.
9. Chandler, A., Pedreschi, R. *Fabric Formwork*. London: RIBA Publishing, 2007.
10. Erdine, E., Kallegias, A. ‘Design by Nature: Concrete Infiltrations’, in Martens, B., Wurzer, G., Grasl, T., Lorenz, W.E., and Schaffranek, R (eds.), *Real Time - Proceedings of the 33rd eCAADe Conference*, Vienna, Austria (2015), 513-520.
11. Mitani, J. Suzuki, H: Making Papercraft Toys from Meshes using Strip-based Approximate Unfolding. University of Tokyo, 2004.
12. http://www.tdmsolutions.com/rhinonest/. Accessed 12 May 2016

PULSE:

Integrated Parametric Modeling for a Shading System From Daylight Optimization to Additive Manufacturing

Milou Teeling, Michela Turrin and Paul de Ruiter

Delft University of Technology
Delft, Netherlands
milouteeling@gmail.com
{m.turrin, p.deruiter}@tudelft.nl

ABSTRACT

This paper presents a parametric approach to an integrated and performance-oriented design, from the conceptual design phase towards materialization. The novelty occurs in the use of parametric models as a way of integrating multidisciplinary design constraints, from daylight optimization to the additive manufacturing process. The work focuses on the case of a customized sun-shading system that tailors daylighting effects for a fully glazed façade of the alleged PULSE building.

The overall workflow includes preliminary analysis on simplified models and an initial parametric model to run computational optimization loops. The output consists of individually unique sun-shading panels, optimized for varying daylighting requirements based on programmatic distribution and specified viewing areas. The resulting geometric complexity was resolved through subsequent detailed parametric models; implementing the structural design requirements and integrating the constraints dictated by the additive manufacturing process, including the necessity to minimize material and 3D-printing time. This paper focuses on a particular part of the overall workflow, describing the support provided by parametric modelling to control geometric complexity and multi-disciplinary requirements.

Author Keywords

Multi-disciplinary design optimization; daylighting; additive manufacturing; performative facades.

1 INTRODUCTION

A number of precedent projects have investigated both static and kinetic solutions for optimized building skins, specifically with regard to daylighting performance through design tools and computation. Some studies aim for the improved performance of daylight harvesting, tackling issues of human comfort and energy efficiency [3]. Others study the performance-based shading capacity of intelligent and kinetic features in building skins [4, 22] while exploring complex geometry for improving building performance, as a potentially more optimal approach [19]. The built projects include the dome of the Louvre Abu Dhabi museum [24], and the Esplanade Theaters in Singapore [21], among others. Numerous precedents address the urgent needs for a more sustainable built environment based on optimized performances.

Nevertheless, most designs of traditional shading devices highly depend on modularity and the related reduction of customized unique items. This restriction is mainly dictated by the traditional production techniques, which are usually unable to deliver customized elements at affordable costs. Unfortunately, this often prevents the designer from customizing the sun shading according to specifically desired performances.

On the contrary, customized shading devices could potentially be beneficial for the performances of the building. Shading systems have major impacts on solar gain, daylight control and visual connections. For any of these concerns, the indoor requirements are not homogeneous throughout all indoor spaces of a building, as each indoor area may have different requirements. Hence, a uniform sun-shading system across the façade may not satisfy these appropriately, leading to discomfort or excessive energy consumption for climate control.

In recent years, the potentials of digital manufacturing for the building industry are creating opportunities to overcome the need of repetitive modularity and standardized components. Specifically, additive manufacturing is showing remarkable potentials to create tailored products with high complexity in shape and variations. As such, it allows producing customized elements, each of which can be unique at no additional cost.

The combination of parametric models, performance simulations and the additive manufacturing process also offers the opportunity to generate a library of generic scenarios, sharing the same systematic workflow, making them re-applicable to multiple specific design cases. The benefit of these generic parametric geometries is that they can be optimized based on the performance requirements of

each specific design case and produced by means of additive manufacturing. An example of previous studies on is [8].

The methodology presented in this paper is based on several parametric models. Via the parametric models, the shading system can be applied onto different façades and optimized according to any orientation and conforming to different indoor daylight-requirements. The paper focuses on the workflow for handling the optimized complex geometry of the shading of a large building façade via parametric models, toward 3D-printing of individually unique modules. The handling of all multi-disciplinary constraints is a challenging task. The paper identifies the difficulties encountered through the integration of multi-disciplinary requirements and related results from the performance simulations introduced at various stages of the computational design process; and it demonstrates the entire workflow until 1:1 prototyping.

The paper focuses on a case study, the PULSE project. Within the specificities of the case study, the paper argues that an integrated and highly collaborative process is essential to identify the optimal geometry for making the transition from the digital geometry to the fabrication output possible. The PULSE project allows discussing the digital workflow at length and through demonstrating the influence of the collaboration. In doing so, the paper underlines the importance of defining the priority and timely integration of design criteria that inform the order of geometric operations.

The paper is structured as follows; first an analysis of precedents and relevant references is provided in section 2; then the specific case of the PULSE building is described in section 3; the digital design process of the PULSE shading is presented in section 4; finally, discussion and conclusions are provided in section 5.

2 BACKGROUND AND PRECEDENTS

In this paper, geometric complexity and systematized customization controlled through digital models are tackled for the sake of enhancing performance.

Recently, the potentials of additive manufacturing (particularly 3D-printing) to produce complex building components tailored to specific requirements and desired building performances are rapidly emerging. Although the research relating to the application of 3D-printing in the construction industry is still in its infancy [26], relevant precedents have investigated its potentials for a number of building components. Among the examples, structural nodes are optimized and 3D-printed [6, 20]. Here, the geometric complexity resulting from the structural optimization is concentrated in localized components. Further potentials are highlighted in [18]. Focusing on facades, [23] investigate the tool-less production with additive manufacturing that allows for new shapes and less, but higher integrated functional parts, such as fittings, offering a better performance with lower material consumption. Recent studies also investigate to what extent 3D-printing technologies can be successfully applied to the construction of large/scale structures, including full buildings [5, 12, 13, 16, 25].

As [26] indicates, depending on the technologies used in the 3D-printing process, there are five distinct types. These are stereo-lithography, fused deposition modeling (FDM), inkjet power printing, selective laser sintering and contour crafting. For each of these, the implementation in the building industry faces various challenges commonly related to economic feasibility and scale of the printed components. This research aimed at pushing the boundaries of relatively inexpensive technology toward reliable building applications, making it competitive with more traditional shading systems. As such, FDM was selected. In the case of FDM, one of the highest challenges relate to the post-processing in case of support material to be removed and to the uncertainties of the long term behavior of the printed materials, especially in case of plastics. In [5], a new material is discussed, to print at a building scale a glass reinforced plastic, claimed as light, solid, anticorrosion, anti-aging, waterproof and insulating.

As compared to the precedents, the uniqueness of the case study presented in the paper is the completeness of the digital workflow applied to a large-scale design toward additive manufacturing. This included iterative loops across digital sketching and simulations, advanced multi-objective optimization, multi-disciplinary models coping with constraints dictated by the production process and production files.

In precedents, parametric design has been largely utilized as a method for performance optimization, constraint-handling and integrated modeling of complex geometries. Among the relevant examples are [2, 7, 9, 17]. Precedents using optimization in combination with parametric modeling and simulations are numerous. Regarding simulations for shading systems, [10] provides an interesting overview, whereas [11, 14, 15] focus particularly on optimization.

However, precedents rarely focus on the complete workflow, (from optimization to production). The fabrication of shading devices for building is mostly centered on standardization in order to meet the requirements of traditional production techniques. In contrast, the workflow presented in this paper supports the customization of individually unique modules.

3 THE PULSE PROJECT

PULSE (Practice, Unite, Learn, Share & Explore) is a multifunctional building for the Campus of Delft University of Technology (TUDelft) (see Figure 1). It is designed by Ector Hoogstad Architecten (EHA). It is to be located at the central axis and will facilitate an interfaculty educational center. It will cover an area of 4700m2 and its expected realization date is in 2017. It is designed with the

ambition to be the first building on the campus to reach the target of becoming energy neutral. Several aspects have been investigated to achieve this target. Besides the optimal orientation of the building and its program, the articulation of the façade plays an important role in reducing energy consumption. For various design intentions, the project includes a prominent west/southwest fully glazed façade, which covers an area of 463m2 on the first floor and 647m2 on the second floor. The indoor spaces behind the façade are large open spaces accommodating multiple functions. The functions are distributed on two floors interconnected by an atrium and the program includes traffic space, study spaces and lounge areas with coffee corners. Based on the different programmatic functions, the daylight requirements are different (300, 400, 600 and 800 lux). Also the architectural preferences for the quality of the light are specified, preferring filtered light close to the façade and allowing desirable, indirect light to enter the core.

This research focused on the need for sun-shading and daylighting control on the facade to minimize the heat load on the facade and increase the lighting conditions in the interior. The team involved in the project for the design of a 3D-printed version of the sun-shading device was a large multi-disciplinary team, including experts from TUDelft regarding computational design, 3D-printing and structural design; and from Yaşar University involving evolutionary optimization; the architects from EHA; and other external parties for 3D-printing facilities.

The overall digital workflow for the sun-shading of the façade can be summarized in the following interrelated phases: a) the initial concept and the preliminary simulations; b) the parameterization of the model; c) the multi-objective optimization; d) the selection of optimized design options and the structural analysis; e) the tests for 3D-printing; f) the integral parametric models; g) the final configuration and production of 1:1 scale prototype. Section 4 of this paper presents phase f) and partially g). The following sections 3.1, 3.2 and 3.3 provide a brief presentation of the phases a) to e).

Figure 1. Render of PULSE Building on TUDelft campus. Image Courtesy of Ector Hoogstad Architecten

3.1 Preliminary Analysis and Optimization

Based on local weather data and preliminary building simulations for solar radiation, the initial shading concept was defined. It consisted of a cloud of sun-shading elements in front of the façade. The shape evolved from a traditional horizontal shutter into a concave element because it increases its reflective capacity. Later tests indicated that pulling the maximum points along its concave surface to the side proved more beneficial as well. These studies resulted into an asymmetric panel that could accommodate different widths along its axis.

In order to identify the meaningful design variables for parameterization, a second set of preliminary simulations were run, this time on parametric models. Daylight studies were done using Rhino and Grasshopper for geometric modelling; Diva and Ladybug (plug-in for Rhino and for Grasshopper) to simulate daylight. A series of systematic analyses were conducted by running daylight simulations for interval values of each design variable, in selected times of the year (different hours and different seasons). This way, the solution space was sampled to better understand the trends between geometric features and daylight performances of each different functional zone. Additionally, a large number of geometric configurations were saved and inspected with the architects upon criteria that were not included in the simulations (such as visual connections with the outdoor and aesthetic appearance of the façade). Based on this process, appropriate design variables (and their numeric ranges) were identified prior to optimization.

Based on the identified significant variables and on the studied daylight requirements, a final parametric model for optimization was built in Grasshopper by a team at Yaşar University; and connected to a genetic algorithm optimization solver developed at Yaşar University. The optimization objectives included the minimization of the areas of the shading modules (in order to save material and time when 3D-printing) and the target lux values for each different functional zone (in order to maximize the amount of time in which the targets are reached, based on daylight only). Divided by the total hours of operation, the obtained percentage demonstrates the efficiency of the solution.

To obtain a higher resolution, the functional zones were further subdivided into squares to which these target illumination values were assigned. The illumination at each of the tiles is simulated for all hours of operation throughout the day. With minimal-tolerance (testing only for approximate target values of 300, 400, 600 and 800 lux), the best performing solution reaches 17% (see Figure 2).When the tolerance is adjusted to instead include a range of target values, this percentage increases significantly.

Several optimization runs were performed by using a large computer server physically located at EHA while being controlled from distance from Yaşar University; and at TUDelft. Each new run included improvements of the

models and algorithms. Using the output of the optimization runs, several design options located on the identified Pareto fronts were inspected (an example is in Figure 2). The related 3D models were visualized by the architects and assessed also based on criteria not included in the fitness functions of the optimization. As a result, a design solution was chosen for further development, as it was identified as the most promising one.

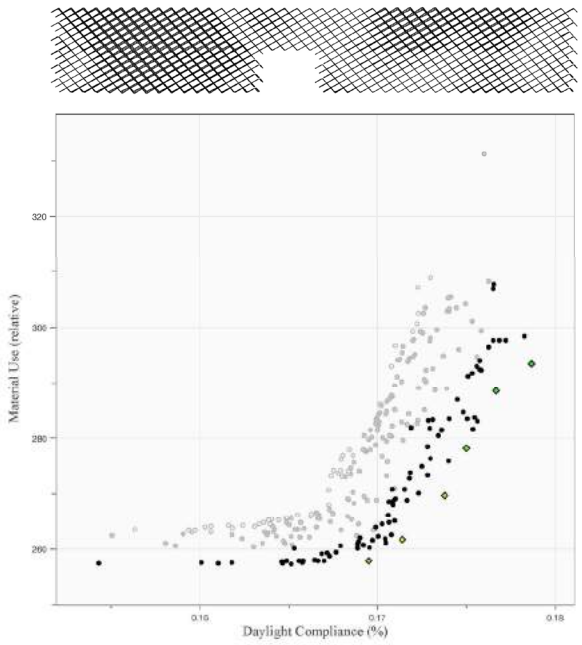

Figure 2. Results of the optimization and a related 3D model.

3.2 3D-printing

After the preliminary simulations and concept development, the relevance of selecting a production technique that could accommodate the variances in each of the modules became evident. 3D-printing was selected as the most advantageous to produce these gradual geometric differences resulting from the optimization process. Moreover, it was considered a relevant research agenda for the construction industry, as the team experimented on the limits and potentials of the technique to be applied in a large-scale outdoor project. Eventually, it also opened related topics, for example regarding recyclability of the materials, among others.

The 3D-printing process was approached with specific demands, as the production was bound to fit the timeline of the construction site; the modules were meant to be translucent; the total budget was limited. In addition, the suspended panels demanded a lightweight material, forcing the team to further minimize material usage. When coping with such demands at a large-scale, several complications add to the geometric definition of the panel, some of which were unforeseen in the early stages.

To proof the concept of using FDM for the manufacturing of the large amount of panels, a big 3D-printer was custom designed and built by Leapfrog 3D-printers. The goal was to be able to manufacture a single panel within the limited timeframe of 8 hours, thereby enabling the production of two panels per day. With hundreds of panels to be produced, the effective, expedient and low cost manufacturing of the panels was key to the viability of the project. As such, multiple 3D-printers would be necessary, also making the custom design of affordable 3D-printers essential.

The first constraint entailed the maximum printable volume of the printer (2100x560x560mm), which is not to be exceeded by the dimensions of the panel. This was taken into consideration in the early stages of the optimization constraints, guaranteeing that each panel would fit in the printer.

Secondly, the thickness of the panel was limited to the size of the custom build 2.2mm-nozzle of the large 3D-printer. As the nozzle completes each section, the final maximum thickness of each panel will be no more than 6mm. Since it is still time-consuming and relatively costly to 3D-print, it was crucial to meet the design criteria within these absolute minimal volumetric dimensions.

In order to save more time and material, an additional goal was to minimize the necessity for support-material, thus constraining the angle between each print-layer no larger than 45 degrees, positioning the panel in such a way that nearly horizontal surfaces are avoided. Upon finding the optimum orientation for the 3D-print, the panels needed to be separated and cut, while adhering to the all of the constraints mentioned above.

Several material experiments were carried out to test for printability, durability, structural strength, UV resistance and cost. PVDF proved promising results at small-scale tests, but still requires modifications for full-scale prints. The possibility of enhancing it with fiberglass to reduce the problematic shrinkage of the material is one of the explored options. As of current, successful 1:1 scale prototype 3D-prints have been completed with PET.

In summary, the primary target of the additive manufacturing process is to make the production of hundreds of panels possible within the allocated budget and time. As of recent tests, the approximate time required to produce each of the full-scale prints is estimated at 8 hours.

3.3 Structural System

In the initial stages of the project, several options were discussed regarding the structural approach as well. Although preferred, a self-supporting structure was not feasible with the selected lightweight materials for the additive manufacturing process. Therefore, the first structural proposal was to suspend the panels with a vertical cable system locking each panel into the correct position.

However, in this scenario panels could potentially break, endangering the people below. Rather than using expensive safety cables as a solution, the option of weaving the steel

cable structure through the panels was explored, not only increasing safety but also making them less visible, esthetically enhancing the design. The panels needed to be divided differently, significantly affecting the joint. Instead of producing a single panel, the redesigned panel combined two segments and their cross connection, with the added benefit of strengthening the structural capacity of the panel.

The cable system alternates between a single cable in one direction and two parabola double-cables in the other direction, which cross one another twice per string; once above and once below. The double-cable holds the panels in place and prevents them from rotating. Since the parabola cables are being held apart by the panels, this system requires that they can structurally withstand the inward tension from the two crossing cables.

4 DIGITAL WORKFLOW AND PARAMETRIC MODELS

After the optimization runs, the parametric model contained simplified geometry, although the geometric complexity of the final geometry was anticipated. The primary objective of the post-optimization digital workflow was to reduce the size of each file as much as possible before resuming the further development of the geometry. The output generated by each parametric model is reduced to only necessary information before proceeding to the next model, keeping the size of the operable data manageable. Identifying the segmentation of the parametric models occurred systematically, as each required a different data structure. The following section provides a summary (also illustrated in Figure 3) of each model in order to explain how each panel is geometrically defined according to the design constraints.

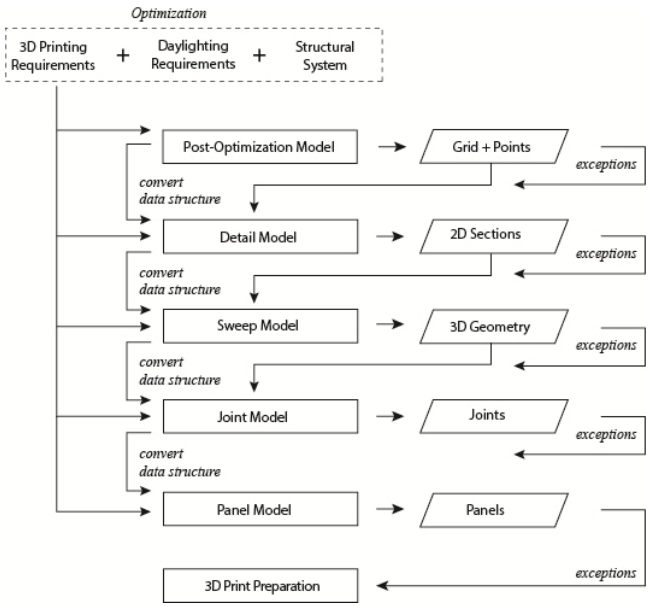

Figure 3. Digital Workflow Flowchart.

4.1 Post-Optimization Model

As a design principle, the diagonal base-grid was generated according to the results of the preliminary daylight studies and the decision to internalize the structural system. The grid controls the orientation and the number of panels in addition to the way the elements are positioned in relation to one another. The optimization was performed on a simplified lofted surface, defined by the dimensions of the grid, resulting in s-shape segments, shaped like the hood of a cobra.

The optimization already incorporated the constraints defined by the integrated structural cable system. For every s-segment, two of the planes intersect the single cable and two planes intersection the double cables of the structural system. In the case the optimization result returned a smaller width than the necessary width between the cables of the double cable system, the optimization result it is overridden to accommodate the cables inside the panel.

The post-optimization model converted the numeric data retrieved from the optimization into a spatial representation, defining the points of intersection and rotation (both in plan and in section) at each of the 4 planes along the s-segments (see Figure 4, top). This point-cloud generated in the post-optimization model was then further used as input for the subsequent parametric models.

4.2 Detail Model

As illustrated, the relationship between the design criteria was first explored at two singular instances in section and only two-dimensionally. Then, the detail model uses the data generated by the optimization results and generates each section on a flat horizontal plane before projecting the two-dimensional geometry onto planes oriented to the directions derived from the post-optimization model. It generates two-dimensional sections located at each plane and defines the width of each section and the appropriate rotation.

The further geometric definition of the sections is entirely informed by structural and additive manufacturing constraints. First, due to the structural system, there are 2 different types of sections, a double cable and a single cable. Secondly, as mentioned, the thickness of the section is derived from the nozzle size (2.2mm) of the 3D-printer, depositing either a single line (3mm) or a double line (6mm). Therefore, the wings are 6mm thick at the tips and are 3mm thick where the inside becomes hollow (see Figure 4, middle).

Due to the anticipated growing complexity of the three-dimensional geometry, the aim was to resolve most of the intricacies emerging from the integration of the design criteria with these planar constructions. The more precise and identical these sections were constructed, the easier it would be the transition from the two-dimensional projection to a volumetric three-dimensional geometry.

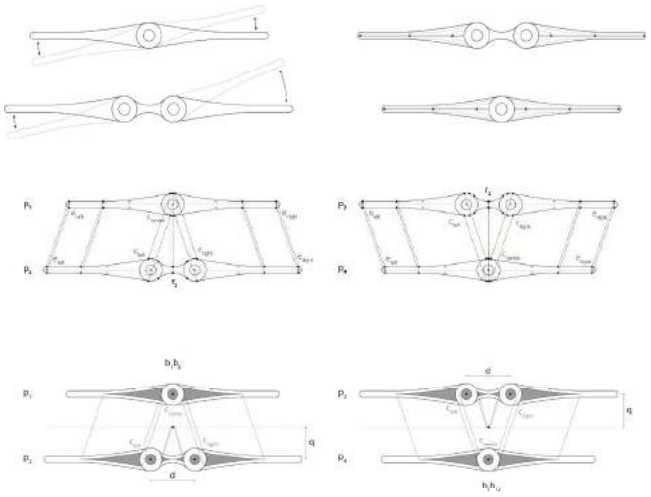

Figure 4. Output from Detail Model.

4.3 Sweep Model

The sweep model uses the sections generated by the detail model to create the three-dimensional continuous surface geometry. The sweep fits a surface through a series of profile curves (sections) that define the surface shape and a series of rail curves that define the surface edges.

The sweep model requires an entirely different data structure. In order to produce the three-dimensional continuous surface geometry, it is necessary to convert the structure from individual s-segments to uninterrupted horizontal branches. The sweep model also generates the hollow inner surfaces by using the offset sections from the detail model. This geometry is subtracted from the solid boundary representation in order to reduce the material and weight of the panel (see Figure 4, bottom).

Upon completion of the sweep model a control-simulation was performed in order to compare the illumination results of the initial optimization with the post-optimization volumetric three-dimensional geometry.

4.4 Joint Model

The joint model produces the joint that occurs at every intersection of the underlying grid between the v-segments and n-segments of each panel (see Figure 5, left-top). The joint internalizes the cable structure to hold the structural system in place and offers structural stability. It needs to withstand both tension forces from the cable system and wind load. To achieve the most equal distribution of these forces, the joint requires a fluid vertical transition between v-segments to n-segments.

According to the additive manufacturing criteria constraining the 3D-print direction, the joint is problematic where it connects the v-segment and n-segment, as it contains horizontal surfaces. Since the two legs of the x-shape panel are printed first, the joint has to bridge a horizontal gap. In order to prevent the need for support material (which is problematic because it adds printing time and material), the bridge between the legs needs to be minimized, resulting in a sharper blend between the v-segment and n-segment (which is undesirable due to structural concerns).

As the goal was aim to minimize material, the joint cannot be solid, so all excess material should be removed. Adhering to the previously established print thickness of 3mm, the inner offset of the joint is created by redrawing the curves according to the previous paragraph. These curves are drawn from a 3mm offset of the original network surface.

4.5 Panel Model

The panel model defines the last parametric relations before exporting the geometry to a format that finalizes 3D-print preparations. It places cutting planes and splits the continuous surfaces from the sweep. Each panel is cut-off according to the size limitations of the 3D-printer, resulting in v-segments and n-segments. Combined with a joint, they form an x-shape panel.

Ideally, this cut-off occurred at the midpoint of each grid element, resulting in a regular x-shaped panel. Unfortunately, this panel exceeds the additive manufacturing criteria restraining the printable angle no larger than 45 degrees. To meet this constraint, the panel is reoriented in such a way that is the legs are not the same length.

In addition, the model resolves the connection between the panels with a tube, ensuring their location and preventing the panel's rotation. The tube is a standardized, straight PVDF cylinder with a diameter of 1.5cm and a length of 10cm. These dimensions are defined parametrically to accommodate various options to be determined later after structural testing and availability of standardized materials.

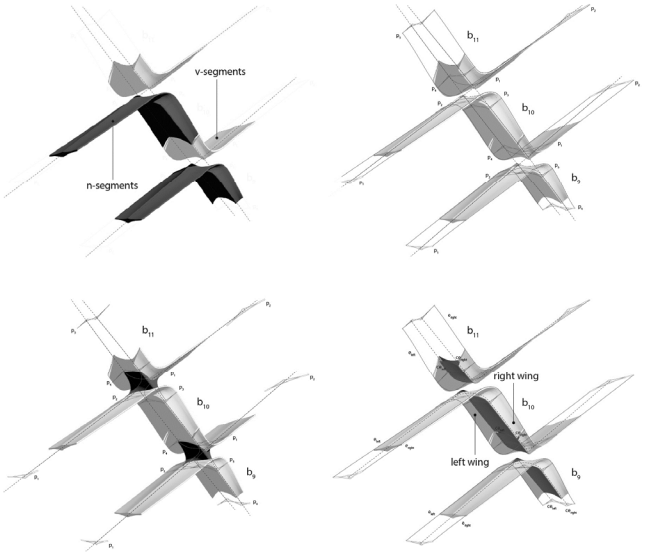

Figure 5. Output from the Sweep, Joint and Panel Models.

Figure 6. Full-scale 3D-printed prototype: one module.

The geometry of the joint model is imported into the panel model and together with the v-segments and n-segments, generates the x-shape. Since the data structures of these three separate pieces do not align, and do not match the desired organization of the panels, the data structure requires revision once more. Once the data matches, the pieces are seamlessly joined as one and exported accordingly. The inner sweeps are also cut, organized and subtracted; resulting into a hollow, bare minimum volume to print. In this case, the organization of the data resembles the order of assembly during construction. The labels are recessed into the planar surface at the cut of each panel and 3d-printed along with the panels. The final model is visible in Figure 7.

4.6 3D-print Preparation

The last step of the digital workflow requires the exporting, organizing and preparing for 3D-printing. From the panel model, each individual panel is repositioned and exported as a separate file to be printed. The polysurfaces are welded into a closed mesh and converted into a .stl file. Evidently, the exported geometry requires thorough inspection and manual fixes before sending it to the 3D-printer.

As such, several samples have been produced across multiple scales, including 1:5 architectural models, an 2 strings of 7 panels as 1:3 assembly models to test the structural systems and finally a successful 1:1 prototype module (see Figure 6).

5 CONCLUSION

The research presented in this paper investigated the digital workflow of the performative-design-to-production process of an optimized sun-shading system. The proposed process exemplified the challenge of integrating multiple design criteria in terms of performance optimization, internalized structure, and manufacturing concerns that resulted into a high geometric complexity. The final geometry (Figure 7) became the calibrated product of a complex, continuously redefined set of mathematically described rules, rather than a preconceived aesthetic image.

As discussed, the design criteria developed over time as part of the natural challenges throughout any collaborative design process. In doing so, the paper argues that this process of identifying the parameters and constraints that informed the design decisions is not a linear, sequential process. The paper argued for the necessary integration of multi-disciplinary constraints through multiple parametric models. In doing so, the juxtaposition of multiple design criteria facilitated the encounter of several conflicts, which could have never been detected if modeled manually through a panel-by-panel approach.

In addition, this research demonstrates the potential use of additive manufacturing at large-scale and its contribution to the design of performative building envelopes. In future research it would be advantageous to streamline the collaboration even further in advance to ensure that each of the identified design criteria is considered simultaneously, rather than sequentially. Particular additive manufacturing constraints became a decisive constraint too late in the process, where it should have been incorporated from the beginning. As of today, more tests are necessary with regard to the selected material (PVDF) and also to decrease the printing time. Upon evaluation and towards possible future phases of the case study the primary concern is to reduce the complexity of the geometry to ensure 3D-printability.

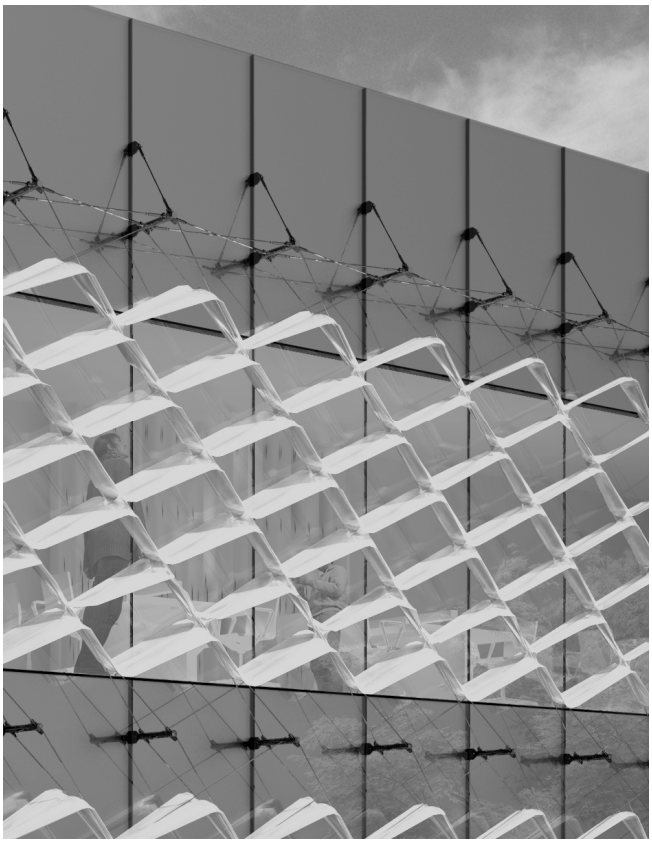

Figure 7. Detail of the PULSE Sun-shading System.
Image Courtesy of Ector Hoogstad Architecten

ACKNOWLEDGEMENTS

Special thanks to the team from Ector Hoogstad Architecten, in particular project architect Lennaert van Capelleveen, Laurence van Benthem, Daniel Diez-Ausias and Rena Logara for facilitating the project. David Maimone contributed to the preliminary daylight analysis. The daylight optimization was carried out by Ioannis Chatzikonstantinou and his team from Yaşar University. Pirouz Nourian helped defining the mathematical models behind the geometry. Peter Eigenraam designed the structure and determined the structural parametric constraints. Mark van Erk contributed to involving manufacturing aspects and preparing the geometry for 3D-printing. Leapfrog provided 3D-printing support.

REFERENCES

1. Adriaenssens, S., Gramazio, F., Kohler, M., Menges, A. and Pauly. M. Foreword. *Proc. of Advances in Architectural-Geometry* (2016)
2. Aish, R. Woodbury, 2007. Multi-Level Interaction in Parametric Design. *Proc. 5th Int. SG,* (2007), 25–27.
3. El Sheik, M. Intelligent Building Skins: Parametric-based algorithm for kinetic facades design and day-lighting Performance integration. *Thesis, USC School of Architecture,* (2000).
4. Emami N., Khodadadi A. and von Buelow, P. Design of Shading Screen Inspired by Persian Geometric Patterns: An Integrated Structural and Daylighting Performance Evaluation. *Proc. of IASS-SLTE* (2014).
5. Feng, L.Y. Study on the Status Quo and Problems of 3D-printed Buildings in China. *Global Journal of Human-Social Science Research*, 14(5) (2014).
6. Galjaard, S., Hofman, S., Perry, N., and Ren, S. Optimizing Structural Building Elements in Metal by using Additive Manufacturing. *Proc. IASS* (2015).
7. Hudson, R. Strategies for Parametric Design in Architecture: An Application of Practice Led Research *Ph.D. Thesis, University of Bath*. (2010)
8. Karagianni, L., Turrin, M., Knaack, U. and Hordijk, T. Additive Manufacturing for Daylight_Towards a Customized Shading Device. *Proc. SimAUD* (2016), 69-76.
9. Kilian, A. Design Exploration through Bidirectional Modeling of Constraints. *Ph.D. Thesis, MIT*. (2006)
10. Kirimtat, A., Koyunbaba, B.K., Chatzikonstantinou, I. and Sariyildiz, S. Review of Simulation Modeling for Shading Devices in Buildings. *Renewable and Sustainable Energy Reviews*, 53, (2016), 23-49.
11. Kirimtat, A., Koyunbaba, B.K., Chatzikonstantinou, I., Sariyildiz, S. and Suganthan, P.N., 2016, July. Multi-Objective Optimization for Shading Devices in Buildings by Using Evolutionary Algorithms. *Proc. IEEE*. (2016), 3917-3924
12. Kothman, I., Kothman, I., Faber, N. and Faber, N. How 3D-printing Technology Changes the Rules of the Game: Insights from the Construction Sector. *Journal of Manufacturing Technology Management*, 27(7), (2016), 932-943.
13. Labonnote, N., Rønnquist, A., Manum, B., and Rüther, P. Additive Construction: State-of-the-art, Challenges and Opportunities. *Automation in Construction,* 72(3) (2016), 347-366.
14. Lavin, C. and Fiorito, F. Optimization of an External Perforated Screen for Improved Daylighting and Thermal Performance of an Office Space. *Procadia Engineering* (2017)
15. Lee, K.S., Han, K.J. and Lee, J.W. Feasibility Study on Parametric Optimization of Daylighting in Building Shading Design. *Sustainability*, 8(12), (2016), 1220.
16. Lim, S., Buswell, R.A., Le, T.T., Austin, S.A, Gibb, A.G.F. and Thorpe, T. Developments in Construction-scale Additive Manufacturing Processes. *Automation in* Construction, 21, (2012), 262-268.
17. Menges, A., Pluripotent Components and Polymorphous Systems: An Alternative Approach to Parametric Design. AA Files, (52), (2015) pp.63-74.
18. Mueller, C.T. 3D-printed Structures: Challenges and Opportunities. *STRUCTURE*, 54 (2016).
19. Pantazis, E., Gerber, D., Wang, A. A Multi-Agent System for Design: Geometric Complexity in Support of Building Performance. *Proc. SimAUD*, (2016), 137-146.
20. Prayudhi, B. 3F3D: Form Follows Force with 3D-printing, *MSc Thesis at the Faculty of Architecture, Delft University of Technology* (2016).
21. Sanchez-Alvarez, J. The Geometrical Processing of the Free-formed Envelopes for the Esplanade Theatres in Singapore. *Proc. IASS* (2002).
22. Sharaidin K., Burry J. and Salim, F. Integration of Digital Simulation Tools With Parametric Designs to Evaluate Kinetic Façades for Daylight Performance, *Proc. of eCAADe,* 30, 2 (2012), 691-699.
23. Strauss, H. and Knaack, U. Additive Manufacturing for Future Facades. *Journal of Facade Design and Engineering*, 3(3-4) (2016), 225-235.
24. Tourre, V. and Miguet, F. Lighting Intention Materialization with a Light-based Parametric Design model. *International Journal of Architectural Computing*, 8(4), (2010), 507-524.
25. Rutkin, A. Watch as the World's First 3D-printed House Goes Up. New Scientist. 221 (2960), (2014) 24.
26. Wu P, Wang J, Wang X. A Critical Review of the Use of 3-D Printing in the Construction Industry. *Automation in Construction*. 68, (2016), 21-31.

Simulation in Complex Modelling

Mette Ramsgaard Thomsen[1], Martin Tamke[1], Paul Nicholas[1], Anders Holden Deleuran[1], Phil Ayres[1], Riccardo La Magna[2], Christoph Gengnagel[2]

[1]CITA, Royal Academy of Fine Arts, School of Architecture
Copenhagen, Denmark
mette.thomsen@kadk.dk

[2]Department for Design and Structural Engineering / UdK
Berlin, Germany
gengnagel@udk-berlin.de

ABSTRACT

This paper will discuss the role of simulation in extended architectural design modelling. As a framing paper, the aim is to present and discuss the role of integrated design simulation and feedback between design and simulation in a series of projects under the Complex Modelling framework. Complex Modelling examining how methods from the parallel disciplines engineering and computer science can broaden our practices and transfer central information modelling concepts and tools. With special focus on new hybrid structural morphologies and material fabrication, we ask how to integrate material performance, engage with high degrees of interdependency and allow the emergence of design agency and feedback between the multiple scales of architectural construction.

This paper presents examples for integrated design simulation from a series of projects including Lace Wall, A Bridge Too Far and Inflated Restraint developed for the research exhibition Complex Modelling, Meldahls Smedie Gallery, Copenhagen in 2016. Where the direct project aims and outcomes have been reported elsewhere, the aim for this paper is to discuss overarching strategies for working with design integrated simulation.

Author Keywords

Complex Modelling; lightweight simulation; design integration; Finite Element analysis

ACM Classification Keywords

Design.; Algorithms; Performance

1 INTRODUCTION

The current forming of a shared digital design practice has led to the emergence of new methods in which simulation both acts as a means by which to enable feedback in the design chain by informing early design decisions, corroborating intuition and rectification of design decisions. In this sense this new practice has employed multiple understandings of simulation; lightweight simulation using fast and less exact methods for early stage design integration and heavyweight simulation using more verifiable and exact calculation method for final design evaluation [1]. This paper examines how this dual practice has traditionally paired particular kinds of simulation tools to either of these practices and how new advances in the way simulation is undertaken challenge this otherwise simple separation.

The paper aims to understand the fundamental differences introduced into architectural design, as we enter an expanded digital design chain equally concerned with design at the scale of the material, the element and the structure. Rather than understanding simulation as duality between lightweight and heavyweight, simulation here becomes a recurrent and distributed event occurring across the modelling environment bringing together different scales of design agency and employing varying levels of precision as well as different tools of calculation. By using examples from the research investigation Complex Modelling [2], the paper will examine how the advancing of digital design practice, the contemporary evolution of our design tools and the stronger understanding of our problems spaces allow us to reconceive how simulation can become part of design strategy.

2 SIMULATION IN DESIGN

Architectural design practice is facing increasing demands in terms of predictability and performance of its outcomes. Simulation lies at the core of this emerging practice of performative architecture [3], as it allows for the quantitative evaluation of a project's performance. Today, different means of simulation cover a broad range of architectural concerns, from design to construction and operation, including the simulation of a design's environmental, structural and material performance and its fabrication and assembly. This means for the new practice, that simulation is understood as an integrated part of the whole chain from design to production and as bridging different disciplines including architects themselves. The incorporation of simulation potentially disrupts traditional design practice by introducing feedback and cyclical thinking in a process that is otherwise characterised by an ideal of linear progression and division of labour separating design generation and analysis.

Design integrated simulation produces computational workflows, which grant simulation models different degrees of design agency [4]. In an analytical track, simulation models are used to investigate the performance of a proposal post design. This approach is exemplified in the Dermoid project [5]. The project utilises the bending

behavior of short plywood elements to form larger trusses arrayed in a reciprocal open topology. The overall structural behaviour of the design in terms of deformation and bending stresses in the trusses is simulated with Finite Element Analysis (FEA). , aThe results are nd in turn explored by the designer, who take decisions on how to alter the design, if design goals are not met yet. In a generative track, simulation is a part of an autonomous design process. This approach is exemplified in The Rise [6]. Here, the 6m high bending active structure is developed in a computational design system based on the simulation of a growth system and built from bundled strands of rattan. The simulation is devised as an artificial energy metabolism, in which a first set of branches are "grown" according to locally available "energy". The performance of the grown branches is then analysed with an integrated and calibrated particle spring system and a new energy level is locally distributed based on the results, before the process restarts.

Computational design workflows on the generative track are generally linked to lightweight simulations, as only these can provide the necessary amount of iterations. The analytical track on the other side is characterised by fewer feedback cycles, in which heavyweight simulation is used to provide accurate and precise answers - at the cost of higher processing time. The question is how to overcome the tie of the generative track to fast, but inaccurate lightweight types of simulation and the analytical track to heavyweight but slow types, when complex architectural problems necessitate generative approaches and a general demand for more frequent and better feedback cycles exists in the profession.

3 THE CURRENT DIVISION INTO LIGHTWEIGHT AND HEAVYWEIGHT SIMULATION

To separate different kinds of simulation we introduce a division into lightweight and heavyweight simulation (Fig. 1). The term lightweight is rooted in computer science, where it describes an algorithm or language, which has a small memory footprint or impact on the overall performance of a computational system. In our field lightweight simulations are similarly characterised by a minimal use of computational power. This allows them to be directly integrated into the generative track and workflows of early design stages. Here, they provide a level of accuracy and precision, that is 'good enough' for design decisions, while operating on high levels of abstractions, assumptions and generalisations. The algorithms that underly lightweight simulations are often so general in scope, that they can encompass a wide range of concerns and solve simultaneously questions related to geometry, structure, assembly and fabrication of a design.

In contrast heavyweight simulation is understood as more accurate and precise, but as well computationally heavy, specialised in scope and demanding in terms of knowledge about a design. Typical representatives of lightweight simulations are particle/spring systems commonly used in physics systems. In contrast to FEA, which employs a matrix based method for the solution of the equations of equilibrium and the associated stresses of the structural members as a result of forces, boundary conditions and material properties, particle-spring systems operate on a simplified vector representation of forces and solve the equilibrium of the system iteratively. This reduced approach allows to form find structures [7] or simulate realistic physical behaviour directly in the design environment; for instance with tools like the Nucleus solver within Autodesk Maya™ or the Kangaroo plugin for Grasshopper/Rhino.

Figure 1. Diagram in which the integration of simulation moves along a time based unfolding from lightweight to heavyweight

In CITA the exploration of how to integrate simulation in design has been undertaken across an extensible range of projects employing different material systems and different scales of material interaction [8]. The design of CITA's pavilion at Roskilde [9] exemplifies this workflow. In the design of this bending active gridshell structure, an initial series of particle-spring simulation models supported the connection between a limited number of critical material behaviours and limits to key design parameters within a generative process. These models included numeric calculation of minimum bending radius and utilisation, so that the natural minimum energy bending behavior of tubular elements could be attracted to a non-standard target geometry, connections established to other elements within the structure, and element lengths maintained. At each iteration, bending was calculated for each element and those forces acting on the elements applied only when the bending was deemed within the limits of the material. After a design was established, it was then evaluated using a different software environment. A non-linear FEA model defined with the FEA software Sofistik AG was used to analyse the resulting geometry and bending stresses after the shaping of the gridshell.

A second example is the Tower [10] a 9m tall bending form-active hybrid structure, in which bend 10mm glass-fibre reinforced plastic (GFRP) rods are stacked in layers and inserted into a constraining bespoke CNC knitted surface. The implementation of the K2 physics solver into the computational design model in Rhino/Grasshopper allowed here for a real-time interaction between the designer and the form-finding of the structure. The ability to quickly customise the K2 simulation engine granted the necessary fluid design process. The general nature of the K2 engine allowed furthermore to represent and solve the many layers of design constraints in one modelling environment. This allows us to consider during the design

process simultaneously parameters of shape, structure, production, assembly and to some extent material

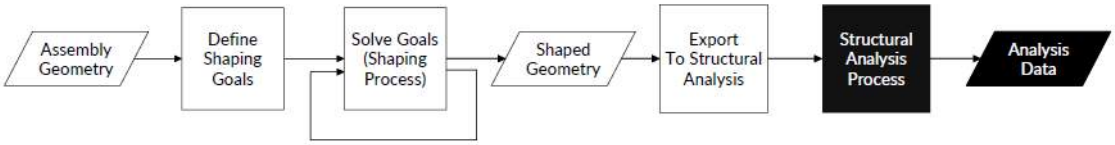

Figure 2. Flowchart of the computational design workflow of the Tower project in which lightweight simulation is used for the shaping process (white) and the subsequent analysis in FEA (black).

behaviour, as the light weight simulation provides feedback on the utilisation of the GFRP rods in terms of bending forces. An accurate analysis of the design in terms of stresses in all building elements and the behaviour of the overall structure under external loads took again part in Sofistik (Fig. 2).

The division of the simulation process into an initial lightweight model for design exploration and a later heavyweight model for validation and verification, sets a focus on interfacing 'handshaking' between the often very different levels of description used in the models. The challenge is to identify and extract information from one model and to port it directly into another as input parameter. Handshaking can here be uni- or bidirectional. It can take place sequentially, as in Dermoid, where the form found design was analysed in FEA and the resulting dimension of elements fed back into the lightweight simulation, or in parallel, when multiple simulation models produce information for other models [4]. The interface between the often mutually inconsistent frameworks of simulation has to be carefully curated and reconciled in overall fitness functions, artificial metabolisms, Hamiltonians or other weighting methods [11].

The previous section between one set of methods for more abstract behavioural descriptions, and another set for more highly specified behavioural descriptions, can be replaced and geometric description. The recognition and exploitation of this overlap – and the extension of domains to which projection-based dynamic relaxation and FEA can be applied - initiates new possibilities for moving between, or combining, simulations - either to become increasingly accurate and precise over a set of investigations, or to simultaneously calculate and combine results drawn from different levels of resolution.

Where these projects have allowed us to understand and prototype the potential for working with different kinds of simulation, both light- and heavyweight, it has also led to a larger research enquiry into how simulation of different levels of realism can interface and handshake along the design chain. Rather than positioning lightweight simulation only at the start of the design chain, and conversely heavyweight simulation only at the end, our new practice asks how these different kinds of design analysis with their differing implementation, speed and ability to couple different frameworks through a manifold of handshake-algorithms can be further leveraged in design practice.

4 PROPOSING A NEW MODEL: INTERFACING SIMULATIONS OF DIFFERENT LEVELS OF FIDELITY

Changes in simulation practice now open the door to less linear differentiations and progressions between lightweight and heavyweight simulation. The separation described in the previous section between one set of methods for more abstract behavioural descriptions, and another set for more highly specified behavioural descriptions, can be replaced by the use of both methods across varying levels of material and geometric description. The recognition and exploitation of this overlap – and the extension of domains to which projection-based dynamic relaxation and FEA can be applied - initiates new possibilities for moving between, or combining, simulations - either to become increasingly accurate and precise over a set of investigations, or to simultaneously calculate and combine results drawn from different levels of resolution (Fig. 3).

In the Complex Modelling project we explore alternative models for intersecting and interfacing different modes of simulation in the design model.

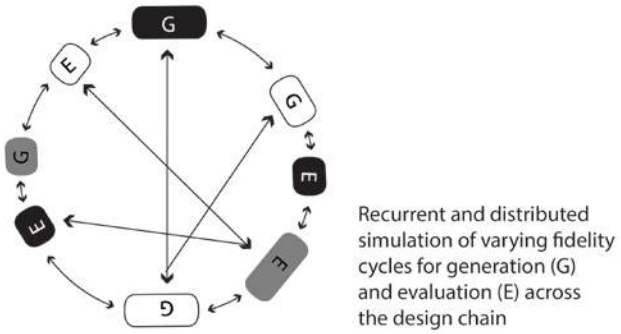

Figure 3. New model in which distributed simulation models of varying degree of realism act in a network and handshake in different ways. The gradient from white to black represents the gradient between high and low fidelity.

The research experiments Lace Wall, A Bridge Too Far, and Inflated Restraint develop and demonstrate this extended ability to specify - at varying degrees of accuracy and precision - material systems within design integrated dynamic relaxation and FEA simulation. Limits around the methods for dynamic relaxation, particularly the capacity to incorporate material information such as Young's Modulus,

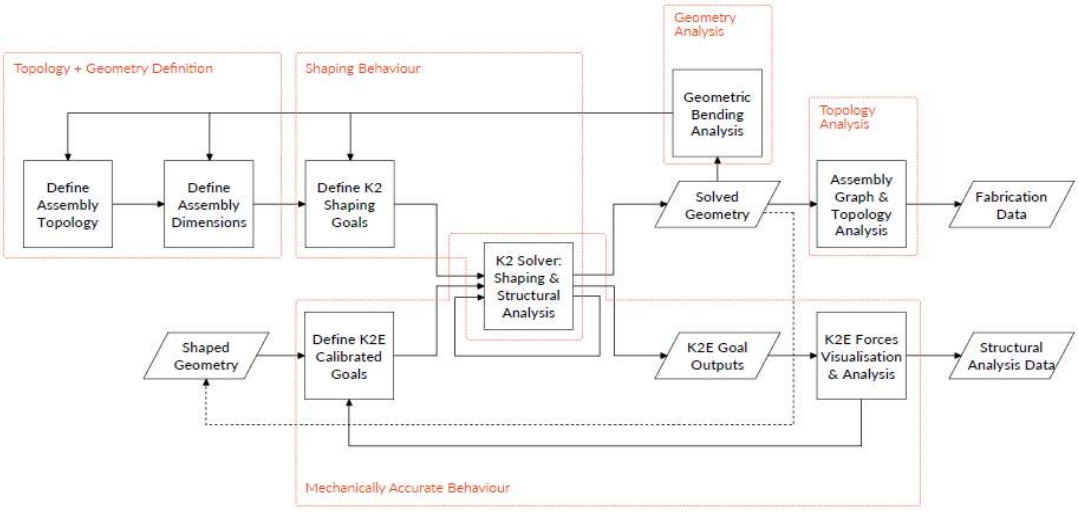

Figure 4: Flowchart of the interactive Lace Wall modelling pipeline, defining different modelling stages and expressing the integrated feedback loops.

have previously restricted its capacity to contribute to higher level quantitative understandings of behaviour. But new approaches using projection based dynamic relaxation extend to include this information: In Lace Wall, the goal solver Kangaroo2 is implemented both for describing form-finding behaviours, used during exploratory design where topology and dimensions are free, and for describing mechanically calibrated behaviours used during accurate structural analysis. The Kangaroo2 API enables designers and developers to integrate the solver and write custom goals with great freedom. Enabling both the development of the K2Engineering plugin [12, 13] and the interactive Lace Wall modelling pipeline [14] where designers are free to handshake between the exploratory and structurally accurate modes of modelling at any time.

In contrast, the limits around FEA tools have been in the other direction: a traditional separation from design tools has implied slow iteration time and encouraged use only in the validation of high-resolution geometries. Current integrations of FEA into the design environment are exploited in A Bridge Too Far to enable fast and iterative feedback, but also to develop more nuanced relationships between the FEA model and the design model – simulations that act on scalar subsets of the model to ask partial questions, and which exploit the fact that often, appropriate answers only require a minimum of information, rather than the whole. In A Bridge Too Far, the integrated FEA tool Karamba is implemented within the design process as part of a search and optimisation loop. Its integration within the 3D modelling environment Rhinoceros allows structural simulation to be informed but also then combined with other considerations in a form-finding and optimisation process.

With the ability to specify the models at varying levels of accuracy and precision, new workflows are enabled. While the simulation methods differ between the projects, the workflows share a common approach that partitions models into networks of sub-models functioning at different levels of resolution, and the curating of connections between these models (Fig. 4). This involves identifying appropriate models, tailoring the specificity of material information and the resolution of geometric definition to those models, at the appropriate resolution, and distributing multiple such models across the workflow. Connections might support a sequential progression of material and design specification from low to high, or one to many: In the case of Lace Wall sub-models are organised by feedback loops. Where upstream models generate topology, geometry and behaviours, central models solve these behaviours, and downstream models generate analysis data to re-inform the upstream models. Enabling a continuous and interactive search loop, where resolution is automatically defined on the fly. Allowing humans or search algorithms to generate fit candidates without having to continuously adjust parameters that do not affect design. Alternatively, connections might support also support the progressive generation of design detail across multiple scales, as in the case of the research structure Stressed Skins [15]. Lastly, connections might extract information in parallel from multiple models and combine this within a single energy descriptor to steer design generation, as implemented in A Bridge Too Far.

Our initial exploration of these workflows has led us to change the way we conceptualise the relationship between methods, and the spectrum on which they sit. When both simulation methods can be employed with greater or lesser quantities of information, lightweight and heavyweight is not the best characterisation anymore. With an increased degree of freedom in how we computationally describe both pseudo behaviours (the description of place-hold behaviours that estimate material performance) and accurate physical behaviours, we are now afforded direct

control of how we define modelling accuracy (i.e. qualitative properties of the underlying model) and precision (i.e. quantitative properties, such as resolution). As such, the simulation spectrum is perhaps better described as being one of fidelity. Rather than arranging these as an incremental process of refinement we can employ these differing means of reproducing behaviour with different degrees of resolution strategically within the design workflow.

5 EXAMPLES OF WORKFLOWS IN COMPLEX MODELLING

These workflows are prototyped and developed through three Complex Modelling projects: Lace Wall, A Bridge Too Far and Inflated Restraint. Where each project finds local means of implementing simulation, then the strategies have in common the partitioning of the model into a network of models, the distributed and recurrent utilisation of different kinds of simulation across the design chain with varying degrees of fidelity, the external verification and validation of the simulations and the establishing of different kinds of handshake operations within the modelling workflow.

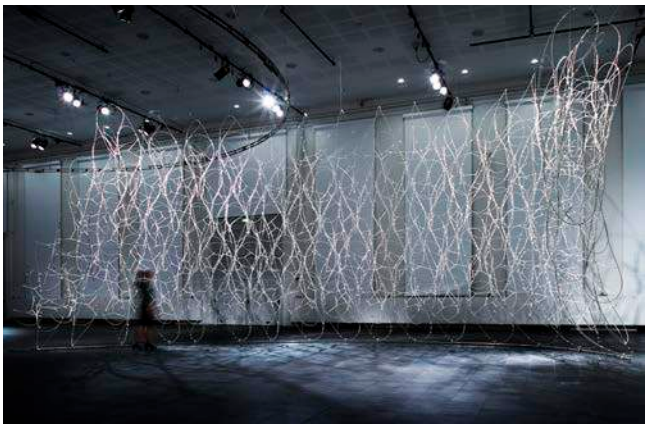

Figure 5. Lace Wall in the Complex Modelling exhibition.

5.1 Simulation in the Lace Wall workflow

Lace Wall belongs to the family of form-active hybrid structures and is a generic and modular space frame-like system, that can be extended in a spatial array to construct large enclosures such as walls, roofs, domes and more complex macro shapes. The material system consists of a minimal inventory of elements: 8mm GFRP rods, textile cables and custom designed high-density polyethylene joints. The rods are bent and joined into 80 discrete units, each stabilised by an internal three-dimensional cable network. While the dimension and topology of the GFRP units are identical, the cable networks are differentiated so as to allow the single units to withstand different local strains in the structure and to constrain each unit into bespoke geometries, that allow them to fit into a desired overall macro shape [16].

Lace Wall investigates computational strategies to design with material systems, that are characterised by a high

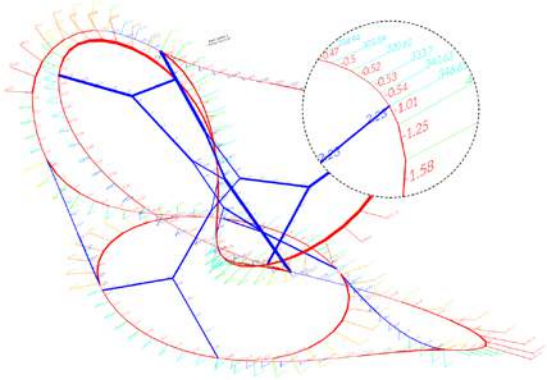

Figure 6. Single unit of Lace Wall after K2E structural analysis with tension (blue), compression (red), stresses and bending stressed displayed.

degree of interdependence of elements and scales. This reciprocal relation limits for Lace Wall the traditional use of small scale physical models for design exploration. Designers get quickly fatigue by the necessary level of accuracy to develop form-active hybrid structures, which are highly sensitive to the smallest imprecision and changes. On computational level the simulation of single units and large arrays of interacting bending active units is similarly challenging, as the final shape emerges only as a result of the interacting forces in the bending active element and the tensioning wires. These can not be captured precisely enough by lightweight simulations and the sheer amount of interacting elements prohibits a handshake to FEA. For Lace Wall it was furthermore of high importance, that the design environment is not restricted to iterations within fixed topologies, as it was the case in Tower [10], but that topologies could be openly explored.

The computational workflow (Fig. 4) of Lace Wall employs, an approach in which a low fidelity simulation, for an initial and approximate form finding, can at any time be exchanged with a high fidelity simulation, for precise determination of the resulting shape and stresses (Fig. 6). The speed of the K2 simulation enables not only a direct interaction of the designer with the bending active structure and immediate feedback on the expected shape and through the K2 loop on the expected performance, but as well to employ generative workflows. Herein topologies for the constraining cable networks can be automatically generated and form found, which provides the means to analyse and qualify the fitness of a candidate. These are collected alongside their fitness parameters in a database for further design iteration. Promising candidates can undergo a more precise analysis with the K2E engine in a second loop.

The models in the workflow share a common data model, where topologies, properties and their performance are encoded in an Object oriented way. This way of representation enables a handshake between the very

different modelling frameworks, within the Lace Wall pipeline.

Core to the development of the workflow, is the constant verification of the computational model against established structural and computational models and theories, as well as the validation of the results against physical probes and prototypes.

Figure 7. A Bridge Too Far in the Complex Modelling exhibition.

5.2 Simulation in the A Bridge Too Far workflow

A Bridge Too Far is an asymmetric bridge, spanning 3 meters and weighing 40kg excluding buttresses. The structure consists of 51 unique planar, hexagonal panels, arranged without framing into an inner and outer skin. The thickness of each panel varies locally, and at maximum is 1mm thick. The project explores an extension to the capacities of thin panelised metallic skins through the use of rigidisation (the selective movement of local areas of the sheet out of plane to increase structural depth) as means to enable novel lightweight and frameless structures, and the improved understanding of underlying processes [17].

The modelling approach seeks to counter and evaluate buckling at the scale of the structure, the panel and the material. The integrated FEA tool Karamba is used to predict behavior and deflections of the entire structure. This design-integrated simulation is validated against simulation using Sofistik as well as empirical load testing of prototypes. A k-means clustering algorithm is used to determine panel outlines, a low fidelity representation that supports evaluation of the coincidence of seams on upper and lower surfaces. An interference model generates high fidelity rigidisation geometries, from which a precise calculation of material properties is made using circle projection. This is done to incorporate the implications of fabrication within the modelling process. All geometric features in the bridge, including those for resisting local footfall, buckling within each panel, and also the structural connections that manage shear forces across upper and lower skins, are fabricated using Robotic Dual Point Incremental Forming (DPIF). The effects of this fabrication process are both geometrically and materially transformative, where stretching and a local increase in surface area corresponds to thinning and a change of yield strength, according to the angle of forming. The impact within the simulation is to add significant variation to information that would more usually be simplified and made uniform.

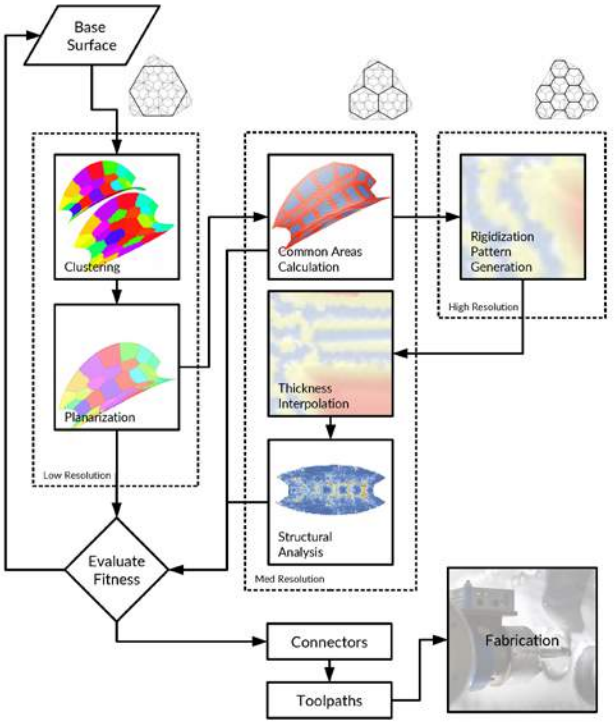

Figure 8. Flowchart of A Bridge Too Far modelling pipeline.

Where previous research at CITA has explored a sequential approach to the definition of shapes and features at different scales, [18], this project has implemented a parallel approach [11]. A custom tree hierarchy class is used to establish geometry-data coupling and support continuity of information flow [15]. The tree supports information flow between models of different geometric resolution and precision, as well as various upstream and downstream methods of data propagation. This approach to communication between models supports a search and optimization loop. Within the loop, geometric (seams, connection size and shape) and material information (yield strength and material thickness) is generated at geometric resolutions that are both lower and higher than that of the FEA simulation, with information down and up-sampled as required. Deflections calculated using Karamba are integrated with measures coming from these other models and combined into an overall measure of energy, which is minimised during the optimisation loop (Fig. 8).

5.3 Simulation in the Inflated Restraint workflow

Inflated Restraint is an air-inflated cable-restrained pneumatic membrane. In this class of structural hybrids the cutting pattern plays a critical role in the scalability,

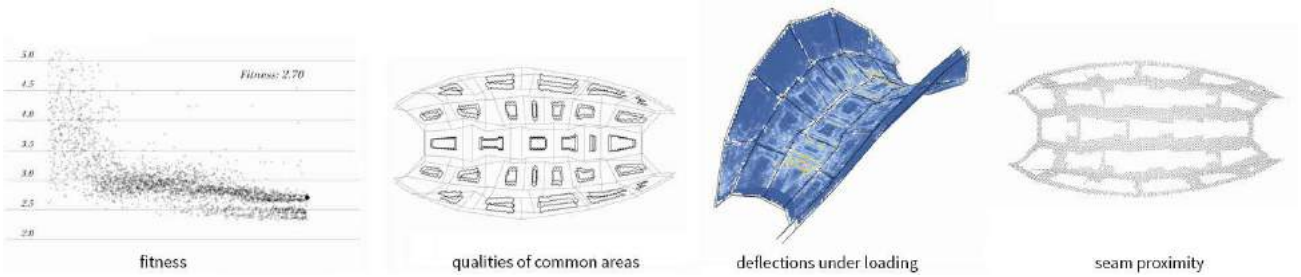

Figure 9: Left: Fitness over time. Right: Fitness criteria that are combined into an overall measure of energy

mechanical performance and resulting aesthetic of the membrane. Architectural membranes are generally characterised by rational patterns with minimal deviation between discrete textile elements. We investigate a method for producing irregular cutting patterns that offer an extension of possible surface languages, achieving defined design volumes with complex surface curvature and the generation of cable restraint topology. To demonstrate this we define a target geometry with areas of pronounced anticlastic curvature. This class of curvature is 'unnatural' to pneumatic systems and embeds an efficacy test for our pattern generation method and fabrication approach. We analyse the mesh curvature of the target geometry to identify and separate regions of synclastic and anticlastic curvature. A k-means clustering algorithm is then used to group mesh faces according to approximate curvature in each of the separated regions. Graph traversal methods (Depth First Search and Dijkstra's Shortest Path) are then employed to further sub-divide the localised curvature regions into individual patches for fabrication. The naked edges of these patches are then dynamically relaxed to smoothen the boundary edge, ready for laser-cutting and sewing.

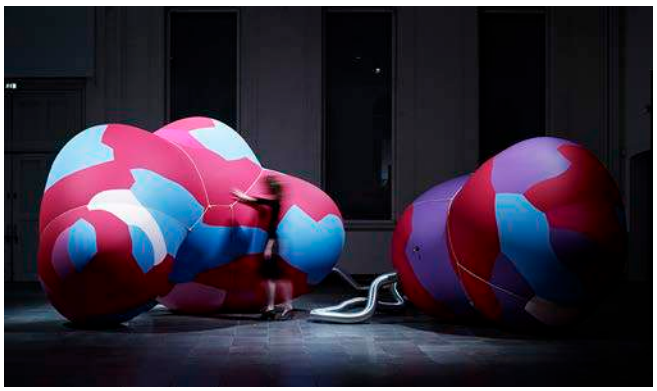

Figure 10. A Bridge Too Far in the Complex Modelling exhibition.

The topology model of the cable restraint is also derived from curvature analysis of the design target model. In this case, we firstly identify areas of anticlastic curvature, the 'lowest' points of the membrane surface, to establish the primary loops of the net. This ensures that they do not exhibit 'slippage' on the membrane when under tension. Further edges are added to the net topology using search criteria that combines finding areas of lowest synclastic curvature (to relieve membrane stress) and being approximately equidistant from each other (to ensure even distribution). In simulation, we 'inflate' the membrane model to verify its interaction with the cable restraint model. Here, the measure of success is that the net does not 'slip' and the two systems find, and maintain, equilibrium across the operating pressure range. The modelling workflow as a whole is verified by comparison with the physical demonstrator. Here, the measures of success are that the inflated surface achieves the desired curvatures, that the membrane has a smooth transition across patches and that there are no areas of compression resulting in unsightly and underperforming wrinkles (Fig. 11).

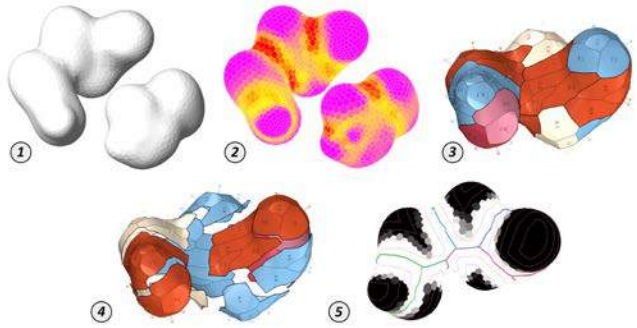

Figure 11. Stages in the modelling workflow. 1. a defined target model; 2. curvature analysis of the design model; 3. subdivision of the surface; 4. breaking into discrete models for refinement; 5. first stage of cable-restraint topology generation.

6 CONCLUSION

Complex Modelling takes point of departure in the understanding that the development of architectural design and its material practices is impeded by our inability to comprehend and capture the complexity of more hybrid and more bespoke material systems. If current building practice is optimised through a modus mass production, Complex Modelling asks how future more complex and more hybrid building systems that take advantage of the complex interactions of stress and strain could look and what the logic of the underlying systems of representation and analysis could be.

The modelling workflow presented here seeks to prototype how future design methods can integrate simulation in ways that support the design of complex and highly interdependent material systems. Where the Complex Modelling projects presented in the paper are highly speculative and rarefied, they explore how advanced computational modelling and its strategic integration of different modes of simulation with varying degrees of accuracy and precision allows us to reconsider how architecture is designed, built and understood.

In this workflow simulation is no longer conceived as a simple division between the practices that belong to generative design thinking or analysis and evaluation. Instead, modelling as a whole is understood as the strategic construction of a network of dedicated sub-models in which simulation models for both design generation and analysis appear as distributed and recurrent events across the design chain. The essence of this practice is that:

- That there are multiple sub-models and that they are composed in an overarching modelling network (workflow)
- That the overarching modelling network integrates different kinds of simulation that operate at different levels of fidelity according to locally available information and needs for design accuracy and precision
- That the dedicated sub-models are locally validated and verified in respect to the particular mode of analysis undertaken
- That information is passed between the models through different kinds of handshakes with different levels of sophistication operating within the models

ACKNOWLEDGMENTS

Complex Modelling is supported by the Danish Council for Independent Research, The Sapere Aude Initiative. We gratefully acknowledge the support of our collaborators, research assistants and interns.

REFERENCES

1. Deleuran, A. H., Tamke, M., and Ramsgaard Thomsen, M. Designing with Deformation: Sketching Material and Aggregate Behaviour of Actively Deforming Structures. SimAUD (2011)
2. Ramsgaard Thomsen, M. Complex Modelling - questioning the infrastructures of information modelling. Complexity & Simplicity - eCAADe Conference, 1, (2016) 33-42
3. Kolarevic, Branko, and Ali Malkawi. Peformative Architecture. Routledge (2005)
4. Tamke, M., Nicholas, P. and Riiber, Jacob. The Agency of Event: Event Based Simulation for Architectural Design. Design Agency: Proceedings of ACADIA (2011)
5. Tamke, M., Lafuente Hernández, E., Holden Deleuran, A., Gengnagel, C., Burry,M and Ramsgard Thomsen, M. A New Material Practice: Integrating Design and Material Behaviour. In Proceedings of SIMAUD (2012)
6. Tamke, M.,Stasiuk, D., and Ramsgaard Thomsen, M.. The Rise—Material Behaviour in Generative Design. Adaptive Architecture. ACADIA (2015) 379–88.
7. Kilian, A., and Ochsendorf, J. Particle-Spring Systems for Structural Form Finding, IASS), 46, 147 (2005)
8. Ramsgaard Thomsen, M., Tamke, M., Ayres, P., and Nicholas, P.CITA works. Riverside Press (2015)
9. Nicholas, P., and Tamke, M. Computational Strategies for the Architectural Design of Bending Active Structures. IJSS, 28, 3/4 (2013)
10. Deleuran, A. H., Schmeck, M., Quinn, G., Gengnagel, C., Tamke, M. and Ramsgaard Thomsen, M. The Tower: Modelling, Analysis and Construction of Bending Active Tensile Membrane Hybrid Structures. Future Visions - IASS (2015)
11. Winsberg, E. Science in the Age of Computer Simulation. University of Chicago Press (2010)
12. Brandt-Olsen, C.Calibrated Modelling of Form-active Structures. Master thesis, DTU (2016)
13. Quinn, G., Deleuran, A.H., Piker, D., Brandt-Olsen, C., Tamke, M.. Ramsgaard Thomsen, M., and Gengnagel, C. Calibrated and Interactive Modelling of Form-Active Hybrid Structures. Spatial Structures in the 21st Century - IASS (2016)
14. Deleuran, A. H., Pauly, M., Tamke, M., Friis Tinning, I, and Ramsgaard Thomsen, M. Exploratory Topology Modelling of Form-Active Hybrid Structures. TensiNet (2016) 71–80
15. Nicholas, P., Zwierzycki, M., Stasiuk, D; Norgaard, E & Thomsen, M. Adaptive Meshing for Bi-directional Information Flows, AAG (2016) 260-273
16. Tamke, M., Zwierzycki, M., Holden Deleuran, A., Sinke Baranovskaya, Y., Friis Tinning, I. and Ramsgaard Thomsen, M. Lace Wall - Extending Design Intuition through Machine Learning, Fabricate (2017).
17. Nicholas, P., Zwierzycki; M., Norgaard, E., Leinweber, S., Hutchinson, C., and Thomsen, M.R. Adaptive Robotic Fabrication for Conditions of Material Inconsistency: Increasing the Geometric Accuracy of Incrementally Formed Metal Panels, Fabricate (2017)
18. Nicholas, P., Stasiuk, D., Norgaard, E., Hutchinson, C., and Thomsen, M. R. An Integrated Modelling and Toolpathing Approach for a Frameless Stressed Skin Structure, Fabricated Using Robotic Incremental Sheet Forming, RobARCH (2016) 62-77

Integrating technical performances within design exploration. The case of an innovative Trombe wall.

Tudor Cosmatu, Yvonne Wattez, Michela Turrin and Martin Tenpierik

TU Delft, Faculty of Architecture and the Built Environment,
Delft, The Netherlands
{T.Cosmatu, Y.C.M.Wattez, M.Turrin,
M.J.Tenpierik}@tudelft.nl

ABSTRACT

The Double Face 2.0 research project aims at developing a novel type of an adaptive translucent Trombe wall. The novelty of the proposed system is based on the integration of new lightweight and translucent materials, used both for latent heat storage and insulation, advanced computational design processes, used to identify the relationship between variations in geometry and their effect in terms of overall performance, as well as proposed fabrication methods based on Fused Deposition Modelling. Various concepts and geometric configurations are explored and improved via a computational design workflow. The exploration is deeply rooted in performance simulations manufacturing constraints and measurements of prototypes. The paper presents the workflow of the overall on-going research project, with specific emphasis on the incorporation of a computational assessment and optimization process. Moreover, it presents the preliminary set of measurements and simulations for thermal performances, their results and related conclusions.

Author Keywords

Simulation-based design; data driven design; building comfort and energy performance.

1 INTRODUCTION

The presented research through design project consists of two sequential stages: the Double Face 1.0 (DF 1.0), which produced a preliminary demonstrator and the DF 2.0, a currently on-going further development and refinement stage. The overall project tackles the integration of technical requirements into the architectural language. In architectural designs, technical requirements are often perceived as limiting constraints rather than inspiring design principles. At contrary, the project develops a workflow for incorporating technical aspects from building physics and from the fabrication process, to support the integration of the engineering performances into the design of the product through an iterative form-finding approach. It does so by focusing on the case of an innovative Trombe wall, conceived as an interior adaptive translucent system. The workflow is being used for multiple design concepts, some of which will be prototyped, and eventually validated via 1:1 demonstrators.

Trombe walls have been implemented as means of passively storing solar heat for more than a century, constantly evolving from the first patent filed by Edward Sylvester Morse in 1881, to the one popularized by the French engineer Felix Trombe in the late 1960's [1]. It generally comprises of a system oriented towards the winter sun composed of an opaque wall (thermal mass), glazing and an air cavity in-between. Through adjustable vents located in the upper and lower part of the wall, air movement can be encouraged creating a convective loop. This allows the heated cavity air to flow towards the interior and the cold air from the interior to be pulled in the cavity.

The proposed Trombe wall is different from traditional Trombe walls for two main reasons: it has the ability to adjust itself towards the heat source or sink and therefore to direct heat absorption and its release where and when needed and it allows daylight transmittance. To achieve these goals, both geometry and innovative materials are investigated. Geometric investigations aim at form-finding as an integral system incorporating multiple design or performance criteria. When complex geometry emerges, fabrication methods such as Fused Deposition Modelling and robotic Fused Deposition Modelling are used. Focusing on the innovative materials, the solid thermal mass of a typical Trombe wall is replaced by phase-change materials (PCM) while the insulation layer consists of translucent aerogel.

PCMs are substances with a high heat of fusion. By changing phase (solid to liquid or liquid to solid) the material can serve as a heat storage [2]. Using PCM as heat storage has a great potential of reducing the energy consumption of buildings [2]. One of the first documented usage of PCM in the construction sector, dates back to 1948 when one of the pioneers of solar energy usage, Dr. Maria Telkes, designed the Dover House [3]. Drums filled with Glauber's salt were housed between the main rooms. Ventilation was used to deliver warm air in winter and cool air in summer. While this system could deliver heat for up to 11 sunless days the target of the DF 2.0 Trombe wall is a daily cycle. More recent projects such as the Wilo headquarters in the Netherlands by Benthem Crouwel Architects make use of the heat-storage capacity of PCM

doubling the thermal mass of the lightweight building to prevent the interior from overheating. In the case of the Floating Pavilion, by Public Domain Architects and Deltasync, PCMs are used in order to pre-cool or pre-heat the fresh air supply. The recharging of the PCM is controlled by air conditioning units. Several researchers have investigated the use of phase change materials in facades [4, 5, 6, 7]. However, all of these researchers considered static non-adjustable systems.

The starting assumption regarding the composition of the layers for our proposed system places the PCM on one side followed by the insulating aerogel layer, protecting it from the opposite side. The elements composing the wall can be oriented making it possible to face the PCM towards the interior or exterior, depending on the climate conditions and daily cycle. During summer days, the PCM will face the interior, charging itself with heat generated by the users while releasing the heat towards the exterior at night. In winter it will face the sun during the day and release the heat towards the interior at night. The ability of the system to be oriented towards the interior or exterior allows for directed and controlled heat transfer.

The design of the system is under development. The process started with an extensive set of measurements and simulations, to understand the basic parameters of the system and to be able to setup a set of form-finding and optimization loops.

2 OVERALL DIGITAL PROCESS

In the DF 2.0 project, advanced computational means (evolutionary algorithms and clustering techniques) and advanced digital manufacturing techniques (customized additive manufacturing) are applied in order to explore complex geometries and their relationship to performance. The computational process of the research project is meant to facilitate the designer to identify the relations between variations in geometry and the resultant performance oscillations and to integrate the engineering performances within the proposed designs. Specifically, the process aims to integrate hard parameters, such as technical performances for thermal behavior and daylight transmittance, and soft parameters, such as aesthetic values and overall appearance.

The hard parameters rely on approximated material properties up to the point where physical experiments as well as simulations produce implementable results. They include material properties of PCM, material distribution and concentration, controlled by geometrical means, and local surface orientation. They need to target conditions regarding necessary volume for best performance of the PCM, translucency or light permeability, surface morphology as well as adaptability of the proposed systems. In combination with design parameters such as visual connection, they are being included in multi-objective optimization loops to identify their influence over the necessary design objectives allowing sufficient space for unexpected design alternatives.

Additionally, the soft parameters are included and assessed through multiple periodic user interviews. While past interviews were based on common representation techniques, future interviews are planned with the support of virtual reality (VR) to facilitate the users in assessing the soft properties of the proposed system while being able to visualize and understand performance aspects

Figure 1 showcases the workflow for the entire research as well as for the current point in the research process. It highlights the integration between the digital design workflow and the inputs from designers and users. The

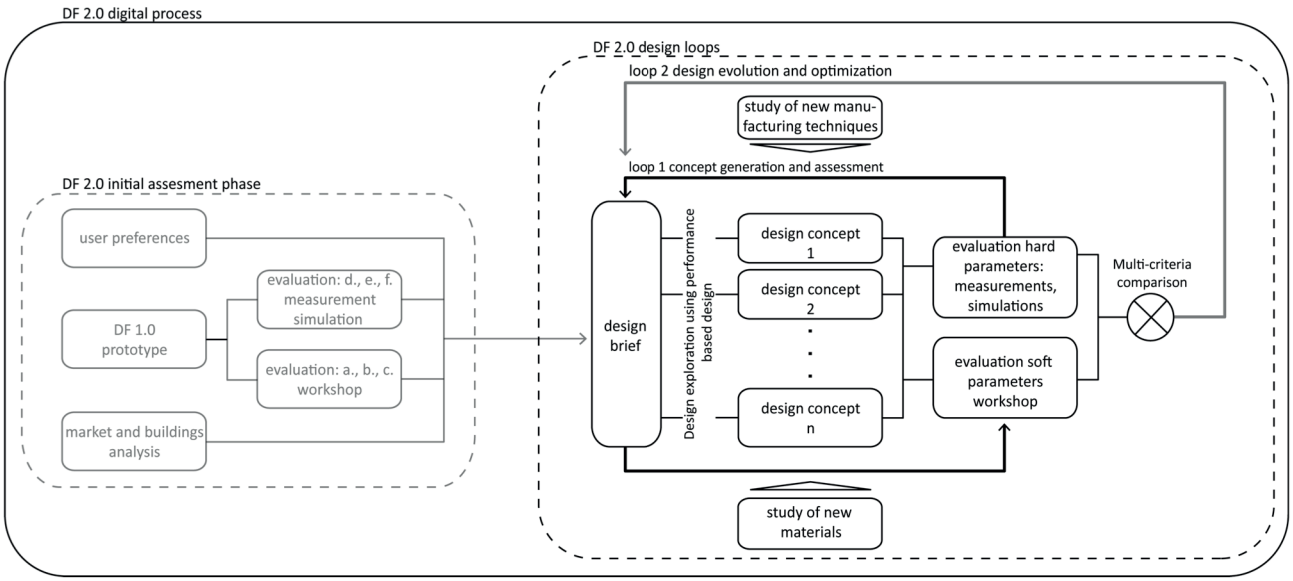

Figure 1. Research process and computational workflow

Figure 2. Demonstrator developed during DF 1.0

overall workflow of the research is divided in two interconnected parts.

The preliminary measurements and simulations were performed during DF 1.0. This phase is represented by the cumulus of user preference studies, market and building analysis and the evaluation through simulation and measurements based on the DF 1.0 demonstrator (Figure 2). This forms a solid base as well as a catalyst for a first concept development phase of DF 2.0 as well as a knowledge pool for informing and enhancing simulation routines to be implemented during DF 2.0.

Secondly DF 2.0 is arranged along 2 design loops: loop 1, concept generation and assessment phase; and loop 2, design evolution and optimization phase. User workshops are introduced within each loop to further asses and fine-tune the concepts, judging design as well as performance related aspects. At the end of each loop a multi-criteria assessment is carried out.

3 PRELIMINARY MEASUREMENTS & SIMULATIONS

This section presents the initial measurements and simulations from DF 1.0 and a second set of simulations from DF 2.0. Several measurements were carried out during DF 1.0 in order to fine-tune assumed material thicknesses as well as establish the specific type of PCM which would allow for an overall better light transmittance to performance ratio.

In parallel simulations using Design Builder v3.4 pointed out that the best tradeoff between unobstructed views and heat storage capacity would lead to a ratio of approximatively 10% opening in the system's overall surface. In order to be able to perform more advanced simulations which would allow for the incorporation of other factors such as movement of the components of the wall, a simulation routine was setup in Matlab/Simulink. The relevant settings are presented in Table 1. For this purpose a small room corresponding to the cardinal orientations in the following order N, E, S, W has been used. The ceiling and floor of the room have been assumed to be adiabatic surfaces. The model takes the use of sun blinds,

calculated time (one winter)	1oct - 30 apr
orientation Trombe wall	south
size of room w*d*h	3.6*5.4*2.7
size window south	80%
size of window north	40%
U-glass	1.65 [W/m2.K]
solar heat gain no sunblind	0.6
people present (7 days a week)	18.00-8.00 h
if PCM panel present	
PCM solid	> 23 Celsius
PCM liquid	> 26 Celsius
% closed wall (no holes)	0,9
thickness of PCM	different per setup
thickness of insulation	0.01 [m]
PCM_c	2000 [J/(kg K)]
PCM_rho	1450 [kg/m3]
PCM_la	0.6 [W/(m K)]
PCM_h	1.8e5 [J/kg]
INS_c	1440 [J/(kg K]
INS_rho	75 [kg/m3]
INS_la	0.012 [W/(m K)]

Table 1. Settings used for the simulations in Matlab

the presence of users, as well as the existence of ventilation into account. As such the model is a full energy performance model including solar gains, internal heat gains, ventilation and infiltration losses, transmission losses through the facades, heat storage in walls, temperature set-points, schedules, etc.

The results are shown in Figure 3. The results give an overview of the amount of energy needed to heat a room. This is 4,78 GJ per winter period. When a Trombe wall of 4 cm concrete is added, the needed energy reduces to 3,71 GJ. When the concrete is replaced by PCM, the needed energy drops to 3,18 GJ. This is a reduction of 33%. The optimum though, lies at a thickness of 1-2 cm of PCM. Here a decrease of 30-32% is achieved.

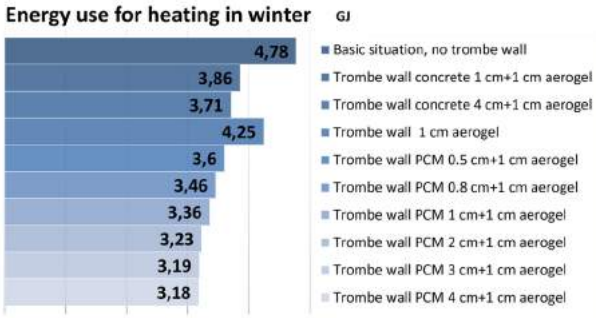

Figure 3. Results regarding the energy use

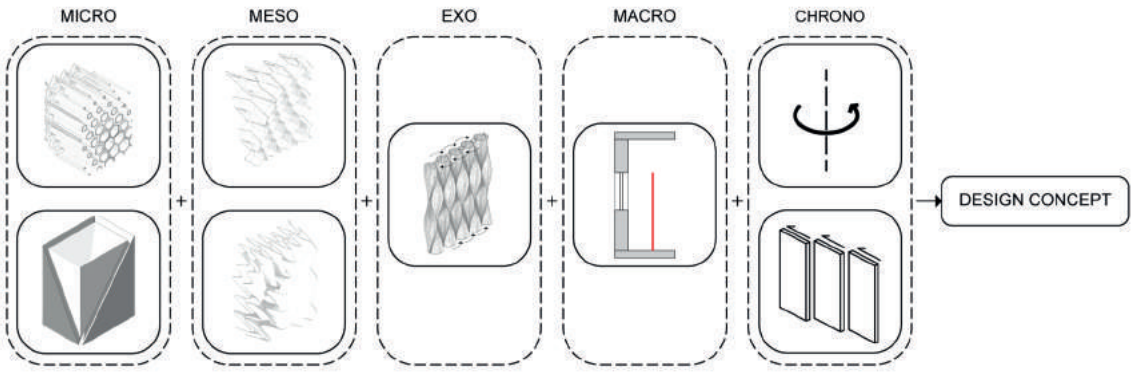

Figure 4. Design concept generation

4 DESIGN WORK

Together with observations from the fabrication spectrum, the preliminary results from simulations and measurements have helped identify multiple levels of design decisions. To make these levels explicit, a mind-map consisting of five categories has been developed. The five categories are: *Micro* referring to the geometrical intricacies at a sectional level; *Meso* regarding the level of detail at the surface level; *Exo* defining a design principle; *Macro* categorizing the possible position within the section of a room; and *Chrono* referring to the type of movement used for adjustment of the wall. The map collects and organizes a broad range of geometric alternative options. For simplicity, Figure 4 summarizes the main principles regarding multiple design scales as well as the concept generation process. Combination of multiple elements per category is possible; nevertheless some of the principles have a certain set of prerequisites embedded in them, acting as constraints for the overall design concept.

User workshops complement the design loops regarding criteria such as: identity, whether the intended use is visible through the chosen design and overall composition; usefulness, whether technical performances are met; and applicability, whether a home or office environment are better suitable for a particular design (Figure 1).

5 FUTURE DEVELOPMENT

Based on the results of the first workshop, the highest scoring concepts are being further analyzed in order to extract either information which might be applicable to other concepts or which will inform the evolution of the existing concepts. The individual concepts will be optimized towards visibility, structural performance, light transmittance and thermal performance. Currently, additional simulations, measurements and further implementation of geometric features within the mind-map are being developed. These will be studied in a layered simulation loop. Simulations regarding airflow and temperature changes within a simplified 2D representation of a room caused by the proposed systems will be investigated with the use of Comsol Multiphysics. Simulations regarding sunlight exposure, radiation values as well as desired transparency percentages will be carried out on a simplified geometrical assembly corresponding to the Macro level (Figure 4) with the use of Grasshopper and relevant plugins such as Ladybug and Honeybee. Resulting simulation data will be visualized and examined within ModeFrontier through the Grasshopper integration node allowing a multi-objective optimization and evaluation loop. Further more detailed CFD simulations will be developed and performed on selected designs in order to validate and improve micro level design decisions in respect to material behavior caused by the proposed geometries. The results of these simulations will be quantified and applied on the designs in an iterative manner.

REFERENCES

1. Smith, D. L. Environmental Issues for Architecture. Wiley 2011
2. Harland, A.; Mackay, C.; Vale, B. Phase Change Materials in Architecture
3. Kosny, J.; Shukla, N.; Fallahi, A. Cost Analysis of Simple Phase Change Material-Enhanced Building Envelopes in Southern U.S. Climates (2013)
4. Castellon, C.; Castell, A.; Medrano, M.; Martorell, I.; Cabeza, L.F. (2009). Experimental Study of PCM Inclusion in Different Building Envelopes. *Journal of Solar Energy Engineering. 131: 1-6.*
5. Kolaitis, D.I.; Martinez, R.G.; Founti, M.A. (2015). An experimental and numerical simulation study of an active solar wall enhanced with phase change materials. *Journal of Façade Design and Engineering 3: 71-80.*
6. Fiorito, F. (2012). Trombe walls for lightweight buildings in temperate and hot climates. *Exploring the use of phase-change materials for performance improvements. Energy Procedia 20: 1110-1119.*
7. Weinläder, H.; Beck, A.; Fricke, J. (2005). PCM-façade-panel for daylighting and room heating. *Solar Energy 78: 177-186*

3D-Printing, Topology Optimization and Statistical Learning: A Case Study

Vishu Bhooshan[1], **Mathias Fuchs**[1] **and Shajay Bhooshan**[1]

[1]Zaha Hadid Architects, Computation & Design Research Group (ZH_CODE)
10 Bowling Green Lane London, UK EC1R 0BQ
{firstname.lastname}@zaha-hadid.com

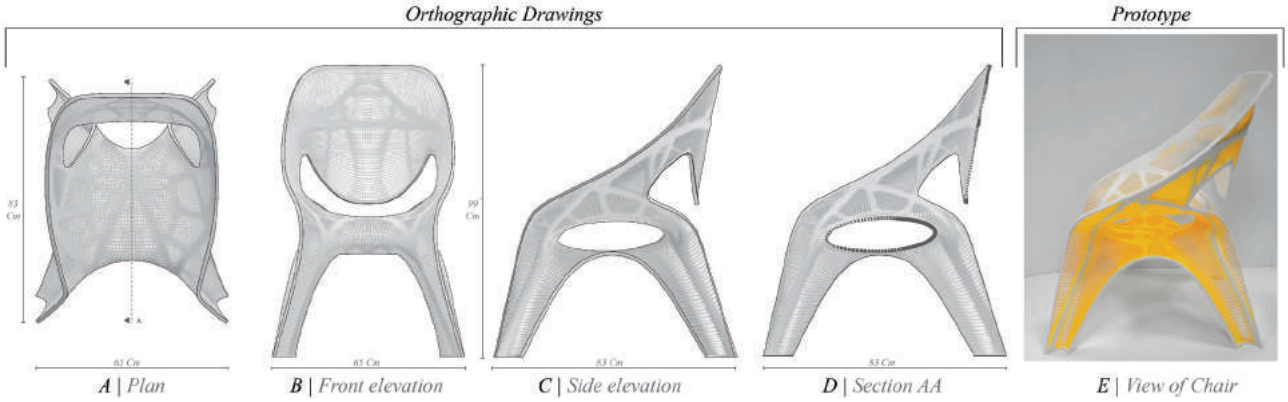

Figure 1: The Chair Prototype

ABSTRACT

This research paper explores the use of 3D-printing technologies in prototyping of Topology Optimization (TO) driven design. The paper describes the integration of TO into an early design work-flow and highlights the difficulties thereof. Due to the high computation times of TO, we outline the use of statistical learning to approximate TO material density results. Specifically, we highlight the use of such techniques for TO of thin-shell, non-volumetric geometries and the incorporation of specific assumptions related to such geometries to improve the functional approximation using statistical methods. We describe the various stages of the design pipeline that benefit from interactive TO.

Author Keywords

topology optimization; 3D-printing; statistical learning; work-flows & digital tools; interactive editing; edit-and-observe;

1 INTRODUCTION

3D-printing, a layer-by-layer additive manufacturing technique [30] is typically used to deliver geometrically precise, functional prototypes in a short period of time. It has emerged as one of the key rapid prototyping technologies in the field of product design [11] and in large scale architectural design [18, 25]. Large 3D-printing companies such as Stratasys [36] most commonly use thermoplastics - *ABS* (Acrylonitrile-Butadiene Styrene) / *PLA* (PolyLactic Acid) - as a material. There have been several recent attempts to investigate alternate materializations like clay & concrete [14], resin & metal [21], glass [20] etc. This along with the development in higher precisions and larger build volumes [43] makes 3D-printing conducive to realize customized designs. Topology Optimization (TO), a field of structural mechanics [28] has found increased application in architectural design in recent times [26, 33, 42]. Its use in architectural design is characterized by the outcome of the simulation being dominantly and visually expressed in the final design. Due to the complexity and intricacy of the results, TO is often constrained to research studies [43]. 3D printing has been used increasingly to materialize TO driven designs [21, 40, 24]. TO faces similar challenges of computational time as other Finite Element Method based simulations, making it unsuitable for interactive edit-and-observe design methods preferred by designers. Statistical learning techniques have been previously applied to alleviate similar problems in Computational Fluid Dynamics [39]. Additionally, there are several examples of using domain-specific information to improve the accuracy of the approximation [41]. Although there have been several recent works to reduce computational times for TO [4, 3] and stand-alone applications for interactive TO [1].

In this research paper, we address the use of statistical learning to develop an intuitive understanding of geometry and structure by correlating TO results with local as well as easily computable global geometrical features. Furthermore, we use this understanding to approximate TO results, for non-volumetric design geometries. Thus, in addition to reducing the computation time of TO, we explain TO results through easily interpretable, geometrically meaningful regression coefficients.

SimAUD 2017 May 22-24 Toronto, Canada

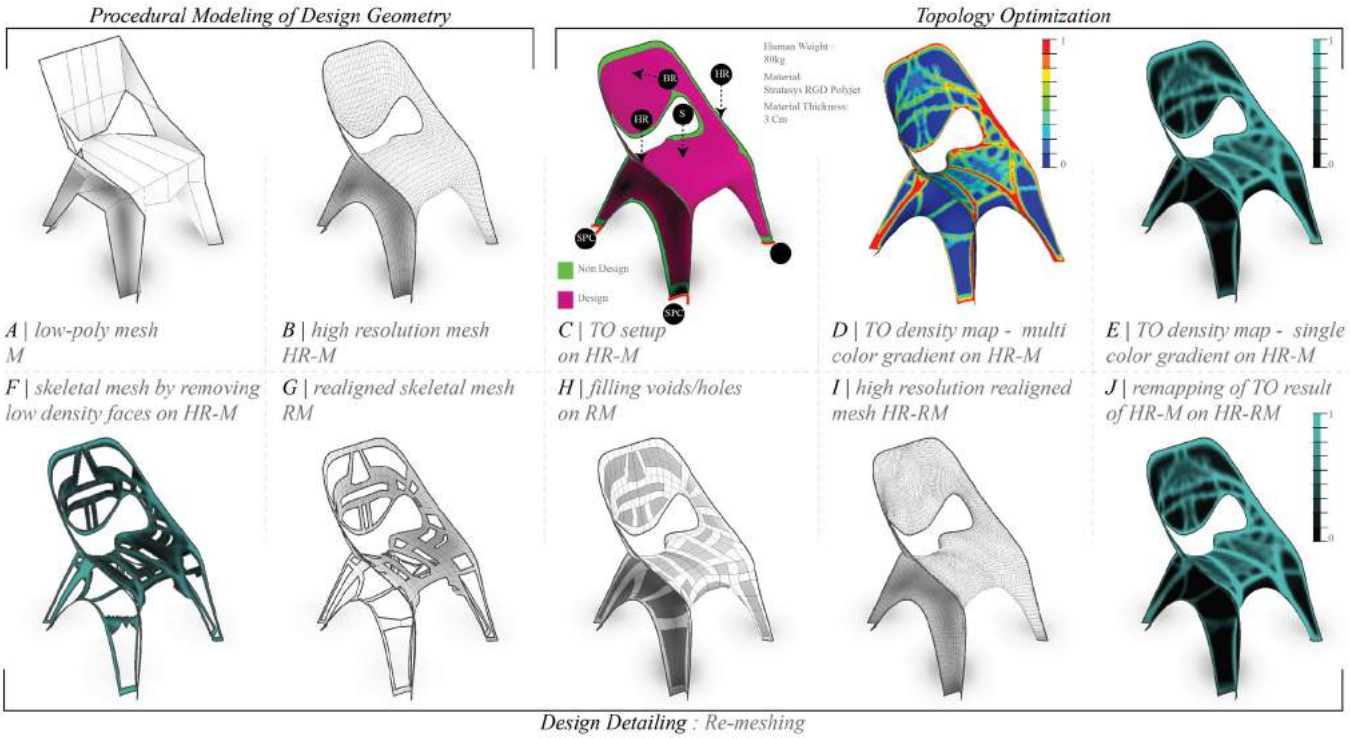

Figure 2. Procedural Modeling, Topology Optimization, and Re-meshing

2 PAPER ORGANIZATION

The paper is prompted by the experiences of using TO for the design and manufacture of a chair (Figure 1) using high-resolution 3D-printing technologies. Section 3 outlines the various stages of the design work-flow that incorporates and highlights the benefits of using procedural modeling of design geometry, TO for structural evaluation and material saving results, re-meshing to produce a structurally aligned geometry and preparation of the geometry for production. In Section 4, we discuss the motivation for using statistical learning to approximate TO results and explain the variables, methods and prediction results. We comment on the extension of the work in both the 3D-printing and statistical learning domain in Section 5, and conclude in Section 6.

3 DESIGN WORK-FLOW

The design work-flow consists of five steps, each of which is described in subsequent subsections.

1. Procedural modeling of design geometry
2. Topology Optimization
3. Re-meshing
4. Parametric design detailing
5. Generating production information

3.1 Procedural Modeling of Design Geometry

Initially, using the process of hierarchical subdivision surface modeling [10], a *low-poly mesh* (M) (Figure 2A) is defined. A manifold M that is predominantly represented by a *quad-faced mesh* lends itself to ease of manipulation of the design geometry and hence helps in creating multiple and quick design iterations. The desired M is then subdivided using the modified Catmull-Clark subdivision scheme inbuilt into Autodesk Maya [35] to create a *high-resolution mesh* (HR-M) (Figure 2B). This improves results from the next step of TO. An iterative perturbation scheme — the so-called *dynamic relaxation* method [6] — is applied to HR-M in order to get an even distribution of quads(Figure 2C).

3.2 Topology Optimization

TO is usually addressed under the heads of size, shape and topology [8]. Each of these have been well researched and documented. For comprehensive understanding on shape optimization, we refer the reader to [29], [7], [15] and to [22], [19] for size optimization.

In this paper we refer to TO by the *homogeneous method* defined as a *distribution problem of isotropic material* which addresses all three aspects of size, shape and topology simultaneously [9]. Given a set of design constraints, support conditions, applied loads, thickness/volume of material, TO is used to *find the optimal layout of a material densities within a specified region* [8]. We have used *Optistruct* [17] and its proprietary optimization algorithm inbuilt in Altair Hypermesh to run the TO simulations.

The process of TO begins by defining the *design and non-design area*. The non-design areas are frozen from the optimization. For the chair, all of the *boundary faces* of HR-M are defined as non-design area and the rest of the faces as design area. All the base *boundary vertices* of HR-M are defined as the support condition which are called as *Single Point Constraints* (SPC). The loads were applied considering

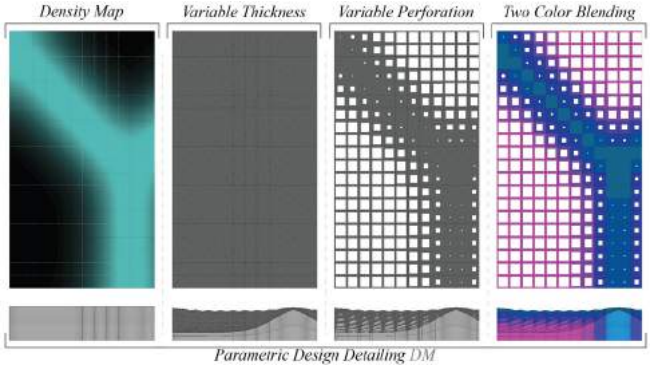

Figure 3. Parametric Design Detailing

an 80 kg human seated on the chair and were classified as load on *seat* (S), *back-rest* (BR) and *hand-rest* (HR) (Figure 2C). The mechanical properties of the material used correspond to the specifications provided by Stratasys - *RGD Polyjet Plastic* [36]. The maximum thickness constraint imposed on the optimization of the chair was 3cm.

3.3 Re-meshing

After the TO simulation , the material distribution map (multi-color gradient) (Figure 2D) showing *material density* per vertex of HRM is converted into a single color gradient (Figure 2E). The density value per vertex varies in the domain of 0 (potential void) to 1 (structural member) [8]. We do a *Re-meshing* of HR-M since the *mesh-edges* of HR-M do not align with the gradient of the TO material density map. A skeletal *Realigned Mesh* (RM) is created using the high material density area of HR-M (Figure 2F-G). Next, the holes of RM (Figure 2H) are filled and converted into a *high-resolution Realigned mesh* (HR-RM) (Figure 2I). The single-color gradient density values of HR-M are then mapped back onto HR-RM (Figure 2J).

3.4 Parametric design detailing

Subsequently, a bespoke algorithm utilizes the material-density information on HR-RM, to create another mesh with varying thickness and perforation (DM) (Figure 3). For the chair, the thickness varies from 3 cm to 1 cm for corresponding vertex density value of 1 and 0 respectively. The perforation were created per face (density value per face computed as average density of all the vertices attached to that face) and the size of the perforation was a percentage of the area of the face. This percentage varied from 0 to 75% for corresponding face density value of 1 and 0 respectively. Since the Stratasys printer could do multi-colored print, the same data of vertex density value are used to create a blend between two user input colors (Figure 3). This process of varying the thickness results in a material saving of 40% in comparison to a geometry of uniform thickness of 3cm. This saving increases to 55%, when thickness and perforation sizes are varied simultaneously.

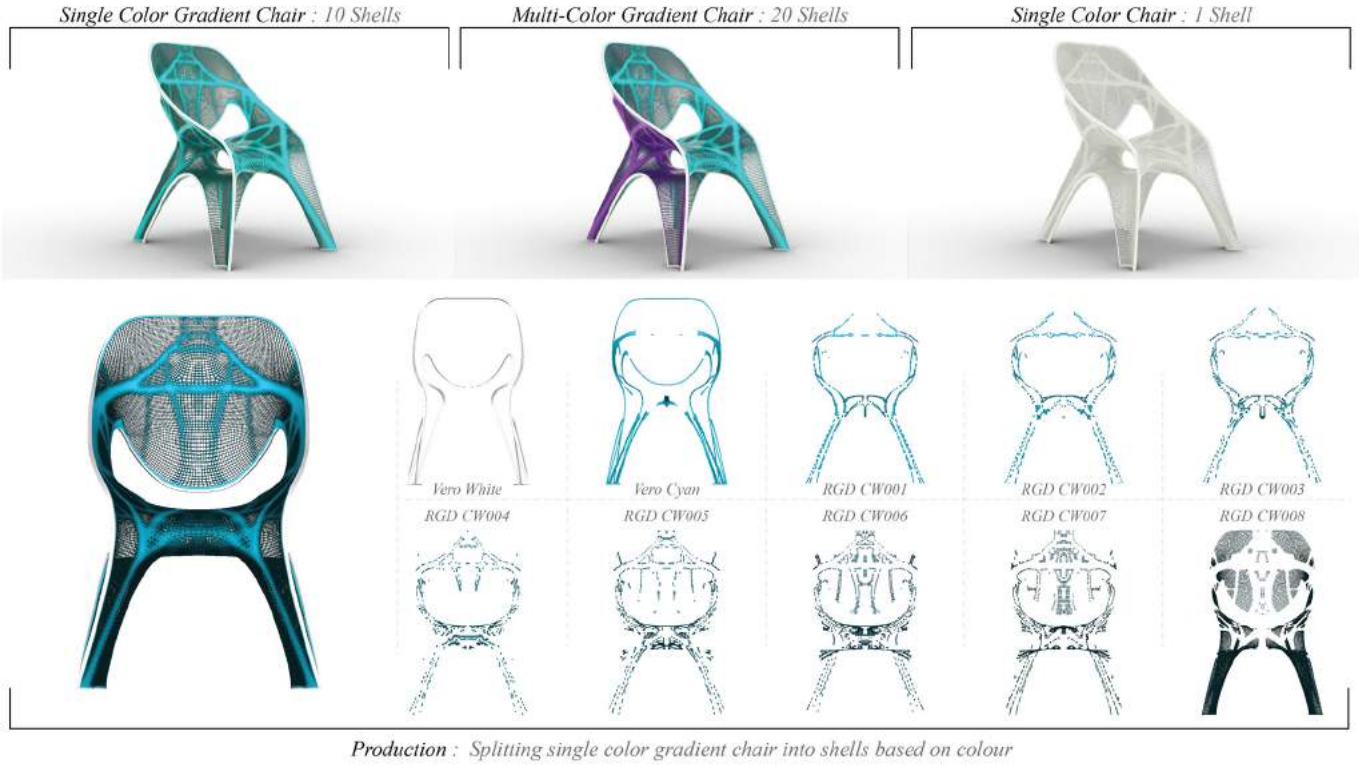

Figure 4. Production Information for 3D-Printing

3.5 Production

The information needed by the 3D-printer was extracted to suit the prevalent industry standard of partitioning design geometry into shells / solids of constant material properties [27]. The number of shells is a function of the number of colors used in the design of the chair (Figure 4) - *single-color gradient chair* (10 shells), *multi-color gradient chair* (20 shells), *single-color chair* (1 shell).

4 APPROXIMATING RESULTS OF TO

TO, as noted in the Section 1, is expensive in terms of computational time. Since the time required to achieve these accurate results is greater than that available in a design work-flow it becomes difficult to integrate TO at the early stage of the design work flow [39]. As such, quick qualitative results that provide interactive feedback to the designer are just as important as the accurate, material-saving results. In order to overcome this difficulty, we looked at statistical learning algorithms to approximate TO results with domain specific data such as *principal curvatures, vertex normals* etc. which are intrinsic properties of the design geometry. Here, we briefly outline our thinking behind the heuristic that was used as part of the statistical learning method. Let us briefly assume the surface to be *funicular*. Then, it is a commonly used approximation to apply the equation describing a deflected membrane stretched by a transverse load ([32, Equation 9.16]). By funicularity, the membrane under pure tension gets inverted "upside down" to a pure compression shell. Thus, we view the surface as a solution of $\Delta z = -w$ where z is the height function of the two variables x, y that parametrize the projection onto the $x-y$ plane, and w denotes the applied load. Let us from now on abbreviate partial derivatives with a subscript. It is well known that the structural properties of a surface can be expressed in terms of the Airy stress function ϕ such that

$$\phi_{yy} z_{xx} - 2\phi_{xy} z_{xy} + \phi_{xx} z_{yy} = -w \tag{1}$$

([2, 3.2.1]) with a function ϕ of x and y. Taking these equations together, one can see that the Airy potential of an equilibrium, compression-only surface can approximately assumed to be the paraboloid $\phi(x,y) = (x^2+y^2)/2$ because its *Hessian matrix* is the unit matrix. Then, (1) simplifies to $\Delta z = -w$. There is the relationship $S = (\sqrt{\det g})g^{-1}\sigma$ ([38] and the corrected version [37]) between $S = \left(\begin{smallmatrix} \phi_{yy} & -\phi_{xy} \\ -\phi_{xy} & \phi_{xx} \end{smallmatrix}\right)$, the metric $g = \left(\begin{smallmatrix} 1+z_x^2 & z_x z_y \\ z_x z_y & 1+z_y^2 \end{smallmatrix}\right)$, and the stress tensor σ. For the particular case where the Airy stress potential is given by paraboloid, the matrix S reduces to the unit matrix. We obtain an approximate explicit formula $\sigma = (\sqrt{\det g})^{-1} g$ or

$$\sigma = \frac{1}{\sqrt{1+z_x^2+z_y^2}} \left(\begin{smallmatrix} 1+z_x^2 & z_x z_y \\ z_x z_y & 1+z_y^2 \end{smallmatrix}\right), \tag{2}$$

expressing the stress tensor in purely local geometric terms. To illustrate this thought by an example, let us suppose, for instance, that the structure is a linear protrusion along the y-axis of a shape that varies only along the x-axis, and the surface is subjected to self-load so that $w = \sqrt{1+z_x^2+z_y^2}$. Then, $z_y = 0$, and (2) means that the compression in a catenary arch satisfies $\sigma = \left(\begin{smallmatrix} \cosh(x) & 0 \\ 0 & 0 \end{smallmatrix}\right)$ in accordance with well-known theory on catenaries and funicular arches [23].

One can prove that the "true" stress tensor $\boldsymbol{\sigma}$ seen as a linear self-maps of the tangent vector space to the structure at any interior point and σ are related by the intertwining relation $\boldsymbol{\sigma} = dz\ \sigma\ (dz)^{-1}$ where dz is the differential of z as a function of x and y. Thus, the eigenvalues of $\boldsymbol{\sigma}$ and σ agree.

Taking these thoughts together, the principal stresses of a compressive structure in equilibrium are approximately the eigenvalues of (2), which are quickly calculated and given by $\lambda_1 = \sqrt{1+z_x^2+z_y^2}$, $\lambda_2 = (\lambda_1)^{-1}$. Thus, the principal stresses and their directions are given in terms of the local geometry, bypassing the need to compute them with a finite element analysis. The quantities λ_1, λ_2 are easily obtained from knowledge of the surface normal n. In fact, since

$$\begin{aligned} n &= ((\nabla z)^T, 1)^T / ||(\nabla z)^T, 1)|| \\ &= ((\nabla z)^T, 1)^T / \sqrt{1+z_x^2+z_y^2} \end{aligned} \tag{3}$$

we get λ_2 by the z-component of the surface normal, and λ_1 by its inverse. Since the vertex normal's z-coordinate is less than its inverse, we view it as a heuristic approximation to the principal stress λ_2, and its inverse as one to λ_1. We expect the result of the topology optimization to be tightly linked to the magnitudes of the principal stresses, and therefore include the quantities (3) into the predictive model even though the chair's structure is not free of bending moment, and is therefore not in compression-only equilibrium.

4.1 Geometric Features for Statistical Learning

We were guided by searching for a possible correlation between the TO material density result and geometric features, as listed below.

1. Locally computable geometric features:
   - the principal curvatures κ_1, κ_2 as the most important local geometric features
   - the z-component of the surface's normal vector as well as its inverse, as motivated by the line of thoughts explained in Section 4
   - the angles between the vertex normal and the direction of the applied load, for each of the applied loads (see Figure 5)

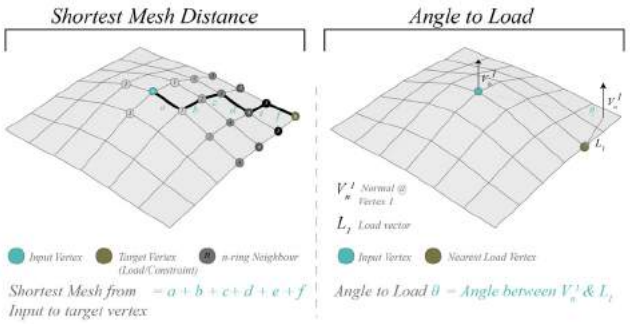

Figure 5. Calculating the Shortest Mesh Distance and Angle to Load

2. Simple globally computable features that are intuitively expected to have an impact on structure
    - the shortest mesh distance to constraint (see Figure 5)
    - the shortest mesh distances to the closest load point, for each of the applied loads (see Figure 5)

In total, our first model was one with nine linear features. In other words, the prediction was based on a *linear predictor* which is a linear combination of these nine features and a constant term called *intercept*. Moreover, we fitted a quadratic model, adding all possible quadratic terms to these , i.e., all two-fold products of any two features out of these, with the only exception being the product between the z-component and its inverse because it is equal to one and would therefore not add predictive value. Likewise, a cubic model incorporated all possible one-fold, two-fold and three-fold products of variables out of these nine variables.

For instance, the linear model featured linear combinations of the principal curvatures κ_1 and κ_2, and therefore made the mean curvature, the sum of κ_1 and κ_2, available as a predictive feature. The quadratic model, in turn, also incorporated the Gaussian curvature, the product of these two.

In total, there were $130 - 8 = 122$ predictors in the cubic model, including the intercept. Since the TO density results, obtained using the same TO setup explained in Subsection 3.2, were distributed on the unit interval $[0, 1]$ and therefore not normally distributed, linear regression had to be discarded. Instead, the density result had to be "*binned*" or "grouped". We applied a grouping threshold of 0.32, the median of the learning data's densities in such a way that both bins had the same size. For a refined analysis, the high density values were further subdivided into two groups of the same size, yielding three groups with the thresholds 0.32 and 0.63. Thus, there was a binary prediction target {low, high} and a three-class prediction target {low, middle, high}. For the former, we chose logistic regression, and for the latter ordinal logistic regression. We refer the reader to the vast statistical literature for introductions to these classical concepts, see for instance [16] as well as [13] and the references therein. For logistic regression, the prediction goal is binary, namely to discern between high and low topology-optimized values of the density D. In logistic regression, the prediction is based on the value of the linear predictor

$$\text{Prob}(D = \text{low}) = \\ (1 + \exp(-(\beta_0 + \beta_1 X_1 + \beta_2 X_2 + \dots)))^{-1}, \quad (4)$$

where each X_i is a product of one, two or three features out of those described in Subsection 4.1, β_0 is the intercept, and the β_i are the coefficients which are being fitted by the learning. For multi-class prediction, we used an ordinal cumulative probability model ([31]). In it, one models the ordered stages of the discretized prediction target $D \in$ {low, middle, high} by means of the expression

$$\text{Prob}(D \leq y) = (1 + \exp(\beta_0^y - (\beta_1 X_1 + \beta_2 X_2 + \dots)))^{-1},$$

where $y \in$ {low, middle, high}. Note that only the intercepts are assumed to depend on y. The coefficients β_i are to be estimated.

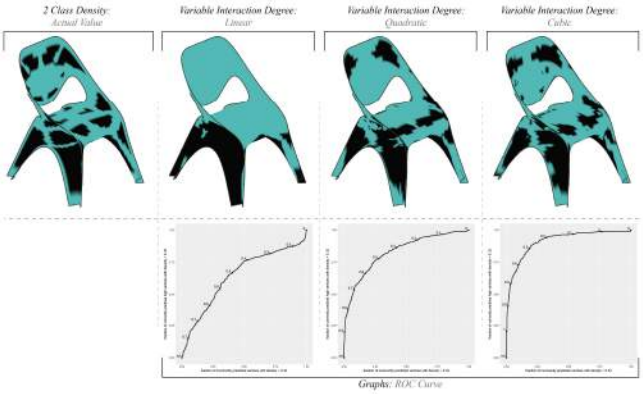

Figure 6. Predictions with Variable Interaction Degrees and corresponding ROC curves. The closer the ROC curve to the upper left corner, the better.

In order to prevent over-fitting, we strictly separated learning and testing geometries: models were either used for training or for testing, but not for both. Specifically, the geometry groups of Figure 7A were used for learning the models, which were subsequently evaluated on the geometry groups of Figure 7BCD.

4.2 Prediction Results

The prediction improved, as anticipated, when passing from the linear over the quadratic to the cubic model (Figure 6). The evaluation of the model was done on the final chair's geometry.

Figure 7 contains predictions of the best model, the cubic model, on alternative geometry. Mostly, the geometric shape of the area formed by vertices with high density was accurately mapped. The model performed better in areas with highly variable geometry, such as the armrests, the backrest, and the legs, whereas in flat regions such as the seat, the prediction was weaker. The best prediction accuracy of up to 84% (i.e., the proportion of correctly classified vertices) was reached on the groups of Figure 7BC which had only minor geometric deviations from training geometries of Figure 7A. However, the geometries with larger geometric deviations of Figure 7D had an accuracy of only 68% to 75%. Prediction with a logistic regression model with linear but without quadratic and cubic terms resulted in the coefficients given in Table 1 containing the coefficients β_i as defined in (4) in the first column. The second column indicates the p value, whose meaning is roughly described as the probability of observing such a high value of the corresponding coefficient by chance

	Estimate	two-sided p-value
(Intercept)	-1.59	
κ_1	-0.02	$< 10^{-40}$
κ_2	0.02	$< 10^{-14}$
shortest mesh distance to constraint(SPC)	-0.66	$< 10^{-10}$
vertex normal z	-2.60	$< 10^{-32}$
shortest mesh distance to load S	0.28	$< 10^{-2}$
angle to load S	0.03	$< 10^{-20}$
shortest mesh distance to load BR	0.26	$< 10^{-3}$
angle to load HR	-0.003	$< 10^{-6}$
(vertex normal z) ^{1}	0.01	$< 10^{-8}$

Table 1. Estimated coefficients of the linear logistic model

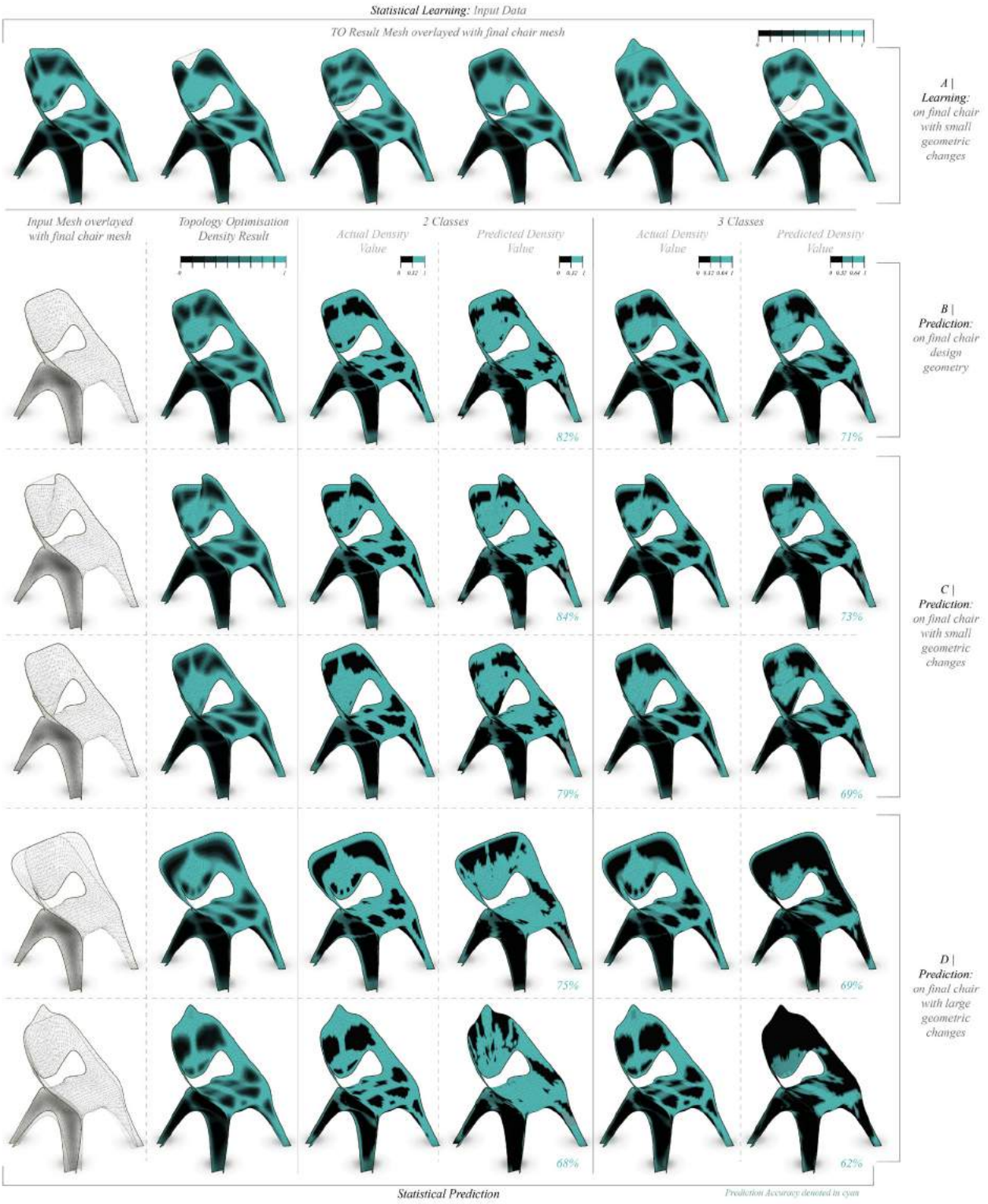

Figure 7. Statistical Learning and Prediction Results

if the true coefficient was zero, i.e., if the corresponding variable had no real influence on the prediction target.
Table 1 contains a few remarkable results. The magnitudes of the influences of κ_1 and κ_2 are the same but their signs are opposed to each other, implying that their difference has predictive value rather than their sum, the mean curvature. The

influence of the shortest distance to the constraint is negative, implying that the density increases close to the constraint, as expected. The distances to the loads, however, have positive influence. The vertex normal's z-coordinate, the heuristic approximation to the second principal stress λ_2 has negative influence, its inverse has positive influence. All features are highly statistically significant (p-values < 0.05). The most powerful model, the cubic one, however, is harder to interpret since in it, each variable occurs often, in different products.

5 FUTURE WORKS

The objective of using TO in the early design work-flow, production of geometry for multi-color 3D-printing and finding correlation between geometric features and TO density results using statistical learning were successful. However issues raised and results obtained during these processes have scope for development under the domains explained below.

Automation of Re-meshing

The process of re-meshing (Subsection 3.3) is currently done manually. We propose to develop on research of *skeletal extraction* [5] to automate the process of extraction of skeletal mesh based on the TO results.

3D-Printing

The current production process prohibits the usage of smooth gradients, due to the limited number of colors available in the material color catalog [36]. The constraints of the printer provided by Stratasys also governed the use of constant material properties for the production shells in the 3D-printed prototypes. We propose to build on research of *voxel based/ data driven material* [12] as a transfer of production information with the printer in order to create smooth gradients in color and multi-material prints. Our design work flow incorporating TO is easily amenable to generate data on material property variation based on structural results.

Statistical learning of structural properties

The current prediction performs reasonably well as long as the learning and the predicting geometries remain within a given series of related geometries. We plan on expanding the prediction radius to more distant or distorted geometries than those the model was learned on. In that vein, we envisage to add further co-variables to those enumerated in Subsection 4.1 in order to improve the prediction. To be more precise, let us recall that the coefficients of the higher order terms indicate the best-fit description of the surface in terms of the graph of polynomials of higher degree [34]. These coefficients provide good candidates for further locally computable geometric features that are empirically correlated with structural features.

Another venue for future work is the challenge to predict the principal stress directions. In a first step, it is possible to derive an immediate good guess of the principal stress directions on funicular surfaces, along the lines developed in Section 4. The approximation might be improved by finding better ways of local guesses of the Airy function associated with the geometry and the loading conditions, thereby implying the stress tensor field.

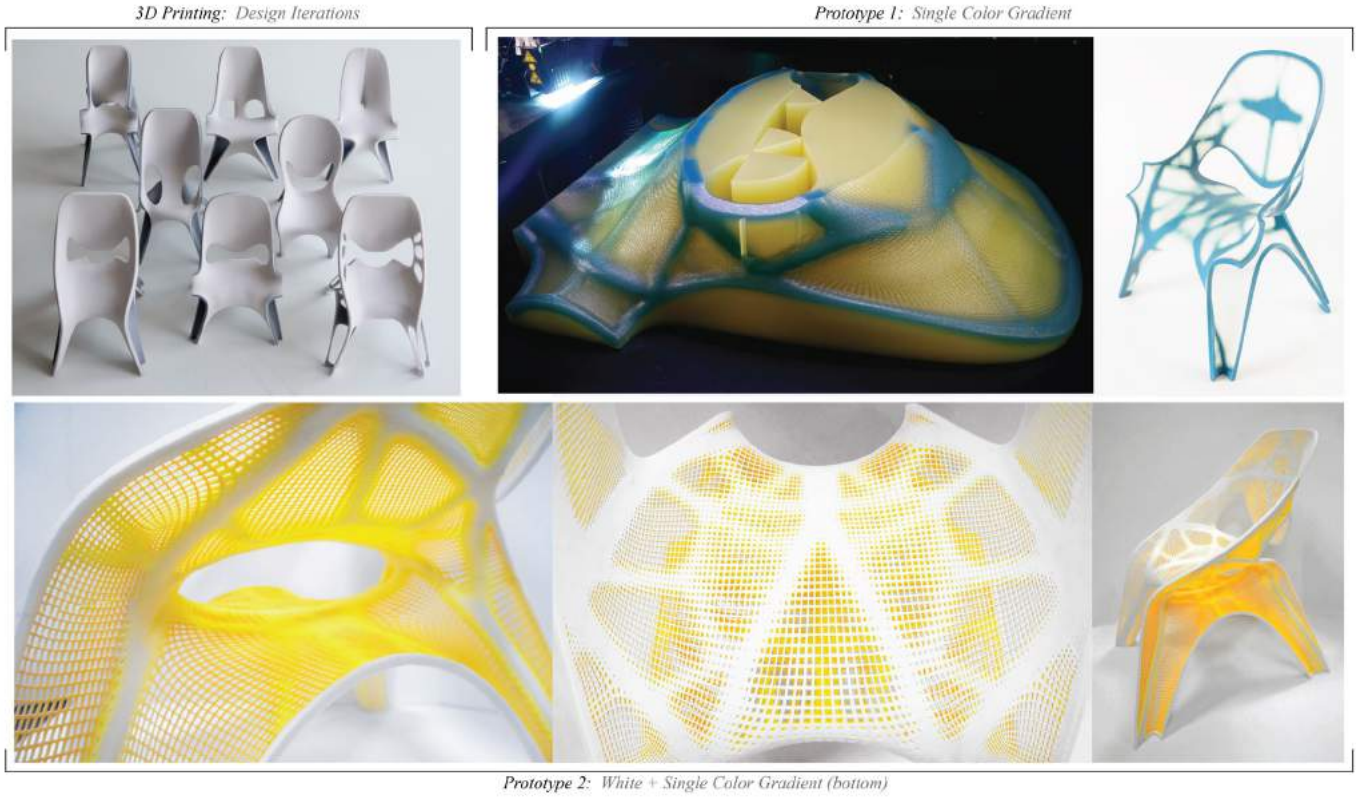

Figure 8. 3D-Printed Chair Prototypes

6 CONCLUSION

The successful realization of TO-driven design prototypes with multi-color 3D-printing (Figure 8), integration of TO into a design friendly environment (Autodesk Maya) and the description of a novel method to approximate TO results for mesh/surface-based geometries using statistical learning are the primary contributions of this paper. In addition, we have highlighted how the regression results might be used to improve an intuitive understanding of the relationship between geometry and structure.

ACKNOWLEDGMENTS

This research was carried out with the support and guidance of Zaha Hadid Architects, especially Patrik Schumacher. We would like to thank Stratasys, our research collaborator and technical support on 3D-printing, and Altair for technical support on Hypermesh.

REFERENCES

1. Aage, N., Nobel-Jørgensen, M., Andreasen, C. S., and Sigmund, O. Interactive topology optimization on hand-held devices. *Structural and Multidisciplinary Optimization 47*, 1 (2013), 1–6.
2. Adriaenssens, S., Block, P., Veenendaal, D., and Williams, C. *Shell structures for architecture: form finding and optimization*. Routledge, 2014.
3. Amir, O., Aage, N., and Lazarov, B. S. On multigrid-cg for efficient topology optimization. *Structural and Multidisciplinary Optimization 49*, 5 (2014), 815–829.
4. Andreassen, E., Clausen, A., Schevenels, M., Lazarov, B. S., and Sigmund, O. Efficient topology optimization in matlab using 88 lines of code. *Structural and Multidisciplinary Optimization 43*, 1 (2011), 1–16.
5. Au, O. K.-C., Tai, C.-L., Chu, H.-K., Cohen-Or, D., and Lee, T.-Y. Skeleton extraction by mesh contraction. *ACM Transactions on Graphics (TOG) 27*, 3 (2008), 44.
6. Barnes, M. R. Form finding and analysis of tension structures by dynamic relaxation. *International journal of space structures 14*, 2 (1999), 89–104.
7. Bendsøe, M. P. Optimal shape design as a material distribution problem. *Structural optimization 1*, 4 (1989), 193–202.
8. Bendsoe, M. P. *Optimization of structural topology, shape, and material*, vol. 414. Springer, 1995.
9. Bendsoe, M. P., and Sigmund, O. *Topology optimization: theory, methods, and applications*. Springer Science & Business Media, 2013.
10. Bhooshan, S., and El Sayed, M. Use of sub-division surfaces in architectural form-finding and procedural modelling. In *Proceedings of the 2011 Symposium on Simulation for Architecture and Urban Design*, Society for Computer Simulation International (2011), 60–67.
11. Chua, C., Teh, S., and Gay, R. Rapid prototyping versus virtual prototyping in product design and manufacturing. *The International Journal of Advanced Manufacturing Technology 15*, 8 (1999), 597–603.
12. Doubrovski, E., Tsai, E., Dikovsky, D., Geraedts, J., Herr, H., and Oxman, N. Voxel-based fabrication through material property mapping: A design method for bitmap printing. *Computer-Aided Design 60* (2015), 3–13.
13. Friedman, J., Hastie, T., and Tibshirani, R. *The elements of statistical learning*, vol. 1. Springer series in statistics Springer, Berlin, 2001.
14. Gosselin, C., Duballet, R., Roux, P., Gaudillière, N., Dirrenberger, J., and Morel, P. Large-scale 3d printing of ultra-high performance concrete–a new processing route for architects and builders. *Materials & Design 100* (2016), 102–109.
15. Haber, R., Jog, C., and Bendsøe, M. P. A new approach to variable-topology shape design using a constraint on perimeter. *Structural Optimization 11*, 1-2 (1996), 1–12.
16. Harrell, F. *Regression modeling strategies: with applications to linear models, logistic and ordinal regression, and survival analysis*. Springer, 2015.
17. Hypermesh, H. Optistruct. *Altair Hyperworks 10*, 0 (2008).
18. Inhabitat. Dubai debuts world's first fully 3d-printed building. **https://goo.gl/QLAJ8v**.
19. Kaveh, A., and Talatahari, S. Particle swarm optimizer, ant colony strategy and harmony search scheme hybridized for optimization of truss structures. *Computers & Structures 87*, 5 (2009), 267–283.
20. Klein, J., Stern, M., Franchin, G., Kayser, M., Inamura, C., Dave, S., Weaver, J. C., Houk, P., Colombo, P., Yang, M., et al. Additive manufacturing of optically transparent glass. *3D Printing and Additive Manufacturing 2*, 3 (2015), 92–105.
21. Larmann, J., and MX3D. Mx3d 3d printed steel bridge. **https://www.dezeen.com/2015/06/13/joris-laarman-3d-printed-bridge**.
22. Lee, K. S., and Geem, Z. W. A new structural optimization method based on the harmony search algorithm. *Computers & structures 82*, 9 (2004), 781–798.
23. Lockwood, E. H. *A book of curves*. Cambridge University Press, 1967.
24. Markopoulou, A., Aguirre, R., Dubor, A., and Khanuja, J. Institute for advanced architecture of catalonia, large scale 3d printing. **=**https://iaac.net/research-projects/large-scale-3d-printing/3d-printed-bridge/.
25. Materials. chinese company 3d prints 10 recycled concrete houses in 24 hours, Jun 2014. **http://www.designboom.com/technology/3d-printed-houses-in-24-hours-04-24-2014/**.
26. Nahmad Vazquez, A., Bhooshan, S., Inamura, C., and Sondergaard, A. Design, analysis and fabrication of expressive, efficient shell structures: a prototype exploring synergy between architecture, engineering and manufacture. In *Proceedings of the IASS-SLTE 2014 Symposium "Shells, Membranes and Spatial Structures: Footprints"*, IASS SLTE (2014).
27. Oxman, N. Variable property rapid prototyping: inspired by nature, where form is characterized by heterogeneous compositions, the paper presents a novel approach to layered manufacturing entitled variable property rapid prototyping. *Virtual and Physical Prototyping 6*, 1 (2011), 3–31.
28. Rozvany, G. Aims, scope, methods, history and unified terminology of computer-aided topology optimization in structural mechanics. *Structural and Multidisciplinary Optimization 21*, 2 (2001), 90–108.
29. Rozvany, G. I., Zhou, M., and Birker, T. Generalized shape optimization without homogenization. *Structural optimization 4*, 3-4 (1992), 250–252.
30. Sachs, E., Cima, M., Cornie, J., Brancazio, D., Bredt, J., Curodeau, A., Fan, T., Khanuja, S., Lauder, A., Lee, J., et al. Three-dimensional printing: the physics and implications of additive manufacturing. *CIRP Annals-Manufacturing Technology 42*, 1 (1993), 257–260.
31. Sall, J. A monotone regression smoother based on ordinal cumulative logistic regression. *ASA Proceedings of the Statistical Computing Section* (1991), 276–281.
32. Selvadurai, A. P. *Partial Differential Equations in Mechanics 2: the Biharmonic Equation, Poisson's Equation*, vol. 2. Springer Science & Business Media, 2013.
33. Søndergaard, A. e. Design, analysis and realisation of topology optimized concrete structures. *Journal of the International Association for Shell and Spatial Structures 53*, 4 (2012), 209–216.
34. Spivak, M. A comprehensive introduction to differential geometry, vol. ii. houston: Publish or perish, 1979.
35. Stam, J. Exact evaluation of catmull-clark subdivision surfaces at arbitrary parameter values. In *Proceedings of the 25th annual conference on Computer graphics and interactive techniques*, ACM (1998), 395–404.
36. Stratasys. Stratasys material catalog. **http://usglobalimages.stratasys.com/Main/Files/Material_Spec_Sheets/MSS_PJ_PJColorMaterials.pdf?v=635785241190888627**.
37. Vouga, E. Self-supporting surfaces. In *Generalized Barycentric Coordinates in Computer Graphics and Computational Mechanics*, N. S. Kai Hormann, Ed. CRC Press, 2017, to appear.
38. Vouga, E., Höbinger, M., Wallner, J., and Pottmann, H. Design of self-supporting surfaces. *ACM Trans. Graph. 31*, 4 (July 2012), 87:1–87:11.
39. Wilkinson, S., and Hanna, S. Approximating computational fluid dynamics for generative tall building design. *International Journal of Architectural Computing 12*, 2 (2014), 155–177.
40. XtreeE. Space truss design and optimization. **http://www.xtreee.eu/2015/08/26/space-truss-design-and-optimization/**.
41. Yu, T., Simoff, S., and Jan, T. Vqsvm: A case study for incorporating prior domain knowledge into inductive machine learning. *Neurocomputing 73*, 13 (2010), 2614–2623.
42. Zaha-Hadid-Architects. Volu dining pavilion. **https://vimeo.com/147482144**.
43. Zegard, T., and Paulino, G. H. Bridging topology optimization and additive manufacturing. *Structural and Multidisciplinary Optimization 53*, 1 (2016), 175–192.

Matrix Architecture: 3D-Printed and Simulated Kirigami Matrices & Auxetic Materials

Madeleine Eggers[1,2], Jingyang Liu[1,2], Jasmine (Chia-Chia) Liu[3,2] ,

Ben Norman[4,2] and Jenny E. Sabin[1,2]

[1]Architecture
Cornell University
Ithaca, USA

[2]Sabin Design Lab
Cornell University
Ithaca, USA

[3]Material Science
Cornell University
Ithaca, USA

[4]Computer Science
Cornell University
Ithaca, USA

ABSTRACT

This paper explores the possibilities of kirigami geometry — folding with the addition of strategically placed cuts and holes — through simulation and kinetic and adaptive architectural assemblies. Typical kinetic assemblies consist of rigid components connected by mechanical joints that offer limited range of motion and tend to require mechatronic actuation. While mechanical motion is adequate for specific applications, mechanically motile systems lack the adaptive potential, elasticity, and embedded intelligence of adaptive structures. We propose to focus on the design of flexible matrices as a way of moving away from stiff, mechanical unitized systems and toward pliable, continuous 2D and 3D structures that can elastically change geometry in response to external stimuli without the need for external mechatronic energy input. As a proof-of-concept, we have produced an integrated panel-and-hinge assembly in which the panels and hinges are not discrete, mechanically connected components, but are instead functional zones of a continuous matrix. In addition, by controlling aspects of the individual units (panel size, hinge geometry, spacing, unit shape), we can induce larger-scale behavioral changes in the whole matrix.

Author Keywords

adaptive architecture; kirigami; simulation and modeling; computational design; 3D printing; material design; programmable matter; auxetic materials

1 INTRODUCTION

As part of two projects funded by the National Science Foundation in the Sabin Design Lab at Cornell University titled, eSkin and Kirigami in Architecture, Technology, and Science (KATS), this paper is one product of ongoing trans-disciplinary research spanning across the fields of architecture, cell biology, materials science, physics, electrical and systems engineering, and computer science. This paper explores the possibilities of kirigami in kinetic and adaptive architectural assemblies. Kirigami is similar to origami, but includes the addition of cuts and holes. The origin of the word comes from the Japanese kiru, “to cut,” a geometric method and process that brings an extra, previously unattainable level of design, dynamics, and deployability to self-folding and -unfolding materials from the molecular to the architectural scale.

ColorFolds, a project produced by Sabin Design Lab 2014-2015, is our largest deployable structure generated with kirigami geometry. The assembly responds in a controlled, kinetic mode to contextual feedback, expressed through optical color and transparency change. The generative design process for ColorFolds began with an examination and study of kirigami processes as a means of creating doubly-curved surfaces through a simple implementation of gradient folding conditions. ColorFolds is an interactive folded assembly prototype composed of a lightweight, tessellated array of interactive components that fold and unfold in the presence or absence of people. ColorFolds was a successful prototype in the exploration of kirigami geometry and form, but the design relied heavily upon mechanical hinges. Shown in 1, complex mechatronic systems including linear actuators and several mechanical devices are integrated to actuate folding response to environmental input. This is essentially allocating almost all of the response control to fragile, error-prone mechatronic elements. A primary issue concerns scale: in order to effectively scale kirigami inspired foldable material assemblies like ColorFolds into deployable building materials, mechatronic systems are problematic. They are too fragile, maintenance and energy-heavy, and costly to support large-scale assemblies of folding panels. To address this issue, we have directed our research toward panel-and-hinge assemblies that integrate the hinge and panel as one composite in order to both decrease reliance on mechatronics and electrical energy for actuation and strive toward a

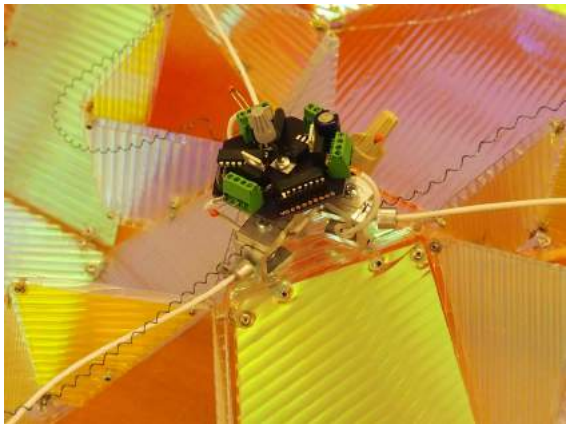

Figure 1. Mechatronic actuator from Sabin Design Lab’s 2014-2015 project *Colorfolds.*

SimAUD 2017 May 22-24 Toronto, Canada

programmable material capable of controlled, elastic response to stimuli.

To further our research on kirigami with our findings from ColorFolds, our goal is threefold: 1) Create a flexible assembly that is not composed of rigid parts, but instead integrated and elastic, 2) Simulate the flexible assembly at a larger scale to understand its global behavior and 3) Create a customized pipeline enmeshed with material feedback between simulation, computational analysis, and the creation of new physical tests. These goals produce findings that inform our testing and representation of open, deployable and scalable structural elements and structures [1]. This paper describes the methods of our 3 step experimental loop: 1) design and prototyping of kirigami material composites [2, 3]. FEA verification with physical testing and 3) larger scale kirigami simulation [4,5]. The results contain relevant images of the physical models, experiments, and simulations of our process.

2 MATERIALS AND METHODS

2.1 Computational Model Design

The primary aim of our computational model is to design patterns with auxetic properties. Auxetic materials are structures with negative poisson ratio. That is, when tension is applied on the pattern, the model becomes thicker and stronger, unlike conventional materials that stretch and weaken with the addition of tension forces. To achieve this, the kirigami pattern consists of two parts: slit cuts and hinges, each defined by a series of tunable parameters. The slits are described by vertical length and the separation between the edge of one slit and the center of the adjacent slit. By changing these parameters, a series of flat sheets with auxetic perforations are created. The geometry is illustrated in Figure 2 (as developed in a research paper by Spencer Magleby of Brigham Young University).

To achieve auxetic properties, every square needs to rotate concurrently. In the physical tests, we found the connection between squares prone to rupture as this is where stress is concentrated, causing failure in rotation. Thus, spring-like hinges are designed to enhance the strength of the linkages. The geometrical shape of the hinge and the width of it are flexible. The mechanical properties that determine the auxetic performance of the model, such as Young's Modulus and Poisson's ratio, can be modified through changing the shape and width in the hinge geometry. Finite element analysis (FEA) is performed on a single hinge to optimize the physical behavior and auxetic performance of the model. In addition to the stretching and compression force, the hinge also undertakes bending force when deformed to approximate a curved surface. When the hinge behaves in a bending-dominated mode of deformation, its thickness and width are key factors in determining the strength of the linkage, as can be seen in Figure 3 (as first conceptualized by Cho et al. in 2014 [2]).

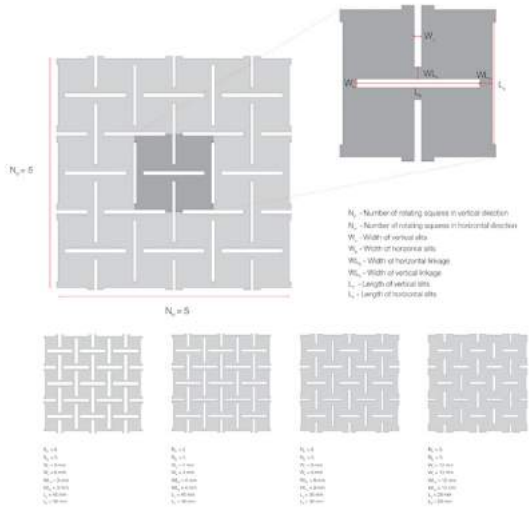

Figure 2. Parameters of slits within the kirigami model that provide auxetic characteristics.

Figure 3. Parameters of hinge parts in kirigami matrices.

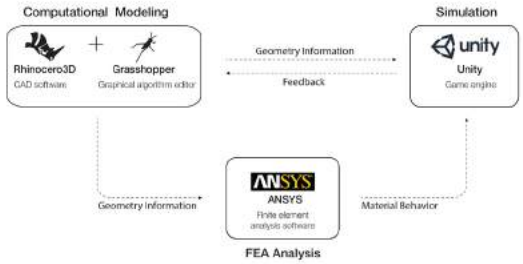

Figure 4. Work-flow diagram depicting key tools and dialogue between programs.

The computational model is generated in Grasshopper for Rhinoceros, a visual programming language run within Rhinoceros 3D computer-aided design (CAD) application. Next, FEA is performed by engineering software, ANSYS, to simulate ideal material properties and to verify experimental results of the models. ANSYS is an engineering simulation software commonly used in industries to predict the life cycle and to simulate the performance of a product. For example, mechanical engineers may use ANSYS to simulate the strength of car structures before the physical crash tests, in order to save time and money in the design process. By changing parameters of slits, hinges and rotation of squares in Grasshopper, a series of 3D models can be created, as can be seen in Figure 3. These are concurrently simulated and analyzed via the connections between Rhino, Unity3D, a customizable graphics platform with advanced physics engine, and ANSYS for finite element analysis. The workflow diagram showing the coordination between different software can be simplified and visualized in Figure 4.

Material Prototyping

To test at the material scale, physical models are 3D printed out of ABS plastic and then cast into a thin sheet of silicone to form composite assemblies. The plastic models are meant to be geometrically flexible – variegated geometries enable stretching and buckling, even when printed in a rigid material like ABS plastic. The ABS plastic sheets are composed of two zones: a panel zone and a hinge zone. The panel and hinge are materially identical and are printed simultaneously, with the goal of integrating the panel and hinge into one continuous system. The ABS sheets are cast into shallow silicone sheets after they are printed, where the process is shown in Figure 5.

2.2 Scaled Unity3D Simulation

Biaxial stretching of the sheets is then simulated in Unity3D. Unity3D is typically used as a game engine. However, it is also used in other fields for its rendering and physics simulation capabilities. Abstractions of the kirigami sheets were created in Unity as rigid bodies. Rigid bodies are the class in Unity that allow objects in the simulated environment to react to physical forces. Performing simple tests on these computational models allows us to understand the global behavior of our kirigami matrix.

First, a script was written to produce a grid of two-dimensional springs connected by Unity joints according to the slit parameters predetermined by our kirigami model. The Unity joint class connects two rigid bodies and behaves as a physical hinge. Pulling and twisting tests were performed on varying grid sizes to mimic our physical tests. The pulling experiments, involve setting the top row as anchor points and applying gravity to the remaining cells. These two-dimensional simulations give us insights into how the lattice cuts respond to simple manipulations on a larger scale.

Next, a script was written to produce a grid of three-dimensional rigid bodies. Halved spheres were included at hinge locations to represent the physical hinges. Moving to three dimensions and adding space between panels allowed for bending and compression tests. Active bending tests were performed by anchoring the bottom row highlighted by the red bounding box in test A of Figure 6. Gravity is then applied to the remaining cells. Tension tests were performed by anchoring the top row in test B of Figure 6 and applying gravity to the remaining cells.

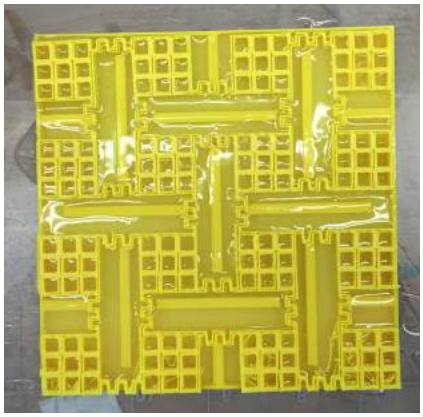

Figure 5. Cast of ABS matrices into shallow silicone sheets.

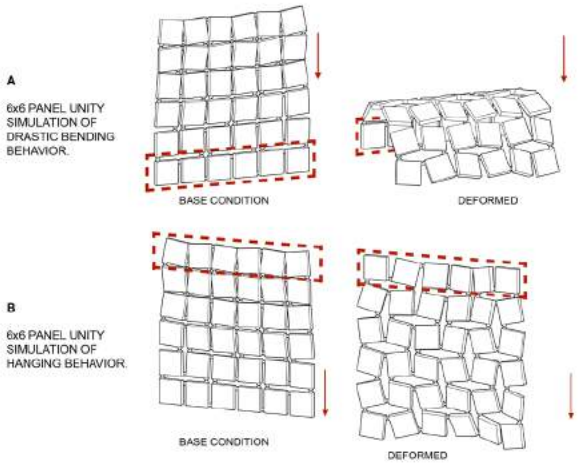

Figure 6. Bending Test A and Stretching Test B.

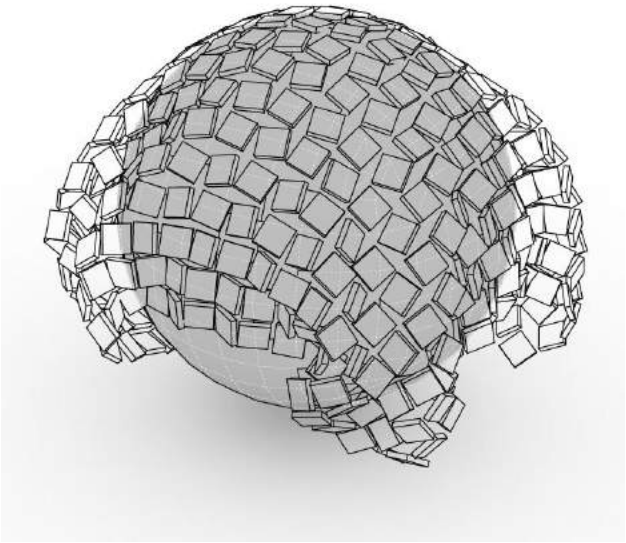

Figure 7. A simulated kirigami sheet measuring 20x20 units, draped over a sphere in Unity.

Unity's lightweight physics engine makes it possible to drape kirigami sheets over simple geometries like the one shown in Figure 7. Stiffness of the hinges can be changed to test how more rigid sheets behave when deformed.

2.3 Experimental Loop

In order to optimize the hinge geometry in the physical design process, an experimental loop was developed. To constrain the variables in optimization, three different models with different quantities of hinges were designed and printed. FEA was performed on the three models with the use of ANSYS software. To verify the FEA results, stress and strain tests were performed using a Vernier Force Sensor and the Young's Modulus Graphs were generated with comparisons between the results of physical testing and FEA. After verifying the results, Young's modulus data were compared between the three models and optimized as a controllable attribute of the panel. Finally, the optimization results were input into Unity for large-scale structures design. In turn, a feedback loop is generated for the next round of geometry and material design.

ANSYS performs finite element analysis by creating meshes on our CAD model geometry. After defining the boundary conditions such as the applied forces and fixed points on the model, rigorous mathematical calculations were done on the edges of every mesh. The calculation continues until the numerical solutions on the meshes converge. Finally, the software post-processes the mathematical solutions into clearly visualized graphs and 3D contour plots. The user-friendly interface of ANSYS allows various definitions of boundary conditions. Loads, edge-fixed supports, and face-fixed supports were set for the static structural loading condition. Von-Mises stress, directional and total deformation, strain, and safety factor were selected for the output of the results. Von-Mises stress is a particular engineering stress that predicts the yielding conditions of materials, and safety factor determines if the material will reach the failure point when experiencing loads. While Von-Mises stress and strain were used to calculate Young's modulus of the model, directional and total deformation, as well as safety factor, enable in depth understanding of the material properties.

Then, physical experiments were further designed to compare the numerical results from previous physical tests with FEA results. The designs of the physical experiments were critical in constraining the variables and obtaining quantitative data. Two different experiments were set up for the validation of FEA - stretch test, and compression test.

Stretch test is set up as in Figure 8.A. The model is pinned at the corners on a 2D horizontal plane and forces were applied on the opposite (left) end with a 3D-printed jig in order to distribute the force evenly. A Vernier Dual-Range force sensor was attached to the force-applying end, and a camera was set up above the model. Certain force quantities were applied with the documentation of the force sensor, and the camera records the deformation of the model.

The compression test features 3D printed jigs in the setup as shown in Figure 8.B. The material composite was put inside the 3D printed jig so that the bottom surface of the model is supported and forces were applied on the top of the model. The 3D printed jigs were designed to constrain the model in a 2D plane. Quantitative forces were applied with the use of weights, and a camera was set up to record the results as in the stretch test.

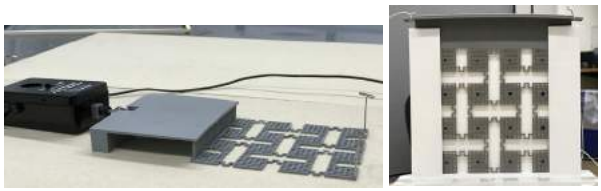

Figure 8. A. Stretch test setup (left). B. Compression test setup (right).

To post process the experimental results, camera images with different stresses were layered, shown in Figure 9. Centers of the local grids were marked, and strain is calculated by measuring the location of the marked center. Nominal strain in x, y directions were then derived from the universal engineering strain formula:

$$\varepsilon_{xx}^{[i,j]} = \frac{x^{(i+,\,j)} - x^{(i,j)} + x^{(i+,\,j+,\,)} - x^{(i,j+,\,)} - 2L_2}{2L_2}$$

$$\varepsilon_{yy}^{[i,j]} = \frac{x^{(i,j+,\,)} - x^{(i,j)} + x^{(i+,\,j+,\,)} - x^{(i+,\,j)} - 2L_2}{2L_2}$$

Stress was obtained by dividing the force sensor data with the surface area of the model. Young's modulus was then computed by taking the ratio of various stress and strain.

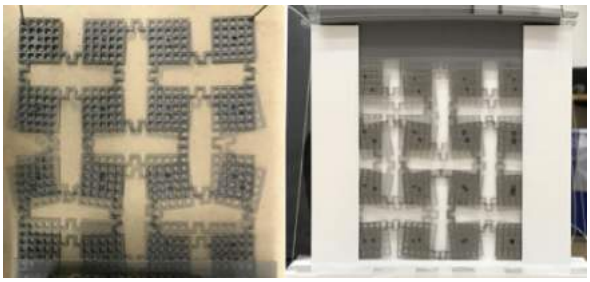

Figure 9. Post processing method for stretch test (left), compression test (right).

3 RESULTS

FEA were performed on a single hinge for studying the mechanical behaviors, avoiding geometric failures, and optimizing auxetic properties. The results are shown in Figure 10. The spring-like geometry was then determined to maximize the auxetic properties, where corner fillets avoid stress concentration. Then the sheet geometries were determined as in Figure 11.

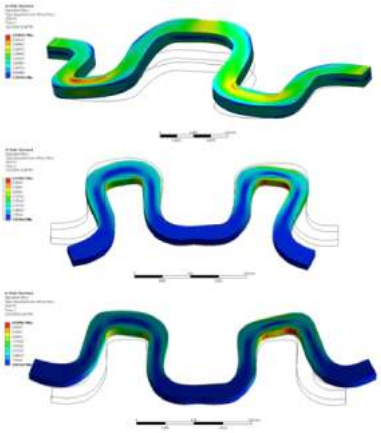

Figure 10. Von-Mises stress contours on a single hinge in FEA. Top to bottom: tension, compression, bending.

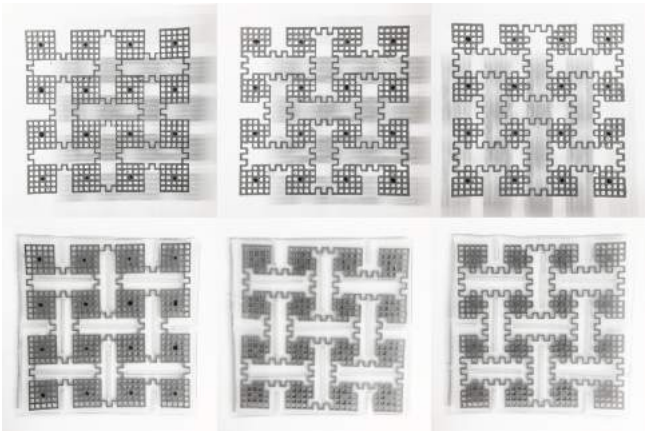

Figure 11. Final ABS and silicone matrices, differentiated by the number of grid units, the hinge travels into the adjacent panel. Across Row 1, Left to Right: 0 unit hinge, 1 unit hinge (on either side), 2 unit hinge (on either side). Bottom row: corresponding panels cast into silicone.

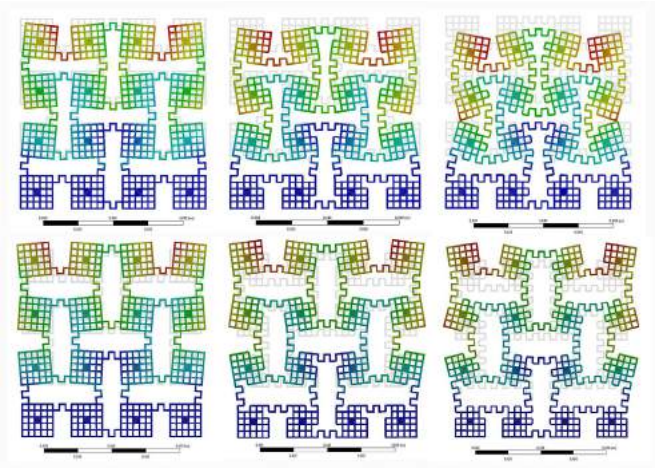

Figure 12. FEA results of tension test (upper row) and compression test (lower row). Non-deformed models were also included in light gray, behind the false-color results.

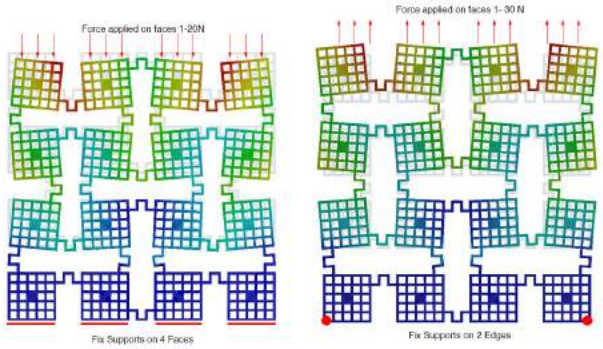

Figure 13. FEA Compression Test Setup (left), FEA Tension Test Setup (Right),

FEA were performed on both tension and compression tests, and visualized results can be seen in Figure 12. The setup for FEA can be seen in Figure 13. In tension tests, fixed supports were applied to the two corners to simulate the pins in the experiment. Force is a variable ranging from 1N to 30N applied to the 4 faces on the opposite end. In compression test, fixed supports were applied to the 4 faces on one end while the force is a variable ranging from 1N to 20N on the 4 faces on the other end. In both experiments, directional deformations were extracted with probes, and post-processed into local strain. Stresses were extracted as Von-Mises engineering stress.

FEA results demonstrate correct verification and validation with the experimental results. In verification, FEA results and experimental results, both included in Figure 14, show similar behavior in both tension and compression tests. The small deviations between the two datasets are possible effects from uncontrollable friction and gravity. To validate the results, the behavior of stress strain curves is consistent with actual material properties with an ultimate tensile stress (UTS) and a failure point. Variations in hinges show huge effects on the Young's modulus. Young's Modulus data evaluated at UTS in both compression test and tension test

are on the same magnitude with a standard deviation of 5.12. Hinge 0 has a Young's Modulus of 1.04 MPa, hinge 1 of 0.53 MPa, and hinge 2 of 0.454 MPa.

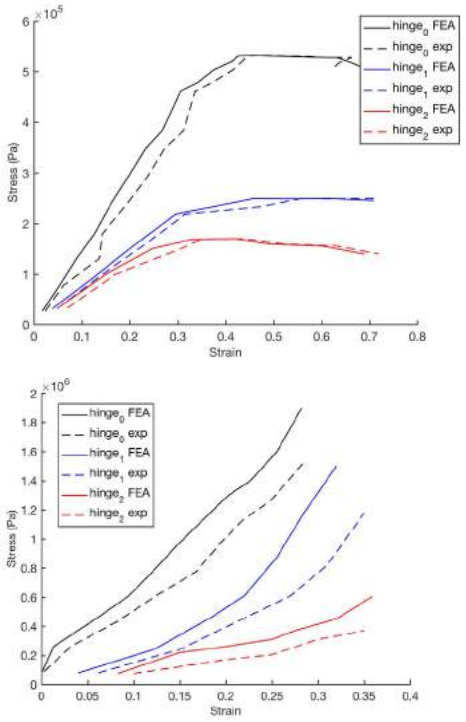

Figure 14. Stress Strain Curve of PLA Model From Stretch Test (top) and compression test (bottom).

4 DISCUSSION

The stress strain curves in the experimental loop show how the hinges affect Young's Modulus, and how the material properties were modified by the kirigami geometry. By comparing the data from the three different models, it is observed that Young's Modulus decreases as hinges were extended into the models. That is, the models are significantly more flexible as hinges were merged into the models.

The three model behaviors in the stretch test show two distinct regimes for typical solids: linear elastic regime, and the non-linear elastic regime after the yielding point. The kirigami models show a significantly higher failure stress, and a longer non-linear elastic regime before failure than a typical PLA block material. Hinges and cuts in the kirigami models behave as springs, which provide damping to the entire model when forces are applied. The damping properties make the kirigami models stronger than normal materials. Impregnating an ABS sheet with silicone, impacted stretching performance of the sheet as a whole by turning discrete bending moments into indeterminate, sheet-wide stresses. The integration of silicone into the plastic assembly may have distributed tension more evenly than the plastic sheet on its own, while also increasing resistance as a whole. In this way, the ABS plastic components function in a way analogous to a skeletal system, while the silicone acts as the 'muscles' and membranes that stretch with and stabilize the underlying plastic structure.

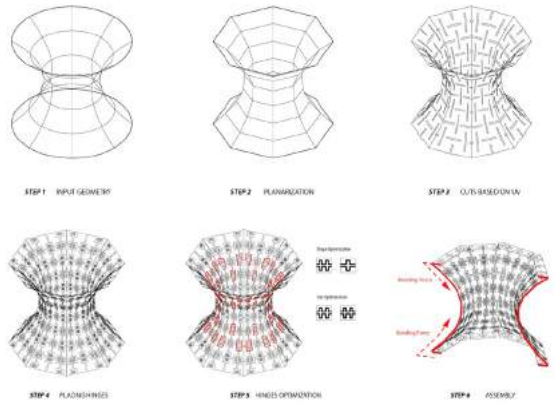

Figure 15. Process of embedding kirigami pattern onto a hyperbolic surface.

5 CONCLUSION

The goal for ColorFolds was to design deployable and scalable structures that respond in a controlled, kinetic mode to contextual feedback. We have established an adequate pipeline for simulating our kirigami structures in order to understand their behaviors on a global scale for larger architectural assemblies. With the pipeline we established, we can utilize the robustness of finite element analysis software ANSYS and the simplicity of physical simulation software Unity to achieve both quantitative and qualitative feedback. The pipeline can also be served as a cooperative platform to integrate both designers and engineers. Our next step is to inform generative design iterations with quantitative data from larger scale simulations in order to optimize and strategically design kirigami cuts and folds while addressing fabrication constraints and desired global curvature. Informed by our research described herein, our current investigations address 2D flat sheet to 3D form.

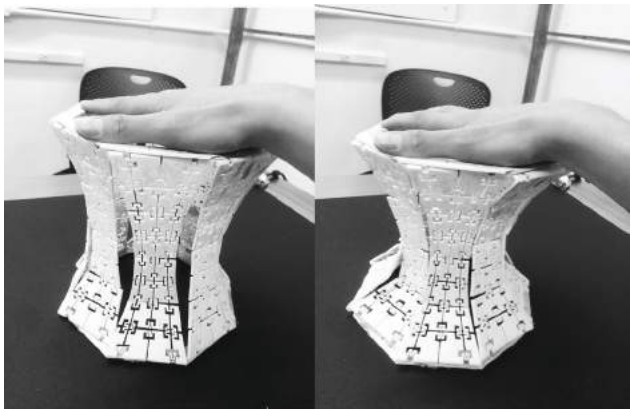

Figure 16. Physical prototype demonstrating that cuts and hinges allow the auxetic hyperbolic surface to be stretched and compressed to eliminate tolerance.

A developable hyperboloid shape was used as an input to test the feasibility of the computational model and the design-simulation-analysis loop, as theoretically demonstrated in Figure 15, and physically demonstrated in Figure 16. The given hyperbolic NURBS (Non-uniform rational B-spline) surface was first approximated by the planarized NURBS with degree of one. The planarization guaranteed that no bending or stretching force was exerted on the hinges. The surface was then divided into six sub-surfaces based on UV subdivision, cuts were placed aligned with UV curves and hinges were placed on the intersection. Each sub-surface was flattened and printed with inextensible plastic material ABS. In Figure 16, the tolerance caused by flattening and assembly was eliminated by the auxetic property enabled by embedded cuts and hinges.

Another immediate goal is the development of a simulation environment that is fully integrated with Rhino Grasshopper. Following this, large-scale physical prototypes can be produced using the programmable matrix, and optimized for different stretching behaviors in discrete zones. This matrix has the potential to become a deployable, 'adaptive' building material capable of optimized and differentiated expansion and contraction based on the properties of each unit. This improved process will greatly benefit large-scale applications that incorporate programmable material composites capable of controlled, elastic response to stimuli. Our ultimate goal is to generate a fluid and intuitive computational pipeline to facilitate a design process that is enmeshed with material and geometric feedback. Our work follows the concept of "Interact Locally, Fold Globally," necessary for deployable and scalable architectures. Using mathematical modeling, architectural elements, simulation, design computation, and controlled elastic response, this work showcases new techniques, algorithms, and processes for the assembly of open, deployable material systems and architectural surface assemblies.

REFERENCES

1. Sussman, D. M., Cho, Y., Castle, T., Gong, X., Jung, E., Yang, S., & Kamien, R. D. (2015). Algorithmic lattice kirigami: A route to pluripotent materials. *Proceedings of the National Academy of Sciences*, *112*(24), 7449-7453.
2. Cho, Y., Shin, J. H., Costa, A., Kim, T. A., Kunin, V., Li, J., ... & Srolovitz, D. J. (2014). Engineering the shape and structure of materials by fractal cut. *Proceedings of the National Academy of Sciences*, *111*(49), 17390-17395.
3. Castle, T., Cho, Y., Gong, X., Jung, E., Sussman, D. M., Yang, S., & Kamien, R. D. (2014). Making the cut: Lattice kirigami rules. *Physical review letters*, *113*(24), 245502.
4. Deng, D., & Chen, Y. (2013). Assembled additive manufacturing–A hybrid fabrication process inspired by origami design. *Solid Freeform Fabrication*, 174.
5. Nelson, T. G., Lang, R. J., Pehrson, N. A., Magleby, S. P., & Howell, L. L. (2016). Facilitating deployable mechanisms and structures via developable lamina emergent arrays. *Journal of Mechanisms and Robotics*, *8*(3), 031006.

A Performance Based Computational Method for Assembly Design of Reciprocal Architectural Systems with 2D Elements

Omid Oliyan Torghabehi[1], Peter von Buelow[1], Alireza Seyedahmadian[2]

[1]University of Michigan
Ann Arbor, Michigan, United States
{oliyan, pvbuelow}@umich.edu

[2]Quarra Stone Company
Madison, Wisconsin, United States
aseyed@quarrastone.com

ABSTRACT

In this research a computational method is developed to study the form-finding process of non-standard reciprocal systems with 2D elements based on the current methods on the morphology of reciprocal systems with 1D elements. The developed form-finding methods will be used in a performance based form exploration process for geometrical and structural performance enhancement. The proposed computational framework will explore new potentials for variations in the assembly design of these systems through the introduction of new geometric parameters both at the component level and the assembly level within the form exploration process. The proposed method integrates parametric assembly design with structural analysis in a stochastic optimization process to explore the design space while minimizing the total weight of the structure. The results of the form exploration process will be stored for the post processing phase in which the solution space is explored to study the variation of the emerging assemblies. In this paper the proposed method is explained and implemented via two case studies towards the further exploration of the concept.

Author Keywords

Performance based design, Reciprocal systems, Associative assembly design, Form-Finding, Finite element analysis

1 INTRODUCTION

The principle of reciprocity is based on the use of loadbearing-elements which support one another along their spans rather than at their ends, and which compose a spatial configuration with no clear structural hierarchy [14] (Figure 1).

From a historic stand point, primitive reciprocal systems were used in early construction methods as reciprocal frames both in the East and the West. In Europe, structural reciprocity has mainly been used, at least until 20th Century, to span distances longer than the length of available timber beams, so called, short beams [3].

In eastern culture interest in reciprocal structures derives mainly from the use of interwoven strips of bamboo for the realization of baskets, an old tradition that has been transferred to the building scale.

From primitive reciprocal structures to modern freeform spatial reciprocal configurations significant research has been done on the form finding, analysis and fabrication of these systems. However, the majority of the research in this field focuses on the study of reciprocal systems with 1D elements leaving the potentials of 2D and 3D element assemblies unexplored. Based on the current literature, the foundational research can be categorized into the two following groups.

1.1 Research on the morphology and geometry of reciprocal spatial structures

The main literature in this category focuses on physical prototyping and experimental study of reciprocal systems through geometrical variations. Which includes studies on different elemental configurations through physical prototyping to be used in reciprocal systems [1], and morphological study of reciprocal systems with planar elements through prototyping and physical studies [8, 13] and also the structural study of different configurations of spherical and fractal reciprocal systems with 1D elements [5,15].

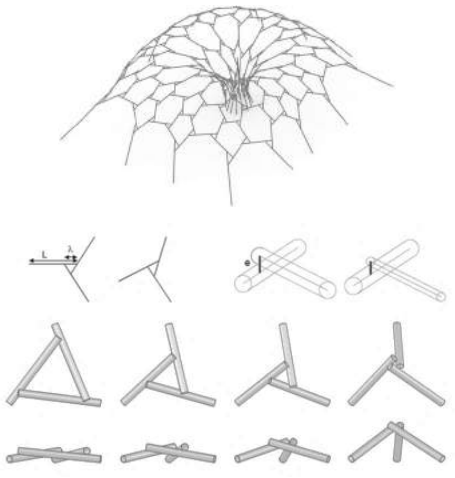

Figure 1. An example of a reciprocal system with 1D elements [9].

SimAUD 2017 May 22-24 Toronto, Canada

1.2 Research on form-finding and morphogenesis of such systems using computational tools

The core of the research in this category focuses on computational methods for the form-finding and analysis of reciprocal systems. Which includes form finding process based on surface tessellation and constraint formulation for reciprocal cells coupled with dynamic relaxation [4, 7, 10, 16, 19]. Song et al. developed a tool for form finding of reciprocal systems based on two-dimensional pattern creation and conformal mapping on three dimensional forms [17, 18].

This current research focuses on the morphology of reciprocal systems with 2D elements and proposes a performance oriented method for the design of reciprocal systems with planar elements, which is relatively an unexplored ground. Building on the existing literature on the morphological study of reciprocal systems with planar elements [2], these systems can be classified in five categories. a) Reciprocal systems with individual planar elements, b) reciprocal systems with planar elements consisting of groups of linear elements, c) reciprocal systems with planar configurations with bending capacity at connections, d) reciprocal systems with truss like combinations of elements, and e) reciprocal systems with hybrid modules integrating two or more of the previous configurations (Figure 2).

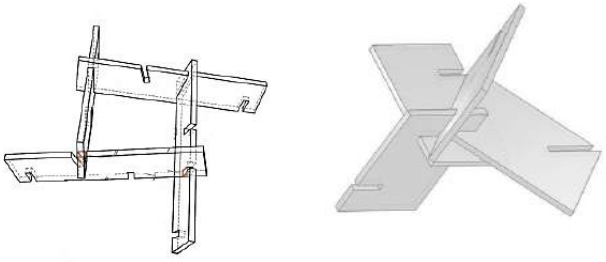

Figure 2. Reciprocal assembly with planar elements (left), group of planar elements in a 3D assembly [13].

The five categories explained above are entirely based on physical prototyping rather than computational modeling, nevertheless it is a valuable classification of these systems based on their configurational behavior, and a good starting point for computational modelling and form finding. The change from configurations with 1D elements to 2D and 3D elements effects both the form finding process as well as the structural behavior of these systems, which requires a different simulation and form finding process in each case [2,11].

This current research uses the stated categorization focusing on the translation of form finding methods for 1D elements towards the development of computational form finding method for reciprocal systems with 2D members.

2 METHODOLIGY

The unique characteristics of reciprocal systems, such as self-equilibrium, modular assembly, inherent three dimensionality and potential for generative growth, qualify these systems as sources of ideation for innovative assembly design and performance integration. However, the key to take advantage of these potentials is a consistent design framework which not only can accommodate geometric form exploration and performance feedback but also provides flexibility to change the conventional reciprocal concept towards the emergence of better performing assemblies. To realize this goal, a computational method for the assembly design of reciprocal systems with planar elements is introduced and implemented in two case studies. This method integrates parametric assembly design with FE analysis and a performance feedback loop in a from exploration process which explores the design space while minimizing the total weight of the structure (Figure 3).

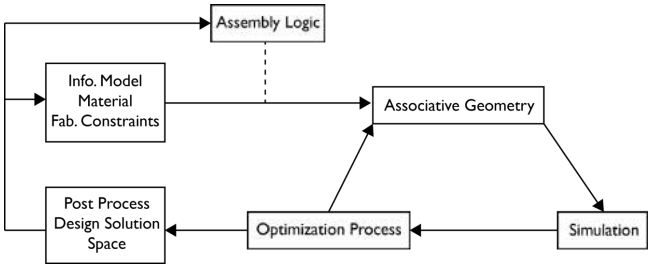

Figure 3. Form exploration workflow and design considerations.

Through the introduction of a rotational parameter for planar elements in the assembly of the second case study new typologies of the structure are explored through the form exploration process.

The rotational parameter compromises the structural behavior however it opens opportunities towards the development of new assembly logics.

2.1 Geometry Definition and Parametric Modeling

The first case study is a flat reciprocal structure with a structural depth in the mid-span comprised of four membered reciprocal modules (Figure 4). The 2D conformal pattern mapping method for reciprocal systems with 1D elements is used to model the associative parametric geometry [17,18]. A 2D parametric pattern of the structure was created in the XY plane and this pattern was mapped on a surface with a parametric depth in the mid span. Subsequently, the mapped members where extruded in the Z direction to create the 2D planar elements (Figure 4).

This parametric model has four controlling parameters. a) the reciprocal parameter which controls the opening of the reciprocal modules based on their engagement length. b) the thickness parameter which controls the thickness of the elements, c) The structural depth parameter which controls the depth of the members by controlling the mid-span depth and d) the depth on the edge (Figure 5). This parametric model will be used in a form exploration process with performance feedback and a database of the results to study the variation of form through the form finding process.

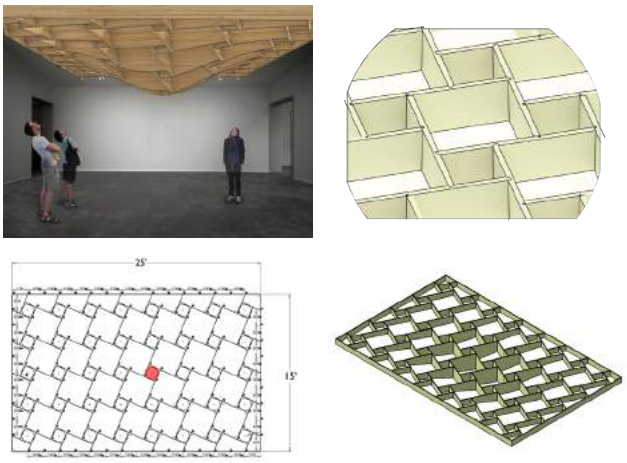

Figure 4. First case study, 2D parametric pattern, local and global geometry.

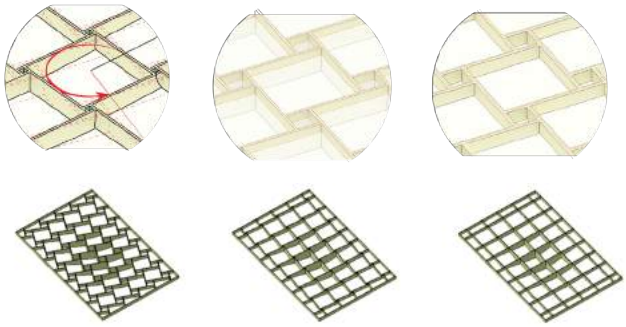

Figure 5. Design parameters, reciprocal parameter (left), Depth parameter (middle), Thickness parameter (right) , geometric variations based on the reciprocal changes.

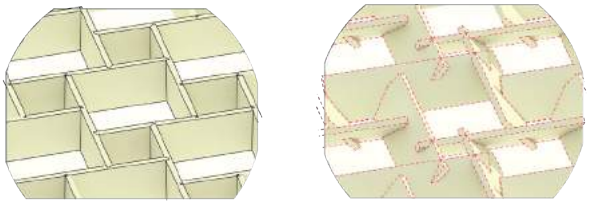

Figure 6. Rotational parameter and transformation of the reciprocal to non-orthogonal configuration.

The second case study uses the same 2D pattern with uniform depth, in this case a rotational parameter is introduced to the model where planar elements rotate around their longitudinal axis based on an angular parameter. This angular parameter is an important agent which transforms the reciprocal geometry allowing the assessment of non-orthogonal typologies of modules within the form exploration process (Figure 6).

2.2 Simulation Model

Structural models of the two case studies are created with fixed boundary conditions on four edges. A 30 psf snow load and a 15 psf cladding loads are applied to the structures in addition to the self-weight. Northern red oak wood material properties are used for the analysis for both case studies (Figure 7 and Figure 8). The common method for the analysis of reciprocal structures is a simplified 1D elemental representation with simple pin connections which does not accommodate three dimensionalities of modules and partial moment distribution of the notched connections.

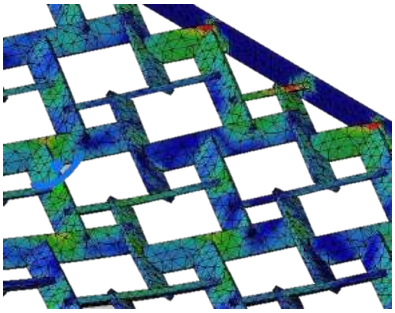

Figure 7. Detailed 3D Finite element mesh and analysis results.

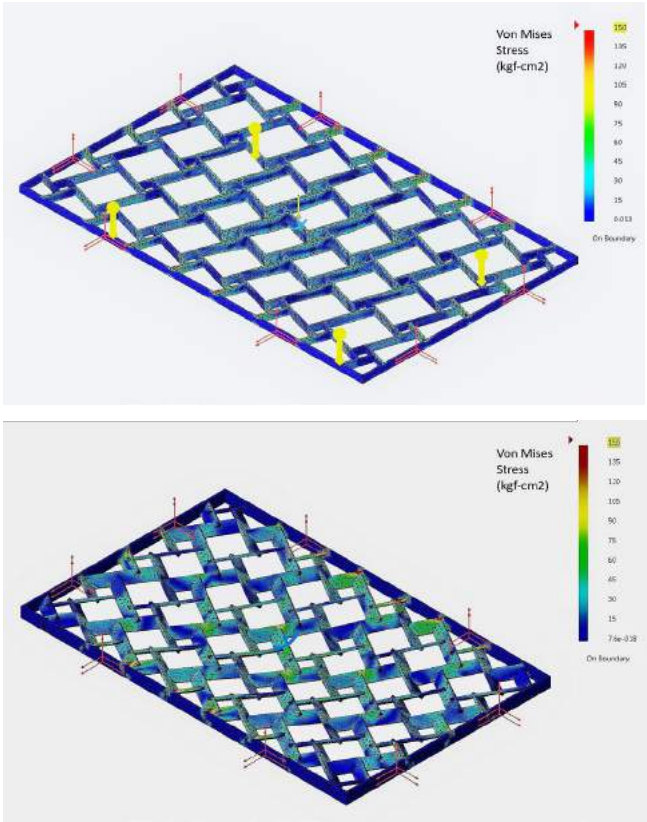

Figure 8. Structural model and Fe analysis results.

In this study a three-dimensional finite element analysis is applied for the structural analysis of the reciprocal structure (Figure 7 and Figure 8). A fine 3D finite element mesh accommodates the three-dimensional geometry of the rotated connections and also correct representation of stress concentrations and guarantees a more accurate structural analysis of the structure. Moreover, the 3D finite element analysis of the assembly accommodates detailed connection

design and analysis which is an integral part of design for fabrication (Figure 7).

The analysis results (maximum stress and maximum deflection) is fed back into the optimization process which informs the design parameter changes for the next iteration.

2.3 Form Exploration

Computational optimization methods for form exploration are primarily suited for well-defined design problems, and the choice of method is often a tradeoff between computing time and the nature of the solution space. However, in architectural design, the definition of a parametric model and boundary conditions and solution domains together with the understanding of how the optimization project actually performs the search for the suitable shape, is more important than reaching an optimal result [6]. In this regard population based form exploration methods which incorporate a database of solutions have become more popular in the form exploration processes. In the current study, CATIA (a software package developed by Dassault Systemes for CAD, CAM and CAE) has been used for the analysis and optimization process. The Product Engineering Optimizer (PEO) workbench, is used to integrate parametric modeling and FE simulation with feedback of results into the optimization process. The optimization algorithm changes the design parameters stochastically towards convergence to the optimal solution. Moreover, the simulation data in each step of the optimization process is stored for post processing and exploration of the design space.

Simulated Annealing (SA) is chosen among the available optimization algorithms in the PEO workbench. The stochastic nature of SA can accommodate the nonlinearity of the proposed optimization problem and improve the exploration of the design space. The results of the form exploration for 400 iterations are stored in a database for post processing. The optimization formulation for the case studies are given in Table 1 and Table 2.

Minimization Target Function	Total Mass (kg)
Constraints	Max Von Mises < 300 (kg/cm2) *Max Displacement < 2 (cm)*
Variable Bounds	*0.5 (cm) < Reciprocal < 70 (cm)* *1 (cm) < Mid-span depth < 20 (cm)* *5 (cm) < Edge Thickness < 30 (cm)* *1 (cm) < Thickness< 8 (cm)*

Table 1. Optimization formulation definition for the first case study.

Through the iterative optimization process design parameters are changed based on the performance feedback towards the minimization of the total mass of the structure and a range of design solutions are explored and stored for post processing towards the further study of geometric configurations with corresponding structural and geometric performances.

Minimization Target Function	Total Mass (kg)
Constraints	Max Von Mises < 300 (kg/cm2) *Max Displacement < 2 (cm)*
Variable Bounds	*0.5 (cm) < Reciprocal < 70 (cm)* *5 (cm) < depth < 50 (cm)* *1 (cm) < Thickness< 8 (cm)* *1 (deg.) < Rotation < 70 (deg.)*

Table 2. Optimization formulation definition for the second case study.

3 RESULTS AND DISCUSSION

In this section, we study the numerical results of the optimization with a focus on the geometric variations and changes in the design parameters of the reciprocal assembly for each case study.

The results of the optimization process for the first case study are shown in (Figure 9), which shows mass minimization of the reciprocal structure with respect to the optimization constraints. The minimization process converges at around 400 iterations.

Some of the critical design solutions are shown in the process of form exploration to demonstrate the geometrical variations.

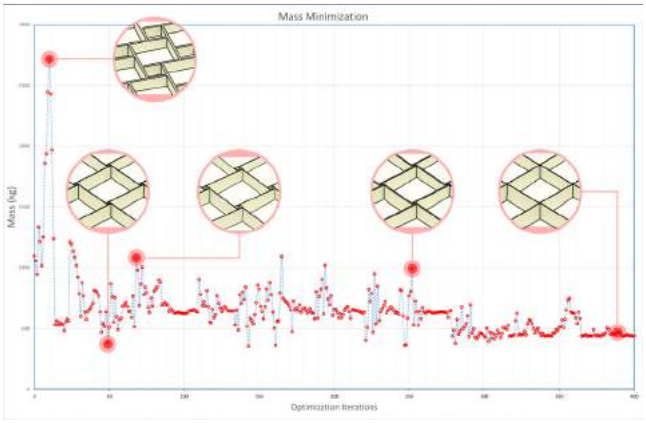

Figure 9. Optimization results for the first case study.

In this case study the numerical results indicate that the local optimum solution has the minimum engagement length (Figure 9). This case study is specifically interesting as it demonstrates the transition of the discrete reciprocal geometry with larger engagement lengths to a more continuous configuration close to a gridshell as the engagement length decreases towards zero in the process of optimization. This transition shows the behavioral connection between these two types of structural systems,

Moreover, theoretically this transition from a discrete geometry of a reciprocal system to a continuous geometry of a gridshell is a proof of convergence to the global minimum for the optimization process as existence of a more continuous load path in the geometry increases the loadbearing efficiency of the system.

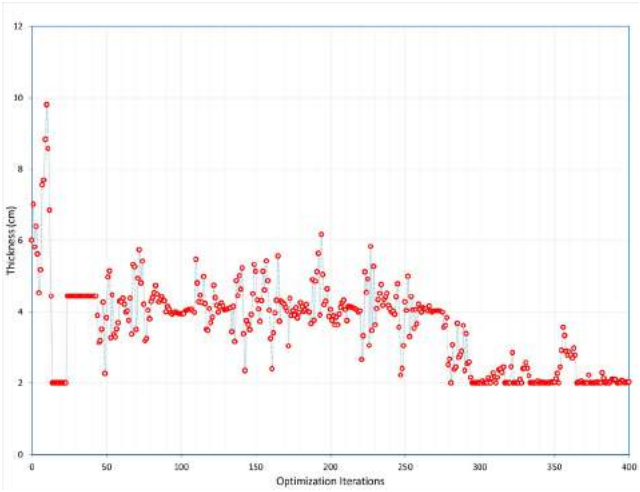

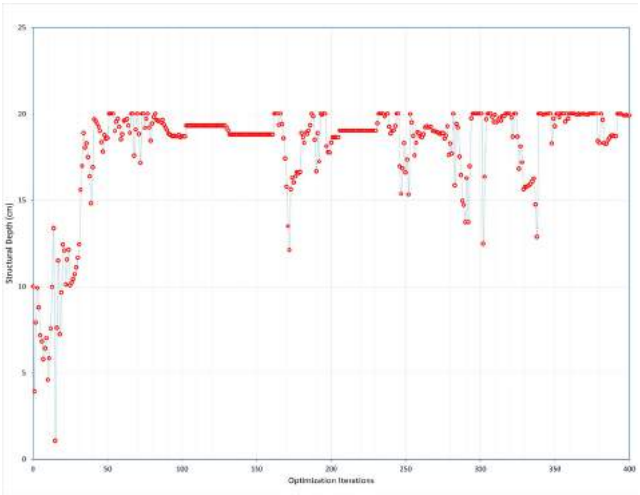

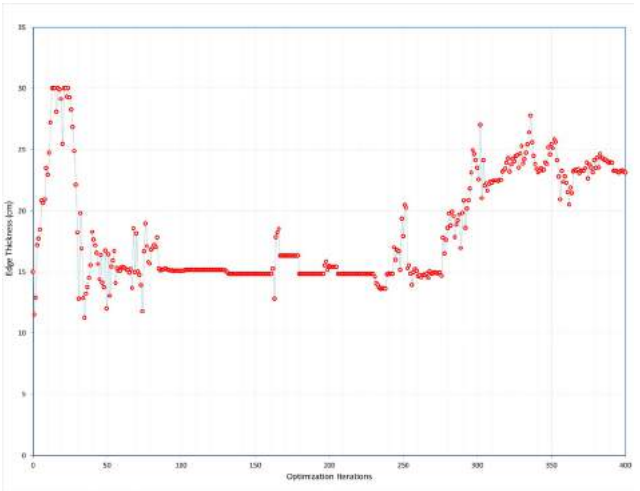

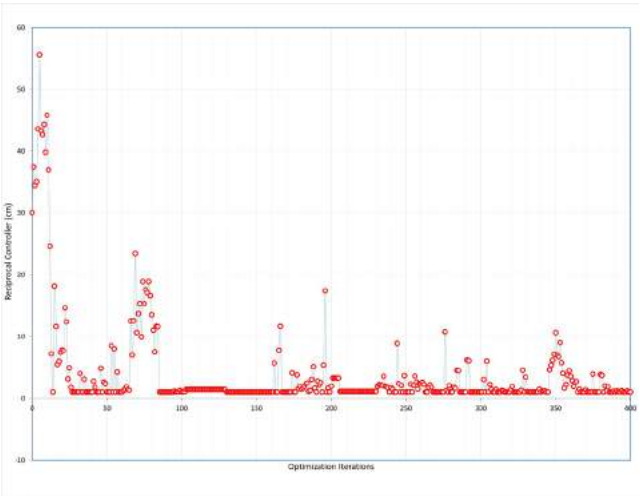

Figure 10. Design parameters through the optimization process.

Figure 10 shows the design variables variations through the process of optimization as it shows the interaction of depth, thickness and reciprocal parameters towards the optimal combination.

Subsequently to testing the convergence of the process through the first case study, this process can be used to, incorporate a rotational parameter which transforms the modular assembly of the reciprocal system. The transformation of the geometry can be studied through the optimization process as is shown in Figure 11.

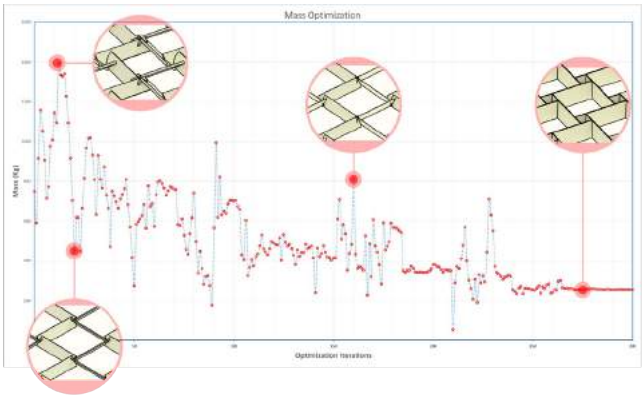

Figure 11. Optimization results for the second case study and geometric transformation.

As stated earlier, the focus of the second case study is to change the standard assembly of reciprocal systems, this change has been implemented through the introduction of a new geometric parameter which rotates the reciprocal elements around their longitudinal axis. The rotational parameter changes the orthogonal configuration and also the aperture of each cell which effects the structural performance of the system.

The numerical results show that the optimization process converges to an orthogonal reciprocal configuration as the

rotation parameter is approaching zero, which corresponds to the fact that a larger rotation decreases the structural depth and consequently, the loadbearing capacity, However, this rotational parameter controls the aperture of the reciprocal cells, which as an example can be used as a design parameter for the shading performance of the structure. In this regard the post-process of the optimization results can provide a selected pallet of structurally well performing design solutions which provides a range of shading performance. Moreover, monitoring the geometrical variations in the optimization process, which produces non-orthogonal configurations, can be a source of inspiration for new assembly logics for non-standard reciprocal systems design.

4 CONCLUSIONS

In the current research a computational method is introduced for the design and form finding of reciprocal systems with planar elements. The method integrates parametric modelling with FE analysis through a stochastic search algorithm with performance feedback. The method is implemented for form exploration in two case studies where a database of the solution space is stored and explored in the post-processing phase.

In the first case study an orthogonal flat reciprocal structure is modeled and optimized for minimal weight. The main design parameter for the form exploration is the engagement length of the planar members which define the geometric variations of the optimization results. The optimization process converges to a reciprocal system with minimum engagement length, which shows the transition of the discrete reciprocal geometry to a more continuous configuration close to a gridshell. This transition implies the behavioral connection between these two types of structural systems which is confirmed numerically by the optimization results. In this regard, it is important to emphasize that while gridshell structure provides more stiffness and strength in comparison to its reciprocal counterpart, it requires long continuous members with limited integrative design potentials. However, a reciprocal system benefits from modular assembly design of relatively short members to span long distances which also accommodates local changes to assembly configuration in the structure. This flexibility adds the potential for an integrative design approach incorporating other design possibilities (e.g. daylighting, acoustics) within the geometry of the structure.

In the second case study a rotational parameter is introduced in the parametric assembly which creates non-orthogonal assemblies in the process of form exploration. In the post-processing step the assembly changes are monitored throughout the optimization process, this process is specifically interesting as it demonstrates how the introduction of a new geometric parameter can accommodate morphological and behavioral changes in the primitive geometry, which in turn can be utilized as a design generator for new assembly logics in a novel reciprocal assembly design approach. The simulation shows that the overall structural capacity of the structure is reduced by introducing the rotational parameter, however, the non-orthogonality of the reciprocal members induced by the rotation parameter change the aperture of reciprocal cells in the structure. Moreover, through the study of the geometric variations in the exploration process we can see how the introduction of new geometric parameters can assist in the ideation of new assembly logics for non-standard reciprocal systems which provide more flexibility for integrative design. Moreover, the proposed methodology can accommodate more accurate connection design and analysis into the process as a performance metric for a better understanding and fabrication of novel assemblies.

The future goal of this research is to integrate physical prototyping and digital tools to develop a performance based method for the computational design and fabrication of reciprocal systems with 2D and 3D elements, which can accommodate multiple performances through the optimization of geometric configurations with the consideration of modular assembly.

REFERENCES

1. Baverel, O., & Larsen, O. A review of woven structures with focus on reciprocal systems-nexorades. *International Journal of Space Structures* 26, 4 (2011), 281-288.
2. Baverel, O., & Pugnale, A. Reciprocal systems based on planar elements: Morphology and design explorations. *Nexus Network Journal16, 1* (2013), 456.
3. Bowie, T. The sketchbook of Villard de Honnecourt, 1960.
4. Douthe, C., & Baverel, O. Design of nexorades or reciprocal frame systems with the dynamic relaxation method. *Computers & Structures* 87, 21 (2009), 1296-1307.
5. Douthe, C., & Baverel, O. Morphological and Mechanical Investigation of Double-Layer Reciprocal Structures. *Nexus Network Journal* 16, 1 (2014), 191-206.
6. Gerber, D. Parametric Practices: Models for Design Exploration in Architecture. PhD dissertation, Harvard University Press, Boston, MA, USA, 2007.
7. Kohlhammer, T., & Kotnik, T. Systemic behavior of plane reciprocal frame structures. *Structural Engineering International* 21, 1 (2011), 80-86.
8. Parigi, Dario. Design and fabrication od a free-form reciprocal roof. *IASS 2016 symposium*, (2015).
9. Parigi, D., & Kirkegaard, P. H. The reciprocalizer: an agile design tool for reciprocal structures. *Nexus Network Journal* 16, 1 (2014), 61-68.
10. Parigi, D., & Kirkegaard, P. H. Design and fabrication of free-form reciprocal structures. *Nexus Network Journal* 16, 1 (2014), 69-87.

11. Parigi, D., & Pugnale, A. Three-dimensionality in reciprocal structures: concepts and generative rules. *Nexus Network Journal* 16, 1 (2014), 151-177.

12. Parigi, D., Sassone, M., Kirkegaard, P. H., & Napoli, P. Static and kinematic formulation of planar reciprocal assemblies. *Nexus Network Journal* 16, 1 (2014), 37-59.

13. Pugnale, A. Reciprocal systems based on planar elements. Exercises and Solutions in Statistical Theory, (2013), 456.

14. Pugnale, A., & Sassone, M. Structural reciprocity: critical overview and promising research/design issues. *Nexus Network Journal* 16, 1 (2014), 9-35.

15. Sánchez-Sánchez, J., Pallarés, F. E., & Rodríguez-León, M. T. Reciprocal Tree-Like Fractal Structures. *Nexus Network Journal* 16, 1 (2014), 135-150.

16. Sénéchal, B., Douthe, C., & Baverel, O. Analytical investigations on elementary nexorades. *International Journal of Space Structures* 26, 4 (2011), 313-320.

17. Song, P., Fu, C. W., Goswami, P., Zheng, J., Mitra, N. J., & Cohen-Or, D. Reciprocal frame structures made easy. *ACM Transactions on Graphics* (TOG) 32, 4 (2013), 94.

18. Song, P., Fu, C. W., Goswami, P., Zheng, J., Mitra, N. J., & Cohen-Or, D. An Interactive Computational Design Tool for Large Reciprocal Frame Structures. *Nexus Network Journal* 16, 1 (2014), 109-118.

19. Thönnissen, U. A form-finding instrument for reciprocal structures. *Nexus Network Journal* 16, 1 (2014), 89-107.

Augmented Assembly for Tessellated Structures

Parantap Bhatt[1], Nicolo Bencini[2], Spyros Efthymiou[3] and Antoniya Stoitsova[4]

[1]AA Emtech
London, UK
Parantap.Bhatt@
aaschool.ac.uk

[2]AA Emtech
London, UK
Nicolo.Bencini@
aaschool.ac.uk

[3]AA Emtech
London, UK
Spyros.Efthymiou@
aaschool.ac.uk

[4]AA Emtech
London, UK
Antoniya.Stoitsova@
aaschool.ac.uk

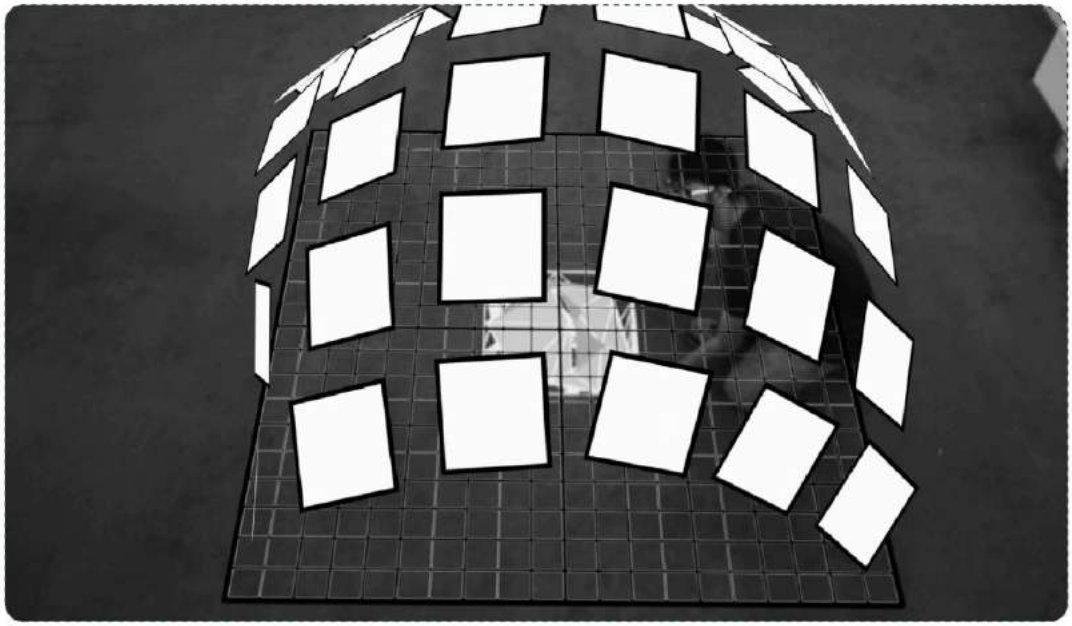

Figure 1. Digital experiments: Using augmented reality to overlay digital simulation of the structure on actual site.

ABSTRACT

This paper focuses on describing how augmented reality (AR) and object tracking methods can become tools for overlaying real-time information, for assembly of structures with tessellated geometries. Within this context, guided assembly is explored as an alternative to the energy intensive construction and demolition processes currently used in the building industry. For the research, sheet folding is chosen as the process upon which all assembly data is based on, and object tracking and augmented reality software are used as tools to guide the assembly of the proposed system. Experiments across multiple scales are conducted to study various methods of translating digital geometric information into a series of physical guided manipulations, which form the techniques for achieving a correct degree of folding within the component. Through large scale assembly tests, the viability of using guided assembly techniques as well as the potential of applying them in construction scenarios is assessed. The paper concludes with a description of benefits and drawbacks in which such technology may be used for, and outlines suggestions for further developments of the system to become a viable tool for construction assembly.

Author Keywords

Digital Design Strategies; Smart Geometry; Computational Design, Human-computer Interaction; Interactive Environments; Augmented Reality

ACM Classification Keywords

H.5.1 MULTIMEDIA INFORMATION SYSTEMS; I.4.1 DIGITIZATION AND IMAGE CAPTURE; I.6.8 TYPES OF SIMULATION

1 INTRODUCTION

Off-site manufacturing and fabrication techniques have improved the efficiency of the construction process, by allowing the creation of unique building components to tight tolerances. These methods have introduced automation into parts of the construction process; however there are limitations in terms of their adaptability and on-site use. Furthermore in fully automated assembly processes, most of the tools are suited to only one particular task but and are not able to adapt to different scenarios [1]. These issues along with problems of material management, coordination and assembly sequencing of the components once they leave the factory environment; have affected the efficiency of the overall process and hinder the introduction of

automated techniques onto the construction site [2]. On-site operations that cannot fully or partially be automated (and often involve human labourers) can be supplemented through the use of technologies which allow for the integration of the digital data and assemblies. This guided assembly process is not a different form of building construction, but the addition of a new layer of transferring construction data onto current methods [3]. "Assembly differs from construction in that it requires very little skill; it does not rely on information passed on through experience or development through apprenticeship. Assembly comes from a hierarchical understanding of groups of assemblies that are all connected through a series of steps." [4]. Guided assembly under this context is described as a "Process of planning and producing a designed part via an aid of information" [5]. In the past, physical guides such as paper manuals, diagrams for sequences or conductors who would orchestrate the sequence were the major controllers of guided assembly. However, modern technologies capable of storing and relaying large amounts of data, have replaced these analog guides with digital information. With rise in personal mobile devices capable of carrying large amounts of construction data, the link between building component and assembly data is being bridged [6].

Robotic fabrication has also helped implement and realize architecture through automating the whole construction process. However an isolated environment works well for robotic construction rather than a more organic on-site process that deals with a lot of behavioral and environmental factors. Complex computation and artificial intelligence can surely help overcome such challenges but it would require substantial time & cost. Hence, products like Microsoft Holo lens and Daqri Smart helmets are trying to explore augmented and mixed reality as another set of technological implementations [7] which enhances the construction process by supplementing operations that cannot fully or partially be automated. "The term Augmented Reality (AR) is used to describe a combination of technologies that enable real-time mixing of computer-generated content with live video display." [8] These systems involve the use of sensors and cameras to track objects in their immediate context and relay real-time construction information or assembly logics to the user, with the scope of improving the accuracy and reducing the duration of construction. Under the context of this research; augmented reality and object tracking applications are explored as a potential viable link between digital data and the construction site.

The aim of this paper was to assess the feasibility of using object tracking and augmented reality as real-time assembly aids, as well as the potential of applying this technology to construction scenarios. Through a series of experiments on different scales, methods of overlaying construction information were tested; and a guided assembly sequence for a tessellated structure was developed.

2 MATERIAL SYSTEM : GEOMETRIC EXPLORATIONS

The technique of sheet folding was chosen as the manipulation to be explored as it requires high precision and is therefore mostly restricted to factory environments. Geometry explorations were carried out using a set of regular and semi-regular tessellations. Specific attention was given to the non-periodic Ron Resch folding pattern due to its inherent characteristics - flexibility and ability to form variety of surface curvatures with regular primitives. These patterns were explored in detail through a series of physical and digital tests.

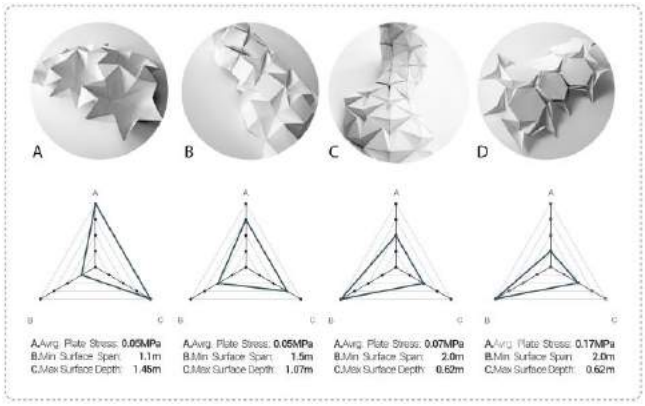

Figure2. Physical experiments showing different tessellated patterns and surface explorations.

The patterns were tested in Finite Element Analysis software and evaluated according to several criteria – *1)* average plate stress, *2)* achievable span, *3)* structural depth *4)* control in digital simulations context. Each model was tested on gravity load as aluminum folded plate with 4mm thickness, approximate size of 1.5m x 1.5m. Pattern B (fig.2) ranked second according to criteria *1,2* and *3*, however it achieved significantly better results in terms of accurate digital representation. Due to its overall high performance it was selected as the base geometry for further geometrical and physical investigations on an aggregation scale.

The surface aggregation experiments (fig.3) were aimed at investigating how components' locking in crucial locations and change in boundary conditions affect the overall geometry. The goal was to extract the parameters controlling the system's performance in terms of its structural stability and to establish the potentials and limitations of the system which would inform the construction assembly.

Several surfaces containing the same number of components were tested under gravity load. The chosen material was 2mm aluminum rather than 4mm aluminum in order to reduce the model self-weight. Components were locked following first and second principal direction stress lines. It was established that positive curvature geometries achieve lower deformations when locked following second principle stress lines and negative curvature – according to first principle stress lines.

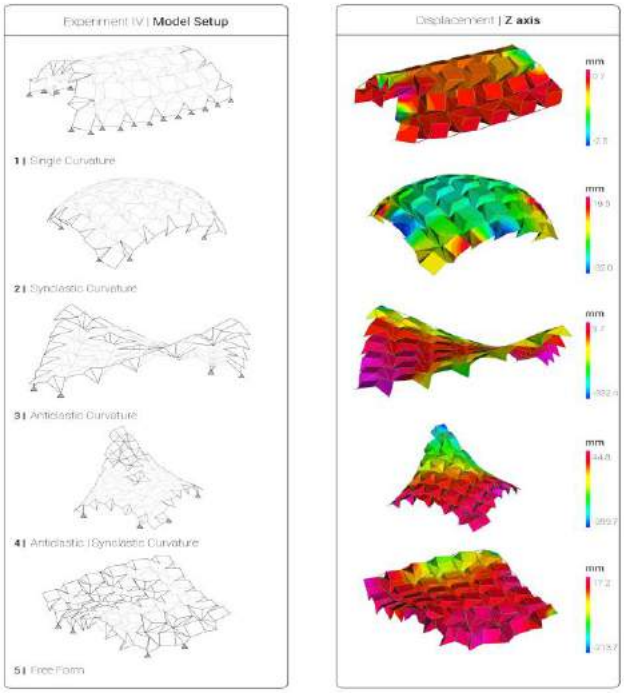

Figure 3. Finite Element Analysis aggregation experiments

A locking algorithm was developed based on the principles for achieving structural stability. First the position of the anchor points for the targeted surface is identified. Then gravity load is applied and stresses in first and second principal direction are determined. The pattern is locked in the positive curvature area when principal in-plane compressive stress values are higher than 60kN/m. In the negative curvature areas components are locked in the case of tensile force lower than 30kN/m. The locking algorithm was directly linked to a custom Augmented Reality assembly tool and used as construction sequence guide.

2.1 MATERIAL SYSTEM : FOLDED SHEET ASSEMBLY

Through alteration of assembly data which dictated the shape of the component, its aggregation logic and position in the overall structure; variations in the global form were achieved. Computational models in the form of spring-based physics simulations were used as a tool for generating the geometries from which the digital information for the guided assembly sequence was abstracted. These digital spring models allowed mapping of the folded patterns onto predetermined forms; however since the face edges behaved like elastic springs the exact edge lengths would vary and tolerances within the system had to be allowed to accommodate differences between the simulated and actual material behavior. Through a series of digital and physical studies, it was determined that lengths within tolerances of 5% greater or less than the edge's actual length would produce folding simulations that could be achieved physically. Furthermore the assembly process had to be adapted to account for these tolerances; and methods through which the relevant assembly data was projected onto physical space were developed through a series of assembly experiments.

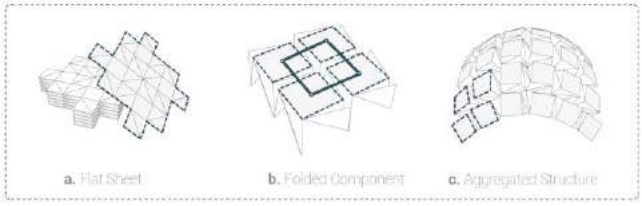

Figure 4. Assembly phases of the material system from component to structure.

3 EXPERIMENT SETUP

The Unity game engine and Vuforia Augmented Reality extension [9] were used as digital tools for translating the geometrical characteristics of physical objects into digital data and vice versa. As the first stage of object tracking image targets were uploaded into the software and were tracked by the camera to acquire an object's location and rotation data from physical models. The size of the target varied from 10x10cm to 50x50cm depending on the scale of the experiment and the tracking requirements. Live video feed was sent to the object tracking software through a HD web camera for smaller scale experiments and a Canon 450D camera for larger setups. Portable display devices were not explored as means of relaying information to the user since the focus of the research was mainly directed towards construction sequencing and therefore the data was relayed to the user from a stationary screen. The results and observations retrieved using these techniques were strictly related to the software and hardware used.

Figure 5. Experiment setup for a 100x120cm test (top) and a 200x200cm test area (bottom).

4 EXPERIMENTS

The experiments were divided into 3 sets which were aimed at exploring different aspects of the assembly process. These experiments were concluded with the construction of a 200x200 cm structure consisting of 9 components.

The first set of experiments involved a series of accuracy studies which were used to understand the capabilities and limitations of the setup as well as its possible applications as a construction aid. The second set of experiments involved a series of small scale studies aimed at understanding the sequence of instructions and manipulations which were used to fold one component into a predetermined form. This information was then used to develop a folding sequence for a single component. Once the folding sequence had been determined a final set of assembly experiments were conducted to study the effectiveness of AR and digital object tracking as a viable tool for the preparation and assembly of the proposed folded sheet system on a larger scale.

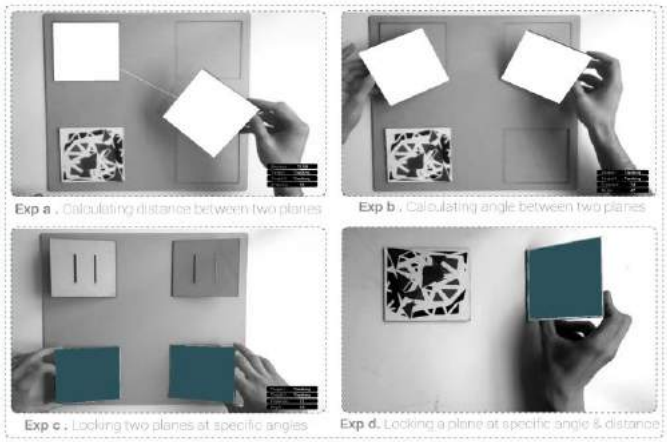

Figure 6. Accuracy tests with overlaid digital information.

4.1 Accuracy Tests

These tests were conducted with 10x10 cm trackers in a test area of 100x120 cm with controlled lighting conditions and an HD webcam as an input device.(Fig.6) The software's capability of measuring distance and rotation were analyzed and the minimum tolerances were recorded. It was shown that on a small scale, the position of one target in relation to another was measured with an accuracy of up to 2mm and its rotation was measured with an accuracy of up to 3°. It was concluded that with the setup used, the distances and rotations were measured with good accuracy under ideal conditions, but in low-light environments the software's ability to track the target was reduced and this resulted in inaccurate readings.

4.2 Folding Experiments

A set of folding experiments were then set up to explore a method by which the process of folding can be enhanced through the use of object tracking and Augmented Reality. These experiments were conducted with a similar setup to the previous experiments with 10x10 cm trackers in a test area of 100x120 cm with controlled lighting conditions and an HD webcam. The aim of these experiments was to understand which overlaid instructions were most successful in assisting the folding process (Fig.7). The first folding experiment explored shaping and locking of an individual component by simultaneously positioning as well as orienting all of its four faces into their final state, using overlaid digital aids. AR guides in the form of rectangles projected on top of the physical model were displayed through the laptop monitor and were used to indicate the correct location and rotation of each individual face. Color indicators were also used to indicate that the correct position and rotation angles had been reached. While this setup was able to direct the folding of the faces into the correct configuration, it presented some limitations in that it was difficult to manipulate all the faces at once while trying to match their orientation and position to the target.

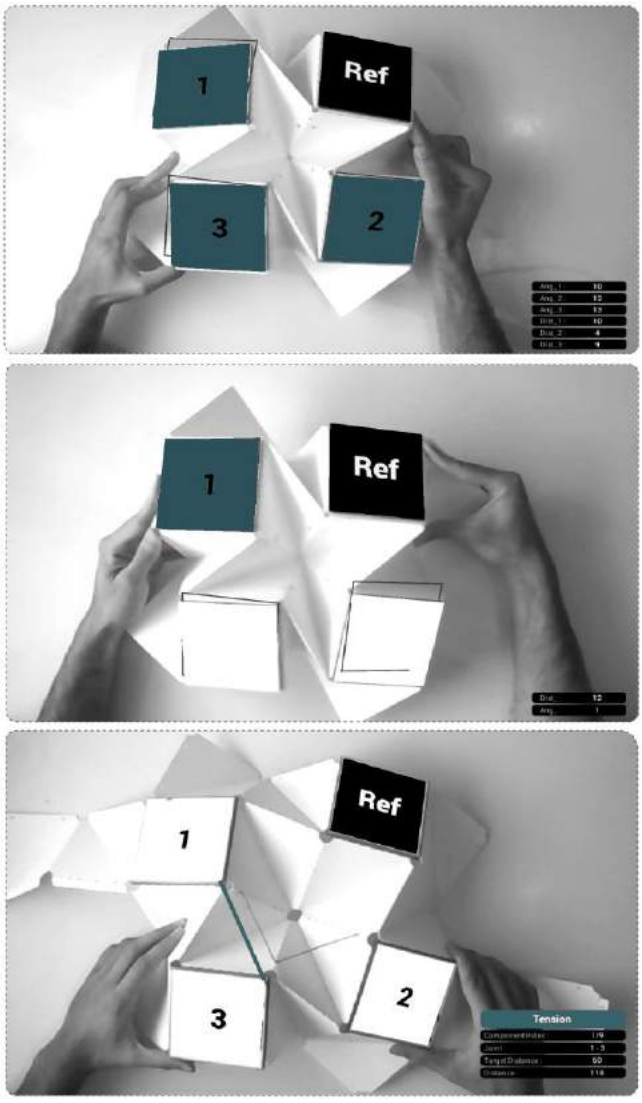

Figure 7. Folding experiment to lock components simultaneously (top), successively (middle) & sequentially (bottom).

The second folding experiment explored the formation of an individual component by successively positioning and rotating each of its four faces into their final state. It was noted that the folding sequence played an important role in the efficiency of these experiments. A numbering system was used to indicate the order in which the elements needed to be placed, whereas projected rectangles and color indicators were used to signify the correct position. This process improved the duration of the folding sequence as the user was able to lock the component more efficiently than in previous experiments.

Although, it was possible to form the geometry and match the correct rotation angles; it was still quite challenging due to the hardware and software inaccuracies which resulted in high tolerances of up to 5° being required for the process to be achievable. These high tolerances resulted in inaccurate folding configurations and it was therefore concluded that to improve the efficiency of the overall process the numbering was necessary.

The final folding experiment would attempt to achieve the component's final form by relaying only the distances of a face in relation to its neighbours rather than its location and rotation data. The goal was to achieve the final shape through locking of the least number of components and therefore speed up the overall process. Furthermore, the user interface was updated to indicate the sequence of elements which needed to be locked rather than indicating when the face has reached its target position. These additions facilitated the assembly process as it proved to be much easier to position the faces based on their distances in relation to their neighbours; rather than their location and rotation. The updated user interface also proved to be successful in relaying the locking order as well as what kinds of locks were needed. It was noted that in certain cases the component would not form the target shape even if all the locks were inserted as the effect of the neighbouring components within the aggregation was required for it to achieve its desired form. For this reason, the locking elements could be designed to allow for a degree of settling that would occur when the components are aggregated.

4.3 Assembly Experiments

The final set of assembly experiments were conducted on a larger scale than the previous setups with 30x30 cm trackers in a test area of 300x300 cm and a Canon 450D as an input camera. These experiments were used to determine which folding methods are effective at a larger scale and which level of accuracy can be achieved. The effectiveness of the proposed construction method was studied in 3 scenarios which related to the different stages of the assembly process: the component preparation stage, the site preparation stage and the component aggregation stage.

During the component preparation stage the folding sequence determined in previous experiments was explored on larger scale components and the accuracy of the AR setup was assessed. A 200x250 cm preparation area was set up with a Canon 450D camera used as a stationary input device. The overlaid instructions were used to fold the component into the required shape and to indicate which part of the component needed to be locked. On-screen color indicators were used to signal when the component face was in the correct location. As in previous experiments, each face was indicated as being in the correct position when the distance between it and surrounding faces was equal to that of the digital model. For the purpose of these experiments different tolerances were tested where a 0% tolerance meant that the user interface would indicate that the component's tracked face is in the intended location when its distance from the surrounding components is exactly equal to the intended distances (Fig.8). This experiment was repeated 10 times with variations in tolerances. It was found that at this scale, it took one person an average of 5 minutes to fold the component into the required shape and that the ideal tolerance for the distance between intended face location and the actual face location was 5%. Tolerances below 5% were not possible to achieve due to the limitations of the object tracking software and hardware whereas tolerances above 10% resulted in inaccurate component folding. It was also noted that the time for folding was initially above 10 minutes however with practice and repetition a constant 5 minute folding time was achieved even with tolerances lower than 5%. As with the previous folding experiments, in certain cases the component was not able to form the indicated shape as the effect of the neighbouring components within the aggregation would be required for it to achieve its desired form. It was also noted that in certain cases failure of the digital model to accurately simulate the components' material behavior led to differences between the physical and simulated component. For this reason it was concluded that locking elements should be designed to allow for a degree of flexibility and settling of the component.

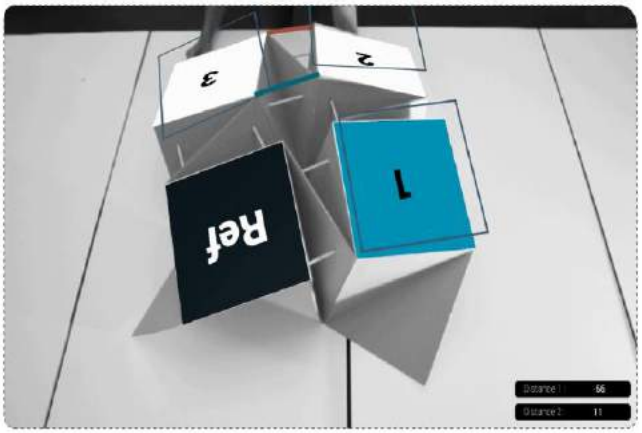

Figure8. Assembly experiment set 1: where the component was locked using digital guides.

The site preparation experiments explored the use of AR as a tool for locating the entire structure on site as well as for

the setting up of structural props for the system. These experiments were used to locate a 200x200 cm structure within a 300x300 cm test environment. A 50x50 cm tracker was used as the target for the base of the structure which was used to orient and locate a digital model of the structure as well as act as the base grid for locating and positioning the structural props (Fig.9). It was found that it was possible to use the proposed object tracking methods on the larger scale required by these experiments. The digital model served as a good indication of the location of the structure in relation to the base tracker and was used successfully to locate the structure in physical space. However perspective issues, where the digital perspective of the model did not match the perspective of the physical world became noticeable on larger scales which resulted in an inaccurate representation of the final form. It was therefore noted that the software was capable of giving visual indications of the position of the structure however it was not able to accurately locate it within space due to tracking issues experienced in larger scale environments

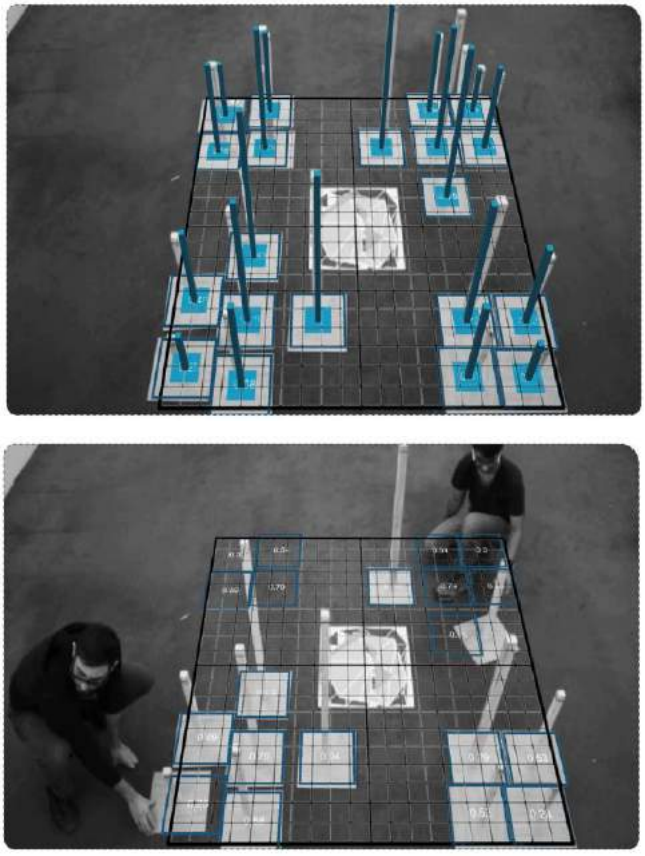

Figure9. Site preparation experiment where different lengths of scaffoldings are placed according to their position on site.

As the camera used was kept in a stationary position, the perspective was kept constant and once the structure had been located on-site, the tracking behaviour of the base target was turned off so as to lock the digital model in relation to its surroundings. This was done to keep the model stable and reduce the flickering that was occurring due to the software's limitations on larger scales. The setup was then used to indicate the location and height of the structural props through the overlaying of a digital assembly grid on the recorded physical environment. It was possible to accurately position each of the props in their correct location using the overlaid information.

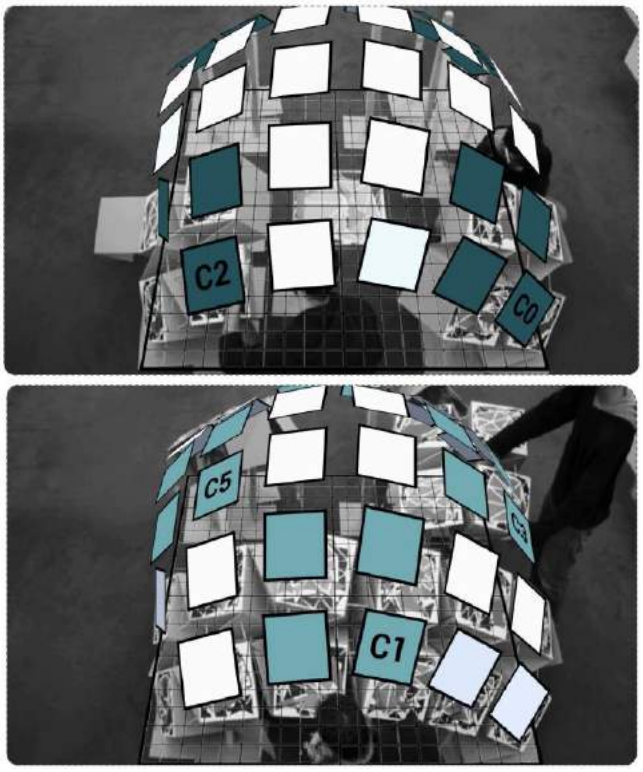

Figure10. Screen capture from the assembly experiments where locked components were assembled using digital guides to relay their desired location and assembly sequence.

The final stage of the assembly sequence involved the aggregation of components to form the intended 200x200 cm structure. The data needed for constructing this structure consisting of 9 components was summed up to 125 different distances and 60 different angles to lock. The main aim of this experiment was to assess the capability of using AR to relay this data to the assembler and outline the construction sequence for the efficient assembly of the structure. Once the flat sheets had been folded into the required shape and the structural props had been set up using the previously outlined methods, AR was used to relay the assembly sequence to the assemblers and give a visual indication of the structure's final form (Fig.10). It was noted that at this scale it would not be effective to use AR as a tool for accurately locating each of the individual components in their correct location; however it was found that the software is capable of relaying assembly sequence

data and assisting component management. It was also noted that once the structural props had been placed in the correct position and the components had been accurately folded into shape, the exact position and orientation of each individual component was not needed to assemble the overall structure. The setup was also successful in relaying the predetermined assembly sequence to the assemblers as well as the location of each component within the structure

5 CONCLUSION

Throughout this research, augmented assembly techniques were evaluated directly in relation to the chosen material system and towards specific design ambitions. All of the observations were linked to the prototypes material, experiments setup and the chosen scales. It is important to note that these conclusions are related to the available resources and knowledge base of the authors at the time of the research. However, the observations and derived conclusions were later used in order to comment on the potential benefits, possibilities and limitations of using digital augmentation in assembly processes.

5.1 Conducted Experiments

The developed process was used effectively within controlled environments up to a scale of 200x200 cm. The best results in terms of time and accuracy were achieved when tolerance allowances were built into the system. It was therefore concluded that it is important that the design of the component itself forms part of the development of a digitally guided assembly sequence. Moreover, it was observed that manipulations which involved measuring distances were easier to guide using AR than those involving rotations. Accuracy was also slightly better whilst controlling distance over rotations. It was therefore noted that for the process to be efficient and as accurate as possible, both the component and its method of assembly should have minimum complex geometrical measurements and manipulations. The overall system should either allow a degree of flexibility or limit for configurations to be achievable. The type of digital information overlaid should also stay simple and easy to follow. From the conducted assembly experiments, it was found that each component took roughly 5 minutes to fold and lock by using the developed AR process. The required time was relatively short and did not require any previous knowledge. On the contrary, the complex geometrical manipulations required to achieve the desired configurations were difficult to execute with traditional methods of translating 2D plans. It was observed that the user was experiencing difficulties in distinguishing the different elements as well as translating the two dimensional plans into the desired form thus increasing the required time dramatically. Overall, the developed AR process was successful in suggesting the desired configuration for each component as well as its final position on the surface in a relatively efficient and accurate way. Through colour indications and relevant data screen projections that were offered to the user, the assembly process was managed without the need of specific project related knowledge or any form of printed information in the form of drawings. On the other hand, the developed process exhibited important limitations in terms of achieved accuracy and tolerances as well as luck of scalability of the overall method. Further experiments should be carried out in order to extensively compare the augmented process with traditional assembly techniques as well as with automated methods such as robotic driven assemblies.

5.2 Augmented Assembly process

Although significant benefits in the developed assembly method were clearly identified, the process revealed limitations that would make its adaptation into large scale projects challenging; as it requires construction accuracy. Those limitations were mostly due to object tracking inefficiencies that would not allow acceptable accuracy levels or large scale digital readings and projections. It was also observed that the above mentioned inefficiencies could be tracked back to poor lighting conditions, large distances, camera characteristics and image targets quality and size. It is important to note that even through optimizing some of these elements, the results were not significantly better in terms of accuracy. Moreover, the inability to accurately simulate material behaviour digitally created inaccuracies between the digital and physical world. This fact further affected the accuracy of the assembly experiments as small differences between the physical and digital models resulted in configurations which were not possible to achieve or reproduce. It is therefore concluded that this process cannot be implemented as is, in cases were relatively big tolerances are unacceptable and of significant importance. Potential improvements in order to make the process more applicable for a larger scale were identified. Firstly, portable controlled environments could be set up on site thus allowing more reliable readings and assembly instructions. Secondly, sophisticated equipments like multiple cameras and laser readings combined with computer vision implementations could be used to calibrate and improve the accuracy issues. Thirdly, further technological additions to the system could involve the use of embedded technologies such as RFID trackers or 3D scanning to supplement the AR data and increase the efficiency and data extraction process. Finally, the most important aspect is that this type of process can prove to be beneficial and reliable enough in cases where the desired structure was designed having this same process in mind. More specific, a structure that would allow pre-defined tolerances or easily achievable configuration settings would be ideal. In these cases, the augmented system could be used effectively to identify each distinct element, illustrate the information for the individual configurations and suggest the overall assembly sequence and order.

Under this context, it is concluded that augmented assembly processes are able to act as a bridge between the

design studio and the construction site by extending the capabilities of current assembly methods. This approach did not attempt to compete or replace automated or semi-automated assembly techniques but rather enhance or compliment them. In specific, for smaller scale components that can be manipulated by humans, for non-repetitive assembly tasks, for assemblies that need to be reconfigured frequently and for structures that include large number of similar components that can take different configurations are some of the cases that this technology could be largely successful if implemented properly. Places that do not have easy access to automated machinery or cases that the assembly cost should stay relatively low could also be considered.

Further developments for the described system would include explorations into the use of the tool for the post-construction evaluation of a material system in order to assess its performance. Moreover, the augmented process could be used to guide a disassembly sequence. In addition, as the results from these experiments were limited to stationary setups in indoor environments, an exploration into the use of mobile devices as assembly guides in outdoor environments should also be explored and evaluated. Finally, experimentation with different configurations - assembly systems other than folding could be studied on various scales so as to assess the flexibility of augmented assembly methods.

ACKNOWLEDGMENTS

We would like to thank Michael Weinstock, George Jeronimidis and Evan Greenberg their advice during the research. A special thanks to all our colleagues and mentors at the AA; who helped us develop and discuss the topic in greater depth. The research paper contains transcripts from the dissertation "Transient Systems: Exploring Aided Assembly techniques for reconfigurable structures" developed by the authors at the Emergent technologies and Design programme at the Architectural Association in London, UK.

REFERENCES

1. Tang.A, Owen.C, Biocca.F & Mou.W; Experimental Evaluation of Augmented Reality in Object Assembly Task: *Inň Proceedingsň ofň Internationalň Symposiumň onň Mixedň andň Augmentedň Reality*, Springer Publications, USA, (2002)

2. Durmisevic.E and Yeang.K; Design for Disassembly in Architectural Design Special Issue: *Patternsň ofň ArchitectureňVolumeň79*, Issue 6, , John Wiley & Sons Publications, UK , pages 134–137, November/December 2009

3. Gines.M & Beorkrem.C; The Transformation of Architecture: Design for Dis-assembly: *InňProceedingsňofň theň 2010ň ARCC/EAAEň Internationalň Conferenceň onň Architecturalň Research*, Washington DC, USA, 2009

4. Kieran.S and Timberlake.J; Refabricating Architecture: How Manufacturing Methodologies are Poised to Transform Building Construction, New York: McGraw-Hill Professional Publishing, USA, 2003

5. Engelke.W; How to Integrate CAD/CAM Systems: Management and Technology, P.234-238. CRC press ,USA, 1987

6. Mekni.M & Lemieux.A; Augmented Reality : Applications, Challenges and Future Trends in *Proceedingsňofňl3thňInternationalňConferenceňofňappliedň computerňandňappliedňcomputationalňscience*, Malaysia, 2014

7. Moar. J, Category on Devices and Wearable in *Consumerň &ňEnterpriseňsmartňglasses:ňOpportunitiesňandňforecastsň 2015-2022,ň*Juniper publications, Canada, 2016

8.Azuma.R, *Aňsurveyňofňaugmentedňreality,ňInňPresence:ň Teleoperatorsňandň Virtualň Environments* vol. 6, no. 4, pp. 355–385, 1997

9. Software details on Unity gaming engine (unity3d.com) and Vuforia developers portal (developer.vuforia.com).

Visualization of Building Performance using Sankey Diagrams to Enhance the Decision-Making Process

Aly Abdelalim, William O'Brien
Human Building Interaction Lab, Carleton University, 1125 Colonel by Dr., Ottawa, ON K1S 5B6
AlyAbdelalim@cmail.carleton.ca, liam.obrien@carleton.ca

ABSTRACT
Nowadays, there are various building energy performance optimization methods available to designers. The aim of these methods is to vary building parameters to optimize the energy performance of the building in the early design stage and during operation and to choose the appropriate alternatives evaluated through multi-criteria objectives. However, current visualization methods have some limitations in evaluating simulation results in relation to non-performative or qualitative analysis. This paper investigates the feasibility of using Sankey diagrams to visualize and understand the upstream and downstream performance impacts of building design decisions. The current target audience is primarily architects and design engineers. The aim of this paper is to provide a workflow to obtain, analyze, and visualize energy flows obtained from simulation outputs. The developed workflow is applied to large office commercial reference building models that comply with the national energy code of Canada for buildings. Samples of Sankey diagrams are presented to visualize the impact of changing building/system components on the whole system performance and demonstrate energy-saving strategies.

Author Keywords
energy flows in buildings; HVAC loads; visualization of energy flows; Sankey diagrams.

1. INTRODUCTION

Energy demand in commercial and intuitional buildings accounts for 14 percent of the total energy consumption in Canada [1]. Optimization of building parameters (such as geometry, orientation, materials, and construction) in early design stages or components (such as mechanical, electrical, and control systems) during operation is crucial to reduce energy use and greenhouse gas emissions [2]. Moreover, communicating these interrelationships to decision makers and other stakeholders is critical to achieve high-performance building design. Integrating parametric modeling into the process of energy performance analysis helps designers evaluate different alternatives through complex multi-criteria objectives [3].

On the visualization side, the most common visualization techniques used for parametric design of buildings are interactive parallel coordinates plot, binning and carpet plots, voxel-plot, superimposed line graph plot, line chart, bar graph, and color mapping.

Jeong et al. [4] developed an integrated environment combining BIM and the results from object-based building energy simulation (BES). Their method helped in visualizing energy simulation results of each building component one at a time in BIM environment. Moreover, objects such as infiltration, ventilation, solar radiation, and occupants were not included in their study. Asl et al. [5] developed an integrated parametric BIM-based system to interact with cloud-based whole building simulation and daylight tools to optimize the building energy performance using a multi-objective optimization. Their system helped designers to explore different design alternatives using a visual programming interface and to assess the energy performance to select the most appropriate window design. Interactive parallel coordinates plot was used in their study to visualize various iterations to be evaluated by users. Raftery and Keane [6] presented a new visualization technique of building performance data by combining binning with carpet plots. Pratt and Bosworth [7] developed a multi-scalar visualization technique that could help users understand the effect of changing building parameters on energy performance. Three-dimensional interactive voxel-plot and superimposed line graph plot were used in their study to visualize the output simulation results. Pratt and Bosworth claimed that an effective visualization method is needed when inspecting a high order (more than three variables) search space.

Moreover, Pratt and Bosworth [7], Srivastav et al. [8], and Hab et al. [9] claimed that conveying simulation results in the form of tables and graphs is not useful to non-expert designers in the field of building science. Elnimeiri and Nicknam [10] visualized the results of environmental and structural performance using color mapping, which enabled the design team to understand the effect of different designs. Recently, Autodesk developed Insight 360 tool [11], which empowers users to evaluate different design scenarios that could lead to a better building performance.

The above-mentioned visualization methods have some limitations in evaluating simulation results in relation to non-performative or qualitative analysis [7]. Moreover, the current visualization tools typically do not provide a comprehensive understanding of how each component

SimAUD 2017 May 22-24 Toronto, Canada

affects the whole system performance, including upstream and downstream building systems.

Sankey diagrams are a useful and rarely-utilized method to represent energy performance at all levels of the build environment. These diagrams consist of arrows that represent the magnitude and direction of the flow (i.e. energy flow) from source to sink [12]. Furthermore, Sankey diagrams can provide relative magnitude of the flow, input and output of interacting systems, energy recovery, and spatial representation. There are various applications of using Sankey diagrams in visualizing energy flows. On the campus level, Sankey diagrams were utilized to visualize energy, mass, greenhouse gases, and utility cost in a companion paper by Abdelalim et al. [12]. In another companion paper, Sankey diagrams were utilized to visualize energy flows and associated costs on the building-level by using measured and calibrated model data [13]. Belzer [14] used Sankey diagrams to visualize energy flows from source to end-use in the building sector. Dynamic Sankey diagrams were also used to visualize internal and external flows through building envelopes [15]. Schlueter and Thesseling [16] integrated Sankey diagrams into building information modeling (BIM) to visualize instantaneous energy and exergy. Sankey diagrams were also integrated to limited number of building design and analysis tools to visualize predicted energy use, such as CASAnova [17] and Sefaira [18]. On the HVAC system level, Sankey diagrams were utilized to visualize real HVAC performance of a large commercial building [19]. Sankey diagrams were also used in the work by Perez-Lombard et al. [20] to visualize energy flows in a typical constant air volume systems installed in office buildings in Spain. The current applications/tools utilizing Sankey diagrams to visualize building-level energy performance used set of nodes to represent inputs and outputs of energy at the building rather than multi-staged nodes. Moreover, the current tools have some limitations in comparing multiple designs simultaneously.

Recently, an online survey was conducted to assess usability and effectiveness of visualizing energy flow and the associated cost using Sankey diagrams on the building-level. The survey was applied to a sample user group (42 participants). The sample group consisted of 13 energy managers, 12 design engineers, 6 researchers/lecturers, and 11 other related professionals. 78 percent of the participants supported the notion that Sankey diagrams helped in: 1) visualizing building-level energy flows and costs, 2) understanding the interrelated variables that affect building performance, 3) identifying system inefficiencies, 4) quantifying and understanding the impact of unmeasured energy flows, and 5) making operational problems more visible and quantifiable in order to identify opportunities for energy savings and facilitate decision making.

This paper investigates the feasibility of utilizing Sankey diagrams in visualizing building energy performance and to understand the upstream and downstream impact to allow various design variants to be evaluated and facilitate the decision-making by architects and design engineers. The target audience is often policy makers and other non-technical professionals without a building physics background. Thus, communicating relative energy flows is important to provide them with a basis for informed decision-making.

This paper proposes a workflow to obtain, analyze, and visualize energy flows obtained from simulation outputs. The developed workflow is applied to large office reference building model that complies with the National Energy Code of Canada for buildings (NECB) (as the base case) for Ottawa climate zone (ASHRAE Climate Zone 6) [21]. Reference building models are used for

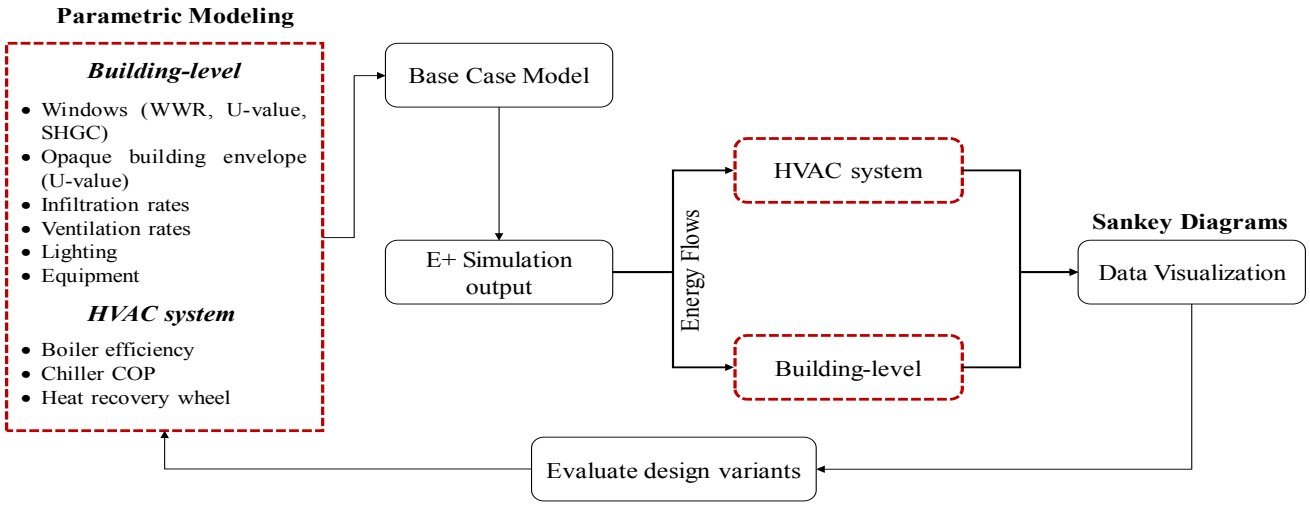

Figure 1. Flowchart showing the process to visualize energy flows on building-level and HVAC system using Sankey diagrams and evaluate different design variants

building code development, research, and design guides. Sankey diagrams are used to inspect the energy-saving opportunities for the base case. Different design scenarios are proposed and compared to the base case model energy performance. Samples of Sankey diagrams are presented to visualize the impact of changing building/system components on the whole system performance and demonstrate energy-saving strategies. The proposed Sankey diagrams consists of multi-staged nodes, rather than merely inputs and outputs, to provide a greater understanding of how each building component/system consumes energy and relates to the others. Moreover, the paper discusses the potential of each design option in terms of energy savings using Sankey diagrams. The paper also discusses the technical challenges of creating Sankey diagrams from simulation data.

2. METHODOLOGY

The aim of the proposed study is to utilize Sankey diagrams to visualize building energy performance on the building-level and building system level (HVAC system) obtained from simulation outputs. The paper proposes a workflow to obtain, analyze, and visualize energy flows obtained from simulation outputs as shown in Figure 1. EnergyPlus 8.6 (E+) was selected as the BPS tool due to its technical documentation and versatility and capability of simulating complex building systems [22]. In this paper, a large office building model that complies with the National Energy Code of Canada for buildings (NECB) for Ottawa climate zone was used as the base case model. The workflow consists of:

1) Converting sub-hourly data into annual energy flows by selecting the appropriate output variables and meters that are listed in Section 2.2.
2) Aggregating energy flows: some variables, such as (windows heat gain/loss and transmitted solar radiations, heating coils, conduction heat gain/loss rates people sensible heating and latent energy gains, air stream nodes, zone infiltration total heat gain/loss energy, and surface heat storage loss/gain rate) provides output for each zone or element. Thus, zones or elements for each variable were summed up.
3) Checking the energy balance. This process was performed by adding energy flows entering and leaving the building. As EnergyPlus provides dynamic simulation results (i.e. not steady-state for each hour). Thus, output variables such as energy input or extraction of radiant panel, boiler, chiller, and heating and cooling coils were modified to maintain energy balance for each hour and also maintain daily and monthly energy consumption.

The following sections provide details on the selecting base case model and the required simulation output variables and meters that creates Sankey diagrams.

2.1 Setting Up the Model

The purpose of this section is to provide information on the selected EnergyPlus 8.6 (E+) base case model. The base case model represents large office Canadian reference building provided by Natural Resources of Canada [23]. Table 1 shows base case model details summary. Figure 2 shows base case model for large office building used for Ottawa climate. AMY (actual meteorological year) weather data was used for Ottawa, Canada [24]. Schedules for internal gains used are based on American Society for Heating, Refrigerating and Air Conditioning Engineers (ASHRAE) 90.1.

Table 1. Base case model details summary

General	Bldg. type	Large office
	Floor Area (m^2)	14,252
	No. of stories (including basement)	12
	No. of thermal zones (4 perimeters and 1 core zones/typical floor)	56
	Window to wall ratio (WWR) for all orientations:	44.57
Building Envelope U-value ($W/m^2.K$)	Roof	1.881
	Walls	0.454
	Below grade walls	3.663
	Intermediate floor and basement floor	1.881
	Windows (double glazed (6mm) with 6mm air gap: clear from inside and tinted from outside)	3.045
	Window (SHGC)	0.368
Internal Gains	People: (person/m^2) office/mechanical rooms	0.05/0.00495
	Lighting: office/mechanical rooms (W/m^2)	10.9/13.29
	Equipment: office/mechanical rooms (W/m^2)	7.5/1
Infiltration Rates	Floor per exterior surface area ($m^3/s\text{-}m^2$)	0.00025
HVAC air loop	The building is conditioned by four air handling units (AHUs). AHU-fan efficiency is 55%. No heat recovery is installed. Air distribution system is single duct VAV-box	
Space Cooling	Two electric EIR chillers with COP of 2.5 and a cooling tower single speed. The building relies on free outdoor cooling when the outdoor temperature is below 28°C	
Space Heating/Hot water	Hot water delivered from a boiler using natural gas (83% thermal efficiency). All zones are equipped with radiant panels	
Thermostat settings	heating/cooling setpoints are 22°C to 24°C, respectively. heating/cooling setbacks are 18°C to 27°C, respectively.	

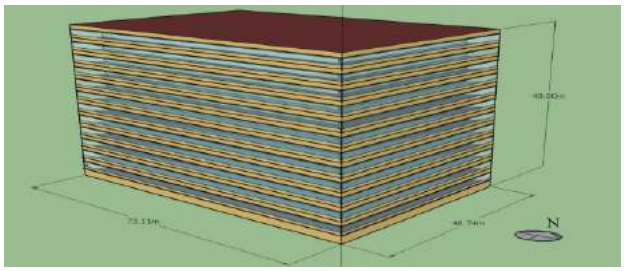

Figure 2. Base case model for the large office building

2.2 Simulation Outputs

Energy simulation tools provide numerous output variables and meters, from which the user has to choose the appropriate ones based on the required analysis. Table 2 shows the outputs that were used in this study in order to create Sankey diagrams.

Table 2. Hourly simulation output variables used in the study

Output variable	Description
Boiler	Heating energy Gas energy Ancillary electrical energy
Chillers	Chillers electricity Evaporator cooling energy Condenser heat transfer rate
Cooling tower	Fan energy Heat transfer rate
Pump	Pump electric energy Pump fluid heat gain
AHU	AHU-fan energy Humidifier Heating coil Cooling coil Heat exchanger (heat recovery) Outdoor air node energy Exhaust air node energy Return air node energy Mixed air node energy
Baseboard	Total heating energy
People	Sensible heating energy Latent energy
Windows	Heat gain Heat loss Transmitted solar radiation
Infiltration	Zone infiltration total heat gain Zone infiltration total heat loss
Lighting	Electric energy
Equipment	Electric energy
Opaque envelope	Outside surface heat loss Outside surface heat gain

3. DATA VISUALIZATION

This section includes samples of data visualization of energy flows on the building-level and one of the air handling units (AHU) and plant loops for the base case model using Sankey diagrams for winter and summer seasons as shown in Figure 3. The Sankey diagrams presented in this paper focused on hourly data obtained from EnergyPlus (E+) simulation outputs. Sankey diagrams should be read based on the direction of the flow (i.e. from left to right). For instance, during winter, heat is added to the building from left side and leaving rightward. While during summer, heat is extracted from the building. All forms of energy in these diagrams were converted to one common energy unit (MWh). The Sankey diagrams were rendered in a browser using Scalable Vector Graphics (SVG). The layout was derived from D3's Sankey layout code developed by Google Developers that provided more flexibility in organizing nodes, colors, and font sizes [25].

For the base case, the exhaust air from the AHU recorded the highest source (~60 percent) of heat loss during winter season. This is due to the lack of heat recovery wheel (HRW) installed. Moreover, approximately 21 and 17 percent of the heat was lost through opaque envelope and windows, respectively. While, that the results show that the amount of heat was added by windows was 7 percent. This is due to the high windows USI-value. During summer season, the highest source (31 percent) of heat gain was from lighting. While, approximately 22, 18, and 17 percent of heat was added by windows, equipment, and opaque envelope, respectively. It was also found that lighting is responsible for approximately 51 percent of total internal heat gain. Moreover, the internal heat gains are responsible for 60 percent of mechanical cooling energy provided.

The next step in this study is to change some building/system components to optimize the building energy performance. Based the above analysis, windows and lighting will be modified on the building-level. While on the building system level (Heating, Ventilation, and Air Conditioning (HVAC)), a HRW will be installed to take advantage of the exhaust air in the AHU. These parameters are listed in details in the next section.

4. PARAMETRIC MODELING

There are various parameters that could be modified on the building-level and building system level to optimize the building energy performance. Table 3 shows different design variants implemented in this study. Each design variant was applied independently and compared to the base case.

Table 3. Design variants details

Design variants	Parameters	Level
Base case (BC): (grey)	Details mentioned in Table 1.	
I1: (red)	Windows: reduce U-value to 1.903 W/m^{2}K and SHGC to 0.252	Building
I2: (blue)	Lighting: reduce light power density to (5.45/6.65 W/m^2) for (office/mechanical room)	Building
I3: (green)	Install rotary heat recovery wheel (HRW)	HVAC

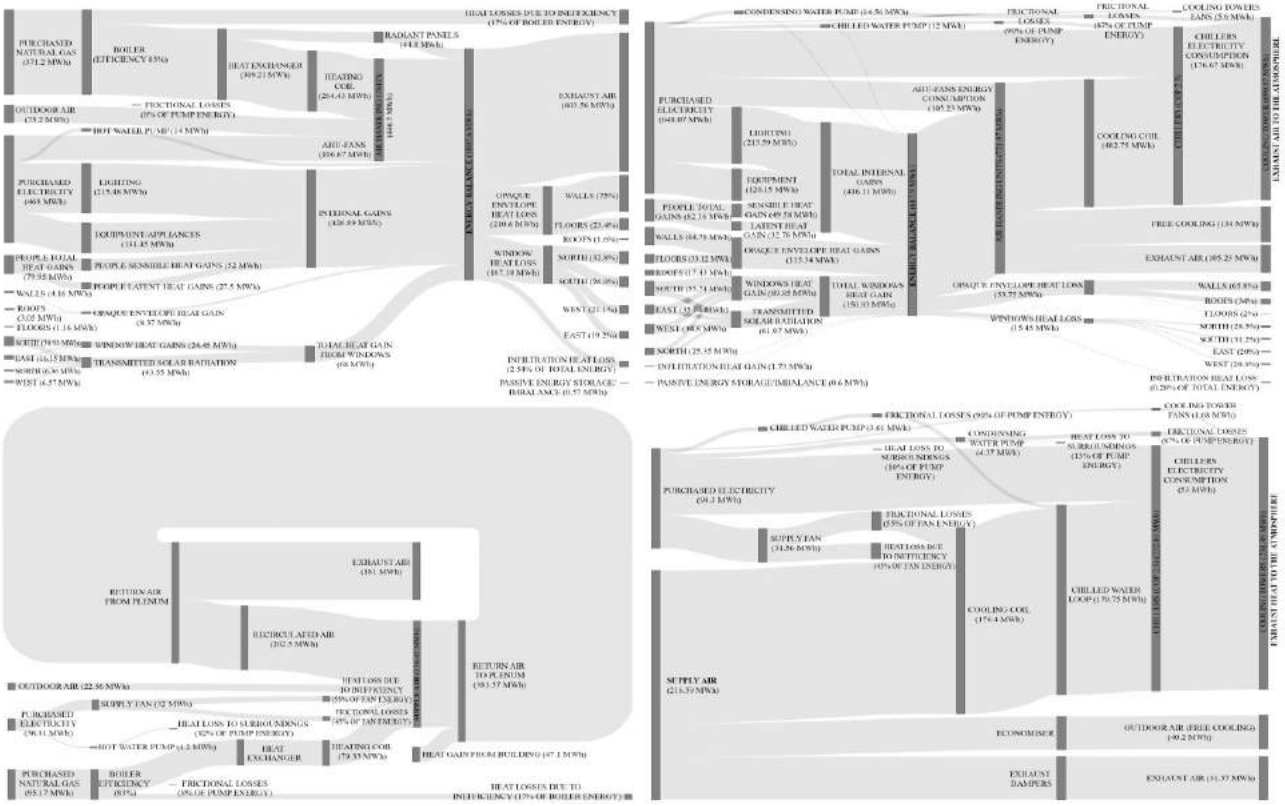

Figure 3. Sankey diagrams showing energy flows on the building-level for the winter season (top left) and summer season (top right), and energy flows on the HVAC system for the winter season (bottom left) and summer season (bottom right) for the base case (BC)

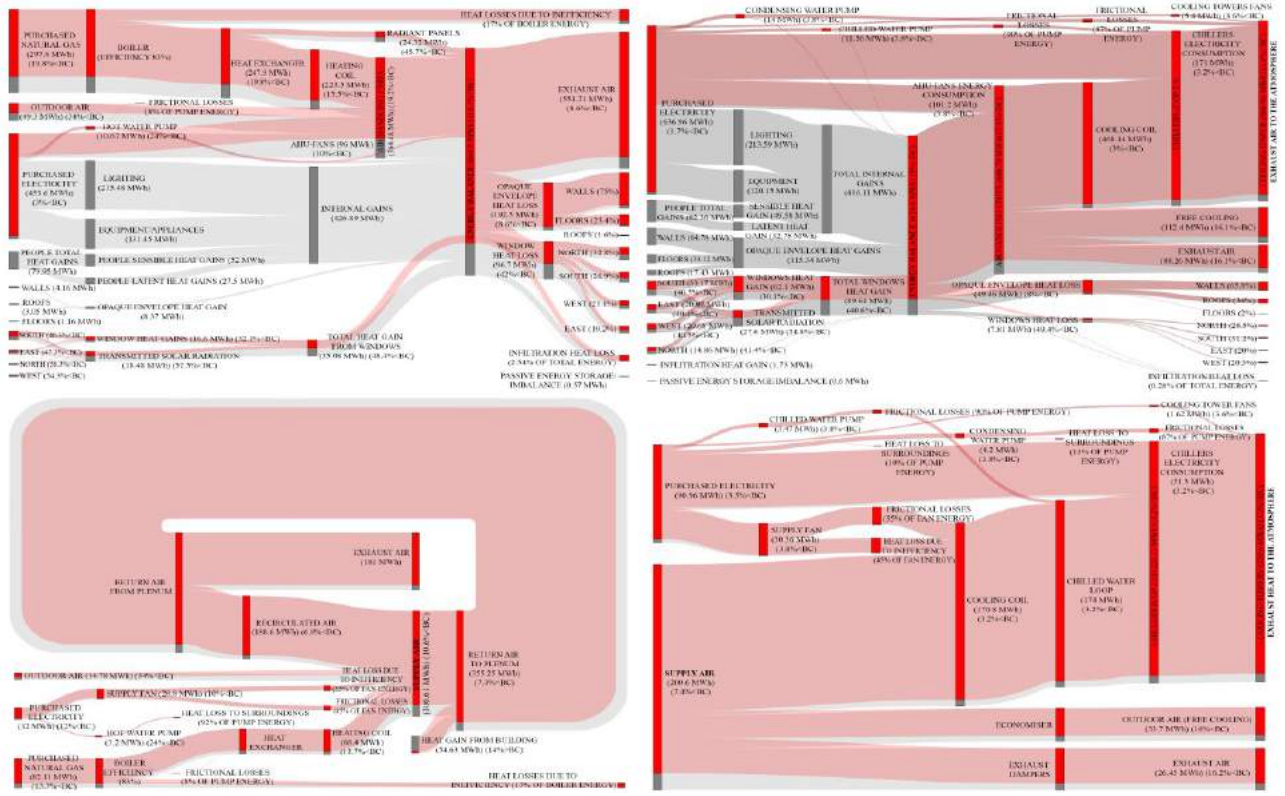

Figure 4. Sankey diagrams showing energy flows (grey for BC and red for I1) on building-level for the winter season (top left) and summer season (top right), and energy flows on HVAC system for the winter season (bottom left) and summer season (bottom right)

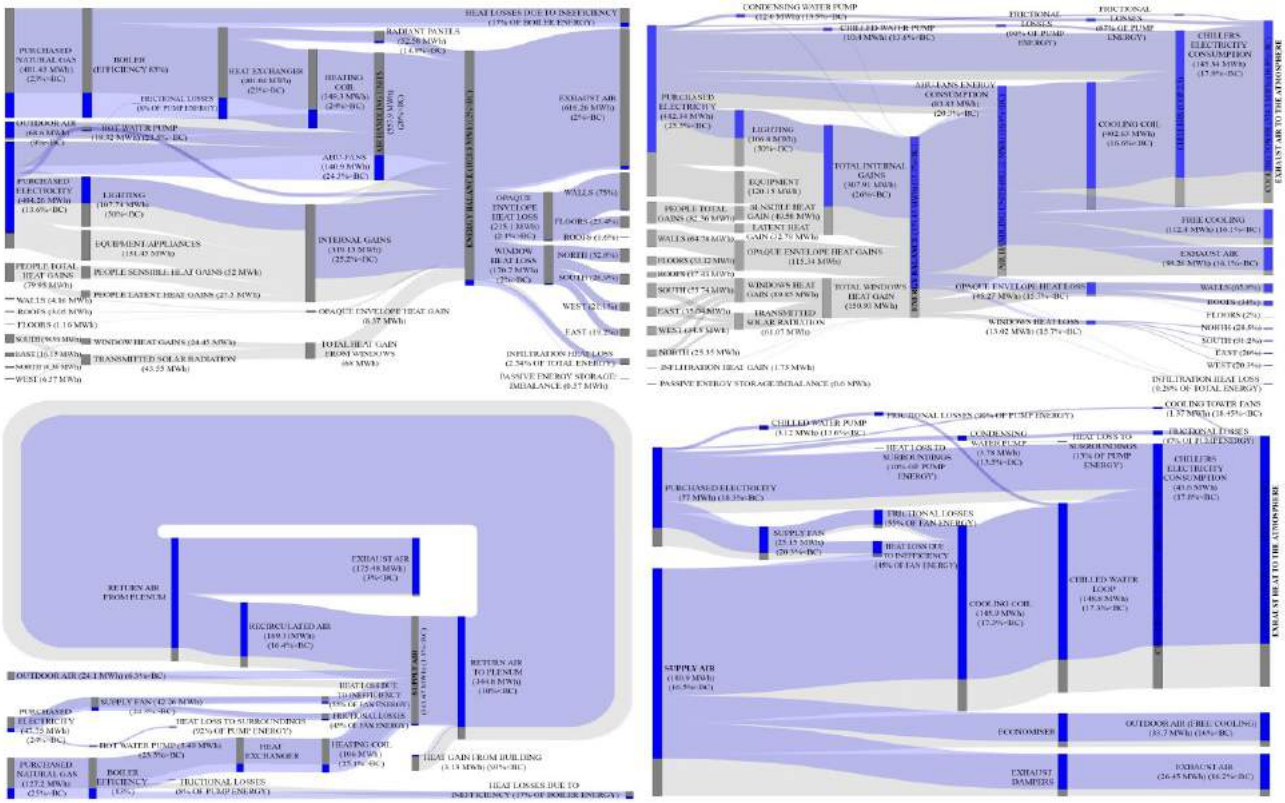

Figure 5. Sankey diagrams showing energy flows (grey for BC and blue for I2) on building-level for the winter season (top left) and summer season (top right), and energy flows on HVAC system for the winter season (bottom left) and summer season (bottom right)

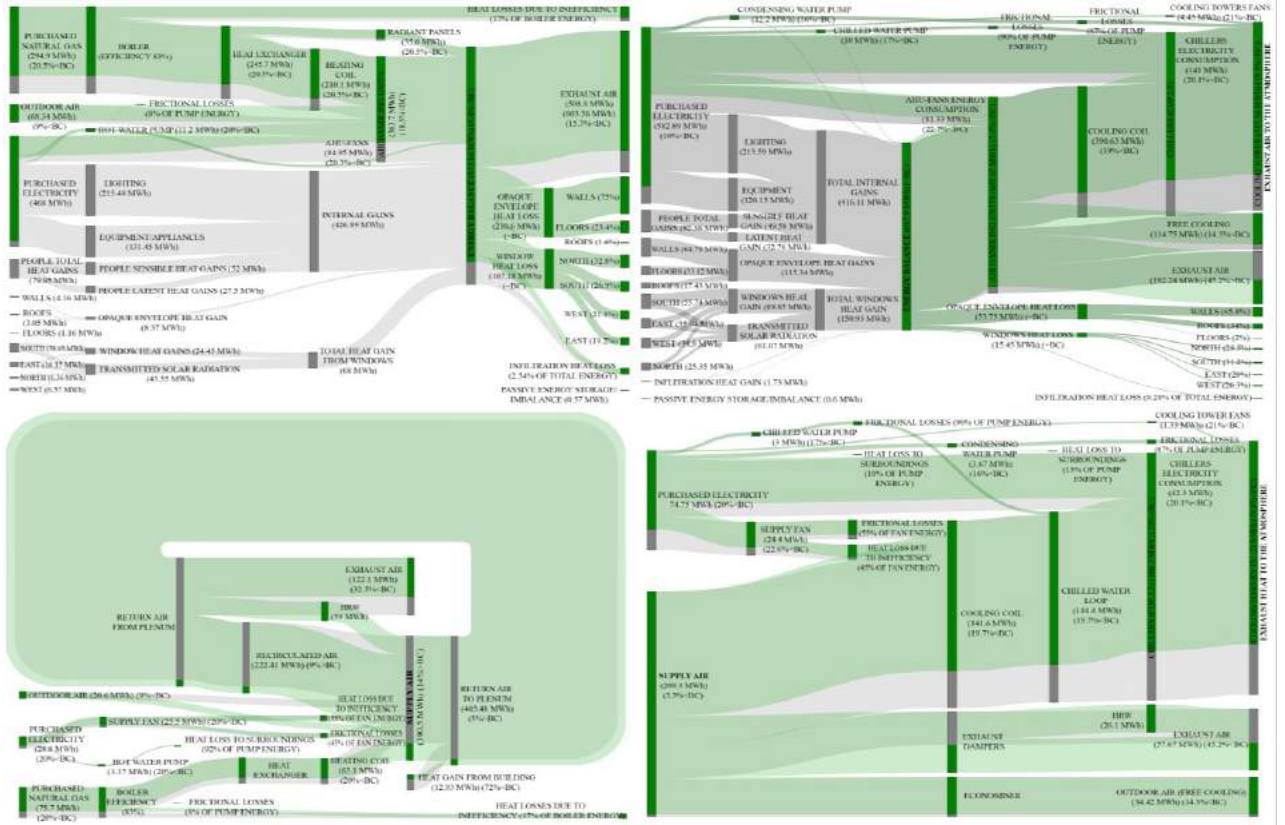

Figure 6. Sankey diagrams showing energy flows (grey for BC and green for I3) on building-level for the winter season (top left) and summer season (top right), and energy flows on HVAC system for the winter season (bottom left) and summer season (bottom right)

5. DISCUSSION

The aim of this study was to investigate the feasibility of utilizing Sankey diagrams in visualizing energy flows on different spatial resolutions obtained from simulation outputs. A workflow was developed to obtain and analyze vast data sets obtained from simulation outputs and convert them to energy flows to create Sankey diagrams. Large office Canadian reference building was used as the base case. Sankey diagrams showing energy flows for base case on building-level and HVAC are shown in Figure 3. From the analysis mentioned in Section 3 on the base case (BC), parameters such as windows, lighting, and HRW were selected to be modified based on their significance on heating and cooling loads. The three proposed design variants are (I1, I2, and I3). Sankey diagrams were utilized to compare different design variants to the base case model energy performance. Energy flows on building-level and HVAC system for winter and summer seasons for I1, I2, and I3 are shown in Figure 4, Figure 5, and Figure 6, respectively. Grey, red, blue, and green colors were used to represent the energy flows of base case, I1, I2, and I3, respectively.

In the base case, the windows were responsible for 17 percent of heat loss during summer. While during summer, the amount of heat gain from windows was 22 percent. Thus, the first design variant (I1) aimed at decreasing windows U-value from 3.045 to 1.903 (W/m^2K) and SHGC from 0.368 to 0.252. During the heating season, window heat losses and heat gains were reduced by 42 and 48.4 percent compared to the base case, respectively. As the ratio of window heat losses to heat gains was 2.45:1, energy consumption by radiant panels, AHU-heating coils, and AHU-fans were reduced by 45.7, 15.5, and 10 percent compared to the base case, respectively. This design variant (I1) resulted in a reduction of 19.8 percent of natural gas consumption by the boiler compared to the base case. During cooling season, it was found that heat gains and losses from windows were reduced by 40.6 and 49.4 percent compared to the base case, respectively. Despite the fact that window heat gains were substantially reduced, the chillers electric energy consumption was only reduced by 3.2 percent compared to the base case. Moreover, AHU-fans, chilled water pump and condensing water pump electric energy consumption were reduced by 3.8 percent. This is due the fact that window heat gains accounts for approximately 22 percent of the total energy gains. Moreover, the reduction recorded for the heat loss from windows caused an increase in the amount of energy on the building-level that should be extracted by mechanical system.

In the base case during summer season, the highest source (~31 percent) of heat gain was from lighting. Thus, the second design variant (I2) aimed at reducing lighting power density by 50 percent. As a result, during summer season, the electric energy consumption by AHU-fans, cooling tower fans, chillers, chilled water pump, and condensing water pump were reduced by 20.3, 18.45, 17.8, 13.6, and 13.5 percent compared to base case, respectively. However, during winter days, this reduction in internal gains from lighting caused an increase of 23 percent to natural gas consumption by the boiler. Despite the increase in heating energy, the lighting power consumption was reduced by 50 percent for both seasons and substantial reduction were recorded for cooling system components.

In the base case, the exhaust air from AHU was responsible for approximately 60 percent of heat loss during winter days due to that there is no HRW installed. Thus, the third design variant (I3) focused on installing heat recovery wheel (HRW) in the air handling units in order to take the advantage of the hot and cold air exhausted from the AHU in order to save energy required for heating and cooling. During winter days, the natural gas energy consumption was reduced by 20.5 percent compared to base case. While during summer days, the chillers electric energy consumption was reduced by 20.1 percent.

Compared to pie charts and other conventional graphs, Sankey diagrams facilitate the visualization of not only proportions but also the direction of flow of energy within buildings and their systems. For instance, Sankey diagrams were able to visualize the amount of lighting energy to the total internal heat gains. Moreover, it can visualize the amount of mechanical cooling required to remove internal heat gains. Moreover, Sankey diagrams demonstrated its usability and effectiveness to compare one design variant at a time or all design variants in one diagram. This could help different users evaluating different design alternatives.

6. CONCLUSION AND FUTURE WORK

The aim of this study was to investigate the feasibility of utilizing Sankey diagrams in visualizing building energy performance obtained from simulation outputs. The study proposed a workflow to obtain, analyze, and visualize energy flows obtained from simulation outputs Large office reference building model that complies with the national energy code of Canada for buildings for Ottawa climate zone was selected as the base case model. Different design variants were proposed and tested against the base case model independently. The proposed Sankey diagrams helped in visualizing building energy performance and to understand the upstream and downstream impact to allow various design variants to be evaluated by users (such as architects, and design engineers). Moreover, it helped in visualizing the impact of changing building/system components on the whole system performance and demonstrate energy-saving strategies.

One of the challenges in creating Sankey diagrams was creating feedback loops. The D3's Sankey layout code used has some limitations in creating feedback loops, so

these loops were added manually using image editing software. Future steps for this research include: developing tool(s) for automating the process that creates Sankey diagrams from simulation output files, and developing interactive Sankey diagrams by allowing the user to select the spatial and temporal resolutions.

ACKNOWLEGEMENTS

The generous support of Autodesk and the Natural Sciences and Engineering Research Council of Canada are acknowledged. Furthermore, this research would not be possible without the tireless ongoing support of Carleton University's Facilities Management and Planning.

REFERENCES

1. Natural Resources Canada (NRCan), "Energy Efficiency Trends in Canada, 1990 to 2009", 09 July 2012. Available: http://oee.rncan. gc.ca/publications/statistics /trends 11/chapter3.cfm. [Accessed 27 October 2016].
2. Hayter, S. J., Torcellini, P. A., Hayter, R. B. and. Judkoff, R. "The Energy Design Process for Designing and Constructing High-Performance Buildings," in *Clima 2000/Napoli 2001 World Congress*, Napoli, 2001.
3. Asl, M., Zarrinmehr, S. and Yan, W., "Towards BIM-based Parametric Building Energy Performance Optimization," in *Proc. ACADIA 13: Adaptive Architecture*, Cambridge, 2013.
4. Jeong, W., Kim, J. B., Clayton, M. J., Haberl, J. S. and Yan, W., "Visualization of Building Energy Performance in Building Information Models," in *Proc. ACADIA 13: Adaptive Architecture*, Cambridge, 2013.
5. Asl, M., Bergin, M., Menter, A. and Yan, W., "BIM-based parametric building energy performance multi-objective optimization," in *Proc. eCAADe 32*, pp. 1-10, 2014.
6. Raftery, P. and Keane, M., "Visualizing Patterns in Building Performance Data," in *Proc. 12th International IBPSA*, Sydney, 2011.
7. Pratt, K. B. and Bosworth, D. E., "A Method for The Design and Analysis of Parametric Building Energy Models," in *Proc. 12th IBPSA*, Sydney, 2011.
8. Srivastav, S., Lannon, S., Alexander, D. K. and Jones, P., "A Review and Comparison of Data Visualization Techniques used in Building Design and in Building Simulation," in *Proc. 11th International IBPSA*, Glasgow, Scotland, 2009.
9. Hab, K., Schweitzer, S., Prieto, D. F., Hagen, E., Engel, D., Bottinger, M. and Scheler, I., "Visualization of Building Performance Simulation Results: State-of-The-Art and Future Directions," in *Visualization Symposium* (PacificVis), 2014.
10. Elnimeiri, M. and Nicknam, M., "A Design Optimization Workflow for Tall Buildings using Parametric Algorithm," in Council on Tall Buildings and Urban Habitat, Seoul, 2011.
11. Autodesk, "Better Building Performance," Autodesk, 2015. Available: https://insight360.autodesk.com /oneenergy. [Accessed 27 October 2016].
12. Abdelalim, A., O'Brien, W. and Shi, Z., "Visualization of Energy and Water Consumption and GHG Emissions: A Case Study of a Canadian University Campus," *Energy and Buildings*, 2015.
13. Abdelalim, A., Shi, Z. and O'Brien, W., "Energy Flow Analysis on A Multi-Zonal Building Scale using Sankey Diagrams," in *Proc. eSim 2016*, Hamilton, Canada, 2016.
14. Belzer, D., "Energy End-Use Flow Maps for the Buildings Sector," Pacific Northwest national Laboratory, Springfield, VA, 2006.
15. Phineas, "Visualizing Internal and External Heat Flow," Sankey Diagrams, 1 September 2015. Available: http://www.sankey-diagrams.com/visualizing-internal-and-external-heat-flow/. [Accessed 10 December 2015].
16. Schlueter, and Thesseling, "Building Information Model Based Energy/Exergy Performance Assessment in Early Design Stages," *Automation in Construction. 18*, 2009.
17. Heidt, F., "CASAnova," 2012. Available: http://nesa1.unisiegen.de/index.htm?/softlab/casanova_e.htm [Accessed 20 February 2015].
18. Sefaira, "Sefaira," 2012. Available: http:// sefaira.com/ our-resources/. [Accessed 18 February2015].
19. Abdelalim, A., Shi, Z. and O'Brien, W., "An Approach towards Developing Methods to Analyze and Visualize Energy Flow of HVAC System," in *Proc. SIMAUD 2016*, London, UK, 2016.
20. Perez-Lombard, L., Ortiz, J. and Maestre, I. R., "The Map of Energy Flow in HVAC Systems," *Applied Energy 88*, p. 5020–5031, 2011.
21. DOE, "Commercial Reference Buildings," U.S. Department of Energy, 2015. Available: http:// energy.gov/eere/buildings/commercial-reference-buildings. [Accessed 27 October 2016].
22. Dong, B., Zheng, O. and Li, Z., "A BIM-enabled Information Infrastructure for Building Energy Fault Detection and Diagnostics," *Automation in Construction 44*, 197-211, 2014.
23. Natural Resources Canada (NRCan), "Canada's energy code", 19 January 2016. Available: http://www. nrcan.gc.ca/energy/efficiency/buildings/eenb/codes/4037. [Accessed 7 November 2016].
24. DOE, "Weather Data Sources," U.S. Department of Energy: Energy Efficiency and Renewable Energy, 2014. Available: http://apps1.eere.energy.gov/buildings/energyplus/weather data_sources.cfm#TMY2. [Accessed 26 October 2015].
25. Google Developers, "Google Developers Charts: Sankey Diagram," Google Developers, 30 June 2015. Available: https://developers.google.com/chart/interactive/docs/gallery/sankey. [Accessed 01 July 2015].

Building performance database to facilitate the integrated design process for net zero energy buildings

Navid Pourmousavian, Samson Yip, Bruno Lee and Andreas Athienitis

Concordia University
Montreal, Canada
S_pourm@live.concordia.ca; samso_yi@encs.concordia.ca;
bruno.lee@concordia.ca; aathieni@encs.concordia.ca

ABSTRACT

There are a variety of international and local programs that encourage the design and construction of sustainable buildings. Irrespective of the energy targets they pursue or their strictness, all affirm the role of integrated building design. Although its benefits are known, in practice it is seldom delivered in its full potential. Two major issues leading to this shortfall have been addressed in this paper. The first is the lack of an appropriate decision-making tool to facilitate conscious integrated design development and the second issue is the lack of a predefined communication framework in which the project can fully benefit from such a tool.

This paper proposes the building performance database, as an effective tool in assisting the project team through the design development of a net zero energy building. A framework consisting of the role of architects and engineers is also discussed to maximize final building design quality, using this database.

To create such a database, an energy and cost model is created for a baseline building. Numerous passive/active parameters with various degrees of freedom are defined and the multi-objective optimization algorithm (NSGA) is used to evaluate the trade-offs between the outputs. The development of this database is demonstrated using a case study.

Author Keywords

Performance-Driven Design; Integrated Design Process; Data Visualization; Multi-Criteria Design Decision;

ACM Classification Keywords

I.6.1 SIMULATION THEORY

H.2.8 DATABASE APPLICATIONS

J.6 COMPUTER-AIDED ENGINEERING

1 INTRODUCTION

Since at least the early 2000s, ideas about how to improve the performance of buildings have led to studies at the research and professional levels of new building design processes that emphasize the close collaboration of project stakeholders to achieve these higher levels of building performance. From early work at the IEA SHC Task 23 [1], this research has expanded to where now many organizations have codified integrated design processes (IDP) or methodologies to improve the building design process to reach these energy goals by holistically addressing the needs of all stakeholders – from the client, professionals, to users [2-4].

Among the common goals that the various approaches to integrated design share is an emphasis on reducing building energy use (and optionally the integration of renewable energy systems). To help achieve this, the proponents of integrated design emphasize overcoming the isolated, linear processes of the traditional/conventional design process by allowing more meaningful integration of input from all stakeholders in a project.

This requires more interaction between the different stakeholders and a willingness to work outside of one's usual expertise or comfort zone to allow potentially innovative solutions to materialize. In an integrated design process, design ideas are discussed, critically evaluated, and refined by all stakeholders in iterative loops to allow the feedback to have meaningful impact on the decisions that move the project forward.

However, it is this iterative nature that may be difficult to negotiate/navigate. Typically, at the beginning of any building design project, it is the architect who takes the lead in establishing building form and the ordering principles of the architectural program. While architects may be sensitive to the energy requirements of a building, the expertise for the energy modeling is usually the responsibility of the engineering team. Therefore, it is essential that these two teams – at a bare minimum – work closely together to achieve design strategies that satisfy both the architectural and energy requirements of the building. And often, the combination of different factors like building form, building function, site conditions, client preferences, project delivery methods, time constraints, budgets, etc. make a new design project different or unique enough for the design team that they cannot fall back directly on immediately relevant prior experience or design precedents that can help with the new design project at hand. This leads to a collaborative process where there are numerous rapid exchanges between the

SimAUD 2017 May 22-24 Toronto, Canada

architects who drive the early design exploration and the energy simulationists who provide needed design support. The search for initial design options may not necessarily rely on a predetermined framework due to the unique factors that constitute any building project. Paradoxically, it at this early design stage when not enough is known about the potential design solution to produce an accurate energy model that building energy simulation can be the most insightful. Through trial and error, invoking many iteration loops is one way to mitigate this problem.

However fraught with unknowns the initial design steps are, as the design progresses, certain objectives and design criteria become fixed and the number of unknown or undecided variables is reduced. At the earliest stage possible, a systematic study of the design space may be feasible to optimize potential design solutions based on established objectives – too soon in the process will risk having to restart the optimizations due to rapid design evolution; too late and the optimizations will only serve as *aṕosteriori* justification of decisions already taken.

Of the architect-engineer relationship: at earliest design stages architects may not be able to fully benefit from building energy simulation [5, 6]. This may explain the popularity of simple design tools. But another likely reason is that simplified tools are compatible with their design workflows [7] and the rapid pace of early design exploration when building energy concerns are just one of numerous variables that have to be considered, and calculations are required quickly. However, as the number of design uncertainties is reduced, increasing accuracy is needed in the building energy simulation tools. At this point, it would be beneficial to exploit BPS to its fullest – as a design-support tool instead of a design validation tool.

Motivation

Many studies have been conducted to identify the barriers hindering a successful IDP. IEA SHC task 23 explored the nature of IDP and developed a design process guideline as well as corresponding methods and tools in order to facilitate the IDP. One of the main outcomes of this task was a multi criteria decision-making tool (MCDM-23). The tool assists the designers in the evaluation of alternative design solutions by comparing their performance to a desired value [8]. However, this evaluation takes place after some design alternatives have been generated; the tool does not actually assist in generating those designs. It still relies on a trial and error approach in which the design is modified if the performance is not satisfactory and then re- evaluated by the tool. Also this tool does not guarantee that the best trade-offs between conflicting objectives will be found. For example, net zero energy performance may be reached in a project, but there is no guarantee that there are no better options in terms of cost or other functions.

In another study, Attia et al [9] in addressing the fact that most of the building performance simulation tools, are post-design evaluative, created a simulation-based decision support tool that integrates energy simulation into early building design. The tool's strength is its capacity to inform design prior to decision making. However, their target audience were architects with little experience in building energy efficiency and therefore, the tool was limited to a narrow search space and the only objective introduced was energy.

Lee et al. [10] presented a performance-based design workflow to support decision making in terms of energy performance, cost effectiveness, and environmental impact. The full factorial design space exploration investigation covers the whole life cycle of industrial halls. This full factorial approach mitigates bias in the design process since the design solutions are results of data driven reasoning based on large-scale simulation, which is possible due to the unique set of characteristics of industrial halls.

By targeting the IDP as a key to a successful collaboration between stakeholders, this paper proposes a performance driven workflow in which the building design team can benefit from a multi-criteria decision database, early in the design phase of a new building – in particular, a net zero energy building which includes active and renewable systems that design teams seldom encounter in conventional practice. This study targets the integration of the work between both architects and engineers, to ensure the target objectives are satisfied in an efficient workflow. This requires another important issue to be addressed. Traditional tables and graphs are argued to be inefficient for the communication and representation of the possible solutions [11]. This paper presents these solutions, in an interactive parallel plot, in which the designers can filter out different design parameters based on design objective, and see the effects on the outputs.

2 PERFORMANCE-DRIVEN WORKFLOW

The workflow presented in this paper, is an efficient way to integrate the architectural and engineering work early in the design process with the target to maximize the final quality of the building design.

In typical workflows, building performance simulation tools are used to evaluate a limited number of designs that have been developed to a level of completeness permitting such evaluation. In contrast, this proposed workflow suggests to create a database of design solutions respecting the main objective targets at the earliest possible moment in the conceptual design phase to assist the design team in making major decisions undergirded by building performance simulation. The design team provides all the required inputs such as building geometry and passive and active design requirements which are integrated to form the base building energy model (Figure 1).

By defining the design parameters parametrically, with meaningful degrees of freedom, and quantifying required metrics for each objective function, such as the incremental cost associated with each design parameter, a pool of

candidate configurations is created. With clearly defined objective functions, agreed upon as important by all stakeholders, optimization methods can be used to find the tradeoffs between different design configurations. All the solutions are collected in a database, which can be used as an interactive tool, to facilitate decision making.

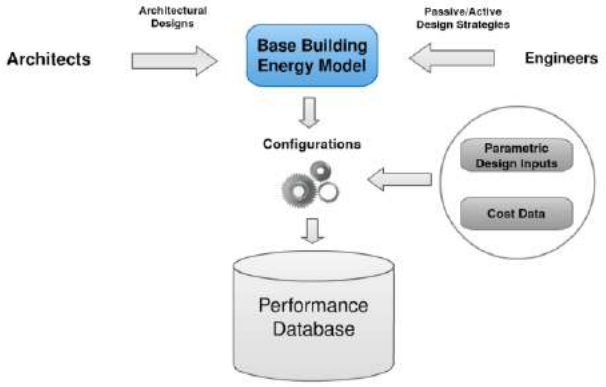

Figure 1. Data Workflow

3 DATABASE CREATION

The creation of the database starts with the definition of the objective function. In this paper, the two objective functions defined as the main drivers of the database are: Net energy and life cycle cost. The energy simulation is performed with the EnergyPlus whole building performance simulation tool [12]. Life cycle cost is approximated in a Microsoft Excel spreadsheet using data from RSMeans 2016 [13]. The optimization is conducted using Modefrontier software. Figure 2 illustrates the architecture of the developed workflow.

The following sections describe the definitions of the objective functions, the energy and cost models, and the optimization algorithm.

3.1 Defining the objective functions

There are a variety of targets, can be selected based on the client preferences and/or project specific characteristics. It may be based on a program specific targets, such as LEED credits, PassiveHouse criteria etc. In order to ensure that the final design outcomes are in-line with the design targets, it should be clearly defined at the beginning of the project. In this paper, two objective functions are defined as the main objective functions to design a net zero energy building:

Net energy

This objective function is defined to predict the balance of energy in the building. It calculates the amount of energy generation minus the total energy consumption of the building.

$$\text{Net energy} = (E_{generation} - (E_{heating}+E_{cooling})/COP_{average} - E_{appliances})/\text{Floor Area}$$

$E_{generation}$: Energy generated by the photovoltaic system,

$E_{heating}$: Heating load of the house,

$E_{cooling}$: Cooling load of the house,

$E_{appliances}$: Energy consumption of lighting, appliances, and domestic hot water heating.

The net energy is divided by total floor area and is reported in kWh/m^2 which is the most common unit used by practitioners in this field. A net energy of zero means that the house is a net-zero energy house on an annual basis. Any number higher than zero would mean the house generates more electricity than it consumes annually.

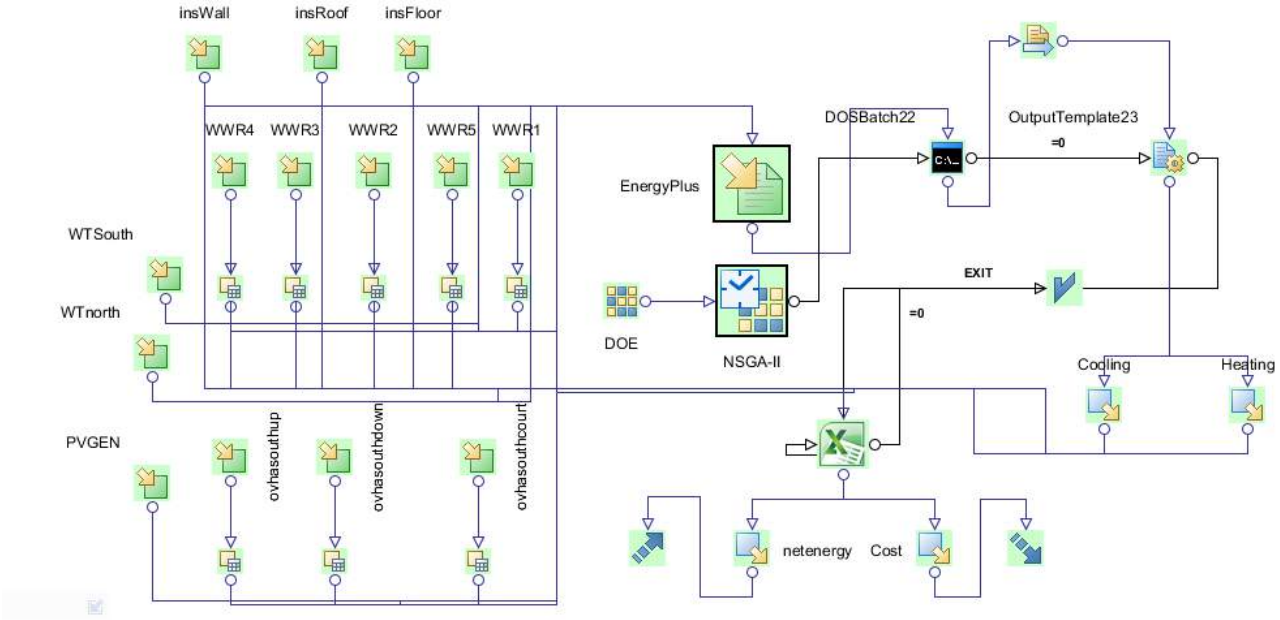

Figure 2. The Architecture of the workflow in Modefrontier

Life cycle cost

There are different pathways to make a net zero energy house in every climate. To find the right balance between passive and active strategies, it's crucial to account for the total cost of every design configuration. To assess the cost of each design option, a life cycle cost analysis has been performed. This objective helps the designers, to find out the most affordable pathways to a net zero energy building. Life cycle cost (LCC) as defined by NIST Handbook 135 [14]:

$$LCC = \sum_{t=0}^{N} \frac{C_t}{(1+d)^t}$$

represents the total present-value of each design configuration in a predefined number of years (N) selected as the studies period. C_t is the total cost in each year (t), including the initial cost, replacement cost, operational and maintenance cost as well as the residual value of each design configuration at the end of the studied period. The discount rate (d) in this formula is used to simply translate the cash flow in future, to the present value.

More details regarding this objective is beyond the scope/intent of this paper, since it is simply used to indicate the application of the proposed workflow.

3.2 Energy model

Based on the complexity and nature of the objective functions, different methods/tools can be used to evaluate the performance of each design configuration. It can be as simple as some rule of thumbs or comprehensive simulation studies.

In this paper, EnergyPlus is used to accurately model the building physical characteristics. The heating and cooling loads included in the Net Energy objective function are the outputs extracted from the EnergyPlus simulation results. For the purpose of this demonstration, an average annual COP of an air source heat pump has been assumed for the heating and cooling systems in order to predict the energy consumption. In a more comprehensive study, different HVAC systems and the cost associated with each one, can be among the design variables. However, the studied design variables presented in Table 1, are meant to be indicative of possible design variables and not to cover all the potential passive and active strategies. All the design variables are set to satisfy minimum code requirements for the base model, however, through an optimization process, the performance of various configurations are investigated over a specified range. Table 1 shows the design variables used in the energy model for conducting the optimization algorithm in this study.

3.3 Cost model

The cost model is not meant to predict the total cost of the construction, but instead to evaluate the incremental cost associated with each strategy for creating a net zero energy building. In this regard, the cost of adding more insulation, installing higher performance windows and different photovoltaic arrays are extracted from RSMeans 2016 database. In this paper, an Excel spreadsheet is used to calculate the Life cycle cost, as defined in previous sections.

	Unit	Lower Band	Upper band	Description
Wall R	m^2K/W	4.5	13.5	Effective insulation value of the wall
Roof R	m^2K/W	7	19.5	Effective insulation value of the roof
Floor R	m^2K/W	4.5	13.5	Effective insulation value of the floor
WWR	%	10	80	Window to wall ratio
Overhang	m	0	1.5	South windows overhang depth
Window Type	-	1	8	Based on manufacturer data sheets
PV Capacity	kW	5	11	Photovoltaic DC capacity

Table 1. Design parameters studies in the energy model.

3.4 Optimization Algorithm

The proposed workflow should provide a set of optimal possible configurations, to assist the design team in making conscious decisions. Therefore, optimization is necessary to explore the design space and to investigate the trade-offs between the conflicting objectives. In this paper, non-dominated sorting genetic algorithm (NSGA II) [15] is selected to perform multi-objective optimization., the choice of the optimization algorithm, doesn't affect the proposed workflow and therefore is not described further in this paper.

4 RESULTS

Using the optimization algorithm, the set of optimal trade-offs between the two objective functions has been recognized. The algorithm performs a number of simulations, to identify the optimal trade-offs. In each level of one criteria, there is only one solution with the best performance in regard of the other criteria. This is known as Pareto front which is highlighted in red, in Figure 3. The other configurations with the blue color, are all the simulation results has been performed to identify the Pareto front which are often called raw optimization data. The solutions with a "Net Energy" higher than zero are circled in Figure 3. These are simply the net zero energy and beyond net zero configurations.

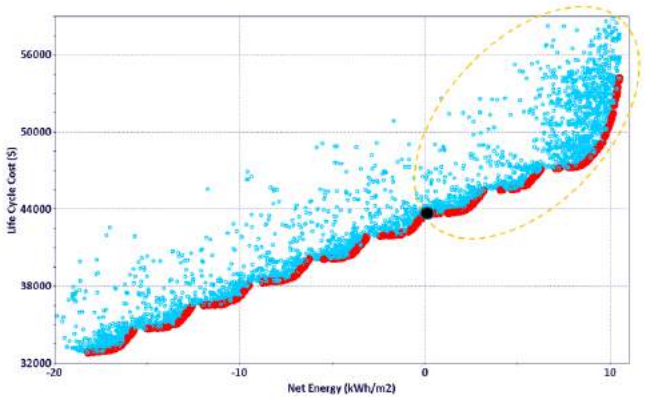

Figure 3. Optimization Results

The lowest life cycle cost configuration that can achieve net zero energy performance is identified by a black dot. There is the possibility to group different categories in this scatter plot, however to fully navigate the design space, this paper proposes the use of parallel plots for representing this database.

Using the parallel plots facilitates the communication between engineers, architects, and other stakeholders. This new design approach enhances the discussion, understanding, and helps achieve data-driven decision-making. In order to easily find the desirable solution during the design development phase, an interactive parallel plot can be used to easily extract the data. Figure 4 demonstrates this parallel plot. The light blue lines represent all the configurations studied and the orange lines represent the Pareto configurations.

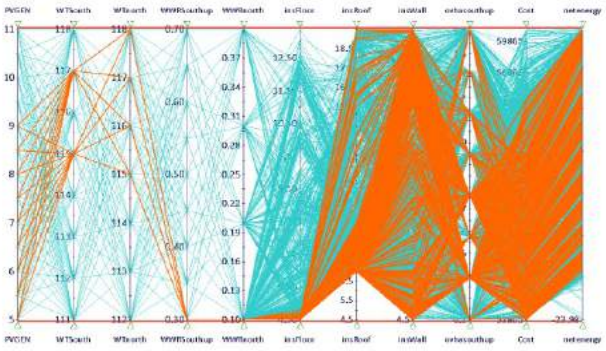

Figure 4. Parallel Plot

It is an interactive database, in which the designers can filter different design parameters and see the effect on the defined performance indicators. In Figure 5, the design has been limited to positive net energy configurations and roof and wall effective insulation values are reduced. It is obvious that the photovoltaic system with higher than 9 kW DC capacity, is not a cost effective solution and further investment should be directed to passive strategies.

The type of the windows also is narrowed down to triple glazed. The percentages of window area on the south and north façades are expected to be 30% and 10% respectively. The overhang depths on the south façade windows range between 0.4 m to 1.1 m depending on the type of window selected. These design parameters can be adopted in the design development phase in order to ensure that the final design is an affordable net zero energy building.

5 CONCLUSION

Although the importance of integrated design to involve all the stakeholders in the design decisions is evident, some difficulties still hinder its achievement. This paper proposes an interactive database to be created and used early in the design, to facilitate and inform the decision making process. The database is a set of optimal design configurations that perform well in regard of the defined objective functions. An interactive parallel plot is also proposed to be used for representing the database and as an effective and easy to use tool for designers.

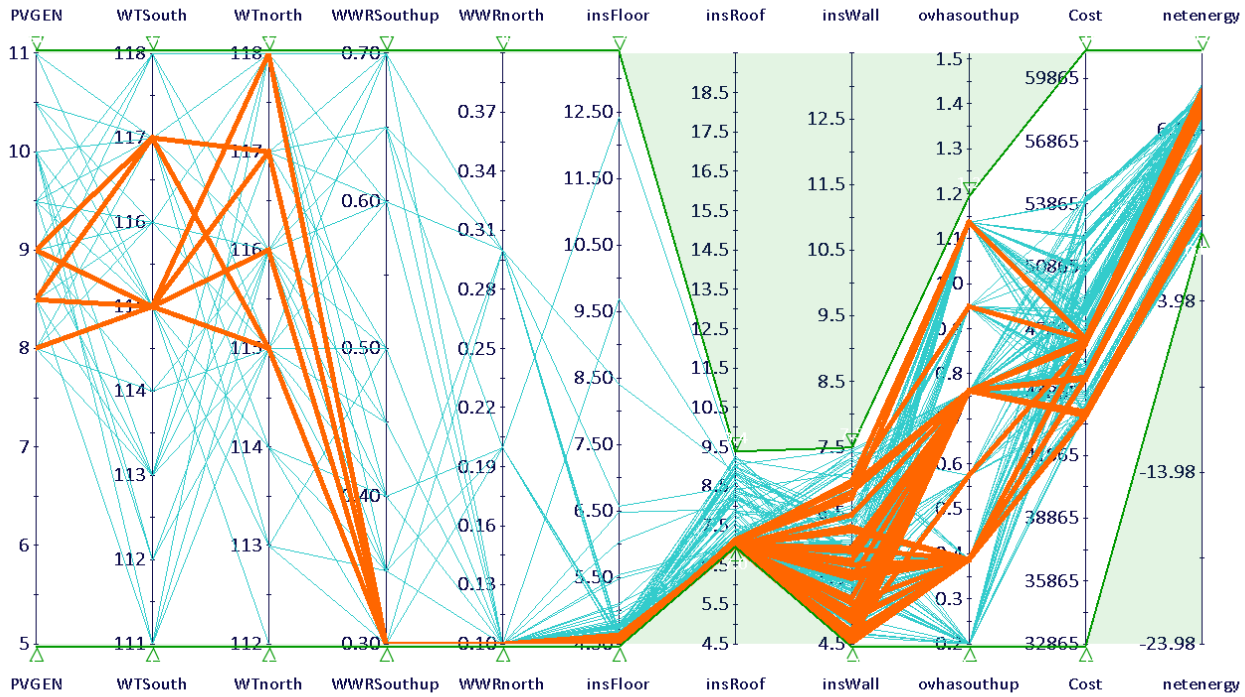

Figure 5. Filtered Parallel Plot

To make full use of the proposed workflow, the following steps should be used:

1. Define the project targets in the pre-design stage of the project by all the stakeholders,
2. Create a base model (energy, cost, etc.) in the conceptual design phase,
3. Study the full range of design variables to mitigate design bias
4. Perform the optimization algorithms to provide a set of optimal design configurations,
5. Create an interactive database as a support tool for designers to generate the design alternatives (in contrast with conventional post-evaluative workflows),

The application of the proposed workflow is demonstrated in the design of a net zero energy building. The approach can be further expanded by visualizing the database of configurations in 3D building models.

ACKNOWLEDGMENTS

This paper has been made possible with the support of the Fonds de recherche du Québec – Nature et technologies (FRQNT), NSERC Smart Net-Zero Energy Buildings Strategic Research Network (SNEBRN), NSERC/Hydro-Québec Industrial Research Chair.

REFERENCES

1. Löhnert, G., A. Dalkowski, and W. Sutter, Integrated Design Process: a guideline for sustainable and solar-optimised building design. Berlin: IEA International Energy Agency, 2003.
2. American National Standards Institute (ANSI) and Institute for Market Transformation to Sustainability (MTS), Integrative Process (IP): ANSI Consensus National Standard Guide, Design and Construction of Sustainable Buildings and Communities, 2012, American National Standards Institute,, Institute for Market Transformation to Sustainability, : Washington, DC.
3. United States Green Building Council, LEED Reference Guide for Building Design and Construction, LEED version 4. 2013, Washington, DC: United States Green Building Council.
4. American Society of Heating, Refrigerating and Air-Conditioning Engineers (ASHRAE),, Standard for the design of high-performance green buildings : except low-rise residential buildings. 2009, Atlanta, GA: American Society of Heating, Refrigerating, and Air-Conditioning Engineers.
5. Donn, M., S. Selkowitz, and B. Bordass, The building performance sketch. Building Research and Information, 2012. 40(2): p. 186-208.
6. Soebarto, V., et al. Capturing the views of architects about building performance simulation to be used during design processes. in 14th International Conference of IBPSA - Building Simulation 2015, BS 2015, Conference Proceedings. 2015.
7. Horvat, M. and J. Kanters, needs of architects regarding digital tools for solar building design, 2012, IEA: Toronto, Canada; Lund, Sweden.
8. Löhnert, G., A. Dalkowski, and W. Sutter, Multi-Criteria Decision-Making, MCDM 23.: IEA International Energy Agency, 2002.
9. Attia S, Gratia E, De Herde A, Hensen JLM. Simulation-based decision support tool for early stages of zero-energy building design. Energy Build 2012;49: 2–15.
10. Bruno Lee, Navid Pourmousavian, Jan L.M Hensen, Full-Factorial design space exploration approach for multi-criteria decision making of the design of industrial halls 2015, Energy and Buildings
11. S. Attia, L. Beltrán, A. De Herde, J. Hensen, Architect friendly: a comparison of ten different building performance simulation tools, in: Proceedings of the 11th International IBPSA Conference, Scotland, Glasgow, 2009.
12. U.S. Department of Energy | Energy efficiency and renewable energy, EnergyPlus, 2015.
13. RSMeans. 2016. RSMeans building construction cost data.Retrieved April 2016. http://www.rsmeans.com.
14. Fuller, S.k., Peterson, S.R., Life-Cycle Costing Manual: NIST Handbook 135, 1995
15. Kalyanmoy Deb, Multi-Objective Optimization Using Evolutionary Algorithms: 1st ed. New York: Wiley., 2001

An Investigation of Generative Design for Heating, Ventilation, and Air-Conditioning

Justin Berquist[1], Alexander Tessier[2], William O'Brien[1], Ramtin Attar[2] and Azam Khan[2]

[1]Carleton University
Ottawa, Canada
{firstlast}@cmail.carleton.ca

[2]Autodesk Research
Toronto, Canada
{first.last}@autodesk.com

ABSTRACT

Energy consumption in buildings contributes to 41% of global carbon dioxide emissions through electricity and heat production, making the design of mechanical systems in buildings of paramount importance. Industry practice for design of mechanical systems is currently limited in the conceptual design phase, often leading to sub-optimal designs. By using Generative Design (GD), many design options can be created, optimized and evaluated, based on system energy consumption and life-cycle cost (LCC). By combining GD for Architecture with GD for HVAC, two areas of building design can be analyzed and optimized simultaneously, resulting in novel designs with improved energy performance. This paper presents GD for HVAC, a Matlab script developed to create improved zone level mechanical systems for improved energy efficiency. Through experiments, GD methodologies are explored and their applicability and effect on building HVAC design is evaluated.

Author Keywords

Generative Design; Genetic Algorithm; Heating, Ventilation, and Air-Conditioning; HVAC

ACM Classification Keywords

J.2 Computer Applications: PHYSICAL SCIENCES AND ENGINEERING; J.6 Computer Applications: COMPUTER-AIDED ENGINEERING

1 INTRODUCTION

Industry practice for the design of mechanical systems in the conceptual phase is limited [5]. Current practice is to select a base design to iterate on. This initial design is often a design previously used by the designer for other projects. To accommodate specific requirements, adjustments are made to the base design as the project proceeds. These adjustments, some of which occur during the construction phase, are often not cost effective, and can lead to inefficient solutions. This common practice of dealing with problems as they arise jeopardizes the potential efficiency of the mechanical system and is exemplified by the significant amount of building energy consumption globally. This paper outlines a methodology utilizing genetic algorithms to develop more optimal HVAC systems, enabling the creation and evaluation of many novel designs during the conceptual phase. By considering and evaluating more designs, more advantageous options can be discovered and selected prior to construction.

SimAUD 2017 May 22-24 Toronto, Canada

2 RELATED WORK

GD is a method that mimics the human approach to design through an algorithmic methodology. Normally, design begins with a set of ideas developed into a design. Throughout the development process, designs are evaluated and improved, by adding new design parameters and constraints, to create a new design iteration. In a similar fashion, GD starts with an initial design or idea, which is then developed into a rule set. The rule set is turned into source code that generates multiple design solutions. With the completed designs, a designer can either alter the source code or the original rule set, depending on how results are evaluated. Figure 1 demonstrates the GD process.

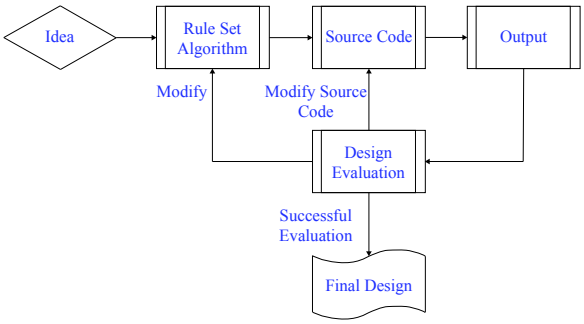

Figure 1. A Flow Chart Representing the Concept of Generative Design

Gu, Singh, and Merrick [10] identify four different GD techniques: shape grammars (SG), L-systems (LS), cellular automata (CA), and genetic algorithms (GA). GAs are a method for solving both constrained and unconstrained optimization problems and are comparable to the concept of evolution by natural selection in biological systems [7]. Of these methods, GAs have been successful at solving various HVAC optimization problems. This can be attributed to the fact that building optimization problems contain several characteristics limiting the applicability of both direct search methods and gradient-based optimization methods [16].

"Some characteristics that building optimization problems may include are a mixture of a large number of integers and continuous variables, non-linear inequality and equality constraints, a discontinuous objective function and variables embedded in constraints that are not in the objective function." [5]

As a result, GAs are prime candidates for solving building optimization problems. Furthermore, GA's possess the abil-

ity to identify optimal trade-offs among multi-objective optimization problems, necessary when considering both energy consumption and LCC.

2.1 Genetic Algorithms

GAs are an optimization strategy based on evolution by natural selection [7], where each candidate solution in the optimization problem is represented by a coded representation of design attributes, analogous to a *chromosome* [1].

GAs create an initial, random population set of these solutions, and continuously iterate until the near-optimal is determined. The five main operations in the iteration process are: evaluation of the fitness function, selection, crossover, mutation and replacement [1]. The effectiveness of each design at solving the problem is determined by its *fitness* [1]. Figure 2 demonstrates the GA process.

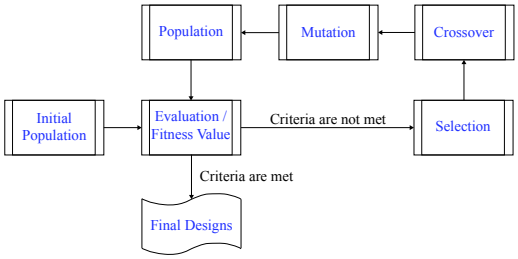

Figure 2. A Flow Chart Representing the Concept of a Genetic Algorithm

Replacement

An initial randomized design population is generated. If the fitness criteria are not met, a new population set is created based on crossover and mutation operations. A new population replaces the old population which is then re-evaluated.

Crossover

An operation that exchanges an aspect of one design with one from another design. This operation is performed probabilistically, and may not occur during a given iteration.

Mutation

An operation that alters an aspect of a design option. For example, if solutions are represented as binary values, a mutation will change the attribute from 0 to 1 or vice versa. Mutations are responsible for keeping variation in the design set and can result in radically different solutions between generations.

Fitness Value

Each design is evaluated and assigned a fitness value based on how well it satisfies the constraints of the given problem. The constraints of the problem can be single-objective or multi-objective during the optimization process.

Selection

The selection operator is used to select design solutions from the current population that will succeed to the next round/iteration. Selection criteria vary, and can include: best single solution, the best in a set of solutions, or even a random selection of solutions.

2.2 Previous Genetic Algorithm Applications

Variations of GAs have been developed and applied to solve energy optimization problems. Caldas et al. [5] developed a Pareto-based genetic algorithm to optimize aspects of building design, resulting in reduced cost and time, while still achieving a desirable design. Their optimization strategy was applied to three areas of building design: building envelope, building form, HVAC design and operation. GA's that utilize the Pareto concept have also been used successfully in energy and building studies (Hamdy et al. [11]).

Different GA methodologies can be applied to the same optimization problem leading to similar results. Palonen et al. [13] applied an elitist non-dominated sorted genetic algorithm (NSGA-II) to the architecture and HVAC system of a Finnish residential house. Hamdy et. al. [11] studied the same residence and instead, applied a modified multi-objective genetic algorithm (PR_GA), utilizing a Pareto-based approach combined with the IDA-ICE 3.0 simulator [11]. This multi-objective problem was focused on lowering the CO2 emissions while maintaining realistic investment costs. Ultimately, the NSGA-II yielded similar results to the modified PR_GA [11] in several runs, appearing to be the most efficient of the GAs according to Deb [8].

Additional studies have been completed that range in GA types: segregated genetic algorithm (SGA), simple genetic algorithm, multi-island genetic algorithm (MIGA), and micro-GA. The SGA was used to route and size ductwork, and was tested using the duct layout in Chapter 32 of ASHRAE (1997) [1]. A modified version of the 'simple genetic algorithm' described by Goldberg was developed to size components in an HVAC system with the goal of reducing the systems life cycle cost [15]. Alvaro Siza's design of the School of Architecture in Oporoto, Portugal was analyzed through a genetic system (GS) that consisted of a micro-GA and used DOE-2.1E as the fitness calculator [4]. The development was created to establish the effect that design choices had on energy consumption. In the end, it suggested similar architectural designs as Siza, but also some varied design concepts, suggesting that the GS could indeed be a beneficial method for exploring various design options during the conceptual design phase. Brahme et al [3] employed differential modeling, homology-based mapping, and generative design agents, to allow the use of building performance analysis tools early in the design. This development was utilized in an office building in Pittsburgh where it generated duct routing options based on equipment location.

3 PROPOSED METHODOLOGY

In previous work, GAs have been utilized to optimize some aspects of HVAC design, however, complete GD for HVAC has not been widely explored. Barnaby et al. [2] explored an automated HVAC system design tool, but design was completed using standard industry practices. In contrast, the proposed approach considers the system from base parameters

and diverges from traditional techniques to find novel designs. These base parameters can be categorized for zone-level design, and include the generation and evaluation of:

1. Building thermal zones
2. Type, number, size and location of diffusers and return grills
3. Sizing and routes of both supply and return ductwork
4. Sizing and location of equipment
5. Sizing and routes of exhaust ductwork
6. Sizing and location of the intake and exhaust louvers
7. The fitness of each design option

Once the building information model (BIM) is available, the required information needs to be extracted. This is currently done manually, however, a gbXML file format can be exported from Autodesk Revit and imported into the Matlab script to obtain all of the required information. Once the information is gathered, the potential thermal zones need to be determined. A thermal zone is defined as an area in the building which has its own temperature control [6]. For each zone, an algorithm determines the type of room, room load requirements, room orientation, and room adjacency when grouping rooms into thermal zones. Figure 3 displays the concept of rooms having to be the same type, orientation and adjacent to each other in order to have a chance to be grouped together.

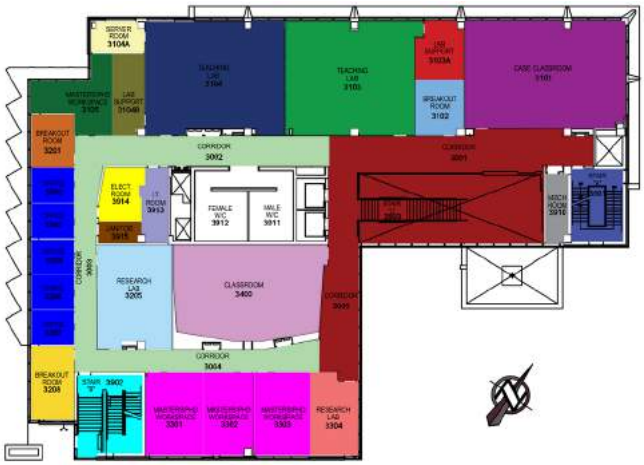

Figure 3. Example zoning for the third floor of the Canal Building

Room Type

The type of room is important when exploring zoning options. Some rooms cannot be zoned together due to certain codes and standards i.e. bathrooms require their own exhaust systems as they are in the third air class category and air can only be recirculated within its own zone (ASHRAE Std 62.1).

Even when building code allows room types to be grouped together, some combinations should be avoided as they can result in system inefficiency for both heating and cooling seasons i.e. grouping a single occupant office with a multi-occupant office can be problematic depending on the control strategy. If the single occupant office contains the lead thermostat, the multi-occupant office will not be supplied with enough cooling to meet the demand from occupant gains. On the other hand, if the multi-occupant office contains the lead thermostat, the single occupant office may be supplied with an unnecessary amount of cooling. Room averaging could be employed, however, this would result in the single occupant office being over-cooled and the multi-occupant office being under-supplied during cooling mode.

Room Load Requirements

It is important to group rooms together that require similar heating and cooling. A larger discrepancy between required heating and/or cooling for a room will either lead to an unnecessary amount of energy being expended on one room at times, or will lead to uncomfortable occupants. This would result from unsatisfactory amounts of cooling and/or heating being supplied to the other room, depending on the controls scheme, similar to the example in the Room Type section.

Chapter 18 of the 2013 ASHRAE Fundamentals Handbook outlines two methods for estimating the peak heating and cooling load requirements, the heat balance (HB) and radiant time series (RTS) methods [6]. Peak load calculations can be thought of as worst-case scenarios, meaning that the peak cooling occurs when all possible internal gains are present, and the solar radiation and outdoor air temperature are at their highest. However, heat gains from infiltration can be neglected for commercial buildings when positive air pressure can be assumed [6]. Conversely, the room's heating load requirement is calculated in the middle of the night when no solar gains and internal heat gains are present, the outdoor air temperature is at its lowest, and losses due to infiltration are taken into consideration. Once the heat gains are calculated separately utilizing the RTS approach, they can be summed together, resulting in Equations 1 and 2.

$$Q_{PeakHeating} = Q_{Ext} + Q_{Inf} \quad (1)$$

$$Q_{PeakCooling} = Q_{Ext} + Q_{Solar} + Q_{PL} + Q_{L} + Q_{Occ} \quad (2)$$

Several tables from ASHRAE Fundamentals are utilized within the code to determine the internal heat gains from occupants, lighting, and computers. Table 2, section 18.4 [6] represents the energy rate from occupants performing various activities. Standard practice is to assume that the number of occupants present during peak load is equal to the number of seats assigned by the architect. Heating loads due to equipment, specifically desktops and laptops are calculated based on ASHRAE table 8, section 18.11 [6]. Offices are assumed to have one desktop per occupant, and meeting rooms are assumed to have one laptop per two occupants. Maximum lighting per room type is determined from ASHRAE table 2, section 18.5 [6] and used for light heating gains during peak cooling operation. This methodology mainly follows standard industry practice, following the ASHRAE guidelines, however, the outdoor temperatures, and maximum solar radiation based on building location are determined by utilizing the Canadian Weather for Energy Calculations (CWEC) file.

Room Orientation

Although orientation plays a role in the required load for a room it is important to evaluate individually as well. Consider a zone that consists of two offices: one facing south and

the other a south-west corner office. These offices might have similar peak load requirements, but in the late afternoon the corner office will be effected by solar gains at a magnitude that the south office will not experience. However, the south office would unnecessarily receive the same amount of cooling as the corner office during this time in the summer.

Room Adjacency

Although rooms may meet the other three requirements, it is key to examine the grouping possibilities from a practicality standpoint. If one office is nearly on the opposite side of the building, the routing of the ductwork would be almost impossible to construct, and unnecessarily extensive duct runs will decrease the efficiency of the system.

Consider Figure 4, a script was developed which thermally zoned offices based on similar load requirements [14]. The south corner office has similar peak load requirements to two large classrooms on the north side due to the solar gains it receives, and were grouped together by the algorithm. If implemented, this grouping would result in difficult routing for ductwork and unreasonably long runs. Although peak loads are similar, the south corner office will only have similar loads to the northern classrooms during solar noon, and most of the time, will require significantly less cooling than the two laboratories. The problem will be exacerbated when the labs are filled with students and it is not solar noon. Considering the peak load requirements in isolation and neglecting adjacency for thermal zoning can have significant negative impacts on system design.

Figure 4. Thermal Zoning outcome from a previously developed algorithm showing unrealistic grouping of north and south rooms into a single zone.

The number of zones selected has a significant outcome on the initial cost of the building's mechanical system, the efficiency of the system, and the comfort of the future occupants. The more zones there are, the more terminal units are required and the more expensive the system. Secondly, requiring greater consideration as building design progresses, is the efficiency of the system. The least amount of zones possible will result in the least efficient design option, as the occupants will never maintain an identical schedule throughout the year, leading to times when the system is supplying tempered air to empty rooms in order to meet the demand of one office. Thirdly, and rarely considered, is occupant comfort. The more offices contained within a zone, the less control and customization each occupant will have over their comfort. For these reasons, the zoning options that are determined will depend on the relative importance of each of the input parameters, which must be determined prior to running the tool.

Mapping

After the generation of multiple zoning strategies, the HVAC configuration is determined using a mapping process. Figure 5 illustrates the output of the mapping process and displays the layout of nodal points, grid and adjacency lines, and zone boundary lines, similar to Brahme et al. [3]. As done by Brahme et al. [3] the adjacency lines represent the potential paths for ductwork. This methodology builds on the work done by Brahme et al. [3], as the nodal points represent the various options that the GA has when permuting locations for the diffusers, return grilles, and equipment, rather than just for the locations of the terminal units. In addition, this work did not include zone boundary lines which contain all rooms that will be grouped in the same thermal zone, as determined by the previous process. The zone boundary lines assist in the permuting of terminal units, whereas the locations of the terminal units were manually input to generate the duct routing in their case study [3] .

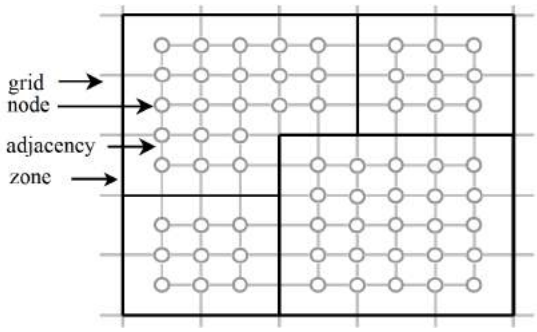

Figure 5. Example Building Mapping.

Due to the combinatorial explosion in the design space, it is important to introduce appropriate constraints, such as constraints on equipment sizing. Directly using the results of the peak load calculations from the *Room Load Requirements* section, results in equipment being sized at a capacity which is rarely required during a year. ASHRAE suggests using the 99th percentile outdoor air temperature when performing the heating load calculation. The justification here is that considerable fluctuations in weather conditions occur from year to year, and using worst case on record could often result in equipment with excess capacity [6] for most normal years. The ASHRAE fundamentals handbook [6] does not address the over-sizing of units that allow for cooled air to pass, such as variable air volume boxes (VAV). Although these terminal units might have to deal with peak cooling loads at some point during the year, it is usually a rare occurrence. Equations 1 and 2 are used to constrain equipment size. Generally, the GA attempts to minimize sizes, finding the smallest

sizing for equipment without jeopardizing comfort during exceptional times of the year, but is constrained to stay within the limits set in these equations.

Diffuser and return grille mapping

At this point, a GA will generate variations for diffusers and return grilles, and determines the range of types, number, size and location within each zone as depicted in figure 6. Each population of diffusers and grilles is required to meet a single objective standard, based on a Computational Fluid Dynamics (CFD) study. Occupant comfort becomes a constraint, and designs resulting in large drafts are eliminated. Furthermore, designs that do not meet the functional requirements of the system will be eliminated from consideration i.e. one constraint is that each room will require at least one diffuser.

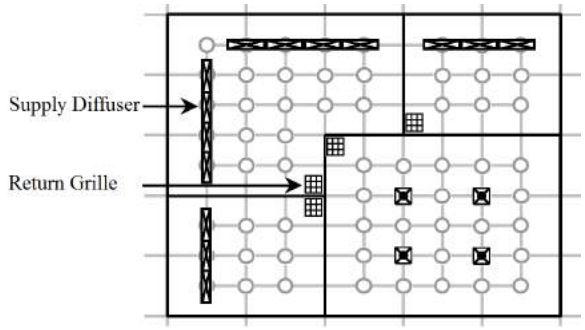

Figure 6. Example mapping of the supply diffusers and return grilles.

A GA will also be required to generate the equipment size and location. At this stage the corresponding supply duct sizing and routing will need to be completed. An example of this is depicted in Figure 7. Once this is completed, the return duct sizing and routing will be determined in a manner which does not interfere with the equipment and supply ductwork. Each design option at this stage will need to be tested for its fitness.

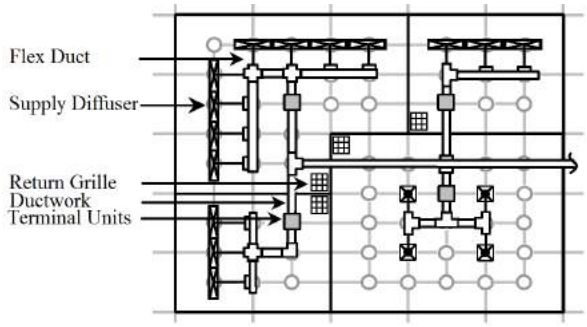

Figure 7. Example mapping of the HVAC system components.

Fitness at this stage is determined through a multi-objective approach utilizing building performance simulation (BPS) in conjunction with a LCC analysis. Each design option is evaluated using this approach. The building performance simulation is created based on the architecture and the design strategies that are generated. These design options will be evaluated based on annual energy consumption associated with the design.

The number of times that the system cannot meet the demand of the building, and the magnitude of deficit is also considered as part of the evaluation. For example, although an extremely under-sized system will not consume as much energy as an over-sized system, it will not be serving its purpose and will not be accepted. A system that does not always meet the demands of the zone could be accepted, for example it is not important to adequately supply cooling to the west façade offices around 7 pm in the summer since occupants have likely gone home.

The LCC of the system will be determined which considers the initial cost, the cost to operate, and the cost to maintain the system. The percent change between LCCs of each design option will be compared to the percent change of the energy consumption to allow for the most efficient design to be selected while remaining cost effective.

The design option's ability to solve the multi-objective problem, or rather its fitness is important to analyze, but it is also beneficial to quantify each design options feasibility/practicality. Designs that propose infeasible solutions ultimately will not be selected, however, slightly infeasible design options can be useful to pass through to the next generation of designs, as they can allow for a new area of the design space to be explored. Infeasible designs can be become feasible with slight variations (repairs) [1]. Different techniques for the introduction of infeasible solutions into the genetic variations can be addressed in different ways. The penalty method is generally considered the most successful method [1]. Alternatively, an SGA approach consisting of two population sets, one that utilizes a severe penalty and another that uses a limited penalty [12] can be employed, allowing feasibly and infeasible genes to interact.

As previously discussed, there is zero tolerance to impractical designs in the final solution set, meaning that each final design option must adhere to the Building Code and ASHRAE Standards, and all options that do not comply will be eliminated from consideration. The path and process to get to these solutions can include imperfections along the way and allow novel designs to be explored. Once the final design options have been determined it will be up to the mechanical designer to decide which design should be finalized utilizing his previous experience and knowledge. He/she will have to decide which design is the most practical and well suited for the given building, considering cost, and efficiency.

Although the above methodology is what is required to have a complete tool for the generative design of HVAC, critical design information can be gathered directly from a Building Information Model (BIM). It is believed that this combination of BIM and GD for HVAC will lead to a more integrated and more efficient building design process.

4 CASE STUDY

A Matlab program was developed to address the first stage of the GD for HVAC process, generating zoning strategies for a given floor plan. This development also included the use of peak load calculations to determine the maximum cooling and heating loads, and the corresponding VAV box sizes. The

Canal Building, located on Carleton University Campus, was utilized as a test subject for this development.

All of the required parameter information regarding the rooms located on the third floor were gathered from a BIM Revit file and the infiltration rate for the entire building was received through a model calibration. The weather data was retrieved through a CWEC file for Ottawa that was found online [9]. The information regarding the building parameters are listed in Table 1 and were manually inserted into the Matlab code, the weather information that the code determined based on the data from the CWEC file is listed in Table 2. Typical values associated with the building parameters are listed in Table 1, non-typical values are listed as "Varies". For example, the windows in the Canal building have a U-value of 3.194 W/m^{2}K, but the window area varies based on the room.

Building Parameters	Values
Room Number	Varies
Room Type	Varies
Potential Occupants	Varies
Room Area (m^2)	Varies
Room Adjacency	Varies
Orientation (N,E,S,W)	Varies
Exterior Wall Area (m^2)	Varies
Window Area (m^2)	Varies
Window SHGC	0.655
Window U-Value (W/m^{2}K)	3.194
Floor to Floor Height (m)	4.2
Exterior Wall Resistance (m^{2}K/W)	4
Infiltration Rate (ACH)	0.2
Cooling Season Setpoint (°C)	23
Heating Season Setpoint (°C)	20

Table 1. Building Parameter Input

Weather Parameters	Values
Max Outdoor Temperature (°C)	33
Min Outdoor Temperature (°C)	-25

Table 2. Weather Data

A section called "User Defined Criteria" was added to allow the user to state preferences for the final design selection. This user defined criteria allows designers some flexibility when generating final design options. Three linearly weighted options influence the GA outcome and design optimization process: initial cost, energy efficiency, and occupant comfort. The weights range from 0 to 4, where a weight of zero indicates no importance, and a value of 4 indicates the highest importance.

Categories are assumed to influence the zoning strategy linearly. Occupant comfort is assumed to increase with the system efficiency, and the initial cost is inversely proportional to the mechanical efficiency. Of these assumptions, occupant comfort is a difficult parameter to quantify and will not generally be related linearly to the number of zones. Although ASHRAE has a recommended range of suitable values for occupant comfort to the number of zones, the specific value should ideally be based on individual occupant preference, which is almost never known prior to construction and can change over a buildings lifetime.

For this case study, user defined criteria was selected based on what is believed to be the current industry practice: a high importance for initial cost, and reduced consideration for system efficiency and occupant comfort. The selected case study values can be seen in Table 3.

Categories	User Defined Weighting
Importance of Initial Cost	3
Importance of System Efficiency	2
Importance of Occupant Comfort	1

Table 3. User Defined Criteria

The user defined criteria was selected in this manner to validate the functionality of the program, however, the intent is to allow for different design outcomes. Although zoning options were generated for the entire floor plan, only results for the five single occupant offices will be examined in this paper. Figure 8 displays these offices and Table 4 displays the zoning strategies that correspond to the user defined criteria.

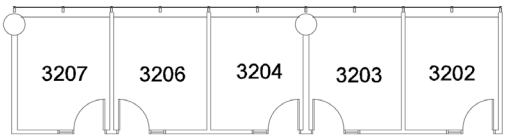

Figure 8. Third Floor Canal Building West Façade Single Occupant Offices

Strategy	Zone 1	Zone 2
1	3202 3203 3204 3206 3207	N/A
2	3202 3203	3204 3206 3207
3	3202 3203 3204	3206 3207

Table 4. West Façade Zoning Strategies

Mechanical design options were generated for the west façade offices based on the three zoning strategies listed in Table 4. Designs were generated using the same type of system that was constructed: a VAV based system with hydronic based radiant heating panels. VAV based systems are commonly selected in designs in order to *avoid over-cooling, most VAV systems are used in conjunction with separate heating systems* [ASHRAE 18.33], such as hydronic-based radiant panels. Table 5 represents the peak cooling load values determined for each of the zoning strategies.

Zoning Strategy	Zone 1 Peak Cooling Load (W)	Zone 2 Peak Cooling Load (W)
1	4,245	N/A
2	1,702	2,550
3	2,550	1,702

Table 5. West Zones Cooling Load Requirements

Zoning Strategy	VAV Supplier	Zone 1 VAV Size (mm)	Zone 2 VAV Size (mm)	Annual Supply & Return Fan Energy Consumption (GJ)	Annual Cooling Load (GJ)	Maximum Temperature (°C)	Days that the Room Temperature Exceeds Setpoint
1	Metalaire	250	N/A	3.31	4.44	23	0
1	Metalaire	200	N/A	1.96	4.43	24.68	5
1	Nailor	200	N/A	1.91	4.44	23	0
1	Nailor	175	N/A	1.28	4.44	24.28	3
2 & 3	*Metalaire*	*250*	*200*	*5.18*	*4.44*	*23*	*0*
2 & 3	Metalaire	200	200	3.78	4.44	23	0
2 & 3	Metalaire	200	150	2.96	4.44	23.59	1
2 & 3	Nailor	150	125	2.16	4.44	23	0
2 & 3	Nailor	125	100	1.67	4.43	25.01	7

Table 6. EnergyPlus Simulation Results

Since radiant panels are the source of heating for these offices, each room's peak heating load will be evaluated individually, rather than on a zone basis, as each room will contain its own radiant panel. These five offices have similar geometry and external wall details. This leads to a similar theoretical peak heating load, which was calculated to be 1,668W.

VAV boxes were selected that could supply the required amount of air to each zoning strategy found in Table 4. The required amount of air is the air flow rate required to meet the demands of the peak cooling loads found in Table 2, based on a cooling supply air temperature of 13 degrees celsius. Multiple supplier's VAV specifications were found online and incorporated into the code. Units from various suppliers are included; Metalaire, Nailor, Kreugar, E. H. Price, Titus, and Turtle Bailey. Once these VAV selections were generated, 38 EnergyPlus simulations were conducted to evaluate these VAV boxes, including the VAVs that were one size smaller. In addition, these VAV sizes were considered to evaluate the various trade-offs that may occur by under-sizing the unit. The setpoint may not be met during the entire cooling season, it may only occur once, which will save a substantial amount of the annual operational cost. Although BPS was performed for all of these suppliers, only the Metalaire and Nailor VAV results are presented in this paper. Results include the annual supply and return fan energy consumption, the five offices annual cooling load, days over the setpoint, and the magnitude of this temperature that were determined using EnergyPlus.

Table 6 represents the Metalaire and Nailor VAVs used in the EnergyPlus simulations. The Metalaire VAVs are analyzed to provide a comparison between the generated VAV results and the as-built design. The as-built design and results are located in the fifth row and are italicized. The Nailor VAV results were included since they yielded the most promising results for the various zoning strategies.

The third zoning option in Table 4, matches the strategy set in place. The VAV box selections that were based on the peak cooling load calculations were very promising, and the Metalaire VAV boxes were similar to those in the as-built, with the exception of one of the VAV boxes which was a unit smaller. The difference in VAV box sizing for the one unit is likely due to the fact that the hallway was grouped into this zone.

Ultimately, the identical zoning strategy and the similarity in the corresponding mechanical design is a strong indicator for the validity and functionality of the code. It confirms the code's capability to thermally zone offices, perform peak heating and cooling load calculations, and select the corresponding VAVs. The EnergyPlus simulations were performed to evaluate each design's fitness for this set of offices. It can be seen from the simulation results that the design that was implemented will always be capable of meeting the cooling demand, however, it yielded the most supply and return fan energy consumption out of the 38 options. VAV boxes operate under several damper positions which allows for specific volumes of air to pass through. VAV's are sized with minimum and maximum air flow through the VAV. Maximum air flow is sized to meet the peak load of a room, while the minimum flow relates to when the system is primarily providing ventilation or recirculation. Given that the system is only ever going to be dominated by the cooling demand for a maximum of 4 months of the year, this minimum air flow plays a significant role in the required supply and return fan energy. Since ASHRAE only requires 8.5 L/s/person (ASHRAE Std 62.1) it is advised to have low minimum air flow rate capabilities from the VAV, as can be seen in Table 6. Consider the same thermal zoning strategy as what was built, but instead utilizing Nailor VAVs. The cooling demand would have always met the cooling demand requirements, but due to significantly lower minimum airflow rate, this would have consumed 58.3% less fan energy in a year.

Instead of using the third zoning strategy, the first strategy could have been utilized. By pairing this strategy with a 200mm Nailor VAV, a decrease of 63.1% of the supply and return fan energy would have resulted. This design option would have been able to meet the cooling demands, but would have offered the occupants less control over their office temperatures, as 5 offices would have been grouped together. Furthermore, if this same zoning strategy was employed, but with a 175mm Nailor VAV, the energy consumption from the supply and return fans would have been 24.7% percent of what was constructed. This was the best solution from an energy consumption standpoint, but would have resulted in 3 days where the setpoint could not have been met. However, the resulting 3 under-cooled days would only have produced max-

imum temperatures of 24.28°C. Although this design is not ideal, the savings that correspond to this design make it a candidate worth considering. These high temperatures occur in the mid-afternoon, and if the occupants have flexible schedules, it might prove acceptable. These are typical considerations for a mechanical designer, however, due to time constraints, they are rarely able to perform sufficient calculations to arrive at these kinds of solutions. This type of development will allow designers the time to evaluate several design options, as opposed to only creating one design. As can be seen from this case study, utilization of this methodology could lead to substantial benefits, including lowering the energy consumption and operational cost.

5 FUTURE WORK

Pairing this development with an Architectural GD system is one of the first steps in the planned future work. Integration of HVAC generative design with Architectural generative design will further improve energy and system efficiency during the most flexible phase of design, the conceptual design phase. This coupling will also eliminate interferences between the two disciplines by shifting the industry standard from a collision detection mentality to an automated collision avoidance process. Mapping of the nodes, grid and adjacency lines, and the corresponding zone boundary lines should be completed, and integrated with an appropriate GA and fitness evaluator for supply diffusers and return grilles.

6 CONCLUSION

While the GD for HVAC code continues development, this research has demonstrated progress and improved capability. Zoning strategies were algorithmically generated and considered the type of room, as well as room adjacency, orientation, and load requirements. The code successfully integrated peak cooling and heating loads, and the corresponding VAV size for each zone into the GD process. When given the same trade-offs and evaluation criteria as those used in an existing building design, the system nearly replicates the existing zone level design. Furthermore, the system produced new design options for consideration, allowing a better understanding of the design space for the end user. By changing evaluation criteria, and considering the shift in design priorities due to new economical challenges, many more alternative designs can be easily generated and evaluated, improving design outcomes.

ACKNOWLEDGMENTS

We would like to thank the Natural Sciences and Engineering Research Council of Canada for their support of the CREATE Heritage Program.

REFERENCES

1. Asiedu, Y., Besant, R. W., and Gu, P. HVAC Duct System Design Using Genetic Algorithms. *HVAC&R Research 6*, 2 (2000), 149–173.
2. Barnaby, C. S., Shnitman, M., and Wright, W. A. HVAC System Design Automation: Issues, Methods, and Ultimate Limits. In *Proc. of Building Simulation '01, 7th International IBPSA Conference* (2001), 1151–1157.
3. Brahme, R., Mahdavi, A., Lam, K. P., and Gupta, S. Complex Building Performance Analysis in Early Stages of Design. In *Proc. of Building Simulation '01, 7th International IBPSA Conference* (2001), 661–668.
4. Caldas, L., and Norford, L. Architectural Constraints in a Generative Design System: Interpreting Energy Consumption Levels. In *Proc. of Building Simulation '01, 7th International IBPSA Conference* (2001), 1397–1404.
5. Caldas, L. G., and Norford, L. K. Genetic Algorithms for Optimization of Building Envelopes and the Design and Control of HVAC Systems. *ASME Journal of Solar Energy Engineering 125*, 3 (2003), 343–351.
6. Callaway, C. *ASHRAE Fundamentals Handbook*. W. Stephen Comstock, 1791 Tullie Circle, N.E., Atlanta, GA 30329, 2013.
7. Chapman, C. D., Saitou, K., and Jakiela, M. Genetic Algorithms as an Approach to Configuration and Topology Design. *ASME Journal of Mechanical Design 116*, 4 (1994), 1005–1012.
8. Deb, K., Pratap, A., Agarwal, S., and Meyarivan, T. A Fast and Elitist Multiobjective Genetic Algorithm: NSGA-II. *IEEE Transactions on Evolutionary Computation 6*, 2 (2002), 182–197.
9. EnergyPlus. Weather Data By Location. `https://energyplus.net/weather-location/north_and_central_america_wmo_region_4/CAN/ON/CAN_ON_Ottawa.716280_CWEC`. Accessed: 2016-07-13.
10. Gu, N., Singh, V., and Merrick, K. A framework to integrate generative design techniques for enhancing design automation. In *Proc. of CAADRIA '10, 15th International Computer Aided Architectural Design Research Conference* (2010), 127–136.
11. Hamdy, M., Hasan, A., and Siren, K. Optimum design of a house and its HVAC systems using simulation-based optimisation. *International Journal of Low-Carbon Technologies 5*, 3 (2010), 120–124.
12. Michalewicz, Z., and Schoenauer, M. Evolutionary Algorithms for Constrained Parameter Optimization Problems. *Evolutionary computation 4*, 1 (1996), 1–32.
13. Palonen, M., Hasan, A., and Siren, K. A Genetic Algorithm for Optimization of Building Envelope and HVAC System Parameters. In *Proc. of Building Simulation '09, 11th International IBPSA Conference* (2009), 159–166.
14. Shi, Z., and O'Brien, W. Building Energy Model using Principal Component Analysis and Affinity Propogation Clustering of Thermal Zones. In *Proc. of Asim '16, 3rd Asia Conference of IBPSA* (2016).
15. Wright, J. HVAC optimisation studies: Sizing by genetic algorithm. *Building Services Engineering Research and Technology 17*, 1 (1996), 7–14.
16. Wright, J., and Farmani, R. The Simultaneous Optimization of Building Fabric Construction, HVAC System Size, and the Plant Control Strategy. In *Proc. of Building Simulation '01, 7th International IBPSA Conference* (2001), 865–872.

The Use and Requirements of Simulation and Data Analytics for Building Energy Efficiency

Zheng Yang, Rishee K. Jain

Urban Informatics Lab, Department of Civil and Environmental Engineering, Stanford University
Stanford, California, United States
zheng.yang@stanford.edu

ABSTRACT

Buildings account for about 40% of total U.S. energy consumption, and 90% of them are energy inefficient to some extent. In order to improve energy efficiency, simulation and data analytics techniques have been widely developed to support building management professionals for efficiency related decisions and actions. However, to date no work has established a comprehensive and clear understanding about the use and requirements of simulation and data analytics for building energy efficiency. This paper proposes a nationwide survey conducted on building management professionals. From the 535 distributed questionnaires, 92 responses were collected. Preliminary results of how decisions are made by building management professionals, how simulation and data analytics are used in their current decision-making process, and how simulation and data analytics should be improved for further leveraging building energy efficiency, are presented.

Author Keywords

building; energy efficiency; survey; decision making; data analytics; simulation; current use; requirement

1 INTRODUCTION

Buildings consume more energy than any other sector in the United States, making improving their energy efficiency integral to our long-term sustainability goals. Since 90% of buildings are energy inefficient to some extent, new laws have sprung up across the country (over 20 cities to date) mandating the disclosure of building energy use data with hopes that such data combined with analytics will translate into energy savings. Simultaneously, numerous building simulation programs have been developed to model how a building uses energy such that management professionals can develop effective energy efficiency measures. In spite such efforts, neither the use of simulations nor data analytics have translated into substantial energy savings. This largely attributed to the fact that building management professionals generally lack the background or interest in data analytics and sophisticated simulation to interpret the results of complex models and processes. It is not clear whether they could make sense of the resulting data deluge and translate data into insights that would inform actions they can take on their building stock. In order to facilitate the use of simulation and data analytics techniques for sustained building energy efficiency, a survey was conducted on nationwide building management professionals. Our survey's four main foci include: 1) what decisions they could make to improve building energy efficiency; 2) what the general procedures to make the decisions are; 3) how simulation and data analytics are applied in current practice to support the decisions; 4) what the requirements and improvements of simulation and data analytics are necessary to benefit their decision-making. The results provide a basis for the further integration and advancement of energy simulation and data analytics techniques to leverage energy efficiency measure design and implementation for building management.

2 RELATED WORK AND MOTIVATIONS

Extensive studies have been conducted to review existing data analytics techniques, such as pattern recognition [1], optimization [2], analogy [3] and artificial intelligence [4], and simulation techniques, such as lighting [5], thermal [6], and CFD (computational fluid dynamics) [7] simulation, available to support the estimation and evaluation of certain decisions and actions for building energy efficiency. A number of surveys have also been carried out in the past to understand the use and trends of building simulation and modeling, focusing on challenges that prevent their wide use [9], user needs and functions for building design [10], data exchange and interoperability [11], and advanced building controls and operations [12]. However, to the authors' knowledge, to date no work exists that has established a clear and comprehensive understanding about the use and requirements of simulation and data analytics in each step of energy efficiency decision-making by building management professionals. Along with the rapid technology evolution, timely and first-hand analysis of application situations, bottlenecks, and demands of simulation and data analytics from professional opinions is of significant value to various studies and applications such as intelligent and sustainable facility management. More importantly, it could provide a reference to ground future advancements and improvements of simulation and data analytics that are specifically targeted to augment energy efficiency decisions and actions. This paper presents the preliminary analysis of survey data collected from a large sample of nationwide building management professionals.

3 SURVEY DESIGN

The survey questionnaire consists of four main sections: 1)

personal information; 2) energy efficiency decision details; 3) practices and requirements for simulation; 4) practices and requirements for data analytics. All the questions are designed based on standard principles including avoiding leading questions, providing mutually exclusive answers, separating double-barreled questions, optimizing sequences of questions, using balanced listings, removing jargons, and marking questions short and clear. All choice questions are open-ended to ensure exhaustive answers. The validity and usability were also examined by iteratively revising and pretesting the questions with random professionals to minimize the bias and misinterpretation of the questions. In total 535 questionnaires were randomly distributed to licensed building management professionals. Until November 30, 2016, 92 responses were collected from the *Quatlrics* platform utilized to deploy the survey

4 FINDINGS AND RESULTS

4.1 Personal Information

This part is designed with the purpose of classifying and analyzing the respondents' personal characteristics. Based on the results (Figure 1), respondents represent a broad range of years of experience from 4 years to 65 years with the average of 23 years. They have a variety of service positions, including (vice) president (22%), principal (chief) energy engineer (22%), energy director (17%), project manager (13%), and building engineer (26%), as shown in Figure 2. In addition, 40% of the respondents are from public sector (e.g. university) while 60% of them are from private sector (e.g. consulting company). Their balanced and diverse experiences and positions demonstrate their qualifications to reliably represent the current practices and requirement specifications of simulation and data analytics for building energy efficiency.

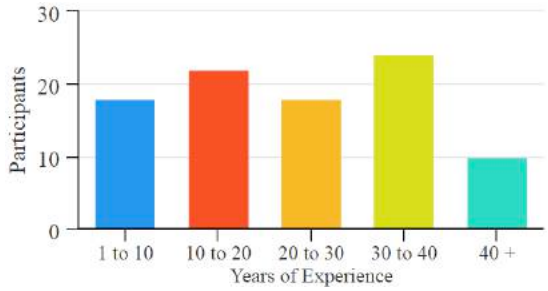

Figure 1. Participants' years of experience

Figure 2. Positions of participants

4.2 Decision-Making Details

This section aims to understand the details of regular decisions to improve building energy efficiency. The types of decisions are presented in Figure 2. It can been seen that the 'building systems and equipment', 'commissioning and energy auditing', and 'operations and maintenance' are the three areas that majority of decisions are made to, followed by 'building utilities', 'building envelop and geometry', and 'additions, alterations and retrofitting'. 'District systems and facilities', 'grid optimization and demand response', and 'community and neighborhood management' are beyond building scale thus receive the least attention.

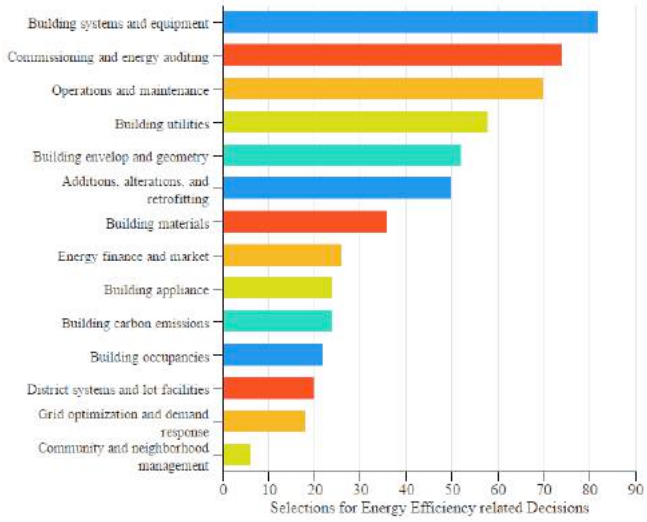

Figure 3. Types of decisions made for building energy efficiency

In terms of team size when making decisions, participants tend to form smaller teams perhaps to enable more efficient and effective decision-making. 40% of participants prefer a team with four or five decision makers. Large group and single person are not the common practices for building energy related decisions.

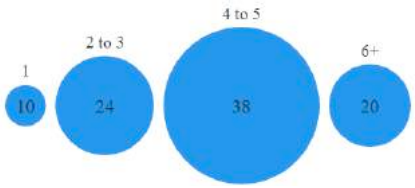

Figure 4. Team size for decision-making

4.3 Use and Requirements for Simulation

This part is for investigating the use and requirements of simulation to support the decision-making for building energy efficiency. Participants were first asked to select the types of simulation techniques commonly applied in their practices. Based on the results in Figure 5, the primary use of simulation is to perform quick and simplified estimates and analysis of building energy process. Less than half of the participants utilize simulation to test assumptions and hypothesis, examine sensitivity and effects of key control parameters, or run analysis at the community/urban scale.

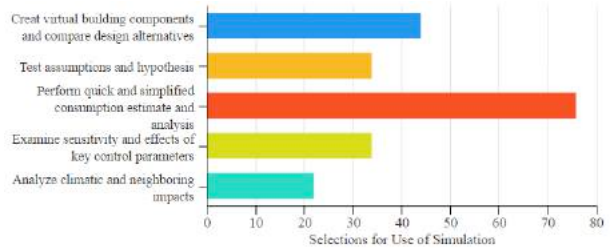

Figure 5. The use of simulation in decision-making

Participants were then asked to rate the usefulness of simulation is each of the seven phases of making decisions. The results show 85% of participants think simulation is necessary to facilitate 'validate and prove the proposals and alternatives'. 61% of them are positive for the function of simulation to support 'generate proposals and alternatives'. Approximately 46% agree simulation is useful to 'perceive and identify problems', 'gather information and improve awareness of situation', and 'evaluate the decision-making'.

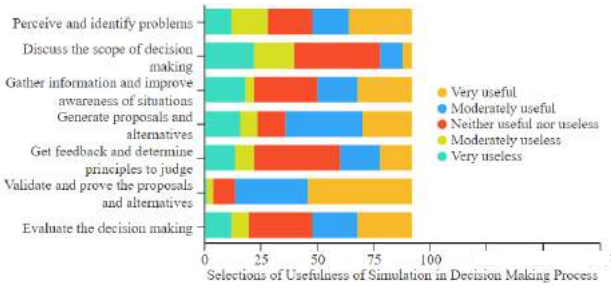

Figure 6. Usefulness of simulation in decision-making process

Next, the main issues that prevent simulation from being widely used in decision-making were identified (Figure 7). 72 participants consider 'efforts and time required time to build models' is the main problem, followed by 'inaccurate and unreliable simulation results'. Both of them are related to the concerns about models' inability to represent unique and real building situations, to some extent attributed to the fact of lacking robust and convenient calibration solutions.

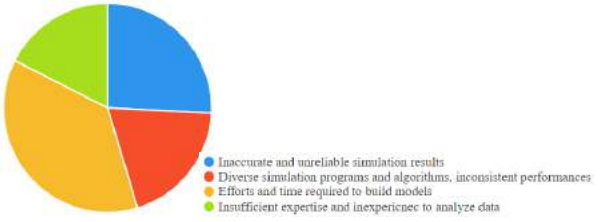

Figure 7. Issues in the use of data analytics

The last question for this part is to determine the levels of importance of criteria to improve simulation for decision-making. Based on the results in Figure 8, 'accuracy and robustness' and 'reduced uncertainty' are considered as the primary requirements by 89% of participants. 'Reduced uncertainty' and 'simple input method for review and modification' receive high number of positive votes like 'extremely important' or 'very important', and should also be given priorities for further improvement.

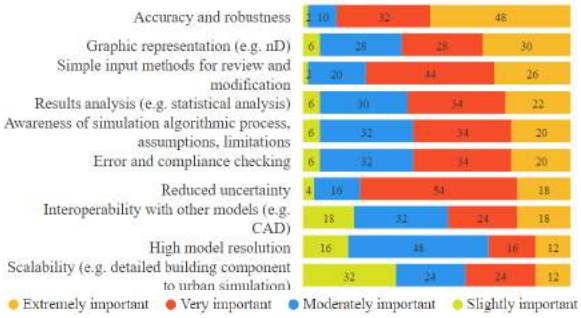

Figure 8. Requirements for further improvement of data analytics

4.4 Use and Requirements for Data Analytics

This part is to understand and analyze the use and requirements of data analytics to support decision-making for building energy efficiency. Similarly, participants were first asked to choose the types of data analytics techniques they have been utilizing in their current practices. It can been seen from Figure 5 the primary use of data analytics stays at the levels of descriptive interpretation, simple data processing and easy calculation, and basic programming. Computational techniques have not been widely accepted by the professionals in the building energy area.

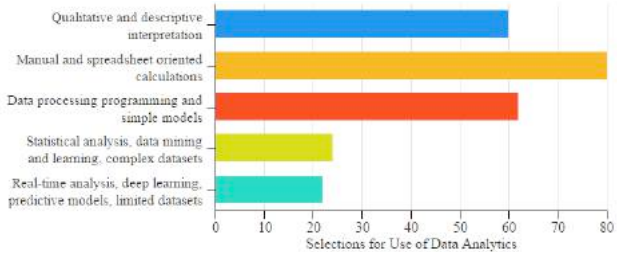

Figure 9. The use of data analytics in decision-making

Given the different phases of decision-making, participants then rated the usefulness of data analytics in each phase to facilitate them make appropriate decisions (Figure 10).

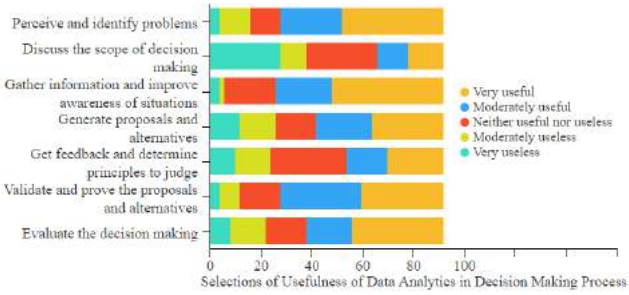

Figure 10. Usefulness of data analytics in decision-making process

Based on the results, 'perceive and identify problems', 'gather information and improve awareness of situations', and 'validate and prove the proposals and alternatives', are considered to significantly benefit from the implementation of data analytics, while 'discuss the scope of decision making' and 'get feedback and determine principles to judge' need less support from data analytics. For the main issues that block the use of data analytics in decision-

making (Figure 7), 60 participants chose 'low data quality, inaccurate and missing data', thus the development of advanced sensing systems and preprocessing techniques is pretty necessary. 44 participants are concerned about the 'hypothesis and biases made in analytics' would hamper the practicality and reliability of solutions to real problems.

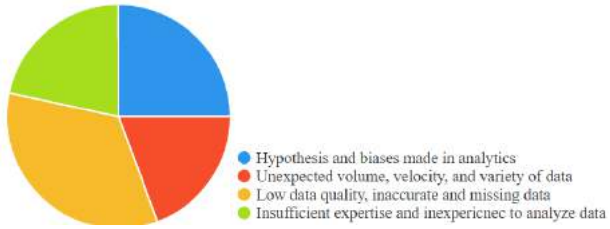

Figure 11. Issues in the use of data analytics

Lastly, regarding the requirements for further leveraging the use of data analytics, participants were asked to rate the level of importance for criteria necessary to support decision-making for building energy efficiency. According to the results (Figure 8), better visualization and strong interpretability are the relatively most urgent, followed by 'informative conclusion extracted', 'transparency of analytics process (e.g. assumptions, limitations, risks) ', and 'quick and easy evaluation of alternatives'. All of the above indicate a strong desire for respondents to better understand the analytics process and possible outcomes for decisions.

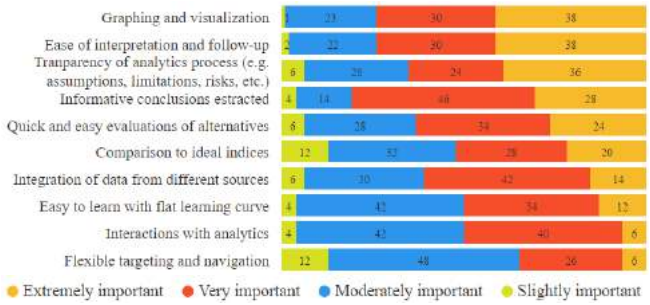

Figure 12. Requirements for further improvement of data analytics

5 CONCLUSIONS AND ONGOING WORK

This paper presents the preliminary results of a nationwide survey of building management professionals that uncovers details on their decisions for building energy efficiency, current use of simulation and data analytics in decision-making process, and requirements for further improvement. The survey is part of a broader effort to improve the awareness of application situations, technical issues, and user demands regarding utilizing simulation and data analytics and effectively support building energy efficiency related decisions. It collects and analyzes data from building management professionals at different levels who have wide range of years of experience. The results provide a concrete basis to further advance and improve simulation and data analytics techniques necessary for leveraging energy efficiency and other applications.

However, only descriptive information was provided in the paper without statistical inference. Comprehensive analysis is being conducted in the ongoing work. First, correlations among different questions (e.g., issues and requirements) will be calculated to identify specific patterns and linkage of responses. Second, analysis of variance and sensitivity analysis will be run to quantify the effects of respondent characteristics on the responses. Third, the relationships between use and requirements of simulation, and those of data analytics, will be investigated to discover opportunities of integrated solutions. Finally, more responses will be continuously collected to converge the analysis results and check whether the opinions are geospatially consistent.

ACKNOWLEDGEMENTS

This material is based upon the work supported in part by the Stanford School of Engineering under a Terman Faculty Fellowship and the National Science Foundation under Grants No. 1461549 and 1642315. Any opinions, findings, and conclusions or recommendations expressed in this material are those of the author(s) and do not necessarily reflect the views of the National Science Foundation.

REFERENCES

1. Kumar R. et al. 2013. Aggarwal R, Sharma J. Energy analysis of a building using artificial neural network: A review. Energy Build. 65: 352-8.
2. Nguyen A. et al. 2014. A review on simulation-based optimization methods applied to building performance analysis. Appl.Energy. 113:1043-58.
3. Li Z, et al. 2014. Methods for benchmarking building energy consumption against its past or intended performance: An overview. Appl.Energy. 124: 325-34.
4. Zhao H., Magoulès F. 2012. A review on the prediction of building energy consumption. Renew. Sustainable Energy Rev. 16(6): 3586-92.
5. Ochoa C.E. et al. 2012. State of the art in lighting simulation for building science: a literature review. J. Build. Performance Sim. 5(4): 209-33.
6. Coakley D. et al. 2014. A review of methods to match building energy simulation models to measured data. Renew. Sustainable Energy Rev. 37:123-41.
7. Foucquier A. et al. 2013. State of the art in building modelling and energy performances prediction: A review. Renew. Sustainable Energy Rev. 23: 272-88.
8. Reinhart C., Fitz A. 2006. Findings from a survey on the current use of daylight simulations in building design. Energy Build. 38(7): 824-35.
9. Attia S. et al. 2012. Selection criteria for building performance simulation tools: contrasting architects' and engineers' needs. J. Build. Performance Sim. 5:155-69.
10. Bynum P. et al. 2012. Building information modeling in support of sustainable design and construction. J.Constr.Eng.Manage. 139(1): 24-34.
11. Elmualim A. et al. 2009. Application of computer-aided facilities management (CAFM) for intelligent buildings operation. Facilities. 27(11/12): 421-8

Relationships Between Variables and Energy Consumption in Different Building Types

Ju Chan Kim[1], Jonathan Salter[2], Ronald Kellett[2] and Cynthia Girling[2]

[1]University of British Columbia
Vancouver, Canada
juchankim.kor@gmail.com

[2]University of British Columbia
Vancouver, Canada
{jsalter, rkellett,
cgirling}@sala.ubc.ca

ABSTRACT

Cities and municipalities have set energy and greenhouse gas (GHG) emissions reduction targets in attempts to manage energy consumption and mitigate climate change. Numerous variables, that vary significantly across climates and design options impact energy consumption in the building sector. It is important to understand the relationships between these variables to reduce energy consumption and GHG emissions. This paper describes ongoing research showing the potential of a parametric simulation approach with regression analysis to investigate and compare relationships among building design variables and energy consumption by building type in the Vancouver region of British Columbia, Canada.

Author Keywords

Energy simulation; parametric simulation; regression analysis

ACM Classification Keywords

I.6. SIMULATION AND MODELING; G.3 Correlation and regression analysis

1 INTRODUCTION

Energy and climate change have been significantly elevated among important global urban planning issues. Many municipalities have set energy and greenhouse gas (GHG) emission targets in attempts to manage energy consumption and mitigate climate change [8]. In parallel, municipalities seek capacity to simulate energy and emissions at urban scales, in combination with measures of land use, transportation and quality of life.

Buildings contribute up to 30% of global GHG emissions and consume approximately 40% of global energy [8]. In 2009, the energy consumed in residential buildings was 17% of total energy used nationwide and released 15% of total GHG emissions in Canada [6].

The United Nations Environment Programme (UNEP) acknowledges the potential of the building sector to reduce GHG emissions to achieve the emissions reduction targets of municipalities and recommends the building sector should be prioritized as a key to reaching emission targets successfully [8]. Because buildings have a long lifespan, operating energy exceeds embodied energy in most cases [1]. Most countries have developed or adopted policies and standards to regulate and encourage reduction in operating energy in the building sector.

Numerous variables, that vary significantly across climates and design options, impact energy consumption in the building sector. Analyzing these variables can help policy makers effectively address energy and emissions reductions and help users make beneficial decisions. Studies have been conducted in different parts of the world looking into these variables [3, 7]. For example, in Canada, only 1% of total energy was used for space cooling and 63% of energy was used for space heating in the residential sector in 2009 [6]. Unfortunately, these studies show limitations in generalizability. They investigated variables in a local context, making results difficult to generalize because of variances in building type, climate, location, etc., which create a unique environment for each case and its use of energy. This paper proposes a method to evaluate variables and predict consequences reflecting local contexts more efficiently by conducting parametric simulations and regression analysis [2].

This paper is a preliminary part of a project investigating effective strategies to reach energy and emissions targets in different types of urban form. Identifying key variables in the built environment for different building types and climate conditions will provide important guidance towards establishing those strategies. We conducted parametric simulations using EnergyPlus and regression analysis to investigate the impacts of different variables on building energy consumption and relationships between and among those variables. Results from the later phase of the project will aid industry professionals and governments to make informed planning and design decisions.

2 METHODOLOGY

Parametric energy simulations were conducted by using EnergyPlus and jEplus. The reference building models (Section 2.2) were simulated parametrically by changing input variables (Section 2.1) in fixed increments while the remaining variables were held constant. To be more time efficient, regression analysis was implemented after the

simulations to predict the results that are not simulated. Phases in the research included the following steps: determining the input variables; setting the reference building models; running the energy simulations; collecting the simulation results; and running the regression analyses.

2.1 Determine Variables

The US Department of Energy (DOE) has categorized the input variables of building energy models by program, form, fabric, and equipment (Table 1) [5]. The variables investigated in this research are: U-value of exterior wall, roof and windows; infiltration rate; lighting; and equipment efficiency (Table 2).

Program	Form	Fabric	Equipment
Location	Number of floors	**Exterior walls**	**Lighting**
Total floor area	Aspect ratio	**Roof**	HVAC system types
Plug and process loads	Window fraction	Floors	Water heating equipment
Ventilation requirements	Window locations	**Windows**	Refrigeration
Occupancy	Shading	Interior partitions	**Component efficiency**
Space environmental conditions	Floor height	Internal mass	Control settings
Service hot water demand	Orientation	**Infiltration**	
Operating schedules			

Table 1. Building energy model input categories

This paper focuses on fabric and equipment variables which could be regulated and controlled by codes and standards. Other variables will be studied in the later stage of the research.

The ranges and distributions for each input variable are summarized in Table 2. These ranges were determined by observing typical buildings built prior to the 1970s when there were no energy efficiency requirements and new construction with strict energy efficiency requirements - the Passive house standard.

Exterior wall

The reference models assigned insulation materials as "Material:NoMass" in EnergyPlus. Therefore, thermal resistance values of insulation were changed instead of changing the thickness in order to have equivalent results of changing U-values.

Roof / attic floor

Thermal resistance values of insulation in roofs were controlled for high-rise apartment, strip mall and primary school types. Thermal resistance values of attic floors were controlled for single-family detached house and multi-family low-rise apartment types.

Window

To overcome the limitations in controlling the U-value of windows in EnergyPlus, "WindowMaterial: SimpleGlazingSystem" was used. Solar Heat Gain Coefficient (SHGC) and visible transmittance (VT) values were fixed to 0.426 and 0.308 respectively – the default of the ASHRAE 90.1 reference model - when controlling the U-values.

Infiltration rate

The "AirChanges/Hour" method was used for "Design Flow Rate Calculation Method" to control the infiltration rate of zones for reference models in EnergyPlus.

	Variables	High-rise apartment	Single-family detached house	Multi-family low-rise apartment	Strip mall	Primary school
		Input values				
Exterior wall	Thermal resistance of insulation [m2K/W]	[0.6:0.5:6.1] *	[0.1:0.5:6.1]	[0.1:0.5:6.1]	[0.6:0.5:6.1]	[0.6:0.5:6.1]
Roof / attic floor	Thermal resistance of insulation [m2K/W]	[0.6:0.5:6.1]	[0.1:0.5:6.1]	[0.1:0.5:6.1]	[0.6:0.5:6.1]	[0.6:0.5:6.1]
Window	U-value [W/m2K]	[0.8:0.5:5.8]				
	Solar Heat Gain Coefficient (SHGC)	[0.01:0.1:0.99]				
Infiltration rate	ACH rate for zones [ACH]	[0.1:0.5:4.6]	[0.1:0.25:2.35]	[0.1:0.5:4.6]	[0.1:0.5:4.6]	[0.2:1.0:9.2]
Lighting	Lighting power density (LPD) [W/m2]	[1.0:2.0:13.0]				
Equipment efficiency	Boiler efficiency [%]	[50.0:10.0:90.0]				
	Gas heater efficiency [%]					

* [A:B:C] indicates the range of input value is from A to C with increments of B

Table 2. The summary of range of input values modelled

2.2 Reference Building Models

The Pacific Northwest National Laboratory (PNNL) developed prototype building models that comply with ASHRAE Standard 90.1 baselines and the International Energy Conservation Code (IECC) [9]. These models are representative of 80% of buildings constructed in the U.S. which represent 65% of the total building energy consumption. Five of those building types (high-rise apartment, single-family detached house, multi-family low-rise apartment, strip mall and primary school) were used as reference building models in this study (Table 2), more building types will be considered in the future.

2.3 Run energy simulations

EnergyPlus and jEplus [10] were used for this study because a later stage of the research uses the Urban Modelling Interface (UMI) which utilizes EnergyPlus. jEplus automates parametric simulations by batch simulating the EnergyPlus Input Data Files (IDF).

2.4 Assumptions and Limitations

The reference prototype building models do not contain models for the Vancouver (British Columbia, Canada) region, therefore, the Seattle (Washington, U.S.) models with Vancouver weather data were used for the simulations. Effects of thermal mass are not accounted for because we used "Material:NoMass" for envelope constructions and "WindowMaterial:SimpleGlazingSystem" for windows. Calculated U-values may differ from those in compliance with the local energy efficiency codes because the recommended R-values of inside/outside air film varies and simulation tools treat them differently. This paper assumes the reference building models represent the buildings in Vancouver. The method does not currently account for complex interactions between input variables. This will be addressed in future iterations.

3 SIMULATION RESULTS

349 simulations were carried out for this research, and regression analyses were conducted to predict the results of every input values.

3.1 Regression Analysis

The annual end uses of electricity and natural gas were used as the dependent variables and the input variables (Section 2.1) as independent variables for the regression analysis. Figure 1 shows a summary of the relationship between variables and the annual energy end use, as well as their regression equations. Only selected cases of the total end uses are presented for illustrative purposes. All R^2 values exceeded 0.94 meaning the selected regression equations fit the data well. The wall and roof U-values correlate with the end use energy by a linear relationship except for the primary school model. All other variables correlate by a quadratic relationship.

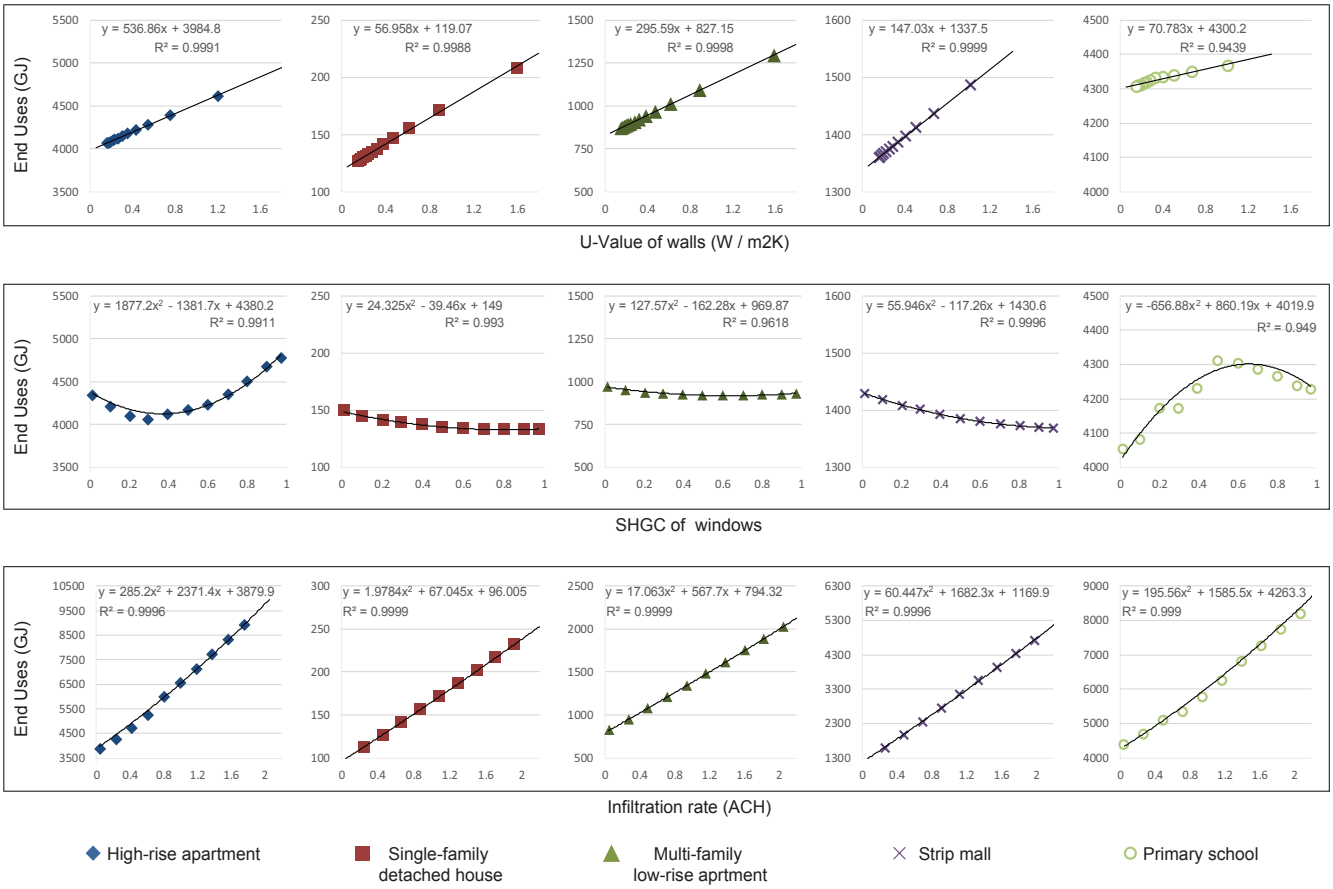

Figure 1. Selected summary of regression analysis

4 CONCLUSION AND FUTURE RESEARCH

The results of this study show that, in residential building types, U-values of exterior wall, roof and windows had significant impact on energy consumption, while in strip mall and primary school types they had less. The SHGC value of windows had a non-linear relationship with the end use energy in all buildings suggesting the importance of windows with the appropriate SHGC for different building types. Among the variables tested, infiltration rate had the highest impact on the end use energy for all building types, particularly for large building types (high-rise apartment, primary school, and strip mall) (Figure 2). This demonstrates significant potential savings on energy and emissions from large buildings if effective policy and practices could be developed to address infiltration in the existing building stock. Preliminary results from a study conducted in the Prince George region of British Columbia suggest that this is more pronounced in less temperate climates common across Canada.

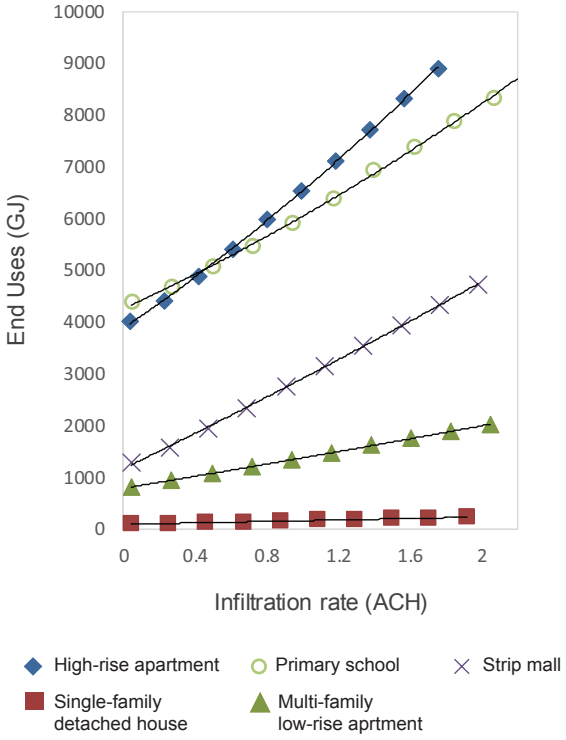

Figure 2. Relationship of infiltration rate and end uses

Current National Energy Code of Canada for Buildings (NECB) or ASHRAE 90.1 standard do not specify the requirements by different building types by climate zones. An accurate understanding of the variables that are most important to different building types could help us adjust regulations and building codes by building type to better realize large energy and emissions savings.

This study shows the potential of a parametric simulation approach with regression analysis to investigate and compare relationships among building design variables and energy consumption. In future work, more building types in other locations across British Columbia will be simulated to make the data representative of different local contexts and a diverse building stock. The end goal of this research is to aid development of effective strategies to reach energy and emissions targets in different types of urban forms and in different climate conditions.

ACKNOWLEDGMENTS

We would like to acknowledge our research partners at UBC and Esri Canada. We would also like to acknowledge funding for this research provided by the Pacific Institute for Climate Solutions, the National Science and Engineering Council, and Esri Canada.

REFERENCES

1. Adams, E., Connor, J., Ochsendorf, J., 2006. Embodied energy and operating energy for buildings: cumulative energy over time. Design for sustainability, Civil and Environmental Engineering. MIT, Cambridge, MA.
2. Bichiou, Y., Krarti, M., 2011. Optimization of envelope and HVAC systems selection for residential buildings. Energy and Buildings 43, 3373-3382.
3. Carvalho, M., La Rovere, E., Gonçalves, A., 2010. Analysis of variables that influence electric energy consumption in commercial buildings in Brazil. Renewable and Sustainable Energy Reviews 14, 3199-3205.
4. City of Vancouver, Renewable City Strategy: our future to 2050. <http://vancouver.ca/green-vancouver/renewable-city.aspx>, (accessed December 03.2016).
5. Deru, M., Field, K., Studer, D., Benne, K., Griffith, B., Torcellini, P., Liu, B., Halverson, M., Winiarski, D., Rosenberg, M., 2011. US Department of Energy commercial reference building models of the national building stock.
6. NR Canada, N.R.C., 2009. Energy Efficiency Trends in Canada 1990 to 2009.
7. Samuelson, H., Claussnitzer, S., Goyal, A., Chen, Y., Romo-Castillo, A., 2016. Parametric energy simulation in early design: High-rise residential buildings in urban contexts. Building and Environment 101, 19-31.
8. SBCI, UNEP, 2009. Buildings and climate change: Summary for decision-makers. United Nations Environmental Programme, Sustainable Buildings and Climate Initiative, Paris, 1-62.
9. U.S. Department of Energy, Building Energy Codes Program Development. <https://www.energycodes.gov/development>, (accessed December 03.2016).
10. Zhang, Y., 2009. Parallel EnergyPlus and the development of a parametric analysis tool, 11th Conference of International Building Performance Association IBPSA, Glasgow, UK

Context-sensitive Personal Space for Dense Crowd Simulation

Omar Hesham and Gabriel Wainer

Department of Systems and Computer Engineering
Carleton University, Ottawa, Canada
omar.hesham@carleton.ca, gwainer@sce.carleton.ca

ABSTRACT

Real-time simulation of dense crowds is finding increased use in event planning, congestion prediction, and threat assessment. Existing particle-based methods assume and aim for collision-free trajectories. That is an ideal -yet not overly realistic- expectation, as near-collisions increase in dense and rushed settings compared to typically sparse pedestrian scenarios. This paper presents a method that evaluates the immediate personal space area surrounding each entity to inform its pathing decisions. While personal spaces have traditionally been modeled as having fixed radii, they actually often change in response to the surrounding context. For instance, in cases of congestion, entities tend to share more of their personal space than they normally would, simply out of necessity (e.g. leaving a concert or boarding a train). Likewise, entities travelling at higher speeds (e.g. strolling, running) tend to expect a larger area ahead of them to be their personal space. We illustrate how our agent-based method for local dynamics can reproduce several key emergent dense crowd phenomena; and how it can be efficiently computed on consumer-grade graphics (GPU) hardware, achieving interactive frame rates for simulating thousands of crowd entities in the scene.

Author Keywords

Crowd animation; Personal space; GPGPU; Interactive.

ACM Classification Keywords

I.6.5 [Simulation and Modeling]: Model Development;
I.3.7 [Computer Graphics]: Animation;

1 INTRODUCTION

Dense crowd simulation is an area of research concerned with assessing and predicting the motion of large groups of people within a limited physical space. The applications range from use in gaming and film production, to designing public spaces and assessing quality of occupancy, to the safety-critical analysis of the potential for stampedes and crowd crushes.

If you ask two people to walk the same path, they will display deviations from each other. Ask the same person to walk the same path twice, and you would still get deviations from one walk to another. Human motion is seemingly non-deterministic, and hence, pedestrian simulation will always be an exercise in abstraction.

When simulating high-density pedestrian traffic, congestion, or a mass gathering event (e.g. at a concert), macroscopic methods that rely on aggregate parameters (bringing a sense of determinism through bounded stochasticity) can be very effective when analyzing collective motion results, such as rate of egress and density distribution over an area. Because they do not rely on simulating individual entities, those methods are often efficient enough to accommodate large-scale simulations of thousands of entities. By contrast, microscopic methods can reproduce the intricate details of every individual's trajectory, at an increased computational cost. However, as computing hardware continues to evolve to provide performance gains through parallelism and portability through power efficiency, microscopic simulation is becoming increasingly accessible to designers, architects, and event planners, allowing them to readily assess the risks and focus stakeholder efforts around potential congestion issues.

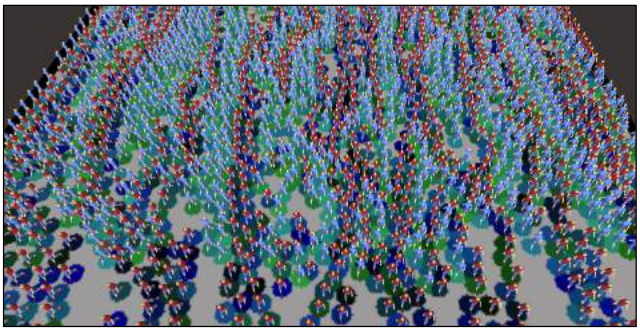

Figure 1. Organically formed lanes in dense bidirectional flow; 2000 entities simulated at 130fps on a consumer-grade desktop.

Here, we present a contribution to the development of micro-scopic methods catered to dense crowd phenomenon (e.g. Figure 1). The relevant background is discussed in sections 2 and 3. Section 4 outlines our contributions and section 5 illustrates our method's results and real-time performance. Finally, the discussion in section 6 reflects on the method's limitations, and hosts opportunities for further discussion and future work.

2 BACKGROUND

Like other physically-based phenomena that exhibit complex interactions between entities over time, crowd motion could only be practically simulated using numerical methods rather than analytical solutions. There are different granularities of motion abstraction depending on the target use case.

Historically, the earliest methods were macroscopic in nature, simulating aggregate behavioural parameters, rather than actual individual trajectories in the scene. They were based on adapting existing fluid simulation models to incorporate aggregate human motion parameters. They were typically computed over an Eulerian grid [20, 25] to provide computational stability and high performance. This granularity of simulation was sufficient to assess and validate collective motion parameters such as egress rate and density distribution over a given scene layout.

Network optimization techniques were also adapted to simulate occupant movement within a predefined multi-compartment environment [15]. Each compartment is treated as a graph node that might represent a section within a room, a hallway, or even an entire building. The edges connecting those nodes would represent the capacity of pedestrians moving between one node to another. By utilizing classic optimization techniques such as finding the shortest path or detecting the max flow, designers could focus their efforts on areas of potential pedestrian bottlenecks better.

To this day, macroscopic crowd methods remain popular in engineering and design applications due to their computational efficiency and the ability to provide a great deal of insight into aggregate crowd dynamics, especially for large-scale projects which involve high crowd counts [6, 13].

With ever-increasing hardware capabilities and improved modeling methodology, the ability to simulate individual entity-to-entity interactions became possible. Unlike macroscopic methods, microscopic methods simulate entities as individual agents with localized rulesets whose emergent behaviour matches that of the aggregate results of macroscopic methods (and more importantly, reality). In microscopic methods, local-neighbourhood interaction rules can have significant effects on the emergent global behaviour.

Some of the earliest examples of this modeling philosophy include Cellular Automata (CA) and the closely related Lattice Boltzmann (LBM) models [1]. In CA methods, the space is typically divided into a uniform grid, where every cell can either be available, have an entity, or represent an obstacle. Every cell's future state is then determined based on the states of the cells in its local neighbourhood. CA crowd models were rapidly developed and adopted, thanks to their parallel-friendly processing and native visualization (every cell is both the computational unit and the visual representation). Nevertheless, this grid-based Eulerian evaluation with discretized stepping and finite directions of motion does not faithfully reflect the fluidity of human motion trajectories.

Lagrangian methods, typically implemented in the form of free-moving particles, perform their computations in-place, avoiding the fixed-grid problem of Eulerian evaluation. Successful efforts in this area were introduced by Reynold's particle swarm model [21] and Helbing's social forces crowd model [10]. Examples of later variations include HiDAC, which incorporates psychological profiles and pushing behaviour [18]; and physical models, which incorporate the simulation of individual locomotive limbs to generate each entity's motion [2].

A fundamental element of Lagrangian-based methods is neighbourhood detection, the process of identifying each entity's neighbours. This is the primary cost differential when compared to Eulerian evaluation where neighborhoods are typically predefined and directly accessible. Certain data structures can be used to accelerate the neighbourhood search through recursive subdivision (e.g. Octrees). Other structures include the Voronoi diagram, which can be used to limit the search area and accelerate neighbourhood detection using GPUs [4, 22]. Beyond identifying neighbours, centroidal particle dynamics can also utilize Voronoi diagrams to compute each entity's response to violations of its personal space [11].

Human motion has been empirically shown to be anticipatory in nature [19]. People continually scan their environment for potential collision events and enact local maneuvers to avoid those predicted events. Agent-based models built on this principle include Reciprocal Velocity Obstacle (RVO) [5], and a velocity-space optimization model (ORCA) [27].

Other efforts try to mimic the human vision-to-motion feedback cycle, by rendering a 1D [16] or 2D [17] depth map from each entity's perspective, and emulating how humans change their trajectory based on that information alone. Vision-based approaches are unique in their realistic depiction of data encapsulation. That is, they realistically model how an entity does not have direct access to its neighbors' state variables; it can only interpret what it can glean from the depth information in its own perspective. Alas, the computational and memory costs of representing each entity's viewpoint can become prohibitive for large-scale simulation.

This paper adopts the centroidal particles approach in [24, 11] for their realistic depiction of personal space compression in congested settings. The following section briefly describes their basic approach, then outlines our contributions, which add anticipatory collision avoidance, and offloads more CPU workload to the graphics card (GPU) for increased performance and higher frame rates.

3 CENTROIDAL PARTICLE DYNAMICS

Centroidal particle dynamics (CPD) for crowd simulation assume that every entity knows its global trajectory or vector [24, 11]. That is, barring any other dynamic entities in the scene, following the global path will lead each entity to its target location in optimal time. Global pathing algorithms, such as A*, are typically used for such broad scale pathing and already take into account the large-scale static elements of the scene (e.g. walls, doorways, obstacles, etc.). CPD methods then enact local rules to attempt to maneuver around

the surrounding dynamic entities in the scene, with the least deviation possible from the ideal global path.

3.1 Personal Space

The basis for CPD crowds lies in explicitly modeling and evaluating every entity's personal space (PS). Studies in France and North America have shown that the average adult PS is ~0.8m evenly around the center of the entity when idling, and ~0.5m when in motion [19, 29]. These numbers vary slightly across cultures [30], and CPD methods can adapt to PS compression around barriers to motion in moving crowds, or points of interest in static crowds (e.g. closer to the stage at a concert) [11]. When two entities approach each other, they equally share (or violate) each other's personal space. CPD methods model local dynamics by having each entity attempt to be at the virtual center of mass (or centroid) of the unviolated portion of its PS, attempting to restore its preferred PS area over time.

The Centroidal crowds in [11] model this attempt in the form of a linear force in the direction of the centroid (Figure 2). The personal space definition of shared space can be geometrically represented by constrained centroidal Voronoi tessellation [24]. This tessellation does not need to happen pair-wise; it can be computed over the entire domain of simulated entities (including obstacles), accounting for the aggregate infringement of each entity's personal space. This global tessellation is called the Personal Space Map (PSM).

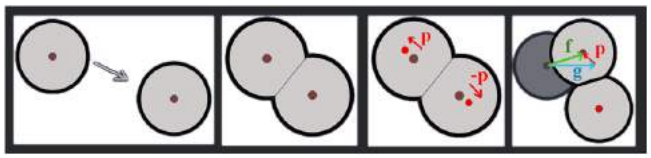

Figure 2. The net force (*f*) experienced by an entity is a linear combination of the global pathing force (*g*), and the penalty force (*p*) which falls along the direction of the new centroid [11].

3.2 Personal Space Map

The global PSM is used to tessellate the space and accelerate the nearest neighbours search [22] by precisely placing and orienting a short-range ray-marching probe in the most optimal position for neighbor detection, without requiring an exhaustive radial search. By contrast, the PSM, illustrated in Figure 3, is used in [11] to avoid the need for any nearest neighbor search explicitly. It does so by relying on the CPD equivalent of data encapsulation: in dense congested scenarios, every entity's local dynamics are informed only by the information within its expected personal space. Hence, regardless of who the entity neighbours are or what obstacle caused the reduction in personal space, every entity will enact the proper local dynamics by only evaluating its expected PS. This high locality also translates to data-parallelism, which could be exploited for acceleration onto a GPU. CPD methods also allow for the modification of the PS base shape (called *PS footprint* in [11]). The modifications include changing the size to accommodate a variety of different entity profiles; reducing the relative Voronoi influence of PS to indicate a more vulnerable pedestrian (e.g. child); and applying an influence map to completely customize how the centroid is calculated (the map is convolved with the integral of the PS area).

Figure 3. A small section of a larger crowd. Right: the crowd's PSM shown as an underlay. PS colors simply encode entity IDs.

We take advantage of this flexibility by proposing our own modifications and contributions to the CPD base PS shapes, and present an implementation that utilizes the GPU compute capabilities of consumer devices (desktop and mobile alike).

4 CONTEXT-SENSITIVE PERSONAL SPACES

This section outlines our contributions to the CPD model, towards more realistic simulation of dense multi-directional flow.

4.1 Asymmetric PS Weighting

Currently, CPD methods use a PS shape that is evenly weighted around the entity, based on the empirical studies in [19] that demonstrate this fact. However, when an entity has its personal space infringed upon outside of its vision, the entity would unrealistically sense this infringement and react as if it had eyes in its back, so to speak.

Our first modification is the use of a multi-area kernel (shown in Figure 4) that splits the shape into two key areas: i) PS area that affects both the entity and its neighbours; and ii) PS area that only affects surrounding neighbours. This asymmetrical shape is an intuitive change that brings about some implications:

- The net separation between entities in motion remains at the ideal ~1m (twice the 0.5m PS radius). The only difference here is that instead of equally sharing the responsibility, the entity with visibility will now shoulder most of the responsibility and corrective efforts to maintain that distance. This is analogous to a driver maintaining a safe distance from the vehicles ahead (there might be some collaboration, but it is mostly that driver's responsibility).
- Because a single entity (the one in the back) is maintaining most of the separation distance, the severity of PS compression around areas of congestion is reduced.

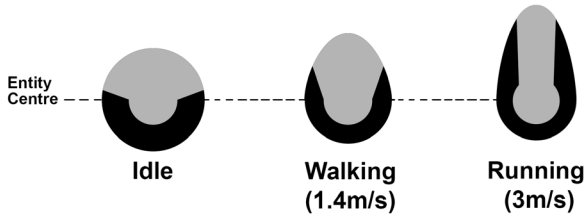

Figure 4. Proposed PS shape: light area affects the entity and its neighbours; dark area only affects neighbors. Lengthening of PS kernel is towards direction of motion as demonstrated.

Additionally, the suggested extension of personal space proportional to the entity velocity was implemented, where the personal space extends by ~0.4m per m/s. This extension is slight for walking speeds (~1.4m/s), but quite noticeable at running or cycling speeds (> 3m/s). Figure 4 illustrates the multipart modification also in relation to speed, to account for the narrowing focus of speeding entities. This is how collision *anticipation* was incorporated into the simulation.

4.2 Resistance to Non-Optimal Bearings

In the linear combination of forces illustrated in Figure 2, we added a resistance element to centroidal forces opposing the optimal global path/objective. This was inspired by the energy-minimization goals set in ORCA [27], and it has reduced the "springiness" of near-miss collisions in pedestrian crossings significantly (especially in bidirectional flow). Therefore, even if the centroid is pointing the entity to face away from the goal -because that is what is locally optimal- the entity will resist this change and instead attempt to wait until more favourable centroidal forces are available.

4.3 Hardware Acceleration via GPU Shaders

Previous CPD methods implemented the PSM using a constrained Voronoi diagram over a discretized surface. The idea was to render every entity PS as a 3D cone viewed from the top [12], and the visible pixels after any intersection will represent the remaining available personal space. This utilization of the graphics pipeline allowed Voronoi-based proximity detection [4] and CPD methods such as [11] to achieve interactive frame rates for thousands of 2D entities in the scene.

In our attempt to accelerate the CPD's PSM computation, the CPU was initially found to be the primary bottleneck, due to the repeated rendering calls made for each entity cone. Each render call came with graphics API overhead and CPU-to-GPU memory transfer costs.

Modern graphics APIs have features that allow instanced rendering. The CPU would send the shape information only once, along with a point cloud of instance locations. Then, the GPU would perform the replication on-chip without needing to communicate again with the CPU over the relatively slow system bus. Unfortunately, this feature could not be naively used for PSM computation because of the dynamic PS shapes, especially with our introduction of velocity-dependent extensions (Figure 4).

With nothing to "instance", we opted instead to develop Geometry Shaders that dynamically generate the PS shapes on the GPU. Geometry Shaders are part of the modern graphics processing pipeline that can programmatically generate new meshes and geometry that the CPU did not initially send. Our geometry shaders accept a point cloud of entity positions along with an array of entity attributes (e.g. current velocity, bearing, comfort speed, etc.) and lets the GPU generate the appropriate voronoidal PS shapes per entity. This reduction in CPU render calls has improved the simulation framerate, as will be shown in Section 5

Furthermore, in order to compute each entity's new centroid position, we opted for a vertex shader (run once per entity, in parallel) that computes the available PS space (and the violated space, by omission) by sampling the previously created PSM (which was input into the vertex shader as a texture). This further resulted in performance gains that improved scalability and significantly reduced the bottlenecks at higher crowd counts (10,000+ entities in the scene).

Sample source code and GLSL shaders are available at http://cell-devs.sce.carleton.ca/publications/ .

5 RESULTS

This section demonstrates how our proposed agent-based method can reproduce several emergent crowd phenomena. Figure 5 illustrates the top view of our simulation of bidirectional flow of a dense crowd (1000 entities) in a corridor. The resulting interlocking pattern is born out of each entity's desire to take the path of least resistance; and in bidirectional scenarios, this simply comes down to avoiding oncoming traffic. As entities traveling in the same direction leave an empty space behind them, the centroid of similarly oriented entities become attracted to fill the void. Hence the appearance of chains or lanes amidst the crowd.

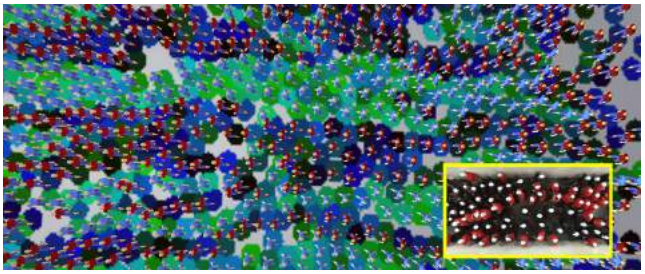

Figure 5. The emergent lane formation produced by our method in a dense bidirectional flow scenario with visually similar forking/joining patterns to those observed in reality (bottom right shows a still frame of real footage [28] of bidirectional flow in a corridor). The entities in both our simulation and the real footage are color-coded to indicate direction of motion.

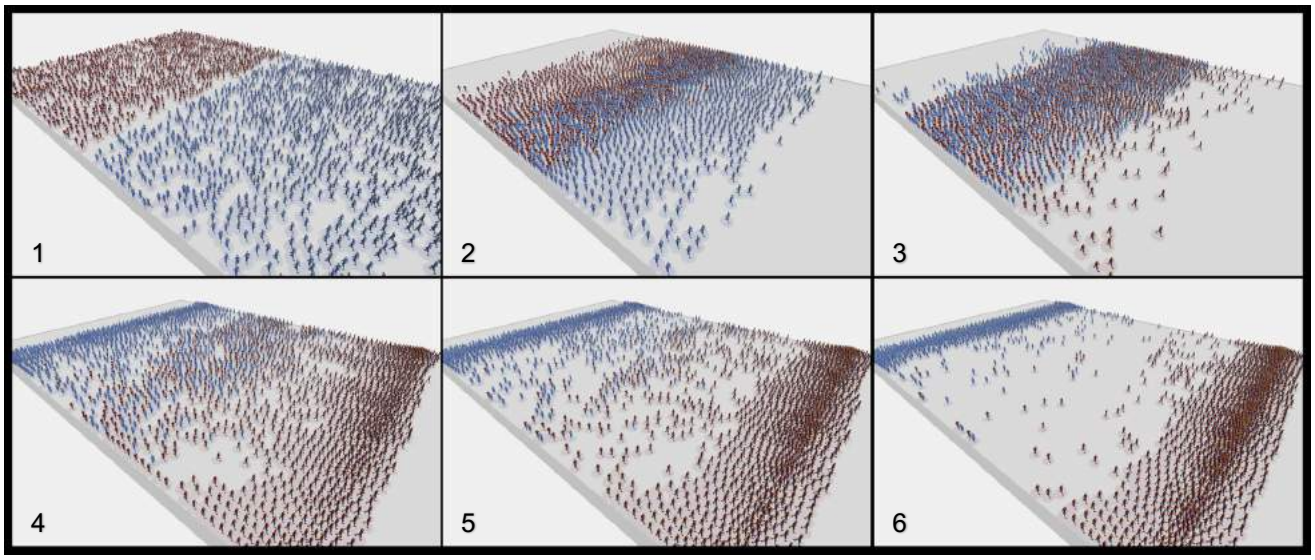

Figure 6. Artificial scenario used for performance testing: blue entities heading north; red entities heading south.

5.1 Simulation Setup

All simulations were run with discrete-time integration, using a quantum of 100ms per frame. Each pixel length represented 10cm of physical space.

The entity PS base radii were kept at 7 pixels (plus 1 centroidal) to achieve the ~0.8m PS idle radius. The shaders described in Section 4.3 were implemented using OpenGL Shading Language (GLSL). Parameters were randomized across the crowd, including the PS radius, comfort speed, and centroidal effect (which alters how aggressive/lenient an entity is about restoring its personal space).

Children were given the same PS radius as adults, but rendered with weaker Voronoi cones (i.e. further away from the PSM top view camera) to reflect the increased the chance of being overpowered by adult personal spaces, or being swept away by strong crowd flow in dense settings.

5.2 Performance

Our testbed consisted of three representative consumer-grade devices with various CPU-GPU configurations:

- Mid-range Desktop: Intel Core i5+ Nvidia GTX1060 GPU
- Laptop: Intel Core i5 (with integrated HD Graphics 4000)
- Mobile: Nexus 6P + Qualcomm Adreno 430 GPU

Table 1 summarizes the average framerate of simulating bidirectional flow over a 600x900 PSM (effectively, a 60m corridor) while varying the number of pedestrians in the scene (Figure 6). The performance gain from implementing our GPU shaders is noticeable, at ~2.6x throughout. While the Android device was capable of simulating higher crowd counts, it was no longer at interactive framerates (< 1fps).

	Non-Instanced Rendering + 2D Sprites			With GPU Shaders + 3D Sprites	
#Entities	**Desktop GTX1060**	**Laptop Corei5**	**Nexus 6P (Android)**	**Desktop GTX1060**	**Gains**
100	160	105	30	450	2.8x
250	125	87	23	338	2.7x
500	90	62	18	266	3.0x
1,000	58	41	13	134	2.3x
1,500	44	31	10	121	2.8x
2,000	33	26	7	89	2.7x
5,000	16.5	12	3	47	2.8x
10,000	10.7	7	-	25	2.3x
15,000	7.6	4.5	-	20	2.6x
20,000	6.2	3	-	14	2.3x

Table 1. Simulation performance in frames per second.

Currently, the simulation performance shows a dependence on the simulation range area. For instance, the 2000 entities in Figure 1 are in a 50x80m corridor (500x800 PSM pixels), which naturally results in faster PSM rendering than the larger PSM area in the Figure 6/Table 1 benchmark. The granularity of PSM pixels can be adjusted to reach performance targets, at the cost of reduced PS fidelity.

Ideally, the simulation performance would be dependent only on the crowd count. We believe the current overhead of essentially simulating empty spaces can be overcome (or hidden) by utilizing multi-threaded CPU rendering calls, as will be possible in upcoming graphics API standards, such as Vulkan [31], the direct successor of OpenGL.

Given the 100ms time quantum, every 10 frames represent 1 second of simulation time. Hence, our algorithm produces faster-than-real-time simulation results for up to 20,000 entities in the scene, and maintains interactive framerates for even higher counts. Performance can be further increased on machines equipped with workstation-grade GPUs.

5.3 Visualization

The shader computation allowed room for real-time 3D sprite rendering. Our simulation can be visualized using existing methods, which generate smoothly rigged and GPU-animated characters [22] at interactive frame rates. For demonstration purposes, we opted instead to create low-cost rigidly-rigged multi-part characters primarily composed of simple primitives, and procedurally animated walk cycles. Animating these composites is only a matter of adjusting a handful of transform matrices (position, orientation, scale, etc.) per entity, rather than fully animating each vertex through smoothed skeletal rigging. The resulting 3D sprites are sufficient for rapid prototyping and iteration, consuming on average 15-30% of each frame time. The results presented in Table 1 include this 3D visualization stage.

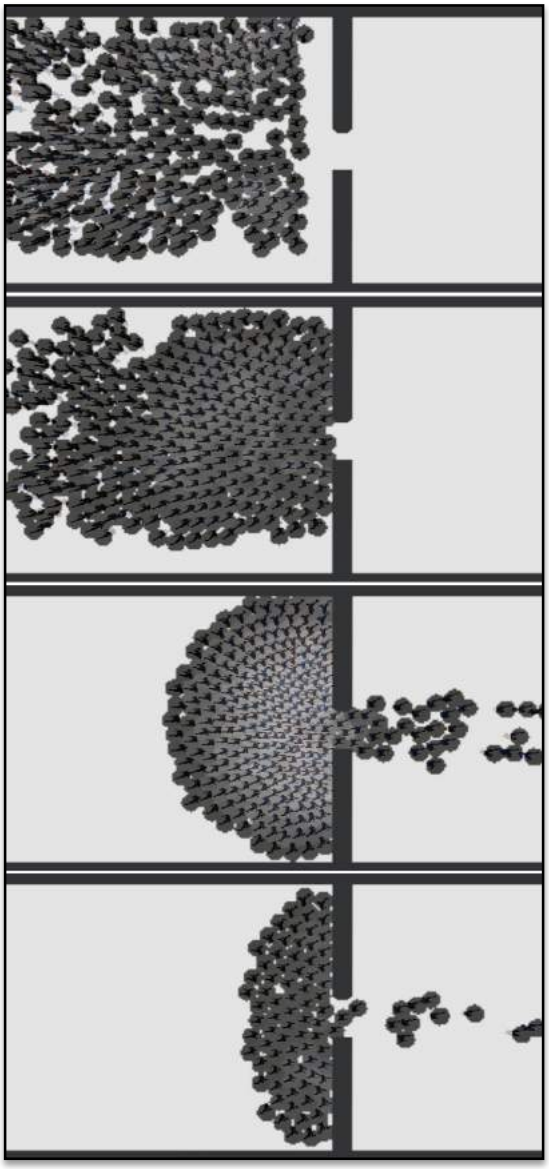

Figure 7. Crowds attempting to pass through a narrow gateway typically begin to arch around that bottleneck.

The PSM can be directly shown as an underlay to visualize the personal spaces used for centroidal force calculations. They can also be used for quick local density visualization by measuring the ratio of the violated area to the ideal PS footprint. Figure 7 illustrates a common emergent crowd phenomenon (arching around pathway bottlenecks), with noticeable compression of personal space near the exit.

This effect aligns with observed PS compression in both moving and static crowds (Figure 8). In addition to arching, densely packed crowds tend to display petal-like formations (as each entity attempts to be situated behind the midpoint of two entities ahead). This increases the entity's visibility of the point of interest (or global path destination), and results in more compact space-filling.

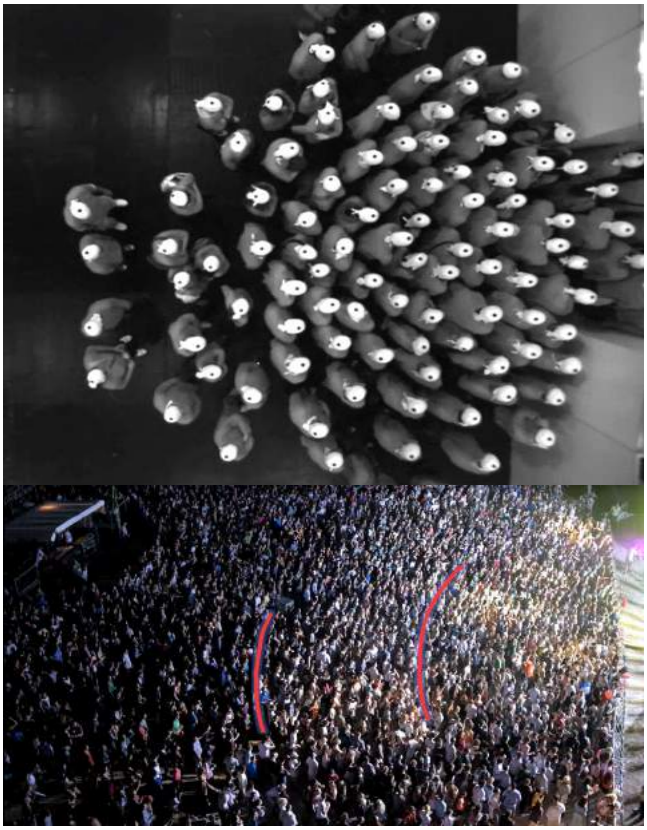

Figure 8. Arching, gradual PS compression, and petal-like formations observed in crowds during egress [28] (top) and while stationary at a concert (bottom). These effects agree with our simulation results.

More experiments, videos, and results can be viewed on the project page at: http://cell-devs.sce.carleton.ca/publications/.

6 LIMITATIONS AND OPPORTUNITIES

Implementation Platform

Our implementation and visualization so far were built on the Java-based Processing framework. Processing is good for rapid prototyping of graphical applications, providing an accessible and cross-platform set of tools for window, file, and UI management, while simultaneously providing access

to low-level OpenGL calls. Also, being Java-based meant that it could be ported directly to Android's platform. Since most of the work is done by GPU shaders, there would not have been much to gain from attempting to use Android's native C++ (NDK) environment.

Although Processing is great for prototyping, it might not be the ideal *deployment* solution. Our method can be made into a plugin for middle-ware engines, depending on the context. For instance, in the film and gaming industry, a worthwhile effort would be to port this to the Fabric Engine [8], which can be run in standalone mode or be made to communicate directly with the scene graphs of major 3D animation packages (e.g. Autodesk Maya and 3ds Max) without rewriting the code for each target platform. The potential overhead when adopting middleware, however, is always an issue that requires careful evaluation.

Heterogeneous and Multi-layered Crowds

The centroidal force indicates a locally preferred bearing and direction of motion for the entity to restore its personal space. However, acting on that centroidal "suggestion" is left up to the entity and its constraints. Human motion is quite flexible with the ability to turn in-place if needed. To extend the simulation to heterogeneous entities sharing the same space, we can still compute the centroidal forces as we did with humans, but the mechanics of following that centroidal "suggestion" might differ (e.g. for strollers, shopping carts, and vehicles).

Those other entities will consume the same rules about personal space, but execute those maneuvers under their own physical constraints (e.g. shopping carts might have a turning radius compared to a human's ability to turn on the spot). To complement this effort, other methods for computing the Voronoi PSM must be tested, since the scene might include lengthy entities whose centroid is no longer a concentric point, but a spine segment. In this case, the jump flooding technique might be a good alternative to Voronoi cones [23].

Another feasible improvement on CPD involves separating gaze from body orientation for situations when, for example, an entity is crossing the road or paying attention to a loud event or scream. The gaze could be computed in its own PSM layer, and it would become another parameter in the context-sensitive personal space adjustments.

Flocking

By design, CPD methods don't produce grouping or flocking behaviour as they focus on dynamics within a personal space. The entities are assumed to be individualistic with their own target destination in mind. This was intentional, to study the effects of centroidal forces in isolation.

By manipulating the global pathing vectors being input into CPD methods, it would be possible to augment (or be augmented by) behaviours such as the ones studied in SAFEgress [3], to account for each entity's familiarity with the environment, social attitudes, and herd dynamics (leader-follower, social order, etc.). This concept also extends to simulating families and friends trying to stay together when at a large gathering or outdoors event.

Validation

Civil safety and threat assessment applications stand to benefit the most from dense-crowd research. Although our method uses empirically-driven parameters to produce visually convincing aggregate behaviour, it cannot yet be reliably used for safety-critical applications. That would require further validation against in-lab scenarios [28] and statistical analysis. There are global statistical properties that can be checked (e.g. governing distributions [14]) and local similarity indices for targeted analysis of smaller areas of interest (e.g. [9]). We echo our earlier assertion that regardless of which method is used, crowd simulation is essentially an exercise in abstraction with no "ground truth" to converge on, yet the increase in accuracy is a worthwhile pursuit, considering the potential applications. A particularly challenging and motivating use case is the prevention of crowd stampedes and crushes. Simulation then becomes an important tool for preplanning barriers and other crowd control measures to prevent such awful disasters in what are otherwise peaceful gatherings [7, 26].

7 CONCLUSION

We presented an improvement to the centroidal particle dynamics (CPD) model that addresses several subtle problems in dense crowd simulation. The contributions include a context-aware personal space kernel that adjusts to the bearing of the entity, its velocity, and destination heading, resulting in a more realistic response to personal space violations and collision anticipation.

The presented implementation aides in scaling the algorithm by utilizing geometry and vertex shaders to offload the computationally demanding personal space map (PSM) and centroidal calculations onto graphics hardware (GPU). This allows for the animation of 5000+ 3D entities at interactive framerates on consumer-grade hardware.

The agent-based simulation produces several visually convincing emergent results for crowd crossings, dense bidirectional flow, and arching near hallway bottlenecks.

ACKNOWLEDGMENTS

This research has been partially funded by NSERC and the first author further supported by an OGS (Ontario Graduate Scholarship). The authors thank members of the Advanced Real-time Simulation lab for their participation and support, and the anonymous reviewers for their insightful feedback.

REFERENCES

1. Bandini, S., Manzoni, S., & Vizzari, G. Crowd Modeling and Simulation. *Innovations in Design & Decision Support Systems in Architecture and Urban Planning*, 105-120 (2006).
2. Brogan, D.C., Metoyer, R.A., and Hodgins, J.K. 1998. Dynamically simulated characters in virtual

environments. *IEEE computer graphics and applications* 18, 5, 58–69.

3. Chu, M.L., Parigi, P., Law, K., and Latombe, J.-C. 2014. SAFEgress: A Flexible Platform to Study the Effect of Human and Social Behaviors on Egress Performance. *SimAUD Proceedings*, SCS 4:1–4:8.
4. De Gyves, O., Toledo, L., and Rudomín, I. 2013. Proximity Queries for Crowd Simulation Using Truncated Voronoi Diagrams. Proceedings of Motion on Games, *ACM*, 87–92.
5. den Berg, J. van, Lin, M., and Manocha, D. 2008. Reciprocal Velocity Obstacles for real-time multi-agent navigation. Robotics and Automation, 2008. *ICRA*, 1928–1935.
6. Duives, D.C., Daamen, W., and Hoogendoorn, S.P. 2013. State-of-the-art crowd motion simulation models. *Transportation Research Part C: Emerging Technologies* 37, 0, 193–209.
7. Fruin, J.J. 1993. The causes and prevention of crowd disasters. *Engineering for Crowd Safety* 1, 10.
8. Fabric Software Inc. Fabric Engine. http://fabricengine.com/.
9. Guy, S.J., van den Berg, J., Liu, W., Lau, R., Lin, M.C., and Manocha, D. 2012. A Statistical Similarity Measure for Aggregate Crowd Dynamics. *ACM transactions on graphics* 31, 6, 190:1–190:11.
10. Helbing, D., Farkas, I., and Vicsek, T. 2000. Simulating dynamical features of escape panic. *Nature* 407, 6803, 487–490.
11. Hesham, O. and Wainer, G. 2016. Centroidal Particles for Interactive Crowd Simulation. *Proc. SummerSim, Society for Computer Simulation International*, 7:1–7:8.
12. Hoff, K.E., III, Keyser, J., Lin, M., Manocha, D., and Culver, T. 1999. Fast Computation of Generalized Voronoi Diagrams Using Graphics Hardware. *Proceedings of the 26th CGIT*, ACM, 277–286.
13. Huerre, S., Lee, J., Lin, M., and O'Sullivan, C. 2010. Simulating Believable Crowd and Group Behaviors. *ACM SIGGRAPH ASIA 2010 Courses*, ACM.
14. Karamouzas, I., Skinner, B., and Guy, S.J. 2014. Universal power law governing pedestrian interactions. *Physical review letters* 113, 23, 238701.
15. Kisko, T.M., Francis, R.L., and Nobel, C.R. 1998. Evacnet4 user's guide. *University of Florida*.
16. Moussaïd, M., Helbing, D., and Theraulaz, G. 2011. How simple rules determine pedestrian behavior and crowd disasters. *Proc. of the National Academy of Sciences of the United States of America* 108, 17.
17. Ondřej, J., Pettré, J., Olivier, A.-H., and Donikian, S. 2010. A Synthetic-vision Based Steering Approach for Crowd Simulation. *ACM transactions on graphics* 29, 4, 123:1–123:9.
18. Pelechano, N., Allbeck, J.M., and Badler, N.I. 2007. Controlling Individual Agents in High-density Crowd Simulation. *Proceedings of the 2007 ACM SIGGRAPH/Eurographics SCA*, 99–108.
19. Pettré, J., Ondřej, J., Olivier, A.-H., Cretual, A. & Donikian, S. 2009. Experiment-based Modeling, Simulation and Validation of Interactions between Virtual Walkers. *ACM SIGGRAPH/Eurographics SCA* 189–198.
20. Peschl, I.A.S.Z. 1971. Passage Capacity of Door Openings in Panic Situations. *BAUN*.
21. Reynolds, C.W. 1999. Steering behaviors for autonomous characters. *Game developers conference*, 763–782.
22. Rivalcoba, I. and Ruiz, S. 2013. GPU generation of large varied animated crowds. *Computación y Sistemas* 17, 3, 365–380.
23. Rong, G. and Tan, T.-S. 2006. Jump flooding in GPU with applications to Voronoi diagram and distance transform. *Proc. Interactive 3D graphics and games*, ACM, 109–116.
24. Secord, A. 2002. Weighted Voronoi Stippling. *Proceedings of NPAR*, ACM, 37–43.
25. Smith, R. A. Volume Flow Rates of Densely Packed Crowds. *Engineering for Crowd Safety* (1993).
26. Special Events Contingency Planning. 2005. *FEMA*.
27. van den Berg, J., Guy, S.J., Lin, M., and Manocha, D. 2011. Reciprocal n-Body Collision Avoidance. In: C. Pradalier, R. Siegwart and G. Hirzinger, eds., *Robotics Research*. Springer Berlin Heidelberg, 3–19.
28. Zhang, J., Klingsch, W., Schadschneider, A., and Seyfried, A. 2011. Ordering in bidirectional pedestrian flows and its influence on the fundamental diagram. *arXiv* [physics.soc-ph].
29. Gérin-Lajoie, M., Richards, C.L., and McFadyen, B.J. 2005. The negotiation of stationary and moving obstructions during walking: anticipatory locomotor adaptations and preservation of personal space. *Motor control* 9, 3, 242–269.
30. Chattaraj, U., Seyfried, A., and Chakroborty, P. 2009. Comparison of Pedestrian Fundamental Diagram. *Advances in Complex Systems 12*, 03, 393–40.
31. Khronos Vulkan Working Group, 2016. Vulkan 1.0.37 - A Specification. *Khronos Group*, 11-18.

Modeling Space To Support Use-Pattern Simulation In Buildings

Kartikeya Date, Davide Schaumann and Yehuda E. Kalay

Technion - Israel Institute of Technology, Haifa, Israel
kartikeya.date@gmail.com, deiv@campus.technion.ac.il, kalay@tx.technion.ac.il

ABSTRACT

Event based approaches to simulating use-patterns in buildings require descriptions of space which are not readily available in contemporary BIM or CAD tools. The required description should accommodate a spatialized description of actors, a method for describing how these actors move in the space, and a method for describing and updating features of the space. A modular, extensible system for modeling space and movement of actors using a hierarchical adaptation of the A* search algorithm is described in this paper. This system provides a modular, extensible data model for describing Events and simulating how people move in buildings. The system is demonstrated using an abstract case.

Author Keywords

Discrete Spatial Modeling; Pathfinding; Agent Based Modeling; Building Information Modeling

ACM Classification Keywords

I.6.1 SIMULATION AND MODELING; I.2.4 KNOWLEDGE REPRESENTATION FORMALISMS AND METHODS; J.5 ARTS AND HUMANITIES: Architecture

1 INTRODUCTION

Since Building Information Modeling (BIM) became part of mainstream architectural practice in the first years of the 21st century, new types of analysis of design proposals have become possible [4, 5, 13]. This analysis involves using, and often extending, the core data models available in commercial BIM software to analyze proposed design solutions for their acoustic performance, energy efficiency, ability to exploit daylight and other (usually physical) aspects of building performance. While substantial advances have been made in these analyses, less progress has been made when it comes to simulating how people use buildings.

Simulating how people use buildings is a challenging task for several reasons. First, apart from the fact the people are complicated entities which are difficult to model in their full rich complexity, the environment they operate in is also continually changing in unpredictable ways. Second, current BIM systems do not natively include data models for people. Third, the model for spaces in BIM is not easily used in its present form for modeling how people move in space. Fourth, people do not always behave exclusively as individuals. Sometimes they behave as part of a group. This means that pure agent based approach, in which every person is a more or less autonomous individual agent, quickly become unmanageably complexity as the use-patterns approach realistic intricacy.

One recent approach to managing complexity in the simulation of use patterns in buildings (for example, a doctor's round in a hospital ward) involves modeling in each use-patterns as an Event [16, 17, 18, 19]. An Event is conceptualized as a coordinator of individual agents and their activities in a given space. This allows the specification of individual and group behavior. Events are described using three separate elements - spaces, actors and activities. A detailed discussion of the Event formalism is beyond the scope of this paper. This question is considered elsewhere in these proceedings [15].

A common approach in agent based simulation (in particular) has been to rely on the boundary representation geometry provided by CAD or BIM software and then deploy agents by implementing a form of the Navigation Mesh [8, 14] to enable traversal. The approach adopted in this paper seeks to reverse this relationship by describing space in such a way that the description of actors is constitutionally spatialized.

Existing models for describing space (such as the boundary representation commonly used in CAD) have three specific shortcomings which need to be overcome so that Events can be modeled. First, the model must enable spatialized descriptions of actors. Second, the model must enable spatial distribution of relevant features of the space (relevant physical and social characteristics, henceforth, costs) to describe the state of the world. Third, the model must enable the description of a mechanism by which this spatial distribution of costs can be updated as the state of the world changes.

The formalism proposed in this paper is demonstrated through an abstract case which has been fully implemented in Python, a general purpose object-oriented programming language. This formalism can be used to describe multiple Events in a shared space. In the future, this formalism can be used to set up specific use cases, for example as an optimization problem. However, this is not demonstrated in the current work which is focused on the detailed description of the formalism.

2 DESCRIPTIONS OF SPACE

For at least the last 500 years, the traditional method of describing architectural design proposals has been using a

SimAUD 2017 May 22-24 Toronto, Canada

3D orthogonal model which can then be viewed orthogonally via plans, sections and elevations. The floorplan is a horizontal section cut through the proposed building such that the desired level of the building (ground, first, second, terrace etc.) is visible. This representational method enables non-redundant description of spatial and built elements of buildings. BIM systems (such as the Autodesk Revit system) are constituted by an object model which enables the description of various constitutive parts of buildings like slabs, beams, columns, windows, doors, trusses, staircases as parametric objects. It also allows rooms and spaces to be represented. Most simulations used to analyze building design proposals involve analysis which depends on the built elements of buildings. Simulating use-patterns in buildings requires syntactical and semantic representation of both spatial and built elements of buildings.

From the point of view of analyzing use, space syntax is a mature approach which is used widely in architectural design and planning disciplines [11, 12]. Space syntax uses a configurational approach in which built environments are broken down into component parts and are then studied as networks of choice. These networks are represented using graphs which describe relational properties of spaces (for example, connectedness). This configurational approach allows space syntax to be used at a variety of scales ranging to individual buildings to road networks. Space syntax based approaches are commonly used to simulate navigational aspects of complex buildings such as airports, museums and hospitals. While this approach accounts for relational aspects of buildings, it does not intrinsically describe formal aspects. Space syntax is inherently not a model of space; it seeks to model relationships in space.

Chris Yessios developed the void modeling approach which involves describing buildings as combinations of volumes (voids) enclosed by walls. The void modeling system consists of void primitives which can be combined using the Boolean operations of difference, intersection and union. Yessios developed the *FormZ* 3D modeling software using this approach. [22]

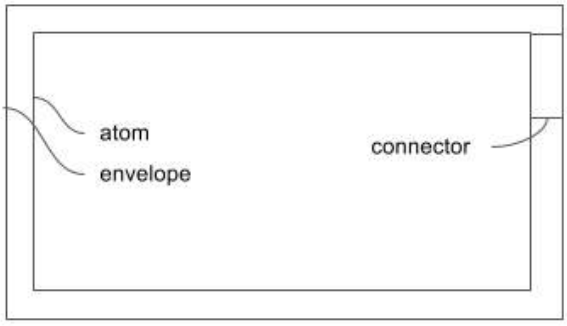

Figure 1. The SFA Classification System developed by Sabu Francis. [6]

Sabu Francis developed a fractal system for classifying spatial and solid elements of buildings in a non-redundant way. In this system (see Figure 1), spaces are classified as *atoms* (the space in a room), *envelopes* (the enclosure wrapping an atoms or a group of atoms) and *connectors* (an element connecting atoms to envelopes, or to other atoms). The built elements can be represented as the Boolean operation: (*envelopes* - (*atoms* + *collectors*)). This taxonomy is implemented in the 3d building information modeling software *The Architect's Desktop*. [6]

The systems developed by Yessios and Francis describe spatial elements explicitly. Of all the participants in building design and construction industry, architects belong in the small minority which is concerned primarily with spaces and not with the built elements. This is why efforts like those by Yessios and Francis to place the model of space at the center of their computer aided modeling system are significant. In both systems built elements (slabs, columns, beams, walls, windows, doors etc.) are inferred implicitly as a consequence of the spatial design. Spaces are defined by specifying their geometrical boundaries. However, while the data models underlying these systems are useful for developing alternative design proposals, they require a model overlay in order to be able to store data which can be used to simulate how people might use behavior. Systems for simulating use patterns require not only the capacity to store information within spaces, but also to update information during the simulation.

Video game developers use 3d modeling systems to develop their 3d 'assets' which constitute their game worlds. Approaches developed the field of video game development to adapt computer aided design models for simulating users fall into three broad categories. Voronoi tessellations can be used to represent dynamic two dimensional environments in which the number of tiles (or polygons) varies as the number of elements varies. Polygons are inserted and removed, and the mesh is rebuilt to account for each change [14, 21].

A second approach is to use waypoints. Waypoints constitute a graph of locations within the space along which movement is possible. Waypoint graphs can be constructed either manually or by writing rules for their generation to describe expected use patterns in spaces.

The third approach is to generate fixed grids (usually square, hexagonal or triangular) over the space and generate search graphs and maps of feature distributions from this fixed grid. Feature maps (or in the terminology of the current work, cost maps) consist of two parts. First, they include spatialized distributions of a feature. Second, they specify rules for how these features change over time in the given space. For example, if an open plan office space is being evaluated, it may be useful to map noise spatially and specify rules for how different uses (such as impromptu meetings) generate different levels of noise. A search graph over this open plan office could account for all the tiles (or cells) which are occupied by furniture, and are therefore not traversable.

This is potentially the most flexible approach as it involves specifying all the possible locations for storing information at the outset. At the same time, it is less efficient than the voronoi tessellation based navigation mesh approach precisely because it requires the definition of a far larger number of possible locations at the outset, thereby increasing the potential search space.

So far we have seen two models for describing space by Yessios and Francis, whose purpose is to facilitate architectural modeling, a configurational model for network analysis in space syntax which is developed for the purpose of evaluating relational aspects of spaces, and models for storing spatial information in order to make a space walkable from the video game development perspective. While boundary representation based models are suitable for architectural designing, we argue that they are not sufficiently flexible for simulate use given the following twin requirements: (a) that the description of space be easy to search and (b) be capable of storing richly textured feature information (costs) which is amenable to being systematically updated. This latter requirement is not met in the waypoints or more generally the navigation mesh based approach. The fixed grid approach has two shortcomings. First, it is less efficient than the boundary representation based approach. Second, it does not, yet, accommodate semantic hierarchies of spaces which are a feature of architectural design proposals. The model described in the next sections responds to the limitations identified in this review.

3 SPACE AND ACTOR MODELS

The proposed model consists of *cells*, *zones*, and *thresholds*. Space is constituted by a two-dimensional array of cells. A single cell can have up to 8 neighboring cells. Each cell is identified by its global grid location. The top left cell has grid location (0, 0). The cell on the bottom right has grid location (x-1, y-1), where x in the number of columns of cells and y is the number of rows of cells. (Figure 2)

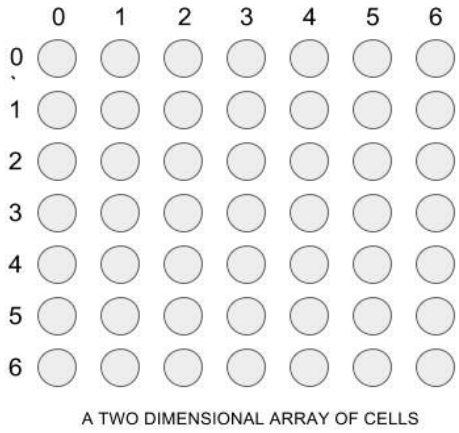

Figure 2. A two-dimensional array of cells with a global coordinate system

A zone is a collection of contiguous cells. A threshold is also a collection of contiguous cells. To draw the architectural analogy, if a zone represents a room, then the threshold represents the space between two rooms - a wall, a doorway, a door, a window or any other type of connecting element. For the purpose of modeling movement, it is essential to identify which of part of the threshold is traversable, and which part is a barrier.

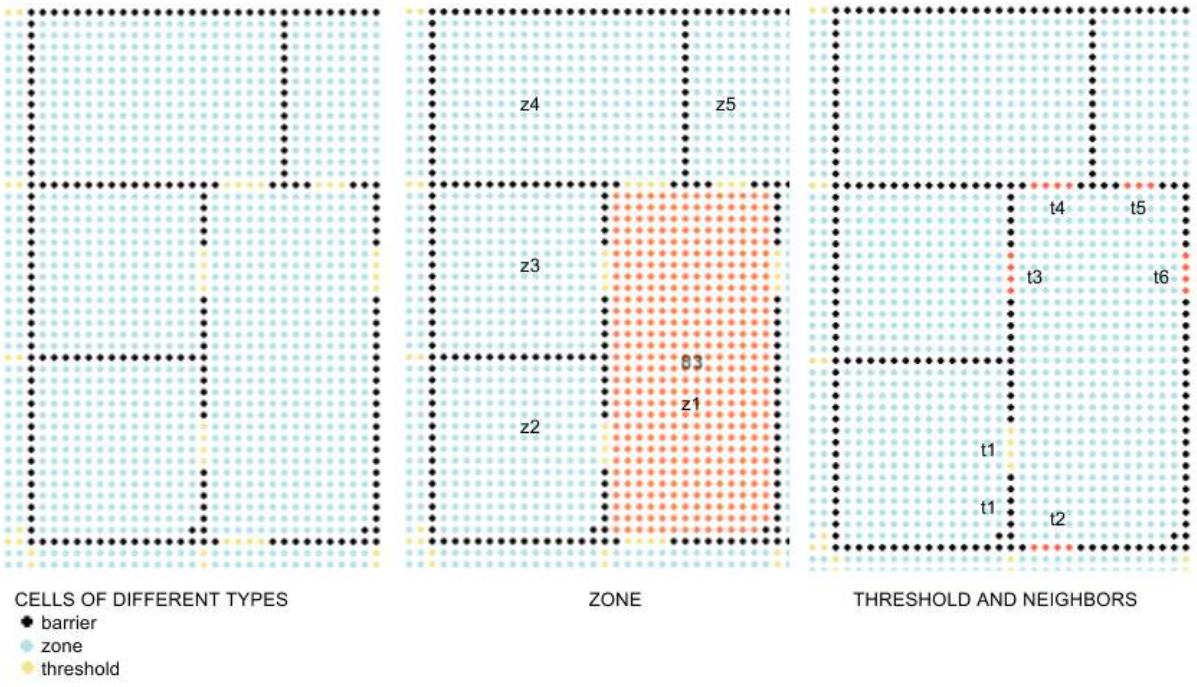

Figure 3. Space is described as an array of cells organized into zones and thresholds.

In Figure 3 (left) the cells which make up the non-traversable parts of a threshold are shown in black. Traversable threshold cells are shown in yellow. Zone cells are shown in light blue. In Fig. 3 (middle) a single zone (z1) is highlighted in red. In order to be connected two zones must share at least one traversable threshold. Reading Fig. 3 (middle and right) together, note the following:

Zone z1 has thresholds t1, t2, t3, t4, t5 and t6.

Zone z3 has threshold t3

Zone z4 has threshold t4

Zone z5 has threshold t5.

It follows that threshold t4 has the following neighbors:

t5, t6, t3, t2 and t1

Threshold t3 has the following neighbors:

t4, t5, t6, t1 and t2

To move from, say zone z3 to zone z5, thresholds t3 and t5 have to be crossed. To move from any zone to any other zone, at least one shared threshold must be crossed.

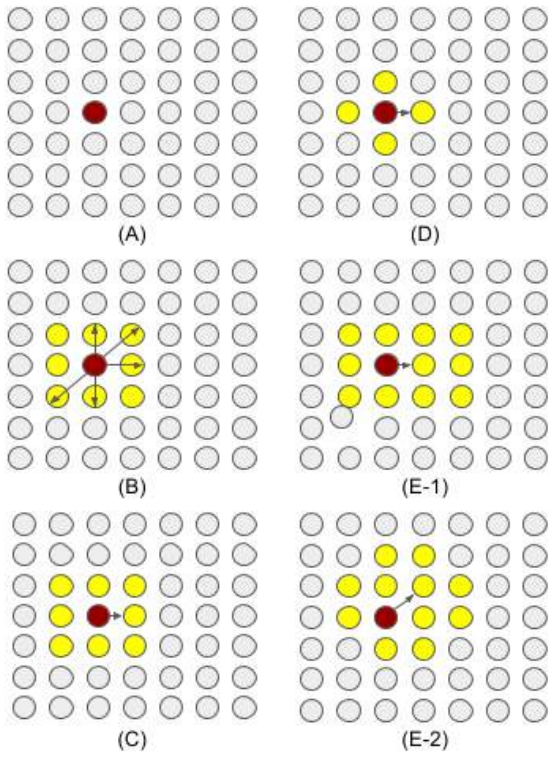

Figure 4. Spatialized descriptions of actors showing varying degrees of detail

Actors can be described in this system at varying degrees of detail depending on the purpose of the simulation. In the simplest form (Figure 4(A)), an actor occupies exactly one cell. The actor can move one cell in one of eight possible directions. The cells immediately surrounding an actor can also be specified as the actor's 'personal space'. This personal space can be the actor's Moore neighborhood (Figure 4(B)), or von Neumann neighborhood (Figure 4(C)). The actor can also be assigned a "front" and a "back" by designating one of the neighboring cells the "front" and the opposite one "back" (Figure 4(D)). In this way, turning can be simulated. The actor's personal space does not need to be symmetrical. Humans have superior perception of what is in front of them than in other directions. These aspects can be modeled as well (Figures. 4(E), 4(F)).

The mechanism also permits the scale of the cell grid to be chosen keeping the human scale in mind. This is an essential requirement from an architectural standpoint. For example, there may be problems for which it will be suitable to design the simulation such that each actor has 26 neighbors and not 8 (a neighborhood of depth 2).

The proposed system for describing cells, zones, thresholds and actors in this section is designed to be modular, extensible and flexible. It enables use-patterns (Events) to be described over different levels of detail and can be easily generated from a floor plan or a BIM model. Its approach to describing actors is spatial (instead of describing actors and then assuming that they can exist in a space).

4 SIMULATING MOVEMENT

Movement is simulated by locating the path (a list of contiguous cells) from the starting point to a specified target. The pathfinding system used to find this path uses the well-known best first search algorithm A* as its point of departure. The A* algorithm is an advancement on Dijkstra's shortest path algorithm and was first described by Hart, Nilsson and Raphael in 1968 [10]. In order to speed up the search, A* uses a heuristic function which produces an estimate of the distance of a given cell n to the goal cell. Given an admissible heuristic function (an admissible heuristic function is one which can be shown to never overestimate the distance to the goal cell from a given cell), A* is optimal. Apart from its uses in the field of robotics, the A* algorithm has been widely used in video game development. A number of variants have been developed to account for various types of search spaces, hierarchical or otherwise, memory constraints and to take advantage of off-line processing wherever possible [1, 2, 8, 9].

In the current instance, the search is designed to account for changes in the features of the search space. Before describing the search method itself, the cost map system is described. Each cost map has two parts. The first is a map of the spatial distribution of the given feature over the space of cells, zones and thresholds. The second is a rule specifying how the spatial distribution of costs is updated during the simulation. A maximum of eight moves is available to an actor in a given cell. Each option is evaluate according to the set of relevant cost maps. The rules for updating costs can be designed at the level of the cell. But they can also be aggregated to the level of the zone, or even to the level of a group of zones such that a given feature at a given cell location adopts the value of the zone to which that cell belongs. The method of

organizing a feature depends on what type of feature it is. For example, the noise generated by a conversation, or by someone playing music at a cubicle in an open plan office is to be simulated, a cell level feature map may be more appropriate. But if the feature is a class of cubicle, then a cell in a space may more properly adopt the class of the zone to which it belongs.

Events may be required to account for multiple categorically different costs. During the search, these cost maps are used to identify available cells for movement. Availability can be established in multiple ways. Let us consider the case of 3 costs A, B, and C. It may not be always be possible to reasonably reduce these costs dimensionally to one figure. In such a case, if the order in which the costs are to be considered is specified, then each available cell in the neighborhood of the current cell can be systematically evaluated according to this sequence of cost maps. This evaluation can be specific to the actor for whom the path is being calculated, or they could be specific to the definition of the Events within which the current movement is taking place.

Once all the cost maps have been accounted for, all remaining acceptable cells are evaluated based on the heuristic function, which in this case is the shortest distance between the current cell and the goal cell. When the calculation is complete and the path is found, the actor advances one step along the path.

The path search is divided into two steps (see Figure 5). In the first step, only the threshold level path from the current cell to the goal cell is calculated. In the second step, the path from the current cell to the next threshold cell in the threshold level path is calculated by evaluating only the zone in which the current cell belongs. The threshold level path guarantees that next intermediate threshold cell target will always belong to a threshold attached to the current zone. Once this zone level path is calculated, after taking into account all relevant cost maps, the actor has identified the next move.

The search space for the threshold level search is a graph of threshold cells. Any threshold usually connects 2 zones, z1 and z2. The exceptions would be for 'U', 'T', 'L' or '+' shaped thresholds which could connect more than two zones. Currently, such thresholds are allowed in the system. The near-optimality of the hierarchical search is severely affected by presence of such thresholds. From an architectural point of view, the decision to allow these types of the thresholds may be appropriate for some simulation problems, but for any problem in which the movement decision is of central importance, they will not be appropriate. For all such simulation problems, a threshold should connect exactly two zones. The design of the threshold graph is described as follows.

Let a given threshold be t0, and let it be made up of three cells (c1, c2 and c3). It follows that all the thresholds attached to the two zones are neighbor thresholds to t0. Suppose that there are 2 such thresholds, t1 (containing cells a1, a2 and a3), and t2 (containing cells b1, b2 and b3). In this case, the threshold graph TG will contain 9 nodes - c1, c2, c3, a1, a2, a3 and b1, b2, b3. The edges will be given as follows:

TG[a1] = (b1, b2, b3, c1, c2, c3)

TG[a2] = (b1, b2, b3, c1, c2, c3)

TG[b1] = (a1, a2, a3, c1, c2, c3)

TG[c1] = (a1, a2, a3, b1, b2, b3)

And so on.

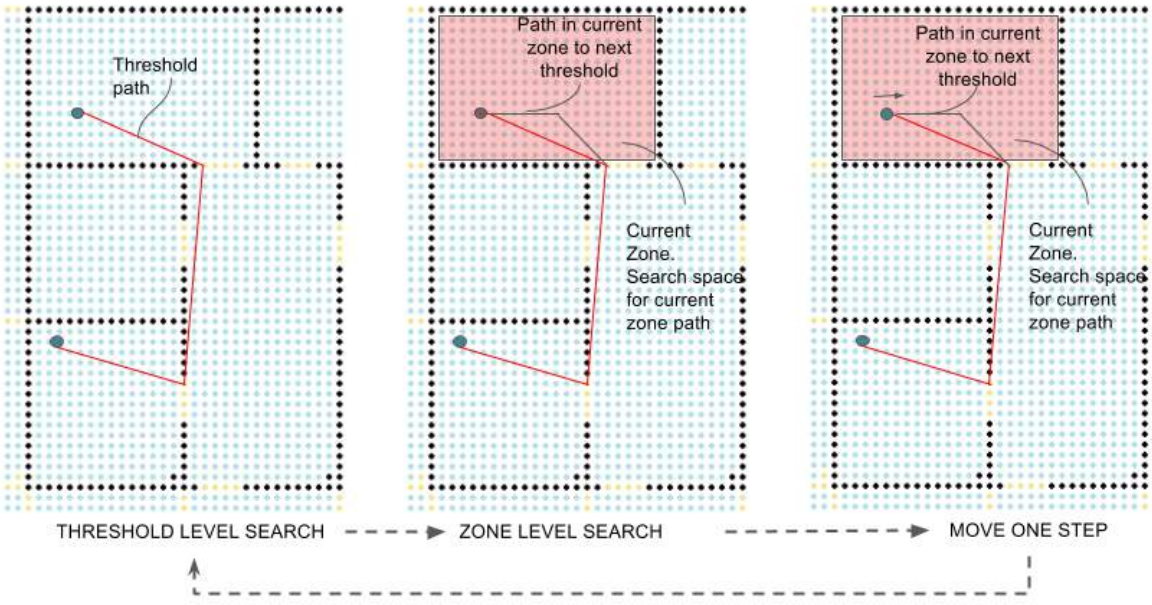

Figure 3. Space is described as an array of cells organized into zones and thresholds.

When this graph is searched using A*, it will return a path which will include at most one cell per threshold. The regularity of the square grid ensures that this path will be optimal over the threshold graph. After the threshold level path is determined, the next step is to determine the path from the current cell to the first threshold cell in the threshold path. The search space for this path is always the zone to which the current cell belongs.

Once the zone level path has been determined, the current state of the world can be said to have been evaluated for the purpose of making a decision as to which neighboring cell the actor should move to next. The actor moves to this neighboring cell. At this point, depending on the simulation problem, it may become necessary to evaluate the state of the world again (since other Events will also have progressed during this time step, and the state of the world may have changed as a result). However, it is possible to evaluate costs differentially. Some cost maps may be evaluated before each move, other cost maps may be evaluated only when zones are crossed, and so on.

5 CASE STUDY

This case study brings together all the parts of the system described thus far. The layout in Figure 6 is an office space consisting of rooms and corridors which have been organized into zones and thresholds. The black cells are non-traversable barriers (walls). Each blue actor is seeking a green actor. In this implementation, there are three distinct costs. Each cost propagates spatially using a random walk. For the purpose of this case study, in order make it easier to visualize a multi-agent situation, every blue actor is assigned the same threshold for the three costs. The light blue cells belong to a zone. Wherever they are not drawn, the cost in that area is higher than the actor's cost threshold and hence is not available to the actor. This is a demonstration of the way the cost mechanism shapes the movement of the actors. The orange path is the threshold-level path while the blue path is the zone level path.

In this case study an Event is not implemented. The task for each blue actor is to reach the green actor assigned to it. If a threshold or zone level path is not available, then the blue actor is instructed to keep trying until a path becomes available. Each actor has a personal space of its immediate 8-cell neighborhood. An actor cannot enter any other actor's personal space unless it is that actor's target.

In each time step of the simulation, first the cost is updated. Second, for each actor, the two-step search is conducted and the actor takes a step. In this version of the simulation, the agents are not collaborating. Nor are they pursuing any group goal. However, each actor is aware of other actors which might be in it its way.

The simulation is implemented in *Pygame*, an open source game engine developed in Python; an open source object oriented programming language.

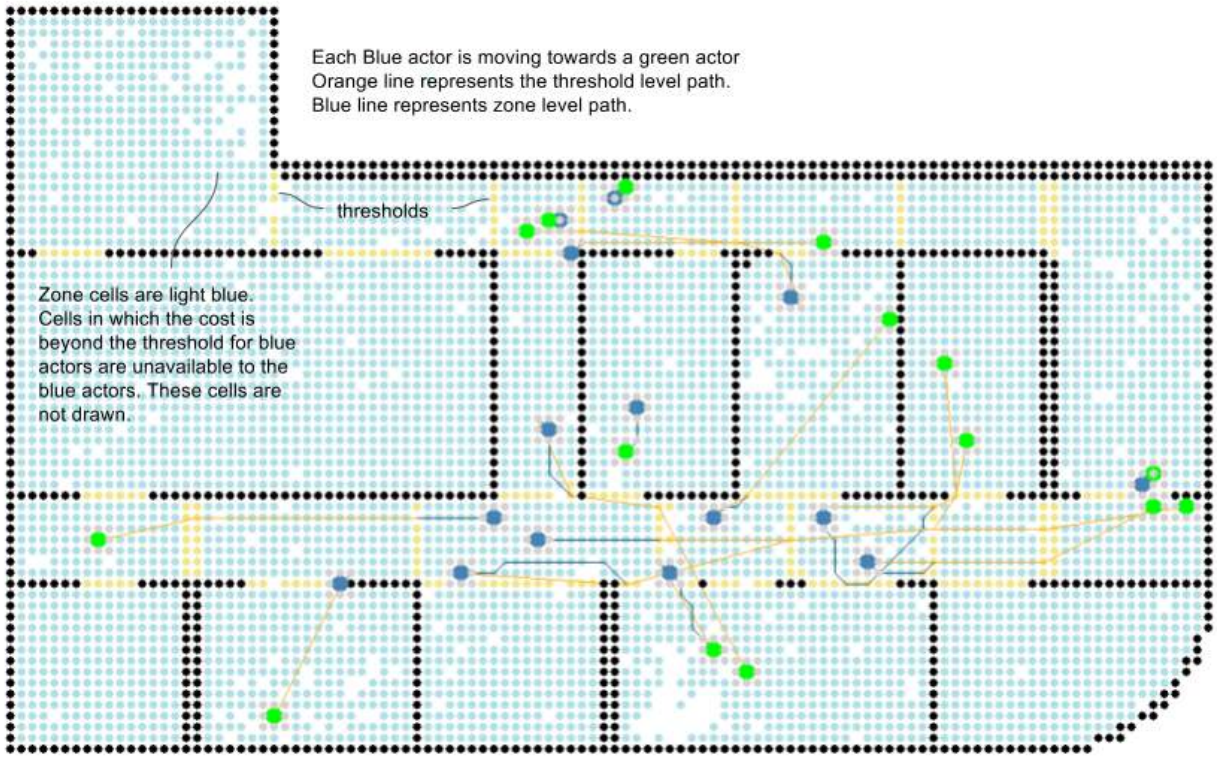

Figure 6. Case Study showing multiple agents navigating a floor plan amid multiple costs

6 DISCUSSION

A modular, extensible system for describing space, actors and the movement of actors in space has been demonstrated in this paper. The system requires the building information present in a floor plan. It organizes architectural spaces into zones, which are collections of cells and are connected by different collection of cells called thresholds. The movement of actors towards targets in the space is modeled using a hierarchical adaptation of the A* best-first graph search algorithm.

Even though this search is hierarchical, it still requires the actor to draw conclusions about far away thresholds. For instance, imagine a path from one corner room in a large building to the opposite corner of that floor of the building. It is conceivable that the threshold level search will produce paths based on costs existing at the time close to the target, which the actor could not possibly 'know' about. The modularity of the proposed system allows the Event to assign partial search spaces or partial targets based on additional information about the space, the actor or the governing Event. As an example, a search space consisting only of those zones which the actor can see from its current cell location could be assigned to such a partial search.

The system demonstrated in this paper can model how many people move in a multi-dimensionally dynamic space. Domain specific information about actors, spaces, the costs which define the domain in question and the Events which occur in that domain can also be overlaid on the elements of this system.

Zones (and their attached thresholds) are conceived as the fundamental aggregation of cells in this system. Any domain, from a hospital, to prison, to a concert hall could be described using zones and thresholds. Each of these domains can be described using this system irrespective of their specific functionalities. This conceptual data model can support domain specific descriptions of buildings as long as these descriptions can be provided in terms of spaces, actors and Events. Domain specific information can be codified using the cost mechanism as long as the cost can be appropriate spatialized and the way in which the cost propagates spatially can be formalized. The cost mechanism can be used to represent physical attributes of a space as well as social and social-psychological concepts.

7 FUTURE WORK

The extensible, modular nature of the proposed system means that further conceptual work is possible to refine the functionality depending on the class of problems being simulated. Currently, no widely agreed taxonomy of building use simulation problems exist. The most widely studied problem is the problem of emergency egress [3, 7, 20]. The novelty of the Event based approach, which the systems proposed in this paper have been designed to support, enables the consideration of a wider variety of building use situations, from routine everyday uses in complex spaces like hospital wards, to more specific problems like evacuations. As these problems are considered, further refinements in the current system may prove to be advantageous.

Two immediate areas are apparent based on the current work. Further work is required to develop a systematic taxonomy of cost maps. This will involve a taxonomy of feature types and a taxonomy of the rules by which these features are updated. This taxonomy needs to be developed from the architectural standpoint. Further work is also necessary for conceptualizing how zones may be grouped. For example, consider a hospital ward with a nurse's station, a day room, and a busy corridor, all forming a large open space. These could be conceptualized as three separate zones with appropriately organized connections (some may be both traversable and visual connections, others may be only visual connections). But for some problems, it may be appropriate to consider groups of zones as a higher level of semantic classification.

ACKNOWLEDGMENTS

This research is supported by a European Research Council grant (FP-7 ADG 340753) and by an Israel Science Foundation grant (1450/16).

REFERENCES

1. Botea, A., Bouzy, B., Buro, M., Bauckhage, C. and Nau, D. 2013. Pathfinding in Games. *Artificial and Computational Intelligence in Games.* S.M. Lucas, M. Mateas, M. Preuss, P. Spronck, and J. Togelius, eds. Schloss Dagstuhl–Leibniz-Zentrum fuer Informatik. 21–31.
2. Botea, A., Muller, M. and Schaeffer, J. 2004. Near optimal hierarchical path-finding. *Journal of Game Development. 1, 1* (2004), 7–28.
3. Chu, M.L., Parigi, P., Law, K.H. and Latombe, J.-C. 2015. Simulating individual, group, and crowd behaviors in building egress. *SIMULATION. 91, 9* (2015), 825–845.
4. Eastman, C.M. *Building Product Models: Computer Environments Supporting Design and Construction.* CRC Press, Boca Raton, Boca Raton, Florida, 1999.
5. Eastman, C.M., Teicholz, P., Sacks, R. and Liston, K. *BIM Handbook: A Guide to Building Information Modeling for Owners, Managers, Designers, Engineers and Contractors.* John Wiley & Sons, Hoboken, NJ, USA, 2011.
6. Francis, S. The Importance Of Being Abstract: An Indian Approach To Models. *Architectural Computing from Turing to 2000: 17th eCAADe Conference Proceedings* (1999), 101–109
7. Gwynne, S., Galea, E.R., Owen, M., Lawrence, P.J. and Filippidis, L. A review of the methodologies used in the computer simulation of evacuation from the built environment. *Building and Environment. 34, 6* (1999), 741–749.

8. Harabor, D. and Botea, A. Hierarchical path planning for multi-size agents in heterogeneous environments. *2008 IEEE Symposium On Computational Intelligence and Games* (2008), 258–265.

9. Harabor, D. and Grastien, A. The JPS Pathfinding System. *Proceedings of the 5th Symposium on Combinatorial Search (SoCS)* (2012), 207-208.

10. Hart, P.E., Nilsson, N.J. and Raphael, B. A Formal Basis for the Heuristic Determination of Minimum Cost Paths. *IEEE Transactions on Systems Science and Cybernetics. 4, 2* (1968), 100–107.

11. Hillier, B. *Space is the Machine: A Configurational Theory of Architecture.* Cambridge University Press, Cambridge, 1999.

12. Hillier, B. and Hanson, J. *The Social Logic of Space.* Cambridge University Press, Cambridge, 1984.

13. Kalay, Y.E. *Architecture's New Media.* MIT Press. Cambridge, Massachusetts, 2004

14. Pelechano, N. and Fuentes, C. Hierarchical Path-finding for Navigation Meshes (HNA*). *Comput. Graph. 59, C* (2016), 68–78.

15. Schaumann, D., Date, K. and Kalay, Y.E. An Event Modeling Language (EML) to simulate use patterns in built environments. *Proc. SimAUD 2017* (2017). *In press.*

16. Schaumann, D., Morad, M.G., Zinger, E., Pilosof, N.P., Sopher, H., Brodeschi, M., Date, K. and Kalay, Y.E. A computational framework to simulate human spatial behavior in built environments. *Proc. SimAUD 2016* (2016), 121-128.

17. Schaumann, D., Pilosof, N.P., Date, K. and Kalay, Y.E. 2016. A study of human behavior simulation in architectural design for healthcare facilities. *Annali dell'Istituto Superiore di Sanità.* 52, 1 (2016), 24–32.

18. Simeone, D., Kalay, Y.E., Schaumann, D. and Hong, S.W. An Event-Based Model to simulate human behavior in built environments. Digital Physicality: *Proceedings of the 30th eCAADe Conference* (2012), 525–532.

19. Simeone, D., Kalay, Y.E., Schaumann, D. and Hong, S.W. 2013. Modelling and Simulating Use Processes in Buildings. *eCAADe 2013: Computation and Performance–Proceedings of the 31st International Conference on Education and research in Computer Aided Architectural Design in Europe*, Delft, The Netherlands, September 18-20 (2013), 59-67.

20. Tan, L., Hu, M. and Lin, H. 2015. Agent-based simulation of building evacuation: Combining human behavior with predictable spatial accessibility in a fire emergency. *Information Sciences. 295*, (2015), 53–66.

21. van Toll, W.G., Cook IV, A.F. and Gerearts, R. A navigation mesh for dynamic environments. *Computer Animation and Virtual Worlds (CAVW) 23, 6* (2012), 535-546.

22. Yessios, C.I. The Computability of Void Architectural Modeling. *Computability of Design*. Y.E. Kalay, ed. John Wiley & Sons, Hoboken, NJ, USA (1987). 141–172

An Event Modeling Language (EML) to simulate use patterns in built environments

Davide Schaumann, Kartikeya Date, Yehuda E. Kalay

Technion – Israel Institute of Technology, Haifa, Israel
deiv@campus.technion.ac.il, kartikeya.date@gmail.com, kalay@ar.technion.ac.il,

ABSTRACT

In this paper we contribute a method to model and simulate use patterns in built environments. The aim is to assist architects in analyzing the implications of design decisions as far as human behavior is concerned, prior to committing to a building construction.

Use patterns are modeled using Events, computational entities that encapsulate descriptions of the dynamic unfolding of human behavior patterns in a designed space, over time. An Event Modeling Language (EML) allows modeling Events in a modular and hierarchical fashion. Event building blocks can be assembled into larger compositions describing context-dependent behaviors at increasing level of detail.

We demonstrate the approach in a hospital domain, where multiple use patterns involving collaborative activities unfold in space, while adapting to the dynamic conditions of the spatial and social environment.

Author Keywords

Use patterns; human behavior simulation; multi-agent system; Event-based model; building occupancy.

ACM Classification Keywords

I.2.11. DISTRIBUTED ARTIFICIAL INTELLIGENCE: Intelligent agents, Multiagent systems; I.6.5 MODEL DEVELOPMENT; J.5 ARTS AND HUMANITIES: Architecture; J.6 COMPUTER AIDED ENGINEERING: Computer-aided design (CAD)

1 INTRODUCTION

Understanding the relationship between the people and the environment they inhabit is a primary task in architectural design. People move and interact in space affecting the surrounding environment, and in turn being affected by it. Predicting this relationship by the time a building is designed rather than after it has been built is an important, yet challenging task. It is important because it allows architects and engineers to maximize occupants' physical comfort, social well-being, and job performance, while minimizing the costs of production, the overall maintenance, and the collective impact on the natural environment. It is challenging because human behavior is stochastic, dynamic and context dependent. It responds to the *form* of a built environment (e.g. its geometry and materials), to its *function* (e.g. hospital, airport, station), and to the individual attitudes, preferences, and cultural traits of the *users* that inhabit it.

At present, during the design process, considerations about human behavior are often based on partial, or even speculative information. As result, the actual building use process might not match the expected one, leading to loss of money, underperforming buildings, and user dissatisfaction. The aim of this research is to define a method to model and simulate use patterns in built environments to analyze how a proposed design will affect and be affected by the patterns that occur in there.

Use patterns are modeled using Events, computational entities that encapsulate descriptions of the dynamic unfolding of human behavior in a designed space, over time [15, 13, 11]. Different from other approaches where behavior emerges from the sum of individual agents' decision-making processes, here behavior is directed by Events, which coordinate the performing of collaborative activities, while accounting for agents' individual goals and abilities.

This interpretation of the word "Event" is consistent with previous work in the field of human behavior simulation [15, 13, 11]. A different interpretation is found in the Computer Science literature, where an "event" is an instantaneous occurrence handled by a system.

In our previous work, we demonstrated an application of Event-based modeling for simulating the interaction between planned (scheduled) and unplanned (unscheduled) Events [13, 14]. Here we describe a systematic method for modeling Events, namely an Event Modeling Language (EML). The EML allows modeling Events in a modular and hierarchical fashion. Event building blocks can be assembled into larger compositions describing context-dependent behaviors at increasing level of detail.

In this paper, we describe the EML and we demonstrate its application for modeling behavior patterns in a generic hospital ward.

2 BACKGROUND

2.1 Use patterns in built environments

According to Alexander, the character of a place is given by the standing patterns of behaviors that keep on happening there [1]. Such patterns are anchored to the spatial and social context of the setting: they manifest themselves in

space, but they originate from the social and cultural habits of the people who use the space. To analyze the dynamic interplay between a physical setting, the human inhabitants, and the patterns of events that happen there, Barker proposed the concept of *behavior setting*, a spatially bounded self-regulated system composed by people and inanimate objects [3].

Based on these theories, we define building use patterns as observable, spatiotemporal, context-specific descriptions of how people use built environments, which tend to recur multiple times and in different forms in the life of a setting. Building use patterns present the following characteristics. First, they have a structure that defines a particular sequence of action to perform, the conditions of the environment to perform such actions, the people that participate in the pattern, and the spaces in which the pattern can be performed. Second, they can adapt to the characteristics of the people that are involved in the pattern, to the spaces in which they are performed, and to dynamic changes in social and environmental conditions of the setting. Third, they are recurrent in different forms and times of the day. Fourth, they can be abstracted into more general patterns that describe how people use spaces at different levels of detail.

This research aims at modeling building use patterns in a computational fashion and at simulating them to analyze in what ways a proposed building design affects and is affected by the patters' unfolding in space and time.

2.2 Simulating use patterns

Different kinds of simulation methods have been developed to represent various aspects of human behavior in built environments. Multi-agent system (MAS) approaches in particular have been used to represent people movement and activities in space by means of goal-oriented agents able (to different extents) to interact among them and with the surrounding environment [17]. These methods have been applied to represent different types of situations, from egress behaviors [5], to more holistic building use processes, such as daily activity schedules [8, 16]. While in the first case the behavior emerges from agents' individual decision-making in response to the local surrounding conditions (e.g. the location of the fire and family members in an egress situation), in the second case, behavior originates from the performing of global, deterministic, pre-calculated activity schedules.

Even though these latter simulation types hold promise to convey a more comprehensive overview of how people use buildings over time, due to the complexity in the coordination of a large number of agents, individual agents' behavior tends to be less responsive to the dynamic social and spatial context. Agents involved in separate activities that cross paths in a building corridor, for instance, will not be able to interrupt their current tasks and initiate a spontaneous discussion, preventing the simulation from considering the consequences of such behaviors, for instance in terms of spatial bottlenecks or social interactions.

To address these issues, Schaumann et al [13, 14] proposed the Event-based model, a form of representation that allows describing building use processes by means of Events, computational entities that coordinate the convergence of people in space to perform collaborative, goal-oriented activities. Compared to other MAS models, Events dictate what agents should do, rather than an alternative view where agents make independent intelligent decisions. Rather than in agents, perception-action capacities are therefore embedded in non-human Events, affording a higher-level view that can coherently coordinate the actions of multiple actors that depend on one another (Figure 1).

In our previous work we demonstrated the application of the concept of Event to model the interaction between planned Events originating from a building schedule, and unplanned Events, originating from the serendipitous interaction of people located in the same space at the same time. Here we focus on developing an Event Modeling Language (EML) to systematically model Events in a modular, hierarchical and well-structured fashion – required conditions for a successful modeling approach [9].

To do so, we turn our attention to Artificial Intelligence (AI) research in video games, where advancements have been made in modeling coordinated realistic behaviors of Non Player Characters (NPC) in response to the dynamic actions of human-controlled avatars [7]. In this context, different types of modeling approaches have been developed to represent agents' decision-making strategies in dynamic environments.

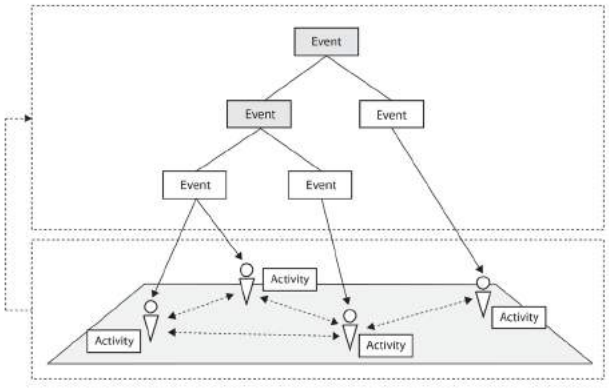

Figure 1. The Event-based model

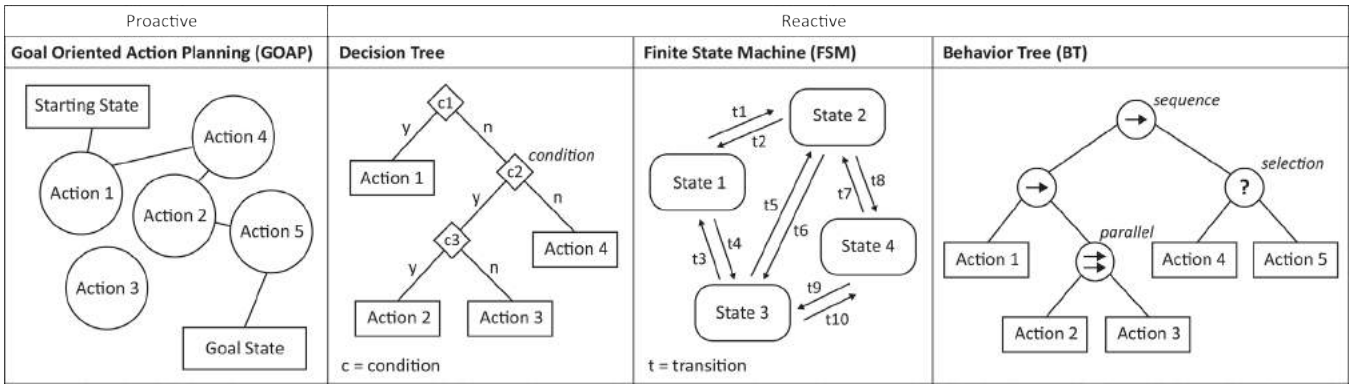

Figure 2. Decision-making in multi-agent environments

2.3 Decision-making in multi-agent environments

Decision-making involves selecting an action (or sequence of actions) that agents perform to accomplish a goal [12]. Different methods have been developed for this purpose (Figure 2). These methods can be either *proactive* or *reactive*.

In *proactive* planning systems the sequence of actions is calculated *on-line* by specifying an initial state of the world, a desired one (defined as *goal*), and a set of executable atomic actions (e.g. move to a target, or use some equipment) that, when combined into larger sequences (defined as *plans*), will eventually lead to the goal accomplishment.

To simulate behaviors that adapt to an ever-changing environmental context, plans must be periodically recalculated. Due to the fact that people move, meet, use resources, and modify the state of the environment (e.g. by opening a window, or locking a door), there is no guarantee that a plan calculated at a certain moment in time will still be valid at another moment in time, when the world will be in a different state. Hence, when simulating complex building use patterns, proactive planning systems require logical and computational efforts (a) to generate a coherent plan for multiple agents using a space at the same time, and (b) to address combinatorial explosion problems that arise in the process of generating plans from atomic action units.

In *reactive* planning systems agents choose among a discrete set of actions available at each moment in time, encoded in the form of condition-action pairs. Even though plans are calculated *off-line*, they incorporate pre-calculated adaptations to the surrounding environment, addressing the logical problems of creating coherent plans, and the computational problem of generating plans on-line. Furthermore, they often use hierarchical representations to describe behaviors at increasing level of detail.

In the context of video games, different AI methods have been developed to model structured, hierarchical representations of reactive actions incorporating adaptations to surrounding environments. Examples of such methods include Decision Trees, Finite State Machines (FSM), and Behavior Trees (BT).

Decision trees use a tree-like representation to describe a finite set of actions that an agent can perform, in response to a set of conditions. After performing each action, new conditions are evaluated to decide the next action to perform. Using this system for simulating building use patterns, however, presents several limitations. First, trees can only be navigated in a linear fashion, meaning that the same node can never be visited twice. Second, each specific transition must be specifically modeled, including the one required to exit a branch of the tree. Both conditions may cause trees to be very long and complex to manage.

FSMs describe a finite set of states in which the system can be, and a set of transitions among states. In every instant, one state of the FSM is active, and all possible transitions are evaluated. If a specified condition is verified, the transition is executed, activating a new state and canceling the former one. States can also be described in a hierarchical fashion, by encapsulating into a state the description of other states. Different from decision trees, states can be selected multiple times, allowing for modularity and re-usability. Similar to decision trees, each transition must be explicitly encoded, leading to complexities in management and extendibility (every time a new behavior is added, all transitions must be explicitly modeled).

BTs use a tree-like representation to model behaviors hierarchically. Each behavior is composed of a list of sub-behaviors (defined as a children nodes), which inform the parent node upon failure or completion. The parent node, in turn, updates its own status and may trigger a different sibling node [4]. Different from the previous approaches described, transition rules are encoded in different node types, as follows: *sequence* nodes trigger one child node after the other; *parallel* nodes, triggers multiple child nodes at the same time; *selection* nodes use priority values to select among a list of competing children. This system allows modularizing both actions and operations on the actions to describe a flexible mechanism able to generate representations of structured activity patterns, which respond to dynamic conditions.

3 EVENT MODELING LANGUAGE (EML)

3.1 Motivation

The proposed EML leverages insights from the aforementioned decision-making systems to define a systematic method for modeling Event-based use patterns in a modular, hierarchical and well-structured fashion. The aim is to address problems of complexity and manageability in representing how people use buildings over time.

In particular, we leverage insights from behavior trees whereby parent nodes coordinate the performing of children nodes in a modular and hierarchical fashion. Similarly, Events are conceived as modular building blocks that encapsulate the logic for the performing of behavior patterns at a specific level of abstraction. Events can be combined into larger compositions in a hierarchical fashion, to describe human behavior patterns at increasing level of detail. While lower-level Events (children nodes) describe general use patterns, higher-level Events (parent nodes) provide more detailed description of the context in which the patterns occur, making their performing more context-dependent.

3.2 Components

The EML components are four, and namely the *spaces*, *actors*, *activities* and *Events*. *Spaces* provide a setting for human behavior. They are divided in zones [6], discrete spatial units able to calculate and store information about their function (e.g. a patient room, or nurse station) and their current use, including who is using the space (e.g. doctors, nurses, patients), for what purpose (e.g. social, clinic, assistance), and under which environmental condition (e.g. people occupancy, noise, smell, light).

Actors are synthetic characters that move and interact in space. Each actor has a specific role (e.g. a doctor or nurse in a hospital setting), some properties (e.g. politeness), and a status (e.g. tiredness) that varies depending on the current state of the world or the activities performed. Both spaces and actors can communicate with each other during the simulation to update their individual statuses. This information can be then used by activities and Events to direct agents' behaviors accounting for the dynamic changing in the social and spatial context.

Activities are atomic executable goal-oriented actions that direct the behavior of one or more actors in space. They resemble the "action" components in the different decision-making systems illustrated in Figure 2.

As it is done in [2], parametric values guide the performing of activities, allowing them to be reused in different circumstances to describe different types of use patterns. While performing a task, an activity is responsible for monitoring a set of performing conditions, and end-conditions, which describe respectively the conditions that need to be met while the activity is running (e.g. the actor tiredness should not exceed a specific threshold value), and the conditions that need to be met to successfully complete the activity (the actor is close to the target).

Events organize activities into larger compositions, and associate them to specific input parameters (e.g. actors and spaces) to define domain-specific building use patterns. Similar to activities, Events can also be composed into larger compositions and associated to specific input parameters to describe building use patterns at increasing level of detail. The resulting composition is a tree where activities are leaf nodes, and Events are parent nodes.

The context-dependent meaning of the use patterns is not explicitly encoded in the nodes themselves. Instead, it is defined at the level of the parent node, which organizes them in a particular order, and triggers them using specific parameters. This prevents the efforts of encapsulating the context-specific meaning into each node, leading to a complex, non-modular system.

To model use patterns, Event nodes perform the following tasks: (a) They associate children nodes to a set of *preconditions*, which describe a required state of the world to perform the action, and *postconditions*, which describe both the changes in the state of the world that might occur as consequence of the node performing, and the relevant information related to the action performing (e.g. duration or number of interruptions due to external circumstances). While preconditions are checked before initializing the node, postconditions are executed after its completion. (b) They define a set of input parameters that are used to drive the node performing, such as particular actors, spaces, equipment or expected duration. (c) They select a specific operator (described in the following section) that manages the node performing. (d) They trigger the appropriate node, and monitor its execution. Depending on the result (e.g. succeed or fail), the Event updates its own status.

3.3 Grammar

Events organize children nodes using a *sequence*, *parallel*, or *selection* operators. The *sequence* operator triggers child nodes one after the other. After performing each node, the control goes back to the parent, which checks the current state of the world, and modifies, if necessary, the children's input parameters. The parent node is completed if every child is completed.

The *parallel* operator triggers all children nodes at the same time. The node is completed if every child is completed.

The *selection* operator decides which child to perform among a list of competing children. After verifying the children precondition, the parent selects the children to perform using different possible criteria, including the first available child, a random one, or using priority values calculated for each child. In this case, the parent node is completed if one of the children nodes is completed.

3.4 Notation

An EML notation describes a tree-like representation where nodes can be triggered sequentially (*sequence*), concurrently (*parallel*) or selectively (*selection*), as represented in Figure 3. Encapsulation is conveyed through L-shaped lines that connect a parent node with a list of child nodes. Sequentiality is conveyed through horizontal lines that connect sibling nodes. Concurrency and selectivity are conveyed by representing nodes positioned one above the other.

The EML notation can be used to convey information about the behavior of a system, or its structure. Accordingly, the notation can be used to describe Event instances, where semantics emerged, or the structural components, where semantics is yet to emerge. In the first case, the leaf nodes in Figure 3 will represent Events, such as "doctor and nurse checking a patient in a patient room". In the second case it will represent an activity "meet", which is associated to specific actors (doctor and nurse) and a specific space (patient room).

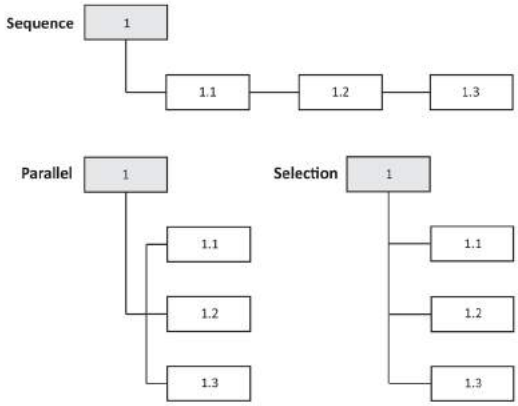

Figure 3. EML notation system [13]

4 CASE STUDY

4.1 Introduction

We demonstrate an application of the EML to model representative use patterns in a generic hospital environment. In this kind of setting, use patterns present a structured yet adaptive nature in relation to the social and spatial context, such as the presence or absence of other people in space, or interruptions that may disrupt the activities' performing.

Data about use patterns has been collected by means of direct experience observations and interviews with doctors, nurses and hospital managers. This process helped us identifying a list of generic patterns happening in internal medicine wards.

In this study, we provide a detailed description of the modeling of three activities and four Events, and we illustrate how these building blocks can be used to model larger building use patterns. Then, we simulate the modeled patterns in an abstracted representation of the Internal Medicine Unit in the Sammy Ofer Heart Building, at the Tel Aviv Sourasky Medical Center.

4.2 Modeling Activities

We describe the modeling of three activities, namely *Move*, *Meet*, *Do*, and four Events, namely *Group Move*, *Check Patient*, *Gather*, and *Visit Patient* (Figure 4).

The *Move* activity directs an actor movement from its current position to a target, using a path-finding algorithm. Since the state of the world constantly changes, the path to the target is recalculated at each time step. The activity requires as input an actor, a target, a distance from the target where to stop, and an eventual equipment unit to push/carry. The activity is completed if the distance between the actor and the target is equal to the specified value. Its duration depends on the building layout, on the actors' properties (e.g. age, tiredness, etc.), and on the environmental conditions. A more detailed description of the movement algorithm is provided in [6].

The *Meet* activity coordinates the meeting of multiple actors in a specific space, involving specific equipment. It takes as input the actors involved, some equipment (e.g. a table where to sit), the current use property of the space in which the activity can be performed (e.g. social), and the duration of the action. The duration, however, is "expected" rather than "actual", since interruptions may occur, which may prolong the activity duration. During its performing, the activity constantly monitors that space-use property of the space, to make sure the activity can be performed. The activity is completed when the meeting duration ends.

The *Do* activity describes an action performed by an actor that does not require moving in space, and which may involve particular equipment. It can be used to describe an actor working at a desk, resting in bed, preparing food, or waiting for somebody to arrive. Similar to the Meet activity it requires as input a space-use property that supports the activity performing, and an expected duration. The activity fails if the space-use property differs from the specified one, and it succeeds when the activity duration ends.

The *Group Move* Event directs the coordinated movement of different actors in space. It consists of a parallel operator that oversees many Move activities. After being triggered with specific input, it assigns preconditions and postconditions to each child node, and it triggers them using the information received as input, or calculating specific information. While the preconditions check for the actors' proximity to the target, the postconditions record the walked distance and the duration of the activity. This information can be used by the actors to update their own status. The Event makes sure that all the actors arrive to the target, and it directs the behavior of the other actors in case one of the group members is interrupted by other tasks.

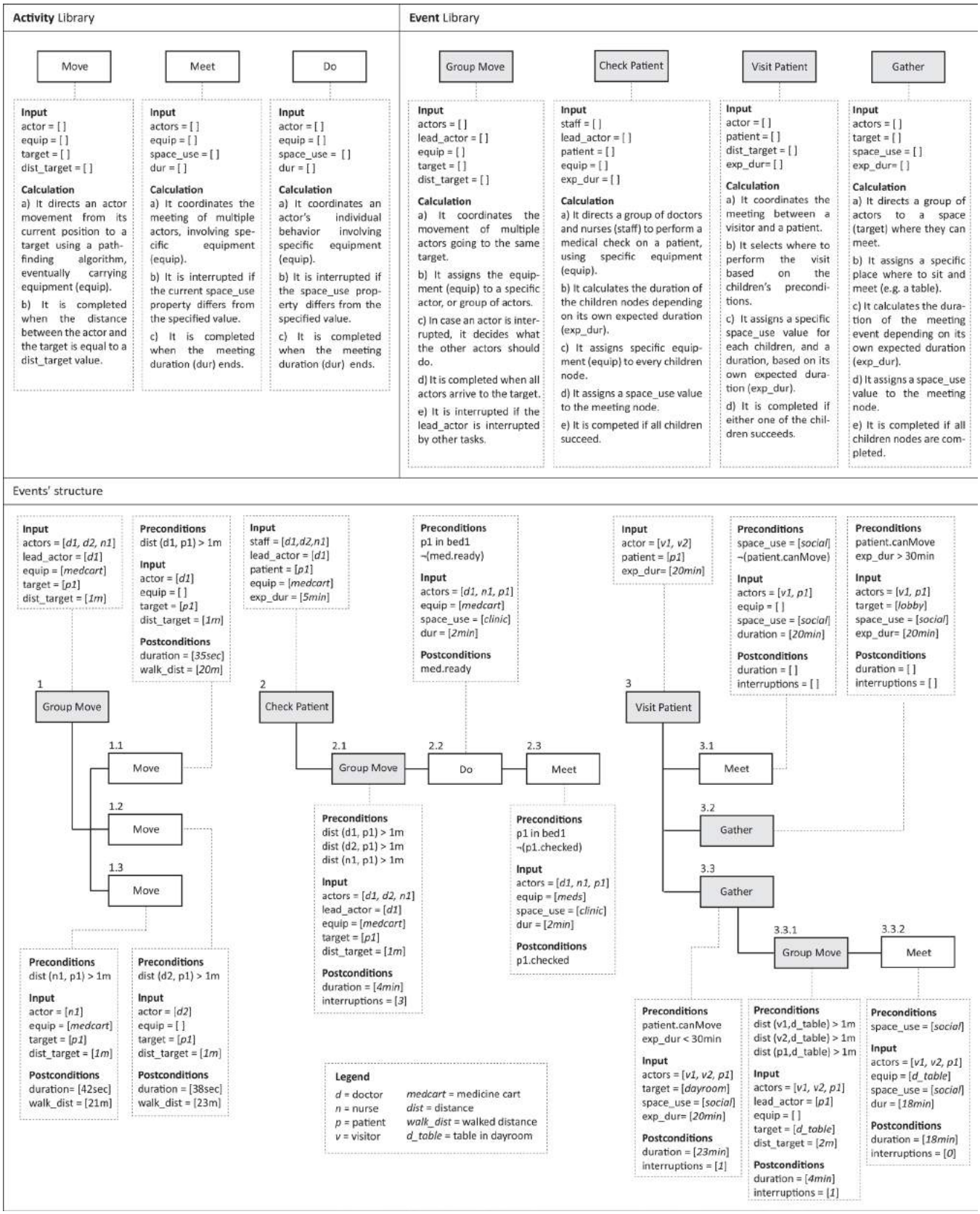

Figure 4. The EML combines activity and Event building blocks into larger compositions to describe building use patterns.

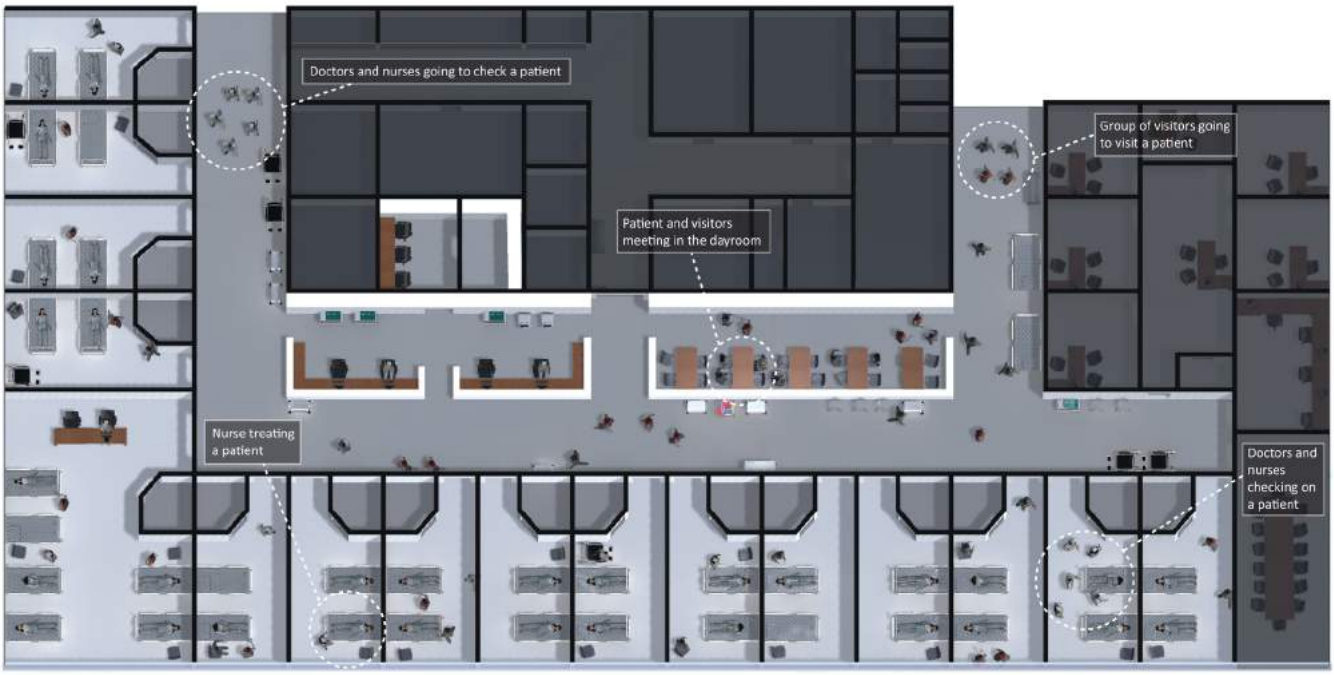

Figure 5. Simulating building use patterns in an abstracted representation of a hospital ward.

The *Check Patient* Event directs the behavior of a group of doctors and nurses to check on a patient. It consists of a sequence of a Group Move Event, a Use activity, and a Meet activity. The first node coordinates the movement of the medical staff to the patient. The second directs a nurse in preparing a special treatment using a medicine cart. The third directs the treatment action. One of the Event tasks is to assign a specific duration to the Use and Meet nodes (2.2 and 2.3 in Figure 4) accounting for its expected duration and for the time it took to complete 2.1. After completing 2.1, in fact, the control goes back to 2, which assigns specific input value to 2.2, and then to 2.3.

The *Visit Patient* Event directs the behavior of a visitor visiting a patient. It consists of a selection operator that decides where the meeting should take place in the room (3.1), in the lobby (3.2) or in the dayroom (3.3). The parent Event assigns to each child node a set of preconditions, postconditions, and input parameters such as the target where the activity should take place, and a space-use value. One of the preconditions checks if the patient can move. This property is stored in the actor. The other precondition involves the expected duration. If it is less then a certain value, the activity will take place in the lobby (3.2), else it will take place in the dayroom (3.3). A *Gather* Event is responsible for directing the behavior of the patient and visitor to the chosen space and coordinate their meeting.

These patterns have been further assembled in larger compositions to model (a) a doctor round, where two groups of doctors and nurses systematically check all the patients in the ward, (b) a random number of visitors entering the word to visit patients, (c) nurse treating patients, and (d) nurse aides assisting patients.

4.3 Simulation

Figure 5 displays a simulation of different use patterns in a hospital ward. Each pattern affects the way other patterns unfold. For instance, the presence of many people in the corridor may cause social interactions between doctors and visitors, leading to prolonged times for doctors to arrive to a patient, potentially leading to shorter checking durations. The presence of many people in a dayroom, instead, may lead to a lack of available tables to sit, which in turn will cause a patient and visitor to sit a the lobby.

The manifestation of certain behavior patterns may also prevent other patterns from occurring. A medical check, for instance, causes a space-use property to change from *social* to *clinic*, potentially leading to the interruption of social events occurring in the patient room.

The simulation was facilitated by a host of computational tools: Autodesk Revit was used to model the space and equipment geometry; 3DS Max was used to model the actor geometry and animations; Unity 3D was used to model the profile of spaces and actors, as well as the activities and the Events, using C# as a scripting language.

5 CONCLUSION AND DISCUSSION

The paper introduces an Event Modeling Language to model building use patterns in built environments. Compared to previous methods, it allows simulating structured set of collaborative activities, which adapt to the surrounding context. A case study demonstrates the approach for modeling representative use patterns in a generic hospital environment.

The simulation enables measuring different types of building use metrics, such as the time space are used or left unused, the walking distances traversed by the different actors, the number of social interactions. We argue that the proposed system holds the potential for generating useful information that can be used in architectural design to evaluate different design options (as argued in [9]).

Even though we applied the EML for modeling only few representative patterns, the modularity and scalability of the system make possible to model Events at increasing level of complexity.

Like any other programming endeavors, however, modeling Events is more of an art, than a science. In the different modeling phases, different considerations need to be made about how large events should be, and how general. While large Events can group complex calculations in one coherent set of instructions, they may be too specific to be re-used in different occasions. Oppositely, smaller Events can be re-used several times, but their design might require efforts in defining calculations that adapt to different types of input parameters.

Eventually, the Event-based model should be used to simulate longer time spans of a single workday. Future work may involve the development of a scheduling mechanism, which defines a sequence of Events to perform based on urgency factors. At the same time, the system should be able to resolve conflicts among Events that compete for the same resources (actors, spaces, equipment).

More generally, large efforts should be directed towards the development of a systematic method to collect data about human behavior patterns in existing settings, modeling them using the proposed approach, and validating the simulation results using established techniques.

ACKNOWLEDGEMENTS

This research is supported by a European Research Council grant (FP-7 ADG 340753) and by an Israel Science Foundation grant (1450/16). We are grateful to Julia Pavlov for her work in the different model implementation phases.

REFERENCES

1. Alexander, C. *The Timeless Way of Building*, Oxford University Press, 1979.
2. Badler, N. Schuler, W. Zhao, L. Palmer, M. Parameterized action representation for virtual human agents, Embodied conversational agents, (2000), 256.
3. Barker, R. G., *Ecological Psychology: concepts and methods for studying the environment of human behavior*. Stanford University Press, 1968.
4. Champandard, A. Behavior trees for next-gen game AI. Game developers conference, audio lecture. (2007).
5. Chu, M.L. Parigi, P. Latombe, J. and Law, K. SAFEgress: A Flexible Platform to Study the Effect of Human and Social Behaviors on Egress Performance. *Proc. SimAUD*, (2014), 35-42.
6. Date, K. Schaumann, D. Kalay, Y.E. Modeling Space To Support Use-Pattern Simulation In Buildings. *Proc. SimAUD*, (2017), *in press*.
7. Diller, D.E., Ferguson, W., Leung, A.M., Benyo, B., Foley, D. Behavior modeling in commercial games. *Behavior Representation in Modeling and Simulation* (BRIMS), (2004), 68.
8. Goldstein, R. Tessier, A. Khan, A. and East, K. S. Space layout in occupant behavior simulation. *Proc. IBPSA-AIRAH Building Simulation Conference*, (2011), 1073–1080.
9. Harel, D., 1987. Statecharts: A visual formalism for complex systems. *Science of computer programming 8*, (1987), 231–274.
10. Hong, S.W. Schaumann, D. Kalay, Y.E. Human behavior simulation in architectural design projects: An observational study in an academic course. *Computers, Environment and Urban Systems 60*, (2016) 1–11.
11. Kapadia, M., Shoulson, A., Steimer, C., Oberholzer, S., Sumner, R.W., Gross, M. An event-centric approach to authoring stories in crowds, in: Proceedings of the 9th International Conference on Motion in Games. ACM, (2016), 15–24.
12. Millington, I. Funge, J. *Artificial intelligence for games*. (2016), CRC Press.
13. Schaumann, D. Kalay, Y.E. Hong, S.W. Simeone, D. Simulating Human Behavior in not-yet Built Environments by means of Event-based Narratives. *Proc. SimAUD*, (2015), 7-14.
14. Schaumann, D. Gath Morad, M. Zinger, E. Putievsky Pilosof, N. Sopher, H. Brodeschi, M. Date, K. Kalay, Y. E. A Computational Framework to Simulate Human Spatial Behavior in Built Environments. *Proc. SimAUD,* (2016), 121-128.
15. Simeone, D. and Kalay, Y .E., An Event-Based Model to simulate human behaviour in built environments. *Proc. eCAADe,* (2012), 525-532.
16. Shen, W., Shen, Q., & Sun, Q., Building Information Modeling-based user activity simulation and evaluation method for improving designer–user communications. *Automation in Construction 21*, (2012), 148-160.
17. Wooldridge, M. Jennings, N. R. Intelligent agents: Theory and practice, *The knowledge engineering review 1*0, (1995), 115–152.

A Building Database for Simulations Requiring Schemata

Gabriel Wurzer[1], Jelena Djordjic[2], Wolfgang E. Lorenz[1] and Vahid Poursaeed[3]

[1]TU Wien
Vienna, Austria
{*firstname.surname*}@tuwien.ac.at

[2]Moser Architects
Vienna, Austria
lela.simanic@gmail.com

[3]Iran Univ. of Science and Techn.
Tehran, Iran
poursaeed_v@arch.iust.ac.ir

ABSTRACT

Obtaining spatial representations of existing buildings for use in simulation is challenging: To begin with, getting permission to access submitted construction plans can take a long time. Then these might only be available in analog form, making it necessary to scan and vectorize them at the regulations office. The resulting representation might still not be adequate for simulation, requiring further extraction of relevant features and enrichment by additional information in order to fit the simulation domain. In our work, we have specifically targeted simulation types that work with schemata (e.g. occupancy, work and egress simulations). Our contribution lies in restructuring the aforementioned workflow so as to (1.) minimize time and effort spent on digitizing and to (2.) automatically derive schemata – sets of boundary polygons which (3.) can be further enriched by attributes. These steps are embedded into a web-based building database which allows uploads and queries per web interface as well as web services. The query interface furthermore includes (4.) the ability to download the schemata both in vector as well as raster form so that they can be used for both discrete and continuous-space approaches. Apart from acting as data provider, the database furthermore (5.) allows for spatial predicate functions which may be used for analysis of a space program.

Author Keywords

Simulation; database; spatial representation; web services.

ACM Classification Keywords

H.2.8 DATABASE APPLICATIONS / Spatial databases and GIS

1 INTRODUCTION

Schemata form the basis for a wide range of simulations that need spaces to be represented simply as boundary polygons (continuous-space simulations) or collections of cells (discrete-space simulations). Such a representation could be derived from data-rich models (i.e. Building Information Models [BIMs] for architecture; Geographical Information Systems [GIS] and Web Mapping Services [WMS] for the urban case), however, these might not be available when dealing with existing buildings for which no digital plans exist. Improving the workflow for getting a digital schema from an analog plan was thus our primary goal – technically achieved by the implementation of a web-based building database that can process images into schemata and allows for elaborate queries via web interface and web services. In more detail, we have

- looked at the current workflow for obtaining schemata from analog plans, carefully restructuring and automating individual steps so as to minimize time and effort spent (see section 'Restructuring and Automating the Digitization Process'),
- incorporated the resulting schemata into a web-based building database which lets us enrich the data further by uploading attribute tables and other media (see section 'Database Representation'),
- devised a query and data retrieval interface in the form of a web interface and RESTful webservices, providing a way for users and applications to interact with the data (see section 'Query and Data Retrieval Interface').

In order to argue for the applicability of our method, we have tested both import and retrieval using a showcase setup (see section 'Showcase'). We further provide a discussion that outlines limitations of our approach (see section 'Discussion') before concluding.

2 RELATED WORK

Many authors have already tried to infer spatial representations from image data: Koutamanis' work [2] is occupied with semantic recognition of building elements from sketches while others employ a rule-based vectorization strategy in floor plan images [3, 4]. In contrast to these approaches, we use a polygon-based vectorization algorithm [5] which has no contextual knowledge specific to architecture. Since it works on monochrome bitmaps, the user needs to separate different features by at least one pixel, which is reasonable if we assume that the interior polygon is shown and walls are simply left out.

Apart from technique used for recognition, the actual representation used for schemata might differ: For example, Tabak [6] uses a circulation graph to which he attaches spaces as single nodes. Our representation uses spaces rather than a circulation network, however we can get the schema as raster and transform the midpoint of each cell into a network node. Once connected to its neighboring nodes, the network can then be used for navigation between different spaces. Dijkstra and Timmermans [1] have used a

similar approach (network of decision points), but these nodes served as intermediate goals for lattice-walking agents.

3 RESTRUCTURING AND AUTOMATING THE DIGITIZATION PROCESS

Depending on regulation, one may need a permission to access the submitted construction plans of a building. The current workflow shown left in Figure 1 thus begins with a supposedly lengthy task "obtain permission". Since we assume that we work with non-digital plans, the next step lies in a visit to the regulations office in which the plans have to be scanned or photographed and optionally stitched in a post-step. Next comes the vectorization part, which tries to identify and restore geometry. However, this process is lossy and might not be adapted to hand-drawn plans which are typical for older structures. It can thus safely be assumed that some geometry will be omitted or recognized only in part. We expect that a bit of manual work in restoring or completing features is part of the process, which also involves deleting parts of the geometry that are not relevant (task "extract relevant features"). With that, the vectorization is complete. One may still want to add attributes to certain features, e.g. room names (if not correctly recognized), functions and so on.

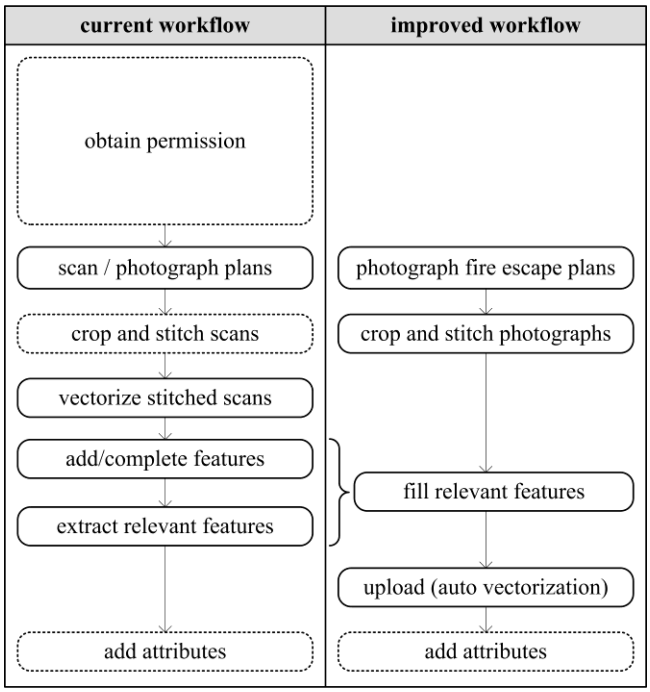

Figure 1. (left) current workflow (right) improved workflow.

When improving the current workflow, we saw our biggest challenge in the initial permission step. There are two ways in how to circumvent this, (a.) by photographing the fire escape plans without asking for permission or (b.) to scan floor plans shown in printed literature. However, the last option seems only feasible for historical architecture, since magazines and books publishing contemporary buildings tend to depict only certain areas or levels. Thus, we stick with the first case - to photograph fire escape plans (see right in Figure 1) since we aim at recent architecture. Because our photographs will likely contain areas and not a whole floor, we must stitch them together in a post step.

The biggest difference between the current and improved workflow comes in the next step: Rather than vectorizing and completing features in a post-step, we fill each extracted space (a simple flood-fill operation in a drawing package) with a known color (or a set of colors, if multiple space are to be marked as belonging to one common area). Details that are not relevant (e.g. doors, equipment) may need to be cleared beforehand since the schema is only concerned with boundaries. A further way in which superfluous details can be eliminated is to clear all pixels that are not in the range of colors used to signify spaces.

The color-coded images are now uploaded to the database which performs an automatic vectorization. In that process, it assigns an id and color to each resulting feature. The vectorization we use guarantees that all features are found if there is at least one pixel between separate elements. The result is registered as vector layer of a certain name (e.g. "schema") at a certain level (e.g. 1) of a certain building. We use naming conventions on the image file in order to extract this information.

In a post-step, one may assign attributes to individual spaces or areas by specifying a mapping of the form (color, *...attributes...*) or (feature id, *...attributes...*) interactively or by upload of a spreadsheet.

4 DATABASE REPRESENTATION

The database acts as a repository that stores uploaded schemata per building and level. It furthermore offers the possibility to upload other media (e.g. images, spreadsheets, documentation) which are registered on a per-building basis. An graphical outline is given in Figure 2.

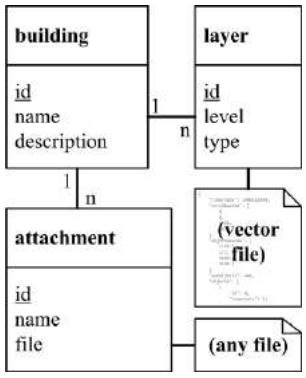

Figure 2. Database representation and linked files.

Technically we use the sqlite database to store all metadata concerning buildings, layers and attachments. The actual vector data is represented as files containing Javascript Object Notation (JSON), attachments are written out as files in their original formats.

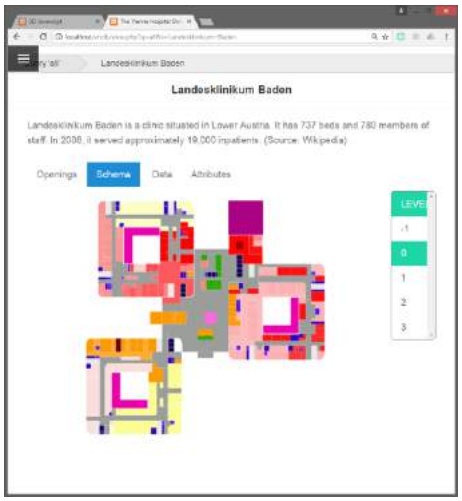

(a)

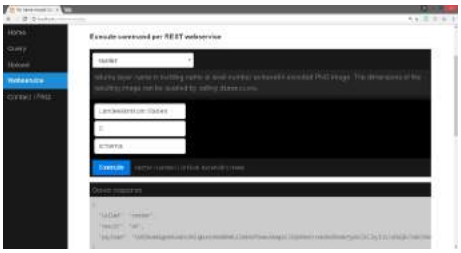

(b)

Figure 3. (a) Web-based query interface with 2D content viewer. (b) Web service call with results shown online.

(a)

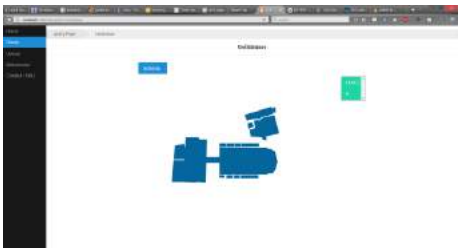

(b)

Figure 4. (a) Touched-up fire escape plans and (b) 2D viewer displaying the ground floor of our institute.

5 QUERY AND DATA RETRIEVAL INTERFACE

Until now the changed workflow proposed by the authors does little more than to vectorize image data with some added constraints (1 pixel separation between spaces) such that these become distinguishable. The true power of the building database lies in leveraging the information for producing extracts in both raster and vector form, offer spatial predicates based on the imported data and to be interfaced in multiple forms, either

- through a web interface which allows end-users to query and view content in 2D (see Figure 3a) or
- a web service which enables applications to interact with the database (see Figure 3b for a web-based service call and response).

The interaction lies in mapping/transforming geometries to the client coordinate system (by scaling the whole geometry or extracting a portion, given by a window) in both vector and raster forms (by rendering geometries to a raster map), and to map colors and indices to attributes (through attachments in spreadsheet form listing [color, *...attributes...*] or [feature id, *...attributes...*]). Another area of queries lies in spatial predicates which are concerned with topological queries (e.g. neighboring spaces), realized internally through the use of an adapted form of the Dimensionally Extended nine-Intersection Model (DE-9IM) which is common in GIS systems.

The query interface does not carry a state, which is assumed to be supplied by the client. In more technical detail, our web service expects to be called in RESTful form, through

{functionňame}/parameter1/parameter2/.../parameterNň

which is received by a PHP stack and mapped to a range of service routines. The results of each call are given in JSON, giving a wide range of web-based clients the opportunity to interact with our database.

6 SHOWCASE

In order to argue for the applicability of our method, we have gone through all of the proposed steps and got a benefit in terms of time spent digitizing and effort involved in getting the gathered data ready for simulation. Our test was split into two phases, (1.) gathering input using fire escape plans, which were digitized automatically and (2.) writing client programs that would access data stored in the database.

For the first task, we scanned the fire escape plan of our own institute, which took 28 minutes for outlining a single floor. The touched-up data is shown in Figure 4a and 4b and is discussed in due course (see 'Discussion').

For the second task, we imported a building from existing floor plans. A data query in vector and raster form was instantaneous, in the order of milliseconds. It enabled programs (see Javascript and Netlogo 3D in Figures 5a and 5b) to utilize a rich scale of options to choose from when

mapping into an own coordinate space and, at the same time, use the set of spatial predicates available via the data interface of the database.

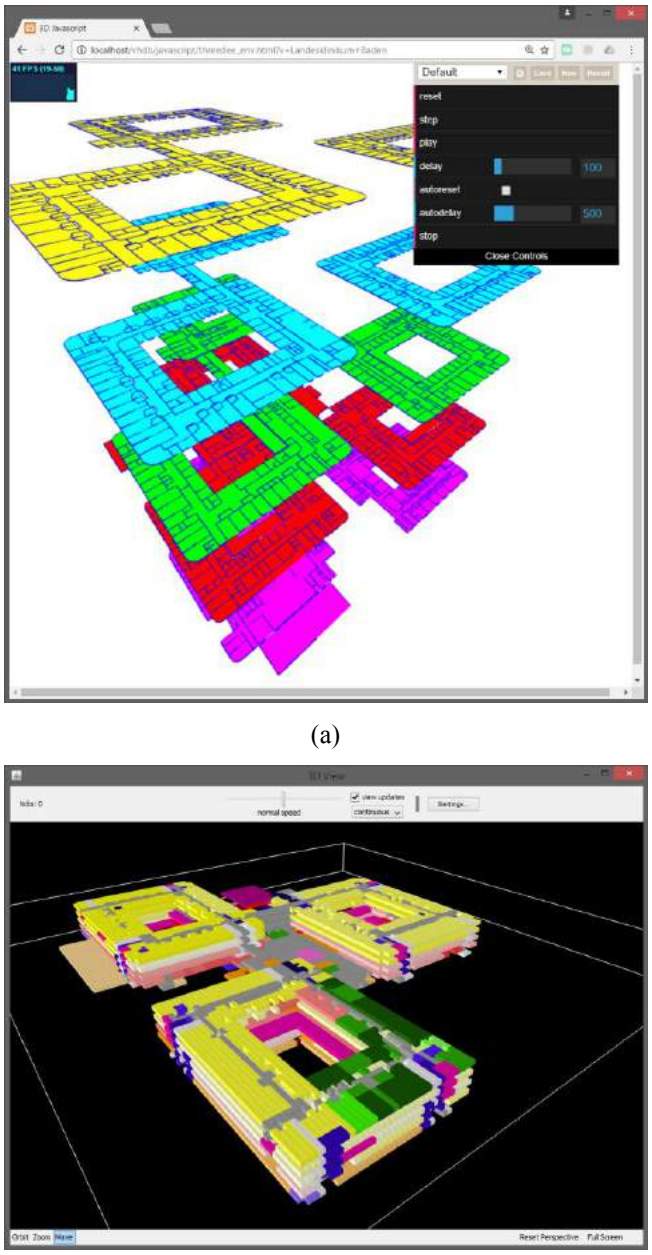

(a)

(b)

Figure 5. (a) Javascript [three.js] and (b) Netlogo 3D viewer accessing the database via web servives.

7 DISCUSSION

Apart from all technical assumptions, it is clear that we presume that we can enter all levels of a building for photographing fire exit plans. This optimistic strategy is driven by the fact that a simulation study is typically conducted in a project context where the client actively supports the retrieval of plans.

The second discussion point lies in the contribution of the method. It is clear that some of the mentioned concepts could be achieved by redrawing features in a vector program, however, the proposed service architecture offers additional functions that make the proposed system valuable as content provider, freeing simulation of having to implement certain functionalities on their own. With that, we are aiming at a service architecture enabling client programs to scrap some of their code when connecting to databases, which is a good outlook for the development of the field.

8 CONCLUSION

We have presented an improved workflow for obtaining digital schemata from analog images. The proposed process is integrated into a building database that offers additional functionalities for querying, transforming and annotating that data and is accessible via a web interface and web services. The applicability of our method was showcased by conducting all steps from data acquisition to usage of the data in a simulation.

REFERENCES

1. Dijkstra, J., Timmermans, H. Towards a multi-agent model for visualizing simulated user behavior to support the assessment of design performance, *Automation in Construction 11*, 2 (2002), 135–145
2. Koutamanis, A. Recognition of Building Elements in Free-Hand Sketches. *Proc. 26th eCAADe*, 2008, 419-426.
3. Lu, T., Yang, H., Yang, R., Cai, S. Automatic analysis and integration of architectural drawings, *Int. Journal of Doc Analysis and Recognition 9*, 1 (2007), 31-47.
4. Macé, S., Valveny, E., Locteau, H., Tabbone, S. A System to Detect Rooms in Architectural Floor Plan Images, *9th IAPR Int. Workshop on Document Analysis Systems*, 2010, 167-174.
5. Selinger, P. Potrace: a polygon-based tracing algorithm (2003). http://potrace.sourceforge.net/potrace.pdf. As of 1st March 2017.
6. Tabak, V. *User Simulation of Space Utilisation*, PhD Thesis, Technical University Eindhoven, 2008.

Double-Skin Facades and Daylight Simulations: Comparative Study of Facade Typologies and Effects on Natural Light in Different Climates

Ajla Aksamija

University of Massachusetts
Amherst, USA
aaksamija@umass.edu

ABSTRACT

This article discusses results of a research study that investigated daylight performance of glazed double-skin facades (DSFs) in various climate types. The objectives of the study were: 1) to analyze the daylight levels in different types of DSFs (box window, corridor type, and multistory) in four different climates; 2) to compare daylight performance against the conventional single skin glazed facade (curtain wall); 3) to investigate the effects of facade orientations on daylight; and 4) to investigate the impacts of facade characteristics (different depth of air cavities in DSFs) on daylight levels. The research methods consisted of daylight simulations in Radiance software program of an office space, which would be enclosed by the investigated facade types. Multiple models were developed to investigate different typologies of DSFs, depth of air cavity between the two skins, orientations and climate types, as well as sky conditions, totaling a dataset of 336 simulation models. Daylight simulations were performed for sunny, overcast and cloudy sky conditions, for four different locations (Miami, San Francisco, Chicago and Duluth). Results indicate that all types of DSFs would decrease daylight levels compared to a conventional curtain wall; however, the air cavity depth and DSF facade type have a significant impact on the daylighting performance. Moreover, the results show that the discrepancies are largest in the area closest to the glazed facade. The article presents detailed results and discusses the effects of each variable on daylight levels.

Author Keywords

Double-skin facades; simulations; daylight; building performance

ACM Classification Keywords

I.6.1 SIMULATION AND MODELING

1 INTRODUCTION

Double skin facades (DSFs) are an emerging type of building facades, aimed at improving thermal performance of glazed envelopes. Different from conventional single glazed facades, DSFs consist of three distinct layers – interior glazed wall system, ventilated air cavity, and exterior glazed wall system. The ventilated air cavity serves as a thermal buffer between interior and exterior glazed wall. Basic DSF types are box window, corridor type, shaft box, and multistory facades [1]. The physical behavior of the DSFs depends on the typology, as well as the ventilation mode of the air cavity and material components. Ventilation mode can include natural ventilation, mechanical and mixed mode.

Since the DSFs consist of three distinct layers, the hypothesis for this research was that daylight levels would be decreased compared to a conventional curtain wall. The assumption is based on the premise that light transmittance reaching the interior space would be decreased in DSFs. However, it is not clear how different types of DSFs or relative orientation would affect daylight performance in various climates.

2 LITERATURE REVIEW

DSF systems provide a visual connection to the surrounding environment, as well as access to daylight [7]. Recent studies affirm DSFs' positive impact on energy efficiency [5]. DSFs are highly glazed, requiring the consideration for glare when attempting to provide daylight to interior spaces [3]. However, systematic research studies that evaluate daylighting performance of DSFs are currently very limited.

Viljoen et al. studied a 32-story Brussels DSF office building to evaluate daylighting performance [8]. Thirteen DSF assemblies were tested using scale models and computer simulations, assuming unobstructed sky view, assessing how far the daylit zone could extend into the office. Direct daylight was excluded from measurements assuming that occupants would use blinds to prevent direct sunlight from entering the building. A comparative study between a scale model and computer simulations using Radiance provided results. Results were analyzed for 50% daylight availability, as well as 35% for comparison using a standard CIE overcast sky [8]. It was concluded that the components of a DSF, a light shelf, reflectivity, perforation of materials, and location of walkways had significant effects on daylighting. Findings also indicated that glazing orientation and surface area would have significant impacts on daylighting [8]. The findings of this research study are applicable to buildings with DSFs, but lack comparison with single glazed facade daylighting.

Shameri et al. simulated daylighting conditions of twelve existing DSF offices located in tropical, subtropical, and temperate climate zones [6]. The analyzed facades had cavity depths ranging from 0.8 m to 2.5 m (2.6 ft to 8.2 ft), with glazed areas ranging from 70% to 100%. For simulations, light transmission values of all interior and exterior windows were assumed to be 0.76. Overcast illuminance values of 19,000; 12,000 and 6,000 lux (1,710; 1,080 and 540 fc) were used, and simulations were run using IES VE. The unique design of each DSF was found to cause significant differences in daylighting characteristics. At 12,000 and 6,000 lux (1080 and 540 fc), all models failed to achieve the minimum indoor illuminance requirement of at least 200 lux within 75% of the office space. The DSF with the smallest cavity depth (0.8 m or 2.6 ft) was found to perform best at 6,000 lux (540 fc) [6]. All DSF models failed to achieve standard indoor illuminance requirements (75%) of the office space. Daylighting percentages of 70%, 53%, and 32% at outdoor illuminance values of 19,000; 12,000 and 6000 lux (1,710; 1,080 and 540 fc) were observed.

Konis evaluated a 56,200 m^2 (605,000 ft^2) office building in San Francisco [4]. The northwest and southeast facades are fully glazed, allowing 0.67 visible light transmittance. The southeast facade is a DSF assembly. The northwest facade is a DSF with laminated glass and plastic fins used to block direct solar radiation in the afternoon. Roller shades were installed on the southeast facade in an effort to reduce glare and are manually operated. The study was conducted for a two to three-week period on upper floors and did not alter roller shade configurations, nor electrical lighting control patterns. On-site observations and an in-depth questionnaire provided subjective results, recording responses at four times per day. Subjective responses were paired with measurements of global horizontal illuminance and vertical luminance. Daylight illuminance levels were calculated by subtracting electrical lighting contributions from physical illuminance measurements. Participants were generally dissatisfied in the northwest perimeter zone due to views of direct sun, glare from unshaded upper windows and neighboring building surfaces, and the translucent fins. Respondents along the southeast perimeter noted glare associated with direct views of the sun, as well as reflections of the solar disk on the second skin facade. The daylight autonomy metric was used to evaluate daylight availability, requiring 75% of occupied spaces to be daylit [4]. Daylight transmission to the core zones was found to be insufficient based on subjective and physical measures. Daylight only contributed 15% of the total illuminance measured in core zones. Roller shade positioning and visual discomfort responses indicated that exterior solar control devices on the northwest and southeast facades provide inadequate glare control for occupants. The fins were sources of visual discomfort, reflecting an image of the solar disk [4]. Both the northwest and southeast exterior shading devices were unable to provide glare control for occupants leading to high use of interior roller shades, thus reducing the design intent of the high visual transmittance to maximize daylighting.

Most studies indirectly address daylighting while evaluating the performance of other effects of DSFs, leading to limited results and evaluations that pertain to specific buildings. A broader understanding of DSF impacts on daylighting is unavailable, thus was the focus of this research.

3 RESEARCH OBJECTIVES AND METHODS

The objectives of this research were to investigate the daylighting performance of three different typologies of DSFs (box window, corridor and multistory) in four different climates, and to compare to single skin facade (conventional curtain wall). Moreover, the objective was to investigate the impacts of DSF characteristics on daylight, specifically orientation and air cavity depth.

3.1 Research Questions

The research questions that were addressed include:

- How does the daylighting performance of DSFs (box window, corridor type and multistory) compare to that of conventional curtain wall?
- How is daylighting penetration depth affected by climate?
- How do different sky conditions impact DSFs' daylight performance?
- Does air cavity depth have a significant impact on DSFs' daylighting performance?
- How are daylighting values impacted by different facade orientations?

3.2 Research Methods

Modeling and simulation tools were utilized in the study to evaluate daylighting performance for box window, corridor type and multistory DSFs. The results were compared against the baseline model, consisting of a standard curtain wall (single skin facade). Figure 1 shows the basic properties of these different types of facade systems. Box window DSF consists of horizontal divisions between different levels, as well as vertical divisions and an air cavity between the two glazed surfaces. Corridor type DSF has horizontal divisions between different levels, but air can move freely within the air cavity within each individual level. Multistory DSF does not have any horizontal or vertical divisions, and air can move freely between different levels within the air cavity. In all DSF scenarios, curtain wall with double insulated glazing unit was placed on the interior side of the facade, while single glazing was situated on the exterior.

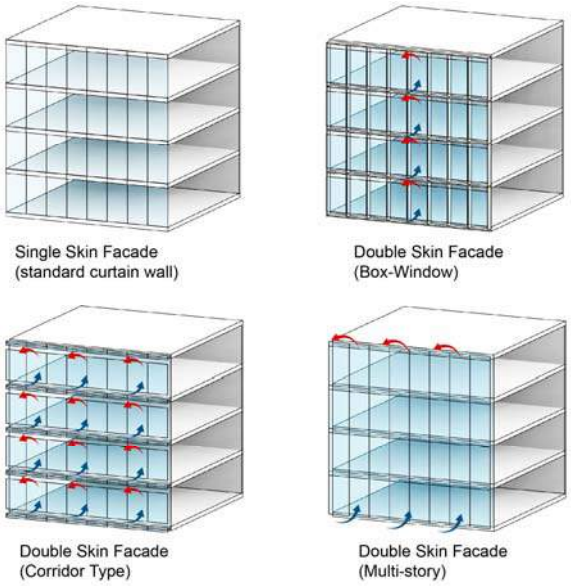

Figure 1. Double skin facade diagrams.

A detailed model of an office space was created in Revit, with an area of 12.6 m by 12.6 m (40 ft by 40 ft), and 3 m (10 ft) height. Different models were created to represent office space that would be enclosed with investigated facade types. Specifically, conventional curtain wall and DSFs with 0.6 m and 0.9 m (2 ft and 3 ft) cavity depths were modeled. Interior materials consisted of white paint on walls, carpet as flooring, and acoustic tile for the ceiling. This model was then imported into Ecotect, where the Radiance plugin was used to simulate daylight levels. Radiance takes into account geometry of the space and facade components, materials, time and date and sky conditions into account, and calculates lighting levels and glare indices.

All DSF facade systems used 25 mm (1 in.) double low-e insulated glazing unit (IGU) with argon gas fill on the interior side of the facade, and 13 mm (1/2 in.) single tempered glazing on the exterior side. Single skin facade consisted of 25 mm (1 in.) double air low-e IGU. The framing members for the typical curtain wall and the interior layer of the DSF included aluminum mullions. The outer layer of the DSFs did not include aluminum framing members—the assumption was that structural silicone would be used for glazing, and that the structural support for the facade would be provided by point-supports and cables. Exterior glazing visual transmittance was 0.79, while interior facade glazing was 0.63. The walls of the office space were modeled white plasterboard with a color reflection coefficient of 0.56, while floor and ceiling with a reflection coefficient of 0.59.

Four U.S. cities were used for daylight simulations: Duluth, Chicago, San Francisco, and Miami. Each city represents a different climate zone and latitude. These cities were selected to investigate differences between different climates and latitudes. The outdoor illuminance values that were used as inputs for the simulations are dependent on the latitude, date and time for each location, and are listed below.

Duluth is located in the humid continental Koppen climate zone (Dfb) and IECC zone 7. The daylight hours for Duluth range from 15:51:56 hours (summer solstice) to 8:32:13 hours (winter solstice). Typical outdoor illuminance is 72,800 lux (6,763 fc) during the summer, and 6,400 lux (595 fc) during the winter. Summer months are significantly sunnier than winter months. Chicago is located in the humid continental climate Koppen zone (Dfa) and IECC zone 5. The daylight hours of Chicago range from 15:13:43 hours (summer solstice) to 9:07:43 hours (winter solstice). Typical outdoor illuminance is 73,000 lux (6,782 fc) during the summer, and 7,300 lux (678 fc) during the winter. Monthly mean sunshine hours range from 318.4 hours in July to 106 hours in December. Summer months are significantly sunnier than winter months. San Francisco is located in the cool-summer Mediterranean Koppen climate zone (Csb) and IECC zone 3. The daylight hours of San Francisco range from 14:46:57 hours (summer solstice) to 9:32:50 hours (winter solstice). Typical outdoor illuminance is 77,300 lux (7,181 fc) during the summer, and 8,800 lux (818 fc) during the winter. Monthly mean sunshine hours range from 235.1 hours in May to 160.6 hours in December. The months of March through July experience more sunshine than the months of July through March. Miami is located in the tropical monsoon climate Koppen zone (Am) and IECC zone 1. The daylight hours of Miami range from 13:44:53 hours (summer solstice) to 10:31:46 hours (winter solstice). Typical outdoor illuminance is 82,000 lux (7,618 fc) during the summer, and 12,000 lux (1,115 fc) during the winter. Monthly mean sunshine hours range from 301.3 in May to 216.1 in December. Little variation occurs in monthly mean sunshine hours.

The baseline model was a standard curtain wall, while all other models were enclosed by different types of DSF (box window, corridor type, and multistory). Each facade type was simulated under three different sky conditions: overcast, partly cloudy, and clear conditions for each location with global illuminance values derived from the weather file. Each DSF was tested with 0.6 m and 0.9 m (2 ft and 3 ft) cavities. The models analyzed four different orientations (north, south, east and west). Simulations were run for the following dates: July 21, January 21, and October 21, at a time of 2 PM for all locations. A value of 500 lux (45 fc) was used as the minimum threshold for the office space to be lit by daylight. A dataset of 336 simulations was produced. Figure 2 shows typical results (floorplan view), while Figure 3 shows three dimensional daylight distribution within the interior for one of the models.

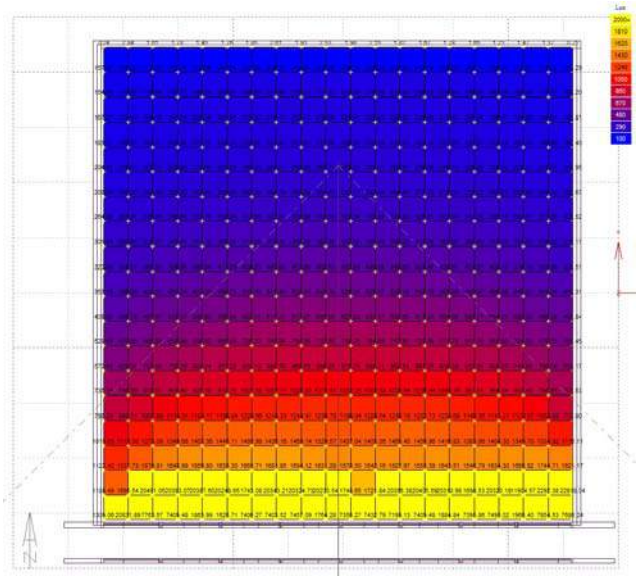

Figure 2. Radiance output (floorplan view).

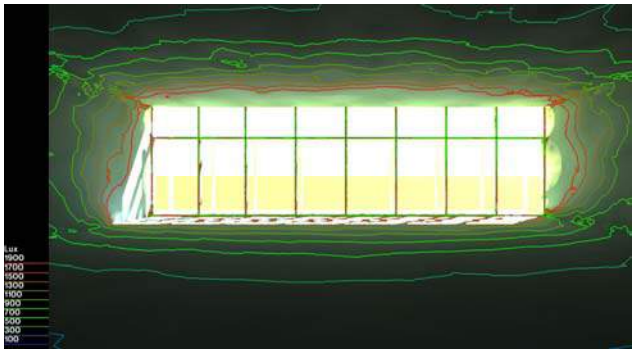

Figure 3. Radiance 3D daylighting visualization.

4 RESULTS

Results of simulations indicated daylight levels (in lux) within the interior space for all models. The data was analyzed, and daylight distribution within the interior space was plotted to visualize results and compare each facade type's performance. DSFs reduced the amount of daylight passing through the building skin significantly compared to conventional single skin facade. However, multistory consistently was the best performing DSF type. The following sections discuss results in more detail, as well as daylight performance threshold analysis.

4.1 Daylighting Results

All graphs show a decreasing amount of daylight as distance from the facade increases within the office space. Selected graphs are shown in Figures 4 to 8. However, the differences in daylighting values between DSFs and the single skin are reduced as the distance from the facade increases.

Outlier daylight values were observed on the southern and western facades during summer months. These anomalies in data indicate direct sun passing through the facade, which can cause glare. Miami was the only location in which southern exposure glare was not observed during summer months, possibly due to its latitude and high position of the sun.

The box window facade exhibits the most consistent daylight results. It typically causes lower daylighting levels closer to the facade than other DSFs, but extends daylight deeper into the space for more northern latitudes, compared to other DSFs. This facade type appears to eliminate glare, except during the summer on the western facade.

Duluth

Duluth exhibited lower lighting levels in the northern and eastern orientations compared to other locations. Figure 4 shows daylight distribution within the interior space for intermediate cloud conditions, north orientation, and 0.6 m (2 ft) deep air cavity for all investigated DSFs. In the southern and western orientations, it experienced higher lighting levels than the other cities during the summer, due to the lower sun angles. In the same orientations during the fall and winter, Duluth experienced similar or lower lighting levels than the other cities. North and east facades had considerably lower lighting levels than the south and west facades, regardless of the season.

Summer months displayed anomalies in data in the western orientated model closest to the facade, with very high daylighting values. These months also feature a dramatic difference between the typical facade and DSF's on the western and southern facades, notably in July. During the summer months, the southern facade experiences some of the highest daylight values observed close to the facade. However, these values quickly decrease 2.4 m (8 ft) from the facade. Minimal differences were observed between the 0.6 m and 0.9 m (2 ft and 3 ft) air cavity depths for the box window DSF, while the multistory and corridor type experienced greater variation.

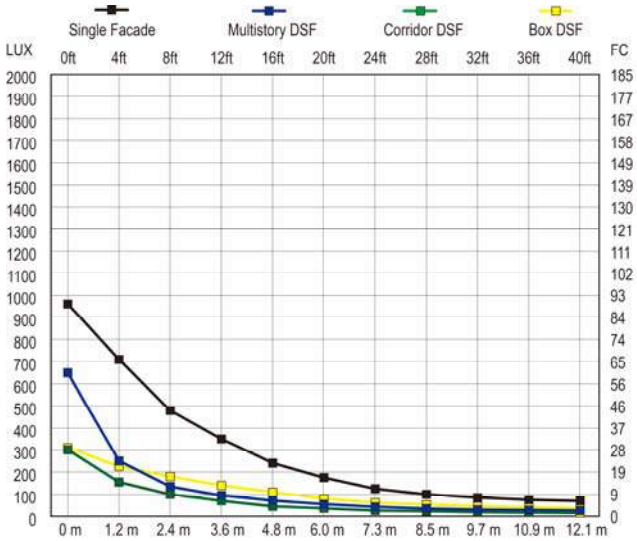

Figure 4. Daylight distribution results for Duluth, October, north facing, 0.6 m (2 ft) DSFs' cavity.

Chicago

Chicago's results were similar to those of Duluth. North and east facades had considerably lower lighting levels than the south and west, regardless of the time of year. Figure 5 shows daylight distribution within the interior space for partly cloudy conditions, south orientation, and 0.6 m (2 ft) deep air cavity for all investigated DSFs.

The month of July featured anomalies in data in the western and southern orientations close to the facade. The southern and western facades did not receive extremely high daylight levels during the intermediate months, as opposed to the summer. The 0.9 m (3 ft) air cavity DSFs in the south and west orientations have higher daylight values, particularly closer to the office perimeter, 0 m to 6 m (0 to 20 ft) range.

In general, the daylight performance of the single skin facade is the best, followed by the multistory DSF, the corridor DSF, and finally the box window DSF. In most cases, the 0.6 m (2 ft) box window DSF outperformed the other DSF types, while the 0.9 m (3 ft) box window DSF performed the worst. The multistory DSF consistently has the highest daylight values closest to the facade, but reduces as the distance from the facade increases.

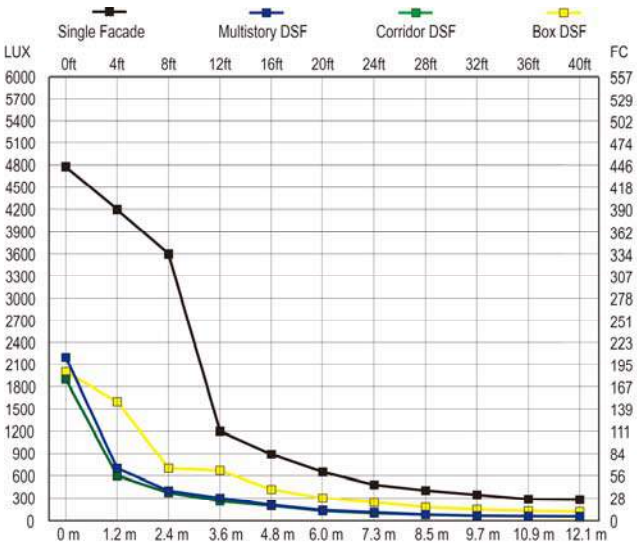

Figure 5. Daylight distribution results for Chicago, October, south facing, 0.6 m (2 ft) DSFs' cavity.

San Francisco

DSF performance during summer months is worse compared to previously mentioned cities, as the decreasing latitude results in the sun being higher in the sky, and less direct light reaching the interior space. The box window DSF with 0.6 m (2 ft) air cavity brings in the most light across the full depth of the space, except immediately adjoining the facade, where the multistory DSF outperforms all others.

The west orientation during July experiences the greatest variation in light levels, while all orientations during January experience the least variation. The multistory DSF performs best with a 0.9 m (3 ft) air cavity depth and outperforms all other DSFs. As with Duluth, an anomaly in the multistory DSF occurs on the south facade during the intermediate months, as seen in Figure 6, where a rise in daylight values occurs 3.7 m (12 ft) from the facade.

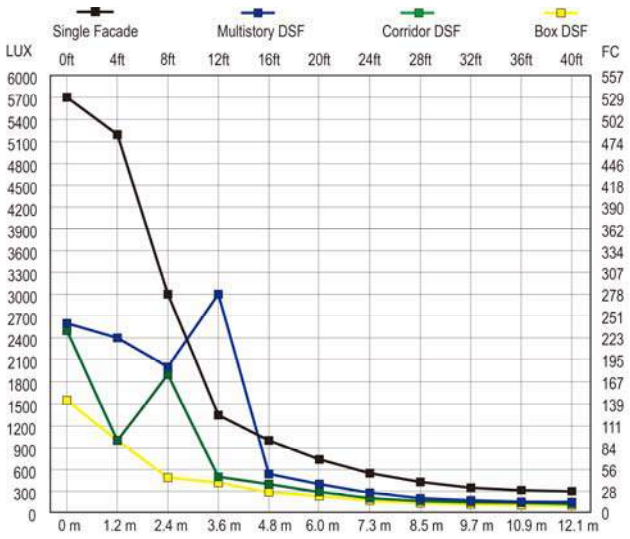

Figure 6. Daylight distribution results for San Francisco, October, south facing, 0.9 m (3 ft) DSFs' cavity.

Miami

Miami's daylighting results are unique in comparison to the other locations. The north and east facades feature lower lighting levels than the south and west during summer months, as is typically the case with the other locations. Figure 7 shows results for north orientated facades, and with 0.9 m (3 ft) air cavity DSFs. The southern orientation is the only case that does not exhibit extremely high daylight levels close to the facade in July (for all facade types), as seen in Figure 7. However, the western orientation exhibits high values during the summer months.

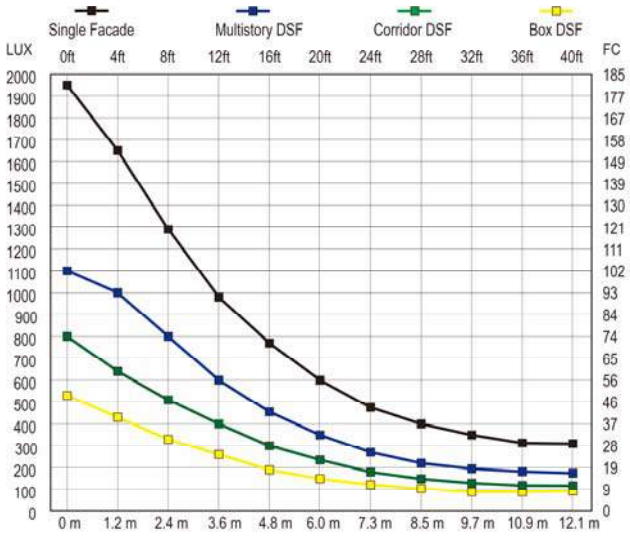

Figure 7. Daylight distribution results for Miami, July, north facing, 0.9 m (3 ft) DSFs' cavity.

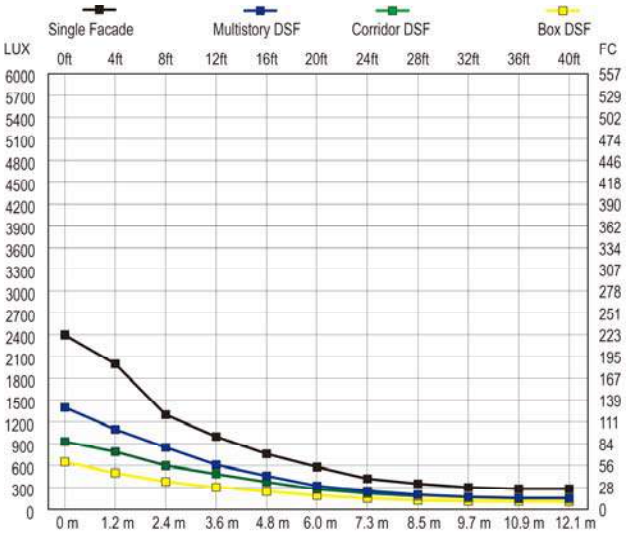

Figure 8. Daylight distribution results for Miami, July, south facing, 0.9 m (3 ft) DSFs' cavity.

In general, the daylighting performance of the single skin facade is the best, followed by the multistory DSF, the corridor DSF, and finally the window box DSF. The box window appears to most effectively transmit light into the interior when a 0.6 m (2 ft) depth of air cavity is used. The box window DSF with a 0.9 m (3 ft) air cavity performs poorly when compared to other facade types.

The multistory DSF performs best closer to the perimeter, but its performance significantly reduces farther from the facade, where it reaches equal or lower levels of light compared to other DSFs, depending on the cavity depth. Both the multistory DSF and corridor DSF perform better than the box window closer to the perimeter, but values quickly diminish as distance increases. Both the multistory and corridor type DSF perform better with the 0.9 m (3 ft) cavity configuration.

Miami features winter lighting levels that are higher than the other cities analyzed. The north orientation during the winter months sees the most consistency in lighting levels for all DSF types with 0.6 m (2 ft) air cavity.

4.2 Daylighting Performance Threshold Analysis

Daylighting performance was analyzed using a 500 lux (46 fc) threshold to observe what percentage of the office space would be adequately daylit for each simulation model.

North Facade

The north facade data indicates that the multistory and corridor DSFs perform better with a 0.9 m (3 ft) cavity, while the box window performs best with a 0.6 m (2 ft) cavity, as seen in Table 1. During July, the northern locations saw greater variation in the results for different DSF types (Duluth: 0% - 30%), while southern locations indicated more uniform results across five of the six investigated DSF types (Miami: 21% - 37%).

During intermediate and winter months, the daylighting performance at higher latitudes decreased significantly, while performance in lower latitudes saw less of a reduction. During January, results indicate that 54% of the investigated scenarios would not have sufficient daylight (0% of the floor area received more than 500 lux). Similar results are evident for intermediate months, especially for the box window and corridor DSF types. There is a significant reduction in performance between the 0.9 m (3 ft) and 0.6 m (2 ft) multistory facade during summer months. During intermediate and winter months, 0.6 m (2 ft) multistory DSFs perform more consistently across all latitudes than their deeper counterparts, although at reduced light levels. The 0.9 m (3 ft) box window DSF is the poorest performer, with observed daylighting values consistent at 0%.

Orientation	Time	Facade Type	Duluth	Chicago	San Francisco	Miami
North	July	Single	46%	54%	56%	57%
		2 Foot Multistory	7%	14%	17%	24%
		3 Foot Multistory	**30%**	**33%**	**35%**	**37%**
		2 Foot Corridor	6%	7%	8%	21%
		3 Foot Corridor	13%	14%	16%	22%
		2 Foot Box Window	10%	13%	17%	22%
		3 Foot Box Window	0%	0%	0%	4%
	October	Single	18%	24%	23%	30%
		2 Foot Multistory	4%	5%	4%	7%
		3 Foot Multistory	**5%**	**7%**	**8%**	**17%**
		2 Foot Corridor	0%	0%	0%	2%
		3 Foot Corridor	0%	0%	3%	1%
		2 Foot Box Window	0%	0%	0%	0%
		3 Foot Box Window	0%	0%	0%	0%
	January	Single	17%	24%	27%	52%
		2 Foot Multistory	**3%**	4%	6%	8%
		3 Foot Multistory	0%	**5%**	**14%**	**20%**
		2 Foot Corridor	0%	0%	0%	2%
		3 Foot Corridor	0%	0%	5%	7%
		2 Foot Box Window	0%	0%	0%	6%
		3 Foot Box Window	0%	0%	0%	0%

Table 1. North orientation: percentage of the floor area daylit above 500 lux (46 fc) at ground level.

East Facade

The east facade performs similarly to the northern facade (Table 2). Data indicated that the multistory with a 0.9 m (3 ft) cavity performs the best in most cases, out of all DSF types, as seen in Table 2. The multistory with a 0.9 m (3 ft) cavity provides enough daylight for 27-36% of the investigated office space. During intermediate months, 11-20% of the floor area has sufficient natural light, while 0-23% during winter months. This facade shows less variation in daylighting values in Miami across seasons, while northern latitudes see a larger variation from summer to winter. The 0.9 m (2 ft) multistory DSF shows minimal variation in percentages across different latitudes; values observed decrease during intermediate and winter months, but remain relatively consistent across latitudes. The 0.9 m (3 ft) box window DSF performs poorly, with daylit percentages of 0% observed across all times of year. The 0.6 m (2 ft) box window and corridor DSFs admit some daylight during summer months (0-24%), but admit an average of 0% during intermediate and winter months.

Orientation	Time	Facade Type	Duluth	Chicago	San Francisco	Miami
East	July	Single	46%	50%	54%	55%
		2 Foot Multistory	7%	13%	15%	16%
		3 Foot Multistory	**27%**	**30%**	**31%**	**36%**
		2 Foot Corridor	0%	6%	8%	10%
		3 Foot Corridor	16%	17%	24%	20%
		2 Foot Box Window	6%	10%	20%	24%
		3 Foot Box Window	0%	0%	0%	0%
	October	Single	23%	27%	29%	31%
		2 Foot Multistory	7%	6%	7%	7%
		3 Foot Multistory	**11%**	**12%**	**26%**	**20%**
		2 Foot Corridor	0%	0%	0%	0%
		3 Foot Corridor	0%	0%	3%	4%
		2 Foot Box Window	0%	0%	0%	1%
		3 Foot Box Window	0%	0%	0%	0%
	January	Single	16%	23%	26%	33%
		2 Foot Multistory	**7%**	4%	5%	8%
		3 Foot Multistory	0%	**4%**	**14%**	**23%**
		2 Foot Corridor	0%	0%	0%	2%
		3 Foot Corridor	0%	1%	1%	7%
		2 Foot Box Window	0%	0%	0%	6%
		3 Foot Box Window	0%	0%	0%	0%

Table 2. East orientation: Percentage of the floor area daylit above 500 lux (46 fc) at ground level.

South Facade

The southern orientation provides significantly higher daylighting percentages than north or east orientations, shown in Table 3. It was observed that locations with higher latitudes indicated higher light levels during July and October, while lower latitudes showed greater levels during the winter. Both summer and intermediate results indicate that significant daylighting can be achieved, with less variation across seasons compared to other orientations. However, winter months show a significant reduction in daylighting values. Results indicate the 0.9 m (3 ft) cavity multistory DSF performs best, compared to other DSF types, with 37-46% of the space daylit above 500 lux during summer months. During intermediate months, daylighting values rage from 40-49% of the floor area, while the values during winter range from 0-20%. The second best performing DSF varies for each season. The 0.9 m (3 ft) corridor DSF performs well in the summer, 0.9 m (2 ft) box window in October, and the 0.6 m (2 ft) multistory in the winter. The northern latitudes saw less variation across all DSF types compared to the southern latitudes. Winter months provide the lowest levels of daylighting, with daylit floor percentages being around 0% for more than half of the DSF types. Overall, southern oriented DSFs perform best during intermediate and summer months.

West Facade

The west facade results indicate that this particular orientation has the highest potential for DSF daylighting during summer months, shown in Table 4. However, all of the data indicated large amounts of daylight within 1.2 m (4 ft) perimeter zone from the facade. This contributed to higher light levels deeper in the space, but if solar shading is used to control glare, light levels would be reduced further into the space. This was the only orientation where the single glazed facade resulted in values of 100% for all climates. During the summer, the 0.6 m (2 ft) box window DSF performed the best in Duluth (67%) and Chicago (66%), while the 0.9 m (3 ft) multistory DSF performed the best in San Francisco (54%) and Miami (52%). During the intermediate months, the 0.9 m (3 ft) multistory DSF performed the best (35-37%), while in January, it performed the best in all locations except Duluth. West oriented DSFs offer the highest daylighting values compared to other orientations during summer months. Minimal daylighting percentages are provided during winter months (although higher than north and east orientations).

Orientation	Time	Facade Type	Duluth	Chicago	San Francisco	Miami
South	July	Single	70%	70%	60%	55%
		2 Foot Multistory	34%	25%	24%	24%
		3 Foot Multistory	**46%**	**45%**	**45%**	**37%**
		2 Foot Corridor	25%	18%	17%	13%
		3 Foot Corridor	42%	30%	29%	28%
		2 Foot Box Window	40%	38%	33%	24%
		3 Foot Box Window	23%	20%	15%	11%
	October	Single	63%	60%	64%	64%
		2 Foot Multistory	18%	16%	20%	18%
		3 Foot Multistory	**49%**	**42%**	**44%**	**40%**
		2 Foot Corridor	18%	14%	15%	15%
		3 Foot Corridor	37%	30%	30%	30%
		2 Foot Box Window	38%	37%	38%	34%
		3 Foot Box Window	36%	24%	20%	20%
	January	Single	17%	22%	26%	33%
		2 Foot Multistory	**3%**	4%	6%	8%
		3 Foot Multistory	0%	**5%**	**15%**	**20%**
		2 Foot Corridor	0%	0%	0%	2%
		3 Foot Corridor	0%	0%	1%	7%
		2 Foot Box Window	0%	0%	0%	6%
		3 Foot Box Window	0%	0%	0%	0%

Table 3. South orientation: percentage of the floor area daylit above 500 lux (46 fc) at ground level.

Orientation	Time	Facade Type	Duluth	Chicago	San Francisco	Miami
West	July	Single	100%	100%	100%	100%
		2 Foot Multistory	40%	42%	36%	36%
		3 Foot Multistory	51%	56%	**54%**	**52%**
		2 Foot Corridor	33%	35%	30%	27%
		3 Foot Corridor	43%	46%	44%	37%
		2 Foot Box Window	**67%**	**66%**	50%	47%
		3 Foot Box Window	29%	36%	28%	27%
	October	Single	49%	58%	49%	56%
		2 Foot Multistory	7%	15%	16%	17%
		3 Foot Multistory	**37%**	**35%**	**36%**	**37%**
		2 Foot Corridor	8%	10%	10%	13%
		3 Foot Corridor	27%	29%	27%	27%
		2 Foot Box Window	25%	32%	28%	30%
		3 Foot Box Window	7%	14%	16%	15%
	January	Single	17%	22%	27%	32%
		2 Foot Multistory	**3%**	4%	5%	8%
		3 Foot Multistory	0%	**5%**	**13%**	**20%**
		2 Foot Corridor	0%	0%	0%	2%
		3 Foot Corridor	0%	0%	0%	7%
		2 Foot Box Window	0%	0%	0%	6%
		3 Foot Box Window	0%	0%	0%	0%

Table 4. West orientation: percentage of the floor area daylit above 500 lux (46 fc) at ground level.

5 CONCLUSION

The purpose of this research was to investigate the effects of different DSFs on daylighting performance. The research focused on several objectives: 1) to analyze the daylight levels in different types of DSFs (box window, corridor type, and multistory) in four different climates; 2) to compare daylight performance against the conventional single skin glazed facade (curtain wall); 3) to investigate the effects of facade orientations (north, south, east and west) on daylight; and 4) to investigate the effects of specific characteristics (different depths of air cavity in DSFs) on daylight levels. Research methods consisted of simulations and modeling. Detailed models were created in Revit and were used for daylight simulations in Radiance to calculate daylight levels.

Results indicate that all types of DSFs would decrease daylight levels compared to a conventional curtain wall, however, the differences between lighting levels are dependent on the orientation, air cavity depth, facade type and climate. Moreover, the results show that the discrepancies are largest in the area closest to the glazed facade. The 0.9 m (3 ft) multistory DSF consistently performed the best across most locations and orientations. For northern latittudes, box window DSF with 0.6 m (2 ft) air cavity performed the best.

Glare is also more likely to occur at higher latitudes, and vertical and horizontal divisions in box window and corridor DSFs can block some of that glare depending on the facade type and orientation. North DSFs exhibited less variation in light levels, due to the absence of direct sunlight entering the space.

Cavity depth appears to influence DSF daylighting in ways that were not anticipated. Multistory and corridor type DSFs showed noticeably better performance with 0.9 m (3 ft) cavities compared to 0.6 m (2 ft) cavities. Box window DSFs showed better performance in a 0.6 m (2 ft) configuration than with a 0.9 m (3 ft) cavity.

Further research could connect simulation data to measured performance, where existing DSFs could be investigated and measured lighting levels could be used to investigate relationships between orientation, facade typology, climate and effects on daylight. However, one of the major challenges is to identify existing buildings that have similar types of DSFs in different climate types.

REFERENCES

1. Aksamija, A. *Sustainable Facades: Design Methods for High-Performance Building Envelopes*. John Wiley & Sons, Hoboken, NJ, USA, 2013.
2. Bueno, B., Wienold, J., Katsifaraki, A. and Kuhn, T. Fener: A Radiance-Based Modelling Approach to Assess the Thermal and Daylighting Performance of Complex Fenestration Systems in Office Spaces, *Energy and Buildings 94*, 1 (2015), 10-20.
3. Ghaffarianhoseini, A., Ghaffarianhoseini, A., Berardi, U., Tookey, J., Li, D. and Kariminia, S. Exploring the Advantages and Challenges of Double-Skin Facades (DSFs), *Renewable and Sustainable Energy Reviews 60,* 2016, 1052-1065.
4. Konis, K. Evaluating Daylighting Effectiveness and Occupant Visual Comfort in a Side-Lit Open-Plan Office Building in San Francisco, California, *Building and Environment 59*, 2013, 662-677.
5. Pomponi, F., Poorang A., Piroozfar, Southall, R., Ashton, P. and Farr, E. Energy Performance of Double-Skin Facades in Temperate Climates: A Systematic Review and Meta-Analysis, *Renewable and Sustainable Energy Reviews 54*, 2016, 1525-1536.
6. Shameri, M., Alghoul, M., Elayeb, O., Fauzi M., M. Zain, M., Halizawati A. and Sopian, K. Daylighting Characteristics of Existing Double-Skin Facade Office Buildings, *Energy and Buildings 59*, 2013, 279-286.
7. Shameri, M., Alghoul, M., Sopian, K., Fauzi M., Zain, M. and Elayeb, O. Perspectives of Double Skin Facade Systems in Buildings and Energy Saving, *Renewable and Sustainable Energy Reviews 15*, 3 (2011), 1468-1475.
8. Viljoen, A., Dubiel, J., Wilson, M. and. Fontoynont, M. Investigations for Improving the Daylighting Potential of Double-Skinned Office Buildings, *Solar Energy 59*, 4 (1997), 179-194.

Geometry-Material Coordination for Passive Adaptive Solar Morphing Envelopes

Sarah Mokhtar[1], Christopher Leung[1] and Angelos Chronis[2]

[1]University College London
London, United Kingdom
sarah.mokhtar.15@ucl.ac.uk, christopher.leung@ucl.ac.uk

[2]Intitute for Advanced Architecture of Catalonia
Barcelona, Spain
angelos.chronis@iaac.net

ABSTRACT

The cost-intensive and mechanical complexity natures of the adaptive facades of the past decades drifted designers and researchers' interest towards passive material-based actuation systems [5, 6, 10]. Architectural applications using the latter showed, however, a few limitations restricting the output possibility space to options that rely entirely on one material's phase characteristic. This study aims to investigate the potential of expanding a shape memory alloy-actuated facade's output from one that is limited and hardly controllable in the case of entirely passive actuation to one that can produce a specific desired performative target. This is explored through coordinating between geometry-movement connections of an adaptive component of four integrated shape memory alloys, which work on tailoring the geometry-material-climate relations of the responsive system. The research findings suggest that the integration of geometry, material, and their connections in the design of a SMA solar morphing envelope lead to the development of a wider range of behavioural system outputs. The variety instilled through these added dimensions promoted diversity and adaptability of output for a flexible range of responses and higher performative gains.

Author Keywords

Material Computation; Requisite Variety; Solar Morphing Envelopes; Smart Materials.

1 INTRODUCTION

The cost-intensive and mechanical complexity natures of the adaptive facades of the past decades drifted designers and researchers' interest towards passive material-based actuation systems [5, 6, 10]. Architectural applications using the latter showed, however, a few limitations restricting the output possibility space to options that rely entirely on one material's phase characteristic.

The Adaptive Skins and the Self-Adaptive Membrane projects [3, 12] constitute examples of applications utilizing solar radiation as the thermal trigger for shape memory alloy (SMA)[1]-actuation of their components. Each component was developed as an integration of several shape memory alloys (SMAs), and thus created wider geometrical possibilities through larger degrees of freedom on the components scale, overcoming the linearity of their material activation. These reflected the potentials of diversifying the material-based actuated components' outputs through careful design of the geometry-system relations.

The shift in the perception of materials' innate capabilities favour the understanding of this domain as computational, rather than mere situational convenience. A material can be recognized as an entity being at one state at any moment in time, the actual state; while having other available virtual states. Triggering the latter into actuality requires catalysts that can either be the manifestation of an essence or the force driving it into obtaining a certain form [2]. DeLanda explains that:

"a richer conception of causality linked to the notion of the structure of a possibility space gives us the means to start thinking about matter as possessing morphogenetic powers of its own".

An unveiling of these powers would thus require an understanding of the underlying system's production mechanism, and its possibility space's structure which includes its stable states and transitions between them [2]. By identifying the material system's rules and input variability, the resulting material's behaviour[2] can potentially be computed, predicted, or defined.

The material behaviour's complexity and the successful attempts in architectural applications suggest there are implications of material computation's concept for expanding the possibilities of its applicability through understanding, controlling and diversifying material triggers.

This study aims to investigate the potential of expanding a SMA-actuated facade component's output entirely passively from one that is limited to one that is capable of producing a specific desired performative target. This is explored through coordinating between geometry-movement connections of a 4-SMAs adaptive component, which works on tailoring geometry-material-climate relations of the adaptive system.

[1] SMAs are alloys that undergo lattice phase transformations, deforming in cold temperatures and recovering shape when heated [8].

[2] Considered as the computational system's output.

2 METHODOLOGY

To investigate the potentials of geometry-material-climate for a façade system actuated by shape memory alloys (SMAs), a case study context and its desired performative outputs are identified followed by a simplified SMA thermal model, pre-calculation of solar irradiation values for SMAs, and a coordination computational model used to carry out the study.

2.1 Case Study SMA Shading Structure

A generic 9 by 6 shading grid for a south-oriented façade in Cairo-Egypt climate is utilized using shape-memory actuated geometries of 400mm square panels [7]. Nine shading forms, shown in Figure 1, are considered, actuated using 4 shape memory alloys located on the four corners of the panel, illustrated in Figure 2. This system's design and performance evaluation (daylighting, solar incidence and openness) carried out in an in-depth previous study [7] was used to identify twenty desired performative configurations to test in this research. Each configuration consists of a façade combination of two of the nine shading forms, one for the upper portion of the façade grid and the other for the lower portion.

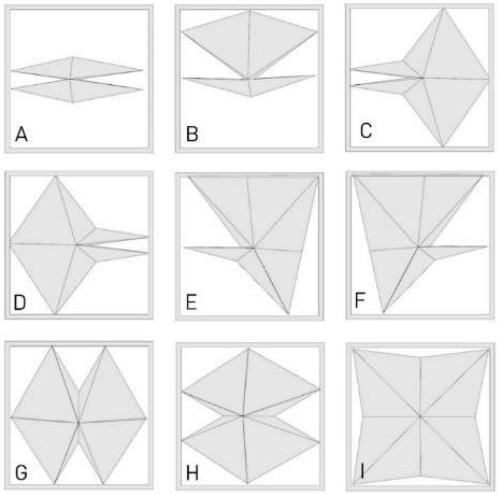

Figure 1. Nine Investigated Geometries [7]

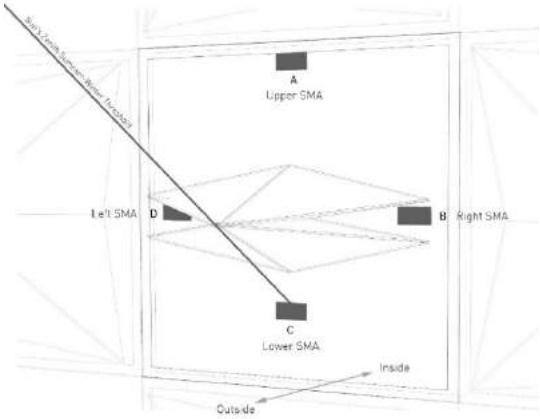

Figure 2. SMA Geometry Locations [7]

2.2 Simplified SMA Thermal Model

Modelling the SMA behaviour was necessary for the prediction of the actuation dynamics and material limitations. Due to the complexity and ambiguity in SMA behaviour models, a simplified approach was used for the estimation of the material temperature in the exterior environment. These calculations were performed for comparative objectives, contrasting different states under selective configurations, rather than for exact predictions.

According to the first law of thermodynamics, a system's total energy is conserved [4, p.13]. In general terms, under equilibrium conditions, the heat stored in the material can be defined as the thermal energy generated by an external source minus thermal losses due to conduction, convection and radiation as defined in Equation A from [11]:

$$\rho C V \frac{dT}{dt} = Q_e - Q_{conduction} - Q_{convection} - Q_{radiation} \quad \text{(A)}$$

where:

ρ	density of the SMA	in $kg \cdot m^{-3}$
C	specific heat capacity of the SMA	in $J \cdot kg^{-1} \cdot K^{-1}$
V	volume of the SMA	in m^3
T	temperature of the SMA at time t	in K
Q	thermal energy	in J

Q_e, where solar radiation is the source of external heat, the incident solar radiation on a material's surface is calculated; while the absorbed portion of that energy can be identified in correspondence with the material's capacity to absorb as described in Equation B from p.10 [4]:

$$Q_e = G_{abs} = \alpha s G = \varepsilon s G \quad \text{(B)}$$

where:

Q_e/G_{abs}	thermal energy absorbed by SMA	in W
α	absorptivity of the SMA	
s	surface area of the SMA	in m^2
G	solar irradiation	in $W \cdot m^{-2}$
ε	emissivity of the SMA, defined as equal to absorptivity in equilibrium	

For a large number of applications, $Q_{radiation}$ effect can be neglected, while $Q_{convection}$ can be expressed in Equation C from [11]:

$$Q_{convection} = hs(T - T_e) \quad \text{(C)}$$

where:

Q_{conv}	convective thermal energy loss	in W
h	heat-exchange coefficient between the SMA and medium	in $W \cdot m^{-2} \cdot K^{-1}$
T_e	temperature of the surrounding	in K

A common neglect of conduction for metallic alloys is justified by the assumption of temperature uniformity in the material because of its low internal heat conduction resistance. A 0.01 value for the Biot number is considered a

verification of the validity of that assumption, calculated with Equation D from [11].

$$B_i = \frac{hl}{k} \quad \text{(D)}$$

where:

B_i Biot number
l characteristic length, as wire diameter in m
k thermal conductivity of the SMA in $W \cdot m^{-1} \cdot K^{-1}$

The heat transfer SMA equation, modelling the SMA behaviour, can thus be simplified to Equation E as follows:

$$\rho CV \frac{dT}{dt} = \varepsilon sG - hs(T - T_e) \quad \text{(E)}$$

The heat exchange coefficient h, in convection, can be defined as function of the SMA thermal conductivity and characteristic length, defined as the wire volume per surface area as expressed in Equation F from [11]:

$$h = \frac{\lambda N_u}{l} \quad \text{(F)}$$

where:

λ thermal conductivity of the convective medium in $W \cdot m^{-1} \cdot K^{-1}$
N_u Nusselt number, defining the heat-exchange ratio in free convection

The Nusselt number, though, can be calculated using the characteristic Prandtl and Grashof numbers for the convective medium, air, were defined in Equation (G) from [11]:

$$N_U = \left(0.6 + \frac{0.387(G_r P_r)^{\frac{1}{6}}}{\left[1+(0.559/P_r)^{\frac{9}{16}}\right]^{\frac{8}{27}}} \right)^2 \quad \text{(G)}$$

where:

P_r Prandtl number for the convective medium
G_r Grashof number for the convective medium

Because of the phase change transformation and hysteresis of the SMA behaviour, the exact behaviour required further calculations of latent heat and adjustment of some temperature-dependent properties. Integrating the added stress from the component's weight would be necessary for an exact temperature, but was assumed here to be a light weight material hence negligible. Geometric properties were identified based on the required actuation length for the full geometry movement, suitable spring diameters and thicknesses. Due to the more common availability of SMA with various activation temperatures commercially produced and the possibility of their tailoring to the design needs, a range of temperatures were considered ranging from 20 to 100℃.

Despite the wide variation in shape memory alloy types in terms of composition and transformation temperatures and their differentiated properties, thermal properties considered were values provided by a SMA material supplier for the most commonly used type, emissivity value estimated by experimental testing and air properties from similar SMA research [11, 13].

The following Table 1 identifies the geometric and physical properties of the SMA used for the approximate material behaviour modelling.

Table 1. Thermal and Physical SMA Characteristics and Convective Medium

Property	Value	Unit
SMA Thermal Properties		
Density ρ	6450	$kg \cdot m^{-3}$
Specific heat C	837	$J \cdot kg^{-1} \cdot K^{-1}$
Thermal conductivity k	18	$W \cdot m^{-1} \cdot K^{-1}$
Emissivity ε	0.82	-
Air Properties (20℃)		
Thermal conductivity λ	0.0257	$W \cdot m^{-1} \cdot K^{-1}$
Grashof number G_r	0.3903	-
Prandtl number P_r	0.713	-
Geometric and Calculated Properties		
Surface Area S	0.003142	m^2
Volume V	3.93×10^{-7}	m^3
Nusselt number N_u	0.739	-
Characteristic length l	5×10^{-4}	m
Heat-exchange coefficient h	38	$W \cdot m^{-2} \cdot K^{-1}$

2.3 SMAs Solar Irradiation Pre-Calculations

Per the thermal model examined in the previous section, the estimation of SMA temperature required two main input variables: the air temperature and the incident solar radiation on each SMA for a designated time and geometry. A representative time sample of the year was identified as hours ranging from 08:00 to 17:00 on the 21st of March, June, September and December, the equidoxes and solstices.

For each of the possible geometrical configurations, a solar irradiation analysis was carried out using Radiance engine through Ladybug[3] for the 40 selected hours of study, of which a sample is illustrated in Figure 3. The corresponding air temperature values were then extracted from Cairo EnergyPlus weather file. These radiation and air temperature values were pre-calculated and saved to reduce the necessary computational time for the coordination impacts investigations.

[3] Ladybug is an open source plugin that help evaluate and visualize environmental performance using imported data from EnergyPlus weather files [9]

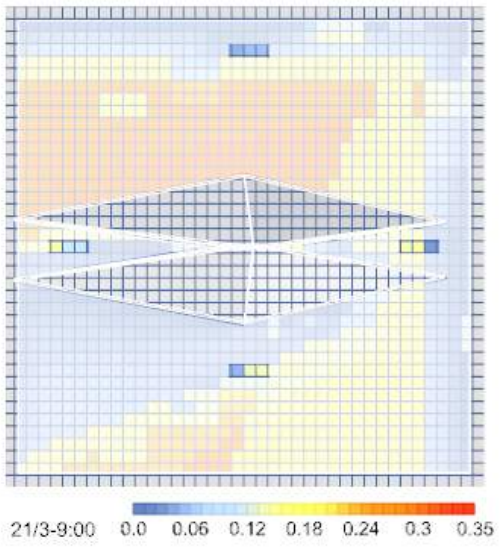

Figure 3. SMA Solar Irradiation Simulation

2.4 Coordination Computational Model

This section describes the methodology used to generate the SMA system characteristics necessary for the production of the desired adaptive output. These characteristics include the actuation temperatures of the four SMAs as well as their corresponding connections between actuators and movement. This approach regards the material system solution as an outcome of the interaction between the context, the performance, the material and the geometry, as illustrated in Figure 4.

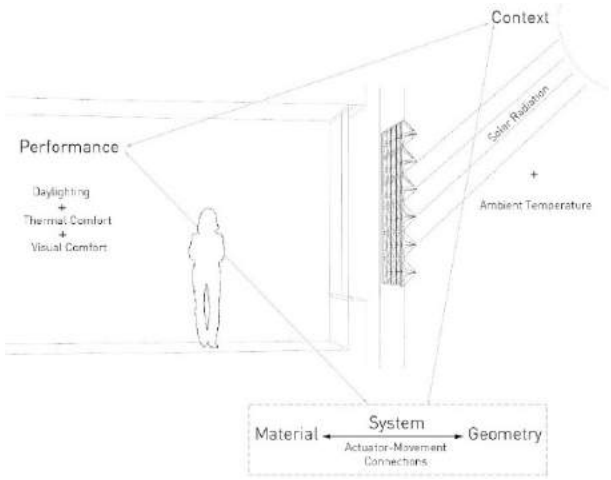

Figure 4. Context-Performance-Material-System-Geometry Interactions

All the connection configurations were identified, where one actuator can only be responsible for the deployment of one or two sides, shown below in Figure 5. The rationale behind excluding the combinations where one actuator can move three or four sides was that it reduced the variability highly desired in this research. This resulted in SMA systems consisting of two, three or four SMAs depending on performative need and behaviour. Finding the most conforming connection system and corresponding actuation temperatures required going through four phases.

The first phase of actual SMA temperature calculations was based on the SMA thermal model discussed in the previous section. For the 40 hours studied (ranging from 08:00 to 17:00 on the 21st of March, June, September and December), the upper and lower portions of the façade were each characterized by one geometrical configuration. For each hour and for each geometry, a two-dimensional array indicated the 4-SMAs incident solar radiations represented in a 2x2 matrix in the following order: $\begin{bmatrix} Upper\ SMA & Eastern\ SMA \\ Lower\ SMA & Western\ SMA \end{bmatrix}$.

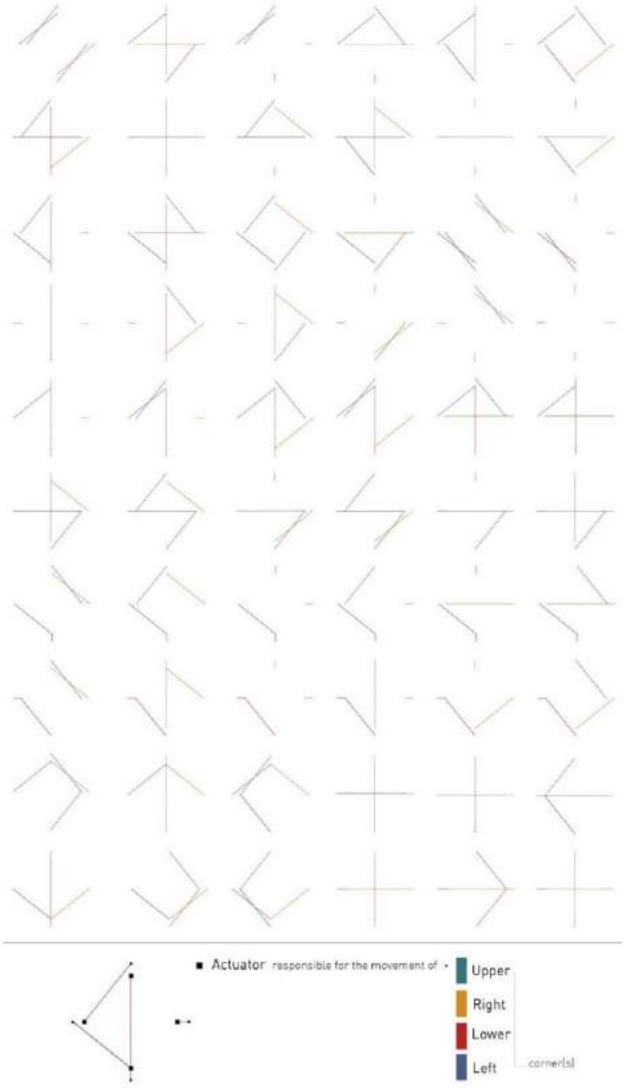

Figure 5. Actuator-Movement Connection Configurations

The calculations were carried out such that T_p in the equation was taken as the air temperature for 08:00 assuming minimal radiation in earlier hours of day; while for all other hours, T_p corresponded to the SMA temperature at the previous state.

The second phase required, in addition to the SMA actual temperatures, two other sets of arrays for each geometry: the geometrical configurations (deployed side:1, undeployed:0), the actuator-connection alternatives, which indicated the actuator responsible for the corresponding movement (index:0-3). For each actuator-movement connection, for the sides connected to each actuator, a search was excecuted through the desired geometric configurations' list for the instances at which this side's geometry is deployed. For all the hours of deployed movements, the SMA temperatures of the corresponding actuator are aggregated in a list. The choice of the suitable temperature was then based on three alternative methods; the minimum, the most common and the average. This approach generated, for each connection type, a two dimensional array indicating the 4-SMAs suitable activation temperatures.

The generation of the resulting SMAs façade combinations, the third computational phase, used the defined 4-SMAs activation temperatures as the threshold to identify deployment status of each compoment 's side, and thus the geometrical configuration. These forms were then, in the fourth phase, compared to the original desired output matrix using four evaluation metrics: the compatiblity of the final geometries, the compatibility of the 4-SMA in deployment, the variety of possible forms within one day and within a year.

3 COORDINATION RESULTS

Large variations were observed between the ambient temperature and the four SMA temperatures over the year, as well as between each other for the same recorded hour. A range of difference expanding from 0 to 15 degrees Celcius was determined, with the largest variations reported in September and during radiation peak hours of winter. Figure 6 shows these variations for the most performing case as identified in the previous section.

Twenty of the highest performing cases were tested as desired output to generate most compatible SMA systems and identify their respective activation temperatures and connection types. Figure 7 and Figure 8 show the result of two samples, illustrated as a comparison between the desired geometrical states for each hour and the actual output achieved through the developed computational process. For each façade portion, a diagram was supplemented to identify the actuator-movement connections, the activation temperature of each SMA as well as an evaluation of their compatibility and diversity.

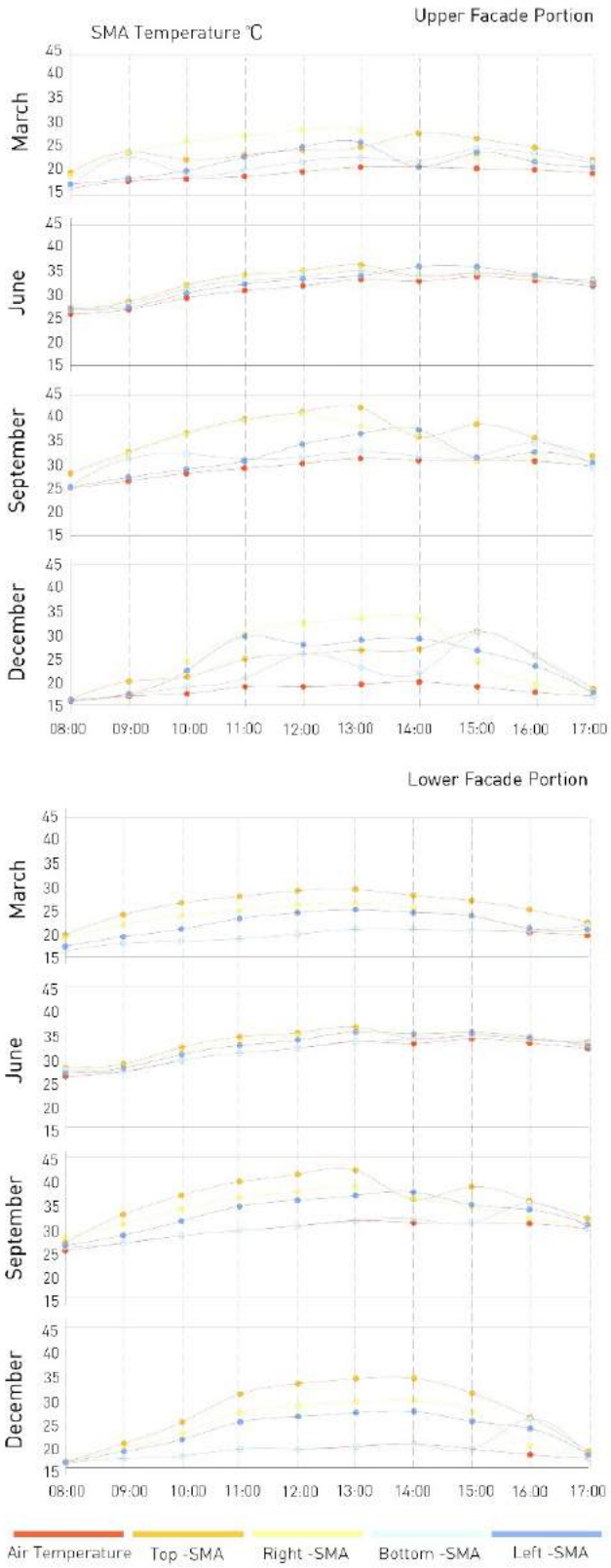

Figure 6. Variations between Ambient and 4-SMA Temperatures

Figure 7. Sample Compatibility SMA Systems for Performative Case – A

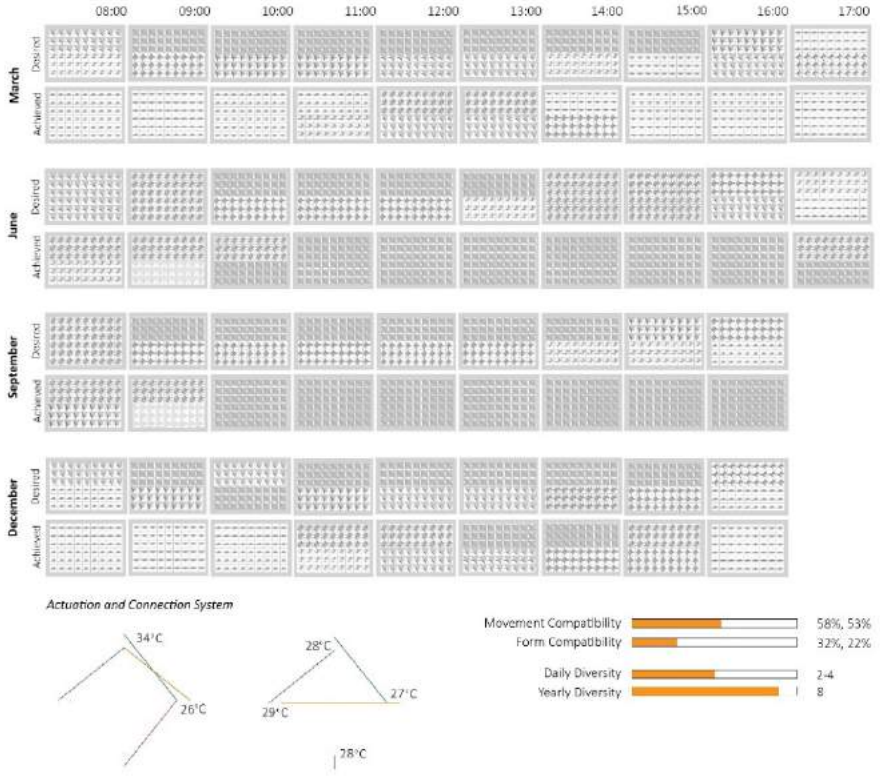

Figure 8. Sample Compatibility SMA System for Performative Case – B

4 DISCUSSION

The strategy used to engineer the SMA shading skin for the desired adaptability was developed to reach a tailored unique solution, a constraining restriction leading to maximum component and SMA compatibilities of 44% and 67% respectively. It is important to note that these calculations excluded all the cases which achieved higher compatability rates, up to 87%, but which only used the closed configuration in most hours. A more flexible targeted output would be more convenient for the façade's initial performative objective which achieves higher compatibility rates and daylighting values.

Additionally, high diversity rates were achieved for the cases with highest compatibility, reaching up to 4 different forms within one day and up to 6 during the year. The resulting behavioural diversity provided evidence for the design premise and the rise of a novel understanding of material-based shading systems as ones that can produce more than just binary outputs on the component's scale.

Partial results are illustrated below in Figure 9 showing the relation between actuator-movement connections and the evaluation criteria.

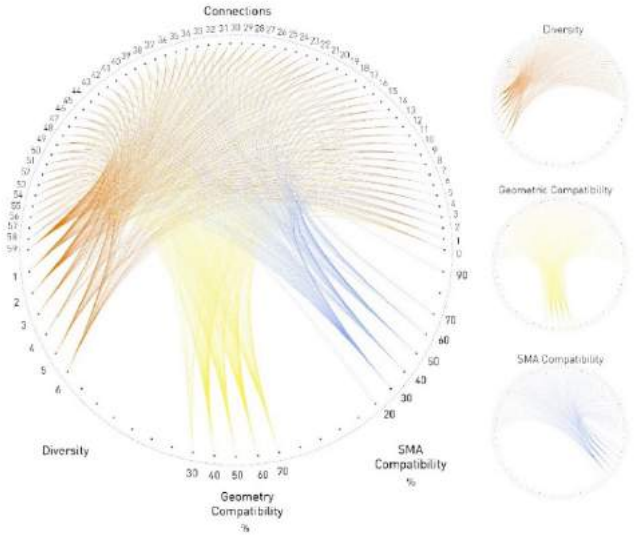

Figure 9. Actuator-Movement Connections Evaluated

The most conforming and diverse cases were identified by a characteristic range of temperature selection methods, activation temperatures and connections. The most common calculation strategy for the activation temperatures was through the identification of the most common within the list with an approximate 80%, followed by the average and none used the minimum method.

Activation temperatures, although calculated in the scope of this study for a comparative purpose, ranged between 18 and 37℃ which indicated the relevance of varying activation temperatures for higher ranges of acceptable systems. However, the highest performing system solutions showed a significant portion of varied connections with all actuators that have similar activation temperatures; demoting this differentiation potential to an important but secondary level of impact.

Connection differentiations between actuators and movements provided insights into the possibilities that this approach unveiled and the degree of adaptability improvement it added. The standard connection, with each actuator connected to the closest movement, was rarely successful; showing the higher resulting ranges achievable by allowing actuators to be responsible for one or two non-direct movements. Despite the variation relevance, about 40% of the connections did not show in the best compatability results, which reflects that some may be eliminated from the search with no major impact on the solution performance.

The solar radiation simulation along with the computational model methodologies provided the means to carry out this research; however carried several constraints. These mainly include their entire dependence on the accuracy of the digital simulations of Cairo's weather file and on the negligable impact of climatic factors other than temperature and radiation such as humidity, wind and others.

The complexity, inaccuracy and experimental base of the developed SMA thermal models in the literature [8] as well as the need for comparative rather than accurate behavioural predictions for this particular study provided a grounded rationale for the use of a significantly simplified model of the actual SMA behaviour. The inaccuracies in material temperature estimations were mainly affected by the determined values for emissivity and convective heat transfer, the assumption of their constant values during the martensitic and austenitic phases and the hysteresis effect. An estimate of 0.82 emissivity was used constantly, while the literature has shown a 9% emissivity variation between martensitic and austenitic states [1]. Determining the SMA convective heat transfer coefficient was the subject of many attempts in material science research and the predicted values varied significantly. The Velazquez and Pissaloux's model was used to determine the convective heat transfer coefficient used in this study's thermal model as a function of the Nusselt number under 20℃ free air, SMA thermal conductivity and characteristic length, reaching a value of 38 $W \cdot m^{-2} \cdot K^{-1}$. The implication of such a wide range of error for this estimation gave rise to the problematic arena of modelling SMA exact behaviour. However, since the study's objective was comparative and based on large time intervals, the simplified thermal model used was found adequate for this specific objective although better predictions could have been made by incorporating physical measurements and more developed thermal models.

The flexibility and adaptability present because of tailoring possibilities of phase temperatures and engineering properties based on composition, had an important impact on

the SMA's system computability capacities. If restricted to only one or two different temperatures, the resulting compatibility rates that this study showed would have been significantly lower.

5 CONCLUSION

The study showed that the integration of geometry, material, and their connections in the design of a SMA solar morphing envelope lead to the development of a wider range of behavioural system outputs. The variety instilled through these added dimensions promoted diversity and adaptability of output with a flexible range of desired responses. Despite the site-specific nature of this research, its findings are transferrable to similar hot dry climates with minimal sky coverage and comparable seasonal and hourly variations, and its study methodology is applicable to any context.

The positive impact of connection variations in achieving diversity provided insight into their computational potential which can be augmented through further studies into designing them as series of inputs capable of producing logical operations through either mechanical or sequential linkages. Research into material capacities for such architectural applications as well as experimental testing of real scale devices in targeted climates would allow for the development of a tailored and verified thermal model for SMA behaviour under targeted conditions. The latter will allow for better behavioural predictions thus higher conformance with performance objectives and provide insights into limitations of transferring this design approach to a constructible working material system.

REFERENCES

1. Costa Sa, M., Da Silva, E., Da Silva, F., Da Silva, T.: Emissivity Measurements on Shape Memory Alloys. Presented at the *2016 Quantitative InfraRed Thermography*, January (2016)
2. DeLanda, M.: *The New Materiality* (2015)
3. Gonzalez, N., More, S.: Self-Adaptive Membrane: Kinetic Passive System. Institute for Advanced Architecture of Catalonia (2015)
4. Incropera, F., Lavine, A., Bergman, T., DeWitt, D.: *Fundamentals of Heat and Mass Transfer*. John Wiley & Sons (2011)
5. Kolarevic, B.: *Actualising (Overlooked) Material Capacities* (2015)
6. Kolarevic, B., Parlac, V.: Adaptive, Responsive Building Skins. In: *Building Dynamics: Exploring Architecture of Change*. pp. 69–88. Routledge (2015)
7. Mokhtar, S.: Material-Based Actuation of Facades: An Adaptive Performative Approach. University College London (2016)
8. Otsuka, K., Wayman, C.: *Shape Memory Materials.* Cambridge (1998)
9. Roudsari, M., Pak, M.: Ladybug: A Parametric Environmental Plugin for Grasshopper to Help Designers Create an Environmentally-Conscious Design. In: *Proceedings of BS2013*. pp. 3128–3135. , France (2013)
10. Speck, T., Knippers, J., Speck, O.: Self-X Materials and Structures in Nature and Technology, (2015)
11. Velazquez, R., Pissaloux, E.: Modelling and Temperature Control of Shape Memory Alloys with Fast Electrical Heating. *Int. J. Mech. Control. 13* (2), 1–8 (2012)
12. Verma, S., Devadass, P.: Adaptive Skins: Responsive Building Skin Systems based on Tensegrity Principles. AA School of Architecture (2013)
13. Technical Characteristics of Flexinol Actuator Wires. Dynalloy Inc., California

A Methodology to Analyze Building Envelopes Based on Discomfort Glare

Navid Hatefnia, Marjan Ghobad

PJCarew Consulting
Cape Town, South Africa
{NavidHatefnia, Marjan.Ghobad}@gmail.com

ABSTRACT

This article proposes a method to analyze the effect of façade surfaces on selected interior area at eye level based on daylight glare probability. By highlighting the critical parts of a façade in terms of indoor discomfort glare issue, this method helps architects to improve the design by adjusting the façade elements, openings and material transparency. Since the demand for the optimized usage of the internal spaces has recently increased it has been gradually becoming more and more important for architects and designers. Consequently, glare is one of the main criteria to consider indoor visual comfort conditions. The analysis identifies the positions on the facade where the daylight comes from and causes discomfort glare, after several bounces, corresponding duration and times, therefore facilitates the design decisions for appropriate solutions.

Although this analytical method is not the only way to analyze and mitigate discomfort glare and it is not solving all the daylight issue, it considers discomfort glare and shows the direct relation between façade design and interior visual discomfort which leads to the design decisions. In the following, the method is applied by a series of Python algorithms in Rhinoceros which are simplified in terms of computational limitations and two practical examples are described.

Keywords

Daylight; Visual Discomfort; Glare Probability; Optimization; Façade Analysis; Discomfort glare

ACM Classification Keywords

I.6.1 SIMULATION AND MODELING (e.g. Model Development).

1 INTRODUCTION

Design teams in the construction industry typically react to comfort issues arising in modern buildings. More and more, designers are trying to answer this simple fundamental question: "How can we best analyze the key causes of building occupant discomfort in the design stages to avoid the problems after construction?" Nowadays, significant improvements of computational analysis are making it easier to predict and design for occupant comfort satisfaction. This paper focuses on one of the aspects of occupant visual comfort, which is, discomfort glare caused by daylight (direct and diffuse). In this regard, discomfort glare should be defined first and then its impact on occupant comfort should be comprehensively understood in order to understand the basis of the glare analysis method.

The International Commission on Illumination (CIE) defines glare as: "Visual conditions in which there is excessive contrast or an inappropriate distribution of light sources that disturbs the observer or limits the ability to distinguish details and objects" [1].

Several factors have an impact on discomfort glare experienced by a person such as angle between the viewpoint and the source of light, view direction, source luminance size, background luminance, eye adaption and so on. These are referred to as discomfort glare indices. This paper focuses on one of the major causes of discomfort glare: daylight into spaces, which in turn creates direct and indirect reflection in the interior spaces. Daylight falling on a surface or directly on the eye might cause discomfort. For instance it is suggested in IES standard LM-83-12 illuminance that direct solar exposure over 1000 lux will cause discomfort [3].

Analysis of discomfort glare in interior building spaces is important because of its impact on the performance and productivity of the occupant. It is clear that the efficiency of an occupant's performance on visual tasks depends on their visual comfort. Hence, it is crucial to maximize occupant visual satisfactions by incorporating natural light into the design of internal spaces while decreasing the discomfort glare which may be achieved through accurate evaluations of daylight and discomfort glare indices in parallel.

There are several challenges in the existing methods for glare analysis and the majority of studies related to glare simulation rather than directly leading to the design solution. Kleindienst and Andersen [4] showed the aspects of vertical illuminance and contrast. In the latter, discomfort glare is generally analyzed in the indoor spaces for only one point in specific time and one view direction or just simulation for all time steps using the respective weather

data, usually utilizing Radiance rendering to simulate the visual field. For instance, Evaglare tool can be used to evaluate glare, which is based on user assessments and calculates daylight glare probability (DGP) [6]. Another method evaluates glare in terms of average luminance in the field of view [2].

Although one can obtain discomfort glare through gathering data such as background contrast, visual field, surface luminance, etc. there hardly seem to be a direct solutions to mitigate the discomfort glare problems and the majority of studies suggest a try and error approach to minimize the discomfort glare probability.

This paper describes a method to determine and record the light paths that bring daylight into spaces and cause discomfort glare on any point of interest as a human eye. Then the intersection of an analytical surface with those paths are highlighted to show the critical parts of the surface for the designer to facilitate the design decision. This analytical surface should be considered in a location with the possibility of adjusting the transparency like facades, openings, windows, skylights, etc. Hence, this method doesn't solve all the glare issues in the building and it just addresses the discomfort glare issues that come through the analyzed surface. This method not only makes a data-base of necessary data matrices for further discomfort glare analysis, but also leads the architect directly to a level of design consideration and solutions in an early design stages.

To apply the method computationally, a series of python algorithms were designed in Rhinoceros. The purpose was to test and develop the method. Hence, algorithms had to be simplified in terms of computational time and restrictions in several parts like limiting the bounces, low resolution (amount of rays) and materials variety. Two cases are then described in this paper that the method is applied by python algorithms. In the examples, it is identified that where the greatest impact can be made for the majority of the year so that design focus and resulting budget can address this for greatest initial impacts. The method is not intended to resolve all instances of discomfort glare and cannot guarantee a discomfort glare free environment caused by a number of aspects beyond this paper. In addition, this method will only assist in identifying those potential locations and the time of year when discomfort glare might occur.

2 METHOD

That being said, there are some solutions to prevent discomfort glare that can be used by designers in the initial design stages. One common solution is to use an obstacle in a light path that cause glare like placing an object between the source of light and the view field into the space. This correlates with the first human reaction against glare; that is, placing a hand on top of the eyes, therefore, mitigating disability glare but still providing vision or in another scenario putting papers on windows to prevent discomfort glare. Reduction of contrast in the internal space within the vision field also decreases the glare probability; this is achieved by scattering the bright light from the luminance source in the whole space. Orientation of openings can also be taken into consideration by building designers. The openings can be placed strategically in order to allow daylight into the space with less possibility of causing discomfort glare issues. Another effective mean for discomfort glare mitigation comes from proper space planning. Internal spaces can be placed strategically on a floor plate according to their functions and occupancy schedule. Since occupants may use these spaces at different times of the day for different periods, when and where glare may become an issue is analyzed within the different spaces and the results can be taken into account during the space planning process.

To assess the discomfort glare phenomena on each point of interest as a human eye, it is necessary to gather all the lights data from surrounding area. The idea is to project the surrounding objects light on a unit sphere centered at the point of interest. A simple technique to obtain the results is to emit a number of vectors (or rays) homogenously from the point of interest to the surrounding entities; similar to the backward path tracing method to find the relative sky patch (simulated divisions of actual luminous flux from sun and sky) as the light source. Distributing rays homogenously makes a valuable possibility to determine the solid angle between points of interest and surrounding surfaces as one of the glare equations variables and also accelerates the post processing glare computation and analysis in next steps.

Furthermore, after gathering all surrounding variables, the data can be filtered by period of time and visual field domain or just simply get a total discomfort glare probability for all directions through the year on each point. In this paper the DGP equation (Eq.1) by Wienold and Christoffersen [6], metric is used to evaluate and compute glare from daylight. Where E_v is the vertical eye illuminance [lux]; L_i the luminance of source [cd/m2]; ω_s the solid angle of source; P is the position index.

$$DGP = 5.87 \times 10^{-5} E_v + 9.18 \times 10^{-2} log\left(1 + \sum_i \frac{{L_{s,i}}^2 \omega_{s,i}}{{E_v}^{1.87} {P_i}^2}\right) + 0.16 \quad (1)$$

The method is structured based on the following sequential steps: First, a point of interest, say point p, should be considered in a three-dimensional space, which normally can be assumed as the eye level of a human body. This point is the origin of the vectors that will be emitted to the surrounding entities. The process can be followed by distributing equally-spaced "guide points" on a unit sphere centered at point p, as depicted in Figure 1. Each point on the surface of the sphere is a guide to a vector originated from point p. If the extension of a vector reaches a surrounding surface, then the surface is considered to be

seen by point p and its illuminance and distance will be included in further calculations.

The ratio between the number of the rays hit a surface and the total number of rays (or guide points) will determine the solid angle from point p to the surface. In fact, the guide points through which the rays are passing to hit a surface represent the projection of the surface on the unit sphere. The resolution of this projected image can be improved by increasing the number of guide points (and consequently the number of rays/vectors) (Figure 1). Then the backward path-tracing method is employed to determine the source of light for each path from the sky patches data. Backward path-tracing needs to be done once then all paths are recorded as a list of data considering the related sky patch index and the series of materials emissivity that redirect each path. Next step is just to change the sky patch light source data and to add the results based on the analysis period. This method's step significantly accelerates the computational process.

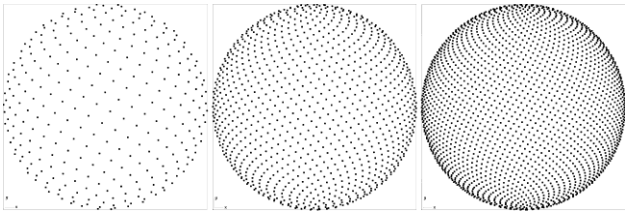

Figure 1. Equally-spaced guide points to start backward path-tracing in different resolutions

Light paths are traced backward from the spectator's eye to the light sources. In this method sky division results yielded from Radiance are used as light source [5]. In principle, forward ray tracing could be employed just the same, but for a great number of scenarios, the former approach is more feasible by considering the required computation time. The most intuitive parameter is the number of "ambient bounce" (ab). The parameter instructs how many surfaces a ray can bounce of or transmit through before it is discarded and directly effects on the background luminance and consequently on discomfort glare evaluation. This backward ray tracing can be followed and recorded as lists of paths and their relative sky patches with their source of light data. It is then possible to follow these paths and vectors back from the analysis point, to define the path and direction of the daylight causing the discomfort glare to be viewed by the point.

Assuming that the main source of discomfort glare is daylight from openings into spaces, so if this light could be prevented or diffused in the first step, then a majority of potential indoor discomfort glare issues would be decreased. This method is already applied practically by people who paste paper on windows or paint some parts of the skylights to avoid glare issue. This paper, therefore, proposes a computational method to analyze a surface between the selected area and the light paths. However, the challenge of barrier surface analysis is not only analyzing it but also to find a way to optimize it. The method has to provide a means to find out when glare is an issue and more importantly, provide an indication of the directions of where the "discomfort glare" is coming from based on the openings of the spaces and the sky as the light source. This is achieved through a geometric solution during the daylight design process, which can assist building designers in understanding of glare in occupied spaces better and generating corresponding solutions. The following steps form parts of the proposed method.

The initial step in the proposed methodology is similar to almost other simulations through geometric modelling. A basic virtual model is built to scale and placed in the desired orientation along with all the surrounding buildings or other overshadowing components on the site.

An appropriate barrier surface is then assumed based on the part of the building which the designer wish to improve the openings in order to mitigate the discomfort glare. This can be any surface from the complete building envelope, a façade of the building, a window as Figure 2, etc. and can be changed later without running the backward path tracing process again by recording all the paths for further post processing. This surface is then divided into multiple sub-surfaces depending on the desired resolution of the analysis.

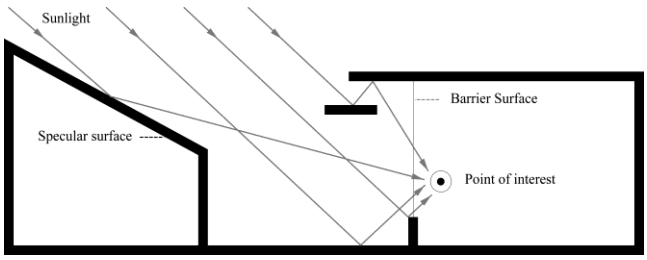

Figure 2. Discomfort glare analysis on the barrier surface

A series of points are selected to be analyzed inside a space, at eye level, based on where the designer wants to limit the discomfort glare issue. For instance, these points are the equivalent of building occupants sitting in an office.

Afterwards, a time schedule is set for the points, since, as discussed above, discomfort glare may not be a problem at all times depending on the building occupant schedule and activities. For example, spaces which are mostly used during lunch periods do not need to be analyzed for glare at times other than being used. The luminance of individual sky patches for a given sky condition, for each hour of the year, can be calculated by using the Perez sky model. After generating the sky, paths which make discomfort glare are intersected with the analytical surface. The intersection of paths with the analytical surface results in a number of points on the geometry.

The points are then converted to matrices and analyzed by overlaying more information about the site, building, sun positions, etc., depending on the desired outcomes by the designer. For instance, amount of intersected points in each sub-mesh is counted to analyze the importance of each sub-

mesh. Angle of intersection is one of the most important parameters for understanding the paths of the light causing the discomfort glare. Sun radiation can show the intensity of the light, if desired.

Gathering all surrounding information for each point of interest and recording all the data matrices for whole year or any period of time makes the data accessible to discomfort glare analysis in any direction by filtering and limiting the domain of data based on the desired visual field direction. This limitation can be done simply by the common approach which is fisheye view field, 180 degree filtering the sphere vectors based on the view direction, or in advanced methods by actual human visual field which is wider in horizon than vertical direction. After adjusting the input and limitation is done, the data can be calculated for the background light and the light source to complete the glare equation. Limiting the view domain might increase the computation time in first stages but doesn't allow the user to compare different view direction later. Repeating this process determines that the glare probability for different directions for each point of interest and shows the glare probability which come from each path to the points on each sub-mesh.

In the other word, the proposed method records all paths which bring light to each point of interest and a database of directions, bounces, material information, light sources and reflectance. This database is used to analyze the parameters that make discomfort glare issue from the first stage that light comes in to next stages that shows the material situation and specularity. Determining the barrier surface as an analytical database highlights the critical parts that discomfort glare comes from and effects on analysis points. Hence, the database would be considered to improve the surface performance as an opening rather using adaptive adjustable kinetic devices which take orders from the main achieved data base for whole year in an advanced approach or simply changing the transparency of the envelope and reshape the openings to minimize the indoor discomfort glare issue by a fixed design.

3 PRACTICAL PROJECTS

Two examples are provided where the above-proposed method has been applied. Algorithms were simplified in terms of computational time and restrictions in several parts like limiting the bounces, low resolution (amount of rays) and low variety of materials. In these examples, it is identified that where the greatest impact can be made for the majority of the year so that design focus and resulting budget can address this for greatest initial impact. As an example, external facades of atria often have a smaller surface area than the glazing between occupied areas and the atria, therefore addressing potential discomfort glare could be more cost effective when that plane is considered for intervention. The method is applied to assist in identifying those potential locations and the time of the year when discomfort glare might occur.

3.1 Analyzing Glare In Indoor Spaces

The building in question is an office building being built in Johannesburg in South Africa. Analysis of the building envelope has been done, where discomfort glare mitigation is one of the important comfort criteria to consider in the design process. The purpose of discomfort glare analysis in this example is to identify which areas of the façade are more likely to allow daylight through the space, which has been caused discomfort glare on the points of concern inside the building. As it has been described previously, a series of points are selected inside the building on the areas where discomfort glare would be a major cause for concern. In this case, these points are at the sitting eye level (1.2m) and one meter aside from the facade on the floor plate.

The west façade has been selected as the analytical surface on the light path between the internal space and the light source in this example, as shown in Figure 3-a. The paths of the light are traced backward from the analysis points to the light source and the intersection of these paths, with the façade are obtained. Overlaying the results of the daylight coefficient calculations, or the duration of discomfort glare occurrence allowed the design team to identify the level of transparency of the façade at these points (Figure 3). The façade adjusted to decrease the discomfort glare issue on points of interest by redesigning the openings based on the analytical method (Figure 3, d). However, based on the other daylight simulations some parts needed to be open and they selected from the parts that make less discomfort glare and in some parts the material adjusted to be translucent and not clear to decrease the discomfort glare issue. The results also showed the hierarchy of using blinds in different locations to decrease the discomfort glare issue for period of time that is needed (Figure 3, c). As a result, the amount of discomfort glare issue significantly decreased.

3.2 Analysing Glare Probability Relative To A Skylight

In this example, the method is applied during the design of a skylight to provide natural light to spaces inside a building while decreasing the effects of discomfort glare. The purpose of this analysis is to not only understand the parts of the skylight where the glare-causing light is coming from but also consider from which direction it is coming. After selecting the points inside the space, a virtual plane was created as the analytical surface above the skylight. The light paths were traced back to find the corresponding intersection points on the barrier surface but more importantly, the angle of intersections of the vectors generated by the paths recorded. Although the basic calculations show indeterminate outcome, the results shows two main groups of directions of the light paths which have the highest glare probabilities. In order to reduce the discomfort glare probability, relaxed mesh adaptive algorithms were employed on the analysis surface to optimize the analysed surface rather being a horizontal plane (this is done by selecting the intersected direction vectors as input forces), thus providing possible solutions

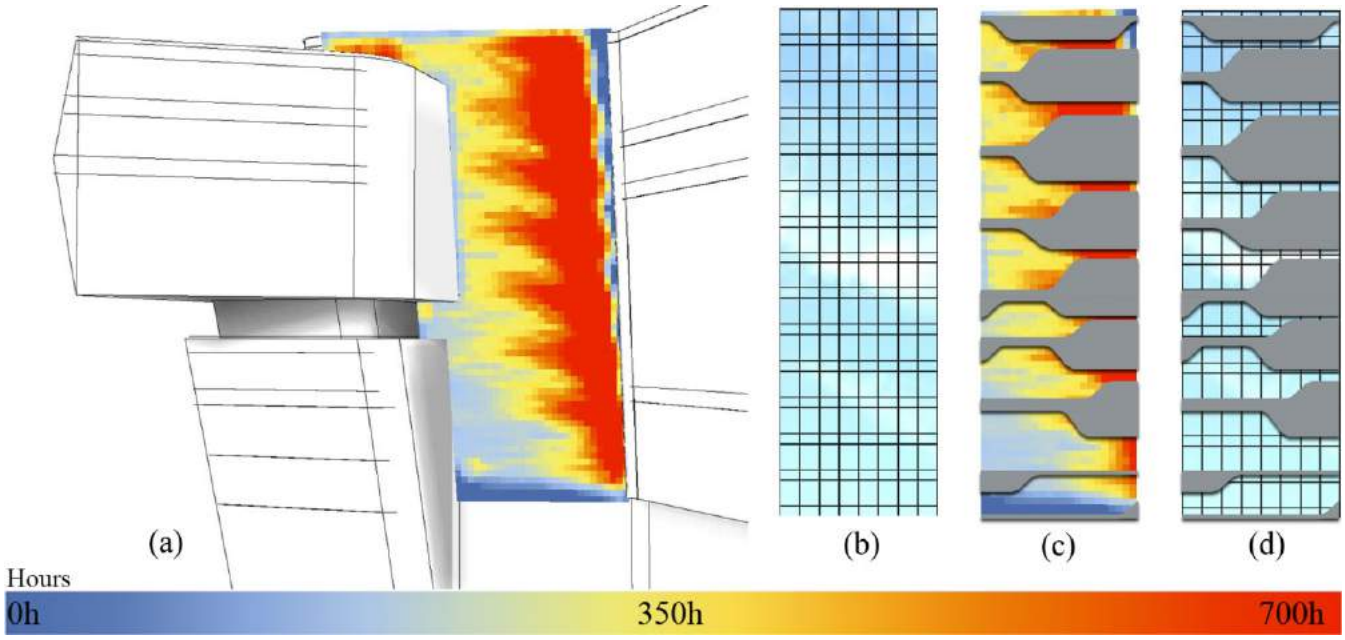

Figure 3. Discomfort glare analysis on the South-West façade

for the skylight surface to respond to the discomfort glare-causing light rays. As a result, the skylight surface started to show "bumps", as shown in Figure 4-c. This process consequently assisted the project team in optimizing their design and selecting a solution based on other factors such as costs and ease of installation as shown in Figure 4-b as an external shading device.

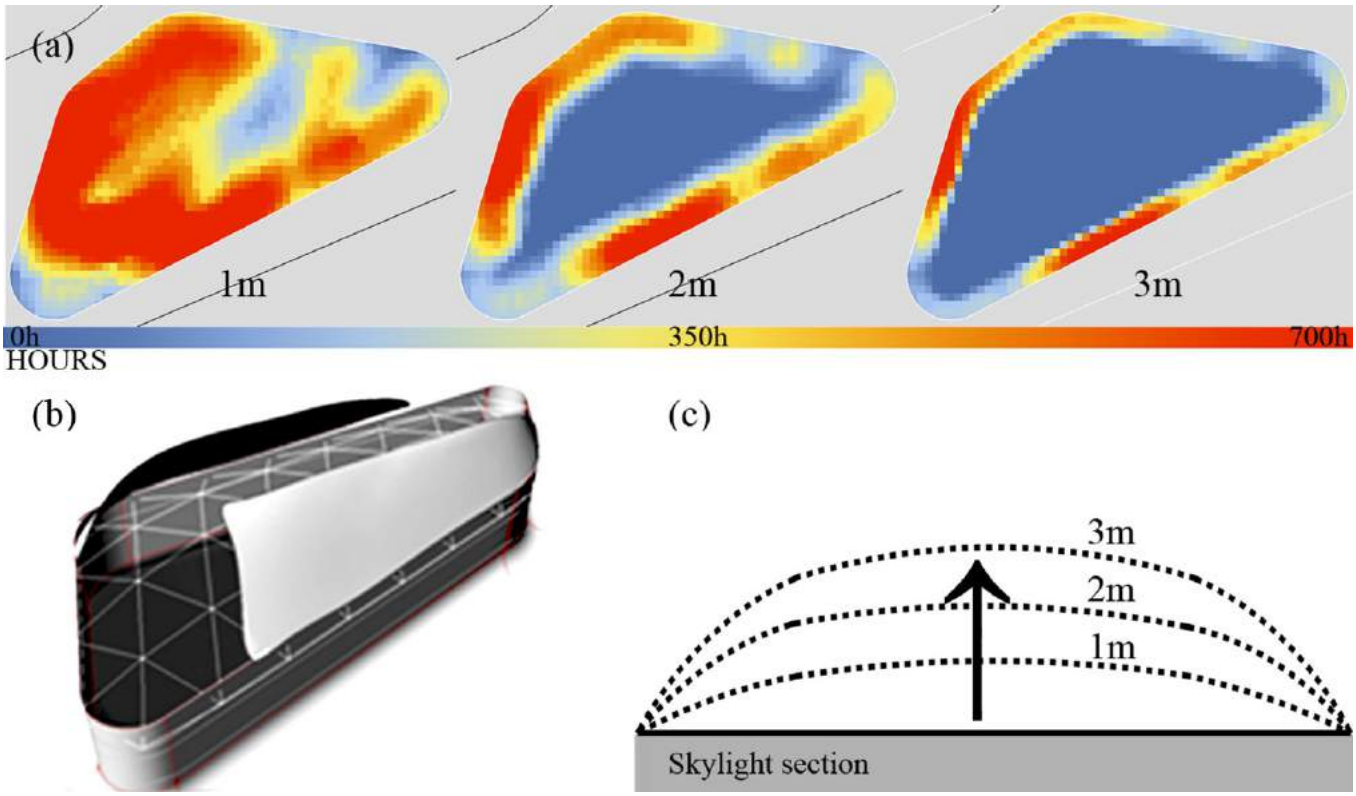

Figure 4. Discomfort glare analysis on the skylight

4 CONCLUSION

The proposed discomfort glare approach is performed by the evaluation of a barrier surface to find effective locations which will decrease the indoor discomfort glare issue. The methodology remarkably expedites the computation of discomfort glare by not solving all the glaring surfaces. The surfaces are selected based on their location in space with respect to the interior planning layout, occupancy schedule, usage, etc.

The barrier surface can be considered as a building envelope, a façade, an overhang or even a window to determine which part plays a more significant role in discomfort glare. As a direct guideline, a designer would immediately find out about the effective factors that can decrease the discomfort glare issue. Moreover, it is important to take into account the interior daylight in the daylight analysis. The surface analysis also works as a database to record all data for post-processing steps. This database can be used to manage automatic shading devices over a whole year and for any part of the façade.

Furthermore, recording the angle of light path can assist designers to manage discomfort glare by adding external surfaces in the right places. Different types of data could be recorded simultaneously when light path reaches surfaces. Other factors such as materials emissivity can also be examined to reduce discomfort glare by highlighting important interior surfaces that affect the light paths.

The various assessment of the barrier surfaces creates great opportunities for further analysis on lots of related issues involved in the occupant visual discomfort in internal spaces. Also, considering the fast growing demand for accurate prediction ability in visual comfort simulation, the proposed approach has the potential to be employed in near future as an effective method to design building envelopes, shading devices, etc. in early stages by architects and designers.

ACKNOWLEDGMENTS

We would like to show our gratitude to the support of the PJCarew consulting. The opportunity that PJC gave us for this research is highly appreciated. We are also grateful to our colleague, Yogeshwar Gooljar, for his great comments that really improved the manuscript.

REFERENCES

1. CIE 117-1995 Discomfort Glare in Interior Lighting. CIE. 1995. ISBN 9783 900734701.
2. Eleanor S. Lee, Glenn D. Hughes, Robert D. Clear, Luís L. Fernandes, Sila Kiliccote, Mary Ann Piette, Francis M. Rubinstein, Stephen E. Selkowitz. Daylighting the New York Times Headquarters Building: Final Report: Commissioning Daylighting Systems and Estimation of Demand Response. Lawrence Berkeley National Laboratory, Berkeley, CA. LBNL-57602.
3. IESNA, IES LM-83-12. IES Spatial Daylight Autonomy (sDA) and Annual Sunlight Exposure (ASE). New York, NY, USA, IESNA Lighting Measurement, 2012.
4. Kleindienst S.A., Andersen M., 2009, The adaptation of daylight glare probability to dynamic metrics in a computational setting. *Proc. Lux Europa 2009 – 11th European Lighting Conference*, Istanbul, Turkey.
5. Ward G, Shakespeare R. *Rendering with RADIANCE: arts and science of lighting visualization*. Morgan Kaufmann; 1998.
6. Wienold, J., Christoffersen, J. Evaluation methods and development of a new glare prediction model for daylight environments with the use of CCD cameras, *Energy and Buildings 38* (2006): 743-757.

Hybrid Workstations: Establishing Interactive and Responsive User-Interfaces for Daylight Applications

Emad Al-Qattan, Liliana Beltrán and Wei Yan

Texas A&M University
College Station, TX, USA
{emadkkqattan, lbeltran,
wyan}@tamu.edu

ABSTRACT

The research project presented in this paper explores the benefits of utilizing a hybrid workstation in a daylight design application. The prototype developed for this work links a physical design object with digital modeling and simulation tools. The aim of the work is to integrate physical and material properties of kinetic design objects in the digital workflow. Additionally, the hybrid system utilizes smart hand-held devices to provide designers with a user-friendly interface to control modeling parameters. The developed workstation provides real-time interactive features and live responses to visualize and evaluate design options in both the digital and physical environments. The proposed work demonstrates unique possibilities for daylight applications, which will assist designers in making informed decisions regarding both the aesthetics and the performance of a kinetic architectural system.

Author Keywords

Parametric Design; Human-Computer Interaction; Daylight Design, Ubiquitous Computing; Physical Computing.

ACM Classification Keywords

B.7.1 TYPES AND DESIGN STYLES (Input/output Circuits); B.7.2 Design Aids (Simulation); C.5.3 MICROCOMPUTERS (Portable Devices, Workstations); I.2.9 ROBOTICS (Kinematics and Dynamics); H.1.2 USER/MACHINE SYSTEMS;

1 INTRODUCTION

Currently, architects are challenged to seek alternative design solutions to meet climatic and social changes. Research has shown that architectural elements with kinetic capabilities (e.g. façade, shading, etc.) may provide a solution to address such conditions in addition to their stimulating visual appearance [6].

Existing works investigating kinetic architectural elements span from geometric studies to software tool development. A drawback in conventional digital workflows is the separation between physical studies, CAD implementation, and simulation procedures [11]. Conversely, the work included in this paper attempts to establish and utilize hybrid workflows to address the gap between design tasks through linking physical and digital design objects together. A design object in the context of this work refers to the digital and physical representations of an architectural element.

The research further investigates hybrid workflows with the aim to enhance the users' interactive experience when manipulating geometry and conducting simulation studies. The work involves integrating smart hand-held devices to provide designers with a customizable and an intuitive interface to control modeling parameters. The hybrid workstation will assist designers in relating physical geometry with digital simulation results, which will provide them with the means to comprehend the complexity associated with designing a kinetic architectural system for a daylight application.

A prototype is developed to test the proposed workflow; and it includes two main parts, the *artifact*, and the digital environment. The artifact consists of a physical design object and a *Physicalй Computing* system. The physical computing system is broadly defined as the platform to communicate between both the digital and physical environments; and it is composed of sensors, actuators, and microcontrollers [9]. The digital environment consists of a 3D modeler, a visual programming environment, and a daylight simulation engine (Figure 1). The link created between the system's components is established through visual programming, which uses a wireless *Localй Areaй Network* (LAN) for data communication. The work will enable designers to control and manage computational tasks using an everyday, personal, and convenient device.

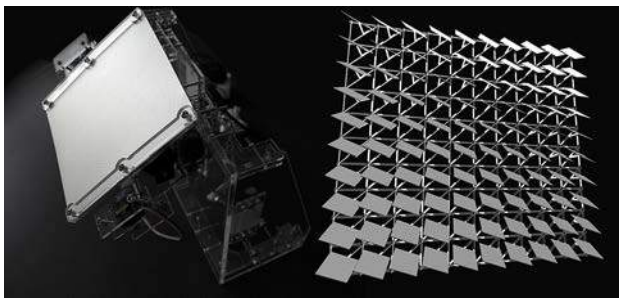

Figure 1. Hybrid Workstation, artifact (left) linked to a digital parametric model (right).

2 RESEARCH CONTEXT AND RELATED WORKS

The proposed hybrid workflow is considered as a *Mixed Reality* (MR) approach in design. The notion of MR can be illustrated as a linear spectrum that is defined by two ends; the virtual environment at one end and the real environment at the other [8]. However, real-time interaction and live responses provided by the proposed hybrid workstation aligns with the notion of *embodiment* where the two ends of the MR spectrum meet to create a loop [2,12].

Earlier works included in this paper demonstrate a few of the many attempts to develop and investigate kinetic elements for addressing environmental design issues; which involve creating computational workflows, hybrid workstations, and software tool improvements. Each of the following examples discussed below highlights an essential component in a hybrid workflow, which will help in informing the progress of the proposed work.

The experiment by ElGhazi and Mahmoud investigates kinetic origami patterns for creating a façade shading element. The work involves conducting physical studies as well as digital simulations [3]. Models of the kinetic unit were physically made and folded. The geometry's response provided an understanding of its physical behavior. Afterwards, the unit, and its folding motion, were recreated in the digital environment for conducting daylight simulations. The experiment demonstrates the value of physical studies in visualizing and realizing an object's kinetic features. Nevertheless, the work shows a linear process where digital and physical workflows are separated.

Another experiment by Kensek involves establishing hybrid workflows for studying the environmental impact on BIM models [7]. The work consists of a digital architectural model and an artifact. The workflow links Revit geometry with a physical computing system using Dynamo and the Revit API. Physical design objects are integrated with sensors that measure CO2, lighting, and humidity levels to activate geometric responses in both the digital and physical environments. The hybrid workflow also uses simulations to optimize design solutions. The use of environmental data with radiation analysis and optimization tools provide unique possibilities for studying kinetic object responses in a digital design workflow. Yet, further investigations of the kinematics involved in the study may provide insight for designers to understand geometric behavior (such as in the case of ElGhazi and Mahmoud) when utilizing such a method.

The work by Plotnikov et al. demonstrates a hybrid workstation with tangible capabilities that links physical forms with simulation tools to evaluate thermal comfort and vision in an urban setting. [11]. The work demonstrates real-time interaction and digital feedback, and an approach to associate physical geometry with digital geometric and non-geometric information. The work demonstrates a high-level integration of software tools to assist designer in their work. Yet, the experiment demonstrates a unidirectional link; physical forms do not display actuation (such as in the case of Kensek).

3 RESEARCH CLAIM AND SIGNIFICANCE

Current research shows the different methods to bridge between the digital and physical environments: including patterns studies, form optimization, and urban planning. The proposed work will suggest a hybrid workflow for designing and evaluating kinetic objects for daylighting in the aim of extending the exploration of these studies.

The proposed work will (1) integrate modeling and simulation tools together through a single visual programming workflow to improve designers work experience. Designers will navigate the visual program to perform the different tasks without the need to use multiple and separate applications. Additionally, integrating the tools in a single workflow will allow the designer to manage complex programming procedures through smart hand-held devices (phones, tablets, etc.), which will (2) help them to operate the system more intuitively for visualizing design options, transforming geometry, and controlling modeling parameters. The proposed work finds an opportunity in utilizing the computing capabilities and the customizable interface of smart hand-held devices in this research, as they provide new possibilities for digital design applications.

In summary, the proposed hybrid workstation provides a straightforward approach for users and novice programmers to interact with digital models thought the integration of portable devices in the design process. The hybrid workstation will allow for real-time interaction, and live physical and digital feedback. associating physical qualities of kinetic systems (geometry, motion, and materials) with digital simulation readings.

4 RESEARCH METHOD

A prototype of the hybrid workstation is developed to test the proposed system. The process of creating the workstation is broken down in the following sections.

4.1 Criteria Selection

The aim of this work is to design and evaluate a kinetic shading system that can block direct sun, diffuse sunlight, and control vision. The shading system in this experiment is represented as a vertical paneled shading system consisting of an array of 81 square panels that can rotate freely in 3D space. The criteria used for creating the work includes: (1) choosing the hybrid workstation's type and theme, (2) panel geometry and kinematics, (3) project site, and (4) daylight simulation metrics.

Hornecker and Buur's guidelines assist in the process of defining the purpose and audience of the proposed hybrid workstation [4]. The theme that best describes the proposed work is an *expressive representation*, which is defined by the following three points: (1) *representational*

significance, (2) *externalization*, and (3) *perceivedй coupling*. Expressive representation, design objects must provide value and clarity to the user. In this work, design objects provide different types of design information (haptic, visual, geometric, etc.), which together inform the design process. Externalization, design objects must be setup in the hybrid workstation to assist designers in their thinking process by providing them with visual and numeric feedback based on their interaction with the design objects. Perceived coupling, design objects in both environments must complement each other. Digital and physical information provided by the hybrid workstation must relate to each other to create a logical connection for the designer make sense of the system's inputs and outputs.

Following in the process is selecting the geometry's type of kinetic motion to meet the daylighting objectives set by the designer. In this experiment, *rotation* is chosen as the primary type of kinetic panel motion. Panels are created and programmed in both the artifact and digital model to flexibly rotate in all three axes in digital and physical space.

The hybrid workstation enables multiple data entries from users and the environment. The specific data types included in this work are: solar information (digital) and user input (panels' angels of rotation). Users' data is obtained through the smart hand-held device, which controls modeling and simulation parameters set in the digital environment.

4.2 Tools

Software and hardware tools are categorized in four groups based on their application in the proposed workflow.

- Modeling: *Rhino* (3D modeler) and *Grasshopper* (a visual programming environment and plug-in for Rhino).
- Physical Computing system: *TouchOSC* (software application for smart hand-held devices and interface for data communication) [13], *Arduino* (a microcontroller board type MEGA 2560), *servomotors* (two high torque motors and two mini motors).
- Linkage: *Firefly* (software package and plug-in for Grasshopper) [10]. It is used to establish data communication between the physical computing system and 3D modeler.
- Simulation: *Diva* (daylight analysis plug-in for Grasshopper based on LEED v4, which uses Radiance as its simulation engine), and *Ladybugй* (plug-in for Grasshopper to import .epw files and generate visualizations for environmental studies).

4.3 Digital Model

A base-case model is created in Rhino (Figure 2) to test the proposed hybrid workflow. The digital model represents a generic space with a south-facing window. The models' elements will be referenced later in Grasshopper to create the kinetic shading system and to perform the daylighting analysis.

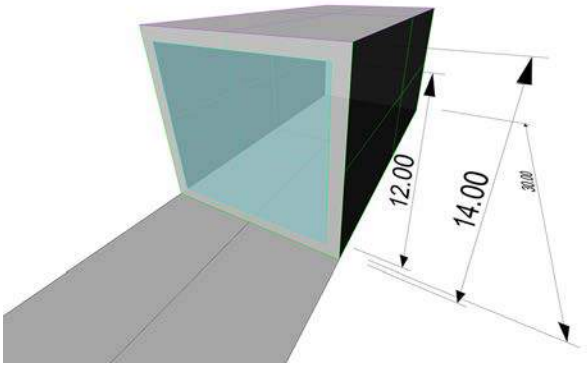

Figure 2. Digital model created in Rhino, measurements are in feet.

4.4 Parametric workflow

A visual programming workflow was created using Grasshopper to (1) integrate modeling and simulation tools, and (2) link the digital model, artifact, and smart hand-held device together. Figure 3 shows the programming logic created in Grasshopper for establishing the hybrid workflow.

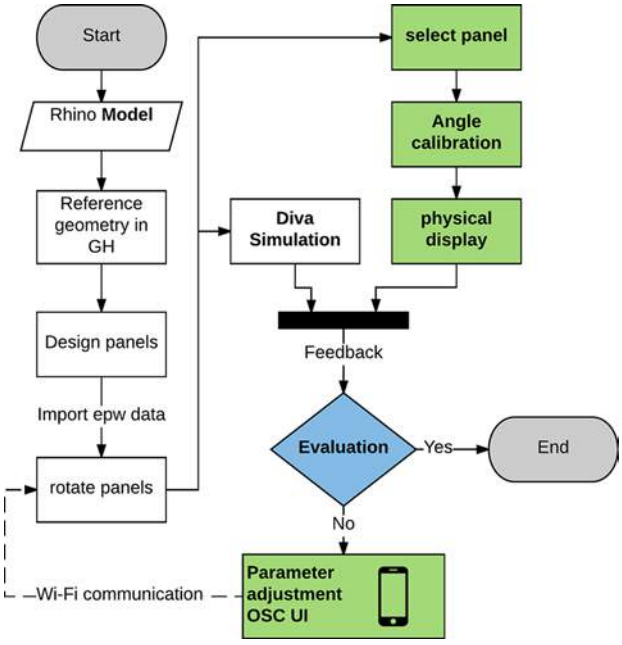

Figure 3. Visual programming workflow in Grasshopper.

The color code used in Figure 3 defines two types of procedures: the first (white blocks) illustrates the common practice of modeling and simulation using Grasshopper or any other visual programming interface; the second (green blocks) illustrates the extended functionality proposed in this work.

The new addition enables the smart hand-held device to manage the hybrid system's data inputs and outputs. The designer will be able to select specific types of geometry from the model, change parameters values, and display kinetic responses physically through the artifact. For

example, the designer can locate a panel in the digital array, display its rotation physically, and changing its angles of rotation in real-time in both models. The smart hand-held device is linked to Grasshopper through a wireless LAN using the TouchOSC application installed on the smart hand-held device.

The base-case's geometry generated in Rhino is referenced in Grasshopper to create a parametric model to be used for generating the kinetic shading system (Figure 4). Afterwards, a relationship between the panels' angle of rotation and the sun's position was established. The parametric relationship will allow the sun to act as an attractor to rotate the panels. The system's mechanical setup and the panels' animated behavior will be further explained in the *Kinematics and Behavior* section.

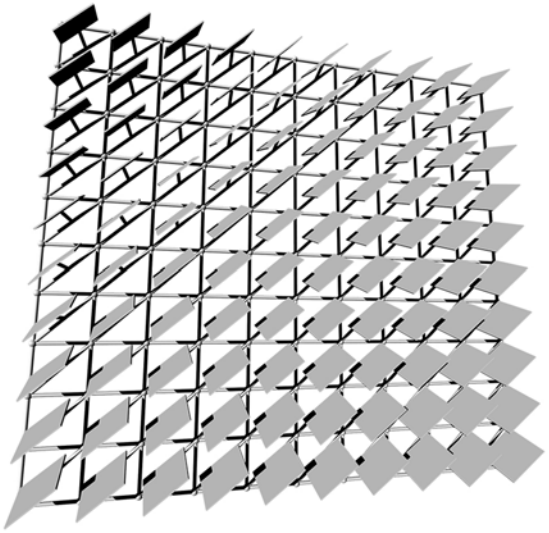

Figure 4. Shading system generated with Grasshopper.

4.5 Artifact

The hybrid workstation in this experiment uses a single physical panel to display the different kinetic responses. The aim of this work is not to physically replicate the shading system in its entirety, but to provide the designer with the means to evaluate an object's physical properties (mechanical performance, material properties, geometry, etc.). Additionally, a single panel at this stage is cost effective and assists the designer to test the functionality of the proposed system. However, further development of the work will involve creating a larger array to help designers obtain a better understanding of a kinetic system's behavior, mechanics, and overall performance in a daylight application. A CAD/CAM approach was adopted to create the artifact. The different components of the artifact (panel, supporting frame, joints, etc.) were designed and prepared in Rhino for laser cutting. The materials used for the artifact are: clear Acrylic for the artifact's support and joints, and a silver coated cardboard with high reflectance for the panel (Figure 5).

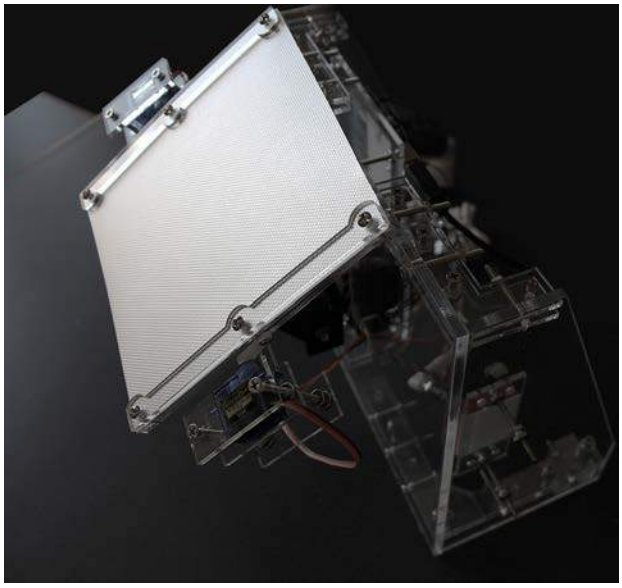

Figure 5. Artifact with a single panel.

The panel is designed to have 3 axes of rotation to meet daylighting requirements. Each panel in both the digital model and the artifact are provided with same number of rotational axes to display a synchronized behavior. The mechanical setup for this work was adopted from an earlier experiment to create complex kinetic motions in hybrid workstations using 2 axes, and it includes using readymade anodized brackets with two high torque servomotors [1]. The brackets enable the physical panel to rotate in two axes with each axis on a separate plane (Figure 6).

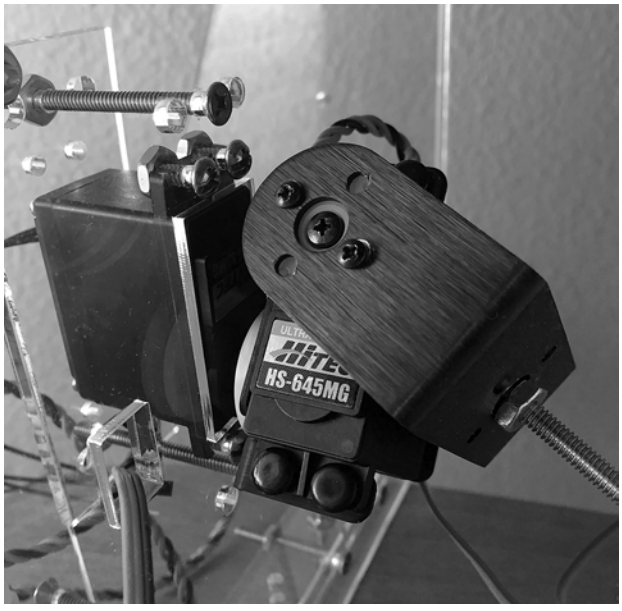

Figure 6. Anodized aluminum brackets for 2 axes rotation attached to two high torque servomotors.

For this work, an additional joint was designed and fabricated other than the aluminum brackets to provide the panel with the third axis of rotation needed. The new joint

is directly attached to the physical panel and uses two mini servomotors to rotate.

Servomotor 1 and 2 (Figure 7), are programmed to rotate the panel to track the sun. The motors will keep the panel's surface perpendicular to the generated sunrays using Ladybug. Servomotor 3 and 4 are directly rotated by the OSC interface, which provides the designer with the option to personalize the shading system's configuration and performance (visual appearance, light penetration, and vision).

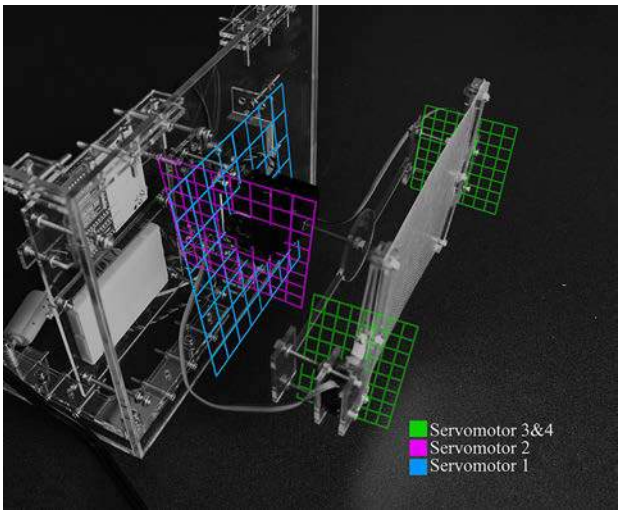

Figure 7. Virtual planes (blue, magenta, and green) created in this view to show how the panel will rotate in physical space. The blue (YZ) and magenta (XZ) grids show the two planes of rotation used to track the sun. As for the green (XZ) plane, it rotates the panel using the OSC interface.

4.6 Linkage and Control System

The link between the artifact, digital model, and smart device is established through Firefly and a wireless LAN. The link will enable real-time communication and live feedback between all three components of the system. The TouchOSC application installed on the smart hand-held device will connect it to the visual program in Grasshopper using Firefly's OSC node. OSC values (user data) received by Grasshopper are calibrated, and then sent to their corresponding modeling parameters and motors in the artifact. Parameter values communicated between the digital model and the artifact are angles of rotation.

Angles of rotation for Servomotor 1 and 2 are obtained from the digital panels' position when tracking the sun, and are sent to the artifact through the computer's USB port. Angles of rotation for Servomotors 3 and 4 are sent to both the digital model and artifact through the established wireless connection.

The smart device's interface is designed using an OSC editor [13]. The interface is customized to include a range of modeling parameters in addition to angles of rotation values (Figure 8).

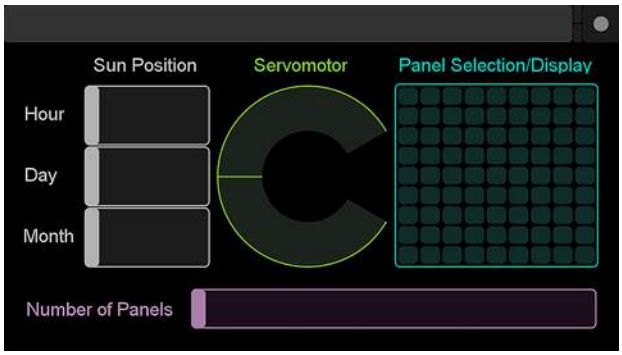

Figure 8. Interface created for the smart hand-held device for the designer to control modeling parameters.

The designer can perform the following tasks using the OSC interface:

- Panel selection: select a panel from the array to physically display its rotation using the artifact (Figure 9).
- Solar information: set the hour, day, and month for conducting daylight analysis and for moving the sun along its path.
- Angles of rotation: send rotation values to Servomotor 3 and 4.
- Number of panels: modify the array by increasing or decreasing the number of its panels.

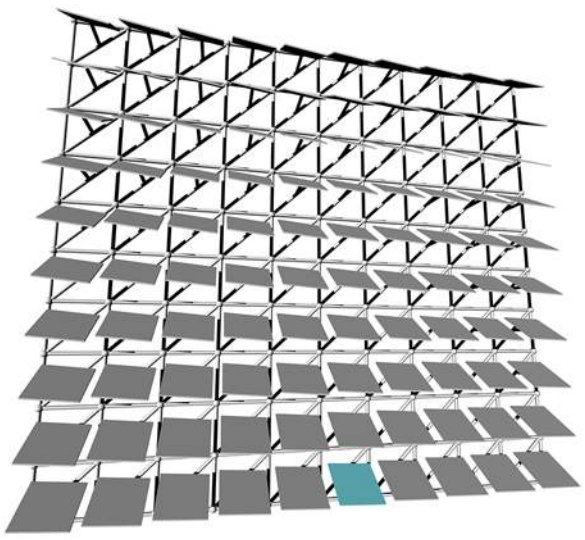

Figure 9. The panel selected through OSC interface will be highlighted in the Rhino scene (panel in the lower row), and its rotation angles will be sent to the artifact automatically.

4.7 Kinematics and Behavior

The Ladybug plug-in will import EnergyPlus weather files (.epw), which include site coordinates, temperature, radiation, solar information, etc. The suggested site for this project is located in College Station, TX, USA. Site coordinates obtained from Ladybug are used to generate a

3D sun path visualization in Rhino, which will be used to program the digital panels' rotation. A point representing the sun's position is generated on the path, which will be used in Grasshopper to create the attractor for rotating the panels.

The relationship between the panels and the sun provide the rotation angles for Servomotor 1 and 2. The process involves generating a vector between the center of the proposed site and the point representing the sun on the path. Afterwards, the vector is duplicated and centered on each panel's surface in the array. In the digital model, each panel is reoriented to face the sun by having its Normal coincident to the duplicated vector. Figure 10 shows the panels rotating to track the sun from 9 AM to 5 PM.

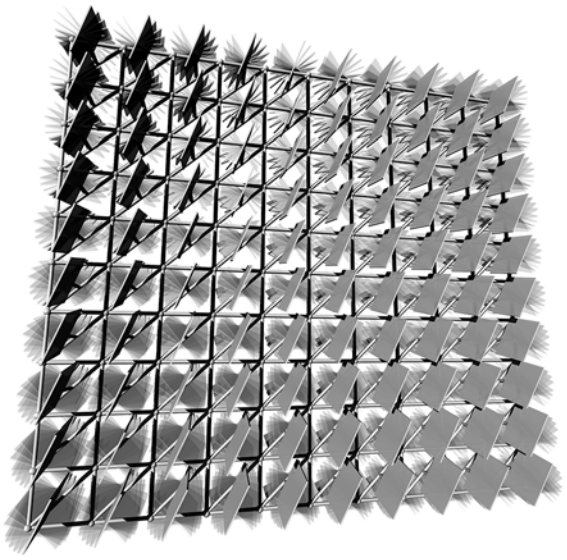

Figure 10. Testing panel rotation between 9 AM and 5 PM, 21st of August.

Angels of rotation values for each panel are not provided in the current Grasshopper program, because the relationship between the panels motion and the sun's position on the path is automated. Therefore, an additional procedure was developed in the visual program to measure the Altitude and Azimuth angles for each panel using the duplicated vectors. The calculated angles are then calibrated to match the servomotors range of motion, and then sent to the artifact. Figure 11 (top and middle images) shows how the physical panel rotates when the sun position is changed in Grasshopper. The Altitude and Azimuth angle values are sent to their corresponding servomotors to display a synchronized behavior in both model.

Figure 11 (lower image) shows how the physical panel rotates using the smart hand-held device by having the user directly providing the angles of rotation for Servomotor 3 and 4. The third axis of rotation is restricted in motion between the angles of 120 to 150 degrees in both the digital and physical models. The aim is to avoid clashes between the panel and its supporting structure.

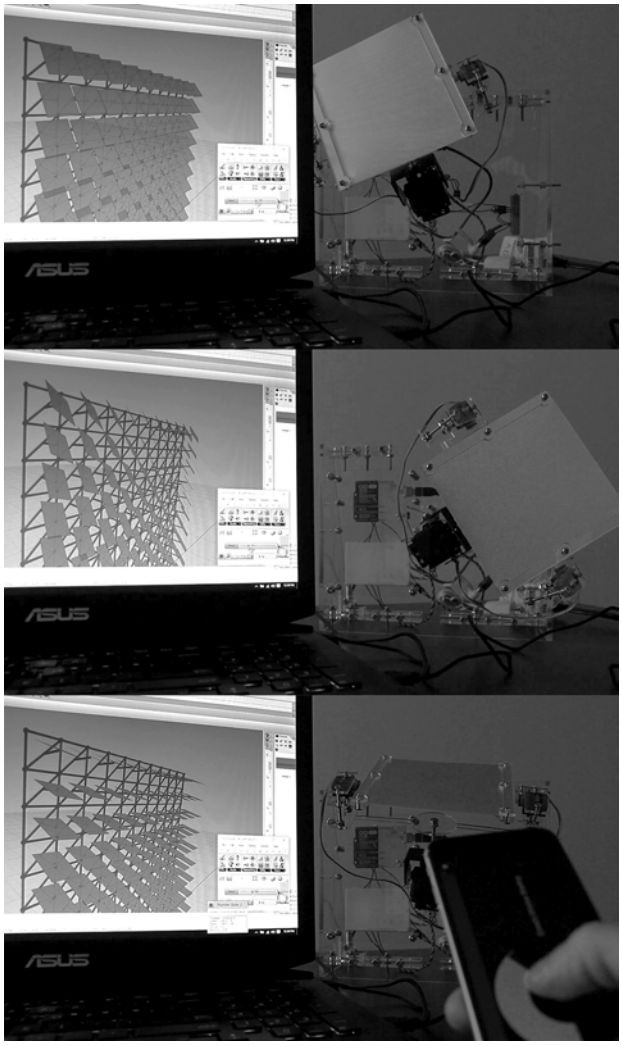

Figure 11. The hybrid workstation with all three components linked with each other. Panel rotated to block direct sun at 2 PM, 21st of December (top image); Panel rotated to block direct sunlight at 11 AM on the same day (middle image); and smart device used to rotate the panels using the OSC dial (lower image).

5 SIMULATION

The aim of the proposed work is to develop a workstation to bridge digital and physical environments together to design and evaluate kinetic objects intended for daylight applications. The prototyping process, previously discussed, explains the making of the workstation. This section will focus on integrating simulation tools with the proposed workflow. The use of daylight analysis tools in this experiment are not used to prove that a specific type of geometry or motion suggests an optimal solution for a daylight condition, it is rather meant to demonstrate the benefits of juxtaposing digital and physical information together to inform the designer's decisions and process.

Ladybug, as previously mentioned, provides interactive visualizations and weather data used to construct the parametric features of the shading system. However, for simulation purposes Diva for Grasshopper is used to

conduct the analysis. Diva's analysis procedures and metrics are setup and accessed through the visual program. For this work, a Climate-Based analysis is used; Grid-based with two feet spacing and a minimum illuminance of 300 lux. Material setup for the base-case objects are selected from the predefined material library provided by Diva: ceiling (GenericCeiling_70), walls (GenericWall_50), floor (GenericFloor_20), window (Glazing_SinglePanel_88), and outside pavement (OutsideGround_20). As for the panels, the material was custom made through the *Radiance Color Picker* [5]. The panels' material was digitally generated by measuring the reflectance value of the physical panel in the artifact using an EXTECH light meter (Figure 12). The digitized material was imported into the Diva library and applied to the panels using Grasshopper.

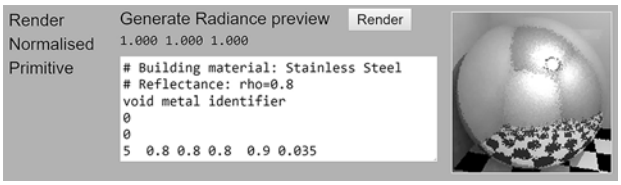

Figure 12. Generated panel material for daylight analysis.

Two types of daylight simulations were performed using Diva, DA (Daylight Autonomy) and False Color. The DA parameters were set to 300 lux and 3 for the ambient bounces. The rest of the parameters were left unchanged (Figure 13).

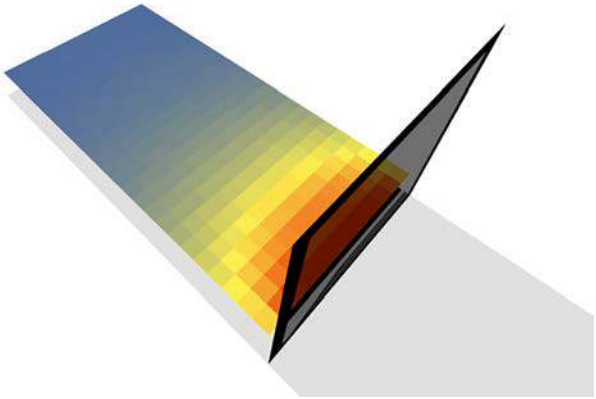

Figure 13. DA results using Diva for Grasshopper.

The parameters for the second simulation using False Color were set to Overcast Sky at 6 PM, 21st of June (Figure 14). The daylight analysis as seen in both the DA and the False color images show that the design does not qualify for LEED points. Therefore, improvements to the shading system is required. Geometric and material modifications can be simply made by replacing the current panel in both the digital model and artifact with a different design option. The changes will not affect the current system. Such a feature will enable designers to examine a wide range of design configurations while having the workstation intact. However, if a different type of kinetic motion is needed then the designer will reconsider using the same artifact.

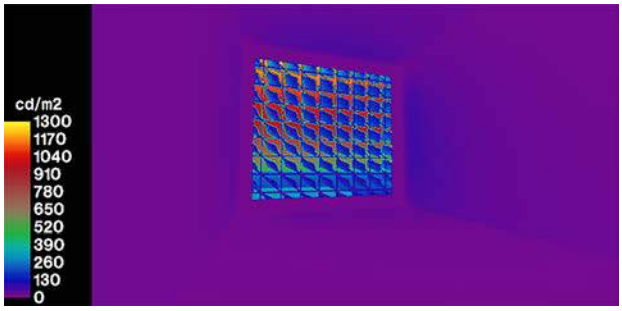

Figure 14. False Color image generated using Diva for Grasshopper.

6 DISCUSSION

Using Diva for Grasshopper in the proposed workflow has shown the possibility of integrating all necessary tools to create a functional hybrid workstation for designing, controlling, and evaluating kinetic objects. However, the current Diva for Grasshopper version (2.0.0.7) provides partial functionality when compared to its Rhino version.

The use of smart hand-held devices enables users to manage complex design tasks through a customizable interface. Setting up the smart hand-held device in this workflow was a straightforward process, uploading a template to the device and connecting it to the wireless LAN. The approach will assist AEC professionals and different parties involved in a project to expressively and remotely partake in the design, review, and evaluation process of a kinetic system.

However, the hybrid workstation has shown limitations and areas of further development. Data translating from one medium to the other required extensive calibration to achieve the desired kinetic behavior. The process also involved going back and forth between the digital and physical models to avoid geometric clashes and misalignments, correcting programming procedures, testing mechanical responses, etc. An issue with the current system, is that Diva did not provide real-time feedback during the designers' interaction; the system had to be paused when the daylight analysis was performed. A similar issue was raised by earlier works utilizing hybrid workstations with simulation tools [7, 11].

The work at this stage establishes the base for conducting further research using hybrid workstations, which involves creating large scale artifacts with sensors for live data logging. Using location specific data will help in evaluating design options in their native context, and properly compare simulations with actual results. Furthermore, earlier research suggests using live weather data to inform geometric responses [7], which smart hand-held devices maybe used to stream such data using the proposed hybrid workstation.

7 CONCLUSION

Conventional GUI applications may provide convenient tools to design and evaluate kinetic systems. Nevertheless, hybrid workstations may provide a valuable addition for digital designs workflows with extended interactive and responsive capabilities. Their ability to associate digital and physical geometric and non-geometric information together will assist designers in the progress of their work.

The work presented in this paper demonstrates an approach for creating hybrid workflows to design kinetic elements for daylight applications. The work focuses on the integration of modeling and simulation tools in a single workflow to combine the commonly separated tasks involved in daylighting (physical studies, modeling, simulation, etc.). The integration provides real-time interaction and response through smart hand-held devices. Additionally, the work provides a concise approach to design, setup, test, and evaluate a kinetic design object to address environmental issues.

REFERENCES

1. Al-Qattan, E., Galanter, P., Yan, W. Developing a tangible user interface for parametric and BIM applications using physical computing systems. *Proc. eCAADe 2016.*
2. Dourish, P. *Where the Interaction is: The foundations of Embodied Interaction*. MIT Press, Cambridge, MA, USA, 2001.
3. ElGhazi, Y.S., Mahmoud, A.H.A. Origami explorations: a generative parametric technique for kinetic cellular façade to optimize daylight performance. *Proc. eCAADe 2016*.
4. Hornecker, E., Buur, J. Getting a grip on tangible interaction: a framework on physical space and social interaction. *Proc. ACM CHI 2006*.
5. JALOXA Radiance Color Picker. http://www.JALOXA.eu/. As of 22 September 2012.
6. Kensek, K.M., Hansanuwat, R. Environment control systems for sustainable design: a methodology for testing, simulating and comparing kinetic façade systems. *Journal of Creative Sustainable Architecture & Built Environment 1 (2011), 27-45*.
7. Kensek, K.M. Integration of environmental sensors with BIM: case studies using Arduino, Dynamo, and Revit API. *Informes de la Construccion 66, 536 (2014), e044*.
8. Milgram, P., Kishino, F. A taxonomy of mixed reality visual displays. *IEICE Transactions on Information and Systems E77-D, 12 (1994), 1321-1329*.
9. O'Sullivan, D., Igoe, T. *Physical Computing: Sensing and Controlling the Physical World with Computers*. Thomson, Boston, MA, USA, 2004.
10. Payne, A. Johnson, J.k. http://www.fireflyexperiments.com/. As of 2012.
11. Plotnikov, B., Schubert, G., Petzold, F. Tangible Grasshopper: a method to combine physical models with generative parametric tools. *Proc. eCAADe 2016.*
12. Salim, F.D., Mulder, H.M., Burry, J.R. Form fostering: a novel design approach for interacting with parametric models in the embodied virtuality. *Journal of Information Technology in Construction 16 (2011) 133-148*.
13. TouchOSC editor. http://www.hexler.net/. As of 2017.

Estimating the Cooling Power through Transpiration of Vining Green Walls in Various Climates

Arta Yazdanseta

Doctoral of Design Program, Harvard Graduate School of Design
Cambridge, U.S.
ayazdanseta@gsd.harvard.edu

ABSTRACT

Limited studies have been conducted on the impact of green walls on the energy performance of buildings. Green walls can reduce the cooling loads of buildings through shading and transpiration. Most studies have focused on the shading effect of green walls. This paper investigates the transpiration effect of green walls. For this investigation, the Penman-Monteith model was modified to estimate the cooling power from transpiration produced by vining indirect green walls in six distinct climatic conditions. The model accounts for green wall design, plant biophysical traits, and environmental conditions. The model shows that under optimal design conditions, green walls can produce a maximum cooling power of 377 w/m^2 through canopy transpiration.

Author Keywords

Green wall design; Cooling power, Penman-Monteith model; Vine transpiration.

1 INTRODUCTION

Vining green walls are a component of green urban infrastructure [1]. They are vertical structures affixed with climbing plants (i.e., vines). The two general types of vining green walls are "direct" green walls, wherein the vines attach directly to the wall, and "indirect" green walls, wherein the vines attach to a vertical structure separated from the wall itself [2].

Green walls are robust passive systems that can cover large surfaces in a relatively short time, are cost effective, and if designed properly, require minimal human intervention and maintenance over their life spans [3-5].

They can reduce the cooling loads of buildings both by minimizing solar gains and by cooling the microclimates surrounding buildings via transpiration [6-10]. In addition, by lowering infiltration rates and convection flows, green walls can reduce the heating loads of buildings [2, 10]. The thermal impact of a green wall on a building depends on several parameters, including plant biophysical traits, the orientation and design of the green wall, and the climatic conditions [1, 3].

On like green roofs, limited studies have been conducted on green walls. Additionally, the majority of the studies that have been conducted focused solely on the cooling from the shading effect of green walls. While the effects of transpiration are widely appreciated, only a few studies have attempted to mathematically model the cooling effects produced from the transpiration of green walls [11-14], and none of the proposed models is sufficiently robust to be used as a design tool.

The objective of this paper is to develop a model that allows designers to estimate the cooling power produced from transpiration by indirect vining green wall designs in different climates. The model accounts for (a) plant biophysical traits, (b) green wall physical design parameters, and (c) six different climate types.

2 THEORETICAL BACKGROUND

The Penman-Monteith (P-M) model is the most dominant method for estimating the transpiration rate of a vegetative canopy. The model has been utilized by the Food and Agriculture Organization of the United Nations (FAO 56 Method) to estimate the transpiration rates of various crop fields [15]. It accounts for environmental variables, plant biophysical traits, and various time scales (hourly and daily) (1).

$$TR_c = \frac{\Delta \,.\, R_n + K_{time} \,.\, \frac{\rho_a . C_p . VPD}{r_a}}{\lambda[\Delta + \gamma(1 + {}^{r_c}/_{r_a})]} \qquad (1)$$

where TR_c is the canopy transpiration rate [mm/h, mm/d], Δ is the slope of saturation vapor pressure vs. temperature [kPa/°C], R_n is the net radiation absorbed by the canopy [MJ/m^2.h, MJ/m^2.d], K_{time} is a unit time conversion (86400 second per day; 3600 second per hour), ρ_a is the density of dry air [kg/m^3], C_p is the specific heat of dry air at constant pressure [MJ/kg°C], VPD is the vapor pressure deficit of air [kPa], r_a is the aerodynamic resistance [s/m], r_c is the canopy resistance [s/m], λ is the latent heat of vaporization of water [MJ/kg], and γ is the psychrometric constant [kPa/°C].

The P-M model treats a canopy as a large, continuous, horizontal leaf without water limitations [15]. Therefore, the model is rather successful when used to analyze large and dense crop fields. However, studies of isolated plants such as those in vineyards and orchards report that the model lacks precision as isolated plants are highly coupled with their surrounding environments [16-19].

SimAUD 2017 May 22-24 Toronto, Canada

2.1 2.1 Penman-Monteith Model Modifications

A few studies have demonstrated that the P-M model can be used to estimate the transpiration rates of green walls. Stec et al. [12] did not modify the model since their experiments were conducted in controlled laboratory conditions with a light source parallel to the canopy. Davis and Hirmer [14] adjusted the model by eliminating the solar radiation term and introducing a new method to calculate r_a such that it more accurately represented the unique design parameters of their green wall.

In this investigation, a variation of the P-M model was used to estimate the transpiration rates, and ultimately cooling power, of green walls. Similar to plants in vineyards, green walls are isolated canopies that are highly coupled with their surrounding environments. Therefore, I have adjusted the P-M model to account for these climatic conditions. The modified variables are highlighted below. All other variables have been calculated following the FAO 56 instructions [15].

Time Scale

The FAO 56 method offers both daily and hourly time step calculations (1). To adjust for the appropriate resolution corresponding with a building scale, the P-M model was adjusted to evaluate monthly time intervals. The monthly estimation can be particularly advantageous when using the P-M model, as some studies have reported that the model can predict the water use of canopies within 1% accuracy. The accuracy of the model is reduced for smaller time steps, such as daily or hourly [16].

Only transpiration during daylight hours was considered since night-time transpiration is negligible. To do this, the daylight hours of the 15th of each month were calculated and converted to the number of seconds in a month (2).

$$K_{time} = N_h . D_m . 3600 \quad (2)$$

Where N_h is the Daylight Hours of the 15th of a month, D_m is the number of days in a month, and 3600 seconds per hour conversion constant. Note that N_h, was calculated using FAO 56 field methods [15]. Subsequently, all environmental variables have been adjusted to the monthly time scale.

Absorbed Net Radiation (R_n)

Solar radiation is the most significant variable impacting the transpiration rate. The P-M model was adjusted to account for the appropriate net radiation that is absorbed by a vertical surface against a building facade. According to FAO 56, the net radiation absorbed by a canopy, R_n, can be estimated by:

$$R_n = R_{ns} - R_{nl} \quad (3)$$

where R_{ns} is the net shortwave radiation [MJ/m^2.day] and R_{nl} is the net longwave radiation emitted from the canopy surface [MJ/m^2.day]. R_{ns} is calculated as a fraction of the total received shortwave radiation, R_s, [MJ/m^2.day], where α represents the albedo of the canopy (4). The FAO 56 model considers the albedo value of a grass field to be 0.23. This value has been used throughout this investigation.

$$R_{ns} = (1-\propto)R_s \quad (3)$$

A vertical surface only collects a fraction of the total radiation received by a horizontal surface. The received shortwave radiation on a vertical surface depends not only on the geographical location and the time of the day, but also on the orientation of the wall. The monthly R_s values were estimated using a solar simulation software, *DIVA for Rhino.* Six climate scenarios corresponding with summer conditions in six U.S. cities were selected (Table 1).

Climate Types	City, State	Monthly Ave. Max. Temp. Range (°C), and Rain (mm)	Average r_l (s/m)
Cool & Humid	Bemidji Muni, MN	20 to 27, > 50	115
Cool & Dry	Cut Bank, MN	20 to 27, < 50	256
Warm & Humid	New York, NY	27 to 32, > 50	128
Warm & Dry	Denver, CO	27 to 32, < 50	152
Hot & Humid	Miami, FL	32 to 40, > 50	91
Hot & Dry	Phoenix, AZ	32 to 40, < 50	125

Table 1. Summer month climate conditions and average r_l

The monthly R_s values for a black, south facing, vertical unit surface were simulated for each climate condition using TMY30 weather files.

To calculate R_{nl}, the FAO 56 accounts for the longwave radiation leaving the surface of the canopy multiplied by a correction factor for air humidity and cloudiness. The monthly R_{nl} was calculated following the FAO 56 equations, but a factor of 0.5 was introduced to adjust for the vertical surface sky view (a horizontal view of gets a coefficient of one).

Aerodynamic Resistance (r_a)

Aerodynamic resistance, r_a, [s/m] determines the transfer of heat and water vapor from a plant surface into the air above the canopy. Although the r_a equation suggested by FAO 56

has proven valuable for short, dense crops, studies on grapevines have reported that the equation works poorly for tall, isolated plants [18]. Several field studies in both "hot and dry" and "cool and humid" climates [16, 18, 19] show a good agreement between the gathered data and the r_a model developed by Thom and Oliver for tall, isolated plants [17]. The Thom and Oliver model was used to estimate the r_a values for this investigation (5).

$$r_a = \frac{4.72[In\left(\frac{Z}{Z_0}\right)]^2}{(1+0.54u)} \quad (4)$$

where Z is the height of measurement of wind speed (normally taken at 2 m above ground), Z_0 is the roughness height (taken as 0.13 times the canopy's height, h (m), [18]), and u is the wind speed (m/s).

Canopy Resistance (r_c)

Canopy resistance describes the resistance of vapor flow through the transpiring canopy [15]. In reality, r_c continuously changes due to rapid stomatal responses to environmental conditions, water availability, and plant geometry [20, 21]. The FAO 56 model requires a fixed canopy resistance to calculate plant transpiration and is given by:

$$r_c = \frac{r_l}{LAI_{Slit}} \quad (5)$$

where r_c is the canopy surface resistance [s/m], r_l is the bulk stomatal resistance of a well-illuminated leaf [s/m], and LAI_{Slit} is the Sunlit Leaf Area Index [-]. The Leaf Area Index (LAI) is a dimensionless value describing the ratio of the area of a one-sided leaf to the unit area of the surface behind the leaf (i.e., the ground or a wall). LAI_{Slit} is the amount of leaf area that receives sunlight and therefore contributes to the transpiration rate of a green wall. LAI_{Slit} is a function of LAI, solar elevation, and leaf angle [20]. Note that for this study a vertically oriented canopy was assumed.

The LAI values for different plant species vary widely. In practice, LAI is empirically obtained through various direct or indirect methods [20]. The FAO 56 model suggests values of 3 to 5 for most mature crops. This assumption seems consistent with LAIs observed for mature green walls [22].

Although the FAO 56 method for estimating r_c is simple, the bulk stomatal resistance values, r_l, can be challenging to obtain, as there are limited studies on urban vine species. Because of this problem, most studies on transpiration rates of green walls use a generic r_l value of woody plants.

This assumption is not correct, since r_l values vary between species and climates. To address this problem, this investigation analyzed records of stomatal resistances of various vine species (agricultural and non-agricultural) in six different climates. Field measured values of bulk stomatal resistance were analyzed from 22 studies for 89 vine species from 11 geographical locations [18, 23-43].

For example, the largest r_l library is for grapevines in warm and dry climates. 25 studies reported r_l values between 100 and 200 s/m (with an average of 151 s/m). Six studies reported r_l values of less than 100 s/m and three studies reported r_l values larger than 300 s/m. The average r_l values from these small "outlier" groups were used to define the range of r_l values over which the model was tested. The average r_l value of 151 s/m from the 25-data point group was used for calculations.

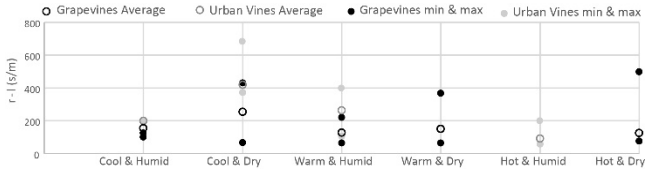

Figure 1. Stomatal resistance averages and ranges per climate conditions for grapevine and urban vines.

Figure 1 shows the average, high, and low r_l values of grapevines and urban vines (non-agricultural vines). Three distinct patterns can be observed. First, as climates become warmer, the r_l range becomes greater. In other words, the difference between the highest and lowest r_l values increases. Second, this trend is exacerbated in dry climates, especially for urban vines. Third, in general, urban vines are more water efficient than are grapevines, meaning that they are more sensitive to humidity and water availability. As a result, their r_l values are larger than those of grapevines. A similar pattern was also observed by Bell et al., wherein they measured the leaf resistances of three urban vines in Maryland, USA for two summers [24].

The r_l library provides a much needed database for designers of vining indirect green walls. It can be used to help calculate a range of possible cooling power performances for both agricultural and non-agricultural vines. Furthermore, it demonstrates the importance of plant biophysical traits in green wall design performance.

3 MODEL VALIDATION AND SENSETIVITY ANALYSIS

The modified P-M model for vertical green walls was written in Engineering Equation Software (EES). The model was verified in two stages. First, the general behaviors of each variable (R_n, VPD, u, r_a, and r_c) and their respective impacts on transpiration rates were studied and compared to H.G. Jones [20]. The modified P-M model shows a good agreement (Figure 2) with the reference. Note that canopy height, h, and roughness was assumed to be 1.5 m (4).

Second, the predicted TR_c values for grapevines in each climate condition were compared to their reported field measured counterparts [16, 19, 44-55]. The results showed a good agreement except for in the cool and dry climate where the estimated TR_c value was approximately half of the reported value (Figure 3). Note that since grapevines do not thrive in humid climates, the TR_c value of a Kudzu vine was used for the warm and humid climate. No comparable vine for the hot and humid climate was found.

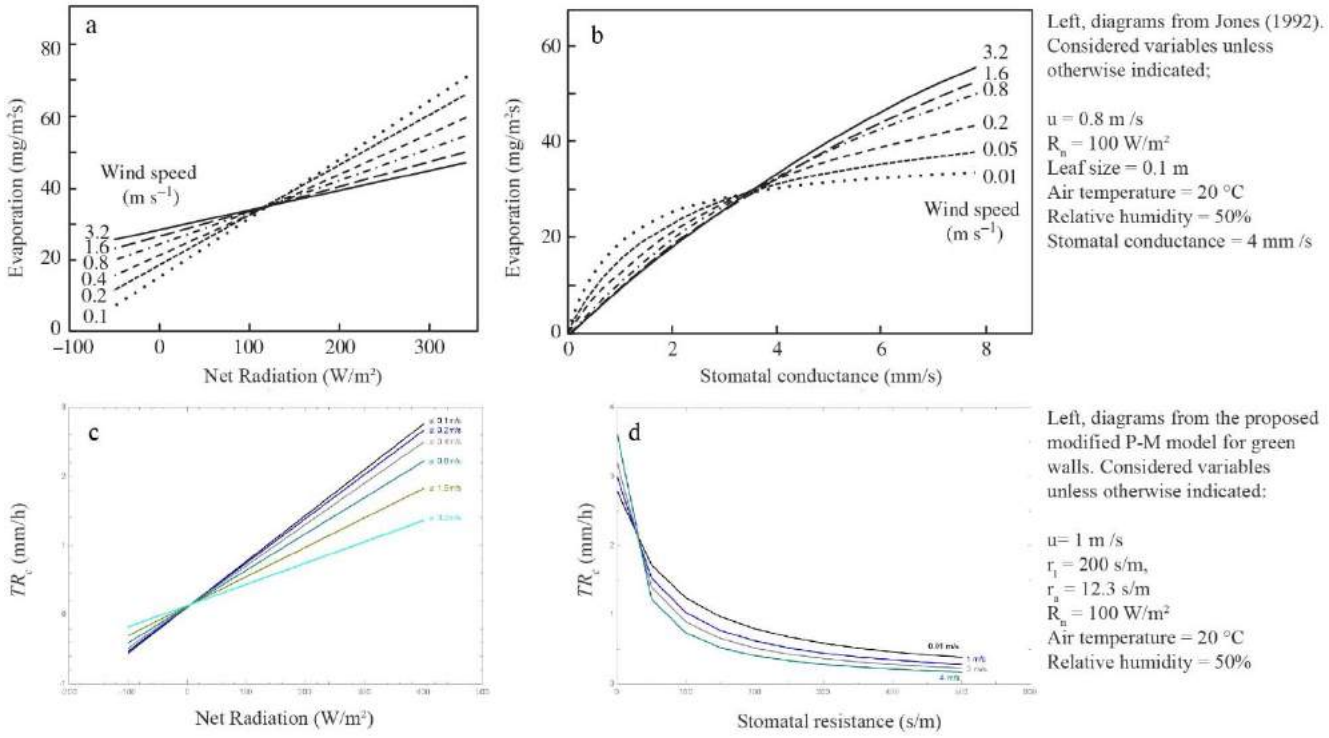

Figure 2. Modified P-M model study. The results (c, d) were compared to H.G. Jones (1992) studies (a, b). a and c: transpiration as a function of solar radiation and wind speed. b and d: transpiration as a function of stomatal conductance (b) / resistance (d) and wind speed. Note stomatal resistance is equal to the inverse of stomatal conductance.

4 GREEN WALL DESIGN OPTIMIZATION

The modified model was then used to identify the optimal green wall design parameters for maximum cooling power in six climates. The parametric studies were conducted using EES software. The cooling power was calculated by converting the transpiration rate (mm/month) from a unit surface of a canopy to cooling power (w/m^2) [15, 56].

The cooling power range of a green wall as a function of r_c and r_a in a hot and dry climate is shown in Figure 4. The dotted lines define the range of possible r_c values for both grapevine species. The largest and smallest r_a values correspond with short grass and forest, respectively. The r_a of 10 s/m represents a typical canopy aerodynamic resistance value for a grapevine in a vineyard (h=1.5 m, Z= 0.13h, and u=2 m/s). The cross over point, r_{cp}, is where the canopy temperature reaches the ambient temperature.

This analysis was conducted for all six climate types. The results show that the greatest transpiration rates occur in hot and dry climates followed by warm and dry, and cool and dry, climates. The humid regions with hot, warm, or cool summers correspond with the lowest ranges of canopy cooling power.

Furthermore, two patterns are apparent from the r_{cp} points. First, their values are reduced for both the dry and humid climates as summer temperatures decrease. This is because sensible cooling becomes more prevalent in cooler climates. Second, in the dry vs. humid climates with similar summer temperatures, e.g., hot and dry vs. hot and humid, the r_{cp} values in the dry climates are consistently larger than are those in the corresponding humid climates. This indicates that in dry climates, r_l has a greater impact on the cooling of a canopy. Under these conditions, latent cooling dominates.

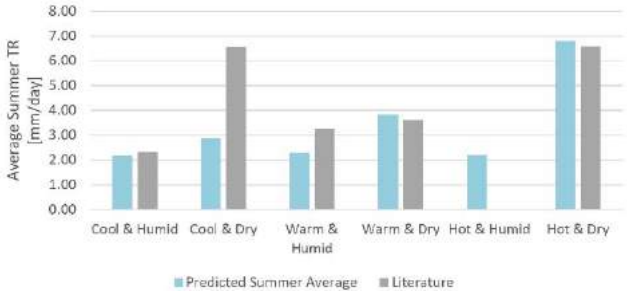

Figure 3. Comparative study of average summer day TR_c from modified P-M model and literature on grapevine canopies (LAI= 5, U=2 m/s, h=1.5 m, r_c= 150 s/m)

Moreover, for all the climate scenarios, transpiration rates increase as r_a decreases. The large r_a values correspond with dense, uniform field conditions, such as grass and crop fields, where plants are poorly connected to their surrounding environments. On the other hand, the small r_a

values represent conditions where the canopy is highly coupled with its surroundings, e.g., grapevines and forests. Theoretically, transpiration rates increase when the height of the canopy increases and wind speed decreases. However, in reality, transpiration is restricted by r_l. For example, forest transpiration is often less than field transpiration since most forest species (especially in coniferous forests) have relatively high r_l values [20].

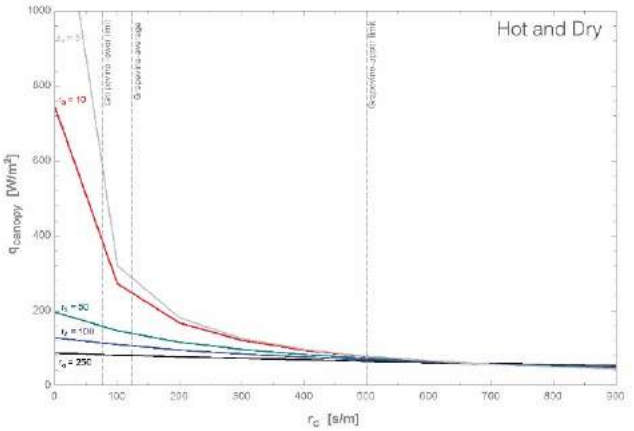

Figure 4. Cooling power as a function of r_c for various r_a.

Since r_c has a direct relationship with r_l and an inverse relationship with *LAI*, canopies with low r_l values and high *LAI* values should have the largest transpiration rates (5). Figure 5 illustrates r_c as a function of r_l and *LAI* in a hot and dry climate. The dotted line represents the r_c value corresponding with a cooling power of 100 W/m^2 and average r_c value of grapevines. Similar study were conducted for other climatic conditions.

Vine canopies in only three out of six climate conditions have the potential to produce 100 W/m^2 or more of cooling power. As expected, the hot and dry climate provides the most robust conditions (designated by the pink box). In this scenario, r_c and r_l can reach values as large as 400 s/m and 370 s/m, respectively. Within this boundary, most sun-loving vine species can produce significant cooling power.

The warm and dry climate provides the second largest boundary. In this environment, the r_c and r_l values of 200 s/m or less can produce 100 W/m^2 or more of cooling power. Most Vitis (grapevine) species can meet this requirement easily. Finally, the r_c and r_l values of approximately 100 s/m can produce 100 W/m^2 or more of cooling power in hot and humid climates. In these environments, most urban vines thrive.

The 100 W/m^2 cutoff point eliminated warm and humid, cool and dry, and cool and humid climates. However, a green wall canopy still produces cooling power in those climatic conditions. The average cooling power values during summer months are approximately 80 W/m^2 for the cool and dry climate followed by 60 W/m^2 for both the warm and humid, and cool and humid, climates.

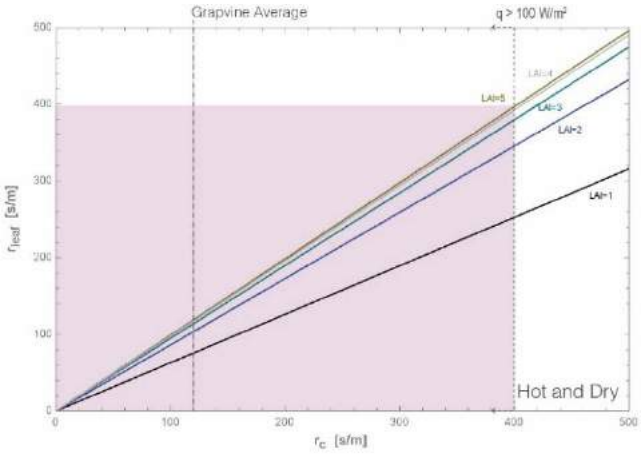

Figure 5. r_c as a function of r_l and various *LAI*.

Furthermore, for low values of *LAI*, the impact of r_l on r_c is significant. As *LAI* increases, the influence of r_l on r_c decreases, since there are more leaves within the canopy to transpire. Note that during summer months, *LAI* values of 3, 4 and 5 are fairly common for green walls.

When provided with a strong support structure, most vines can climb up to 20 m. Although in most cases wind speed cannot be controlled, the height, *h*, of the canopy can be adjusted to reduce r_a. Parametrically studying r_a as a function of *u* and *h* illustrates that as *h* increases, r_a decreases. However, the impact of *h* on r_a becomes negligible as *h* reaches 10 m. As expected, an increase in wind speed, *u,* reduces r_a as long as r_c does not impose restrictions on water vapor loss from stomatal.

Figure 6 illustrates the best design options for maximizing the cooling power of a south facing green wall in the month of June in various climates. The average r_c values, accounting for the possibility of 10% variability, and the corresponding maximum cooling power values, are highlighted with a pink bar and text, respectively. The cooling power values of three green walls with different heights (3 m, 6 m, and 9 m) for no wind (0.1 m/s) and a wind speed of 2 m/s are considered.

The largest cooling power is produced in the hot and dry climate followed by the warm and dry, and hot and humid, climates. Except for in the cold and dry climate, the tallest canopy (9 m) with a wind speed of 2 m/s produces the largest cooling power. The least cooling power is produced in the cold and dry climate where the cooling is mostly provided through convection and not transpiration. This is due to high average r_c values (255 s/m). The r_c values of 100 s/m or smaller can significantly improve the cooling power of a canopy. For all climates, the positive impact of wind on cooling power decreases as the height of the canopy increases. The largest impact of wind on cooling power is when the canopy is 3 m tall. This study suggests that in all climates, wind only slightly improves the cooling power of canopies taller than 6 m.

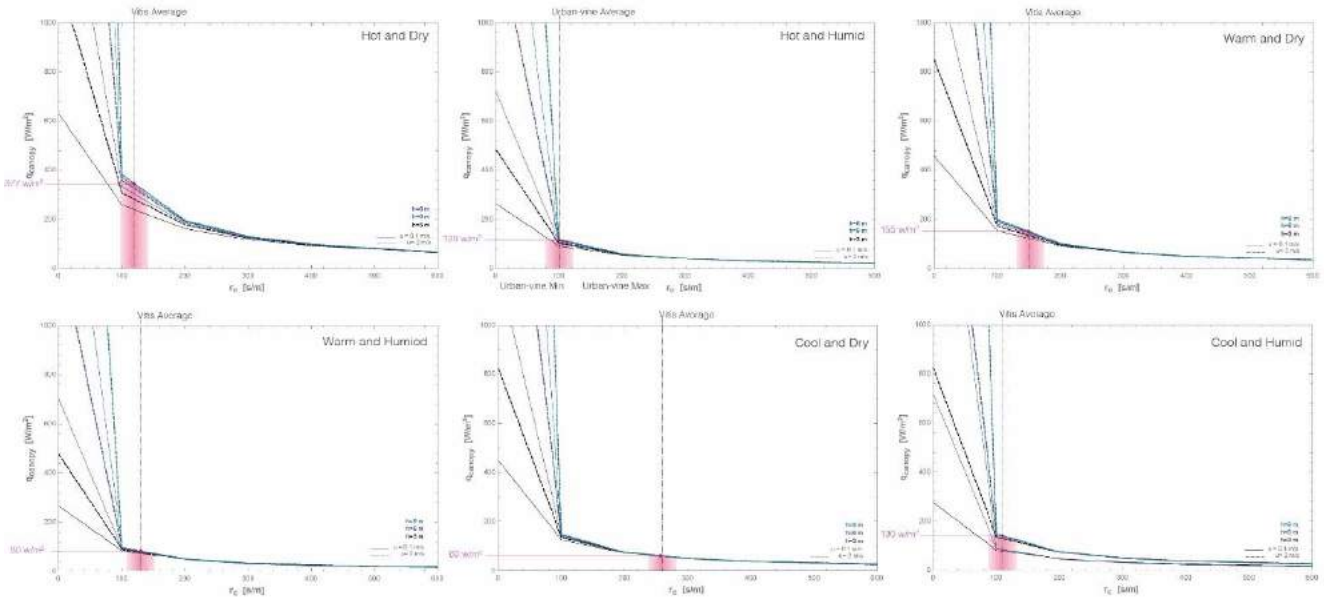

Figure 6. Month of June cooling power of south facing canopy in various climates as a function of canopy resistance (r_c) and aerodynamic resistance (r_a) for various canopy heights (3, 6 and 9 m) and wind speeds (0.1 and 2 m/s). The pink bar represents the average r_c values per climate with 10% possible changes.

Furthermore, in all climates, r_c values of 100 s/m or less greatly improve canopy cooling power. However, the influence of canopy height must be further investigated, as some studies on forests suggest that stomatal resistance increases as height increases [20]. This would result in lower transpiration rates and cooling power rates at higher canopy elevations.

5 DISCUSSION AND CONCLUSION

The modified P-M model described in this paper allows designers to estimate the monthly cooling power produced from a vining indirect green wall. This cooling power can be translated to environmental temperature reduction or, in accordance with occupant thermal comfort boundaries, brought into the building as a passive cooling strategy.

Furthermore, this study illustrates the importance of canopy geometry, plant biophysical traits, and climatic conditions on the performance of green walls as evaporative cooling systems. The optimal designs disclosed by this study and the associated cooling power values per climate type can be used to estimate the performance of vining indirect green walls.

ACKNOWLEDGMENTS

The author wishes to thank Professor Ali Malkawi, Professor Holly Samuelson, and Collin Vierra for their time and support during this research.

REFERENCE

1. Cameron, R.W., Taylor, J.E., and Emmett, M.R., "What's 'cool'in the world of green façades? How plant choice influences the cooling properties of green walls," *Building and Environment*, Vol. 73 2014, pp. 198-207.

2. Perini, K., Ottelé, M., Haas, E., and Raiteri, R., "Greening the building envelope, façade greening and living wall systems," *Open Journal of Ecology*, Vol. 1, 01 2011, pp. 1.

3. Hunter, A.M., Williams, N.S.G., Rayner, J.P., Aye, L., Hes, D., and Livesley, S.J., "Quantifying the thermal performance of green façades: A critical review," *Ecological Engineering*, Vol. 63 2014, pp. 102-113.

4. Mitsch, W. and Jorgensen, S., "Ecological engineering: A field whose time has come," *Ecological Engineering; Ecol.Eng.*, Vol. 20, 5 2003, pp. 363-377.

5. Mitsch, W., "What is ecological engineering?" *Ecological Engineering; Ecol.Eng.*, Vol. 45 2012, pp. 5-12.

6. Cheng, C., Cheung, K.K., and Chu, L., "Thermal performance of a vegetated cladding system on facade walls," *Building and Environment*, Vol. 45, 8 2010, pp. 1779-1787.

7. Hoyano, A., "Climatological uses of plants for solar control and the effects on the thermal environment of a building," *Energy & Buildings*, Vol. 11, 1 1988, pp. 181-199.

8. Holman, J.P.(., *Heat transfer*, McGraw-Hill, New York, 1976, pp. xvii, 530 p.

9. Ip, K., Lam, M., and Miller, A., "Shading performance of a vertical deciduous climbing plant canopy," *Building and Environment*, Vol. 45, 1 2010, pp. 81-88.

10. Price, J.W., Green Facade Energetics, 2010University of Maryland, MD, USA.

11. Alexandri, E. and Jones, P., "Temperature decreases in an urban canyon due to green walls and green roofs in

diverse climates," *Building and Environment*, Vol. 43, 4 2008, pp. 480-493.

12. Stec, W.J., van Paassen, A.H.C., and Maziarz, A., "Modelling the double skin façade with plants," *Energy & Buildings*, Vol. 37, 5 2005, pp. 419-427.

13. Susorova, I., Angulo, M., Bahrami, P., and Stephens, B., "A model of vegetated exterior facades for evaluation of wall thermal performance," *Building and Environment*, Vol. 67 2013, pp. 1-13.

14. Davis, M.M. and Hirmer, S., "The potential for vertical gardens as evaporative coolers: An adaptation of the ' Penman Monteith Equation'," *Building and Environment*, Vol. 92 2015, pp. 135-141.

15. Allen, R.G., Pereira, L.S., Raes, D., and Smith, M., "Crop evaporation–Guidelines for computing crop water requirements–FAO Irrigation and drainage paper 56," *Food and Agriculture Organization of the United Nations, Rome* 1998.

16. Dragoni, D., Lakso, A.N., Piccioni, R.M., and Tarara, J.M., "Transpiration of grapevines in the humid northeastern United States," *American Journal of Enology and Viticulture*, Vol. 57, 4 2006, pp. 460-467.

17. Thom, A. and Oliver, H., "On Penman's equation for estimating regional evaporation," *Quarterly Journal of the Royal Meteorological Society*, Vol. 103, 436 1977, pp. 345-357.

18. Lu, P., Yunusa, I.A., Walker, R.R., and Müller, W.J., "Regulation of canopy conductance and transpiration and their modelling in irrigated grapevines," *Functional Plant Biology*, Vol. 30, 6 2003, pp. 689-698.

19. Yunusa, I., Walker, R., Loveys, B., and Blackmore, D., "Determination of transpiration in irrigated grapevines: comparison of the heat-pulse technique with gravimetric and micrometeorological methods," *Irrigation Science*, Vol. 20, 1 2000, pp. 1-8.

20. Jones, H.G., *Plants and microclimate : a quantitative approach to environmental plant physiology*, Cambridge University Press, Cambridge England] ; New York, 1992.

21. Monteith, J. and Unsworth, M., *Principles of Environmental Physics: Plants, Animals, and the Atmosphere*, Academic Press, 2013.

22. Schumann, L.M., *Ecologically inspired design of green roof retrofit*, ProQuest, 2007.

23. Barker, M.G. and Pérez-Salicrup, D., "Comparative water relations of mature mahogany (Swietenia macrophylla) trees with and without lianas in a subhumid, seasonally dry forest in Bolivia," *Tree physiology*, Vol. 20, 17 2000, pp. 1167-1174.

24. Bell, D., Forseth, I., and Teramura, A., "Field water relations of three temperate vines," *Oecologia*, Vol. 74, 4 1988, pp. 537-545.

25. BOTA, B.J., Flexas, J., and Medrano, H., "Genetic variability of photosynthesis and water use in Balearic grapevine cultivars," *Annals of Applied Biology*, Vol. 138, 3 2001, pp. 353-361.

26. Carter, G.A. and Teramura, A.H., "Vine photosynthesis and relationships to climbing mechanics in a forest understory," *American Journal of Botany* 1988, pp. 1011-1018.

27. Chaves, M.M., Harley, P.C., Tenhunen, J.D., and Lange, O.L., "Gas exchange studies in two Portuguese grapevine cultivars," *Physiologia Plantarum*, Vol. 70, 4 1987, pp. 639-647.

28. Correia, M., Pereira, J., Chaves, M., Rodrigues, M., and Pacheco, C., "ABA xylem concentrations determine maximum daily leaf conductance of field-grown Vitis vinifera L. plants," *Plant, Cell & Environment*, Vol. 18, 5 1995, pp. 511-521.

29. Cuevas, E., Baeza, P., and Lissarrague, J., "Variation in stomatal behaviour and gas exchange between mid-morning and mid-afternoon of north–south oriented grapevines (Vitis vinifera L. cv. Tempranillo) at different levels of soil water availability," *Scientia Horticulturae*, Vol. 108, 2 2006, pp. 173-180.

30. Downton, W., Grant, W., and Loveys, B., "Diurnal changes in the photosynthesis of field-grown grape vines," *New Phytologist*, Vol. 105, 1 1987, pp. 71-80.

31. Edwards, W. and Warwick, N., "Transpiration from a kiwifruit vine as estimated by the heat pulse technique and the Penman-Monteith equation," *New Zealand Journal of Agricultural Research*, Vol. 27, 4 1984, pp. 537-543.

32. Escalona, J.M., Flexas, J., and Medrano, H., "Stomatal and non-stomatal limitations of photosynthesis under water stress in field-grown grapevines," *Functional Plant Biology*, Vol. 27, 1 2000, pp. 87-87.

33. Fichtner, K. and Schulze, E., "Xylem water flow in tropical vines as measured by a steady state heating method," *Oecologia*, Vol. 82, 3 1990, pp. 355-361.

34. Leuzinger, S., Hartmann, A., and Körner, C., "Water relations of climbing ivy in a temperate forest," *Planta*, Vol. 233, 6 2011, pp. 1087-1096.

35. Liu, W., Pool, R., Wenkert, W., and Kriedemann, P., "Changes in photosynthesis, stomatal resistance and abscisic acid of Vitis labruscana through drought and irrigation cycles," *American Journal of Enology and Viticulture*, Vol. 29, 4 1978, pp. 239-246.

36. Liu, W., Wenkert, W., Allen Jr, L., and Lemon, E., "Soil-plant water relations in a New York vineyard;

resistances to water movement." *Journal American Society for Horticultural Science* 1978.

37. Padgett-Johnson, M., Williams, L., and Walker, M., "Vine water relations, gas exchange, and vegetative growth of seventeen Vitis species grown under irrigated and nonirrigated conditions in California," *Journal of the American Society for Horticultural Science*, Vol. 128, 2 2003, pp. 269-276.

38. Quick, W., Chaves, M., Wendler, R., David, M., Rodrigues, M., Passaharinho, J., Pereira, J., Adcock, M., Leegood, R., and Stitt, M., "The effect of water stress on photosynthetic carbon metabolism in four species grown under field conditions," *Plant, Cell & Environment*, Vol. 15, 1 1992, pp. 25-35.

39. Rogiers, S.Y., Greer, D.H., Hutton, R.J., and Clarke, S.J., "Transpiration efficiency of the grapevine cv. Semillon is tied to VPD in warm climates," *Annals of Applied Biology*, Vol. 158, 1 2011, pp. 106-114.

40. Sanches, M. and Válio, I., "Photosynthetic response of two tropical liana species grown under different irradiances," *Photosynthetica*, Vol. 46, 4 2008, pp. 557-566.

41. Schultz, H., "Water relations and photosynthetic responses of two grapevine cultivars of different geographical origin during water stress," *Strategies to Optimize Wine Grape Quality 427* 1995, pp. 251-266.

42. Smart, R., "Aspects of water relations of the grapevine (Vitis vinifera)," *American Journal of Enology and Viticulture*, Vol. 25, 2 1974, pp. 84-91.

43. Winkel, T. and Rambal, S., "Stomatal conductance of some grapevines growing in the field under a Mediterranean environment," *Agricultural and Forest Meteorology*, Vol. 51, 2 1990, pp. 107-121.

44. Braun, P. and Schmid, J., "Sap flow measurements in grapevines (Vitis vinifera L.) 2. Granier measurements," *Plant and Soil*, Vol. 215, 1 1999, pp. 47-55.

45. Intrigliolo, D., Lakso, A., and Piccioni, R., "Grapevine cv.'Riesling'water use in the northeastern United States," *Irrigation Science*, Vol. 27, 3 2009, pp. 253-262.

46. Moutinho-Pereira, J., Correia, C., Gonçalves, B., Bacelar, E., and Torres-Pereira, J., "Leaf gas exchange and water relations of grapevines grown in three different conditions," *Photosynthetica*, Vol. 42, 1 2004, pp. 81-86.

47. Evans, R., Spayd, S., Wample, R., Kroeger, M., and Mahan, M., "Water use of Vitis vinifera grapes in Washington," *Agricultural Water Management*, Vol. 23, 2 1993, pp. 109-124.

48. Eastham, J. and Gray, S.A., "A preliminary evaluation of the suitability of sap flow sensors for use in scheduling vineyard irrigation," *American Journal of Enology and Viticulture*, Vol. 49, 2 1998, pp. 171-176.

49. Poblete-Echeverría, C. and Ortega-Farias, S., "Evaluation of single and dual crop coefficients over a drip-irrigated Merlot vineyard (Vitis vinifera L.) using combined measurements of sap flow sensors and an eddy covariance system," *Australian Journal of Grape and Wine Research*, Vol. 19, 2 2013, pp. 249-260.

50. Patakas, A., Noitsakis, B., and Chouzouri, A., "Optimization of irrigation water use in grapevines using the relationship between transpiration and plant water status," *Agriculture, Ecosystems & Environment*, Vol. 106, 2 2005, pp. 253-259.

51. Forseth, I. and Teramura, A., "Field photosynthesis, microclimate and water relations of an exotic temperate liana, Pueraria lobata, kudzu," *Oecologia*, Vol. 71, 2 1987, pp. 262-267.

52. Erie, L., French, O.F., and Harris, K., "Consumptive use of water by crops in Arizona," 1965.

53. Bucks, D., Erie, L., NAKAVAMA, F., and French, O., "Trickle irrigation management for grapes," 1974.

54. Lascano, R., Baumhardt, R., and Lipe, W., "Measurement of water flow in young grapevines using the stem heat balance method," *American Journal of Enology and Viticulture*, Vol. 43, 2 1992, pp. 159-165.

55. Padgett-Johnson, M., Williams, L., and Walker, M., "Vine water relations, gas exchange, and vegetative growth of seventeen Vitis species grown under irrigated and nonirrigated conditions in California," *Journal of the American Society for Horticultural Science*, Vol. 128, 2 2003, pp. 269-276.

56. Gates, D.M., *Biophysical ecology*, Springer-Verlag, New York, 1980.

Assisting the development of innovative responsive façade elements using building performance simulation

M.L. de Klijn-Chevalerias[1], R.C.G.M. Loonen[1], A. Zarzycka[1], D. de Witte[2], M.V. Sarakinioti[2] and J.L.M. Hensen[1]

[1]Eindhoven University of Technology
Eindhoven, The Netherlands.
m.l.d.klijn@tue.nl

[2]Delft University of Technology
Delft, The Netherlands.

ABSTRACT

Thermal mass is usually positively associated with energy efficiency and thermal comfort in buildings. However, the slow response of heavyweight constructions is not beneficial at all times, as these dynamic effects may actually also increase heating and cooling energy demand during intermittent operation or can cause unwanted discomfort. This study investigates the potential of energy simulations to support the exploration-driven development of two innovative responsive building elements: "Spong3D" and "Convective Concrete". Both use fluid flow (Spong3D: water, Convective Concrete: air) inside the construction to reduce building energy demand by exploiting the use of natural energy sinks and sources in the ambient environment, aiming to make more intelligent use of thermal mass. During the development of these concepts, different simulation tools were used alongside experiments for e.g. materials selection, climate analysis, comfort prediction and risk assessment. By presenting the results from a series of simulation studies and by reflecting on their application, this paper shows how computational building performance analyses can play a useful role in ill-defined R&D processes.

Author Keywords

thermal mass; adaptive façade; building simulation; energy performance; thermal comfort; design decision support; product development; physics-based simulation in design.

ACM Classification Keywords

Design; Experimentation; Performance.

1 INTRODUCTION

Over the last decades, building performance simulation (BPS) has evolved to become an established tool for supporting the design and operation of high-performance buildings [4]. BPS facilitates analysis of the interrelated effects of building shape, construction type, materials, energy systems, weather influences and occupant behavior on building performance. The potential of BPS is most pronounced when it is proactively used for guiding building design decisions towards solutions that combine high indoor environmental quality (thermal, air quality, visual, acoustic) with minimum use of resources (e.g. CO_2 emissions or materials) [5]. However, the traditional, and still most common use of BPS is the application by engineers, for "post-rationalization" and code compliance at a time in the building design process when many influential design decisions have already been made [1, 2].

In an abstract way, the building design process can be described as the activity of conjoining various spatial configurations with different combinations of existing components, technologies and building material assemblies until a solution is found that satisfies all aesthetic and functional requirements [23]. This tendency of selecting from a collection of known or proven solutions often gives little room for conceiving truly innovative building concepts that reconsider the way in which buildings operate. It is increasingly realized, however, that such breakthrough innovations are necessary to meet the 21st century societal and environmental challenges for a sustainable built environment [12]. Building envelopes and utilization of thermal mass play a crucial role in this respect, and the concept of adaptive facades has regularly been identified as being among the most promising developments and trends [7, 11, 18]. As such, there is a growing need to devise innovative façade concepts, with special attention for transforming them into scalable building envelope elements and products, to be able to achieve the biggest overall impact.

Such developments tend to start small but in large numbers. Through projects in architecture schools, design competitions and also in research projects with more technical orientation and via start-ups, a nearly incessant stream of new ideas and proposals for innovative adaptive façade concepts is being generated [15]. Judging from the information available in the public domain, it turns out that, despite its potential, BPS is rarely ever used to support such creativity-driven developments. The following barriers can be perceived:

• The explorative, iterative and diverging features of the R&D process do not match with the analysis- and evaluation-oriented attributes of BPS.

• Many simulation tools do not have the modeling capabilities required to predict the performance of certain novel adaptive features [16].
• There is a mismatch between (i) the amount and level-of-detail of available information about the concept under development, and (ii) what is needed as input for BPS programs [14].
• The output options of simulation programs are perceived to be not informative for timely assistance in the decision-making process [19].
• The time required to obtain accurate predictions is incompatible with the need for quick feedback as the interpretation of the issue to be solved keeps evolving [8].

Despite the abovementioned barriers, the premise of this article is that, provided that it is used in a sensible and sometimes creative way, there is much scope for BPS as a support tool for decision-making throughout various phases of ill-defined, design-oriented R&D projects of innovative responsive façade concepts. This potential will be demonstrated by presenting the development of two innovative building envelope concepts that both aim at making more intelligent use of thermal mass in buildings. These developments are part of the so-called 4TU.Bouw Lighthouse initiative. They are rather unique, multi-disciplinary, one-year research projects, starting with an initial idea as outline, and leading to either a proof-of-concept or proof-of-failure. This paper briefly presents the two concepts, demonstrates the use of BPS throughout various phases of the development, and concludes with a discussion and reflection about challenges and opportunities for more widespread use of BPS to support future innovation processes.

2 CONVECTIVE CONCRETE

2.1 Concept

The main goal of Convective Concrete is to mitigate residential overheating during summer periods by reducing the temperature of constructions through active heat exchange between the building construction and cool outside air at night. To accomplish the on-demand charging of thermal mass, a network of ducts (with attached fans) is embedded in a concrete wall element. This is done by developing customized formwork elements in combination with advanced concrete mixtures [6].

Using Fused Deposition Modeling (FDM), an Additive Manufacturing (AM) process based on material extrusion, the air channels are printed in wax so they can be placed in the formwork before casting the concrete and then be melted after the concrete is hardened (Figure 1). Consequently, the concrete is in direct contact with the air circulating through it and each air channel can be unique in form to optimize the performance of the system. To achieve an efficient activation of the concrete, the element functions like a lung. The convection takes place with separate pipes on both sides of the concrete's core to increase the charge/discharge of the thermal storage process. The airflow rate through the wall elements is controlled with the help of valves and small computer fans, as back-up for the buoyancy effect.

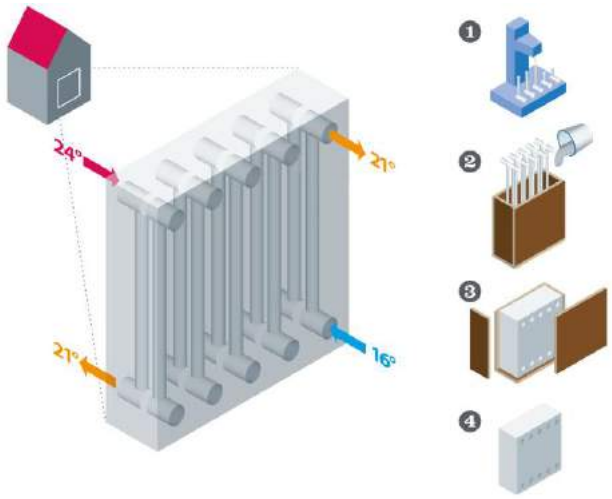

Figure 1. Convective Concrete concept.

2.2 Simulation at the element scale

Although the design process of the research uses experimentation with the making of mock-ups, not all parameters and design options can be extensively tested this way due to time and material constraints. However, computational simulations can help to make decisions on some variables in order to select the most promising properties to further analyze with the mock-up [17]. In this case, a two-dimensional dynamic heat transfer model is used via the simulation program Energy2D to make decisions on the shape and layout of the air channels in the Convective Concrete as well as the properties of the concrete mixture itself. The software program Energy2D is used to solve the dynamic Fourier heat transfer equations for the Convective Concrete case. Energy2D is a relatively new program [25] and is not yet widely used as a building performance simulation tool. To gain more confidence in the predictions with Energy2D, an analytical validation study was first carried out, inspired by the approach described by Hensen and Nakhi [10]. The simulation results never divert from the exact solution more than 0.45 °C and it is therefore considered acceptable to further use this model [24].
Energy2D was then used to visualize the dynamic heat dissipation for various layouts of air channels. Different shapes, sizes and distributions of air channels were tested in a plan view and the isotherms are observed to determine the most efficient configuration. Figure 2 presents the comparison of aligned and staggered air channel distributions paused at the same time during the simulation. From this study, the first mock-up is designed with round air channels with a diameter of 4 cm which are aligned with a spacing of 8 cm between them.

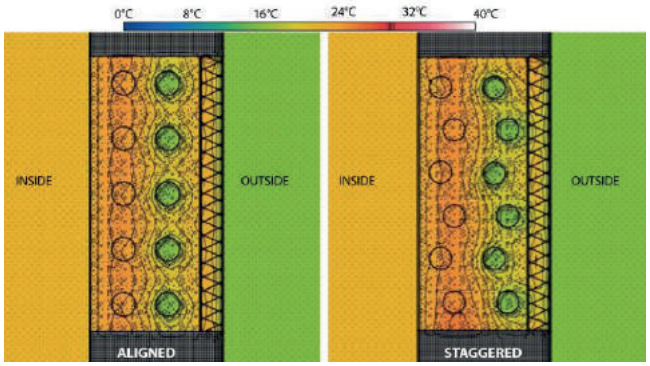

Figure 2. Staggered and aligned distribution of air channels.

The Energy2D model is also used to characterize the thermal time constant of different concrete mixtures in order to select the mixture that will be used for the initial Convective Concrete mock-up. In this study, the temperature for a point in the middle of a 20 cm thick concrete wall is simulated and the wall is subjected to a 10°°° temperature step decrease. The thermal time constant is defined as the time required for this point to change e^{-1} = 36.8% of the total difference between its initial and final temperature. The thermal time constant was evaluated for 70 existing types of concrete with different density and thermal conductivity. The heat capacity of the 70 types of concrete was always 840 J/kg·K.

Figure 3 presents all the examined concrete types according to their thermal conductivity (x-axis) and their density (y-axis). The diameter of the circle represents the time constant recorded during the simulation for every concrete type while the shades of grey categorize the results in different sections of time. The smaller and darker the dot, the shorter the time constant.

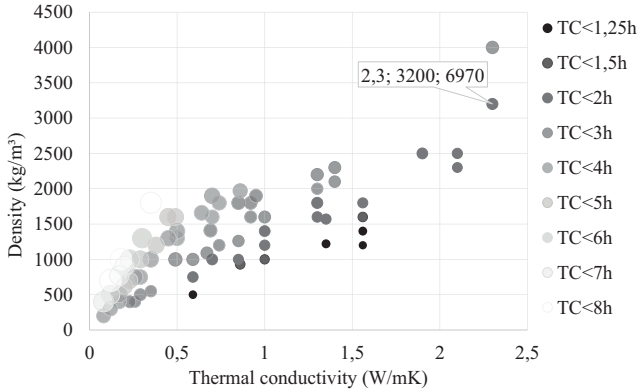

Figure 3. Thermal time constant of 70 concrete types.

This graph allows us to select a concrete mixture that has a high density for high storage capacity purposes while having a relatively quick thermal response with a time constant in the order of 2 hours. As can be seen in Figure 3, the selected concrete mixture has a density of 3200 kg/m^3, a thermal conductivity of 2.3 W/m·K and a time constant of one hour and 56 minutes.

2.3 Whole-building Simulation

While the performance of the mock-up will be measured under controlled conditions, the timespan of the project does not allow to implement and monitor the performance of the system in a real building. This situation can instead be modeled in a whole building energy simulation software. No model pre-exists to simulate the innovative Convective Concrete system, however, some existing models have enough similarities and flexibility to replicate the effects of Convective Concrete.

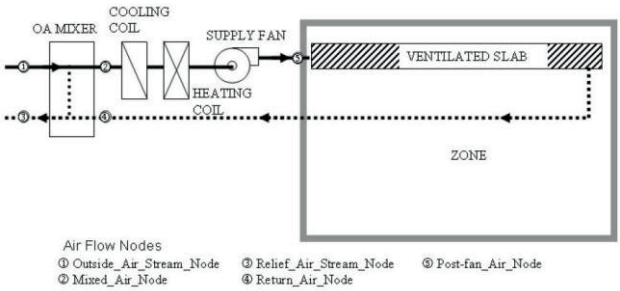

Figure 4. Schematic section representing the operation of the ventilated slab model in EnergyPlus [22].

In this study, the ventilated slab model developed by Chae and Strand [3] in EnergyPlus is used [9]. Since the Convective Concrete does not directly circulate the air of the room, the "Slab Only" mode which is displayed in a schematic manner in Figure 4 is selected. The system is assigned to wall surfaces rather than ceiling. Also, no heating or cooling coils are implemented as the Convective Concrete uses outdoor air directly.

Figure 5 shows the effect of Convective Concrete on a typical bedroom of 9 m^2 when the system starts operating on day 2 at midnight (climate conditions: the Netherlands). The bedroom has two walls exposed to the outside: the south wall has a window while the east wall accommodates the Convective Concrete. Other surfaces are considered adiabatic. The outside air is circulated in the Convective Concrete element and out. This decreases the inside surface temperature of the wall which in turn decreases the temperature of the room. The ventilation in the Convective Concrete is only on when the outside temperature is low enough to cool the element which is mostly during the night. The thermal mass of the high density Convective Concrete keeps the room cool during the day.

With this model, various parameters can be altered in the simulation to visualize their effect. In Figure 5, a low (0.02 m^3/s) and high (0.08 m^3/s) air flow rate are tested. As expected, the high flow rate has a higher cooling effect, reducing the operative temperature up to 2 degrees.

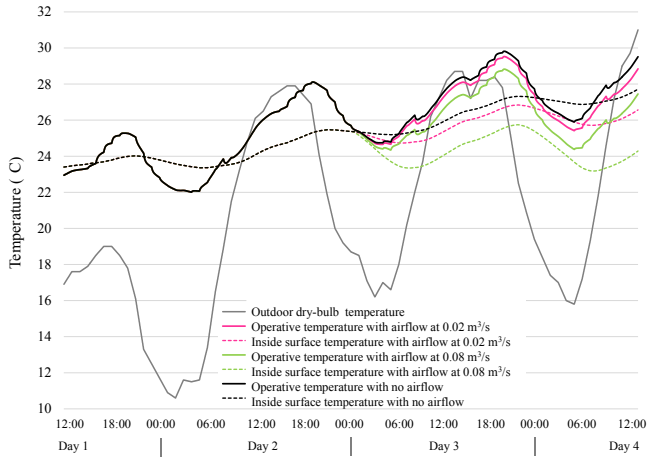

Figure 5. Effect of the Convective Concrete with an air flow rate of 0.02 and 0.08 m³/s compared to the system off.

The model also allows to analyze a longer period of time and different locations. To do this with measurements would require much more time and investments. Figure 6 presents the amount of time the operative temperature in the bedroom is above 24 °C from the 1st of April to the 31st of October, for four different locations which are derived from the climate analysis (section 2.4). The baseline building has a typical brick cavity wall and the same insulation level as the Convective Concrete case. While the Convective Concrete was simulated with the same low and high air flow rate as in Figure 5, the baseline building was also modelled with the possibility to use free cooling by opening the windows at night (from 10 PM to 6 AM and when the temperature outside is at least 3 degrees lower than the temperature inside). For all locations, a high air flow rate is required to present significant improvement of thermal comfort compared to the scenario of opening the windows at night.

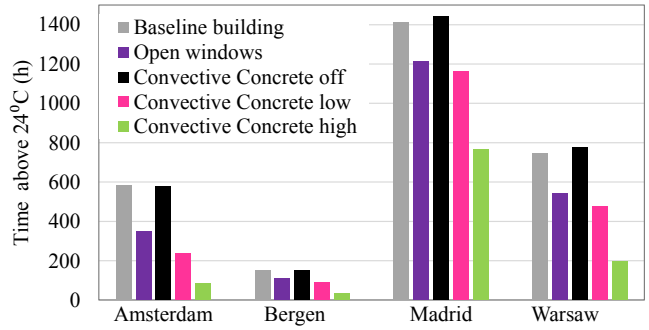

Figure 6. Hours above 24 °C for four locations.

2.4 Climate analysis

When developing a new building envelope system such as Convective Concrete, it is important to identify high-potential locations that have favorable climate characteristics with respect to the operating principles of the system. Convective Concrete is expected to work well in a climate where summer night time temperatures drop well below indoor comfort temperature. In this way, the outside air can effectively cool down the building structure, and help in reducing the extent of indoor overheating during the next day. In addition, it is important that the climate has a moderate degree of summer discomfort. Figure 6 shows that Convective Concrete is best used for peak shaving. For climates that have too little indoor overheating issues, it will be difficult to make Convective Concrete an economically viable investment. In climates that are too warm, on the other hand, buildings will likely rely on active cooling systems to ensure occupant comfort all year round.

Figure 7 shows temperature duration curves for eight European cities, inspired by Medved and Arkar (2008).

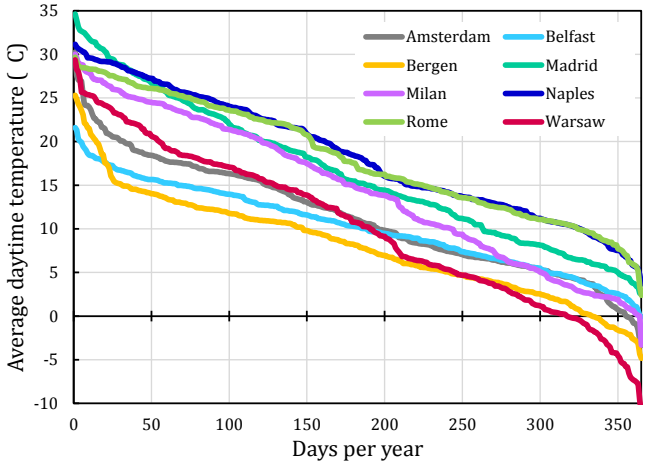

Figure 7. Temperature duration curves of average daytime (08h00 – 18h00) outside temperature.

Each line represents the average daytime outside temperature, taken between 8am and 8pm. The data is sorted from high to low values to investigate the number of days per year that a certain temperature is exceeded. The cities of Rome and Naples are considered as too warm for using Convective Concrete, since the average daily outside temperature is above 20 °C for approximately half of the year. The climate of Belfast, on the other hand, has very mild summers, and consequently little need for summer cooling. The fact that both Warsaw and Madrid have continental climates, can also be observed since they both show a large temperature difference between summer and winter and a steep gradient. Bergen has a short, but rather intense summer season. Convective Concrete could be used to reduce indoor overheating during this period in cities such as Madrid, Warsaw, Bergen and Amsterdam.

To get a better understanding of the temperature difference between day and night, the daily amplitude in outside temperature was calculated for the four locations cited above (Figure 8). During the warmest period in Amsterdam and Warsaw, the temperature swing between day and night varies between 10 and 18 °C. On some days, this is enough to get a significant temperature difference for cooling down interior spaces. There are, however, also warm summer nights in which the free cooling potential will not be

enough to avoid overheating. The city of Bergen has, on average, the lowest day-night temperature difference. Still, in the summer season, this difference is mostly above 10 °C, indicating that there is potential for using free cooling. Madrid experiences a climate with warm summers, but also a large temperature difference between day and night. This seems to indicate that there is potential to use a low-energy cooling system such as Convective Concrete under these climatic conditions.

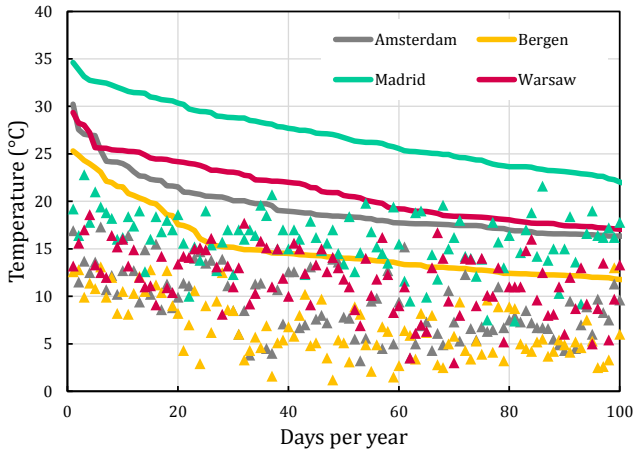

Figure 8. Temperature duration curves with daily temperature amplitude on the corresponding day.

This climate analysis provides an early estimate of the application potential of Convective Concrete in various European climates. Combined with dynamic building performance simulations, much more comprehensive information can be obtained to further predict the performance of the implemented system in our built environment (section 2.3).

3 SPONG3D

3.1 Concept

The Spong3D project investigates the potential of Additive Manufacturing to produce a façade system that fully integrates thermal insulation, heat storage, and distribution system additionally to traditional façade requirements [20].

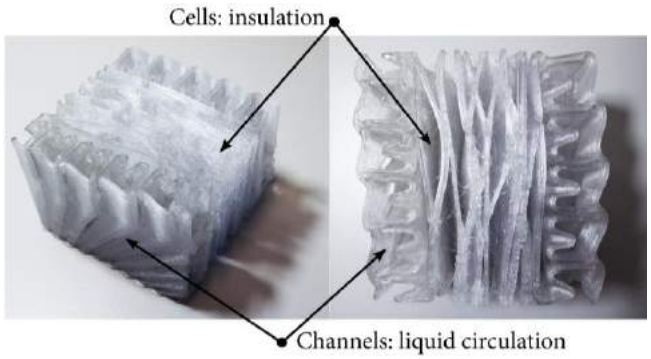

Figure 9. Sample of the structure with its channels and cells.

The proposed system incorporates closed air cavities which are located in the core of the façade to provide thermal insulation and channels on the outer layers which are used to circulate a liquid (water plus additive) that acts as thermal mass. Together, the composition of the channels and the cavities form a complex structure, integrating multiple functions into a single component (Figure 9).

Thanks to two reversible pumps, the liquid can be circulated from one side of the façade to the other with the possibility to be stored in a tank in the middle of each façade panel when necessary (Figure 10).

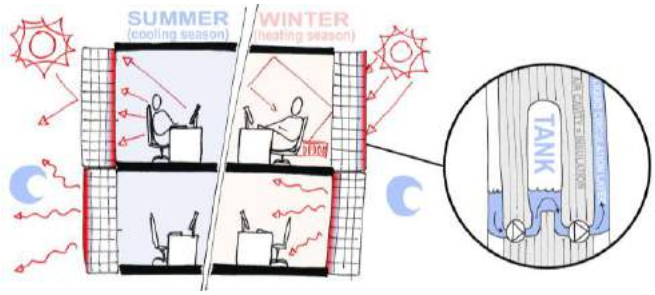

Figure 10. Schematic illustration of the operation of the system.

In a cooling situation, the liquid is first placed on the inside to absorb internal heat gain and is then pumped to the outside layer to discharge its heat to the cool night sky. For heating purposes, the liquid is placed outside during daytime, to absorb any solar heat gain and is then pumped to the inside to release this heat inside the building.

3.2 Simulation at the element scale

The multidisciplinary research team involves experts with various backgrounds, which ensures that every aspect of the requirements expected from the façade system is considered. In this research team, three main disciplines are highlighted: (i) design and 3D printing process, (ii) structural engineering, (iii) building physics and thermal performance. The structural engineers performed impact tests on the 3D printed material which showed unpredictable strength of the material depending on the printing conditions. A significantly higher number of tests was required to make safe conclusions about the resistance of the façade towards impacts. The structure team expressed its concerns and suggested to apply a glass cover on both sides of the façade element to guarantee its protection. On the other hand, the design team argued that adding a glass cover would restrict the freedom of shape allowed by AM. Multiple different arguments were presented by various team members, which made it difficult to make a clear decision on which direction to continue the research. Introducing a façade system that integrates many functions with a single material and manufacturing process is one of the main goals of this project. However, the first goal is to create a façade system that integrates controlled heat exchange, storage and distribution. Therefore the decision of having a glass cover should be determined based on the thermal performance of the system with and without it.

At this stage of the design, Energy2D appeared as a suitable tool to quickly assess the effect of adding a glass cover relative to not having it. The façade was modeled in section in the 2-dimentional heat transfer model. The different parts of the system were modelled with layers of different properties as presented in Figure 11. The different scenarios (e.g. liquid on the outside during summer night) were modelled in different files and the absorption or release of heat was studied over time.

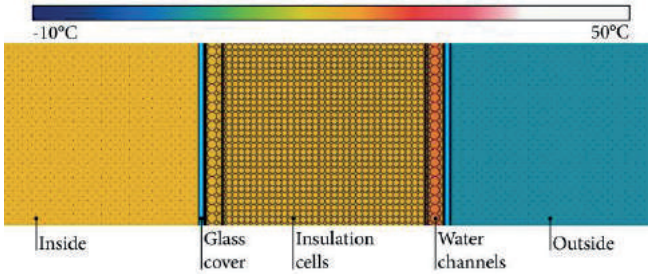

Figure 11. Model of the Spong3D system with glass cover in Energy2D (section)

For each scenario, the glass cover presented an extra thermal resistance which reduced the release or absorption of heat by the liquid layer in the first 10 hours. These simulations allowed to quickly produce quantitative results, leading to actionable information that allowed the research team to move on in a common direction.

3.3 Whole-building simulation

Similarly to Convective Concrete, as explained above, the Spong3D system does not correspond to any existing model from a whole-building simulation program. However, the water layer on the outside operates in a similar way as a solar collector does. It absorbs heat from solar radiation during sunny winter days and exchanges the thermal energy to a liquid with a specified mass flow rate. The same model can be used to investigate heat losses during cool summer night.

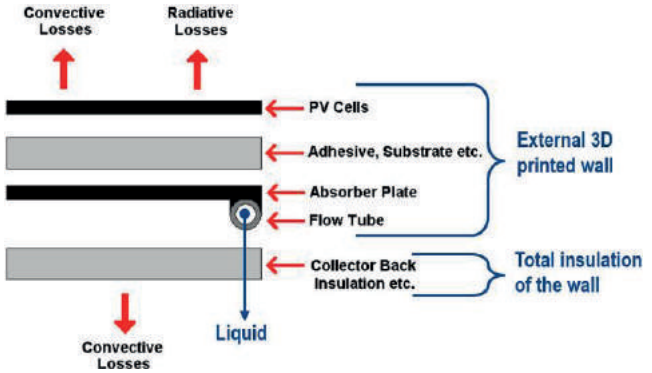

Figure 12. Diagram model of the Spong3D system in Trnsys.

As explained previously, the solar collector model should be unglazed to reduce the resistance to heat transfer. Therefore, the component Type 560 in Trnsys was used. It models a combined PV/T solar collector [21]. As shown in Figure 12, the properties of the flow tube, absorber plate, adhesive, substrate and PV cells are modified to represent the properties of the 3D printed water channel wall which as a thermal resistance of 0.0092 $m^2 \cdot K/W$.

The focus of the simulation presented here is on the summer night and winter day scenarios when the liquid is placed on the outer channels and interacts with the outside climatic conditions.

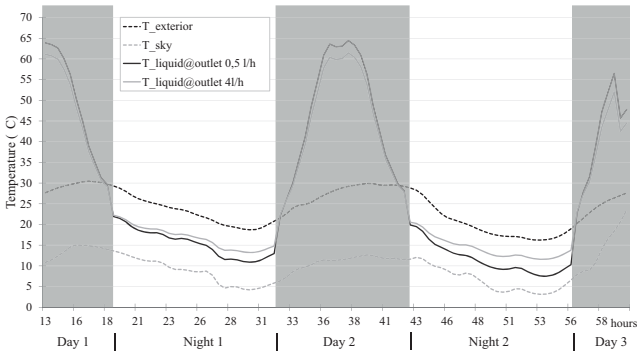

Figure 13. Trnsys results showing the temperature of the liquid during two summer night for two mass flow rate.

The weather file used in this simulation allows to observe the dynamic effects of the climate on the temperature in the channels. Until now, the different scenarios of the liquid being placed in the inner or outer channel layer are looked at separately. But the result of one simulation can be used as input for the other. This model allows to alter various parameters such as: thermal properties of the front cover, mass flow rate of the liquid, thermal properties of the liquid, outside climate conditions.

Figure 13 shows that a lower mass flow of 0.5 l/h releases more heat during the night than a high flow rate of 4 l/h. A similar trend was observed for the scenario of a sunny winter day where a low mass flow rate of the liquid allows it to get warmer than with a high mass flow rate.

3.4 Climate Analysis

As mentioned in section 3.3, the system can be tested in different climate conditions. But simply looking at the weather files can already give a lot of information about the performance of the system in different locations.

As seen in Figure 13, the outside temperature, but more importantly the sky temperature will determine how easily the heat in the liquid will be released to the environment at night during the summer. In winter, it is important to look at the outside temperature and at the solar radiation since the Spong3D system would work best in locations with cold but sunny winter days. Figure 14 presents four color maps created with the Ladybug plug-in for Grasshopper [13]. Each pixel represents one hour of one winter day and is colored according to the legend on the right. The top chart shows the solar irradiance between 200 and 1000 Wh/m^2 and the second from the top shows the dry-bulb temperature from -10 to 20 °C, both for Amsterdam, the Netherlands. The two bottom charts show the same but for Toronto,

Canada. As can be seen, the climate of Toronto benefits from longer and sunnier days than in Amsterdam while the temperature rarely goes above 10 °C.

In conclusion the heating capacities of the Spong3D system in winter would be much more beneficial in Toronto than in Amsterdam as it could be used more often and yield a greater temperature difference.

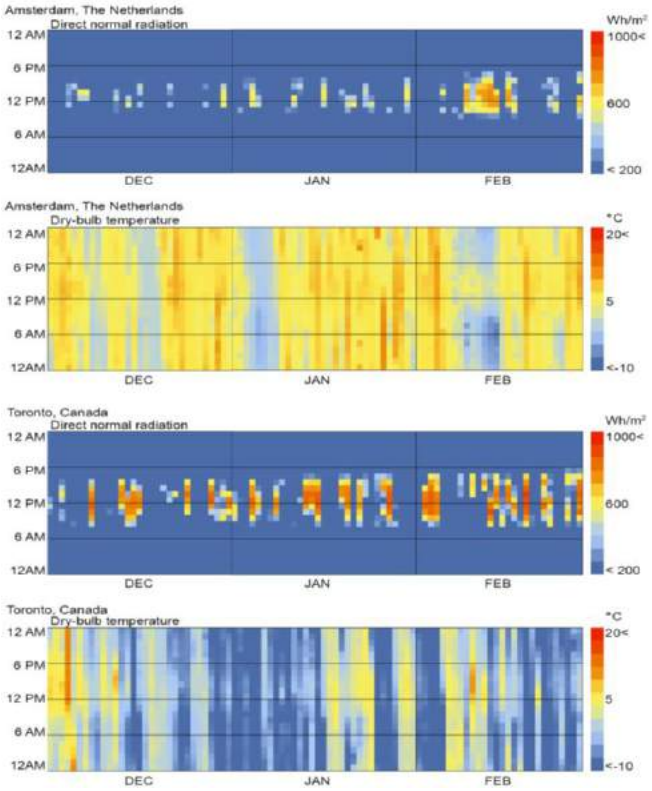

Figure 14. Radiation and temperature flood chart for Amsterdam (top) and Toronto (bottom).

DISCUSSION AND CONCLUSION

This paper has summarized the process and outcomes of simulation-based research activities in the development of two adaptive building envelope systems, with a focus on energy and comfort aspects. Different simulation strategies, with various software programs (i.e. Energy2D, Ladybug, Trnsys and EnergyPlus) were deployed in response to the needs posed by different questions in different phases of the R&D process. The development of both concepts is still work in progress. Modelling and simulation will continue to play an important role in planned follow-up activities.

Literature shows that BPS is occasionally used to support decision-making in product development of innovative building envelope components in industry [17]. It was found, however, that its application in more explorative projects, such as the ones reported in this article, is rare. A perceived mismatch between simulation capabilities and the need for rapid feedback in relation to the ill-defined and evolving nature of explorative R&D projects is believed to inhibit the use of BPS in this context.

The various short simulation studies that have been presented throughout this paper, however, demonstrate that this assertion does not always have to hold true, because BPS can provide valuable feedback to the R&D team, by:

- Providing quick estimates about the performance of multiple problem-solution pairs to offer early information that helps choosing among different development directions.
- Giving the R&D team the opportunity to analyze the energy and comfort consequences of their decisions at multiple spatial scales, from material to whole-building level. The dynamic features of BPS are especially relevant, because due to the high influence of thermal inertia, simple calculation methods and rules-of-thumb may not suffice.
- Enabling the option to conduct virtual experiments and explore what-if scenarios (e.g. different climate conditions) in a quick and cost-effective manner.
- Helping in the definition and design of physical experiments that use available resources efficiently.
- Allowing for the exploration of the performance of materials and components with not-yet-existing properties. This is, evidently, not possible in experimental research.
- Confirming engineering intuition by means of quantitative metrics. Or alternatively, providing physics-based insights in situations where counterintuitive effects are to be expected.

This type of information is not only helpful for making informed decisions when selecting between different design alternatives, it may also help in determining the longer-term outlook of the innovation. For example, simulations can provide quantitative input for business models and identification of high potential niche markets, as well as realistic projections for attracting possible follow-up funding.

It was also demonstrated that systematic analysis of datasets with typical meteorological weather data (TMY files) can lead to additional useful insights. Although the use of TMY files is strictly speaking not a simulation activity, it is closely related to the building simulation field, and therefore also considered in this paper. With the help of such climate analyses, it becomes easy to target most promising application areas, and to tune design specifications in response to these conditions.

Dealing with first-of-its-kind innovative façade concepts often means that the tools available for simulations on the whole-building scale do not have sufficient modelling capabilities to support performance evaluation of these specific elements. It should be noted, though, that many simulation models can be reused outside their initially intended application domain, as long as there is sufficient attention for quality assurance [16]. Using examples of the ventilated slab in EnergyPlus, and a BIPVT collector in

Trnsys, this paper has demonstrated two examples of such a creative use of legacy simulation software.

Both projects that are discussed in this article make use of additive manufacturing as a production method for making prototypes as well as the final product. The application of AM as a rapid prototyping tool has led to many design iterations and a strong interaction with simulation activities. With the growing interest in AM in the construction industry, many promising opportunities are foreseen to further take advantage of the coupling with BPS.

There are several other trends in the field of computational building performance analysis, such as generative and parametric design methods, enhanced simulation domain integration (e.g. thermal, visual and airflow), advanced visualization techniques and the use of building information modeling. It is expected that these developments will help in further reducing the barrier for applying BPS in exploration-driven R&D projects.

ACKNOWLEDGMENTS

The authors want to thank 4TU.Bouw for its support in the form of two Lighthouse project grants. We are very grateful to all Lighthouse project members for many inspiring discussions and for creating the research environment in which this paper could develop.

REFERENCES

1. Attia, S., Gratia, E., De Herde, A. and Hensen, J.L.M. (2012). Simulation-based decision support tool for early stages of zero-energy building design. *Energy and buildings*, 49, pp.2-15.
2. Bernal, M., Haymaker, J.R. and Eastman, C. (2015). On the role of computational support for designers in action. *Design Studies*, 41, pp.163-182.
3. Chae, Y.T. & Strand, R.K. (2013). Modeling ventilated slab systems using a hollow core slab: Implementation in a whole building energy simulation program. *Energy and Buildings*, 57, 165-175.
4. Clarke, J.A. and Hensen, J.L.M. (2015). Integrated building performance simulation: Progress, prospects and requirements. *Building and Environment*, 91, pp.294-306.
5. Clevenger, C.M. and Haymaker, J. (2011). Metrics to assess design guidance. *Design Studies*, 32(5), pp.431-456.
6. Convective Concrete. www.4tu.nl/bouw/en/LHP2016/Convective Concrete
7. COST TU1403. (2017). EU COST Action TU 1403: Adaptive Façade Network, www.adaptivefacade.eu.
8. Dorst, K. and Cross, N. (2001). Creativity in the design process: co-evolution of problem–solution. *Design studies*, 22(5), pp.425-437.
9. EnergyPlus v8.4. www.energyplus.net
10. Hensen, J.L.M. and Nakhi, A.E. (1994). Fourier and Biot numbers and the accuracy of conduction modelling. Proceedings of BEP '94 Conference (pp. 247-256). York: Building Environmental Performance Analysis Club (BEPAC).
11. Hoes, P. and Hensen, J.L.M. (2016). The potential of lightweight low-energy houses with hybrid adaptable thermal storage: comparing the performance of promising concepts. *Energy and Buildings*, 110, pp.79-93.
12. IEA (2013). International Energy Agency, Technology Roadmap: Energy Efficient Building Envelopes.
13. Ladybug. www.grasshopper3d.com/group/ladybug
14. Lin, S.H.E. and Gerber, D.J. (2014). Designing-in performance: A framework for evolutionary energy performance feedback in early stage design. *Automation in Construction*, 38, pp.59-73.
15. Loonen, R.C.G.M. (2017). Overview of Climate Adaptive Building Shells. Online: www.pinterest.com/CABSoverview
16. Loonen, R.C.G.M., Favoino, F., Hensen, J.L.M. and Overend, M. (2017). Review of current status, requirements and opportunities for building performance simulation of adaptive facades. *Journal of Building Performance Simulation, 10(2),* pp. 205-223.
17. Loonen, R.C.G.M., Singaravel, S., Trcka, M., Cóstola, D. and Hensen, J.L.M. (2014) Simulation-based support for product development of innovative building envelope components. *Automation in Construction 45*, 86-95.
18. Loonen, R.C.G.M., Trčka, M., Cóstola, D. and Hensen, J.L.M. (2013). Climate adaptive building shells: State-of-the-art and future challenges. *Renewable and Sustainable Energy Reviews*, 25, pp.483-493.
19. de Souza, C.B. (2012). Contrasting paradigms of design thinking: The building thermal simulation tool user vs. the building designer. *Automation in Construction*, 22, pp.112-122.
20. SPONG3D. www.4tu.nl/bouw/en/LHP2016/SPONG3D
21. Trnsys v17. www.trnsys.com
22. U.S. Department of Energy (2016). Engineering Reference, EnergyPlusTM Version 8.5 Documentation. Section 17.6.16 Ventilated slab.
23. de Wilde, P. and Van Der Voorden, M. (2004). Providing computational support for the selection of energy saving building components. *Energy and Buildings*, 36(8), pp.749-758.
24. de Witte, D., de Klijn-Chevalerias, M.L., Loonen, R.C.G.M., Hensen, J.L.M., Knaack, U., Zimmermann, G. (2017). Convective Concrete: Additive Manufacturing to facilitate activation of thermal mass. *Journal of Façade Design and Engineering*, 5(1).
25. Xie, C. (2012). Interactive Heat Transfer Simulations for Everyone, *The Physics Teacher,* Volume 50, Issue 4, pp. 237-24.

Unifying Visualization of Hydrologic, Thermal and Plant Growth Performance in Green Roofs

Liat Margolis, Andrew Hooke and Vincent Javet

University of Toronto
Toronto, Canada
info@grit.daniels.utoronto.ca

ABSTRACT

Vegetated roofs have become an important component of sustainable building design in many cities across the world due to the range of environmental benefits they provide, including water retention, evaporative cooling, and biodiverse habitat. Not all green roofs are made equal, and the performance metrics of green roofs are influenced by the choice of growing media, planting, and the use of supplemental irrigation, among other factors. There is a need for additional studies on the influence of multiple design variables on multiple performances in green roofs, as well as for visualization and design tools that represent such complex relationships. This paper describes the data acquisition system of a replicated green roof modular array to derive hydrologic, thermal, and plant growth data over a three-year period. Using Rhinoceros™ with Grasshopper® and LunchBox™ plug-in components, as well as a web-based platform, an interactive tool was developed to unify visualization of diverse forms of data. We discuss the tool's merits over current visualization practices and the potential use in green roof design simulation by researchers and design professionals.

Author Keywords

Green roofs; performance; data visualization; sensors; thermal cooling, stormwater management, plant growth

ACM Classification Keywords

Experimentation; measurement; performance; design

1 INTRODUCTION

Vegetated Green roof technologies have been extensively studied worldwide and the level of interest in academic literature continues to rise [5, 14, 24]. As it became widely accepted that green roofs offer a high-performance alternative to traditional non-vegetated roofs, the next generation of research developed, comparing different green roof materials and configurations against once another [10]. A study by Simmons et al. [26] titled "Green roofs are not created equal" maintained that green roof performance varied significantly based on design factors and environmental context. Dvorak and Volder [5] called for many more studies across North American ecoregions to better understand the correlation between plant selection, growing media, and maintenance regimes to develop regional standards and professional practice.

Municipalities across North America have recognized the benefits of green roofs and incorporated supportive policies into their sustainable building programs. Consequently, the green roof industry has grown tenfold since 2003 [7]. However, Hill [10] argues that green roof policies and practices are largely dominated by aesthetic concerns, while infrastructural intentions are rarely defined clearly. For example, vegetative cover is the only performance metrics mentioned in the City of Toronto's Green Roof Bylaw [2]. Toronto's stormwater management policy lists overarching water retention metrics for site planning, but lists green roof technologies as one of many strategies to achieving these objectives [4]. A separate set of green roof guidelines offers principles for increasing biodiversity and ecological habitat value on green roofs, yet does not cross-reference water management policies, or urban cooling objectives [3].

The choice of planting, growing media, and irrigation remains a topic of much debate in both industry practice and academic research. *Sedum* species are commonly selected for their ability to withstand periods of drought [21, 23, 29] and maintain nearly 100% vegetative cover [1]. Other studies found that native grasses and forbs not only offer a practical alternative to *Sedum* [15], but also provide greater habitat for native pollinators [18].

Growing media composition is another widely debated design parameter. Organic matter has demonstrated positive influence on plant growth [17] and water holding capacity [11, 30]. However, many North American manufacturers and municipal guidelines follow the German Landscape Research, Development and Construction Society (F.L.L.) and promote a freely draining mixture of mineral aggregates with a low proportion of organic material [6]. Lastly, while irrigation proves to be a negative factor for water capture [11, 25), it is positively correlated with increased thermal cooling [16, 27], as well as plant growth and diversity [13, 17, 27]. To complicate matters further, Leadership in Energy and Environmental Design (LEED) certification discourages the consumption of potable water for irrigation [9].

Developing consensus among researchers, designers, manufacturers, and policymakers on the 'best' green roof configuration is not necessarily straightforward. And nor should it be, given regional differences in climate, ecology, urban infrastructure, and material availability. On the other

hand, in most cases, green roofs are promoted and employed for their co-benefits [22] thus, a complex understanding of relationships is important.

Two primary gaps in research are relevant in this context. The first is the relatively limited number of studies that examine the influence of multiple independent variables (controlled design parameters) on multiple dependent variable (performance, behavior). With a majority of studies isolating variables, we run the risk of obscuring the complex relationships between soil, plants, water, weather patterns and so on. Secondly, analytical diagrams and visualization models vary greatly with respect to time scales, assumptions, and data sampling sizes, and may not permit comparison, or synthesis. Moreover, visualization is poorly represented in literature that examines the relationship between multiple independent and dependent variables. Overall, there is a need to develop both scientific experiments and visualization techniques that can characterize co-benefits and tradeoffs and provide with decision making tools for green roof design.

2 METHODS

2.1 Experimental Site

The Green Roof Innovation Testing laboratory (GRIT Lab) is located on the fifth-story roof of the John H. Daniels Faculty of Architecture, Landscape, and Design at the University of Toronto, Canada. The lab comprises twenty-three green roof modules (2.36 m x 1.21 m) suspended 0.8 m above the roof deck to accommodate instruments and maintenance requirements (Figure 1).

Figure 1. GRIT Lab experimental site

The study evaluates the relative influence of four green roof design variables on three performances: water capture, thermal cooling, and plant growth. The modules represent all combinations of the four design variables: native grass-forb 'meadow' species versus Sedum (recommended by Toronto Green Roof Guidelines), mineral-based (F.L.L. compliant; recommended by Toronto Green Roof Guidelines) versus 'organic' biologically-derived (wood compost-based) growing medium, 10 cm (minimum requirement by Toronto Green Roof Guidelines) versus 15 cm depth, and irrigation provided daily, sensor controlled, or not at all (see notes on LEED above). Technical drawings and further details on the experimental layout, plant species, and growing media properties have been published [10, 17, 19].

2.2 Data Acquisition

To measure water balance, precipitation is measured by onsite weather station, using a tipping bucket rain gauge (TE525M Texas Electronics), while each green roof module is equipped with a rain gauge (TB6, Hydrological Services) to measure water discharge, and a soil moisture sensor (5TE, Decagon Devices) to measure moisture content in the growing medium. Both rain gauge and soil moisture sensors were recalibrated for accuracy [12]. For the thermal cooling analysis, each module is equipped with five thermistors (109-L thermistor, Campbell Scientific) installed along a vertical center axis to generate a thermal profile for each module (Figure 2). These data are compared to the ambient temperature measured by the weather station using a temperature probe (Campbell Scientific). The data logger, controlling all the sensors, records at five-minute resolution using LoggerNet software since 2013 (Campbell Scientific). Details on sensor equipment and mounting, as well as the thermal cooling study were previously published [16, 19], while the stormwater hydrology analysis is currently in press [11].

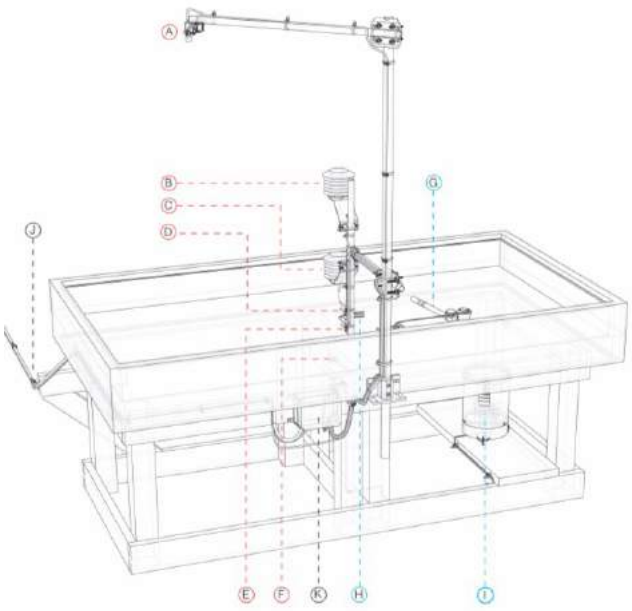

Figure 2. Green roof module and sensor instruments

Plant biomass sampling of cover, structure (height), and density consists of measurements using a pin-frame [17]. Cover is measured twice per module by the proportion of pin touches out of 16 pins, for a total of 32 pins. Structure is measured by number of pin touches at four equal heights

from the top of the growing media up to 60 cm. Density was measured by number of touches per pin for all 16 pins per height interval (Figure 3). In the meadow planting modules, diversity is measured by distinguishing grass and forb species. Biomass sampling has been conducted biweekly during the months of May-August since 2011. These data have been used to determine the influence of the design variables on survivability and richness of each species type [17]. The modules are also photographed biweekly.

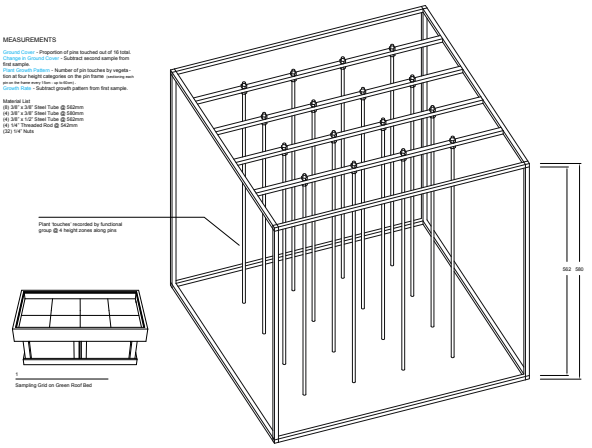

Figure 3. Pin-frame instrument to measure biomass

2.3 Data Visualization

The objective for this data visualization was to produce a unified representation of sensor data and biomass sampling. Sensor data comprises of precipitation and temperature (input) recorded through the weather station, as well as water discharge and temperature per module (output) using measurements from the rain gauge and temperature sensors. The maximum temperature per month was selected for input and output. Only the sensor located at the top surface of the growing media was used, as the difference in temperature at this height proved to the most significant [16]. For water input, the sum of monthly precipitation and irrigation volumes was used. For water output, the total water discharge per module was used. Since temperature and water measurements are expressed in different units (C^o and mm) the data was scaled to produce a graphically comparable model. Biomass data was scaled to indicate proportions, widths and quantity of a stacked set of rings. The scaling values (e.g. 2.03, etc.) were employed strictly to generate clearer visual representation and do not hold empirical significance themselves (Table 1).

The software platforms used to carry out the data modeling are McNeel® Rhinoceros™ with plug-in components including Grasshopper® and LunchBox™. Rhinoceros™ is a NURBS based geometric modeling program developed by Robert McNeel & Associates favored by designers and architects for its ease in generating three-dimensional geometric forms. A plug-in for Grasshopper®, LunchBox™ allows Grasshopper® to parameterize input values and generate line segments in the form of NURBS geometry. LunchBox™ was used to read Excel spreadsheet columns as inputs to contribute to a fully parameterized workflow, resulting in a three-dimensional model output unique to each test module at the timescale of one month. Number sliders in Grasshopper® allowed for the program to switch columns, which represent unique test module and month combinations. Grasshopper® functions were assembled to generate a model based on the values obtained from Excel via Lunchbox™. Grasshopper's 'bake' component transformed the parametric model into a NURBS geometry that is permanent. The model was then generated in Rhinoceros™ and organized by month and year. Rendering software V-Ray (Visual Dynamics® LLC) was used to create PNG images for a web-based interface described below.

Input / output Temperature	**Input Water**	**Output Water**	**Biomass**
Monthly maximum x 2.5	Monthly sum + irrigation / 2.03	Monthly sum / 2860 mm^2*/ 2.03	Cover= pins touched per bed x 11.25^B** Density= number of total touches/ 3 Structure= number of height categories touched + 8
* Size of the bed			
** 360^o (full cover)/ 32 (max number of pins touched per bed)			

Table 1. Scaling calculations for water, temperature, biomass

Biomass data is represented with stacked rings at the midpoint of the model, where the number of rings represents plant structure as per the pin-frame height intervals. The thickness of each ring represents density of plants, and the degree to which the circular ring is whole represents percent cover. Sedum is represented with a bright yellow color and distinguished from grass-forb planting, represented in light yellow and dark yellow colors respectively. Temperature data, represented as the red ribbon, is separated at the midpoint of the model into inputs (max. air temperature per month) and outputs (max. temperature per module per month). The input appears above the biomass data, extending up and to the left, while the outputs extend down and to the right. Both the distance from midpoint and the length of the bar that extends outwards indicate temperature value. Output temperature is compared against the input value and annotated with plus or minus to indicate the extent of thermal cooling. Since Toronto's stormwater policy requires minimum 50% retention of total rainfall [4], the water balance ribbon,

represented in blue, is annotated with plus or minus to indicate 50% of combined monthly rainfall and irrigation (Figure 4).

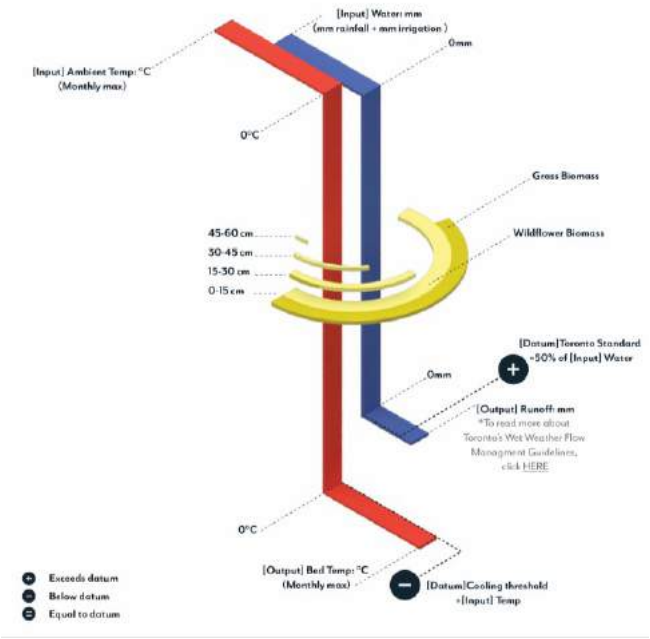

Figure 4. Hydrologic, thermal, and plant growth data are scaled and related in a single model

2.4 Interactive Tool

A web-based platform, titled GRIT Lab Performance Index [8] was developed to visually represent three primary aspects of the experimental design: 1) influence of individual and combined independent variables on dependent variables per month, 2) incremental seasonal and annual changes, and 3) comparison of data and photographs. The interface was developed to allow sorting by the four design variables (growing media composition, depth, planting, irrigation) and by monthly intervals since 2011 (Figure 5). This function permits the user to both isolate and combine design variables and observe their relative influence on hydrologic, thermal and plant growth performance on a monthly basis, using the timeline slider. Monthly intervals were selected to relate biomass sampling rates with sensor data measurements, which visualizes seasonal and annual variations. Data models were only produced for years 2014-2016 as these were the most reliable and complete datasets. These are displayed in a grid for visual comparison. Each model is labeled with its configuration and hyperlinked to a display of numerical values for water and temperature, as well as difference between input and output. The models are cross-referenced to monthly photographs of the green roof modules, which can be independently sorted by the design variables and displayed in a grid layout for visual comparison (Figure 6).

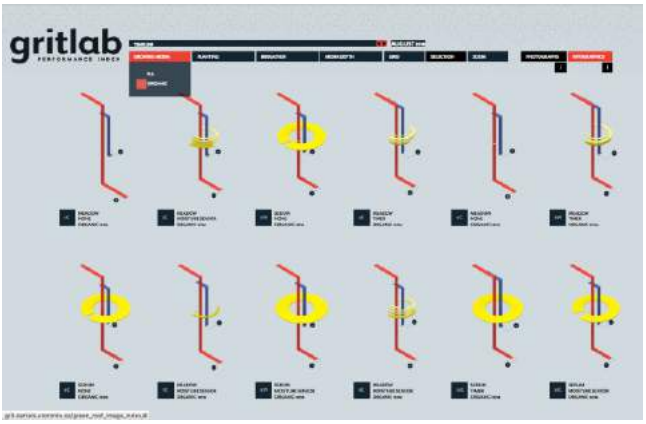

Figure 5. Performance Index data models sorted by design variables (organic media, August 2016)

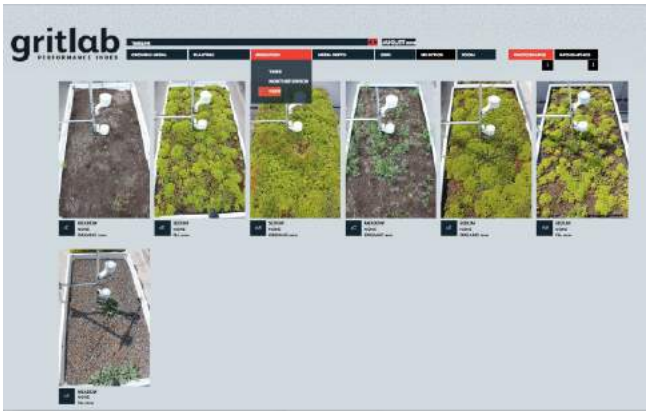

Figure 6. Performance Index photo documentation sorted by design variables (no irrigation, August 2016)

3 RESULTS & DISCUSSION

The outcome of this visualization exercise resulted in a data model and a web-based interface that visually unifies different forms of sensor data on water and temperature with biomass sampling and photographic documentation of different green roof test module. For water and temperature, the model presents the difference between weather data plus irrigation and localized cooling and water discharge. An accompanying display of monthly water volumes and maximum temperature calculates numerical differences between input and output per module (Figure 7). For plant growth, the model visualizes percent cover, but also robustness: structure, density, diversity. The distinct dataset types and associated units were unified and scaled for visual comparison to represent the three co-benefits simultaneously. However, this representation framework is not intended to produce statistical analysis, or conclusive recommendations for 'best' green roof configurations. Rather, the intention is to explore the visualization of the vast quantities of data collected over a three-year period in a manner that would necessitate careful observation and consideration and open up new developments for decision making tools in green roof design.

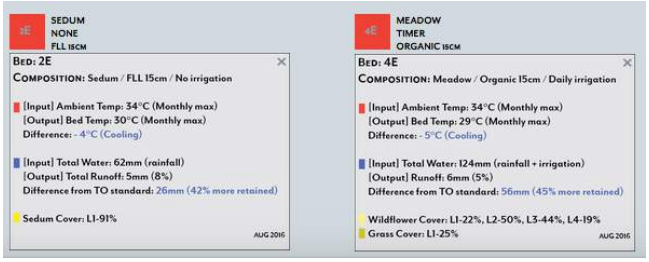

Figure 7. Numerical values and differences for water and temperature input and output

A relatively limited number of green roof studies examine multiple independent and dependent variables despite the core premise of co-benefits, or ecosystem services [22]. Often benefits are examined in parallel and through different models (e.g. scatter plot, bar graphs, regression diagrams), field-specific indexes, and temporal scales [22, 26]. Moreover, visualization that examines the relationship between multiple independent and dependent variables is poorly represented in literature. Lundholm et al. [20] investigated the correlations between ecosystem services and vegetation properties in a modular green roof system using a path diagram. Another more complex method that is increasingly used is structural equation modeling. Both types of modeling present statistical analysis, but have not been used as interactive decision making tools for green roof design. The significance of the representation framework of the proposed tool lies in its integrated and interactive structure, which elucidates the interactions among multiple independent and dependent variables, and facilitates sorting and comparing different configurations over incremental, yet practical periods of time.

The web-based sorting function permits the user to isolate and combine independent variables and observe their relative influence on hydrologic, thermal, and plant growth performance. For example, it appears that irrigation and 'organic' growing media are necessary for high percent cover and structure in the 'meadow' planting, and that the combined effect of these independent and dependent variables increases thermal cooling, while decreasing water retention. With upcoming policies and guidelines in the City of Toronto to create, restore, and enhance high quality wild bee habitats, policies and incentive programs for biodiverse green roof designs may increase. This means that growing media designed to support a range of flowering plants, namely high-nutrient and water-retaining media, as well as irrigation practices may be encouraged. However, given that irrigation negatively affects runoff reduction, employing deeper growing media may improve both retention and plant cover and diversity, as suggested in the data models for June 2015, the wettest month between 2014-2016.

The grid layout facilitates a comparison of different green roof configurations, typically represented in scientific papers as a bar graph with standard error annotation representing the range of measurements. For instance, in addition to the analysis of showing that Sedum planting maintains minimum 90% cover regardless of growing condition [17], the grid layout of monthly data models comparatively shows a more nuanced observation of the incremental increase in structure and density over time when planted in organic media (Figure 8).

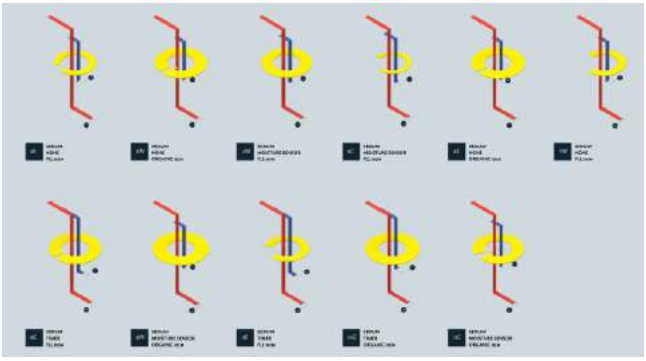

Figure 8. *Sedum* cover, structure and density, indicated by yellow rings, increases in organic growing media (August 2016)

In this context, monthly data was selected to allow observation of incremental change in contrast with annual or bi-annual sums, yet provide with a more practical data resolution than a scatter plot of five-minute, hourly, or daily measurements. Lastly, cross-referencing between data and photographs, and vice versa, allows a quantitative understanding of invisible and dynamic changes, such as temperature and water flow, alongside a qualitative account of the physical and aesthetic manifestation (Figure 9).

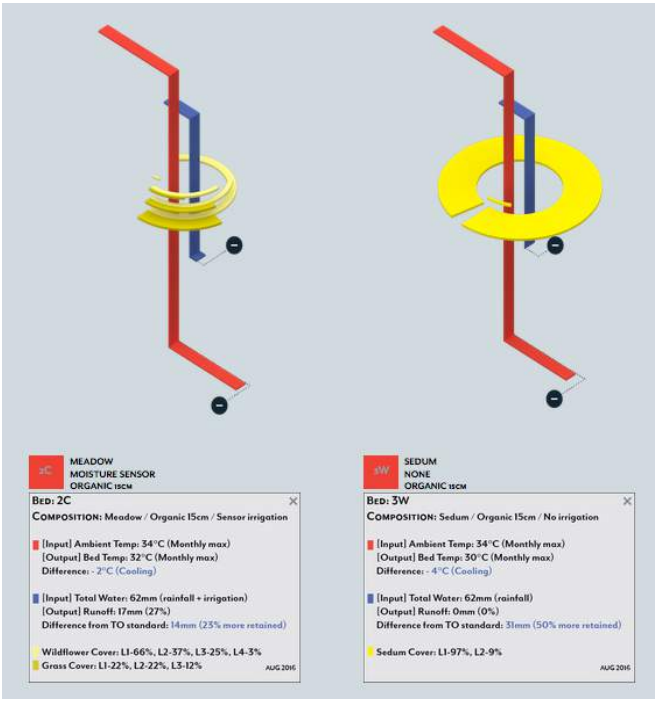

Figure 9. Two 'best' configurations show 4°C cooling and 0% runoff in *Sedum*, 15 cm organic, no irrigation vs. 2°C and 27% in Meadow, 15 cm organic with on-demand irrigation, August 2016

4 CONCLUSION

To help designers and policymakers understand the influence of different green roof materials and configurations on hydrologic, thermal, and plant growth performance in a regional context, we set up a multivariate experiment comparing twenty-three green roof test modules and a network of sensor to collect data on water balance and air temperature, as well as vegetative cover, structure and diversity. We then explored the use of data visualization using Rhinoceros™, Grasshopper® and LunchBox™ platforms to parameterize input values recorded by LoggerNet data acquisition software and manual biomass sampling. A web-based interface was developed to sort according to design variables and monthly increments, and then present the test modules side by side for comparison. We established the rationale for both scientific experiments and visualization techniques that can characterize co-benefits and tradeoffs and provide with decision making tools for green roof design. We then demonstrated the merits of the proposed representation framework over current models, where the integrated and interactive structure reveals the interactions among multiple independent and dependent variables and facilitates the sorting and comparing of different configurations over incremental, yet practical periods of time.

5 NEXT STEPS

As previously noted, the intention of this exercise is to explore the visualization of the vast quantities of data collected over multiple years to elicit new observations and ideas for interactive decision-making design tools. The next steps would be to develop data models for virtual simulation, where the current interface is converted into toggling functions and the photographic documentation serves as the basis for the green roof appearance.

ACKNOWLEDGMENTS

The authors would like to thank Isaac Seah, Ultan Byrne and Melissa Gerskup for their technical assistance. We are also grateful for Scott MacIvor, Jenny Hill, Ultan Byrne, and Robert Wright for their helpful comments. This project was made possible with grant funding from Natural Sciences and Engineering Research Council of Canada, STPGP 447409-13.

REFERENCES

1. Butler, C., and Orians, C. M. Sedum cools soil and can improve neighboring plant performance during water deficit on a green roof. *Ecological Engineering*, 37, 11 (2011), 1796-1803.
2. City of Toronto. Green Roofs. Adopted by Council City Toronto 2009-05-27 by By-law No. 583- 2009.
3. City of Toronto. Guidelines for Biodiverse Green Roofs. 2013. http://www1.toronto.ca/City%20Of%20Toronto/City%20Planning/Zoning%20&%20Environment/Files/pdf/B/biodiversegreenroofs_2013.pdf. 2013.
4. City of Toronto. Wet Weather Flow Management Guidelines. http://www1.toronto.ca/city_of_toronto/toronto_water/files/pdf/wwfmmp_policy.pdf. September 2003.
5. Dvorak, B. and Volder, A. Green roof vegetation for North American ecoregions: A literature review. *Landscape and Urban Planning* 96 (2010), 197–213.
6. F.L.L. Guidelines for the Planning, Construction and Maintenance of Green Roofing – Green Roofing Guideline. 2008.
7. Green Roof for Healthy Cities. How Your Community Will Benefit From Adopting Green Roof Policy (report). http://greenroofs.org. 2014.
8. GRIT Lab Performance Index. http://grit.daniels.utoronto.ca/green_roof_image_index. 2016.
9. Haselbach, L. *The engineering guide to LEED-New construction: Sustainable construction for engineers.* McGraw-Hill, New York, NY, USA. 2008.
10. Hill, J. *Designing Green Roofs for Low Impact Development: What Matters, and Why?* (Thesis). University of Toronto. 2016.
11. Hill, J., Drake, J., Sleep, B., Margolis, L. Influences of four extensive green roof design variables on stormwater hydrology. *Journal of Hydrologic Engineering*. In press.
12. Hill, J., Perotto, M., Yoon, C. Processes of quantifying the hydrological performance of extensive green roofs. *RCI International Convention Proceedings*. 2015.
13. Lazzarin, R.M., Castellotti, F., Busato, F. Experimental measurements and numerical modelling of a green roof. *Energy and Buildings,* 37:12 (2005), 1260–1267.
14. Li, Y., Babcock, R.W. Green roof hydrologic performance and modeling: A review. *Water Science Technology*, 69:4 (2014), 727-738.
15. MacIvor, J.S., and Lundholm, J. Performance evaluation of native plants suited to extensive green roof conditions in a maritime climate. *Ecological Engineering*, 37:3 (2011), 407-417.
16. MacIvor, J.S., Margolis, L., Perotto, M., Drake, J.A.P. Air temperature cooling by extensive green roofs in Toronto Canada. *Ecological Engineering,* 95 (2016), 36–42.
17. MacIvor, J.S., Margolis, L., Puncher, C.L., Carver Matthews J.B. Decoupling factors affecting plant diversity and cover on extensive green roofs. *Journal of Environmental Management,* 130 (2013), 297–305.

18. MacIvor, J.S., Ruttan, A., Salehi, B. Exotics on exotics: Pollen analysis of urban bees visiting Sedum on a green roof. *Urban Ecosystems*, 18:2 (2014), 419-430.

19. Green Roof Innovation Testing Laboratory. http://grit.daniels.utoronto.ca. 2013.

20. Lundholm, J., MacIvor, J. S., MacDougall, Z., Ranalli, M. Plant Species and Functional Group Combinations Affect Green Roof Ecosystem Functions. *PLoS ONE,* 5:3 (2010), doi:10.1371/journal.pone.0009677

21. Monterusso, M. A., Rowe, D. B., Rugh, C. L. Establishment and persistence of *Sedum* spp. and native taxa for green roof applications. *HortScience*, 40:2 (2005), 391-396.

22. Oberndorfer, E., Lundholm, J., Bass, B., Coffman, R. R., Doshi, H., Dunnet, N., Gaffin, S., Köhler, M., Liu, K. Y., Rowe, B. Green Roofs as Urban Ecosystems: Ecological Structures, Functions, and Services. *BioScience*, 57:10 (2007), 823–833.

23. Rowe, D.B., Getter, K.L., Durhman, A.K. Effect of green roof media depth on Crassulacean plant succession over seven years. *Landscape and Urban Planning*, 104 (2012), 310-319.

24. Santamouris, M. Cooling the cities – A review of reflective and green roof mitigation technologies to fight heat island and improve comfort in urban environments. *Solar Energy*, 103 (2014), 682–703.

25. Schroll, E., Lambrinos, J., Righetti, T., Sandrock, D. The role of vegetation in regulating stormwater runoff from green roofs in a winter rainfall climate. *Ecological Engineering*, 37 (2011), 595–600.

26. Simmons, M.T., Gardiner, B., Windhager, S., Tinsley, J. Green roofs are not created Equal: The hydrologic and thermal performance of six different extensive green roofs and reflective and non-reflective roofs in a sub-tropical climate. *Urban Ecosystems*, 11 (2008), 339–348.

27. Starry, O. *The comparative Effects of Three Sedum Species on Green Roof Stormwater Retention* (Thesis). University of Maryland, 2013.

28. Van Mechelen, C., Dutoit, T., Hermy, M. Adapting green roof irrigation practices for a sustainable future: A review. *Sustainable Cities and Society,* 19 (2015), 74–90.

29. VanWoert, N. D., Rowe, D. B., Andresen, J. A., Rugh, C. L., Xiao, L. Watering regime and green roof substrate design affect *Sedum* plant growth. *HortScience*, 40:3 (2005), 659-664.

30. Yio, M.H.N., Stovin, V., Werdin, J., Vesuviano, G. Experimental analysis of green roof substrate detention characteristics. *Water Science Technology*, 68 (2013), 1477-1486.

Microclimate on building envelopes: wind tunnel and computational fluid dynamic analysis of basic and complex geometries

C. Hershcovich, R. van Hout, V. Rinsky and M. Laufer, Y. J. Grobman

Technion, Israel Institute of Technology
Haifa, Israel
cheli@campus.technion.ac.il, rene@technion.ac.il, rinsky@tx.technion.ac.il,
mjlaufer103@gmail.com, yasha@technion.ac.il

ABSTRACT
This paper presents the results of an investigation into the potential of complex geometry to create a microclimate by changing the airflow on building façades.

The current stage of the research focused on developing a set-up and a methodology for examining and comparing the results of a physical wind tunnel test to those of CFD (computational fluid dynamics) simulations. A series of chosen façade geometries was examined using CFD simulations and physical wind tunnel simulations. The numerical simulations were validated by the experimental data. Based on the best performing geometries of the first examined series, new geometries will be developed and tested towards a better understanding of the façade's geometry contribution to the building's thermal performance.

Author Keywords
microclimate; building envelope; thermal insulation; computational fluid dynamics; complex geometry.

ACM Classification Keywords

I.6.1 SIMULATION AND MODELING

1 INTRODUCTION

The traditional approach to the design of building envelopes is based on a combination of layers that combine mass and material properties and create the thermal barrier from the outside. As opposed to the complex cellular structure of natural skins, which use their geometry to increase thermal performance, traditional building envelopes are typically based on flat orthogonal geometry, repetition, limited functions and structural homogeneity.

The following paper presents the results of research that examines the potential to develop a multifunctional building façade that employs complex geometry to create a microclimate on the building façade, which will contribute to its thermal performance.

The early stages of the research developed a theoretical framework for a shift toward building envelopes that are based on complex geometry and validated the potential of this approach with 2D computational fluid dynamic (CFD) simulations [5, 6]. The current stage of the research focuses on the development and optimisation of complex cellular building envelope geometry. It employs and compares results from physical wind tunnel experiments and 3D CFD simulations.

This paper opens with a summary on architectural precedents, existing literature on complex geometry in building envelopes and the results of the previous stages of the research. It then presents the set-up and the methodology of the current stage of the research. The final section discusses the results, the conclusions of the current examinations and the directions worth pursuing in future stages of the research.

2 BACKGROUND AND PRELIMINARY RESEARCH

A precedent and literature review on microclimate and complex façade geometries in architecture was performed in a preliminary research [5, 6]. Architectural precedents in this field can be divided into two types. The first focused on the esthetical aspects of the façade geometry and did not try to postulate better performance because of the facades geometry. Notable examples are the buildings of Antoni Gaudi, Eladio Dieste and Frank Gehry. The other type of designs focused on the material and morphological aspects of the façade to increase the building envelope's performance. Notable examples are the Beijing National Aquatic Center by PTW Architects and KOL/MAC Architecture's INVERSAbrane building envelope [4]. Academic research in this field that was reviewed in the preliminary research focused on green roofs and the effects of vegetation [1], and bio inspired building facades [3, 7-9].

The preliminary research developed a framework for a shift towards using the geometry of the building envelope to create a microclimate on the building façade. It also validated the potential of basic building envelope geometries to generate a micro-climate on the façade [6].

SimAUD 2017 May 22-24 Toronto, Canada

The preliminary research examined only a small number of basic façade geometries. It called for further examination of various types of geometries in order to better define the connection between microclimate and façade geometry. It also suggested that CFD results should be validated using wind tunnel tests with physical models due to the complex nature of air flow on facades.

3 METHODOLOGY

The current stage of the research focused on examining the microclimate developed on various envelope geometries and the potential impact of the microclimate on the thermal performance of the building envelope. The research methodology consisted of two stages. The first consisted of a comparative examination of similar chosen façade geometries in physical wind tunnel and CFD analysis. The aim of this stage is to validate the numerical simulations by experimental data and to select the best performing envelope geometries for further development and optimization. Following successful results in the first stage, the second stage of the research will continue developing the best performing geometries from the first stage using the CFD analysis tested in the first stage. The tile geometries will be initially optimized for thermal behaviour and later also for self-shading to decrease solar radiation. The final aim of the research is to develop a building envelope tile or series of tiles with increased thermal performance, which is generated by the envelope's tile geometry.

3.1 Flow field

Here, the flow impinging on a building envelope was modeled by a turbulent jet impinging on smooth and sculptured flat surfaces using a combination of numerical simulations and experiments. The physical experiments were conducted at the Environmental Multi-Phase Flow Laboratory at the Technion (Figure 1). An axisymmetric, turbulent air jet was created by installing a converging nozzle (contraction area ratio of 100:1) at the end of a small open loop wind tunnel. The exit diameter of the jet was D = 20 mm, and exit jet velocities were U_j = 1, 5 and 10 m/s, corresponding to 1, 3 and 5 Beaufort. Jet Reynolds numbers were Re = U_jD/ν = 1,300, 6,260 and 12,354, where ν is the kinematic air viscosity. The surfaces were installed at H = 10 cm (H/D = 5), where H denotes the distance measured from the nozzle exit. Plate dimensions were ten times those of D while modelled sculptured hole diameters were smaller than D. Flow field measurements were performed using Particle Image Velocimetry (PIV). The PIV system (LaVision GmbH) consisted of a CCD camera (2048x2048 pixels), an Nd:Yag laser (200mJ/pulse), laser sheet optics and acquisition/processing software (DaVis 8.1). A laser sheet (~ 1mm thickness) was created using a cylindrical lens and planar measurements were acquired at 5Hz. At each Re and plate configuration, 450 instantaneous vector maps were acquired having a field of view (FOV) of about 100x100 mm^2. Multi-pass data processing was performed starting with an interrogation window size of 64x64 pixels that was reduced to 8x8 pixels at 50% overlap resulting in a vector spacing of 0.2 mm. In between passes, outlier detection was performed and the data was smoothed using a 3x3 Gaussian spatial filter [10].

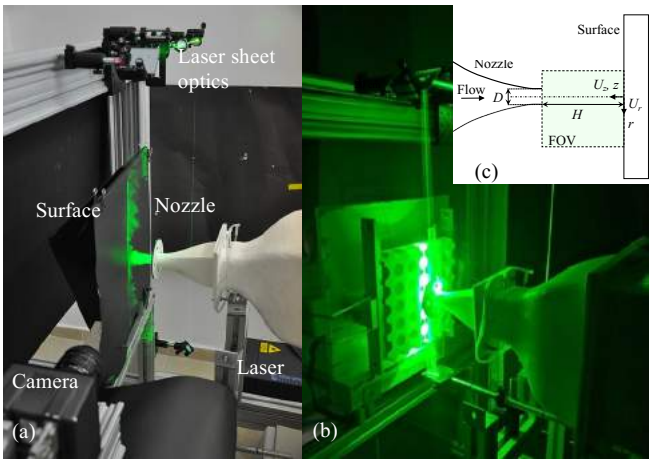

Figure 1. Picture of the (a) experimental PIV setup, (b) flow visualization on sculptured surface and (c) FOV and employed coordinate system

The computer-based simulation employed the commercially available Star-CCM+ 11 CFD package. A 3D simulation was set up with a flat impinging surface. The fluid parameters and jet geometry were modelled to match the experiments. The numerical simulations were based on the Reynolds Averaged Navier-Stokes (RANS) equations that were solved using the V2F model (e.g. [2]) employing a slightly modified k-ε turbulence model and an additional transport equation for the variance of the wall-normal velocity fluctuations. Note that the V2F model was chosen since it has previously shown to offer the most accurate results for impinging jet problems excluding the overly "expensive" Direct Numerical Simulation and Large Eddy Simulation (DNS/LES) methods [11].

In general, a jet flow impinging on a wall results in a stagnation region and a fast developing wall jet, radially extending from the stagnation point. We choose the impinging jet since it is a well-researched flow that may model some of the flow characteristics around a building envelope exposed to atmospheric winds. This setup allows both for the study of the stagnation point heat transfer characteristics as well as in those regions where the flow is parallel to the wall.

3.2 Envelope geometry

Two different sets of geometries were tested. The first set consisted of repetitive basic geometries, similar to the geometries that were examined in the 2D CFD simulation in the early stage of the research [6] (Figure 2).

The second set of geometries was based on selected 3D scans of cacti. The idea was to examine whether the cacti external geometry helps to develop a microclimate in a way

that contributes to its thermal performance. From numerous cacti that were 3D scanned, 3 cacti with different geometry were selected. The 3D scans were rationalized and employed on a flat surface while keeping the exact proportions of the cactus envelope (see figure 3). Similar to the preliminary research, all simulations in this stage were performed on concrete walls, 30 cm thick, which is the typical width used for load-bearing concrete walls in buildings. Wind tunnel simulations were performed on 3D printed models made of gypsum that were printed using a Zcorp printer in 1:25 scale (Figure 3).

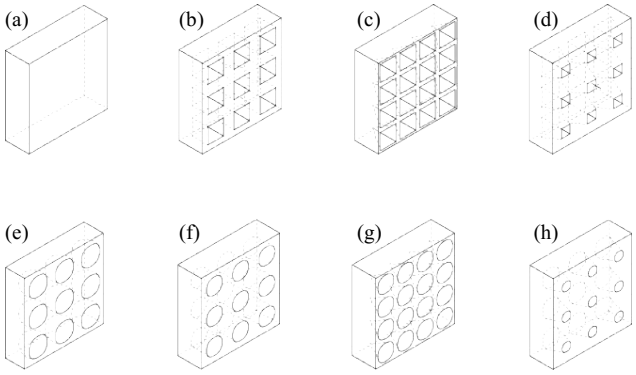

Figure 2. Test tiles: (a) – plane wall; (b)-(d) – rectangular cells; (e)-(h) – circular cells

4 PRELIMINARY RESULTS

As an initial step the measured average flow field of a turbulent jet impinging on a flat, smooth surface was compared to the CFD simulations. An example is provided in Figure 4 that depicts iso-contour levels of the normalized, ensemble averaged axial velocity field, $\langle U_z \rangle / U_j$, and the radial velocity, $\langle U_r \rangle / U_j$, respectively. Note that the $\langle U_z \rangle$ is significant mainly in the incoming circular jet while $\langle U_r \rangle$ is significant near to the wall in the radial direction. As observed, some differences exist but overall the comparison between the simulations and the experiments is satisfactory. Although these are initial results and they will need to be further corroborated against results involving sculptured plates, we anticipate that in future studies the relatively fast CFD simulations can be used to select the most promising results and geometries and wind tunnel experiments will only be used for validation purposes.

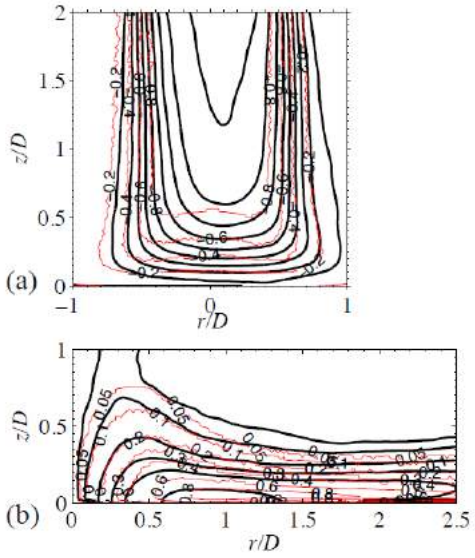

Figure 4. Comparison between numerical simulations and experiments (Re = 6,260, U_j = 5 m/s). (a)$\langle U_z \rangle / U_j$. (b) $\langle U_r \rangle / U_j$. Experiments: Black solid iso-contours; Simulation: Red solid iso-contours. Depicted contour levels relate to simulations but equally apply to experiments.

In addition, Figure 5 shows the contour plots of the normalized Reynolds shear stress, $\langle u_r u_z \rangle / U_j^2$, for a smooth target surface and a sculptured one (Fig. 2e). Here u_r and u_z are the velocity fluctuations in the r and z direction, respectively. Since $\langle u_r u_z \rangle$ is directly associated with momentum transfer and can also be related to the heat transfer by the Reynolds analogy, differences in its distribution will have an effect on the heat transfer characteristics. While the distribution of $\langle u_r u_z \rangle$ is similar in the incoming jet, the influence of the holes can be discerned in the insets in Figure 5. The CFD simulation will be used in the next stage of the research to simulate and calculate the expected heat transfer or thermal insulation performance of the examined geometries and a comparison with the experiments will be made based on the Reynolds analogy.

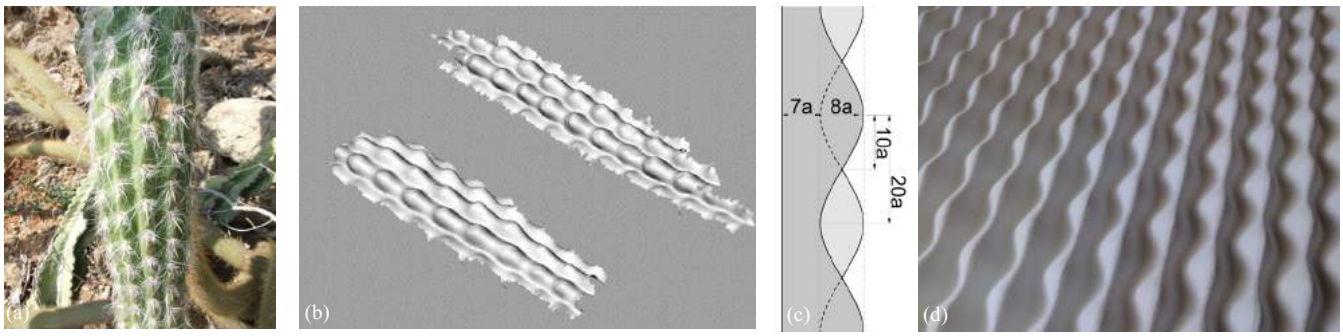

Figure 3. Example of one examined cactus. (a) – type: Oero cactus; (b) – 3d model of Oero cactus created by a 3d scan; (c) – tile section, defined according to the exact proportions of the scan; (d) – a 3d printed gypsum model representing the cactus proportions.

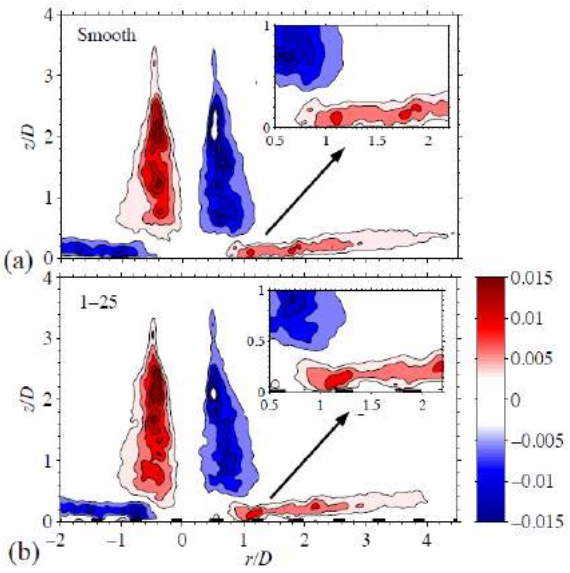

Figure 5. Measured spatial distribution of the normalized Reynolds shear stress. (a) smooth plate, (b) plate with hemispherical dimples having a diameter of 10 mm (Fig. 2e). The impenetrable wall between the holes is indicated by thick black bars at $z/D = 0$ in (b).

5 CONCLUSION

This paper presented the initial results of a second stage of research that examined the potential of using geometry parallel to material to increase the building envelope's performance. The current stage focused on developing a set-up and a methodology for examining and comparing the results of a wind tunnel tests to those of CFD simulations. Initial results in the wind tunnel validated the correlation between both test paving the way to expand the CFD tests in future research towards examining, comparing and optimizing building envelope geometry contribution to the thermal performance of buildings.

ACKNOWLEDGMENTS

The research was supported by the Israeli Ministry of Construction and Housing - grant number 2022402/2015.

REFERENCES

1. Aydogan, A. (2012). Building-integrated active modular phytoremediation system (Doctoral dissertation, Rensselaer Polytechnic Institute). http://gradworks.umi.com/35/30/3530027.html.
2. Behnia, M., Parneix, S., & Durbin, P. A. (1998). Prediction of heat transfer in an axisymmetric turbulent jet impinging on a flat plate. International journal of heat and mass transfer, 41(12), 1845-1855.
3. Badarnah, L., Farchi, Y. N., Knaack, U., Carpi, A., & Brebbia, C. A. (2010). Solutions from nature for building envelope thermoregulation. Design & Nature V: Comparing Design in Nature with Science and Engineering, A. Carpi, CA Brebbia, Editors, 251-262.
4. Grobman, Y. J., & Neuman, E. (2011). Performalism: form and performance in digital architecture. Routledge.
5. Grobman, Y. (2013). Cellular Building Envelopes, in: Chakrabarti, A., Prakash, R.V. (Eds.), ICoRD'13, Lecture Notes in Mechanical Engineering. Springer India, pp. 951–963.
6. Grobman, Y. J., & Elimelech, Y. (2016). Microclimate on building envelopes: testing geometry manipulations as an approach for increasing building envelopes' thermal performance. Architectural Science Review, 59(4), 269-278.
7. Gruber, P., & Gosztonyi, S. (2010). Skin in architecture: towards bioinspired facades. WIT Transactions on Ecology and the Environment, 138, 503-513.
8. Knippers, J., & Speck, T. (2012). Design and construction principles in nature and architecture. Bioinspiration & biomimetics, 7(1), 015002.
9. Laver, J., Clifford, D., & Vollen, J. (2008). High performance masonry wall systems: principles derived from natural analogues. WIT Transactions on Ecology and the Environment, 114, 243-252.
10. Raffel, M., Willert, C. E., Wereley, S. T., Kompenhans, J. (2007). Particle Image Velocimetry, A practical guide. Second Edition Springer-Verlag Berlin Heidelberg, pp. 460.
11. Zuckerman, N., & Lior, N. (2005). Impingement heat transfer: correlations and numerical modeling. Transactions of the ASME-C-Journal of Heat Transfer, 127(5), 544.

Parametric Modeling in Form-Based Urban Design Code for High-Dense Cities

Yingyi Zhang and Marc Aurel Schnabel

Victoria University of Wellington
Wellington, New Zealand
{yingyi.zhang,
marcaurel.schnabel}@vuw.ac.nz

ABSTRACT

The parametric modeling capabilities were established to support architecture design and building processes. While in urban design, it is still in the relative infancy. This paper aims to extend parametric approaches to multi-scenario tests and modification in large scale urban design. Tsim Sha Tsui (TST), a super high-dense area of Hong Kong, here works as a study context. Through marrying Building Information Modeling (BIM) into Form-Based Code (FBC) generation of TST, this research argues that 1) as a critical response to conventional zoning, FBC has potential to be an alternative approach to urban design of high-dense cities; 2) parametric modeling can support FBC implementation with directly visualized consequences that paper-based regulation cannot express; 3) adopting parametric FBC in high-dense cities has both benefits and drawbacks. Thus, this research attempt to fill the gap among the current approaches by generating parametric form-based urban design code for high-dense cities.

Author Keywords

Parametric modeling; City Information Modeling; Form-Based Code; urban design; high-dense.

ACM Classification Keywords

I.6.5 MODELING DEVELOPMENT (Modeling methodologies).

1 INTRODUCTION

The design in urban scale involves a complex interpretation and management of morphological structures, existent and proposed, as well as several kinds of the urban environment form which several urban indicators can be calculated and used for supporting design decision [1]. Parametric modeling for urban design process has been increasingly discussed recently. As a collaborative endeavor, urban design needs to combine various opinions from designers, stakeholders, developers and governments. It is not easy to negotiate different ideas and concerns together and finally achieve a relatively appropriate result that fulfills the demands from different groups. When non-designers are involved into making decisions in urban design projects, the draft scenario or layout proposal need to be directly visualized and flexible enough to be modified.

BIM software has the capability to support urban design in a parametric way. For instance, the project developers are interested in the locations and areas, building densities, exactly floor area ratio, etc. Stakeholders need to know what their living environment looks like. Governments concern on the basic infrastructures, road networks, and the quality of urban space. A three dimension layout with parameters of BIM platform can contribute to providing physical information for different requirements.

The concept of City Information Modeling (CIM) was presented by Beirao in 2009, which is an analogy of BIM. While BIM offers a new paradigm in building design, the current urban design paradigm is still rooted in drafting and illustration methods eventually supported by information technologies of Computer Aided Design (CAD), 3D modeling and visualization [9]. The main idea of CIM, as in BIM, is to link a parametric model of an area with the data related to it providing simultaneously a design environment and an analytical environment where urban spaces can be measured, analyzed and changed interactively along a design process [1]. This paper hypothetically combines the parametric urban design with FBC together to support urban design decisions in a rational and sustainable way.

2 FBC IN HIGH-DENSE CITIES

FBC is a means of regulating urban development to achieve predictable form. It was created as an alternative to conventional zoning and land use regulations by addressing the public realm and urban form [3]. Form-Based Code Institute (FBCI) defines FBC as a land development regulation that fosters predictable built results and a high-quality public space by using the physical form as the organizing principle for the code [8]. In 2008, Parolek raised the relationship and differences between zoning and FBC [15]. He proposed FBC a method to create or recreate a specific urban form primarily by controlling physical form, with a lesser focus on land use, through city or county regulations [12]. He also argues that FBC is a tool for encouraging mix-used zoning, helping improve the quality of the environment, as well as for fighting sprawl and detrimental effects [12].

2.1 Characteristics of FBC

Transect Matrix is the main characteristic of FBC. It defines the hierarchical development scales [4]. Naturalists use a concept called the "transect" to describe the characteristics of ecosystems and the transition from one ecosystem to another; Andres Duany has applied this concept to human settlements, and since about 2000 this idea has permeated the thinking of new urbanists [5]. Figure 1 shows that Transect 1 (T1) to Transect 6 (T6) with the Special District (SD) represent from natural zone to urban core zone. The Transect Matrix provides transect types to describe what the urban space looks like. For instance, Figure 2 shows the regulation plan of Miami based on FBC and conventional zoning. The FBC regulation plan contains more levels from T1 to T6-n, reflecting more details than conventional land-used zoning with five land use types.

Figure 1. Standard transect matrix of FBC [6].

2.2 Examples of FBC

As a practical approach to developing smarter, FBC has been increasingly implemented in different scales. A number of FBC adoptions are clustered in sparse counties of America. For example, the FBC project in Bellevue, Kentucky is a mandatory code for shaping public space and preserving historic downtown character. The organizing principle is Transect Zoning. The City of Bellevue generated the code after a year-long public process, a four-hour visioning exercise, and a four-day charrette in which nearly 200 residents, business owners, developers and policymakers' participated and assembled a vision plan for the project's implementation [2]. Figure 3 maps the locations of the transect types, and Figure 4 provides an example that what are the specific regulations of different transect types.

The East Billings Code in Montana offers the zoning regulations and standards for allowable frontage types, landscape standards, signage, and street types. The code aims to regulate the urban forms through specifying building's parameters to result in a predictable physical built environment. Figure 5 shows the regulation plan of the district code which zones the target site by transect matrix rather than land-use. The idea of conventional zoning is criticized because of rigid and inflexible. Compared with zoning, FBC provides more possibilities for shaping urban space. Parameter regulation examples are expressed in Figure 6.

Large cities with relatively high density have begun to consider FBC as well. Miami 21 Codes is a reprehensive project, which using form-based techniques on a larger scale than ever before attempted [10]. The development includes centers, corridor, downtown, historic preservation, infill, and redevelopment. Since Miami is a center city and it has a larger region that should be regarded as transect 6 (T6) type, the government and urban designers divide the T6 type into a few sub-types from T6-8 to T6-48 (Figure 7). In our research, we take the Miami project as a reference and divide the T6 into subtypes in Hong Kong.

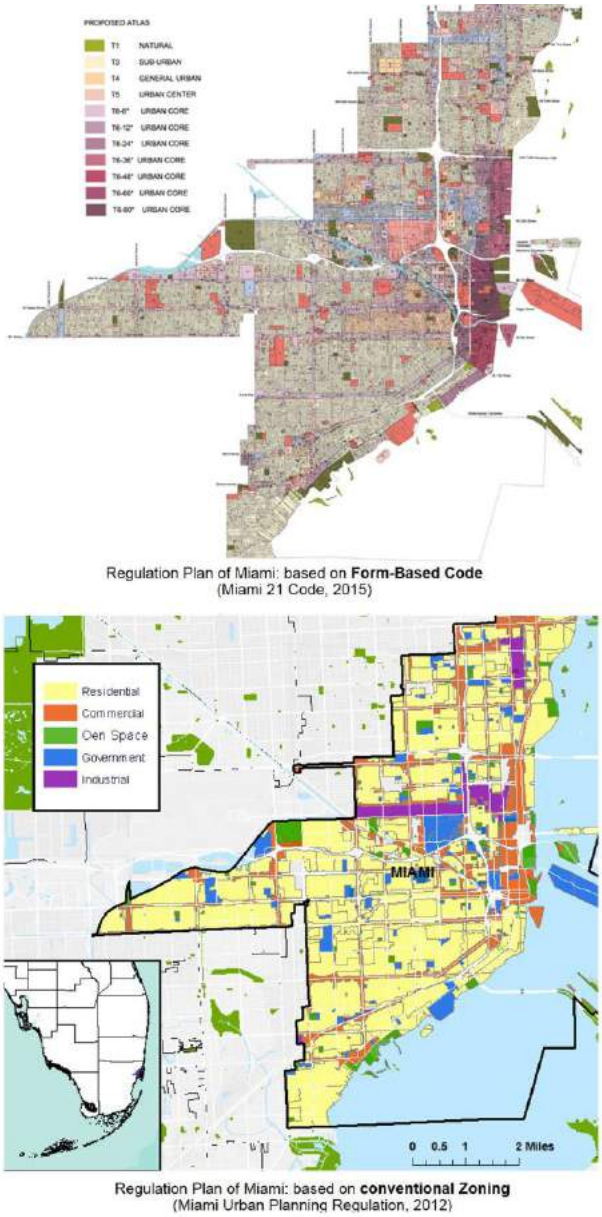

Figure 2. Comparison of regulation plan based on FBC and Zoning [11].

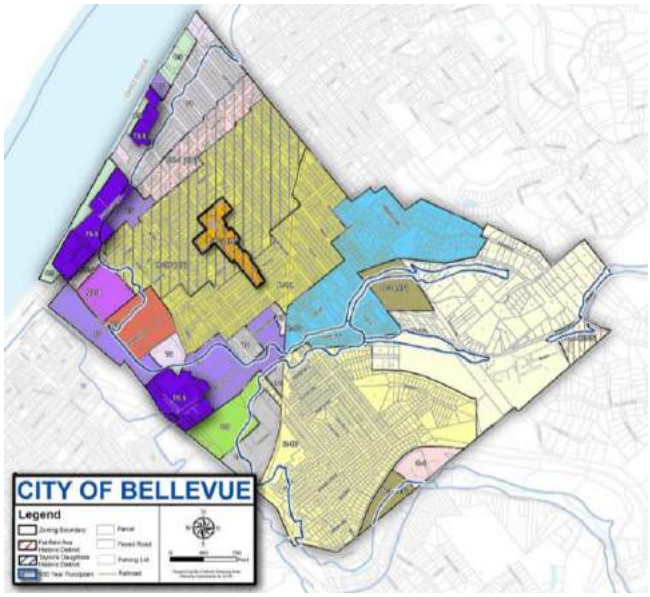

Figure 3. Transect-based regulation plan, City of Bellevue, 2011 [2].

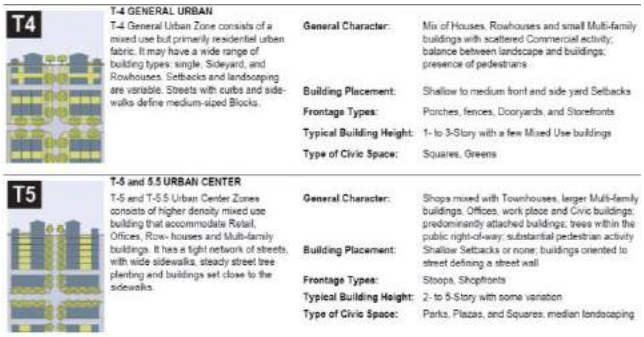

Figure 4. T4/5 (General Urban / Urban Center) descriptions of Bellevue project, 2011 [2].

Figure 5. Five zoning types of the FBC master plan, East Billings Urban Renewal District Code, 2014 [7].

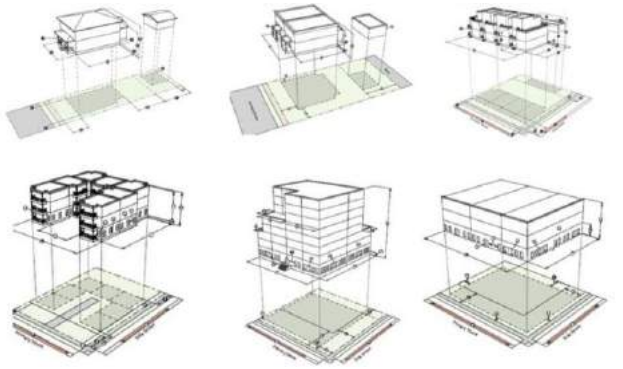

Figure 6. The parameter regulations of East Billings, 2014 [7].

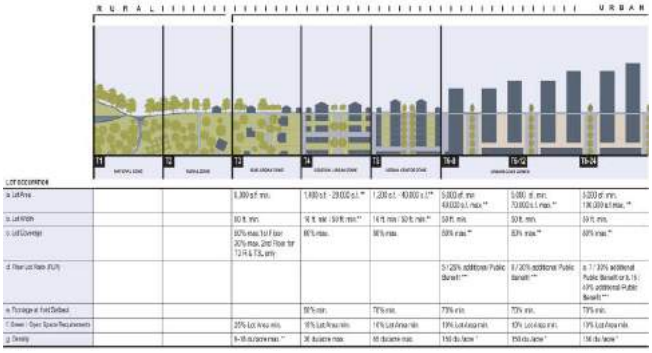

Figure 7. Transect of Miami 21 Codes, 2015 [14].

3 MODELING FOR THE FBC IN HONG KONG

We use TST area, Hong Kong as a study context. As a typical high-dense metropolis region, Hong Kong has one of the most crowded city centers in the world. TST is located at the southern part of Kowloon. From 1860s, some small villages were established here. Nowadays, this district has become a major tourist hub and movement venue of metropolitan Hong Kong [16].

3.1 Building and block forms

The existing building and block forms in TST region of Hong Kong various by location. The buildings of historical streets and neighborhoods tend to have relatively smaller size than newly developing places. The buildings with narrow façade width and different materials create a plenty of impressive street collages in Kowloon Peninsula. Minimized open grounds are enclosed by mix-used towers and skyscrapers.

Most of the blocks are presented as rectangle nets in TST. The short edge ranged from 40-70 meters and long edge 70-200 meters. In each block, the street interface length for the business function is as long as the block's outline. Therefore, the high-dense road grids and detailed block division contribute to generating more commercial space and improve the land's economic effectiveness. The ground floor and first floor stores cannot fulfil the business demands. Different commercial types have been sprawling volumetrically to higher levels.

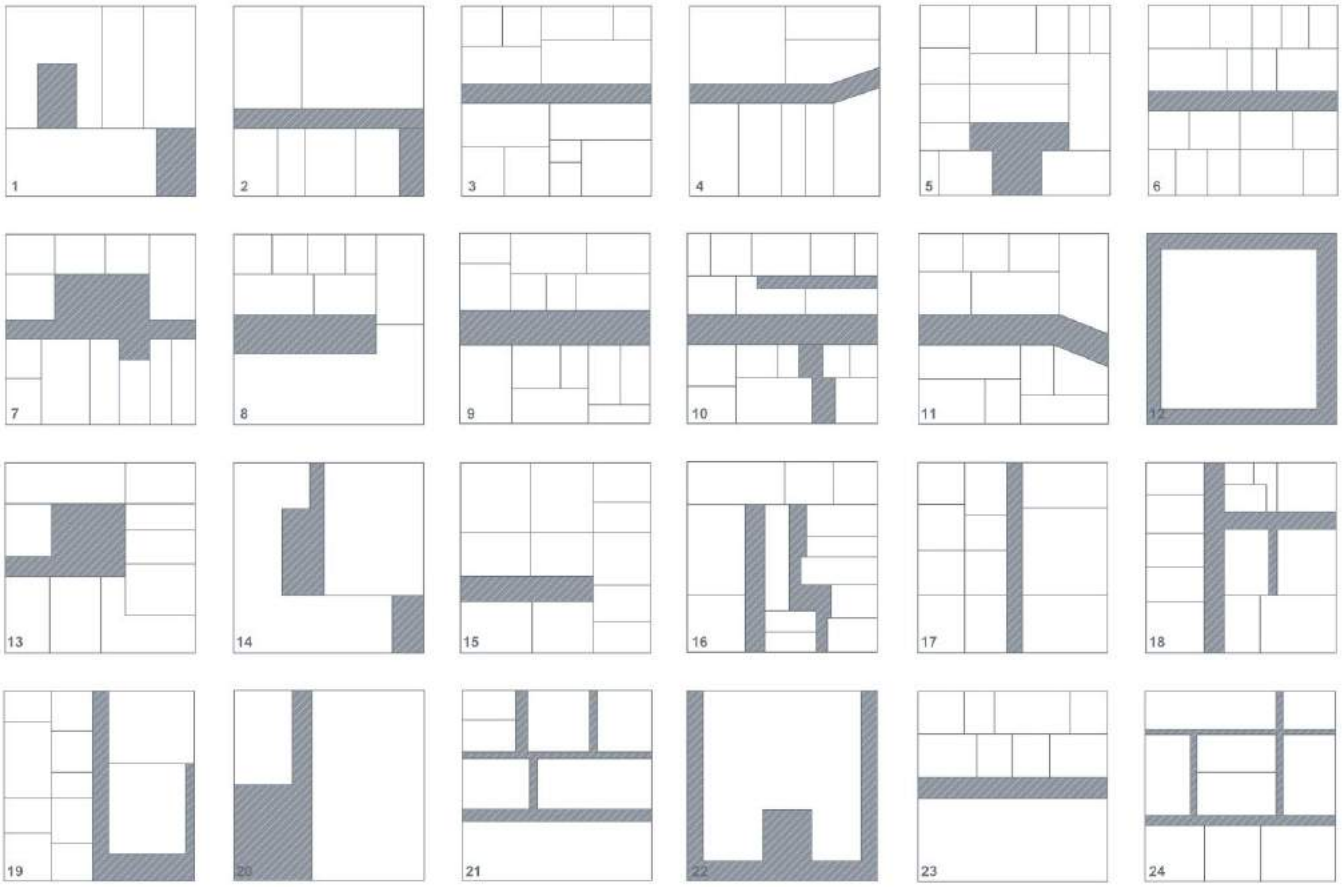

Figure 8. Simplified block forms of TST region.

In this situation, we divide the target site into 24 blocks with approx.100 x 100 square meters, an average size of the blocks, to simplify the figure-ground form as Figure 8 presents. The blocks are numbered in order to conduct the data analysis in next steps.

3.2 Redefine the transects

In the project of form-based urban design code of TST, we use seven variables to measure the transect type of different blocks. The variables are plot ratio, average pavement width, road hierarchy, infrastructure, the depth-width ratio of streets, max height, and connections between buildings. Table 1 shows the statistic outcomes of the 24 blocks in TST.

No.	V1	V2	V3	V4	V5	V6	V7
1	15.81	3	1	1	11.0	110	0
2	9.17	2	1	2	7.5	110	0
3	6.49	2.5	1	1	6.8	110	0
4	15.22	3	1	2	13.8	110	0
5	8.64	3	4	2	3.7	110	0
6	8.00	2	2	1	4.2	110	0
7	8.33	3	3	1	4.3	110	0
8	8.75	2.5	3	2	3.6	110	0
9	5.97	3	5	3	2.8	130	1
10	7.97	3	5	2	2.8	130	0
11	7.53	3	5	2	2.8	130	0
12	13.79	4	5	3	7.2	130	0
13	15.25	2.5	3	1	3.5	130	0
14	8.61	4	4	3	2.8	50	0
15	7.17	2	4	1	2.3	110	0
16	4.14	4	4	3	2.4	110	0
17	6.31	4	4	4	2.1	110	0
18	10.85	2.5	3	2	4.6	110	0
19	5.64	2	3	2	3.6	110	1
20	5.94	3	2	4	3.0	110	0
21	8.90	4	4	4	3.4	110	0
22	6.77	3	6	4	1.7	50	0
23	6.24	2	1	2	5.1	110	0
24	8.21	3	4	4	4.2	110	0

Table 1. Variable values of the existing blocks.

Variable 1: Plot ratio = (gross floor area) / (area of the plot)

Variable 2: Average pavement width (m)

Variable 3: Road hierarchy

Grade	Description
1	One-way street, single lane
2	One-way street, double lanes
3	One-way street, treble lanes
4	two-way street, double lanes
5	two-way street, four lanes
6	two-way street, six lanes and above

Table 2. Descriptions of the road hierarchy.

Variable 4: Infrastructure

Grade	Description
1	fire hydrant; plumbing well; trash can; substation box
2	fire hydrant; plumbing well; trash can; substation box; border tree
3	fire hydrant; plumbing well; trash can; substation box; border tree; street lamps
4	fire hydrant; plumbing well; trash can; substation box; border tree; street lamps; chair; art; etc.

Table 3. Descriptions of the infrastructure grades.

Variable 5: Depth-width ratio of streets = (average building height) / (average street width)

Variable 6: Max. Height based on the existing official design files.

Variable 7: Connections between buildings. Since the existing compacted land uses, the space between buildings is generally narrower than other sparse cities. Some connections are added between towers and skyscrapers from the consideration of structure stabilization, hazard prevention, and convenient transportation on high-rise levels. In FBC method, buildings with connections are more closed to the artificial point of the transect matrix.

The variables need to be normalized because of the different units they have. For example, the pavement width cannot plus infrastructure grade directly since they are not in the same unit of measurement. We use the Min-Max Normalization to normalize data to [0, 1]. The normalized value of e_i for variable E is calculated as:

$$Normalized\ (e_i) = \frac{e_i - E_{min}}{E_{max} - E_{min}}$$

Where

E_{min} = the minimum value for variable E

E_{max} = the maximum value for variable E

If E_{max} is equal to E_{min} then *Normalized* (e_i) is set to 0.5.

Table 4 shows the normalization results:

No.	V1	V2	V3	V4	V5	V6	V7	Σ	x
1	1.00	0.50	0	0	0.77	0.33	0	2.60	0.37
2	0.43	0	0	0.33	0.48	0.33	0	1.57	0.22
3	0.20	0.25	0	0	0.42	0.33	0	1.20	0.17
4	0.95	0.50	0	0.33	1.00	0.33	0	3.11	0.44
5	0.39	0.50	0.60	0.33	0.17	0.33	0	2.32	0.33
6	0.33	0	0.20	0	0.21	0.33	0	1.07	0.15
7	0.36	0.50	0.40	0	0.21	0.33	0	1.80	0.26
8	0.40	0.25	0.40	0.33	0.16	0.33	0	1.87	0.27
9	0.16	0.50	0.80	0.67	0.09	0.44	1	3.66	0.52
10	0.93	0.50	0.80	0.33	0.09	0.44	0	3.09	0.44
11	0.29	0.50	0.80	0.33	0.09	0.44	0	2.45	0.35
12	0.83	1.00	0.80	0.67	0.45	1.00	0	4.75	0.68
13	0.95	0.25	0.40	0	0.15	0.44	0	2.19	0.31
14	0.38	1.00	0.60	0.67	0.09	0	0	2.74	0.39
15	0.26	0	0.60	0	0.05	0.33	0	1.24	0.18
16	0	1.00	0.60	0.67	0.06	0.33	0	2.66	0.38
17	0.19	1.00	0.60	1.00	0.03	0.33	0	3.15	0.45
18	0.58	0.25	0.40	0.33	0.24	0.33	0	2.13	0.30
19	0.13	0	0.40	0.33	0.16	0.33	1	2.35	0.34
20	0.15	0.50	0.20	1.00	0.11	0.33	0	2.29	0.33
21	0.41	1.00	0.60	1.00	0.14	0.33	0	3.48	0.50
22	0.23	0.50	1.00	1.00	0	0	0	2.73	0.39
23	0.18	0	0	0.33	0.28	0.33	0	1.12	0.16
24	0.35	1.00	0.60	1.00	0.21	0.33	0	3.49	0.50

Note: Σ = V1+V2+…+Vn; x = Σ/n; n=7

Table 4. Normalization results of the blocks.

3.3 Result of the transect types analysis

Through adding the statistic outcomes into corresponding blanks, we get the average normalized value in each closed internal from 0 to 1. The outcomes are showed in Table 5.

	T6-1	T6-2	T6-3	T6-4	T6-5	T6-6			
0-0.09	0.1-0.19	0.2-0.29	0.3-0.39	0.4-0.49	0.5-0.59	0.6-0.69	0.7-0.79	0.8-0.89	0.9-1
-	3	2	1	4	9	12	-	-	-
-	6	7	5	10	21	-	-	-	-
-	15	8	11	17	24	-	-	-	-
-	23	-	13	-	-	-	-	-	-
-	-	-	14	-	-	-	-	-	-
-	-	-	16	-	-	-	-	-	-
-	-	-	18	-	-	-	-	-	-
-	-	-	19	-	-	-	-	-	-
-	-	-	20	-	-	-	-	-	-
-	-	-	22	-	-	-	-	-	-

Table 5. Numbered blocks in closed interval.

The whole TST area belongs to T6 (urban core zone) according to the standard FBC transect matrix. Only using T6 to conclude all of the communities and blocks are not sufficient to regulate the urban development. Sub-transect types need to be generated based on the analysis above. There are six subtypes in T6. The blocks scored 0.1-0.19, 0.2-0.29, 0.3-0.39, 0.4-0.49, 0.5-0.59, and 0.6-0.69 are respectively belong to T6-1, T6-2, T6-3, T6-4, T6-5, and T6-6. Sub-types of T6 has been determined. Therefore, the transect matrix of TST is expressed in Figure 9.

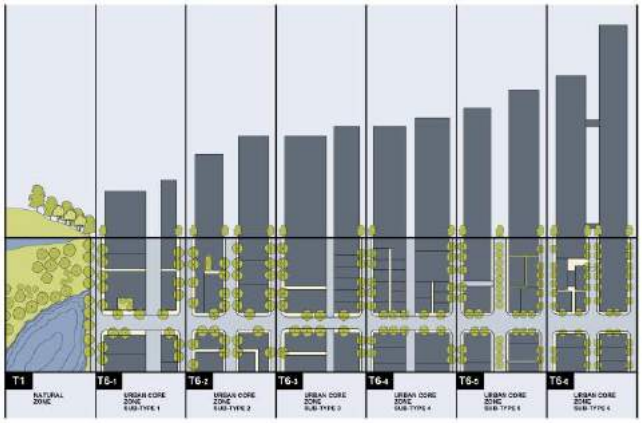

Figure 9. Transect matrix of TST.

However, transect division is not the final objective of FBC. Designers need to make standards for different transect and sub-transect types. That's an innovative point that makes FBC more flexible and elaborate than conventional zoning. Zoning takes land-use as one of the most essential parts. Other regulations are based on the land functions and usage. But, the land use regulation of TST contains limited information, which only consists of land function and height controls (Figure 10-11).

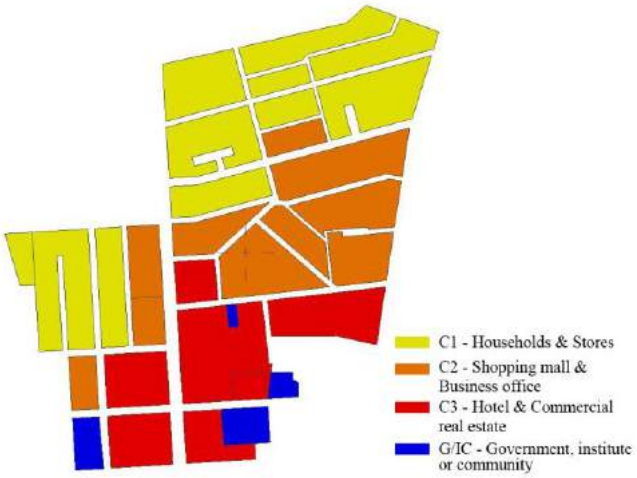

Figure 10. Land-use zoning of TST (reproduced based on Town Planning Ordinance, Kowloon Planning Area No. 1 – Tsim Sha Tsui).

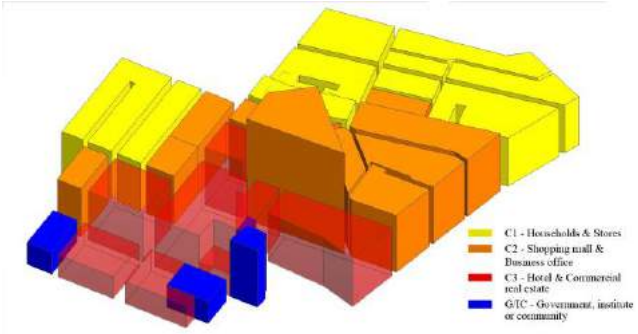

Figure 11. Model of the land-use plan of TST.

The form-based master plan code of TST (Figure 13) has been generated in Autodesk Revit ™ environment based on the calculate results above. There are six transect subtypes and each sub-type has its own locations and characteristics. The 3D model shows in Figure 14. Compare with the model of land-use, the model of FBC contains building forms, micro urban environment, and open space rather than simplified land functions.

After achieving the model of form-based master regulation, there are a few tasks need to conduct in next step in order to create a form-based urban design code. First, generate corresponding standards and regulations for the six transect sub-types from T6-1 to T6-6. Second, using parametric modeling approaches to modify the parameters and test different scenarios. In this research, we use Revit Conceptual Massing as a parametric modeling tool. It can support multi-scenario tests by changing parameters. Third, compare the form-based urban design code and existing regulation files, and then find out if it is possible to replace part of the existing controls by FBC.

Figure 12. FBC master plan of TST.

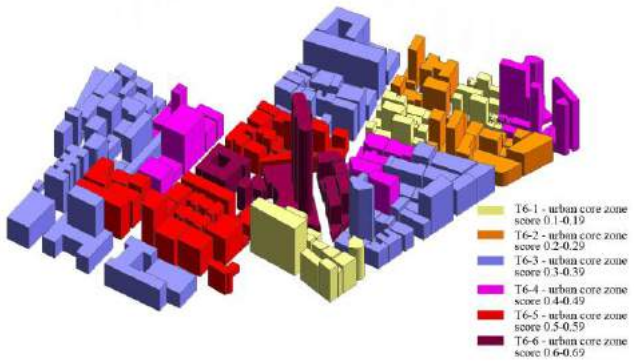

Figure 13. Model of the FBC master plan of TST.

4 DISCUSSION

Using FBC as an urban planning and design approach helps to get a different design code result compared with current zoning of Hong Kong. Conventional zoning aims to control the urban development from a macroscopic perspective. It benefits for government, developers, or experts to review the development processes. Nevertheless, the conventional zoning makes it difficult to impel public participation. Individuals nearly have no chance to take part in the zoning process. FBC is more focusing on microcosmic space features and characteristics. It advocates that urban design is a continuous flow from bottom to top. Public participation is an essential step in the visioning phase of FBC. By figuring out the urban codes in a three-dimension way instead of words and tables, people can understand FBC without any background knowledge. It is also convenient for designers, developers, and communities to be involved in urban development projects with clearly-expressed controls and guidelines.

Form-Based Code has been applied for about thirty years in different scales and contexts, however, combining FBC with parametric modeling tools are just starting. Parametric design techniques offer advantages for engineering and manufacturing processes, architects emerge from applying these methods in their creation of design suggesting solutions at an earlier stage of the process [16]. In FBC processes, especially for high-dense cities, urban designers can also make design suggestions with the help of parametric instruments before implementing.

Another discussion point is the procedures to generate FBC in high-dense cities. Generally, high-dense cities always have intensive road networks. These road networks divide the communities and neighborhoods into small sizes. Form and transects of the small-sized blocks are complex. Using the existing standard transect matrix of FBC is not enough. In this research, we use creative manners, adding sub-transect types based on differing variables, to conduct the FBC of TST. The detailing steps include:

- Site decision
- Dividing the target site into 100 x 100 square meters grids and analyzing the block and building forms
- Setting the variables up to redefine the transect types or subtypes. In this occasion, TST only has T6 type, so we delimit the transect into sub-types
- Data statistic and normalization
- Determining the block locations in each transect subtype and generating the transect matrix
- Modeling the FBC master plan in parametric tools environment. We use Revit, in this case, to test various scenarios considering the opinions from different groups (government, developers, stakeholders, etc.)
- Making customized standards and regulations for each transect subtype to complete the FBC
- Evaluating the FBC and comparing it with existing design controls and regulations

5 CONCLUSION

The research aims to match parametric modeling with Form-Based Code and test it in urban planning and design of high-dense cities. Through using Hong Kong as the study context, this paper concludes that FBC has potential to be adopted in high-dense cities with the support of parametric modeling methods. The possible implementing manners includes combine FBC with local zoning or making FBC as a supplement regulation of existing codes. In further research, more exploration about supporting FBC by parametric modeling tools need to be discussed and evaluated towards the objective of making sustainable and smart cities.

REFERENCES

1. Beirao, J., et al. City Information Modeling: parametric urban models including design support data. ISCTE Lisboa (2012), 1122-1134.

2. Bellevue, KY Form-Based Code. http://formbasedcodes.org/codes/bellevue-ky-form-based-code. As of 15 May 2016.
3. Ben-Joseph, E. and M. J. Kiefer. *The code of the city: standards and the hidden language of place Making*. MIT Press, Cambridge, Massachusetts, USA, 2005.
4. Bum Kim, J., et al. Parametric Form-Based Codes: Incorporation of Land-use Regulations into Building Information Models. *Proc. ACADIA* (2011), 217-223.
5. CNU, Congress for the New Urbanism. What is New Urbanism? http://www.cnu.org/resources/what-new-urbanism. As of 15 Jan 2016.
6. Duany Plater-Zyberk & Company. SmartCode Version 9.2. http://www.growsmarti.org/training/SmartCode%20Version%209.2.pdf. As of 15 Jan 2016.
7. East Billings Urban Renewal District Code. http://formbasedcodes.org/contenct/uploads/2014/06/EBURD-CODE21.pdf. As of 1 May 2016.
8. Form-Based Code definition. http://formbasedcodes.org/definition. As of 22 Nov 2015.
9. Gil, J., et al. Assessing computational tools for urban design: towards a City Information Model. *Proc. eCAADe* (2010), 316-324.
10. Madden, M. E., et al. Place making with Form-Based Codes. http://www.spikowski.com/documents-Miscellaneous/Madden-Spikowski-Article.pdf. As of 21 Jun 2016.
11. Miami 21 Amended Codes. http://www.miami21.org/PDFs/May2015-VolumeI.pdf. As of 12 Dec 2015.
12. Parolek, D. G., et al. *Form-Based Codes: a Guide for Planners, Urban Designers, Municipalities, and Developers*. John Wiley & Sons, Hoboken, New Jersey, 2008.
13. Schnabel, M. A. Parametric designing in architecture: A parametric design studio. *Proc. CAADFutures* (2007), Springer: 237-250.
14. Transect of Miami 21 Codes. http://www.miami21.org/PDFs/May2015-VolumeI.pdf. As of 21 Nov 2016.
15. Zhang, Y. and Schnabel, M.A. Form-Based Code (FBC) modeling for urban design of high-dense cities. *Proc. SimAUD* (2016), 147-152.
16. Zhang, Y. and Schnabel, M.A. Mapping volumetric urban space: a critical development analysis of multi-level morphology of high-dense cities. *Proc. ISAIA* (2016), 1785-1790.

Volatile Data Mining: A Proof Of Concept For Performance Evaluation Of The Built Environment Using Drones

Ramon van der Heijden[1], Alan Tai[2] and Gustav Fagerström[3]

[1]Front Asia
Hong Kong, HK
rvanderheijden@frontinc.com

[2]Front, Inc
Brooklyn, New York
atai@frontinc.com

[3]Walter P Moore
New York, New York
gfagerstrom@walterpmoore.com

ABSTRACT

In this paper we propose a proof of concept for an affordable method utilizing Unmanned Aerial Vehicles (UAV) to acquire visual and thermal images of a building envelope using preprogrammed flight paths. We demonstrate how photogrammetry and sensing technology can be used to create three-dimensional digital models and enrich them with non-geometrical properties. Our main research focus is to gather urban data in novel ways, offering a reading of the city that historically has been hard to observe and quantify, while allowing for a fluid design process regardless of scale and maintaining a reliable storage and retrieval functionality for persistent data. Furthermore we aim to contextualize said method within current practices in building enclosure design, engineering and post-occupancy evaluation. The proposed method is generically applicable and scalable, exemplified by a specific case study conducted during a 4 day intensive workshop in the summer of 2014. We describe how this methodology may be deployed to create Building Information Models (BIM) – and, on a larger scale of data gathering, Urban Information Models (UIM) - from simple data. Finally we will introduce means of obtaining metrics and techniques by which geometric and non-geometric data may be combined.

KEYWORDS

Unmanned Aerial Vehicles; Drones; Thermal Sensing; Photogrammetry; Simulation-Based Design Tools and Methods; Building Comfort and Energy Performance; Urban-Scale Modeling; Building Performance Monitoring

ACM CLASSIFICATION KEYWORDS

I.5.4 COMPUTER VISION; I.6.4 MODELING VALIDATION AND ANALYSIS

1 INTRODUCTION

More than ever, contemporary society relies on sets of data to enhance the way we experience, create and interact with our physical surroundings. The augmenting of real world objects with digitally stored and processed information is currently happening on a multitude of levels, from nanobots delivering drugs to cancer cells, to large scale construction projects being realized by millions – billions – of pieces of data embedded within physical matter [3]. The city is a repository for huge amounts of data, which can be retrieved, sorted and visualized with the ultimate aim to analyze and understand – and ideally improve on – the urban condition. The processing of said data is no mean feat. It presents one of the perhaps most daunting tasks of contemporary computing; how to reliably embed, query and retrieve useful information from inside incredibly large and complex datasets? How to mine for meaning in what oftentimes appears to be little more than noise? Adding to this in the context of building practice, and particularly building enclosures, there are several aspects of data acquisition and interpretation which have significant real-world implications and therefore need detailed consideration and precise implementation.

1.1 Scientific context

In recent years, several strands of research applicable to non-destructive forensics and as-built surveys of buildings have seen much progress:

Thermography and infrared remote sensing

Thermal infrared remote sensing has been in use since the early 1970's as part of the NASA Landsat Missions [14] using Landsat 1 to record, among other things, earth surface temperatures. The current state of this technology has been explored by among others Weng [19] who points out that even after a recent upgrade, Landsat 7 has a best expected sensing technology of 50-60 m spatial accuracy.

A common method for earth based point cloud generation thermography is the one described by among others Lagüela et al. [12] in which a Terrestrial Laser Scanner (TLS) is used to obtain data necessary for geometric representation of a building, while a high-resolution handheld thermographic camera is used to create heat map of the visible surfaces of the same building. Using the gbXML format the geometric and semantic data are then combined into a BIM carrying the thermographic readings as metadata associated with geometric entities. The method creates rich sets of both geometric and non-geometric data, however we believe it has some shortcomings. Firstly, continual access to numerous vantage points is crucial not only for a complete study and for positional consistency between the TLS and thermal readings, as they are obtained by two discrete processes, but also due to the fact that a complete thermographic survey of an existing building's performance requires all the seasons of the year during different times of day to be recorded. Moreover the method describes the need for an intermediate

SimAUD 2017 May 22-24 Toronto, Canada

step in which semantic and geometric data are matched visually, in order to be able to generate the needed structure of the gbXML schema.

Structure from Motion and Photogrammetry

Ham et al. have in their research [10] eliminated this visual matching step and propose an integrated method in which a high resolution digital thermal camera provides the images needed for point cloud construction using a Structure from Motion (SfM) algorithm [11], [15], [18] as well as the thermal imagery. The study shows great promise and is well-grounded in the realities of building practice, however it still faces the same aforementioned challenge of physical access, as well as yielding a final data format of a meta-data enriched point cloud which in our opinion can be suboptimal in building practice for purely practical reasons.

Thermal analysis and moisture management

On the side of the current discourse which is less concerned with the generation of geometry, and instead focuses on in depth scientific evaluation of thermal performance, studies by Fokaides and Kalogirou [6] and Albatici and Tonelli [1] have suggested methods of deriving building envelope U-values (a measure of thermal insulation) directly from thermography, however this requires access to both indoor and outdoor measurements, whereas Boué and Holé [2] have shown theoretically and in a controlled lab environment that thermal conductivity and diffusivity can be determined by single-sided thermography, however one premise for their method is that some knowledge exists of the temperature on the non-accessible side.

UAV and sensing technology

Fraguada et al. [7] as well as Girot et al [8] have recently suggested the usefulness of UAV technology for spatial and non-spatial data retrieval, processing and storage in the context on a landscape or a larger urban scale. The work exhibits a strong notion of synergies between analog versus digital data acquisition and processing, something which also holds a central position in the work of Burry et al. [4] and Muehlbauer et al. [13], both operating in the context and scale of building skins and discrete building components.

2 PROBLEM STATEMENT

2.1 Building Enclosures

As energy codes become more stringent and prescriptive in response to policy change, which in its turn is a reflection of an increased public and political awareness of a rapidly transforming climate and of associated issues of global energy consumption and resource management, the building sector stands out on the global scene with an estimated 24% of global energy consumption and up to 40% in the developed world [16]. Ever more complex technical systems are devised and implemented in response to more stringent demanding energy performance criteria, paired with a seemingly insatiable demand for “signature” architectural design concepts.

2.2 Potential risks

For the aforementioned reasons building enclosure systems are increasingly becoming more bespoke and technically challenging while at the same time needing to exhibit better energy performance. Shortcomings of the building envelope are thus steadily becoming more common, exhibiting performance deficiencies or even failure. A common source for this is the presence of a breach in the thermal seal or the air-vapor barrier. Sometimes the effects are hardly noticeable and may only result in decreased energy performance of the building. However, oftentimes such failure can result in water infiltration and/or condensation, which - depending on climate, season and the makeup of adjacent building systems - may result in anything from toxic mold and harmful emissions from deteriorating building materials to the formation of icicles or even compromise of structural capacity due to freeze-thaw cycles or corrosion of ferrous elements, which both over time cause cracking of masonry and concrete components. Depending on the nature of the building, such manifestations of the laws of physics could be detrimental to the success of the construction project and could lead to claims that well exceed the original construction cost.

2.3 Diagnostic methods

The current approach in the industry is to conduct a forensic investigation by an independent party. A common tool for such investigations is the acquisition of thermal infrared images of the exterior of a building, while intensifying the conditions under which the respective symptoms would presumably be manifested. These conditions could be increasing the interior building pressure and/or relative humidity. These investigations will have to be repeated during different times of day and different times of year. During each investigation, all images will have to be taken from the same locations as preceding runs. The images will have to be analyzed based on the thermal radiation properties of the material as well as the exact buildup of the structure in each area of interest.

The study described below aims to address these points from a building enclosure design and engineering standpoint with a focus on energy performance evaluation and early problem detection. Drawing on the current state of relevant technology developments, the study has three specific aims:

2.4 Data retrieval

The identification and retrieval of crucial real world design data using UAV’s (Unmanned Aerial Vehicles), colloquially referred to as drones. These offer a novel and affordable way to gather data from an urban setting [7], [8]. With a combination of light weight Arduino technology based sensors for thermal radiation, movement, temperature, humidity, airflow and more, it is possible to get a customized real-time feed of real world data streamed right to a regular laptop.

2.5 Geometry

The creation of design geometry and enhancement of it with the design data, using the Elefront plugin. Written as a plugin for McNeel's Rhinoceros and Grasshopper software, this add-on's main purpose is to augment 3D geometry with user defined information. Elefront tools enable a user to read, filter, query and manipulate the 3D model as if it was a database. Rather than storing geometry in a database, Elefront stores data in a geometry base. The open nature of Grasshopper allows for easy formatting of incoming and outgoing data, such that virtually any source of data can be used. Similarly, the output can take shape in a vast array of possibilities. Drawings, schedules and tables are but a few examples of the possible products of a data enhanced model.

2.6 Visualization

The development of a data visualization protocol to capture and describe the results graphically and make them integral to a larger digital modeling context and process.

3 EXECUTION

3.1 Preparation and equipment

Hardware

Prior to the practical experiments being carried out, hardware and software solutions were identified to suit the project needs. Following some trial and error and setting of a budget, the following hardware list was assembled containing off-the-shelf as well as custom built items:

- DJI Phantom 2 drone ("UAV" in paper, u.o.n.)
- 4x16 thermal IR array: MLX90620ESF-BAB-000-TU
- ArduPilot Mega 2.6 ("APM" in paper, u.o.n.) Arduino based microcontroller
- GoPro camera with Gyro-stabilized Gimbal: DJI H3-2D
- 3DR radio signal transmitter
- Single pixel small cone thermal IR sensor: MLX90614ESF-DCIXXX
- GPS + Digital compass

Software and setup

On the transmitting end, the APM 2.5 Arduino based micro controller board loaded with ArduCopter code, was mounted onto the UAV. GPS, compass, sensors and radio signal transmitter were connected to the APM, which sends data through the radio transmitter back to a laptop on the ground using the MAVLINK Micro Air Vehicle Communication Protocol. On the receiving end, our laptop would receive the radio signals through the USB radio receiver and the data would be picked up by the Mission Planner open source software. Mission Planner decodes the MAVLINK message and provides a GUI to visualize all the data received from the APM. We modified the code of Mission Planner so that it also sends data to a Grasshopper Plugin using WCF (Windows Communication Foundation). In this way our Grasshopper plugin would receive a constant stream of data and update the model accordingly. The received information

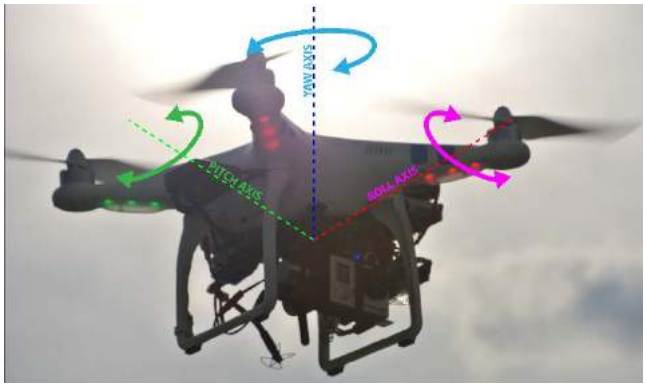

Figure 1. Degrees of freedom during flight.

includes GPS data, altitude (from a combined APM barometric sensor and GPS readings), orientation (APM gyro sensor) and thermal data from the optical sensors. The digital compass would determine the absolute heading, whereas the gyro is part of the IMU (Inertial Measurement Unit) which deals primarily with relative movements.

GPS data would be interpreted as X and Y coordinates using Mercator projection, while the altitude would give the Z coordinate. Gyro and compass data was used to orient the model in space and determine the direction that the sensor is pointing to – the gyro output data is governed by the degrees of freedom for an airplane in flight (Figure 1). This would

Figure 2, 3. UAV carrying gyro-stabilized GoPro and sensors, APM and GPS.

enable the recreation of the viewing cone geometry – or viewing pyramid in the case of our 64 pixel sensor - in CAD space, which would ultimately serve the purpose of collocating the thermal data onto the relevant part of the building mesh generated via photogrammetry by a Structure from Motion (SfM) algorithm (see further *Data collection Readings* and *Geometry* sections).

Figure 4. Photo survey using GoPro.

Figure 6. Mesh models of surveyed urban context created with SfM.

3.2 Case Study

A focused effort was made from the start to keep to lightweight hardware components, so as to be able to have the UAV carry the full payload of all the measuring equipment simultaneously (Figure 2, 3). In addition, all three pieces of optical equipment – GoPro and both thermal sensors – were mounted together so as to be gyro-stabilized. The flight path best suited to photomapping – long sweeping motions, 360 degree views and capturing both sides of a corner, for instance - might not be ideal for the thermal scan in which a more orthogonal front view of a façade is the most efficient method. For this reason it would be necessary to embark on two quite distinctly pre-programmed different flight paths to collect all the data needed

Data Collection

The fully loaded UAV would set out giving a one snap every two seconds photographic documentation of its flight path (stored in the memory card in the camera) as well as a live feed of GPS coordinates. Additionally vector data reporting on compass bearing, the degrees of freedom of the gyroscope (Figure 1) and altitude would be streamed in real time to our laptop's USB radio receiver. During the first part of the flight (Figure 4) the location data would be redundant, as the SfM algorithm used to construct mesh geometry from photos uses only graphic data for point cloud construction and texture mapping. During the flight's second part, the UAV would have to be maneuvered differently; while the photo session needs long sweeping movements and with pictures snapped as close to 360° around the study object as possible, scanning wants a much more orthogonal and systematic coverage of, say, a building's facade. Both of these distinct flight techniques and modes of data collection are equally integral to the ultimate creation of a complete and useful digital information repository, containing geometry as well as abstract data (Figure 5).

4 RESULTS

4.1 Data collection and processing

Geometry

At the end of the first set of flights, two sets of data had been created – an aerial photography survey of the study area and a dataset containing XYZ location coordinates together with orientation vectors for each thermal reading.

The 248 photos were loaded into Autodesk's ReCap, which implements an SfM algorithm running as a cloud-based service (Figure 6) which produced mesh models of the surveyed urban context. Creating a 3d model that is augmented with data is a multi-step process. As described by Van Der Heijden et al. [17] we implemented a method whereby a distributed network of data sources is connected by algorithmically defined relationships (Figure 5). Each Grasshopper node in the graph performs a specific task. The

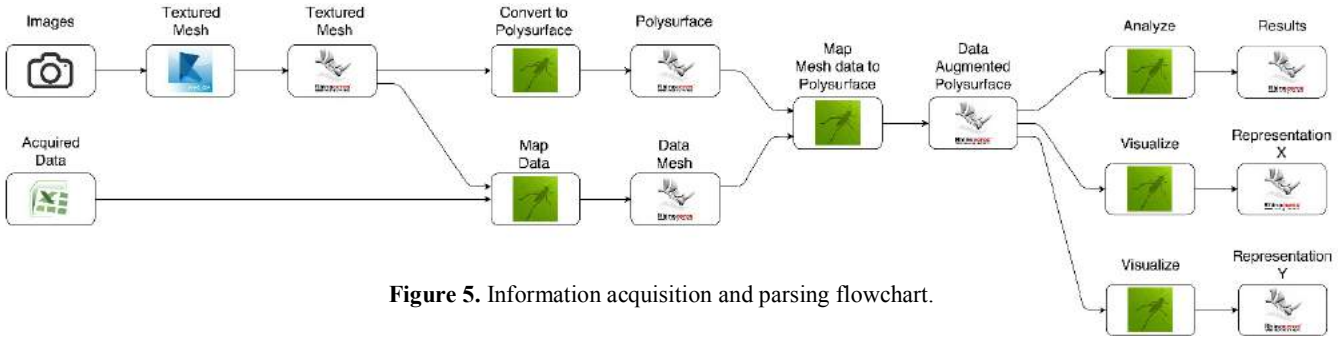

Figure 5. Information acquisition and parsing flowchart.

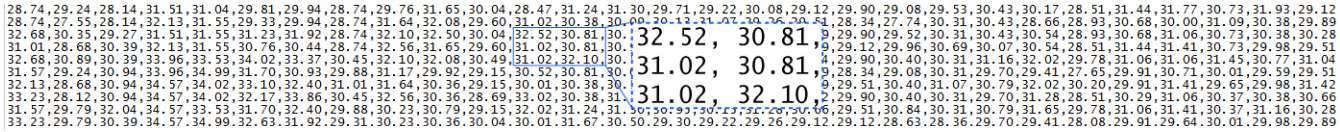

Figure 7. Raw temperature output. Each number corresponds to one pixel's reading (C°).

output is typically another Rhino model which can then in turn be used as input for the next Grasshopper node.

Readings

Thermal building data collected during the second part of the flight was reported as degrees centigrade in a 64 entries per row text file (Figure 7). Through the parsing of GPS, compass and gyro data into XYZ, it was possible to correlate the UAV's position in world space with its readings in CAD space, thus aligning the digital drone with the physical one. In this way we were able to take the CAD mesh building envelope created with SfM, and map back onto it the thermal readings (Figure 8). Thermal readings [C°] were mapped to the CAD mesh faces according to the correspondence between GPS and CAD coordinates, using Elefront. Following this a more granular model can be created, and the constituent parts of the envelope modeled and their material makeup deduced from the mesh thermal values. Finally the readings are stored directly on the geometry in as large a quantity as desired (for instance not only the average surface temperature from this particular study could be stored, but the same preprogrammed flight paths could be repeated throughout the year and the day and the corresponding data stored on one and the same discrete geometry object. The process for imbuing the geometry with the semantic data has been described in detail by Van Der Heijden et al. [17] as well as by Fagerström et al [5] and is based on a dictionary logic in which key-value pairs are attached directly to the geometric entities. A normalized RGB color scale was defined such that the lowest recorded façade surface temperature (around 26°C) would correspond to a 0-0-255 (RGB Blue) while the highest recorded surface temperature of close to 60°C would correspond to 255-0-0 (RGB Red).

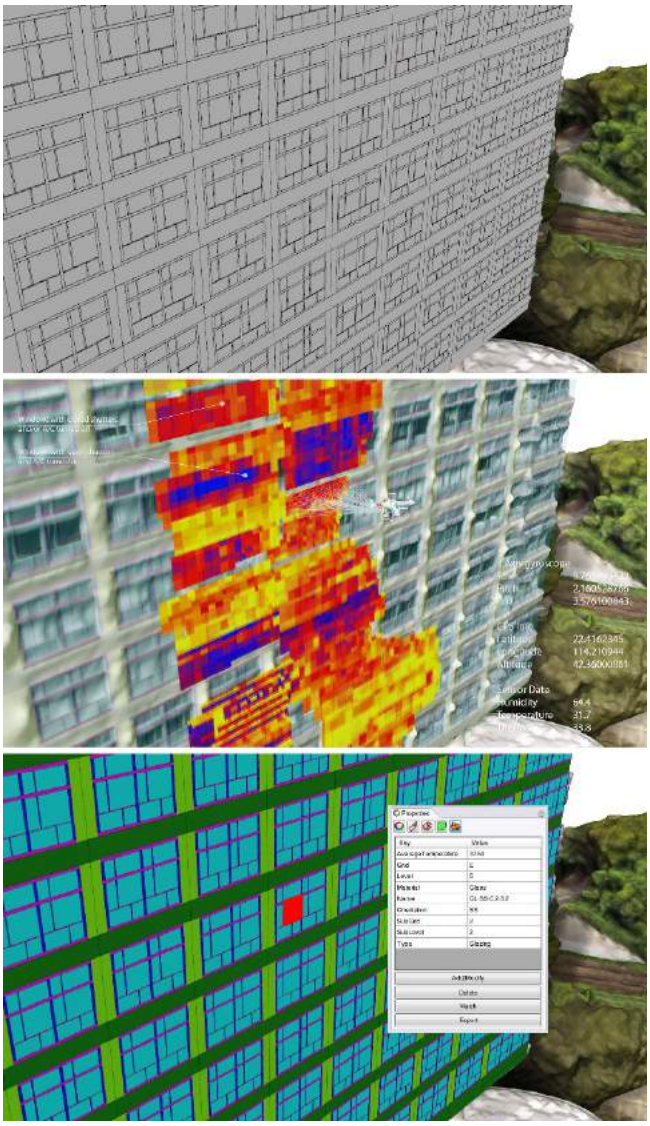

Figure 8.

- Top: Creation of polysurface model elements based on textured mesh.
- Center: Remapping thermal scan data onto mesh geometry.
- Bottom: Mapped temperatures are used to deduce discrete building materials/assemblies and stored within them.

Bearing in mind the case study was performed in south east Asia at the height of summer on a southwest facing curtain wall facade, this scale would need recalibrating for future studies, so as to give an absolute - and comparable between studies - relationship between temperature and color.

This notwithstanding, the readings paint an accurate picture of relative surface temperature differences between for instance an insulated spandrel and a single pane window with or without the air conditioning running.

5 CONCLUSION

Especially in the development of high end residential buildings, or buildings in need of highly controlled environments harboring valuable and delicate items such as art, the potential ramifications of failure of building systems and subsequent remedial and legal proceedings can be quite significant. Therefore, it is essential that any destructive manifestations of compromised performance of the building enclosure be prevented, ideally, or else promptly and conclusively mitigated.

Discovering a problem with the performance of a building façade typically means that parts of the façade need to be dismounted and potentially partially destroyed. This could be

a very costly endeavor and It is therefore of great importance that any suspicions of malfunction be conclusively investigated. Some areas of interest may turn out to be a hidden air exhaust, or some piping that simply runs behind a rain screen. In order to accurately interpret the acquired thermal infrared data, it is of great importance that the data of all consecutive runs is easily comparable against the actual building location and envelope buildup.

Currently this form of forensic investigation involves a labor intensive process of repeated manual image taking from locations that are inherently difficult to access. These images need to be catalogued and manually compared against construction drawings or building models. This is a very costly process and for that reason, it is not conducted on many project which would tremendously benefit from it.

Tying back to the initial problem statement, as professionals active in the building industry and with particular attention to building enclosures, we see this technology inserting itself in three main areas of our practice:

5.1 Adaptive reuse

When the function of an existing building is changed (e.g. industrial to commercial or residential), a series of performance criteria come into play for the adapted building and its envelope, which previously would not have been within its purview. Examples hereof include daylighting, energy performance and access and maintenance, all of which require a detailed understanding of the existing envelope's properties and characteristics.

5.2 Diagnostics and problem mitigation

Any stakeholder in a building project has a high degree of vested interest in the correct execution and performance of building systems. The building envelope can account for as much as 25% of total construction costs – for it to not perform according to expectation is needless to say a potentially disastrous event for design parties, client and contractor alike. Aside from any warranties usually in force post-occupancy, making stakeholders liable to varying degrees for the incorrect functioning of installed systems, there is the equally important aspect of reputation and future relationships between clients, contractor and design parties.

5.3 As-built survey

Even before any problems arise, a post-occupancy evaluation is of great value in order to ascertain workmanship quality and any possible errors in the design itself [9]. It is common practice in building envelope engineering to commission a Performance Mock-Up (PMU) prior to new construction which serves to validate design assumptions and construction means and methods, by way of a series of rigorously performed and recorded tests of waterproofing, air tightness and insulating ability. The method proposed here below effectively becomes a full scale PMU in which, rather than using a mockup, the actual envelope is physically evaluated. This can be particularly efficient in such an event where the design model/s used for energy modeling and final construction documentation are available and can be used as baseline for comparison with the real-world post-occupancy data. Already today, some construction projects make use of physical performance evaluation of the actual built artifact, something which could be complemented by the proposed method. As pointed out by Ham et al. [10], the "assumptions typically made during the modeling stage, once buildings are operating, the actual energy performance deviates from the baseline models." In other words, even when buildings are not exhibiting issues that could be characterized as downright failure in design or execution, the truest measure of their energy performance might still be obtained from a physical post-occupancy survey.

6 FUTURE WORKS

Several recent technological developments have come together to make this type of study possible within the limited time frame and budget given. In no particular order these are Arduino controllers, optical sensors, high resolution digital photography and radio controlled UAV technology. The digital revolution is already well underway both in terms of ubiquity and general equipment cost on many fronts relevant to this research. This notwithstanding, until quite recently a large part of the necessary equipment for the present study was not available at non-professional level prices. This marks an interesting milestone, we believe, as we can now realistically undertake a surprisingly accurate building survey like in the present case study at an upfront cost entirely within consumer reach. In terms of geometrical data acquisition the ability to accurately reconstruct digital meshes from photographs has seen significant progress in recent years. Much of this is thanks to improvements in pure computing power, something the study benefited significantly from taking advantage of cloud computing to turn around a large model in a short time. When it comes to the acquisition and remapping of non-geometrical onto geometrical data, as is often the case when dealing with real world assets, there are considerations to be made between speed and accuracy. Our 64-pixel sensor proved, in spite of its relatively limited optical quality, to be capable of registering data for a larger area at both acceptable accuracy and speed.

At the end of this study, we believe it to hold substantial value as proof of concept for a vast array of applications, from building forensics for restoration purposes through energy monitoring to urban planning. Going in to the study we were aware of the limitations imposed by our equipment; for this reason it is our conclusion that – regardless of measurement precision – the targets were met of obtaining geometric and non-geometric data from a UAV equipped with navigation and sensing technology. This being said, our results make quite clear the limitations imposed by the accuracy of location devices used, something that here was driven by financial constraints. This applies most of all to the GPS and the compass, the readings of which can be thrown off by a number of factors, such as proximity to the building which partially blocks satellite signals, or electromagnetic

interferences coming from all the devices present in contemporary society. Traditional GPS technology can today be used in conjunction with Real Time Kinematics (RTK) satellite navigation technique. Based on measuring the carrier wave's phase it provides positional accuracy down to 100 mm. While a significant improvement in accuracy to traditional GPS technology, RTK is no more impervious to blocked signals than any GPS. For this reason an even more promising technological upgrade to the proposed method would be optical positioning. We can speculate with some certainty that this, together with better exploiting the existing abilities of SfM algorithms to record and store positional and orientational information would improve our method. In doing so, we could eliminate the small but yet existent component of manual fine tuning of position and orientation presently required by the proposed method in order to match geometry and metadata.

Furthermore, as following step we plan to extend the research scope to a wider variety of measured and remapped data, such as wind speed, humidity and lighting conditions. In summary, we believe this study to suggest financially attainable methods to cut down on highly labor intensive – as well as potentially hazardous - activities such as building inspections, translating survey data into 3D-models or obtaining, interpreting and storing building performance metrics.

ACKNOWLEDGEMENTS

The authors would like to extend their thanks to the following people and organizations: SmartGeometry Group. Front, Inc. Chinese University of Hong Kong. Jason Carlow, Christian Lange, Marco Juliani, Megan Ng, Oliver Thomas, Piotr Baszynski, & Luca Maccarinelli, Binsun Hu, Amos Chan, Vincent Ip, Albert Lo, Riyad Joucka, Mariane de Souza, Alison Li, Xinliu Huang. Ian Keough and Autodesk. Katherine Chan, Erik Verboon & Anton Nelson.

REFERENCES

1. Albatici, R. and Tonelli, A.M. Infrared thermovision technique for the assessment of thermal transmittance value of opaque building elements on site, *Energy and Buildings 42*, (2010), Elsevier B.V., Amsterdam, 2177–2183
2. Boué, C. and Holé, S. Infrared thermography protocol for simple measurements of thermal diffusivity and conductivity, *Infrared Physics & Technology 55*, (2012), Elsevier B.V., Amsterdam, 376–379
3. Brynjolfsson, E. and McAfee, A. *The Second Machine Age: Work, Progress, and Prosperity in a Time of Brilliant Technologies*; W. W. Norton & Company, New York, USA, 2014
4. Burry, J., Salim, F., Williams, M., Anton Nielsen, S., Pena de Leon, A., Sharaidin, K., and Burry, M. Understanding heat transfer performance for designing better facades. *Proc. ACADIA 13*, 71-78
5. Fagerström, G., Hoppermann, M., Almeida, N., Zangerl, M., Rocchetti, S., and Van Berkel, B. Softbim: An Open Ended Building Information Model in Design Practice. *Proc. ACADIA 12*, 37-46
6. Fokaides, P. A. and Kalogirou, S.A. Application of infrared thermography for the determination of the overall heat transfer coefficient (U-Value) in building envelopes, *Applied Energy 88*, (2011), Elsevier B.V., Amsterdam, 4358–4365
7. Fraguada, L., Girot, C. and Melsom, J. Ambient Terrain, in Stouffs, R. and Sariyildiz, S. (eds.), *Proc. eCAADe 13*, 433-438
8. Girot, C., Fraguada, L., and Melsom, J. Synchronous Horizons: Redefining spatial design in landscape architecture through ambient data collection and volumetric manipulation. *Proc. ACADIA 12*, 355-361
9. Golparvar-Fard, M., Peña-Mora, F., and Savarese, S. Application of D4AR- A 4 Dimensional augmented reality model for automating construction progress monitoring data collection, processing and communication, *ITcon 14* (2009) 129–153
10. Ham, Y. and Golparvar-Fard, M. An automated vision-based method for rapid 3D energy performance modeling of existing buildings using thermal and digital imagery, *Advanced Engineering Informatics 27,* (2013), Elsevier B.V., Amsterdam, 395–409
11. Havlena, M., Torii, A., and Pajdla, T. Efficient Structure from Motion by Graph Optimization, *Lecture Notes in Computer Science (LNCS) Volume 6312*, (2010), Springer-Verlag, Berlin, Heidelberg, 100-113
12. Lagüela, S., Díaz-Vilariño, L., Armesto, J., and Arias, P. Non-destructive approach for the generation and thermal characterization of an as-built BIM, *Construction and Building Materials 51*, (2014), Elsevier B.V., Amsterdam, 55–61
13. Muehlbauer, M., Cheng, Nancy Y., Khorasgani, M. L., McCarthy, J. and Burry, J. Air Flow Visualisation Towards the Design of Breathing Skins. *Proc. SimAUD 16*, 51-57.
14. Rao,P.K. Remote sensing of urban heat islands from an environmental satellite. *Bulletin of the American Meteorological Society 53* (1972),647-648
15. Snavely, N, Seitz, S, and Szeliski, R. Modeling the world from internet photocollections, *International Journal of Computer Vision 80* (2008) 189–210
16. U.S. DOE. U.S. DOE Buildings Energy Databook, U.S. Department of Energy, 2010
17. Van Der Heijden, R., Levelle, E., and Riese, M. Parametric Building Information Generation for Design and Construction. *Proc. ACADIA 15*, 417-429

18. Wang, Y.-F. A Comparison Study of Five 3D Modeling Systems Based on the SfM Principles, *Technical Report No. 1*, (2011), Visualsize Inc., Goleta, USA, 1–30

19. Weng, Q. Thermal infrared remote sensing for urban climate and environmental studies: Methods, applications, and trends, *ISPRS Journal of Photogrammetry and Remote Sensing Volume 64*(4), (2009), Elsevier B.V., Amsterdam, 335-344

A Case Study on the Relationship between Urban Morphology and Traffic Noise Distribution in High-density Urban Context

Ji Zhang[1], Stephen Siu Yu Lau[2], Chye Kiang Heng[2], Siu-Kit Lau[2] and Hongzhan Lai[2]

[1]Solar Energy Research Institute of Singapore, National University of Singapore
Singapore
serzhj@nus.edu.sg

[2]Dept. of Architecture, School of Design and Environment, National University of Singapore
Singapore
{akilssy, akihck, akilsk}@nus.edu.sg, e0001389@u.nus.edu

ABSTRACT

Noise pollution is one of the key issues that may have significant impact to the physiological comfort and psychological wellbeing of urban dwellers and to urban environmental quality in general in the planning of liveable city to achieve urban sustainability. Applying validated numerical noise mapping technology, a case study of 30 high-density urban residential neighborhoods in Singapore were conducted utilizing an integrated and automated workflow for simulation, analysis and visualization. The results revealed the significant impacts of several key urban planning and architectural geometric parameters on a variety of performance indicators quantifying the traffic noise levels as simulated for outdoor open spaces and building façade. The research findings highlight the need to develop methods and technology to allow reliable and efficient evaluation of urban aural performance in the early stage of planning and design when building typology and urban morphology play a much decisive role in affecting a variety of environmental qualities.

Author Keywords

Building typology, urban morphology, urban aural environment, noise pollution, noise mapping, simulation-based performance evaluation

1 INTRODUCTION

Urban noise pollution is one of the key factors that may affect the environmental quality of urban space resulted in significant impacts on both the physiological health and psychological wellbeing of urban dwellers. The investigation of noise pollution is certainly more relevant to the Asian context due to the high-density urban planning strategy adopted by most Asian cities. The resultant compact urban morphology, as compared to that of relatively lower density cities, leads to closer spatial proximity for various urban functions and their respective sources of noise. This situation is further aggravated by the intensification of traffic noise due to continuous development of massive infrastructure for transportation and by the competing needs for better daylight accessibility, natural ventilation, and unobstructed view etc. in urban planning and architectural design. This poses a great challenge for the planning and design of a built environment of optimized and balanced environmental quality.

Various solutions, such as noise barriers and sound deflectors, have been implemented in many Asian cities to mitigate urban noise pollution. However, most of them are costly afterthought measures and are not integrated with design of buildings and planning of urban infrastructures. Urban planners and architects need to make informed decision to optimize their designs and take proactive interventions to minimize potential negative impacts of noise pollution within a given context. There is also the research need to develop methods and technology to allow reliable and efficient evaluation of urban aural performance in the early stage of planning and design when building typology and urban morphology play a much decisive role in affecting a variety of environmental qualities.

This study examines the relationship between building typology, urban morphology and urban acoustic environment through numerical simulation for selected urban residential neighborhoods so as to identify the key planning and design factors that may have significant impact on traffic noise exposure level and distribution in high-density urban context.

2 METHOD

2.1 Validation of Simulation-based Noise Mapping

Various methods have been developed in different countries to predict road traffic noise level which is one of the major sources of environmental noise, among which the CRTN method [5] has been adopted in many countries and regions, such as Hong Kong and Singapore. The CRTN method takes traffic flow, traffic speed and percentage of heavy vehicles as the primary inputs for estimation of basic traffic noise level beside the road. A series of corrections are applied depending on several factors such as the spatial position of measurement point relative to road, ground cover materials, obstruction screening, façade effect, angle of view etc. Considering that the CRTN method was developed based on data collected decades ago when the traffic conditions and

vehicle compositions were different, validation is needed when applying it in a different context in nowadays.

A three-phase validation study [6] was conducted for four different types of roads in locations along the road and in front of building façade to verify the accuracy of the CRTN method in predicting traffic noise level in the context of Singapore's urban built environment. The descriptors of the measured noise exposure levels are L10 (1-hour) and L10 (18-huor), which denote the sound pressure level exceeded for 10% of the measurement period of 1 hour and 18 hours (06:00 to 24:00), respectively. They were compared with the ones manually calculated following the procedures specified in CRTN and the ones simulated in the noise mapping software CadnaA [4] with CRTN implemented and with the measured traffic data as input.

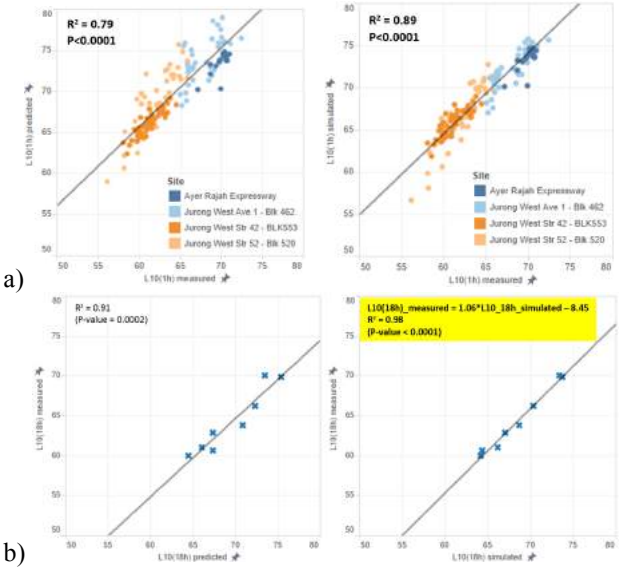

Figure 1. a) Correlation between measured, predicted and simulated L10 (1-hour), b) correlation between measured, predicted and simulated L10 (18-hour).

The results as shown in Figure 1 indicate that CRTN method tends to overestimate noise level as compared to measurement in the context of this study. This is probably related to its source model which was developed based on regression analysis of data collected almost three decades ago. Considering the contemporary traffic condition and composition which might be different from that in Briton when CRTN was established, the progress in noise reducing technology for motorized vehicles and road surfaces, and the high-density physical environment in Singapore, adjustment of the results derived from CRTN method is needed. The regression equation describing the significant relationship between the measured and simulated L10 (18-hour) values (R^2=0.98, p<0.0001) was used to adjust the simulated result obtained from CadnaA to one that is closer to measurement. The range of deviation of simulated results as against the measurement decreased from 3.4 to 5.4 dBA to -1.5 to 0.6 dBA after applying the adjustment.

2.2 Case Study

A case study approach was adopted for the simulation-based investigation of the relationship between urban planning and traffic noise distribution with the scope of study defined as an area of 500m by 500m, which represents the spatial dimension of a typical residential neighborhood surrounded by external roads (Figure 2).

In total, 30 study areas were selected from different neighborhoods in Singapore's HDB1 public housing new towns (Figure 3). The criteria of case selection include homogeneity of building typology, representativeness in public housing planning era, built density no less than 2.0 and site coverage larger than 20%, surrounded by typical urban or neighborhood roads, not been affected by major source of noise other than traffic, etc.

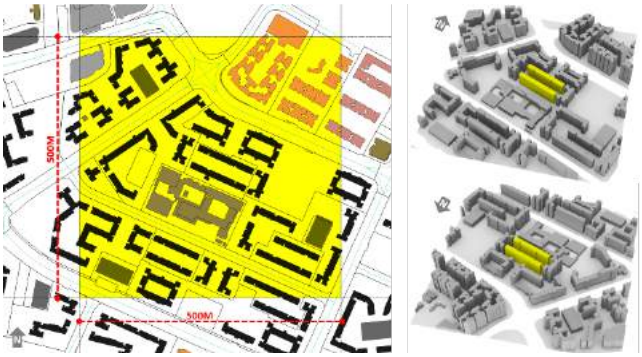

Figure 2. Spatial dimension of the case study area.

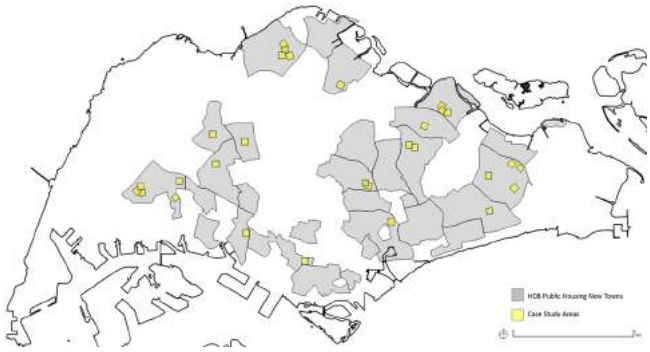

Figure 3. Locations of the 30 public housing neighborhoods selected for the case study

2.3 Planning and Design Parameters and Noise Performance Indicators

A series of parameters that characterize different morphological properties of urban planning and geometric attributes of building typologies were specified for the quantitative analysis.

[1] HDB represents the Housing Development Board, which is the lead government agency supervising the planning, construction and management of the public housing estates in Singapore that accommodates more than 80% of its population including citizens and permanent residents.

The planning parameters include Floor Area Ratio (FAR), the ratio of total usable floor areas to site area that quantifies built density, and the percentage of the study area or buildable area excluding roads within the study area that is covered by buildings, roads, open spaces and hard pavement surfaces that may reflect sounds, respectively. The building geometric parameters include compacity which is the ratio of envelope surface areas to building volumes that quantifies the compactness of urban geometry [1], area-to-perimeter ratio (APR) which is an indicator of building depth [3], and Open Space Ratio (OSR) which indicates the open space shared for unit floor area [2].

Performance indicators to quantify traffic noise exposure levels on both the ground outdoor spaces and building facades were also specified that include the percentage of overexposed areas, the min, max and average levels, the noise levels for 10%, 50% and 90% percentiles of the surfaces. An additional performance indicator was proposed to quantify the potential impact of the noise exposure level as experienced in front of building façade to indoor space: façade noise exposure level per unit floor area, which is calculated as the total façade noise levels divided by total usable floor areas.

2.4 Integrated Workflow for Simulation, Analysis and Visualization

Geometric information such as building footprints, building height, road centre lines and boundaries of reflecting surfaces were imported from Singapore's island-wide GIS database into CadnaA to create the 3D models for simulation.

The horizontal simulation grid was specified as 2x2m at 2-meter height representing traffic noise level potential experienced by pedestrians in outdoor areas. The noise exposure level along building façades was simulated at a distance 1 meter away from façade surfaces with a vertical spacing of 3 meters and horizontal spacing between 0.5 to 3 meters, depending on the length of respective façade (Figure 4). Considering that the existing vegetations are sporadically distributed in the high density residential neighborhoods and their screening effects might be limited due to their porous forms, trees were not modeled and included in the simulation study.

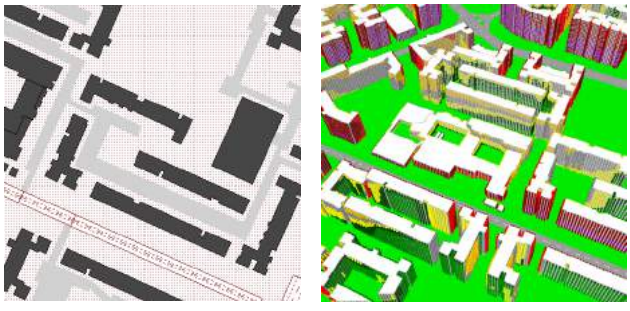

Figure 4. Horizontal and building elevation simulation grids as specified in CadnaA.

Building façades were specified as reflective with a reflection loss of 1 dBA. The ground surfaces were specified as absorbent (G=1) since most of them are covered by lawn or vegetation, except for the surfaces of roads, parking lots and hard pavement which were specified as reflective (G=0). One order of reflection was specified based on comparative study so as to obtain relatively more accurate prediction for areas with no direct and unscreened path to source of noise. With the road centre lines imported, properties of road objects such as width, hourly traffic flows, mean traffic speed and ratio of heavy vehicles were specified based on the measured data obtained from the validation study for the respective types of roads in each case.

A database was created to document the key information derived from the simulation study for each case, such as the key descriptive statistics, histogram and cumulative frequency distribution, and visualization of the noise exposure levels on both building facades and ground surfaces (Figure 5).

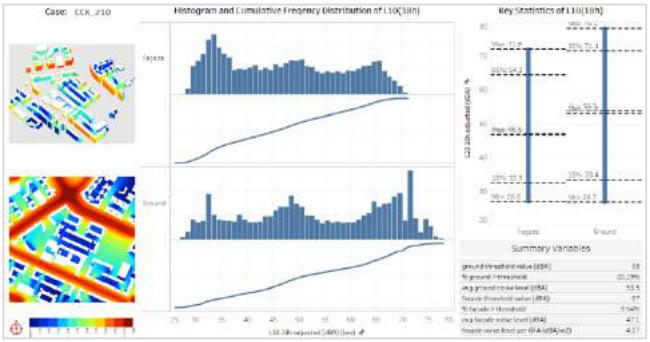

Figure 5. Example of the case study database.

An integrated workflow for simulation, analysis and visualization was created using the Rhinoceros3D software and its parametric modeling and visual programming plugin Grasshopper as the platform (Figure 6). The workflow automatically processes the geometries based on the 3D model created from the GIS data imported and calculates the key planning and geometric parameters for each case. It also calculates the key performance indicators based on the simulation results imported for both building facades and ground open spaces.

3 RESULTS

3.1 Summary of the Cases

Figure 7 shows the visualization of the ground noise exposure level for the 30 cases which indicate that ground areas close to the roads tend to have relatively higher noise levels, whereas the areas within the neighborhood that are shielded by the building blocks tend to have relatively lower noise level.

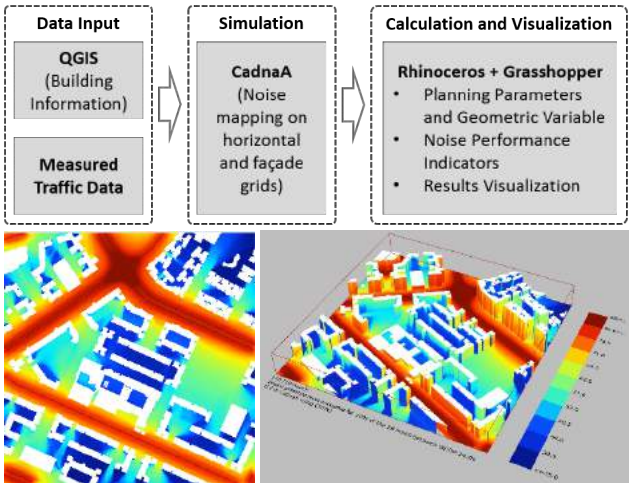

Figure 6. Interface of the integrated workflow for simulation, analysis and visualization of traffic noise levels on ground surfaces and building facades.

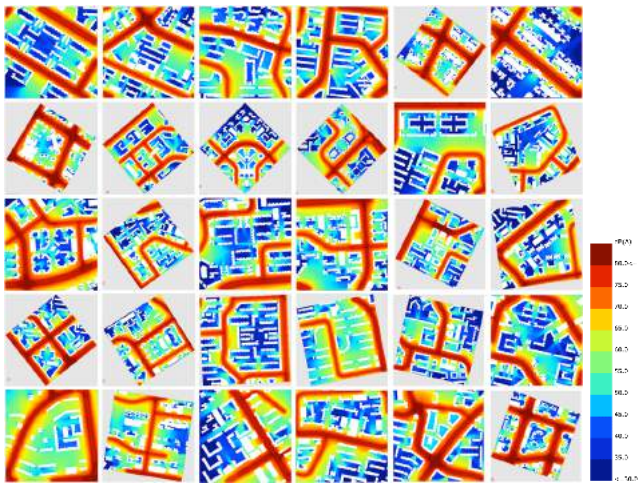

Figure 7. Traffic noise level on ground for the 30 cases.

Table 1 summarizes the key planning and geometric parameters and the performance indicators calculated for the 30 cases. The gross FAR of the cases ranges from 1.65 to 4.59 with an average of 2.81 (Figure 8). Net building coverage ranges from 17.52% to 34.78% with an average of 27.57% that is within the maximum of 40% as specified in planning regulation. This corresponds to a relatively high average open space coverage of more than 60%.

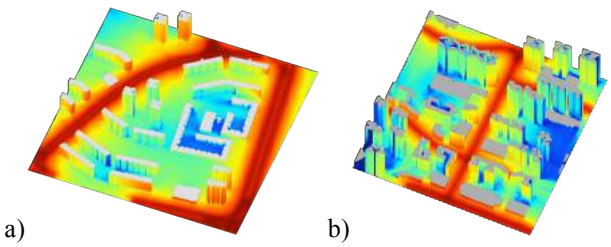

a) b)

Figure 8. The cases with the lowest and highest FAR values: a) Clementi block 356 and b) Dowson block 92.

Table 1. Summary of the key planning parameters and performance indicators.

Key planning and geometric parameters			
	Min	**Max**	**Average**
Net FAR	1.65	4.59	2.81
Gross building coverage (%)	13.67	29.97	22.94
Net building coverage (%)	17.52	34.78	27.57
Gross road coverage (%)	10.81	29.37	16.65
Net road coverage (%)	14.34	38.57	21.57
Gross reflecting surface coverage (%)	21.48	40.19	29.08
Net reflecting surface coverage (%)	29.29	51.56	37.63
Open space coverage (%)	46.78	67.61	60.46
Compacity (m^{-1})	24.41	44.46	32.46
Average area-to-perimeter ratio (m)	2.94	4.84	4.16
Open Space Ratio	0.16	0.51	0.27
Key performance indicators			
	Min	**Max**	**Average**
Ratio of overexposed ground area (%)	12.07	33.18	17.64
Min ground noise level (dBA)	21.4	30.5	25.6
Max ground noise level (dBA)	75.8	84.0	77.6
Average ground noise level (dBA)	49.8	62.4	54.5
10 percentile ground noise level (dBA)	69.0	74.5	71.2
50 percentile (median) ground noise level (dBA)	46.4	66.6	55.8
90 percentile ground noise level (dBA)	28.5	46.6	35.2
Ratio of overexposed facade area (%)	0.05	10.96	3.19
Min facade noise level (dBA)	21.3	30.2	25.7
Max facade noise level (dBA)	67.7	77.8	71.1
Average facade noise level (dBA)	41.8	54.5	47.1
10 percentile facade noise level (dBA)	59.9	67.2	63.6
50 percentile (median) facade level (dBA)	37.8	55.4	46.0
90 percentile facade noise level (dBA)	27.1	43.3	32.6
Facade noise level per unit floor area (dBA/m2)	3.84	7.18	4.85

Averagely speaking, one sixth of the areas within the study zone is covered by roads and close to 30% is covered by reflecting surfaces including roads, car park and hard pavement. The average compacity of 32.46 and the average Open Space Ratio of 0.27 are higher than that for the typical compact urban blocks in the European context reported in a previous study [10], indicating a generally less compact urban morphology with slightly more accessible open space. On the other hand, the average area-to-perimeter ratio of 4.16 indicates a relatively smaller building depth as compared to the European cases.

The average ratio of overexposed ground area is 17.64% regarding the reference threshold value of 68 dBA for L10 (18-hour) [7], which is primarily the spaces corresponding to the road surfaces and the areas immediately adjacent to the roads. The average ground noise level of 54.5 dBA is well below the threshold value. The average ratio of overexposed façade surfaces is only 3.19%, regarding the reference value of 67 dBA [8], which is relatively low, probably due to the large setback of the buildings from road for most of the neighborhoods (Figure 9).

	Noise Exposure Level Performance Indicator	Planning Parameters										Building Geometric Parameters		
		grosss FAR	net FAR	gross building coverage (%)	net building coverage (%)	gross road coverage (%)	net road coverage (%)	open space coverage (%)	gross reflecting surface coverage (%)	net reflecting surface coverage (%)	reflecting surface coverage within site (%)	compacity	avg Area to Perimeter Ratio	Open Space Ratio
Ground Level Performance Indicators for the entire study zone	gross % of ground >= threshold					0.90	0.90	-0.77	0.71	0.76			-0.49	
	net % of ground >= threshold		0.40		0.41	0.88	0.90	-0.82	0.67	0.74		0.37	-0.54	
	min ground level (dBA)					0.64	0.63	-0.49	0.52	0.52				
	max ground level (dBA)					0.38	0.37							
	avg ground level (dBA)			-0.40		0.85	0.82	-0.58	0.72	0.71			-0.40	
	90 percentile ground level (dBA)			-0.61		0.56	0.49		0.62	0.53				
	50 percentile ground level (dBA)					0.87	0.85	-0.67	0.68	0.69			-0.37	
	10 percentile ground level (dBA)					0.74	0.75	-0.66	0.58	0.63			-0.51	
Ground Level Performance Indicators within Site Boundary	% of ground within site >= threshold					0.44	0.47	-0.45	0.37	0.44			-0.41	
	min ground level within site (dBA)					0.64	0.63	-0.49	0.52	0.52				
	max ground level within site (dBA)													
	avg ground level within site (dBA)			-0.50		0.64	0.59		0.58	0.53				
	90 percentile ground level within site (dBA)			-0.65	-0.40	0.46	0.39		0.57	0.47				
	50 percentile ground level within site (dBA)			-0.49		0.57	0.52		0.54	0.48				
	10 percentile ground level within site (dBA)				0.39	0.49	0.53	-0.56		0.37		0.38	-0.50	
Facade Level Performance Indicators	% of façade >= threshold					0.41	0.40		0.38	0.40				
	min façade level (dBA)					0.63	0.62	-0.51	0.46	0.47			-0.39	
	max façade level (dBA)													
	avg façade level (dBA)			-0.63	-0.38	0.49	0.42		0.53	0.43				
	90 percentile façade level (dBA)	-0.44		-0.69	-0.48	0.43			0.56	0.45	0.36			0.51
	50 percentile façade level (dBA)			-0.59	-0.38	0.39			0.42					
	10 percentile façade level (dBA)					0.57	0.56	-0.47	0.45	0.47				
	façade noise exposure level per unit floor area (dBA/m2)	0.57	0.71		0.43	0.53	0.57	-0.60				0.84	-0.91	-0.52

Figure 10. Significant correlation between planning and geometric parameters and the performance indicators.

3.2 Relationship between Planning and Design Parameters and Traffic Noise Distribution Performance Indicators

Figure 10 shows the bivariate correlation analysis between all the planning and geometric parameters and the performance indicators with the Pearson correlation coefficients significant at the 0.05 level highlighted in red for positive correlations and blue for negative correlations.

Generally speaking, building coverage and open space coverage are negatively correlated with a variety of performance indicators, suggesting that higher building coverage and open space provision may lead to lower noise levels on ground and façades. On the other hand, road coverage and reflecting surface coverage are positively related to majority of the performance indicators, which is understandably reasonable as road surface area is directly proportional to traffic flows and more reflecting surfaces may lead to more reflected noise.

The results of linear regression analysis as shown in Figure 11 further confirmed the significant impacts of road coverage, open space coverage, reflecting surface coverage and average ARP on the ratio of overexposed ground area, with the effect of road coverage been the strongest (R^2=0.8, p<0.0001).

The most significant planning parameter affecting the average ground noise level is also road coverage (R^2=0.73), followed by reflecting surface coverage (R^2=0.52), open space coverage (R^2=0.34), building coverage (R^2=0.16), and average APR (R^2=0.16) (Figure 12).

As to average façade noise level, the most significant planning parameter is building coverage (R^2=0.40), followed by reflecting surface coverage (R^2=0.28) and road coverage (R^2=0.24) (Figure 13).

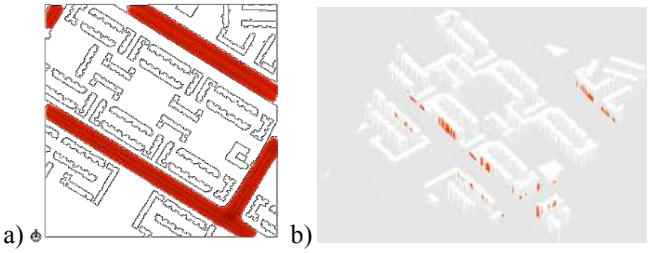

Figure 9. Examples of overexposured areas on ground and building facades as highlighted in red.

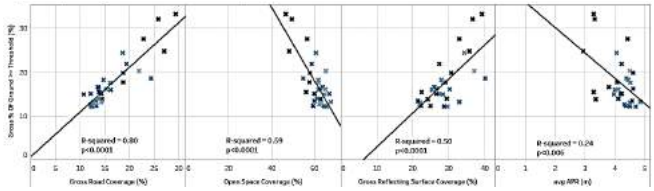

Figure 11. Significant planning and geometric parameters for ratio of overexposed ground area.

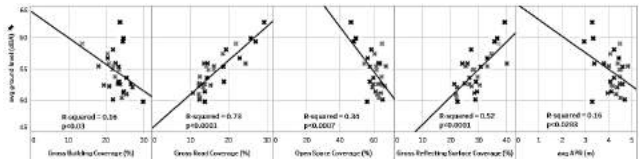

Figure 12. Significant planning and geometric parameters for average ground noise level.

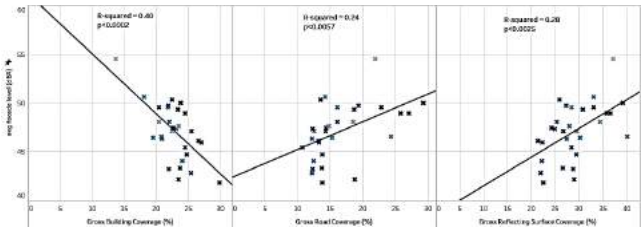

Figure 13. Significant planning parameters for average facade noise level.

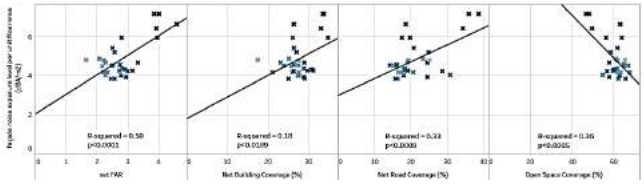

Figure 14. Significant planning parameters for facade noise exposure level per unit floor area.

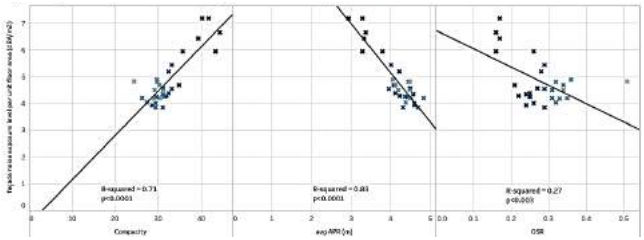

Figure 15. Significant geometric parameters for facade noise exposure level per unit floor area.

Model	R	R Square	Adjusted R Square	Std. Error of the Estimate	Change Statistics				
					R Square Change	F Change	df1	df2	Sig. F Change
1	.953[a]	.909	.899	.30794	.909	86.634	3	26	.000

a. Predictors: (Constant), compacity, grossroadcoverage, OSR

b. Dependent Variable: façadenoiseexposurelevelperunitfloorareadBAm2

Model		Unstandardized Coefficients		Standardized Coefficients	t	Sig.	Correlations			Collinearity Statistics	
		B	Std. Error	Beta			Zero-order	Partial	Part	Tolerance	VIF
1	(Constant)	-5.583	.992		-5.625	.000					
	grossroadcoverage	.066	.012	.339	5.541	.000	.534	.736	.328	.937	1.067
	OSR	6.663	1.354	.509	4.919	.000	-.523	.694	.291	.326	3.066
	compacity	.231	.021	1.178	11.224	.000	.844	.910	.664	.318	3.148

a. Dependent Variable: façadenoiseexposurelevelperunitfloorareadBAm2

Figure 16. Results of multiple regression analysis for the key factors affecting façade noise exposure level per unit floor area.

The performance indicator, façade noise exposure level per unit floor area, provides a measure of the potential impact of building elevation noise level on indoor usable spaces that is unable to be captured by the average façade noise level. As shown in Figure 14. net FAR is the most significant planning parameter for this performance indicator (R^2=0.5), followed by open space coverage (R^2=0.36), road coverage (R^2=0.33) and building coverage (R^2=0.18).

The three geometric parameters also have significant effects on façade noise level per unit floor area as shown in Figure 15, with average area-to-perimeter ratio been the strongest factor (R^2=0.83), followed by compacity (R^2=0.71) and Open Space Ratio (R^2=0.27).

The results of multiple regression analysis as shown in Figure 16 above indicate that gross road coverage, Open Space Ratio and compacity together can account for close to 90% (adjusted R^2=0.899) of the variation in the potential impact of façade noise exposure level to indoor usable floor spaces.

4 DISCUSSION AND CONCLUSIONS

The findings suggest that the overexposed ground surfaces are primarily those covered by roads and those immediately surrounding them. Due to the relatively large building setback (10 to 28 meters), most of the ground areas within the boundaries of the neighborhoods are below the threshold values of 68 dBA. The ratio of overexposed façade surfaces is relatively low, and those areas with a noise exposure level larger than 67 dBA are primarily the facades directly facing the roads.

The results indicate that many planning and geometric parameters examined in this study have significant effects on a variety of noise exposure performance indicators investigated, though to various extents. Reducing road coverage is one of the major factors to reduce the ratio of overexposed areas on both ground and facades in that it is the primary approach to reduce the intensity of traffic noise from its source. However, in urban planning, density and type of roads are usually determined before urban development and they are less easy to adjust. On the other hand, reflecting surface coverage as a positive factor and open space ratio as a negative factor suggest that increase the ratio of open spaces and reduce the area of the surfaces that may reflect noise or replacing them with material such as porous bricks that can absorb noise can effectively reduce the noise level on ground.

The impacts of the planning parameters such as building coverage, road coverage and reflecting surface coverage on façade noise level are relatively lesser. However, built density was found to be positively related to façade noise level per unit floor area, suggesting that increasing built density may potentially lead to more façade noise penetrating into indoor spaces. The building geometric parameters strongly and significantly related to floor area normalized façade noise level suggest that compact building typology with relatively deeper floor plan may lead to lower façade noise level for unit floor area.

These findings echo some of the previous studies investigating the relationship between urban morphology and traffic noise distribution [9]. They provide planners and designers suggestions on potential planning and design factors to adjust so as to mitigate the negative impact of traffic noise on both ground and building façades, especially in the early planning stage when architectural details are not fully developed and building typology and spatial configuration of building clusters matter to a greater extent.

ACKNOWLEDGMENTS

This study is the outcome of the research project "Urban Noise: Performance and Simulation for Urban Typology and Morphology Analysis" (WBS: R-294-000-056-112) which is funded by the Tier 1 Academic Research Fund. The authors

would like to thank the Department of Architecture, School of Design and Environment, National University of Singapore for the funding support for this project.

REFERENCES

1. Adolphe, L. (2001b). A simplified model of urban morphology: application to an analysis of the environmental performance of cities. *Environment and Planning B: Planning and Design 28(2)*, 183–200.
2. Berghauser Pont, M., & Haupt, P. (2004). Spacemate : the spatial logic of urban density. Delft: Delft University Press.
3. Building Performance Research Unit., & Markus, T. A. (1972). Building performance; Building Performance Research Unit, School of Architecture, University of Strathclyde. London: Applied Science Publishers.
4. DataKustik (2016). CadnaA (Computer Aided Noise Abatement). http://www.datakustik.com/en/products/cadnaa/
5. Department of Transport Welsh Office. (1988). Calculation of Road Traffic Noise (CRTN).
6. Lau, S. S. Y., Zhang, J., Lau, S.-K., & Lai, H. (2016). A Comparative Study of Road Traffic Noise based on Measurement, Prediction and Simulation according to the CRTN Method in Singapore. Paper presented at *The 9th Cross-Strait Acoustic Conference*, Macau University of Science and Technology, Macau, China.
7. Mak, C. M., Leung, W. K., & Jiang, G. S. (2010). Measurement and prediction of road traffic noise at different building floor levels in Hong Kong. *Building services engineering research & technology 31(2)*, 131-139.
8. NEA. (2016). General Requirements To Be Complied With At Development Control & Building Plan Stage.
9. Wang, B., & Kang, J. (2011). Effects of urban morphology on the traffic noise distribution through noise mapping: A comparative study between UK and China. *Applied Acoustics 72(8)*, 556-568.
10. Zhang, Ji. (2013) A Study of the Relationship between Urban Form and Environmental Performance for Three Urban Block Typologies in Paris. *Proc. SimAUD 2013*, San Diego, CA, USA.

Multimodal Transportation Performance Certificate (MTPC) for Buildings and Neighborhoods – A Model for Benchmarking the Effect of the Built Environment on the Modal Split in Geographic Information Systems (GIS)

Todor Stojanovski

KTH Royal Institute of Technology
Stockholm, Sweden
todor@kth.se

ABSTRACT

Unsustainable mobility is a major challenge in many cities. To provide information about sustainable transportation, this paper proposes instituting Multimodal Transportation Performance Certificates (MTPC) as assessment method and performance measure for multimodality of buildings and neighborhoods. MTPC measures the Level of Integration (LoI) of the built environment with walking, cycling, public transportation and private car and estimates the modal split in Geographic Information Systems (GIS) based on urban design elements. The benchmarking procedure for MTPC is applied and tested in a suburban neighborhood in Stockholm.

Author Keywords

urban design; element; built environment; indicator; performance; measure; integration; multimodal; transportation; travel;

1 INTRODUCTION

Indicators and performance measures will play a key role in sustainable cities as complex adaptive learning systems [12]. Multimodal Transportation Performance Certificate (MTPC) is proposed as an indicator for buildings and neighborhoods which will provide information about sustainable transportation and multimodality (access to location, integration of different modes with the built environment, competitiveness between transportation modes, energy efficiency and carbon emissions from transportation systems, etc.) to landlords and tenants, urban designers and planners.

Multimodality is defined as ability to travel with a choice of different transportation modes. Modal split is a common measure for multimodality showing percentages of traveled distances or number of trips by different modes of transportation. In transportation planning and forecasting, built environment and land use factors are used to calculate trip generation rates and subsequently modal splits [9, 11, 21]. Many journey planners and web navigation services offer possibilities to see and choose among multiple travel alternatives (by one or many transportation modes). Some journey planners also calculate carbon emissions savings by shifting from private car to public transportation or energy consumption (measured unconventionally in pieces of chocolate) if the traveler decides to walk or bike (see http://www.reittiopas.fi/en/). There are new mobile apps which use location tracking and automatic transportation mode detection to analyze movement of individuals ([14], see http://en.trivector.se/it-systems/travelvu/) and calculate modal split for. Walk Score (http://www.walkscore.com/) is a website that calculates Walk, Bike and Transit Scores for different buildings and cities, based on their proximity to destinations (shops, restaurants, cinemas, etc.). The link between the built environment, factors known as D-variables (Density, Diversity, Design, etc.), and travel is the most researched topic in urban planning [8]. Environmental certification systems for buildings and neighborhoods like LEED (Leadership in Energy and Environmental Design) or BREEAM (Building Research Establishment Environmental Assessment Methodology) include these transportation-related built environment factors in a green building and sustainable neighborhood certification.

To develop MTPC, components of these different methods to assess, measure or visualize multimodality are combined and compiled in the benchmarking procedure applied and tested in a neighborhood in Haninge Municipality, a suburb of Stockholm in Sweden. The following section and subsections describe the study area, methodology and present and discuss the results. The paper closes with conclusion section and directions for further research.

2 ANALYZING MULTIMODALITY IN STOCKHOLM

The neighborhood around Handen Station in Haninge, Stockholm was selected for the multimodality analysis (Figure 1). Haninge, a municipality with roughly 90 000 inhabitants, is a southern suburb of Stockholm, the capital and largest city in Sweden with approximately 2.2 million people living in its metropolitan area. It is a typical suburban neighborhood development project from the 1960-70s with local shopping mall (Haninge Centrum, subsequently upgraded under 1980s) and additional commercial and institutional buildings (library, municipality headquarters, etc.) around commuter rail

station. The suburban neighborhood center is surrounded by residential multifamily apartment buildings.

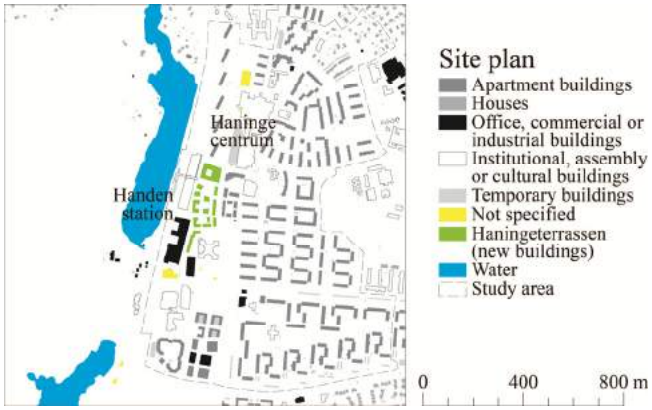

Figure 1. Study area

2.1 Methodology

MTPC shows Levels of Integration (LoIs) of the built environment with different transportation modes (walking, cycling, public transportation or private car) and estimates the modal split based on competition between modes. There are three steps in the analysis/benchmarking procedure: 1) calculation of LoI (for a specific mode) based on built environment factors; 2) assessment of LoI for a particular transportation mode by including competition with the private car or among all modes (modal share); and 3) calculating MTPC for specific mobility groups (Figure 2).

The built environment preconditions mobility, rather than it determines travel. When a neighborhood is developed, certain urban design elements are embedded in the neighborhood (density, mix of uses, parking standards, street widths and speed limits, sidewalks, transit stops, busways or tramways, parking lots and garages, etc.). These design elements support or hinder travel by specific transportation modes. The LoI for walking, cycling, public transportation, private car, etc. is a measure based on few most important factors (urban design elements) on different scales which support these modes. If all crucial factors are fulfilled the LoI is 100%. If all the parking spaces are removed from a neighborhood the LoI with the private car would be 0%. It will be impossible to drive in this neighborhood. If there are parking places the integration is immediately at 100% (congestion on roads can disturbed car traffic, but it will be possible to travel with delays).

LoI (for a specific mode) = Σ weights * built environment factors

Multimodality is characterized by competition among transportation modes on different scales. All modes compete on local scale, whereas only private car and public transportation (sometimes cycling) regionally. The private car is the only mode that competes with every other mode on every scale. It has 100% around the clock accessibility and 100% access to any point network, which makes it perfect benchmarking reference for network transportation systems in undisturbed traffic flow conditions. The formula used for benchmarking of specific transportation modes in respect to the private car as transportation mode with maximum network access is:

LoI (in competition with the private car) = LoI (for a specific mode) / ((LoI (for a specific mode) + LoI (for private car))

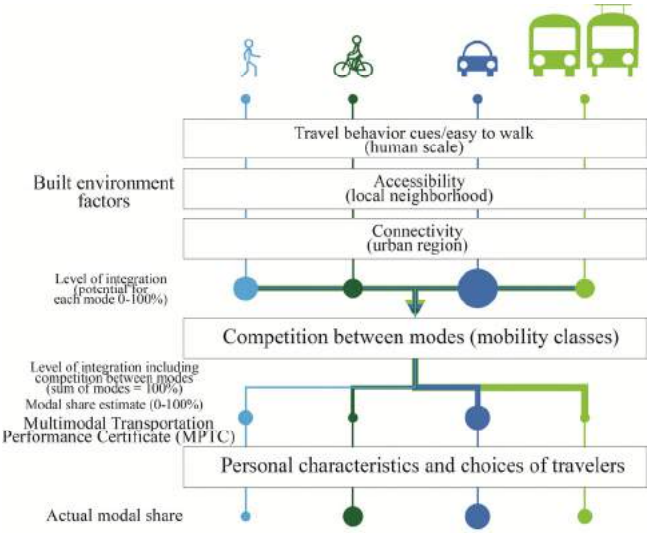

Figure 2. Steps in the MTPC benchmarking procedure

The LoI in the end is analyzed in respect to all the modes:

LoI (in competition with all transportation modes) = LoI (for that transportation mode) / Σ LoIs for all modes

The sum of the LoIs for all transportation modes (competition between modes included) is 100% and it is an estimate of the modal split (based only on built environment factors). The actual modal split is a product of personal characteristics and discrete travel choices of individuals.

MTPC (individual traveler/particular mobility class) = LoI (for a specific mode) * weight (modal preferences)

The LoIs and MTPC are calculated and visualized on map with help of Geographic Information Systems (GIS). The maps and statistics are provided from Lantmateriet (Swedish National Land Survey), municipalities and SCB (Statistics Sweden). GIS are often used in urban analysis, e.g. to visualize and compare sizes of different neighborhoods [19] or assessing urban metrics [20] for measuring Transit-Oriented Development (TOD) and walkability indicators [15, 16], TOD development potential [18], land use-transportation integration [6], etc.

The urban design elements and scales, the weighing of the factors and mobility classes are described in the following three subsections.

Scales of multimodality

The urban life in European cities is mobile and experienced as sequences of spaces (buildings, public or open spaces, neighborhoods, etc.). Buildings are central or peripheral to this mobility sequences, nodes in a local neighborhood or a metropolitan area. To disentangle the complexities between building and neighborhood, local and regional, a theoretical framework of a pattern language [1, 2] is proposed in a mix of urban morphology and environmental psychology. The relevance for MTPC is that the pattern language allows to differentiate between urban design elements on various scales. The human scale is defined by the line of sight. The clear visual acuity of an average person is approximately 100 m. This zone corresponds to the smallest neighborhood defined by neighborly acquaintances and interaction [13, 19], so-called 'social field of vision' [7] or a size of a city block. From a perspective of a human scale, individuals become observers in urban space. Their orientation stems from the immediate knowledge of the environment rather than from maps, or other abstract representations. Different elements become spatial referents for these observers, such as streets, entrances, façades, storefronts, crowds of pedestrians, benches, etc., which in turn requires the use of morphological concepts and elements that understand the city from within (street, setback, street frontage, building façade, sidewalks, building height to street ratio are illustrated on Figure 3, B).

Local scale is defined in terms of home range, an area with destinations (shopping, services, etc.) needed for everyday life [13]. Regional scale implies to a wider zone of commuting, weekend shopping, visiting cultural events, health checks and hospital visits, etc. (roughly the entire metropolitan area). The local and regional scale rely on representations of the city (cartography, mental maps, cartograms, etc.). The design elements (buildings, streets, lots, land use, city blocks, neighborhoods, urban regions) are represented e.g. in GIS by symbols (points, polylines or polygons) and described by attributes (Figure 3, C1). The locations (building, lot, city block, neighborhood) are generalized by characteristics (density, mix of uses, etc. land use factors are attributed to the building too; see Figure 3, C1); and the access to the location can be spatial (C2); network (C3) or topological (C4).

Effect of urban design factors on different transportation modes

The built environment influences travel choices indirectly on the three scales. On local or regional scale, the effect of land use on travel, so called D-variables (Density, Diversity, Design, etc.), is measured with elasticities [8]. On human scale there are behavioral cues or affordances [4, 10]. A bike lane or a transit stop on a street (human scale) will remind the residents of the house that there are possibilities to cycle and available public transportation service, but these residents might never use transit or bike.

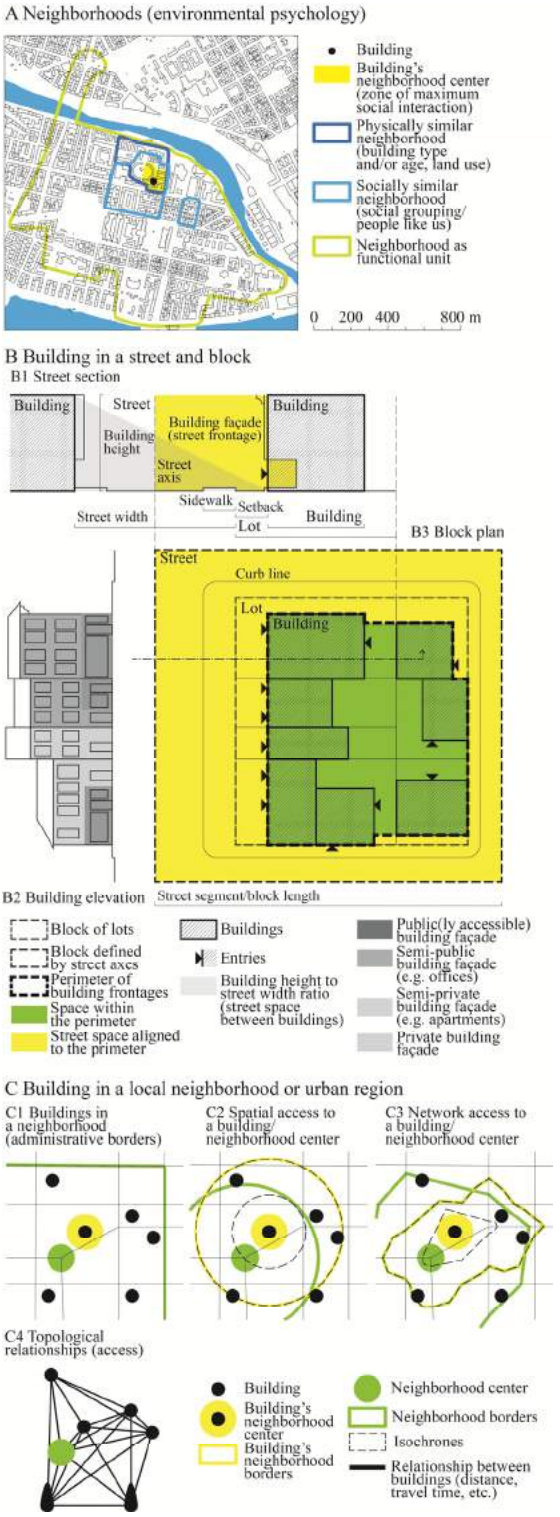

Figure 3. Urban design elements in MTPC

The factors on Table 1 utilize the research on D-variables [8] and draw inspiration from Walk Score methodology (for assessing cycling and public transportation) and LEED for Neighborhood Development (ND) for walkability. Slope is an important factor in Bike Score, whereas the Transit

Score is calculated in respect to weekly departures and type of transit service (not only as Distance to transit).

Urban element	Method
Sidewalk design and continuity	Surveyed (assigned arbitrary)
Pedestrian crossings/street segment length/city block width	I_3 = 200 - city block width (maximum 100 for width lower than 100 m and minimum 0 points for width over 200 m). city block width = city block area ^ (1/2).
Speed limit	Surveyed (I_4 = 100 if speed limit = 30km/h)
Bike parking	Surveyed (bicycle parking racks on a street give I_5 = 100)
Cycling lanes on street/cycleways	Surveyed (street segments with cycling lanes receive I_6 = 100)
Bus line/busway/tramway on street	Surveyed (street segments with bus lines receive I_7 = 50, whereas I_7 = 100 with busways/tramways on street)
Transit stop/station exit on street	Surveyed (city blocks with a transit stop/station exit on the surrounding streets receives I_8 = 100)
On-street parking	Surveyed (assigned arbitrary)
Undisturbed traffic flow (no congestion)	Surveyed (assigned arbitrary)
Building setback	Surveyed (building façade within 0.5 m will yield I_{11} = 100, between 0.5 and 5m I_{11} = 50, and I_{11} = 0 over 5 m)
Building height to street width ratio	Surveyed (if the ratio is 1:3 or lower I_{12} = 100)
Building façade activity/openness	Surveyed (if any part of the building façade is publicly accessible I_{13} = 100)
Lot/block density (residents and jobs)	I_{15} = residents and jobs per ha/100 (if residents and jobs per ha > 100 then I_{15} =100)
Lot/block land use mix (entropy of residents and jobs)	I_{16} = entropy of residents and jobs /0.7*100 (if entropy of residents and jobs > 0.7 then I_{16} =100)
Lot/block off-street parking	Surveyed (assigned arbitrary)
Neighborhood topography (slope)	Two raster maps with cost distance from the central points are created to calculate the travel ratio (TR): 1) without slope; and 2) with slope degree penalty: no penalty was given for 0-0.5 degrees, 50% for 0.5-1, 100% for 1-2, 300% for 2-5, 400 % for 5-10 and beyond 10%-degree slope got 100 times penalty (1000%). By dividing the raster without and with slope penalty it is possible to see how difficult is to reach a destination. A TR of 1 would mean two points on the map connect without slope obstacles, whereas 2 would mean 0-1% slope. I_{19} is normalized (0-100) with the formula: I_{19} = -10 * travel ratio + 110 ratios (the negative values are corrected to 0)
Access to everyday activities	GIS O-D matrix network analysis was used to calculate distances from each supermarket, shop, restaurant, bar, etc. to every building in the neighborhood. Interpolation method (IDW) was used to calculate ranges. I_{16} = 100 if building is within 100 m (buffer tool was used), 60 if between 200-400 m network distance, 30 if within 400-800 m network distance.
Access to event-type activities	Same method as in access to everyday activities, just destinations included in this case churches, libraries, etc.
Access to a mix of activities	GIS service area network analysis in ArcGIS was used. Service area polygons within 400 m to entries with different land uses (shopping, culture, recreation, bars and restaurants, services, education and public spaces) were created and overlaid to sum up the number of land uses: I_{16} = 0 (0-1 uses); I_{16} = 25 (2-3 uses); I_{16} = 50 (4-5 uses): and I_{16} = 100 (6-7 uses).
Access to a local transit stop	GIS O-D matrix network analysis was used to calculate distances from local transit stops to every building in the neighborhood. Each local transit stop received a Transit Stop Performance Benchmark (TSPB) in respect to the frequency and type of service (weekly departures multiplied by 2 for commuter rail/subway/regional bus lines, 1.5 for local trunk buses and 1 for standard buses. The reference for the calculus (TSPB = 100) is Stockholm's busiest transit node (Centralen/T-central/) which has 3374 departures or arrivals per week by bus, 2002 by trunk bus, 6643 by subway and 1302 by commuter rail (weighted sum of 22267). The formula is: TSPB = ln (all weekly departures at the transit stop) / ln (22267). I_{23} = weight for proximity to a transit stop (w)*TSPB Interpolation method (IDW) was used to calculate w: w = 100% if building is within 100 m (buffer tool was used), 60% if between 200-400 m network distance, 30% if within 400-800 m network distance.
Access to a regional transit stop	Same method as for access to a local transit stop
Access to an expressway	I_{23} = 100 if the neighborhood center is within 3 km to an exit to an expressway
Bikable location (regionally)	I_{23} = -20*distance to the metropolitan core (in km) +200 (if distance to the metropolitan core > 10km then I_{23} = 0)

Table 1. Methods used to assess built environment factors.

The weights for different factors are represent on Table 2. The weighting is done accordingly to the 9-point scale commonly used in Multi-Criteria Evaluation (MCE) in GIS where only the top 4 values are used: 9 for extremely, 7 for very much, 5 for moderately and 3 for slightly effects the LoI. The values are arbitrary, but derive from empirical research on the link between built environment and travel [8] and on trip generation based on land use factors [9, 11, 21]. The proportion between scales in the weighting is assumed arbitrary (10-20% for human (visible behavioral cues/scripts), 40-50 for local neighborhood and 30-40% for regional scale).

In the LoI for walking, the street spaces received arbitrary values for design elements (sidewalk design and continuity, speed limit, building setback, building height to street width

ratio and building façade activity/openness). On a city block (the perimeter within building façades) level LoI was calculated as average of the density (residents and jobs) and diversity/residents-job balance (entropy of residents and jobs). The LoI for walking on the map was a product of focal statistics as average values of all the values within a 100 m buffer (average LoI within clear line of sight from that point). The human scale factor (pedestrian crossings) was replaced with street segment length/city block width. Street segment length/city block width correlates with intersection density, a Design variable with strongest effect on walking [8] The LoIs for cycling, public transportation and private car focused on two crucial factors for each scale weighted in the proportion described above.

Urban element	Walking	Cycling	Public transportation	Private car
Sidewalk design and continuity	(3) 5[1]			
Pedestrian crossings/street segment length/city block width	(7) 15			
Speed limit	(3) 5[1]			
Bike parking		(3) 10		
Cycling lanes on street/cycleways		(3) 10		
Bus line/busway/tramway on street			(3) 5	
Transit stop/station exit on street			(3) 5	
On-street parking				(3) 10
Undisturbed traffic flow (no congestion)				(3) 10
Building setback	(3) 5[1]			
Building height to street width ratio	(3) 5[1]			
Building façade activity/openness	(9) 20[1]			
Lot/block density (residents and jobs)	(9) 20[2]		(3) 5	
Lot/block land use mix (entropy of residents and jobs)	(9) 20[2]		(3) 5	
Lot/block off-street parking				(9) 50
Neighborhood topography (slope)		(9) 40		
Access to everyday activities	(9) 20			
Access to event-type activities	(3) 5			
Access to a mix of activities	(9) 20			
Access to a local transit stop			(9) 30	
Access to a regional transit stop			(9) 30	
Access to an expressway				(5) 30
Bikable location		(9) 40		
			Walking (5) 20	
Sum	(51) 100	(24) 100	(27) 100	(20) 100

[1] assigned to street space

[2] assigned to city blocks/perimeter within building façades

Table 2. Weighting of built environment factors

Mobility classes

Multimodality (as set of mobility choices) is individual, since travel needs and preferences differ. Not everyone can drive. Some people love bikes and advocate biking. Other individuals are passionate about driving and cars. Some are nostalgic about trams and trains. Mobility class is proposed term to capture travel preferences and tastes deriving from Bourdieusien conceptualization of social class. Social classes are groups of agents who occupy similar positions in social space and who, being placed in similar conditions and subjected to similar conditionings, have every likelihood of having similar dispositions and interests and therefore of producing similar practices and adopting similar stance [5]. In a context of travel and multimodality, the term mobility class defines groups of agents with same preferences to specific transportation modes.

To analyze the dispersion, the most radical cases of mobility classes (flâneurs prefer to walk, cycling advocates love bikes, bus or rail nerds prefer transit and dedicated motorists drive everywhere) are completed with green travellers (who prefer walking, cycling and public transportation before private car) and rational agents (have equal preference to all transportation modes). The new trends of electrification, automation and sharing create new emerging hybrid modes too (Figure 4).

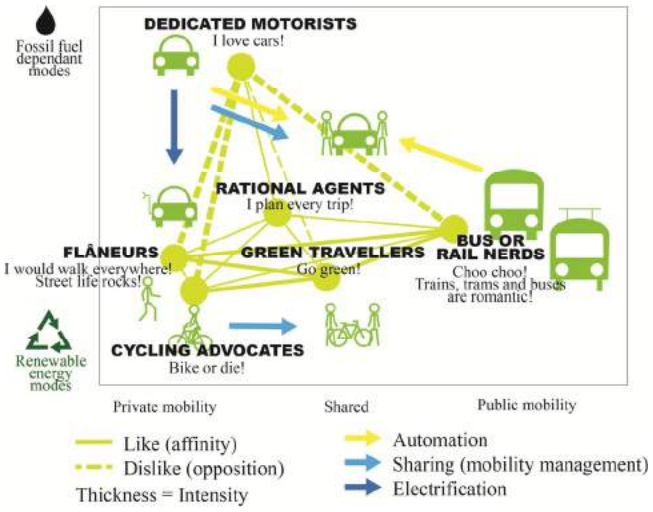

Figure 4. Mobility classes

The mobility classes are furthermore inspired by research on market segmentation [3]. The actual modal split reveals conflicts between preferences (mobility classes or market segments) and possibilities to travel (affected by design elements in the built environment which support or hinder mobility). The preferences of the typical mobility classes are profiled in Table 3.

	Walking	Cycling	Public transportation	Private car
Flâneurs	Like extremely (0.92)	Dislike slightly (0.03)	Dislike slightly (0.03)	Dislike extremely (0.01)
Cycling advocates	Dislike slightly (0.03)	Like extremely (0.92)	Dislike slightly (0.03)	Dislike extremely (0.01)
Bus or Rail nerds	Neither like nor dislike (0.08)	Neither like nor dislike (0.08)	Like extremely (0.75)	Neither like nor dislike (0.08)
Green travelers	Like moderately (0.33)	Like moderately (0.33)	Like moderately (0.33)	Dislike moderately (0.01)
Rational agents	Neither like nor dislike (0.25)	Neither like nor dislike (0.25)	Neither like nor dislike (0.25)	Neither like nor dislike (0.25)
Dedicated motorists	Dislike extremely (0.01)	Dislike extremely (0.01)	Dislike extremely (0.01)	Like extremely (0.96)

Table 3. Weighting of transportation mode preferences for typical mobility classes

Each typical mobility class received a weight based on 9-point scale: 1) like extremely (9); 2) like very much (7); 3) like moderately (5); 4) like slightly (3); 5) neither like nor dislike (1); 6) dislike slightly (1/3); 7) dislike moderately (1/5); 8) dislike very much (1/7); and 9) dislike extremely (1/9). The weight factor was calculated when the weights for different factors were summed for each row and divided with the weight of mode. The sum for flâneurs is 9.778=9+1/3+1/3+1/9 and the weight 0.92=9/9.778.

2.2 Results and discussion

Figure 5 shows maps illustrating different built environment factors and LoIs for walking, cycling, public transportation and private car. The benchmarking procedure produces hot spots for walking and public transportation (the direction from Handen Station to Haninge Centrum, the local shopping mall), and it shows where it is problematic to bike. There are steep slopes and terrain depressions (the square which links to Handen Station via a tunnel and Haninge Centrum's ground floor is below the level where car traffic circulates) where it is difficult to bike. There is no visible congestion or traffic jams around Handen Station and the parking is abundant both off and on-street. The LoI with private car is at 100% throughout the neighborhood.

The LoIs in respect to competition with the private car and all the transportation modes (modal split estimate) are presented on Figure 6. There is no difference with LoIs for specific modes with the LoI considering competition with the private car because is at 100%. The results show the same map as Figure 5. The LoIs in respect to completion to all the transportation modes display an estimated modal shares dispersed geographically (in respect to the built environment factors). Estimated shares of walking vary between 0 and 50% (around Haninge Centrum) with an average between 10-30% whereas cycling is at 10-20%, Public transportation is around 20-30% in proximity to the transit stops and 10-20% further away. Driving and the private car is at 50-60% throughout the neighborhood. The actual modal share at Haninge Municipality is 50% car, 32% public transportation, 5% cycling and 10% walking (SLL, 2016). The results are somewhat reasonable. Since Handen Station and Haninge Centrum are pedestrian pockets of the a predominantly commuting suburb it is possible that the walking share is a bit higher.

Figure 6 also shows how typical representatives of mobility classes would perceive the neighborhoods. The flâneurs who prefer to walk would most enjoy the land use mix in the Handen Station-Haninge Centrum direction. The best location for bus or rail nerds is around the local transit hub on the entrance of Haninge Centrum. dedicated motorists can drive everywhere and this is a great neighborhood for private car. this is a bad neighborhood for cycling advocates. The terrain around Handen Station and Haninge Centrum is difficult and the suburb is too far from the metropolitan core of Stockholm. This neighborhood is good for rational agents who like to combine all the modes, whereas a bit less good for green travelers (who prefer walking, cycling and public transportation before private car).

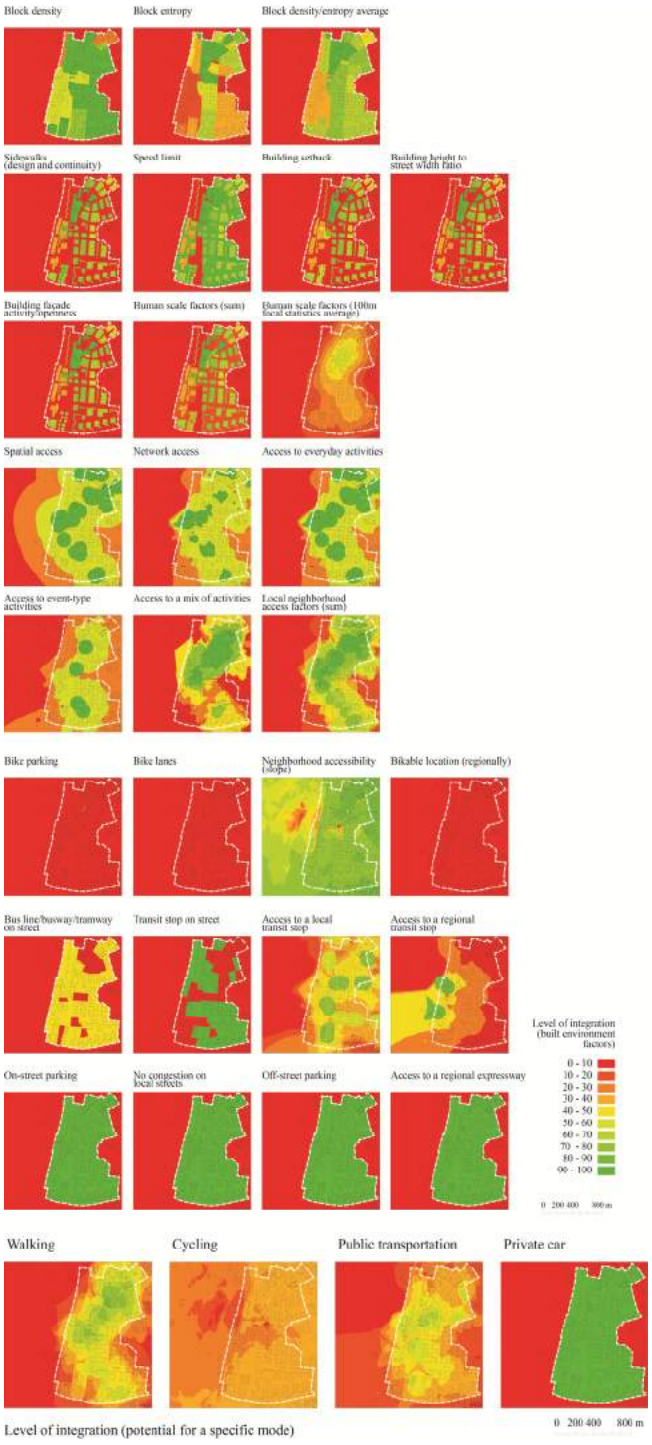

Figure 5. Levels of integration for specific transportation modes

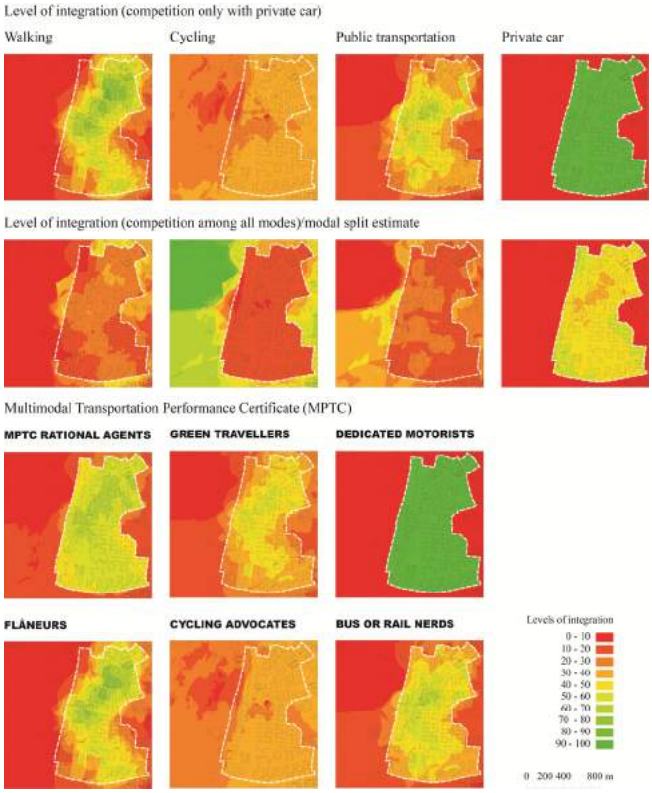

Figure 6. MPTC results (modal split and mobility classes)

3 CONCLUSION

The MTPC benchmarking procedure generates reasonable results for levels of integrations and estimates of modal split (based only on built environment factors). The variation of the LoIs for walking, cycling and public transportation before private car correspond to the actual patterns of movement in the neighborhood. There are many cars. People usually walk between Handen Station and Haninge Centrum. There are not many cyclists.

MTPC aims to provide information to individuals with different mobility preferences. The analysis shows results for most typical mobility classes (flâneurs, cycling advocates, bus or rail nerds, dedicated motorists and rational agents). Many real individuals are located in between these typical personalities. The same weighting procedure can be applied to any travel preferences to calculate tailor-made MTPC.

The predictions of mobility patterns based only on built environment factors must be considered with awareness, because travel directly depends on discrete choices of individuals (economic rationality, personality traits, irrational commitment to specific modes, etc.). Mobility management also plays role in shaping everyday travel. Some cities like Stockholm have developed a culture where public transportation is prioritized. Other cities like Copenhagen have a cultural cycling bias. Strong mobility

cultures influence actual modal shares by boosting specific modes.

The future research is to refine the MTPC benchmarking procedure and test it in other Swedish municipalities in which the metropolitan core is a small or medium sized city. An analysis of low density neighborhoods in large and small city urban regions is also needed to see how the benchmarking performs. In long term the goal is to create a web application which will automatically recognize urban design elements and individual travel preferences in order to provide information about multimodality of buildings and neighborhoods. MTPC can be a framework to localize individual modal splits (from new travel survey mobile apps).

ACKNOWLEDGMENTS

The research on MTPC is supported by a grant from Sweden's innovation agency VINNOVA (2015-03483) and scholarship from Riksbyggen. The author would also like to thank Paul L. Casey, Miguel Torres García and Tigran Haas.

REFERENCES

1. Alexander, C. Ishikawa, S. and Silverstein, M. *A pattern language: towns, buildings, construction.* Oxford University Press, New York, 1977.
2. Alexander, C. *The timeless way of building.* Oxford University Press, New York, 1979.
3. Anable, J. 'Complacent car addicts' or 'aspiring environmentalists'? Identifying travel behaviour segments using attitude theory. *Transport Policy 12*, no. 1 (2005): 65-78.
4. Barker, R.G. *Ecological psychology: concepts and methods for studying the environment of human behavior*, Stanford University Press, Stanford, 1968.
5. Bourdieu P. The Social Space and the Genesis of Groups, *Theory and Society*, vol. 14, no. 6. (1985): 723-744.
6. Dur, F. Yigitcanlar, T. and Bunker, J. "A spatial-indexing model for measuring neighbourhood-level land-use and transport integration." *Environment and Planning B: Planning and Design* 41, no. 5 (2014): 792-812.
7. Gehl, J. *Life between buildings: using public space.* Van Nostrand Reinhold, New York, 1987.
8. Ewing, R, and Cervero. R. Travel and the built environment. *Journal of the American planning association 76*, no. 3 (2010): 265-294.
9. Ewing, R. Greenwald, M.J. Zhang, M. Bogaerts, M. and Greene, W. Predicting transportation outcomes for LEED projects. *Journal of Planning Education and Research 33(3)* (2013): 1-15
10. Gibson, J.J. *The ecological approach to visual perception*, Lawrence Erlbaum Associates, Hillsdale, N.J., 1986.
11. ITE (Institute of Transportation Engineers). *Trip Generation Manual*. 9th edition. Washington. DC, 2012.
12. E. Innes, J. and Booher. D.E. Indicators for sustainable communities: a strategy building on complexity theory and distributed intelligence. *Planning theory & practice 1*, no. 2 (2000): 173-186.
13. Lee, T. Urban neighborhood as a socio-spatial schema. *Ekistics*, (1970): 119-129.
14. Prelipcean, A.C. Gidófalvi, G. and Susilo. Y.O. Mobility collector. *Journal of Location Based Services 8*, no. 4 (2014): 229-255.
15. Schlossberg, M, and Brown. N. Comparing transit-oriented development sites by walkability indicators. *Journal of the transportation research board 1887* (2004): 34-42.
16. Singh, Y.J. Fard, P. Zuidgeest, M. Brussel, M. and van Maarseveen. M. Measuring transit oriented development: a spatial multi criteria assessment approach for the City Region Arnhem and Nijmegen. *Journal of Transport Geography* 35 (2014): 130-143.
17. SLL (Stockholms läns landsting), (2016). Resvanor i Stockholms lan 2015. http://www.sll.se/Global/Verksamhet/Kollektivtrafik/Kollektivtrafiken%20v%C3%A4xer%20med%20Stockholm/SU/Resvaneunders%C3%B6kningen/resvanor-i-stockholms-lan-2015.pdf As of 12 December 2016.
18. Stojanovski, T., Alam, T., & Janson, M. Transit-oriented development (TOD): analyzing urban development and transformation in Stockholm. In Proceedings of the Symposium on Simulation for Architecture & Urban Design. (2014): 1-8.
19. Talen, E. and Shah. S. Neighborhood Evaluation Using GIS An Exploratory Study. *Environment and Behavior 39*, no. 5 (2007): 583-615.
20. Talen, E. Allen, E. Bosse, A Ahmann, J. Koschinsky, J. Wentz, E. and Anselin, L. LEED-ND as an urban metric. *Landscape and Urban Planning 119* (2013): 20-34.
21. Weinberger, R. Dock, S. Cohen, L. Rogers, J.D. and Henson J. Predicting travel impacts of new development in America's major cities: testing alternative trip generation models. *Journal of the Transportation Research Board 2500* (2015): 36-47.

The Mobility Topography Model for Substantializing and Projecting Transportation in Cities

Zachary Trattner, Angelos Chronis, Angel Muñoz

Institute for Advanced Architecture of Catalonia
Barcelona, Spain
zacharytrattner@iaac.net, angelos.chronis@iaac.net, angel@iaac.net

ABSTRACT

Cities are built on transportation strategies. The constructed urban environment is influenced by the accumulation of individual transport choices, and also by the decisions of transportation planners who continue to rely on tools designed to hasten the expansion of car culture. Past experiences incorporating cars, trains, and horses have demonstrated that paradigm shifts in mobility technology impact activity patterns in cities. Autonomous vehicles will certainly revolutionize urban mobility, but the positive and negative consequences of driverless personal transport on cities and societies remain unknown. The probability of a beneficial impact will increase with more and better tools available for analyzing existing transportation habits and projecting future possibilities. The mobility topography model (MTM) introduced in this paper is a multimodal route simulator that evaluates probable modal choice for hypothetical travelers, derived using actual ridership data, transportation infrastructure, and economic conditions. An application has been developed for users to adjust input parameters and quickly project the potential impacts of evolving technologies and changing circumstances. The MTM is flexible, general, and well suited for casting holistic projections of future scenarios, rather than for precise accounting of specific interventions. The model is demonstrated in Singapore today and into the future.

Author Keywords

Transportation; mobility; probability model; autonomous vehicles, urban planning.

ACM Classification Keywords

I.6.1 SIMULATION AND MODELING (Model Development).

1 INTRODUCTION

The widespread acceptance of the car in the early 20th century was a paradigm shift in mobility technology. However, cities around the world are experiencing a multitude of problems from excessive car use, including urban sprawl, global warming, traffic congestion, poor health, and social isolation (Litman 2002). Therefore, it is reasonable to state that the shift to cars was mishandled by past generations of planners, and the same mistakes are being repeated in developing counties today. Meanwhile, many prominent planners acknowledge that when priority was first assigned to the movement of cars over pedestrians, car culture built momentum, inaugurating the development of a two-tier transportation system that persists today.

Recent advances in autonomous vehicles (AVs) suggest that in a few short years, roads will be populated by self-driving cars. Experience tells us that the response of planners to this emerging technology will define the character of our cities and societies for generations. A potential problem is that the main computational tool that transportation planners rely on to predict future use is still the traditional four-step traffic demand model that was developed in Detroit during the 1950s. The four-step model applied the concepts of supply and demand to transportation engineering (concepts that were pioneered in economic theory), and has been used to design roads and mass transit networks based on the needs of vehicles ever since. Without doubt, we will need new, more dynamic tools to develop mobility solutions that are appropriate for cultivating healthy and sustainable cities.

This paper presents the mobility topography model (MTM), a variation on traditional transportation modeling techniques that is designed to give planners insight into the broader effects of technological, infrastructural, and economic developments. The MTM was constructed around the example of Singapore, but the tools and procedures demonstrated here can be applied to any urban environment. Calculations for the first three steps (environment description, trip generation, and route assignment) are conducted in the Grasshopper3D plugin for Rhinoceros3D using a combination of native components and custom Python scripts. The subsequent steps (calibration, mode choice, and topographic visualization) are implemented in Processing as a standalone application with an intuitive, user-friendly interface. This approach is designed to substantialize the invisible mobility layer of cities, so that planners and politicians can intuitively process visual information as opposed to abstract figures. Applying this computational tool to the difficult work of interpreting the probability landscape that emerges from urban transportation systems, the human imagination can pursue innovative solutions to complex mobility scenarios.

2 BACKGROUND

Transportation planners currently have access to several advanced computational techniques for modeling human

mobility, including agent-based models (ABMs) and neural networks. Chen [2] provides a detailed survey of many possible applications for ABMs in architecture, urban, and transportation planning. Agent-based transportation models usually simulate the actual use patterns of individual travelers and vehicles; for example, the model constructed by Aschwanden [1] included digitized representations of street lanes, buildings, and bus stops. The TRANSIMS project is a flexible and comprehensive ABM tool that has found many wide applications including modeling vehicular traffic, pedestrian flows, and emergency egress [13]. However, ABMs are best suited for modeling situations that occur over small time scales and in limited spatial areas, because they depend on repetitively updating the micro-scale decisions of individual automata. Trained neural networks are another advanced computational tool with potential applications in urban planning, such as predicting patterns of urban sprawl [6]. However, the traditional four-step model is the most commonly used tool for planning road capacity, validating public transit demand, optimizing tolls, and more. In essence, the four-step model interprets a city as a network of links and nodes, on which trips are distributed according to demand, and then redistributed based on link capacity until equilibrium is achieved.

When implementing a transportation macro-model, it is common practice to combine household data with distance decay methods or other techniques to generate trips [4]. However, Singapore hasn't published place-of-work data, so this example MTM implementation determines trip rates using alternative methods. To arrive at reasonably accurate trip rates for employed residents, distances are measured from point locations for trip generating occupancies including employment centers, malls, hospitals, airports, etc., and are modified by accessibility indices based on distance from the centroid of the starting zone (Figure 1). Zhou, Kockelman, and Lemp [25] demonstrate the use of an accessibility index to modify trip rates, a feature that is becoming progressively more common in four-step model applications. To limit the potential for extreme results, each trip start point has multiple end points.

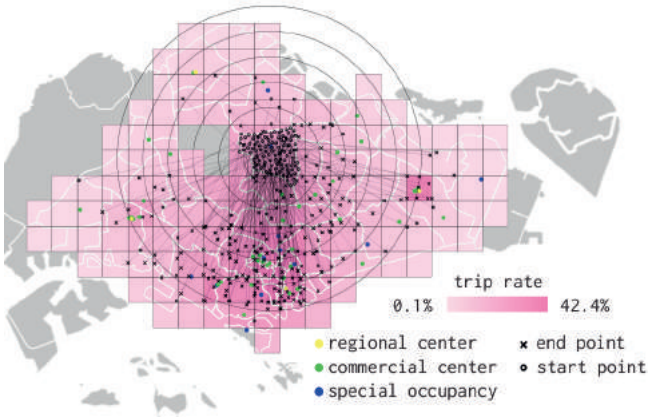

Figure 1. Employment activity trip production map for Ang Mo Kio, a centrally located, residential planning zone.

Four-step models frequently include mode choice probability calculations using probit, logit, or gravity models. The multinomial logit model (MNL) used by the MTM was adapted from the methods used by Koppelman and Bhat [12] to compare discrete utility values for several modes of transportation and determine the most probable choice (Figure 2). The utility value equation includes average monthly household income for each zone as a denominator below calculated trip cost (Figure 3), enabling the model to consider the influence of economic forces like income inequality on mobility. These formulae are well established, and the theoretical basis for the validity of the MTM is derived from the use of these models.

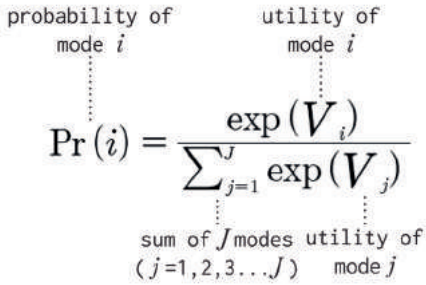

Figure 2. Probability equation derived from MNL.

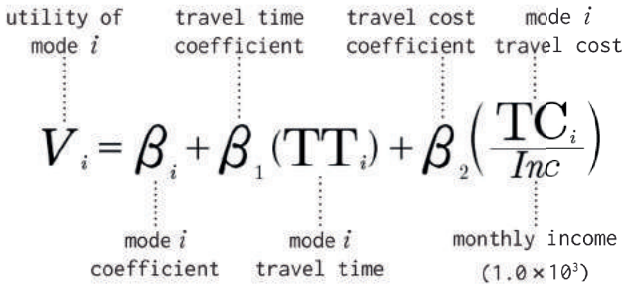

Figure 3. Equation to calculate mode utility using terms for travel time, travel cost, and income alongside mode coefficients.

The resulting probability output by the MNL is analogous to probable modal choice, and is calculated by comparing the utility of different modes. Each mode utility value is calibrated to better represent reality using mode bias coefficients. While logit models have often relied on traditional optimization techniques like Newton-Raphson or steepest ascent methods to determine mode bias coefficients, the proposed MTM uses a genetic algorithm (GA) to determine coefficients. Research confirms the viability of calibrating coefficients using GAs to match a dataset [24]. In this case, the dataset being matched is the actual modal split of residents of Singapore, calculated using ridership data from the 2010 Census of Population [21]. Using randomly generated coefficients does not compromise the validity of the model, because the input values for utility equations have arbitrary units of measurement (hours, dollars), and as such, they naturally require coefficients to become related. Mode bias coefficients also account for social values and other

generally incalculable factors as discussed at length by Koppelman and Bhat [12].

Methods for modeling congestion are a key difference between the traditional four-step model and the proposed MTM. Traditional models rationalize congestion as an imbalance between trip demand and link capacity, and usually depend on equilibrating these two forces by reassigning trips within a feedback loop (McNally 2007). However, empirical evidence indicates that travelers continue to use heavily congested roads. Therefore, this understanding of congestion can fail to accurately represent reality, particularly due to induced demand. Instead, the MTM uses a common sense algorithm (Figure 4) based on causality, which utilizes the concept of congestion indices. A congestion index is a ratio that compares trip duration during peak travel times (morning and evening rush hours) with free-flowing travel (usually from 2-5am). For this MTM application, the base congestion indices were calculated using trips entered into TomTom MyDrive [22], a time-based route calculator that uses data sourced from real GPS devices. In the proposed algorithm, congestion indices are primarily modified by vehicle population, which is in turn modified by additional parameters such as road tolls, ride-sharing ratios, and total population. Congested travel is assumed for 50% of trips, with the congestion index averaged between values at the start and end of each trip [15].

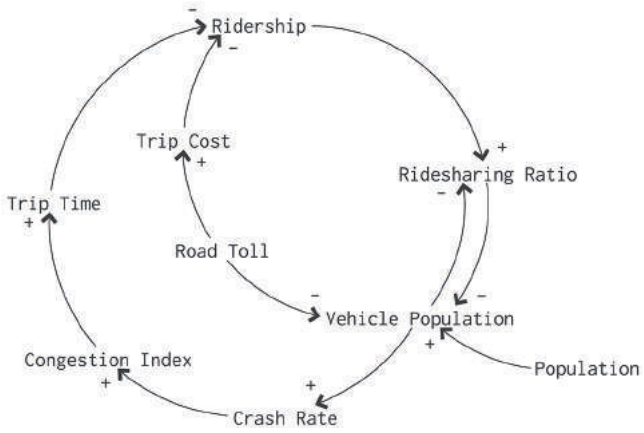

Figure 4. Causal loop diagram of the algorithm to calculate congestion indices for the MTM based on realistic, relevant factors.

Another key difference between the MTM and the four-step model is the speed with which the model can return results. Although four-step model practitioners have become reasonably accurate at predicting traffic demand and link capacity over the past six decades, the process is not optimal. Achieving a high degree of accuracy requires complex networks with long calculation times, and additional steps for advanced methods like time-of-day disaggregation and congestion feedback loops [3]. It is reasonable to conclude that although the four-step model is a powerful tool, it can be cumbersome and even restrictive. Comparing the architecture of the traditional four-step model with the MTM described in this paper reveals the MTM's clear advantages in terms of calculation time (Figure 5). To consider changes to the network, a four-step model must loop back to the trip distribution step, while changes in activity production must be recalculated from the trip generation step [16]. In comparison, once it has been initialized, the MTM can skip the costly trip generation and route assignment steps, giving the user immediate visual response, and a tactile experience.

3 METHODS

Implementing the MTM requires collecting an intensive quantity of site-specific data, including geospatial information for expressways, metro lines, bus routes, and bike paths. A geometric dataset capturing transportation infrastructure in Singapore was assembled in Rhinoceros3D, including data published by the Singapore Land Transport Authority regarding future infrastructure projects. Singapore is an ideal study area because within the last decade, they have built multiple new metro lines, producing several diverse data points for comparison. Singaporean institutions frequently publish high-quality data and are also conducting ongoing research into AVs, which indicates that the city will probably be an early adopter of robot car technology to enable further comparison [11, 20]. The geometric data for existing and future infrastructure was organized chronologically into layers, and a Python script to cycle through the possible configurations while exporting the route data being produced from Grasshopper into JSON format.

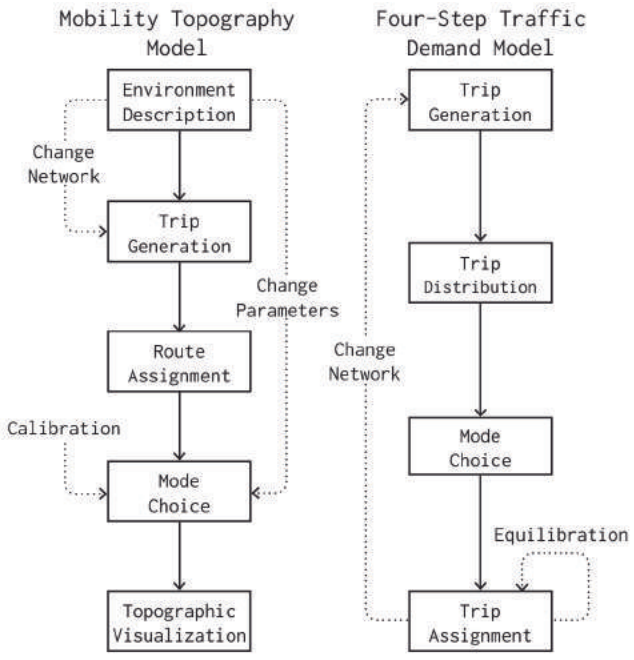

Figure 5. Flow chart comparing the inefficient architecture of the traditional FSM with the innovative architecture of the MTM designed to improve calculation speed and flexibility.

However, options for reconfiguring infrastructure represent only a small percentage of the complete set of adjustable parameters available to the user. The quantity of possible scenarios that can be considered by modifying MTM parameters is endless. For example, vehicle speed can be increased to consider scenarios with AVs travelling at high speeds on dedicated expressways, or set to zero to simulate the complete removal of the expressway network. High-capacity trip generating occupancies like stadiums can be strengthened to anticipate travel patterns for large events. There are also parameters available to consider travel time reliability to understand the possible implications of service disruptions on metro systems, or the effects of severe storms from climate change on bicycle use. The design of the MTM makes it flexible enough to quickly visualize diverse scenarios that traditional models may struggle to consider. Although the calculation method is similar to that of the four-step model it is not intended for same type of precise accounting, but instead for projecting broad trends and their consequences on the urban mobility landscape.

Implementing the following steps (trip generation and route assignment) is very similar to the four-step model. The data aggregated in Rhinoceros3D is processed in Grasshopper via algorithms written using a combination of native Grasshopper components and custom Python scripts (Figure 6). The shortest walk component developed by Piacentino [19] is also used extensively in the route assignment step to calculate optimal routes over expressway, metro, and bike path networks. In addition, a technique previously implemented by Cukier [5] for penalizing transfers between metro lines is applied for calculating metro routes.

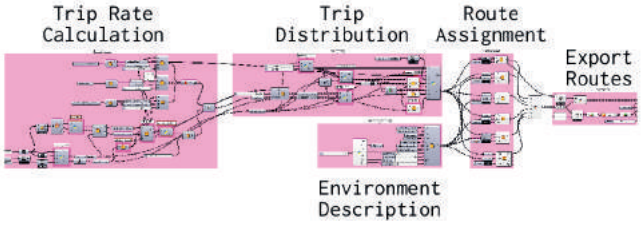

Figure 6. Screenshot of the Grasshopper3D script used to interpret the digitally described environment and to generate route data for subsequent mode choice calculations.

Route data was pre-calculated for every possible combination of a discrete number of infrastructural configurations, and exported in JSON format for use in the subsequent stages of the model. For the following steps of the MTM, the development environment was switched from Grasshopper3D to Processing, a popular Java development environment.

Route data based on Singapore's 2009 infrastructure and urban conditions was compared with ridership data from the 2010 census, and used to calibrate the model´s mode utility coefficients using a GA adapted from a kernel developed by Turner [23]. With each generation of the GA, the time and cost impedance for every trip across every mode was evaluated and combined with a population of coefficients to output a set of mode utility values. Next, these values were converted to modal choice probabilities using the probability equation from Figure 2, and evaluated for fitness. An individual was considered fit if the calculated probable modal split aligned with actual modal split extracted from ridership statistics in the 2010 census for each analysis zone. After finding a solution below the threshold of 0.03%, the GA stored the fittest individual and moved on to the next zone with a fresh population. Once routes were pre-calculated and optimal coefficients determined, these datasets were input to the Processing application designed to facilitate interaction with the MTM. At startup, time and cost values for each route are calculated by the application and stored in memory. Next, these route impedance values are combined in the calibrated MNL, and probability values are output. The most probable mode is determined for each trip start point and the color corresponding to that mode is assigned to a mesh vertex to construct the topographic mobility map visualization.

The application interface was designed to be simple and intuitive, while offering the user complete control over the entire range of mobility model parameters (Figure 7). Although the application is currently focused on Singapore, it can be adapted to model any urban environment. All of the graphical and numerical MTM output data presented in the following section was sourced from interaction with the application.

4 RESULTS AND DISCUSSION

This section is intended to demonstrate the process of analyzing MTM map and data outputs. It investigates the probable impact of AVs on mobility in Singapore with a series of three scenarios that could potentially occur over 30 years of technological and infrastructural evolution.

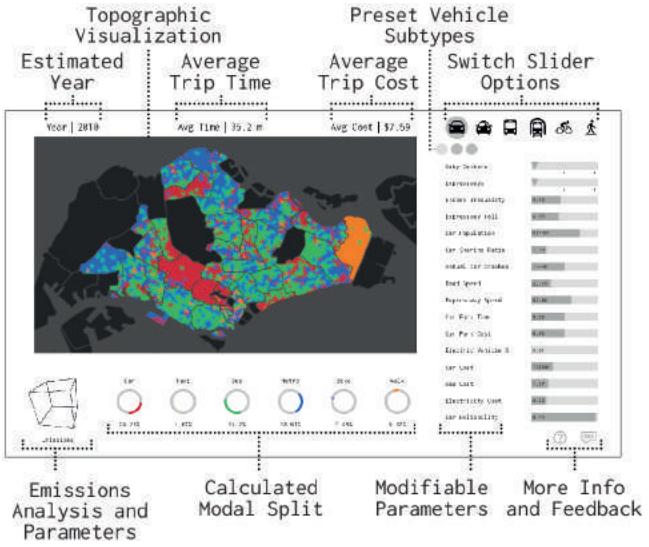

Figure 7. Screenshot of the interactive MTM interface complete with sliders for modifying parameters, a map viewport, and multiple sources of numerical data output.

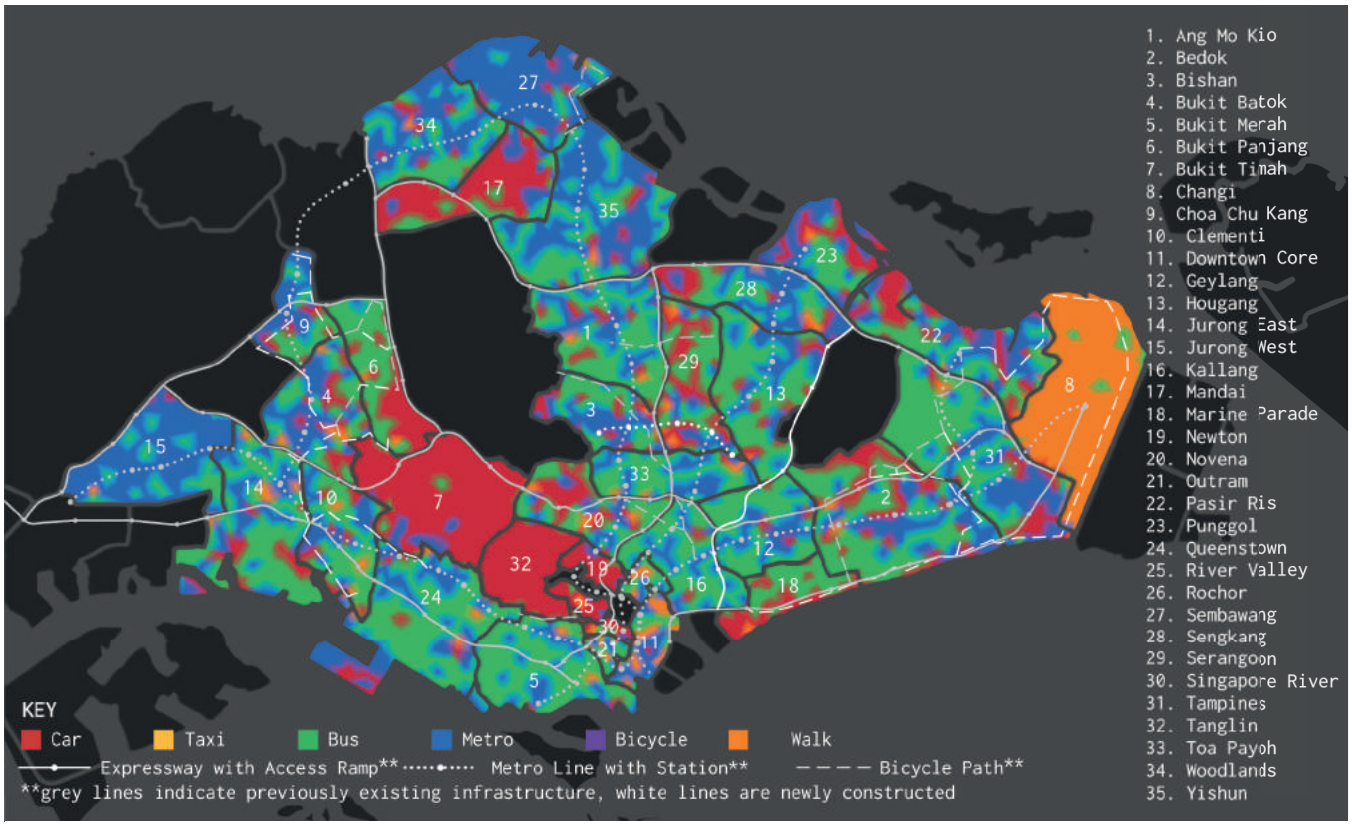

Figure 8. Probable modal choice visualized as a topographic map using data output by the MTM for scenario one (Singapore c. 2010). This mapping technique reveals the mobility layer of cities. Each place is understood as a product of local transportation habits and infrastructure.

- **Scenario one:** a snapshot of Singapore in 2009, based on residents' responses to the 2010 census.
- **Scenario two:** a projection of Singapore in 2025, with several major infrastructure projects completed and AVs in place of manually driven vehicles.
- **Scenario three:** a hypothetical Singapore in 2040, where AVs are present and the entire expressway system has been removed.

When examining the MTM output from scenario one at this holistic scale, several features of the existing mobility topography in Singapore become apparent (Figure 8). Notably, there is widespread reliance on bus travel despite frequent long wait times. Next, the residents of wealthy planning zones such as Mandai, Bukit Timah, and Tanglin are car dependent, while most other districts present a marbled transportation mix. The patterns of dominance apparent around metro lines and car expressways provide satisfactory evidence that the model has been properly formulated. The frequent dominance of walking over other modes visible in the Downtown Core and appearing elsewhere sporadically is a notable feature characteristic of walkable cities such as Singapore. Walking is dominant in Changi, a zone with a small population, low average income, and a large airport. Besides displaying the mobility topography map for Singapore in 2010, this image also introduces the graphic standards that will be used throughout this section. The subsequent diagrams illustrating MTM output display magnified, side-by-side comparisons of the three scenarios under analysis. The areas selected for detailed analysis demonstrate dramatic changes from modifying input parameters.

Scenario two assumes that road vehicles including cars, taxis, and even buses have become almost completely autonomous by 2025. Such a paradigm shift can be represented in the model by modifying parameters including parking time, vehicle speed, perceived cost, and crash rates. When AVs with piloted parking capabilities become prevalent, zero time is spent parking because passengers can travel door-to-door and leave the car to park itself [17]. Average road speeds will also increase slightly for shared streets, since autonomously managed intersections can be navigated without stopping, while expressway speeds may be faster because AVs can drive in platoon formation, reducing both energy consumption and congestion [7, 10]. These reductions in trip time for car journeys increase the probability of car travel.

The concept of perceived cost describes the monetary equivalent for stress caused by the act of driving, and varies according to road conditions and the purpose of the trip [14]. As people become more comfortable in AVs, driver stress will be reduced and time can be spent performing tasks other than driving, changing existing perceptions of the value of travel time. The potential downside of

perceived cost reduction is radically expanded urban sprawl, since travellers would be willing to spend more time commuting if their cars did the work of driving.

A benefit of AVs is that they remove the risk of human error from the roads, and could reduce the frequency of car crashes by 90% [8]. This is represented in the model by reducing the crash cost carried by travellers. Crash cost is a monetary value assigned per kilometer of travel to cover the internal costs of a crash including property damage, medical expenses, lost wages, etc., based on the probable severity of an accident.

A fleet of autonomous taxis could also eliminate the danger of drunk drivers because they would be readily available and cheaper to operate than traditional taxis with drivers. The associated increase in taxi modal share would expand the taxi population and reduce wait times outside of the city center. Research suggests that shared autonomous taxis could reduce the population of privately owned vehicles within urban environments at a ratio of ten fewer cars for each taxi added [9]. The MTM translates this decrease in congestion over surface routes as growth in the attractiveness of car, taxi, and bus travel.

The transportation infrastructure in scenario two has also been updated to include projects that are likely to be completed by 2025, including expanded metro lines, expressways, and bike paths. For this scenario, the total population of Singapore was increased in line with predictions from the *Population White Paper*, causing an increase in congestion experienced across every mode [18].

Year	Calculated Modal Split					
	Car	Taxi	Bus	Metro	Bike	Walk
2010	24.3%	1.7%	34.2%	30.7%	2.5%	6.6%
2025	22.9%	18.4%	28.1%	23.7%	2.0%	4.9%
2040	22.5%	8.1%	25.0%	33.0%	6.9%	4.5%

Table 1. Modal splits for the three different transportation scenarios analyzed in this section.

Year	Average Trip Time (minutes)	Average Trip Cost (SGD)	Annual Transport Emissions (MT CO_2e)
2010	35.2	$7.59	8.1
2025	28.2	$9.65	7.8
2040	31.4	$6.16	5.5

Table 2. Average trip time and cost comparison, along with annual emissions to evaluate the impacts of each scenario.

The third scenario is a more distant projection of Singapore as it might exist in 2040, where the main assumption is that the entire network of restricted-access expressways has been removed. This significant change is simulated by reducing vehicle speed on expressways to zero, forcing the model to consider only direct routes for cars and taxis. Other parameters changed between the second and third scenarios include further incremental improvement in wait times, and slightly reduced vehicle speed over local roads due to higher congestion. Metro and bike infrastructure were also updated to include more bike rental points and reduce bike park times, assuming that more racks will be available. The total population of Singapore is again increased. The resulting output data from these three scenarios is summarized in Tables 1 and 2 above.

To demonstrate the mobility topography analysis process, the first area of focus is the wealthy and car-dependent planning zone Bukit Timah, and the adjacent zones Bukit Batok, Bukit Panjang, Clementi, and Jurong East (Figure 9). The magnified map of 2025 suggests that residents of Bukit Timah would prefer private AVs over mass public transit despite receiving a metro line. Moreover, car dominance in Bukit Timah will not be superseded by cheaper and more readily available taxis, a conclusion that makes sense in the context of Singapore, where car ownership is a status symbol. Meanwhile, residents who previously relied upon mass transit or walking in the suburban, middle income zones Bukit Batok, Clementi, and Jurong East may switch to autonomous cars and taxis for their speed and convenience.

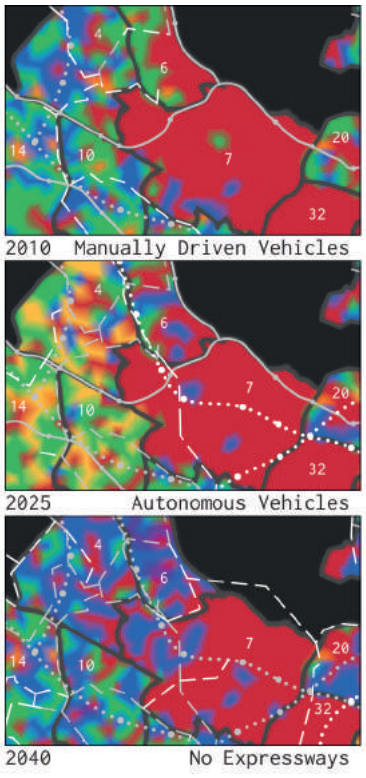

Figure 9. Magnified MTM output for three scenarios focused on luxurious residential district Bukit Timah.

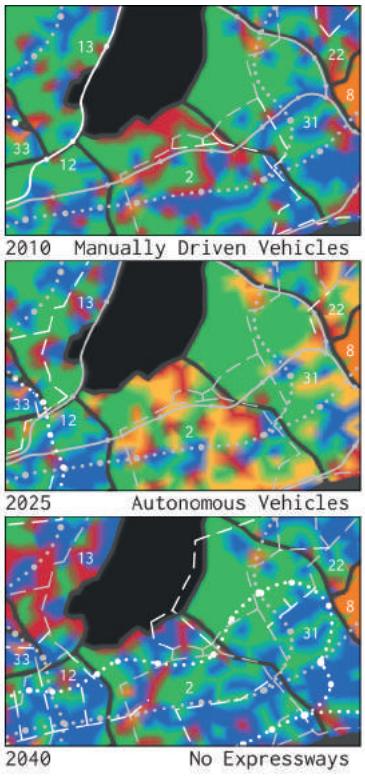

Figure 10. Magnified MTM output for three scenarios focused on dense, affordable residential zones Bedok and Tampines.

However, when expressways are removed in 2040 for scenario three, the MTM suggests that a significant percentage of Bukit Timah's population would finally utilize the local public transit infrastructure. Personal vehicle use in the adjacent zones is also projected to decrease. Notably, the expanded bike path networks of 2040 appear to result in pockets within Bukit Panjang where bikes are the preferred mode of personal transport.

The second area for comparison analysis is focused on the regional center of Tampines, and the adjacent zones Bedok, Hougang, and Pasir Ris (Figure 10). These are densely populated, medium income residential zones where present day occupants rely on a mixture of car, bus, and metro transport for their commutes. When AVs are introduced into this environment, the MTM predicts that much of Pasir Ris and large swaths of Bedok and Tampines would switch to autonomous cars or taxis, despite the 23.8% increase in average cost per trip. Reduced dependence on slow bus transport probably accounts for much of the 19.9% reduction in average travel time predicted by the model. It is worth noting that the substantial increase in the quantity of vehicles present may increase congestion and degrade the quality of life for residents of these areas.

However, without expressways the calculated probability for residents of Tampines, Bedok, and Pasir Ris to travel by car drops dramatically by 2040. The model predicts they would switch to more environmentally sustainable bus or metro transport, while in Hougang, the reduction in vehicle population and congestion is projected to cause a slight increase in car use. The general shift towards mass transit predicted by the MTM comes with an 11.3% increase in average travel time, while the average cost per trip drops by an astonishing 31.1%. The implication of this analysis is that expressways and tolls perpetuate a two-tier transportation system. Wealthier travellers can afford fast personal mobility, while the inhabitants of low and middle income areas are more likely to avoid travelling by car or taxi because of the relatively high cost. Without expressways dividing the social and urban fabrics, the model concludes that mobility would be more democratic and substantially cheaper. Some of the potential benefits in this scenario would be greater social cohesion and growing average personal wealth.

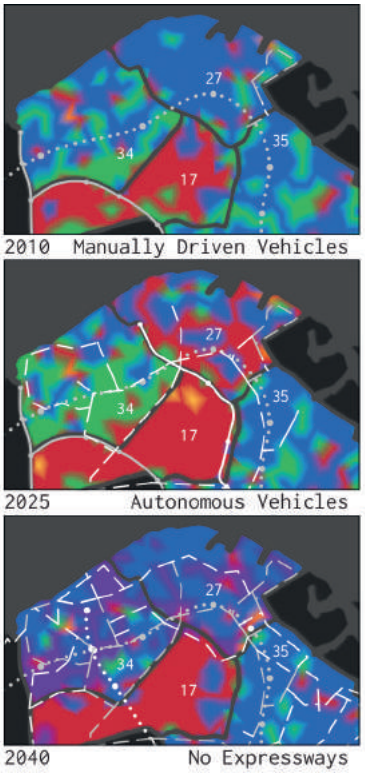

Figure 11. MTM output for three scenarios focused on emerging employment clusters in zones Woodlands and Sembawang.

The emerging regional center at Woodlands and the adjacent zones Sembaweng, Mandai, and Yishun form the third area of focus for detailed analysis (Figure 11). A comparison between the MTM output for 2010 and 2025 reveals that many residents of Sembaweng and Mandai are projected to shift towards car dependence upon completion of the North-South expressway in 2020. The model predicts that residents of Woodlands would prefer to travel by bus rather than by metro in this scenario. This phenomenon is a result of the growing use of autonomous taxis seen in previous analyses, which will reduce the number of vehicles in Singapore. Decreasing congestion on surface routes is projected to lead to a corresponding increase of

bus use in Woodlands.

For the third scenario, the previous increase in car use would be completely negated by the elimination of high-speed expressways. In fact, the MTM concludes that the expanded bike path network will lead to a significant percentage of residents in Sembaweng and Woodlands commuting by bike. This implies that residents might work nearby and not travel to the Downtown Core, thereby changing the wasteful commuting pattern prevalent in cities around the world. The MTM analysis concludes that by combining employment growth in the Woodlands regional center with expressway-free transportation, Singapore could transform into an example of a sustainable mobility city.

5 FUTURE WORK

Although this sample implementation in Singapore includes a substantial amount of data collected from site-specific sources such as Singapore's Land Transport Authority, the MTM could also function with readily available data from Google. Acquiring a reasonable amount of data over Google's API and compiling mobility topography maps would be fast and relatively straightforward for many cities. Differences and similarities in the algorithms and coefficients across diverse socio-cultural regions may become apparent to a trained neural network, and broader theories of urban transportation could eventually be developed. A faster model could also be applied to the task of charting transportation lines to optimize a particular parameter, such as metro ridership or travel time.

An issue with the MTM is its simplistic understanding of multimodal travel. The model does not consider the breakdown of individual trips, instead concentrating on the more general concept of ridership. By definition, a multimodal trip counts towards two or more rides, implying that by focusing on ridership the proposed model considers intensity of use and not actual travel patterns. Future iterations of the model could implement more complete understandings of multimodality by introducing combined modes to the logit model, such as "car and metro" or "bus and bike." Unfortunately, adding additional dimensions increases calculation time exponentially. This could also compromise the accuracy of the coefficients, since GA performance degrades with higher dimensional problems. The model may also benefit from expanding the quantity of routes available for each trip to dynamically redistribute trips away from congested routes.

In the seven years that have elapsed since the collection of Singapore's 2010 census data, the city has added 7 km of expressways, 46.8 km of metro lines, and 124.5 km of bike paths. This rapid pace of transportation infrastructure development presents an opportunity to evaluate the accuracy of the MTM. Singapore's evolving infrastructure will have impacted transportation patterns over the last seven years. If a survey of the present day transportation profile for a significant percentage of Singaporeans agreed with the predictions of the MTM, it would confirm the usefulness of the model as a projection tool. At minimum a survey would offer more data for comparison. The interactive MTM application is hosted online, presently generating a database of feedback for further analysis.

6 CONCLUSION

The intent of this project was to construct a predictive model that would complement the transportation planners existing toolkit. Although the accuracy of this model is unproven, it may still offer valuable perspective to urban planners. The linear structure of the MTM enables faster, more tactile visualization than can be achieved with traditional modeling techniques. The simplified congestion model implemented by the MTM also allows it to simulate a broad range of scenarios without experiencing capacity overloads and "breaking," as a traditional four-step model would. In theory, with further advancement this model could be used to generate optimal solutions to problems that escape the threshold for understanding complexity of the average human urban planner.

At present this project is best described as a mathematical probability model that visualizes the effects of changing variables over several layered geometric networks. It is still a speculative project without empirical evidence to validate its predictions. However, even if it remains merely an intermediary between the deductive abilities of the human imagination and the unimaginable complexity of an urban transportation system, it is still a potentially valuable tool for planners to consult during the decision-making process.

REFERENCES

1. Aschwanden, Gideon. 2012. "Agent-Based Social Pedestrian Simulation for the Validation of Urban Planning Recommendations." *Sigradi*, 332-36.
2. Chen, Liang. 2012. "Agent-Based Modeling in Urban and Architectural Research: A Brief Literature Review." *Frontiers of Architectural Research*, 1: 166-77.
3. Chen, T. Donna, Kara M. Kockelman and Yong Zhao. 2015. "What Matters Most in Demand Model Specifications: A Comparison of Outputs." *Journal of the Transportation Research Forum,* 52 (1): 71-89.
4. Chimba, Deo, Daniel Emaasit and Boniphace Kutela. Oct. 2012. "Integrating Origin Destination Survey and Stochastic User Equilibrium: A Case Study for Route Relocation." *Journal of Transportation Technologies*, 2 (2): 297-304.
5. Cukier, Jerome. 2013. "Interactive Map of the Subway." *Communicating with Data,* Jan. 13. http://www.jeromecukier.net/blog/2013/01/14/interactive-map-of-the-subway/.
6. Diappi, Lidia, Paola Bolchim, and Massimo Buscema. 2004. "Improved Understanding of Urban Sprawl Using Neural Networks." In *Recent Advances in Design &*

Support Systems in Architecture and Urban Planning, 33–49.

7. Dresner, Kurt and Peter Stone. 2008. "A Multiagent Approach to Autonomous Intersection Management." *Journal of Artificial Intelligence Research*, 31: 591-656.
8. Fagnant, Daniel and Kara M. Kockelman. 2015. "Preparing a Nation for Autonomous Vehicles: Opportunities, Barriers and Policy Recommendations for Capitalizing on Self-Driven Vehicles." *Transportation Research Part A,* 77: 167-181.
9. Fagnant, Daniel and Kara M. Kockelman. 2016. "Dynamic Ride-Sharing and Optimal Fleet Sizing for a System of Shared Autonomous Vehicles." *Transportation*. Accepted, Oct. 2015.
10. Fernandes, Pedro and Urbano Nunes. Mar. 2012. "Platooning With IVC-Enabled Autonomous Vehicles: Strategies to Mitigate Communication Delays, Improve Safety and Traffic Flow." *IEEE Transactions on Intelligent Transportation Systems*, 13 (1): 91-106.
11. Kheong, Tan Cheon and Tham Kwang Sheun. 2014."Autonomous Vehicles, Next Stop: Singapore." *JOURNEYS* (12): 5-11.
12. Koppelman, Frank S. and Chandra Bhat. 2006. *A Self Instructing Course in Mode Choice Modeling: Multinomial and Nested Logit Models*. U.S. Department of Transportation.
13. Lee, Kwang Sub, Jin Ki Eom and Dae-Seop Moon. 2014."Applications of TRANSMIS in Transportation: A Literature Review." *Procedia Computer Science,* 32: 769-77.
14. Litman, Todd. 2002. "The Costs of Automobile Dependency and the Benefits of Balanced Transportation." Victoria Transport Policy Institute.
15. Litman, Todd and Eric Doherty. Aug. 2013. "Travel Time Costs." In *Transportation Cost and Benefit Analysis II*. Victoria Transport Policy Institute.
16. McNally, Michael G. 2007. "The Four Step Model." In *Handbook of Transport Modeling.* Emerald Group Publishing Limited.
17. Meier-Burkert, Friederike. 2014. "Piloted Parking." *Audi Urban Future Initiative*. http://audi-urban-future-initiative.com/blog/piloted-parking-future-mobility.
18. National Population and Talent Division. Jan. 2013. *Population White Paper: A Sustainable Population for a Dynamic Singapore*. Singapore: Prime Minister's Office.
19. Piacentino, Giulio. May 2011. *Shortest Walk Gh.* Grasshopper3D. McNeel Europe. http://www.food4rhino.com/project/shortestwalkgh?etx.
20. Rodoulis, Stelios. 2014. "The Impact of Autonomous Vehicles on Cities." *JOURNEYS* (12): 12-20.
21. SINGSTAT. 2010. *Census of Population 2010 Statistical Release 3: Geographic Distribution and Transport*. Singapore: Department of Statistics.
22. TomTom MyDrive. 2016. *TomTom International BV*. https://mydrive.tomtom.com/.
23. Turner, Alasdair. 2009. *Genetic Algorithm.* Processing. http://www.openprocessing.org/sketch/3101.
24. Zhong, Ming, Pawan Lingras, Will Blades and John Douglas Hunt. 2008. "Evolving Parameters of Logit Models Using Genetic Algorithms." In *Canadian Transportation Research Forum.*
25. Zhou, Bin (Brenda), Kara M. Kockelman and Jason D. Lemp. 2009. "Transportation and Land Use Policy Analysis Using Integrated Transport and Gravity-Based Land Use Models." *Transportation Research Record,* 2133: 123-32.

A Pedestrian-centric Design Strategy: Melding Reactive Scripting with Multi-agent Simulation

Xiaoran Huang, Marcus White, Mark Burry

The University of Melbourne
Melbourne, Australia
{xiaoran.huang, mrwhite, mburry}@unimelb.edu.au

ABSTRACT

Over last two decades, walkability has been increasingly recognised as a pivotal component for urban liveability and sustainability. As a result, facilitating pedestrian-friendly environments is now becoming an urgent need for many urban design and planning projects.

This research investigates a computer-aided design strategy to optimise urban forms to enhance precinct walkability. Agent-based modelling (ABM) is used to simulate both mobile pedestrian behaviours and immobile built environments. Urban forms are evolved informed by walking, taking multiple design parameters into consideration. The principle of *reactive scripting* is applied to keep designers in the simulation loop, allowing them to make critical adjustments during the concept design process. Acting as the procedural core, a walking index system based on precedent research is encoded and used for the evaluation process. This method is applied and tested against a practical scenario in Melbourne, Australia. The investigation site is situated on the Arden-Macaulay precinct in Melbourne's inner North, which will be transformed from its former industrial area to a sustainable mixed-use community.

Through this case study we demonstrate how this transformation from industrial to mixed use commercial and housing can be shaped by adopting our pedestrian-centric ABM modelling approach, addressing a range of spatial and temporal urban walkability concerns. The flexibility of our approach and its successful demonstration in the Arden-Macaulay project suggest significant potential for improving walkability in other urban scenarios throughout the world.

Author Keywords

Agent-based modelling; walkability; design method; pedestrian simulation, reactive scripting.

ACM Classification Keywords

I.6.1 Simulation and Modelling; J.6 Computer aided design

1 INTRODUCTION

Walking is one of the most fundamental transport modes. Almost everyone walks, and walking is a constituent part of every journey in the city [1]. There is a growing and compelling body of research concluding that improving pedestrian experience can contribute to forming a healthier, more livable and more sustainable community [3, 11]. Therefore, facilitating a walkable environment has become a considerable objective amongst many city planning schemes.

To evaluate the pedestrian experience, one of the most widely-used methods is the Walkability Index (WI) which translates physical urban attributes into the readable cumulative indices. This system may vary in different urban conditions; scholars and research institutions like Billie Giles-Corti, Lawrence Frank and the Australian Urban Research Infrastructure Network (AURIN) have developed independent WI based on observations and investigations from diverse perspectives [10, 12]. The WI is evident when it demonstrates a static urban scenario, providing intuitive evidence for urban designers and planning consultants. This methodology can be further enhanced, however, since pedestrian friendliness does not solely depend on built environment properties but also individual and social characters [12]. Pedestrian behaviour is dynamic and in many cases include stochastic phenomena that a static description alone is an inadequate representation on its own. Simulating walking movement in a dynamic manner could therefore fill the gap, and it may suggest how certain urban features can positively affect pedestrian experience at the local scale, providing evidence for more appropriate design decisions.

To accommodate this objective, a multi-agent system is proposed in this research. Agent-based modelling (ABM) has been used for pedestrian simulation for more than twenty years and it is considered to be a suitable technique for this purpose [4]. In general, ABM is a system that contains a collection of different agents where each agent is autonomous and follows basic rules. The agents interact with each other during the simulation and during which complex phenomena may emerge, which are usually closer to the real scenario [6]. Developed in the 1940s, ABM was implemented in many fields and has been redefined as an applicable strategy due to various aims: Craig Reynold created an agent-based definition for 'flocking' behaviour in the late 1960s while ABM has been used for stock market and emergency evacuation simulations commencing in the 1980s [17, 5]. Compared with those applications, using ABM in urban design domain is a relatively late story, and only until this century has the computing power

exponentially increased sufficiently for mass-pedestrian simulation to becomes feasible.

Nowadays, ABM tools are more widely applied and designers have many more options than a few decades ago. Nevertheless, the opacity of common agent-based applications is still a considerable concern: usually, educational platforms are easy to access but less powerful while commercial ABM are computationally advanced yet expensive.

In addition, most of standalone toolboxes are difficult to couple with popular 3D urban design modelling environments, which disconnects the ABM analysis from an iterative design process or at very least reduces the number of iterations possible in practical projects.

To overcome these limitations, in this research we aimed to develop a more convenient design-software integrated assistant system in popular 3D modelling software Rhinoceros™ utilising graphical algorithm editor, Grasshopper™, suggesting an eligible operating environment without the steep learning curve of the specialist software. This design strategy also employed the concept of reactive scripting, a programming principle where specified decisions for the designer are waiting for execution only when certain conditions or events are met [7], allowing end-users to set up different criteria to accommodate potential moderations and, in this case, generate revised urban forms accordingly, based on emergent properties that the ABM provokes.

Incorporated with pedestrian ABM and reactive scripts, we have applied this strategy to test a practical case study in the Arden-Macaulay precinct, inner city Melbourne. Enhancing precinct walkability has been set as the predominant task for this project. Different scenarios and additional conditions were employed to examine whether this method is capable of providing swift and appropriate feedback, and ultimately, revealing potential for further design implementation.

2 BACKGROUND AND LITERATURE REVIEW

2.1 Walkability and current assessment method:

Walking is one of the pivotal movements of human beings. Today, although alternative options are available for long range mobility including transportation, walking is still the way we 'finish the last step', and is considered as the most efficient method for short distance movement [12]. Moreover, the significance of walking as a leisure activity has been recognised increasingly in last fifty years [3]. Research linking walking and both physical and mental health [1, 3, 10, 11] have encouraged the government and citizens to improve walking behaviour and understand that people are not just walking as a mode of transit but a way to maintain fitness as well as for relaxation.

Walkability is, in general, a measurement that describes how a natural or a built environment is "friendly" to walking [10] and could potentially be extended to a larger extent to "which the environment is friendly to the presence of people walking, cycling, visiting, or spending time in a particular area." [1] Amongst all relevant research and practices, advantages of enhancing walkability can contribute to following six aspects: Health, Energy Consumption, Happiness, Mobility Choices, Local Economy, and Social Capital [1].

Though there is no universal agreement on what are the definite aspects that influence walkability, it is possible to infer known factors with particular hierarchy. According to related research by Giles-Corti, the perception of determinants of walkability can be classified into threefold: Individual characteristics; Social environment characteristics; and Built environments characteristics [6]. A wide range of actors are involved in the perception of walkability, and the measurements are different in diverse groups. Aschwanden concluded that there are three main methods regarding measuring walkability: crowd-based rating, geographic indicators and graph-based measures [2]. Amongst all these approaches the geographical indicator/environment index measurement is the most prevailing method and has been transplanted into many GIS platforms.

2.2 ABM and Urban Design

In the last two decades, agent-based modelling is becoming an emerging simulation technique in many disciplines. Comprising of actions and interactions between autonomous agents, ABM makes it possible to form and describe a complex system. Unlike the Cellular Automata (CA) models which activities do not actually move or migrate, what typical ABM required are "mobile cells," which would then admit an entire range of action and interaction effects relevant to dynamic environments [4]. Hence, in many desired domains, multi-criteria decision-making, emergent phenomena and adaptive mechanism could be further tested: many have been proven useful, for example, epidemics simulation, market assessment, and social behaviour predictions [13]. In recent years, inspired by burgeoning CAD techniques, designers and researchers were starting to become aware of the power of ABM and implemented it in many prototypical projects [4].

The idea of agent-based modelling can be tracking back to late 1940s. As its procedure is considered extremely computationally intensive, it did not become widely employed until the 1990s. ABM has a direct historical connection with the complex adaptive system (CAS) which initially motivated by investigations into adaptation and emergence of biological and mathematical systems. The term 'agent' and its correlation with CAS have been firstly mentioned in two decades ago [14]. In the 1970s, Thomas Schelling designed one of the earliest agent-based model concepts in his paper "Dynamic models of segregation". While by the late 1980s, the 'flocking model' has been engaged by Craig Reynold, which is considered one of the

first biological agent-based models [17]. With the appearance of high-performative computer and data expansion, ABM was finally entering its era by the end of last century.

The applications of ABM in urban design domain were not properly realised until the late 1990s. Turner, in 1996, was considered as the first one which shows how ABM can be realised in micro-levels of an urban scenario [5]. Thereafter, many prominent agent-based planning models have been proposed by Portugali and Coates [9, 16] and soon, in precinct level, the ABMs have been rapidly tested. In an early time of this century, a space syntax based ABM has been developed by Turner and Penn [15]. This technique assumes pedestrians' movement behaviours are dominated by destination selection, the field of view and steps taken between decision points. In this approach, an agent's action is not only guided by an instant perception of the environment but also by its knowledge of the surrounding environment. In many cases, ABM needs to be compiled with other modelling strategies, and a synthetic methodology has been implemented by Aschwanden where both procedural modelling and ABM are well aggregated and correlated [2]. The procedural models are used to describe a static, and geometrical urban condition while ABMs are applied to enrich the whole scenes with constantly interactive behaviour. To date, most ABMs are complicated and hard to read that the demand for 'lightweight' tools should not be underestimated. PedCatch is a simple agent-based walkable catchment device design by Badland and White [3]. This online application can be easily accessed from different web browsers, and the final output is highly-visualised, allowing different users to evaluate the accessibility from potential nodes.

From academia to industry, different ABM toolsets were designed for many particular objectives. For instance: 'NetLogo' and 'Processing' for interactive design and academic prototypes; Anylogic' and 'Oasys' for sophisticated transport and logistic simulation; 'MASSIVE' and 'Miarmy' for industrial level crowd animation modelling, etc. Amongst all these platforms, commercialised applications are usually more powerful but expensive and hard to access, while open sourced tools are often too 'monotonous' and have less potential to make further extension. In urban design field, especially for concept development process, we are still eager for the proper design-oriented strategy where ABM and standard 3D massing model can be well correlated.

3 METHODOLOGY

This pedestrian-centric design strategy employs a tripartite process where walkability index, multi-agent system and reactive scripting are melding together. It formulates a feedback loop which urban form could continuously be optimised concerning pedestrian behaviour and designer's adjustments, enhancing precinct walking experience under different design speculations. In order to reduce the tool opacity and increase the involvement of designer, this system is fully framed under Rhinoceros 3D, a commonly used modelling software, and its plugin Grasshopper, providing an appropriate strategy when commencing with various design speculations.

3.1 Walkability Assessment

The process began with the evaluation of current urban built environment. Walkability index is applied for demonstrating the physical features within proposed area where criteria/factors are subject to change according to different circumstances. Usually, a city model is required as the start to extracting fundamental information such as road intersection numbers and net dwelling density. This model might not necessarily to be 3D visualised as long as it contains sufficient data. We first developed a prototype in grasshopper to test the viability, started with single proximity factor as a testbed. Site model with road network centre-lines and building footprint has been assigned to the script. For each plot, the script finds an aggregate distance towards any of the attraction points, tells how close a building is to all of the attraction points. We used it to analyse how 'open inner road to public' changes local proximity and visualised the final result with gradient colour (see Figure 1).

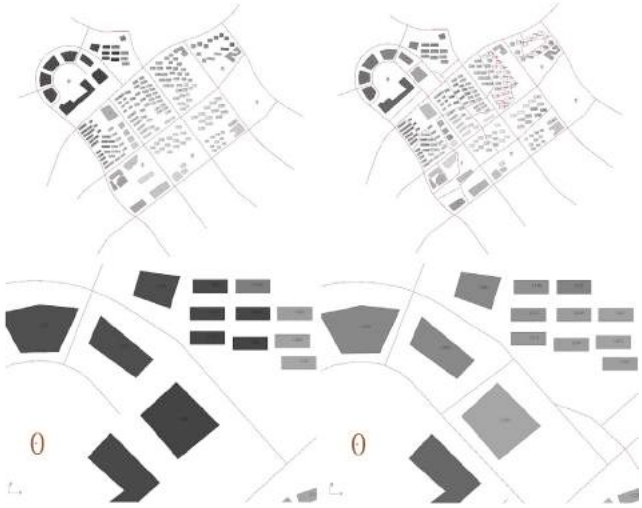

Figure 1. Proximity difference between before 'open up' and after. Lighter grey indicates higher levels of proximity. **Top:** Macro scale. **Bottom:** Micro scale.

Then we intended to encode more complex and sophisticated walkability system into our digital apparatus. The system we proposed is expected to be flexible enough to switch from various of WI standard for different themes. Take Frank's WI for instance, he summarised *Walkability F = Net residential density + 2 * Street Connectivity + Land-use mix + Retail Floor area* [10]. All these data are required as inputs where we can easily extract most of the information from ordinary concept design models (including street network and massing properties). Some attributes like land use and floor number might need to be

further specified and could be acquired without complicated manipulation from GIS platforms or government online datasets.

Street networks are divided into segments for intersection counting while geometrical attributes and Land properties are utilised for other feature calculations, e.g. the net dwelling density is the dwelling units divided by acres in residential use. A grid frame is applied for exhibits cumulative index at each node. To achieve a more accurate and useful analysis, the PedShed method [3] is used to regulate potential walking area for proximity calculation, creating convex hulls which represent real reachable sheds via city networks rather than simplified circles. Finally, the output can be translated as a heatmap which provides a more intuitive evidence to support early design decisions (see figure 2).

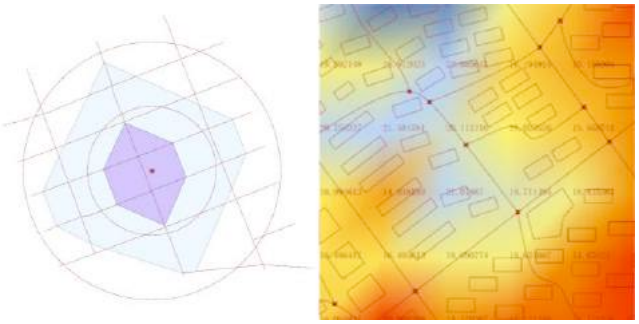

Figure 2. **Left**: PedShed demonstrates real walking catchment for 400m and 800m, compared with traditional circle representations. **Right:** Walkability index heat map within 50m grid frames.

3.2 Pedestrian simulation via Multi-agent system (MAS)

Walkability index can be used to represent how a built environment is friendly to walking, demonstrating pedestrian preferences in a broader context [11]. However, the pedestrian behaviour is usually too complex and cannot be simplified as flowing on the most walkable route only. People often walk to their destinations with diverse purposes, and there are many emerging behaviours in our daily life. For instance, young students may choose the shortest route when they are late for school though the streetscape is less preferred for walking; pedestrians might slow down their speed or quickly stop when picking up phones; shoppers are often wandering around when they have no specific objectives. A multi-agent system can, therefore, introduce individual and social characteristics which allowing designers understand how micro scale features could influence walking experience.

The Multi-agent system we proposed including two major elements: typical mobile pedestrian agent and immobile environment agent, each of them is constructed with different sub-entities. The pedestrian agent is used to mimic the walking behaviour and may contain multiple actors with diverse features. Chen characterised three types of agent behaviour modes: Reactive agent which wandering around without predetermined orientation or itinerary; Proactive agent who has the intention to select destinations, moves and stops due to its own interests; and Motivated agents that quickly move towards a target with a clearly defined purpose. In our system, we decided to construct virtual forces to guide agent's behaviour without applying confined hierarchy as a shopper can be oriented to a certain location but may still sometimes be "wandering" along the street. Those forces are assigned differently with unique weights and possibilities for each agent type, regulating the entropy of the whole system. Basic settings of individual and social characters can be found in table 1.:

Environment agents are immobile entities who can change their conditions or morphologies to interact with pedestrian agents. They can be either artificial entities such as buildings and traffic facilities or natural elements like shade trees or grassland. Those immobile agents are expected as visiting nodes that attract or repel certain types of agents and recording the number of them. All forementioned functions have been realised in Grasshopper with open-source libraries and self-scripted C# components.

To test our model, we ran a benchmark in a theoretical art gallery pavilion where two types of agents, individual visitors and student group, are implemented. The simulation starts from two emitters (individual and group entrances) where artworks (the environment agents) are allocated in the cylinder spaces and interior wall (the boundary). Individual agents are set with higher wandering force and maximum speed while alignment and cohesion forces are particularly applied to students to ensure the whole group steered together. This simplified test articulates the technical availability of this multi-agent system and reveals its potential to model the anticipated behaviours of the pedestrian (see figure 3).

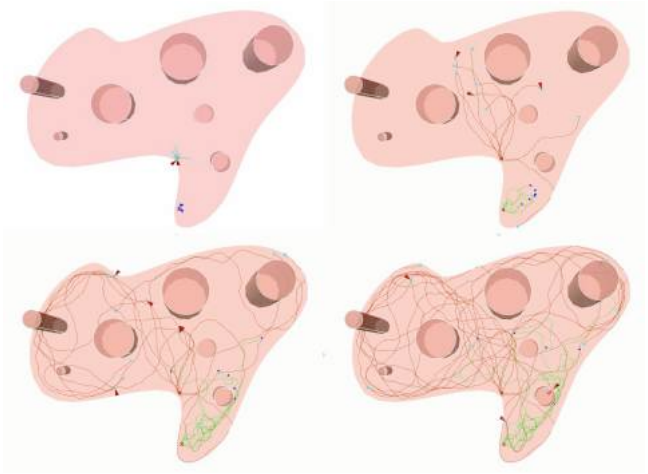

Figure 3. Two types of agents with different settings (red tail = individual agents; green tail = student agents). **Topleft**: step = 0. **Topright:** step = 50. **Bottomleft:** step =100. **Bottomright:** step=150.

Individual agent settings	
Max speed	The highest speed an agent can achieve during the simulation, depends on what unit is used in the 3D model and the interval time of each iteration. e.g. if the ideal pedestrian speed is 1.33m/s and interval is 100ms this figure would be set as 0.133.
Max force	The magnitude of attracting force an agent can receive is restricted by this number.
Max acceleration	How fast an agent speed can be accelerated due to the type of group.
View	The detecting radius for barrel and social forces
Vision angle	The angle of physical vision an agent can perceive, normally set as 180 degrees.
Lifespan	Time steps that an agent can survive. Can be adjusted according to proposed scenarios.
Initial orientation	Initial speed vector for each agent and can be randomized in certain domain.
Mass	Determine how an agent react with steering forces, higher the number lower the impact a force would affected on the agent.
Emitter settings	
Starting point	The place agents will be emitted.
Number of agent	How many agents will be released from one emitter
Creation rate	Related to simulation interval, this rate decides whether agents will emit once or in every nth step
Social force settings	
Wandering	A force that determines the possibility and intensity of random walk.
Obstacle avoidance	Give a contrast force when an agent approaches an impenetrable obstacle.
Collision avoidance	Keep enough distance between agents, generate a perpendicular force when potential collision is detected.
Contain	A force that keeps agents moving in proposed site.
Alignment	Keep agents move towards the average direction of adjacent companies
Cohesion	Keep agents stay in a relatively close position.

Table 1. Basic agent settings.

3.3 Reactive scripting

Contemporary design strategies commonly present static situations which are not capable of accommodating an iterative design process [8]. Especially in the early stage of urban design projects, objectives and criteria may frequently alter that require designers to adapt quickly. With the dawn of the digital era, we now have the potential to ease this problem. Computational design should not be merely considered as the implementation of fancy tools but rather an integrated mechanism keeping designers "in the analysis loop" whilst probing distinct design possibilities. In this research, we were speculating of how to get urban designers involved in the simulation process, allowing setting thresholds and calibrating model parameters to satisfy the ever-changing urban scenarios.

In 1996, Frederic Boussinot and Laurent Hazard crystallised the concept of Reactive scripts and suggested a corresponding event-driven interpreter which can react to several commands in parallel [7]. The two key commands are **event generation** and **await** which triggers execution till prerequisite events occurred, composing multiple complex behaviours in several ways. The pseudocode can be written as following:

generate E; await E; {puts OK!}

When **generate E** is activated, the **await E** command is immediately fired and *OK!* is printed as a consequence.

This mechanism can be extended to the field of digital simulation where designer determines commands and conditions. Execution is triggered when prerequisites are met, and criteria are subject to change between each two iterations. In our case, the urban morphology is a proper testbed where environment agents can be taken as executors and walkability indices of current urban scenario are considered as preliminary inputs. Pedestrian agents are event generators that are moving toward to different destinations. When pre-set terms are met, the executors will respond accordingly, e.g., a certain amount of pedestrian agents traversed an area where WI is less than predefined figure would cause an optimisation function for adjacent urban built environments. During this process, the designer is a part of the feedback loop who can deactivate the executors as some urban environments are culturally or economically significant that need to be reserved. Moreover, the timer component is employed in our script that we can always pause or break the iteration where conditions and execution commands are demanded to be calibrated, facilitating various design alterations during the development process.

4 CASE STUDY

The proposed site Arden-Macaulay is located in Melbourne, Australia and has been primarily an industrial area since the 19th century which economically supported by manufacturing and production (see figure 4). In recent years, the businesses' nature of this area has dramatically

shifted, which leads to an underutilised domain when considering its proximity to Melbourne CBD. By 2030, the population of Melbourne city is expected to increase by a quarter while Arden-Macaulay is considered as a fertile site to accommodate this rapid population growth with a high standard of liveability [1]. It is essential to keep urban environments welcoming and accessible for pedestrian as the city is expected to expand in a sustainable way.

Our design strategy has applied by starting from the walkability index evaluation of existing urban context, utilising valid Melbourne-based index criteria to generate applicable input data (see figure 5).

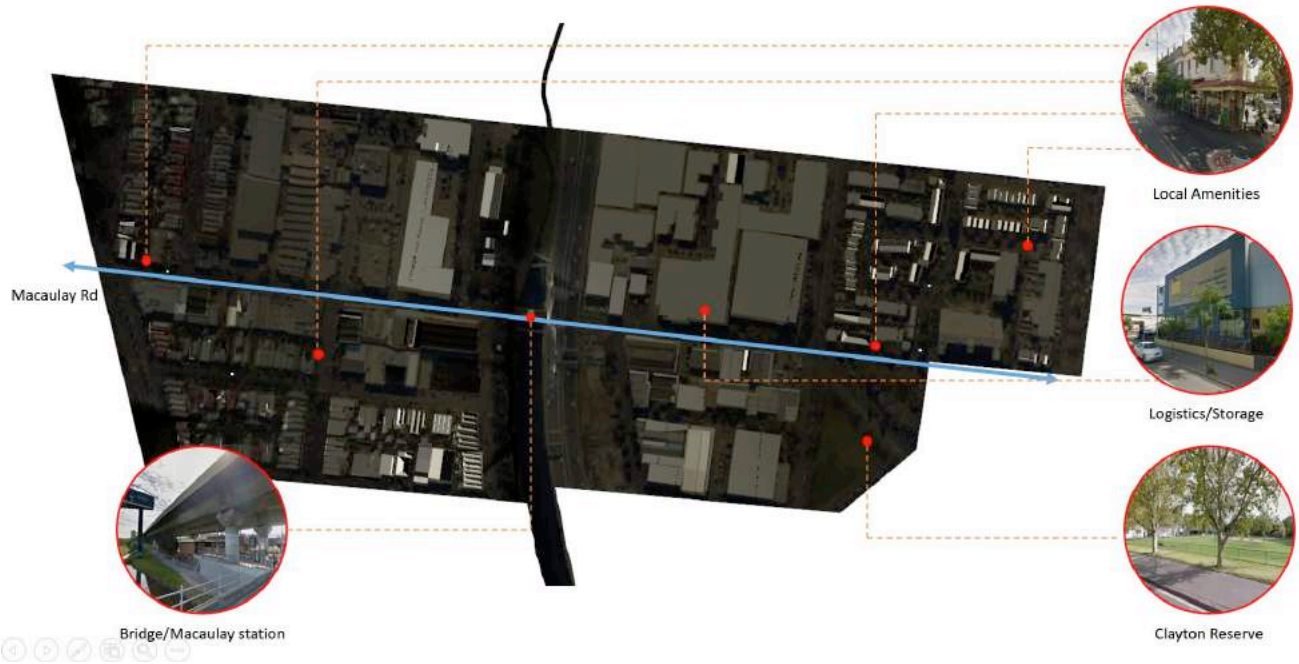

Figure 4. Proposed site with potential important amenities.

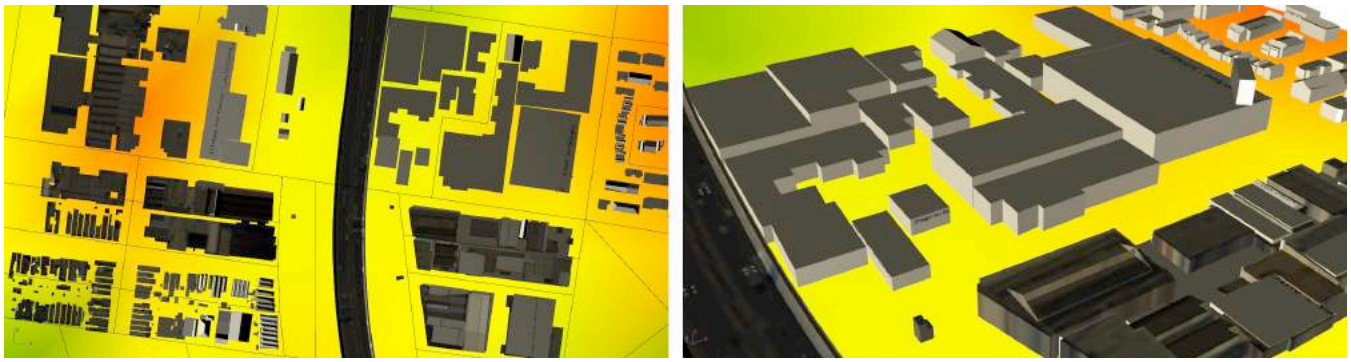

Figure 5. Left: existing walkability index heatmap (red= highest figure). **Right:** current urban morphology along the Moonee Ponds Creek.

We then selected an area with particular walkability issue, which is divided by a local creek and only one bridge has deployed to connecting two separate precincts where new crossings are difficult to achieve due to the toll ways and train lines along the waterfront. In scenario one, the design aim is anticipated by proposing a form transformation of obsolete logistic warehouses which located in the mid-east part of the site. Those urban plots have been assigned as environment agents with reactive commands for shape and land use optimisation alongside with additional constraints, for example. the height limitation. 100 pedestrian agents were applied for the simulation geared with basic social characteristics, median preference for the walkable environment and strong seeking force for retail amenities. At the beginning of the simulation, most pedestrians are keen to target on closer shopping parcels, and long distance movements are infrequent. However, as more agents pass through the adjacent roads of the 'warehouse', environment agents keep reforming by increase floor levels and shift land use properties, boosting local WI and therefore attracts more visitors (see figure 6).

In Scenario 2, we introduced two types of pedestrians which seeking for retail and entertainment facilities respectively. All amenities except reserved buildings are

implemented as environment agents, yet in this circumstance, only height adjustment is allowed that density and FAR (floor area ratio) become the predominant features that influence the walking experience. Though having disparate goals, two pedestrian agent entities are still interacting with each other based on social forces and emerges a complex dynamic equilibrium where building morphologies are evolved in accordance with walking trajectories, enhancing precinct walkability in the whole area (see figure 7). During this process, designers are allowed to intervening the program iteration and set new limitations or thresholds if needed.

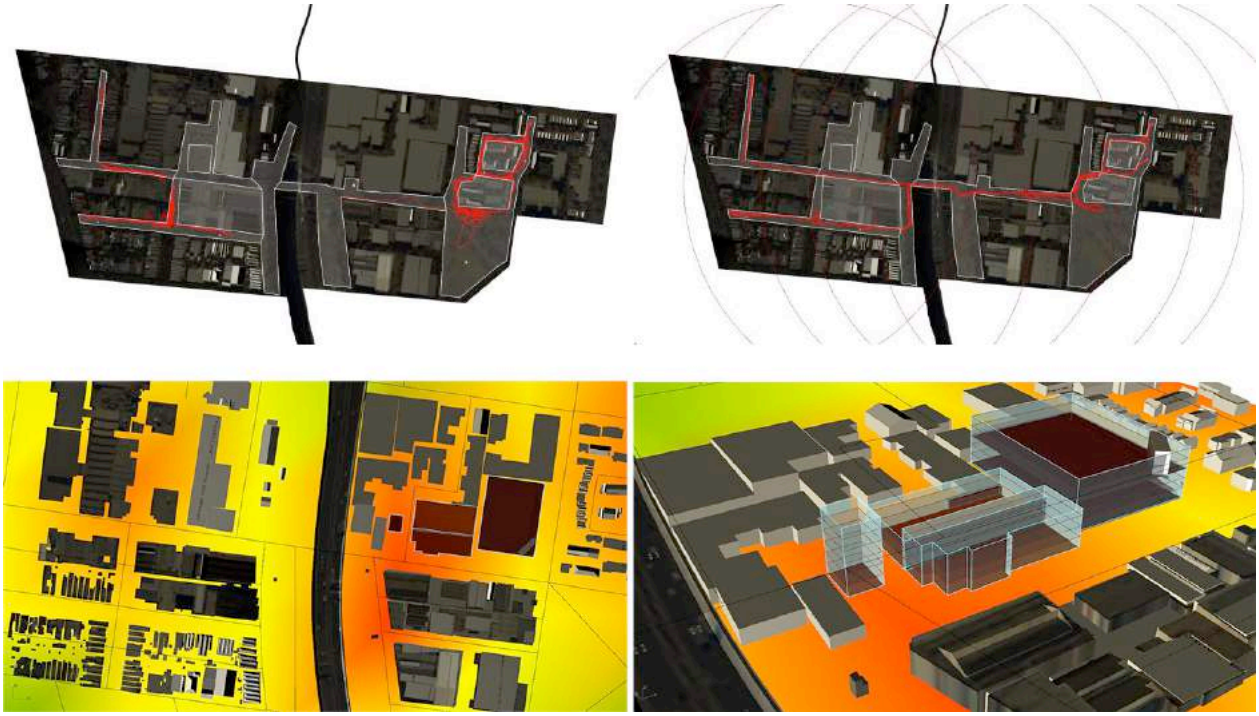

Figure 6. Topleft: step = 150. **Topright:** step = 500. **Bottomleft:** optimised WI. **Bottomright:** optimised form.

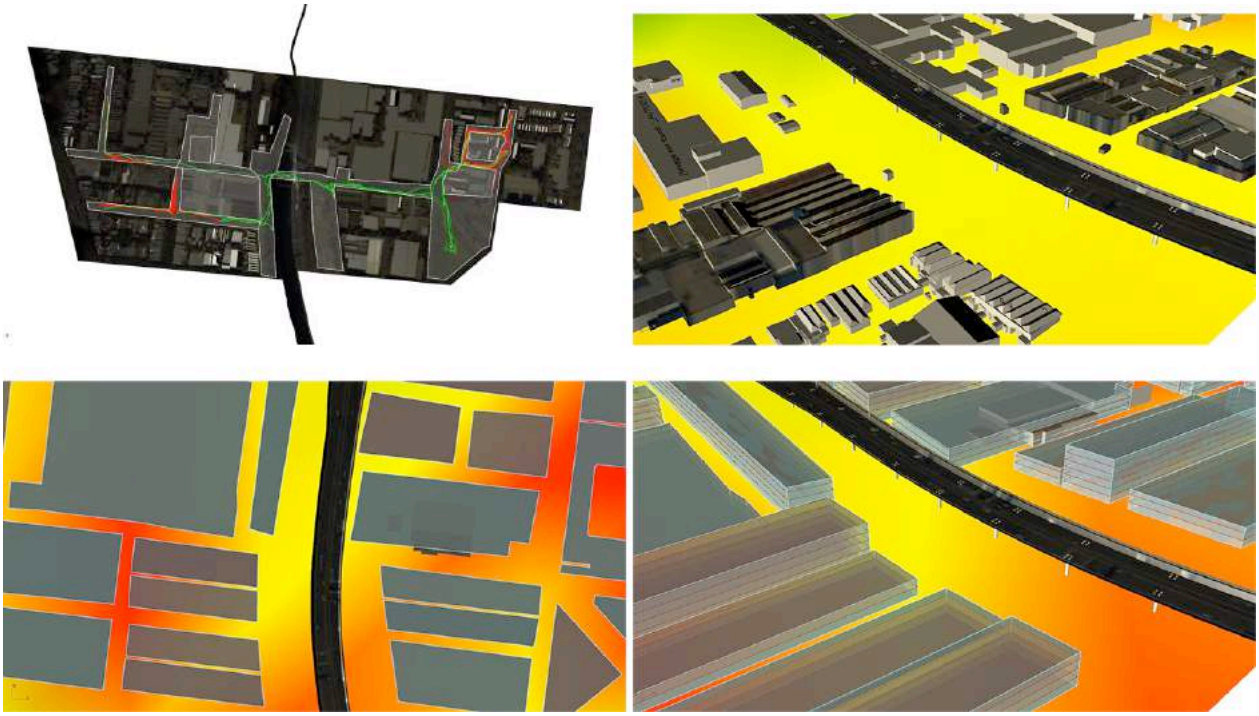

Figure 7. **Topleft:** step = 500. (red=retail agent; green= entertainment agent). **Topright:** existing urban morphology. **Bottomleft:** optimised building foot print and WI. **Bottomright:** optimised form

5 CONCLUSION AND FUTURE WORKS

This research investigated how to integrate reactive scripting and multi-agent system into a walking-prioritised urban design process justified with walkability index evaluation. The results propose a readily available and pragmatic strategy for potentially contributing positively to the discourse of conceptual precinct design and public policy making. A novel dynamic-static coupled methodology structured from individual, social and environmental characters has offered an alternative to conventional top-down approaches where more emergent and spatial-temporal attributes can be articulated and modelled. Self-evolved and optimised built environments are further offered as an outcome from the interaction between both human (designer) and inhuman (system) agencies, facilitating the participation of the designer during the iterative tests which ensure both manoeuvrability and flexibility during 'what if' scenario-based speculations.

The strategy shows substantial potential to engage with the emerging more pedestrian-centric urban design topics. It is currently limited, however, by the demand of abundant data and simplicity of form generation process. For most major cities, urban infrastructure and footprint data can be easily accessed via open-sourced platforms such as Openstreetmap or professional software like ArcGIS™. Nonetheless, for many suburbs and city brownfield sites, it requires a time-consuming in-situ survey to supplement missing data and, therefore, it might be wiser to engage with an alternative approach for walkability assessment, e.g. the crowd rating method.

Also, the morphology modulations in our research are currently based on several simple properties and predefined geometries which are mainly existing building footprints. This restricts the possibility for many urban renewal speculations, and requires further manual adjustment to provide a more pragmatic design output. We continue to discover how to add and eliminate building plots via a genetic algorithm, using a built-in add-on Galapagos to optimise more architecture attributes and properties.

The individual and social behaviours can be further refined and justified via local observation where general patterns are sometimes inadequate to portray local pedestrian characters. Drones and still cameras are increasingly viable for tracking vicinal street walking movements. Trajectory information gained through these devices can be interpreted as deviations (inputs) to regulate the standard model, establishing an interactive pedestrian-centric design process where multi-scale urban simulations are applied.

REFERENCES

1. The City of Melbourne, Walking Plan 2014–17. http://participate.melbourne.vic.gov.au/walkingplan As of November 2014.
2. Aschwanden, G.D.P.A. Health and Place: an analysis of the built environment's impact on walking behavior and health. *Diss.,* ETH Zürich, Nr. 22014, 2014.
3. Badland, H., et al. Using simple agent-based modeling to inform and enhance neighborhood walkability. *International journal of health geographics* 12.1 (2013)
4. Batty, M. *Cities and complexity: understanding cities with cellular automata, agent-based models, and fractals.* The MIT press, 2007.
5. Batty, M. Urban modeling. *International Encyclopedia of Human Geography.* Oxford, UK: Elsevier (2009).
6. Bonabeau, E. Agent-based modeling: Methods and techniques for simulating human systems. *Proc. Natl. Acad. Sci. 99.suppl 3* (2002): 7280-7287.
7. Boussinot, F., & Hazard, L. Reactive scripts. *Proc. RTCSA '96',* IEEE, 1996.
8. Burry, M. *Scripting cultures: Architectural design and programming.* John Wiley & Sons, 2011.
9. Coates, P., Claudia, S. Agent based modelling. *Proc. eCAADe* (1999).
10. Frank, L. D., Sallis, J. F., Conway, T. L., Chapman, J. E., Saelens, B. E., & Bachman, W. Many pathways from land use to health: associations between neighborhood walkability and active transportation, body mass index, and air quality. *Journal of the American Planning Association 72*.1 (2006): 75-87.
11. Giles-Corti, B., Timperio, A., Bull, F., Pikora, T. Understanding physical activity environmental correlates: increased specificity for ecological models. *Exercise and sport sciences reviews 33*.4 (2005): 175-181.
12. Giles-Corti, B. & Donovan, R.J. The relative influence of individual, social and physical environment determinants of physical activity. *Social science & medicine 54*.12 (2002): 1793-1812.
13. Heppenstall, A. J., Crooks, A. T., See, L. M., & Batty, M. (Eds.). *Agent-based models of geographical systems.* Springer Science & Business Media, 2011.
14. Holland, J. H. *Emergence: From chaos to order*. OUP Oxford, 2000.
15. Penn, A, and Turner, A,. *Space syntax based agent simulation.* Bartlett School of Graduate Studies, UCL, 2001.
16. Portugali, J. Toward a cognitive approach to urban dynamics. *Environment and Planning B: Planning and Design 31.4 (2004): 589-613*
17. Reynolds, C. W. Flocks, herds and schools: A distributed behavioral model. *ACM SIGGRAPH computer graphics* 21.4 (1987): 25-34.

The Use of CFD and Wind Tunnel Testing in Wind Microclimate Assessments

Krishan Jayyaratnam, Ruth Shilston and Daniel Hackett

RWDI
Milton Keynes, UK
{krishan.jayyaratnam, ruth.shilston, daniel.hackett}@rwdi.com

ABSTRACT

As Computational Fluid Dynamics (CFD) tools become more powerful and widely available, their use for the assessment of the wind microclimate around buildings has become more prevalent. The key question for wind consultants and planning authorities to understand: is CFD appropriate for this assessment, and what are its limitations in comparison to wind tunnel testing? In collaboration with the Development Division of the City of London, UK, we have conducted a comparative assessment of the wind microclimate around the "Eastern Cluster" of the City using the two tools.

An understanding of the limitations of each tool is crucial and the consideration of parameters beyond the choice of wind modelling tool are at least as influential on the outcome as the choice of tool. The conclusion is that while CFD cannot currently replace established wind tunnel methodology in all scenarios (where strong, gusty winds occur) it can provide a good match in terms of wind comfort. This allows for consultants to use CFD qualitatively, i.e. in early stage designing, or quantitatively for buildings not anticipated being susceptible to strong, gusty winds (with necessary application of professional judgement to determine the likelihood of strong winds causing distress).

1 INTRODUCTION

The interaction of the wind with the built environment has the potential to create conditions at ground level that are uncomfortable (or in extreme cases unsafe) for pedestrian use. This is a particular concern for tall or large buildings where high speed winds, which are down-drafted to ground level and accelerate around the building, create locally windy conditions. The City of London is a prime example of this where windy conditions have already been anecdotally reported in and around the Eastern Cluster.

Lawson [1] remains the definitive reference for conducting wind microclimate assessments in the built environment, and is specified by current planning policy in London [2] in relation to the assessment criteria. Boundary layer wind tunnel testing is also specified in local planning policies within London, and has been the de facto industry standard for use in this type of assessment.

The evolution of computational fluid dynamics (CFD) tools has received attention over the years, with respect to their potential to supplement or replace traditional wind tunnel methods. [3][4][5][6][7] The increasing sophistication (and reduced cost) of CFD in recent years has seen it being increasingly used in practice instead of wind tunnel testing, under the assumption that Lawson's methodology can be sufficiently and robustly replicated in CFD. It is therefore important for consultants and planning authorities to understand the extent to which this assumption is true, and how the tools compare to each other.

This paper discusses the findings of the collaboration between the Development Division of the City of London and RWDI to investigate and compare the two assessment tools of wind tunnel testing and CFD, using the Eastern Cluster of the City as a case study. We will also explore the other important considerations that go into making a robust assessment, with the goal of informing new planning guidance that will be used by the City of London.

2 APPROACH AND METHODOLOGY

An approximately 1km area of the City of London (incorporating the majority of the high rise developments in the City), was tested in a boundary layer wind tunnel at a 1:400 scale, and also simulated at full scale in CFD to allow a comparison of the two assessment tools (Figure 1). 36 angles were assessed for both methods (every 10^{o}).

The wind tunnel test model was constructed from high density foam. In the wind tunnel, the wind approaches the test model over a series of "roughness" elements that are used to shape the wind speed and turbulence profile to represent the real conditions in the City. Wind speed measurements were acquired at 489 locations at street level using Irwin sensors (small pressure sensors which are typically used for urban wind microclimate assessments), and compared with a reference wind speed measurement acquired up-wind of the model at a full-scale equivalent height of 160m above local ground level. Expressing the local wind speeds as ratios allows the model-scale wind speeds to be "scaled up" to full scale for combining with historical meteorological data, or for a direct comparison with the CFD simulation results.

Figure 1. Wind Tunnel Model (left) and CFD Geometry (right)

The CFD simulation was conducted using a steady-state RANS solver (commonly used in these assessments due to lower cost and computing time compared with transient simulations, making them commercially competitive with wind tunnel testing) in OpenFoam, with a k-ε turbulence model. The simulation mesh comprised approximately 17.5 million cells. Wind speed and turbulence profiles were input at the up-wind boundary of the simulation domain to match the profiles used in the wind tunnel.

Following the initial comparison, several aspects of the methodology were varied to demonstrate how relatively sensitive the assessment is to different variables. The meteorological data from London was replaced with that of other cities around the world; the terrain leading up to the Site (represented by the boundary layer wind profiles) were varied; and the quantity of tested/simulated wind angles were changed to investigate their effect on the results of the assessment. By doing this, we have been able to provide some context for how large the discrepancies between wind tunnel and CFD results were, by comparison with other possible variations in the methodology. The results have been used together with the authors' experience of assessing wind in the urban environment to recommend best practice/minimum requirements for a robust wind microclimate assessment, using either wind tunnel or CFD methodologies. The graphics shown in this paper show the CFD velocity ratios for a specific angle as contour plots with the wind tunnel results for the same angle for each sensor location (shown as spheres) overlaid on them.

3 WIND TUNNEL AND CFD COMPARISON

The results from the wind tunnel and CFD assessments have been compared, in order to understand the differences and similarities between the two assessment tools. This is discussed below, using four key areas of the City as examples to highlight the comparisons.

3.1 Eastern Cluster

The Eastern Cluster consists of 6-8 Bishopsgate, 22 Bishopsgate, 1 Undershaft, and 122 Leadenhall. The prevailing south-westerly winds create a pressure difference between the western side and the central and eastern parts of the cluster. As a result, relatively higher wind speeds occur along Bishopsgate and Leadenhall Street (west and south of the cluster) with calmer conditions to the east and centrally within the cluster. Additionally, there are windier conditions along Great St Helens (north of 22 Bishopsgate).

Both types of assessments generally agree well in terms of pedestrian comfort (Figure 2). Locally, there is a notable difference towards the north-west corner of 22 Bishopsgate where the wind tunnel results suggest much calmer wind speeds compared to the CFD simulation. This is a good example of how the detail of the geometry used for each study can affect the outcome. The wind tunnel model includes an extra canopy element, along the northern façade of 22 Bishopsgate which was excluded on the CFD geometry. This canopy helps to reduce the suction effect behind the development and therefore reduce wind speeds along Great St. Helens (Figure 3). Without this element the wind speeds along Great St Helens increase and is illustrated in the higher wind speeds measures in the CFD simulation. It should be noted that this is a localised effect, impacting the wind speeds only in this specific area.

The other notable difference is found in the wake of large buildings or groups of buildings where the CFD results tend to under-predict the wind speeds. This is largely due to limitations of the steady-state CFD in solving flow properties in the wake behind buildings (i.e. areas with high turbulence). This has further implications beyond pedestrian comfort, as this is also an area in which strong, gusty conditions would potentially occur (impacting pedestrian safety).

SimAUD 2017 May 22-24 Toronto, Canada

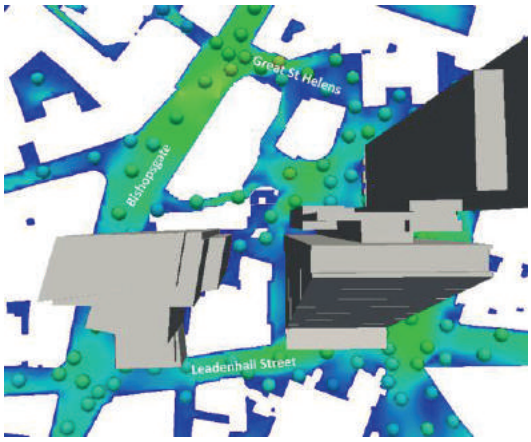

Figure 2. Wind tunnel / CFD comparison (Eastern Cluster). Figure shows mean wind velocity ratio, with wind approaching from 240 degrees

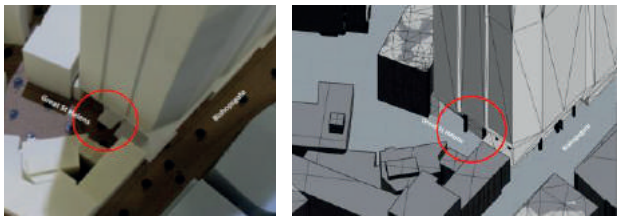

Figure 3. Extra canopy element included in the wind tunnel model (left) and omitted in the CFD model (right)

Summary

With regards to wind tunnel testing and CFD simulations, the highlighted difference in this area of the City was caused by a difference in the geometry. Although some parts of the geometry need to be simplified for the respective studies, some elements will cause significant local differences in the predicted wind microclimate. The level of detail required for a wind study should be appropriate to the assessment and if a comparative study is being conducted between the two assessment tools, then the geometry should be consistent between the two. Furthermore, if simplifications are needed which would impact the results significantly this may mean that one analysis tool is more appropriate than the other for the overall wind microclimate analysis.

Additionally, in areas where there are clusters of high rise developments, the CFD would under predict the wind speeds in the wake region.

3.2 Heron Plaza

Prevailing south-westerly winds accelerate around the north-west corner of 100 Bishopsgate and are channelled along Camomile Street, which is relatively windy compared to the centre of the cluster.

Areas to the north of these two developments are generally calm with the majority of locations having standing wind conditions, which is expected due to the sheltering effect created by these tall developments.

When comparing the raw velocity ratios between the wind tunnel test and CFD simulation, the majority of angles show similar results; however, the CFD under-predicts wind speeds in the wake region of large developments compared to the wind tunnel results (Figure 4).

The largest discrepancies occur between angles 240° (southwest) and 310° (northwest), in the center of Camomile Street between 100 Bishopsgate and Heron Plaza. In the wind tunnel these wind speeds are noted to be higher than in the CFD simulation. Although both wind tunnel and CFD data shown in these plots are a mean value, the wind tunnel results are a mean of all winds (including gusts) during the test whereas the CFD results, as these were run using a steady state solver and as such do not consider the gusts (i.e. transient behavior of the wind).

Conversely, at angle 270°, the CFD suggests there are higher wind speeds close to the southern façade of Heron Plaza compared to the wind tunnel results. The difference is likely caused by a combination of the limited receptor density in this area and the mesh refinement. With a higher distribution of receptors and increased cell density in this area, the wind speed results will likely agree more closely. As this area demonstrates a sharp increase in wind speed over a short distance, the CFD would require an increased density of cells in order to accurately solve the equations of motion in the wake. Similarly, an increased number of receptors in the wind tunnel test would provide a better understanding of the local wind behaviour in this sensitive area.

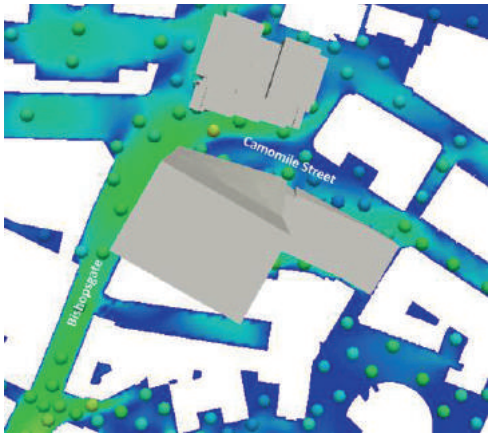

Figure 4. Wind tunnel / CFD comparison (Heron Plaza). Figure shows mean wind velocity ratio, with wind approaching from 240 degrees

Summary

The differences between the wind tunnel results and the CFD simulations in this area are as a result of the wind tunnel testing taking into account gusts (i.e. the transient

behaviour of the wind) whereas the CFD simulations only consider the mean wind speed (i.e. steady state). The higher wind speeds along Camomile Street are dominated by the gusts and therefore are not captured adequately by the CFD simulations.

3.3 South of Eastern Cluster

Compared to other parts of the City, there are relatively calm wind conditions in the area south of the Cluster, along Leadenhall Place, Lime Street and Fenchurch Avenue. The buildings in this area are of a similar height and therefore provide mutual shelter to each other. The prevailing south-westerly winds tend to stay above ground level as the height of these buildings gradually increase from west to east. This area is also fairly well sheltered from the secondary north-easterly wind due to the larger developments to the east and the "cluster effect" encouraging the flow to go around this area as a whole.

When comparing the velocity ratios from the wind tunnel and the CFD simulation (Figure 5), there is a close agreement in the area south of the Eastern Cluster for the majority of wind angles. Generally, both the windier and calmer areas are highlighted in both types of assessments such as the windiness along Leadenhall Street and Bishopsgate compared to the calmer Lime Street and Fenchurch Avenue.

Significant differences start to appear at angles 40 and 50 (i.e. north-east), where the wind tunnel results suggest a higher wind speed at the corner of 52-54 Lime Street. This is similar to the higher wind speeds measured in the wind tunnel on Camomile Street due to the inclusion of gusts. At angles 60 and 70 this area is similarly predicted in both the wind tunnel and CFD. The acceleration of wind round the north-western corner of 52-54 Lime Street is shown clearly with the contoured 'arc' of yellow and the two sensor locations along this arc.

Conversely, at angles 80 and 90, the shape of the 'arc' shifts and reduces in wind speed. This is not highlighted in the wind tunnel results as the sensors are located in areas at the edge of the 'arc' where wind speeds are lower. This illustrates an inherent benefit of CFD, which provides results in all locations, and the importance of careful sensor placement in order to capture the windiest locations in the wind tunnel testing.

At north-westerly angles, 290° to 350°, the high wind speeds at the junction between Leadenhall Street and Bishopsgate is highlighted well between both the wind tunnel and CFD results.

Summary

Generally, the wind tunnel and CFD simulations agree apart from the following:

- The north-west corner of 52-54 Lime Street where the wind speeds are dominated by the gusts and therefore are not captured within the steady state CFD simulations; resulting in lower wind speeds compared to the wind tunnel tests.
- The relatively higher wind speeds around 52-55 Lime Street, where wind tunnel tests did not register the 'arc' around the north-west corner which was predicted in the CFD simulations. This is due to the spacing of the sensor locations around this corner, revealing a limitation of the wind tunnel testing in this scenario.

Figure 5. Wind tunnel / CFD comparison (South of the Eastern Cluster). Figure shows mean wind velocity ratio, with wind approaching from 60 degrees

3.4 20 Fenchurch Street

The wind tunnel results immediately around 20 Fenchurch Street show that there is large change in wind conditions over a short distance as the majority of the surrounding streets have sitting or standing wind conditions. This sudden change in wind conditions, over a short distance, would be noticeable to a person walking through the area.

These wind conditions are caused by typical building-induced aerodynamic effects (such as down-draughting and corner acceleration already discussed above) and by the 'constricted' nature of the area around 20 Fenchurch Street giving the impression that this area is windier than other areas around the City of London. It is also notable that the 20 Fenchurch Street building is relatively isolated from other tall buildings in the area, and so does not benefit from the mutual sheltering effect of other parts of the City.

The CFD results highlight that for a wide range of angles (60° to 350°) the wind speeds at ground level immediately around 20 Fenchurch Street are higher than other areas. Furthermore, it illustrates how these down-draughted winds channel along the narrow streets, creating locally higher wind speeds. For example, when winds are

approaching from 270° (i.e. westerly winds), there are notable higher wind speeds directly at the base of the 20 Fenchurch Street and winds speeds east along Fenchurch Street and Great Tower Street.

When comparing the wind tunnel and CFD results (Figure 6), the methods agree in highlighting the areas of higher and lower wind speeds. As was the case in the previous areas discussed in this paper, locations in the wake of the taller buildings are typically under-predicted in the CFD results.

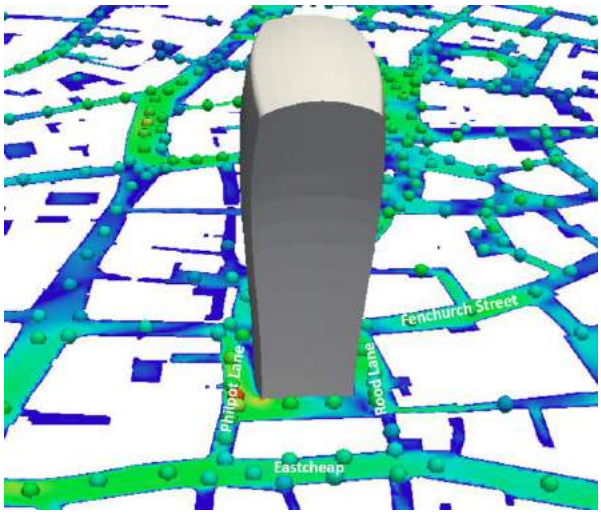

Figure 6. Wind tunnel / CFD comparison (20 Fenchurch Street). Figure shows mean wind velocity ratio, with wind approaching from 150 degrees

At angles 130 to 150, the wind tunnel results highlight a locally higher wind speed to the south-west of the development. The CFD also highlights an area of high wind speeds; however, it is directly at the south-west corner of the development. The wind tunnel results, combined with anecdotal evidence, suggest that this area of windiness may be larger than the area illustrated within the CFD simulation.

These results demonstrate some of the limitations of both tools: the wind tunnel results show data at each sensor location and it is up to the engineer to understand the cause and how far around these areas these wind speeds/conditions extend. However, the CFD results may not represent the actual behavior of the wind in the wake of structures and therefore an understanding of wind characteristics will be needed to distinguish a realistic wake behavior from and unrealistic one. In both cases, it is necessary for the engineer to be aware of the limitations of the chosen method, and to apply experience and professional judgement to ensure the robustness of the assessment.

Summary

The differences between wind tunnel and CFD results are a result of the CFD simulations only capturing the mean wind speed and not considering the gusts. This reduces the area of windiness around the corner of 20 Fenchurch Street as the majority of this area is driven by the "gustiness" of the wind (which is also suggested by anecdotal accounts). However, both tools illustrate the sudden increase in windiness around 20 Fenchurch Street and its surrounding streets.

4 OTHER METHODOLOGICAL CONSIDERATIONS

To provide some context for the magnitude of the differences between wind tunnel and CFD methodologies, a number of other elements of the methodology were varied (namely the modelling of the up-wind terrain, the selection of historical meteorological data, and the number of tested/simulated wind angles). Their effect on the wind microclimate results is discussed below.

4.1 Atmospheric Boundary Layer and Surface Roughness

The atmospheric boundary layer can be described as a variation in wind speed and turbulence with the height above ground. Typically, as the height above ground increases, the mean wind speed increases and tends to a free stream velocity (the distance above ground at which this free stream velocity is reached depends on the surface roughness). Furthermore, the turbulence ("gustiness") of the wind varies tends to decrease with increasing height above ground, being most turbulent close to ground level where the wind is disrupted by trees, buildings or other obstacles.

The slope of the profile varies with approaching terrain and therefore should be selected carefully in order to replicate the expected large scale wind approaching the target Site (based on the Deaves and Harris log law wind profile method noted by Lawson [1]).

To demonstrate the potential difference in the results of the wind microclimate assessment as a result of changing the boundary layer profile, the assessment results were re-analysed using profiles representing open water, open countryside, and sparse suburban terrain, in addition to the suburban terrain used in the primary assessment. The results show that with a more open wind profile, the wind conditions vary (within one comfort category) becoming windier in areas dominated by the mean wind speed and calmer in areas where the turbulence has reduced (Figure 7).

4.2 Meteorological Data Source

Meteorological data is typically collected at airports around the world, and at other meteorological observatories / weather stations. The choice of data source for a wind microclimate assessment should be made to be representative of the wind climate expected at the target Site.

Figure 7. Wind tunnel results around the Eastern Cluster (suburban profile on the left, open profile on the right)

An adjustment to the wind climate needs to be made in order to account for the effects of terrain and topography, both at the meteorological station and at the study area. This is done by conducting a terrain analysis similar to that described in above in Section 4.1.

Meteorological data is typically in the form of hourly or 3-hourly records of wind speed and direction (along with other information such as rainfall, pressure, temperature and cloud cover). This data can be split up ("binned") by speed and direction. The size of these bins gives a model of the frequency of occurrence i.e. bins from the south-west sector will have more recorded events than bins from the north in London. These are then used to weight the influence of the measured wind speeds from the wind tunnel or CFD simulation to determine the overall wind comfort conditions.

The meteorological data represents the largest potential source of uncertainty in a wind microclimate assessment. The following aspects must be carefully considered:

- Choice of meteorological station;
- The period of record;
- Correction of the terrain and meteorological data of the Site; and
- Data quality.

These aspects have potential to change the data used for the wind microclimate analysis significantly and need to be considered carefully when choosing the meteorological source.

This is demonstrated in our assessment by replacing the London meteorological data with data from other cities around the world, some of which are shown in the Figure 8 below for meteorological data taken from New York and Toronto.

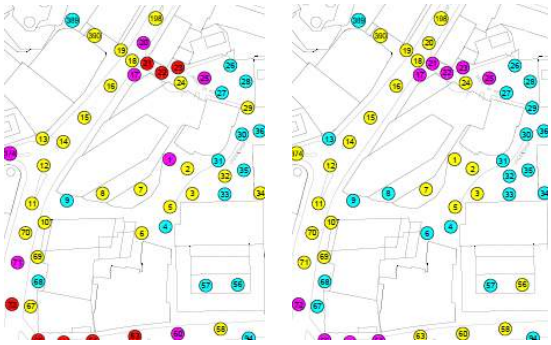

Figure 8. Wind tunnel results around the Eastern Cluster (New York meteorological data on the left, Toronto meteorological data on the right)

4.3 Quantity of Angles

For wind microclimate assessment, the data from the wind tunnel/CFD simulation is merged with the meteorological data relevant to the target Site.

Typically, meteorological data is taken at every 10º or 30º around the compass; therefore, if the wind assessment is carried out from 36 angles this can be directly matched to the meteorological data (interpolation of the data is required if the data is received in 30º increments and the assessment is carried out at every 10º). Conversely, if fewer wind angles are considered, then the meteorological data will be grouped in order to correct for the angles not assessed. This may lead to varying results, depending on the grouping or interpolation of the data.

Wind Tunnel – quantity of angles

When varying the number of angles used for the wind tunnel analysis (12-, 18- and 36-wind angles), there are several locations where the wind conditions change; however, it is noted that these locations were very close to the threshold of the next wind category (and therefore appear to be more sensitive to objectively smaller differences). These changes can cause issues with the acceptability of a location. Changing the quantity of wind angles may change the results at a location and therefore change the usability of that particular space. This would result in recommendations to mitigate the location.

Furthermore, in regards to strong wind exceedances; these are gusts of wind for short durations which occur at a few specific angles and not from a broad range of angles. As a result, these gusts could be missed out if the assessment is based on an insufficient number of angles.

Typically, assessing 36 angles is the most accurate quantity of angles; however, fewer angles can be assessed if justified. For example, if both the target development and surrounding developments have simple geometry; it would be sufficient to test fewer wind angles as the dominating aerodynamics are likely to be captured. With more complex geometries (such as narrow buildings, sharp corners etc.) of the target or its surroundings may

cause narrow bands of wind angles to dominate the aerodynamics. In scenarios such as these, a higher quantity of wind angles should be assessed in order to accurately capture these effects.

CFD Simulation

Typically, CFD simulations are run with 8 or 12 wind angles; however, in RWDI's experience, some consultants consider as few as 4 wind angles, usually selected to be the prevailing wind directions. The reason for the reduced number is often simply to reduce the time taken to undertake the CFD simulation.

Similar to the wind tunnel, this can be appropriate depending on the target development and its immediate surroundings. On the other hand, more complex geometry targets would require a higher quantity of wind angles in order to capture the narrow band aerodynamic effects. A good example of this is 20 Fenchurch Street. From the CFD simulation, there is a sudden change in wind speeds locally around 20 Fenchurch with a small change in wind angles.

There is a large change in velocity ratios when the wind angle is changed from 50° to 60° and to 70°. If a typical CFD simulation is carried out where only the prevailing wind directions were analysed, these sudden peaks in wind speeds would not have been included. Although these wind angles may not be the prevailing directions, due to the high velocity ratios measured, these will still provide a large contribution to the wind conditions.

Summary

The analysis of both the wind tunnel tests and CFD simulations have suggested two keys points in regards to the quantity of wind angles assessed for each study type:

- For wind tunnel tests and CFD simulations, the quantity of wind angles assessed should be determined by the complexity of the target geometry and the geometry of its surroundings; for example, a complex geometry target may require 36-wind angles instead of 16 or 12 in order to capture narrow band aerodynamic effects.
- Both wind tunnel and CFD simulations should consider a larger quantity of wind angles (a minimum of 16) in order to capture a broad range of aerodynamics even if they may occur from non-prevailing wind directions. CFD simulations of fewer wind angles can be appropriate as a preliminary assessment to identify the main wind flow interactions with the target building; however, for a more detailed wind microclimate assessment, more angles should be assessed.

Overall, the higher the quantity of wind angles assessed, the greater the accuracy as narrow-band aerodynamic effects will be captured. However, the quantity of angles can be reduced for smaller developments where the potential for serious concerns related to wind is low.

5 CONCLUSIONS

5.1 Comparison of Modelling Technique

Overall the results of the wind tunnel tests and CFD simulations were largely consistent with areas of high and low wind speeds identified in the same areas across both assessments.

Larger discrepancies were found to occur in the wake of the high-rise developments; and in areas of high wind speed due to corner acceleration or channeling (such as between Heron Plaza and 100 Bishopsgate). This occurs as the CFD has difficulty solving the complex flow features in the wake regions of high-rise developments and around sharp corners.

The wake region is generally under-predicted by the CFD simulation around the City of London, especially to the east of the Eastern Cluster as this area is sheltered by the high-rise developments. This has implications for occasional strong winds (affecting safety) which means steady-state CFD cannot replace wind tunnel testing in all situations.

The CFD simulations allow for a 3-dimensional view of the wind aerodynamics around the City and provide a continuous plot of the wind conditions. Conversely, the wind tunnel results present a limited amount of points to illustrate the local wind conditions and require experience to interpret these results and understand the large scale flow features which drive these wind conditions.

As section 5.6 above describes, wind tunnel tests can provide an analysis on both the comfort and safety conditions around the Site as it simulates the full transient behavior of wind. However, although CFD simulations can solve transient flow, it requires a substantial amount of cost/time and therefore is not typically undertaken by consultants.

5.2 Meteorological Data

The climate data, which identifies the directionality of the wind, determines the majority or the large scale wind flow features around the target. The meteorological data used for the overall wind microclimate assessment should be selected to accurately represent the expected wind climate at the target Site. Additionally, it should include a sufficient period of met data, at least 20 years, if possible as the data may miss infrequent strong wind events that would impact safety.

5.3 Quantity of Wind Angles

Typically, wind tunnel tests asses between 12- and 36-wind angles, whereas CFD simulations typically consider between 4- and 12-wind angles due to the time taken for the assessment. The comparison highlighted that the quantity of wind angles and the specific wind angles chosen resulted in significant differences in the predicted wind microclimate.

Specifically, although assessing 4-5 of the predominant wind directions would capture the prevailing wind behaviour around the City, the smaller scale aerodynamics which would affect localised areas over a narrow band of wind angles would be missed. The assessment of wind comfort and safety is cumulative over the whole season/year and therefore even infrequent winds from angles other than the prevailing wind directions will contribute to the overall result. Additionally, as the strong winds typically occur over a narrow band of wind angles, these would be potentially be missed or under-predicted from the final analysis in a limited-angle assessment.

As a result, the quantity of wind angles used for a wind microclimate assessment should be determined by the complexity of the geometry of the target and its surroundings. Wind conditions around a simple target and surrounding geometry will be dominated by the prevailing winds and is unlikely to have strong winds or other peak wind speeds from the less dominant wind angles. However, a target or its surroundings which has a complex geometry or are orientated in such a way that it is expected the non-prevailing wind directions may dominate the wind conditions, a higher quantity of wind angles should be assessed. For example, a development with sharp corners and extrusions (e.g. large vertical fins) will create a wake which is localised and highly sensitive to directions; therefore, there will be a higher chance of missing the 'peak' wind effect with a larger wind angle increment

5.4 General Conclusions

Overall the comparison between wind tunnel testing and CFD simulations for a wind microclimate assessment showed that although there are some differences between the tools, each can be used appropriately depending on the complexity of the target development and its surroundings. Both play a key part in understanding and quantifying the expected wind microclimate and together can provide a robust wind assessment.

Both the wind tunnel and CFD have their advantages and disadvantages, for example CFD allows for a holistic view of the large scale wind interactions; however, the prediction of wake regions is limited and can result in unrealistic flow features and therefore is a limitation in regards to assessing strong winds and safety. The wind tunnel provides high quality data at the chosen measurement locations however, is limited to the amount of sensors that can be instrumented, which creates a point by point wind microclimate around the City. In each case, it is necessary to understand the limitations of each analysis tool and apply experience and judgment to decide if the output results illustrate the real life full scale aerodynamics.

Additionally, it must be noted that the other elements that make up a complete wind microclimate assessment (which comprise the assumptions made about the effect of up-wind terrain on the boundary layer, the appropriate selection and transposition of historical meteorological data, and other practical elements such as the choice of wind angles to assess) can impact the results of the assessment to a greater degree than the choice of tool. All elements of the assessment must be robust in order to provide an appropriate assessment.

ACKNOWLEDGMENTS

The authors would like to thank the Development Division of the City of London, and the technical teams, model builders, CAD technicians and wind tunnel operators for making the project possible. We would specifically like to thank Ryan Danks for his expert guidance throughout the project.

REFERENCES

1. Lawson, T. V. *Building Aerodynamics*. Imperial College Press (2001)
2. Mayor of London, *Sustainable Design and Construction Supplementary Planning Guidance*. Greater London Authority (2014)
3. Stathopoulos, T., Baskaran, B. A., Computer simulation of wind environmental conditions around buildings. *Engineering Structures Vol. 18*, No. 11 (1996), 876-885
4. Stathopoulos, T., Wu, H., Using Computational Fluid Dynamics (CFD) for Pedestrian Winds. *Proceedings of the Structures Congress, Nashville, TN.* (2004)
5. Bitsuamlak, G., Simiu, E., CFD's potential applications: a wind engineering perspective. *The Fifth International Symposium on Computational Wind Engineering* (2010)
6. Cochran, L., Derickson, R., A physical modeler's view of Computational Wine Engineering, *The Fifth International Symposium on Computational Wind Engineering* (2010)
7. Liu, S. et al., CFD simulations of wind distribution in an urban community with a full-scale geometrical model. *Building and Environment Vol. 117* (2017), 11-23

The Thermal Performance Exploration of Outdoor and Indoor Spaces Using IES & ENVI-met

Amirhosein Ghaffarianhoseini[1], Umberto Berardi[1], Kaamran Raahemifar[1], Ali Ghaffarianhoseini[2], Karam Al-Obaidi[3]

[1] Faculty of Engineering and Architectural Science, Ryerson University, Toronto, Canada

[2] Department of Built Environment Engineering, AUT University, Auckland, New Zealand

[3] Faculty of Built Environment, University of Malaya, Kuala Lumpur, Malaysia

ABSTRACT

Recent studies have frequently reported the relatively high rate of thermal discomfort in urban spaces during summer time in numerous cities. This clearly indicates the crucial need for applying effective passive design and heat mitigation strategies during the early design phase of urban built environments. Reviewing the recent studies in this area, it is found that there is a growing interest in use of ENVI-met simulation for the purpose of thermal performance investigation of urban areas. However, besides the limitations of ENVI-met simulation, the majority of these studies do not fully take into account the impacts of their findings on indoor environments. As a result, this study proposes a new simulation approach using IES and ENVI-met to better understand the design weaknesses of the existing urban settings and explore the circumstances of thermal performance optimization. Hence, looking at two case studies in Toronto and Kuala Lumpur; the study explores and tests the benefits of the proposed two-phase simulation strategy. The output of this strategy can lead to the development of more effective technical guidelines for the design of thermally comfortable urban areas while taking into account the impact of the proposed configurations on both outdoor and indoor thermal conditions.

Author Keywords

Urban Environments, Thermal Performance Exploration, Thermal Comfort, Computational Simulation

ACM Classification Keywords

I.6.1 SIMULATION AND MODELING

1 INTRODUCTION

Design and development of successful urban outdoor environment has become crucially important for promoting outdoor life. However, in many cases, outdoor environments are not highly attractive to the users resulting in low frequency of use due to their thermal discomfort. Hence, it is of significant importance to continuously take into account the effective climate-responsive design principles for achieving thermally comfortable outdoor spaces.

In recent years, a considerable amount of studies has been performed using ENVI-met dynamic simulation [4] to explore the thermal performance characteristics of urban settings and to propose effective guidelines for creating more comfortable outdoor environments [2-3, 5, 7-11]. Nonetheless, despite the great potentials of running ENVI-met simulations as part of the early design stage of projects, particularly its CFD analysis, it also has particular limitations that do not allow fully exploring the thermal interactions in a detailed and fast manner within a reasonable duration of time. Among these limitations, more importantly, the simulations are usually time-consuming depending on the complexity of the model and as a result, testing a large number of different design configurations for optimization purposes is not possible. Moreover, the main focus of the ENVI-met simulations is on outdoor thermal interactions and as a result, while one may achieve a successful design layout for ameliorating the outdoor thermal comfort, the impacts of the proposed design on indoor thermal and energy performance and particularly, indoor thermal comfort, as well as daylight factor are not taken into consideration.

On other hand, recent studies have shown that IES-VE simulations [6] have become significantly widespread due to their strong potentials in assessing the indoor performance of buildings with relatively less strength in CFD analysis and outdoor thermal performance analysis. As a result, in this study, we propose the use of IES-VE and ENVI-met as a two-stage continuous simulation approach to carefully explore the overall performance of proposed designs from both indoor and outdoor perspectives leading to the development of more practical guidelines for building industry.

This paper presents a holistic approach to introduce and test the effectiveness of the proposed simulation approach with the target of concurrently optimizing both outdoor and indoor comfort conditions while achieving more in-depth thermal analysis. It is envisaged that with this proposed simulation approach, future studies in this area, can provide more effective insights for designing urban settings that contribute to the performance optimization of the urban areas from a multifaceted perspective.

SimAUD 2017 May 22-24 Toronto, Canada

2 RESEARCH METHODS

This study attempts to demonstrate the strengths of a two-stage simulation approach using ENVI-met and IES-VE proposed to further enhance the practicality of findings published in recent years using only ENVI-met simulation.

The study has initially conducted continuous field measurement at both focused sites in Ryerson University (Study Area A) and University of Malaya (Study Area B) campuses as shown in Figure 1, following similar studies performed by the authors in the past [1, 12].

It is accordingly argued that while ENVI-met simulations allow researchers to investigate the current status and exploration scenarios for achieving higher level of thermal comfort for the pedestrians, particularly during summer time, these configurations can be further analyzed using IES-VE plus looking at their impacts on indoor environments. Toronto has a humid continental climate with hot and humid summers and cold winters [1] while Kuala Lumpur has a tropical climate with high level of air temperature, humidity and solar radiation [5].

Figure 1. Locations of study areas A and C at Ryerson University and University of Malaya campuses.

2.1 Thermal Analysis Using IES-VE

In this stage, the study investigates the shading levels of the street as a result of the blockage of direct radiations by surrounded building blocks in study area A. As presented in Figure 2, it is shown that buildings are incapable of providing shading during the period of summer while on the contrary, on other months such as December and January when the weather is highly cold and no shading is expected, buildings provide high level of shading at noontime. This simulation shows that the building heights and/or the building orientations during the early design stage can be altered to achieve a more meaningful output while later, ENVI-met simulation can present the thermal interaction and outdoor comfort conditions.

Looking at the variation of shading levels in summer during a single day on July (the month with highest sun position), it can be similarly seen that this orientation and building configuration do not provide shading at any time of the day, particularly for the embedded street, while the street only gets shaded at 18:00. Hence, irrespective of a monthly or daily analysis of shading, IES-VE simulation allows re-adjusting the design, location and orientation of the buildings for achieving more shading (Figures 3, 4 and 5).

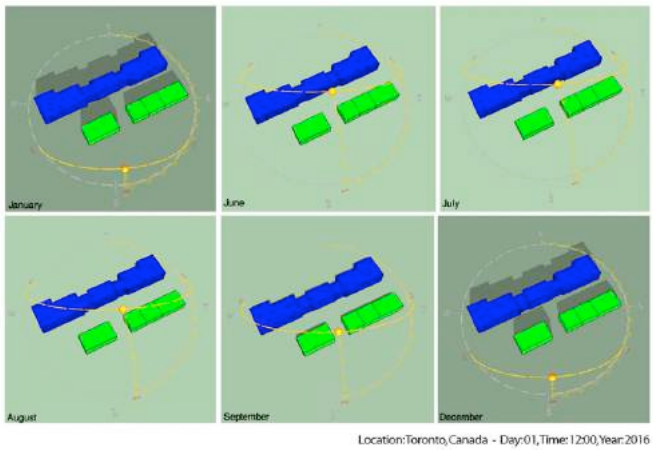

Figure 2. Shading analysis from a monthly perspective.

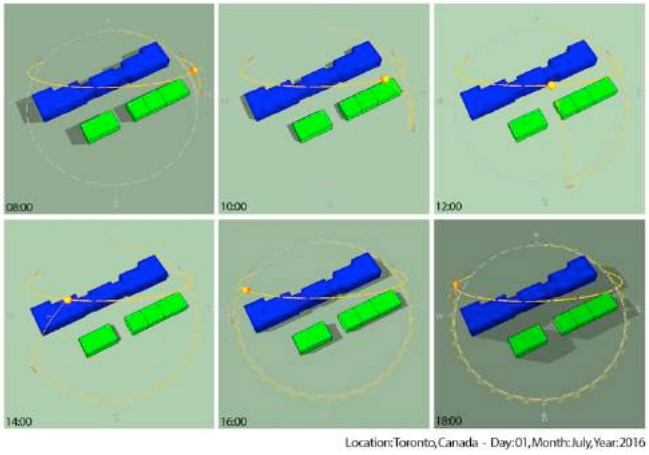

Figure 3. Shading analysis from a daily perspective.

From the perspective of indoor thermal comfort condition of the spaces with the pre-set condition of having all windows (all 90% openable) open continuously with no use of mechanical HVAC systems, the study looks at the current status of natural ventilation and comfort variations. Accordingly, Figure 6 presents that over the course of

summer, indoor temperature ranges between 5 to 35 C besides the extremely wide range of PPD variations (0% to 100%) and PMV values (-3.0 to +2.5). This analysis demonstrates that while in particular days, the indoor spaces can be thermally comfortable, in many other days, the users may feel very hot or cold as the indication of thermal discomfort (Figure 6).

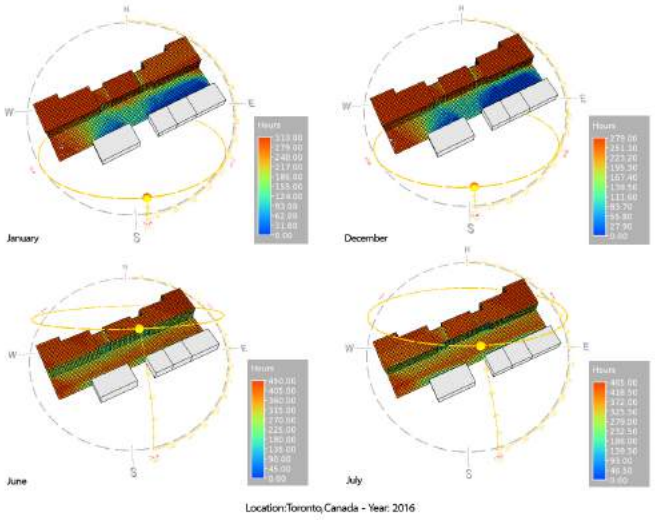

Figure 4. Hours of solar exposure in the hottest and coldest months of the year.

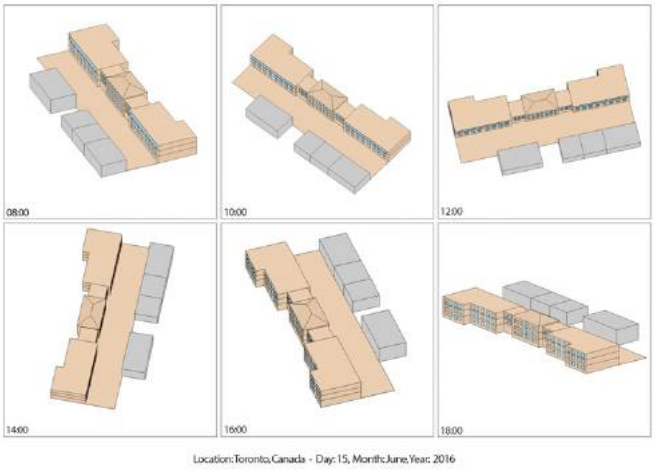

Figure 5. Sun-view position at different hours of a day in summer.

The analysis elucidates that by looking at first days of June, July and August, concentrating on a selected indoor space at the third level in the middle part of the block, an acceptable level of indoor comfort is achieved with PMV values ranging between -1 to +1. Nonetheless, by looking at specific dates such as 14th of June, it can be seen that both dry bulb and indoor temperature values can drop to 4 C resulting in PMV values reaching – 2.6 with up to 90% thermal dissatisfaction. As another evidence of thermal discomfort, looking at 09th of July and 03rd of August, both dry bulb and indoor temperature values can exceed 30 C and as a result, PMV values reach 2 and above leading to a maximum of 80 % thermal dissatisfaction. With the above elaborations, it can be concluded that with the existing design configuration of this building block, its orientation and adjacent buildings, turning off the HVAC systems and only relying on natural ventilation should not be advised.

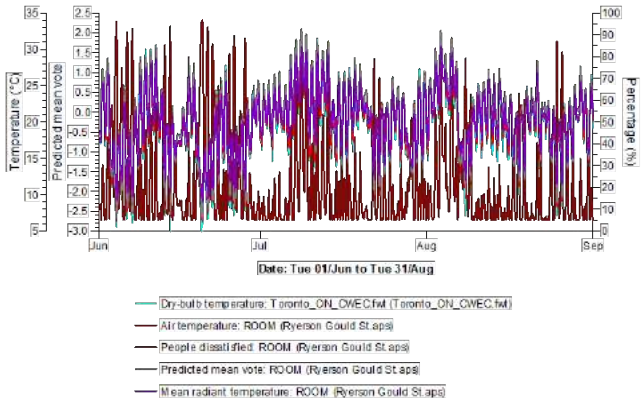

Figure 6. Variation of dry indoor air temperature, PMV, and PPD during the hot months of June, July and August.

Further looking at the variation of calculated data, it can be inferred that over the course of a year, indoor air temperature can get as low as -19 C and as high as 32 C resulting in very hot and cold conditions. The highest record of temperature is in August while it drops to the lowest in January. Similarly, the highest PMV value as 2.09 representing a hot condition occurs in January. This, in the same way, presents the existence of unacceptable thermal comfort conditions in different days throughout the year with the current design condition of this urban building block located within the Ryerson University campus in the city of Toronto (Figure 7).

Further analyzing the current status of thermal performance within the focused urban building block, the study explores the variation of mean radiant temperature (Tmrt) and PMV at the center of outdoor space surrounded by building blocks and the room at the center block located at the top level, as illustrated in Figure 8. Focusing on summer months, it is evidently found that in all three months of June, July and August, there is a significant different between the Tmrt values of indoor and outdoor spaces. Similarly, the variation of PMV values demonstrates that the outdoor space continuously has a considerably higher rate. Furthermore, in many cases, the PMV values of the outdoor space are above 1 representing hot conditions and thermal discomfort. On 11th of July, the highest calculated record of Tmrt for the outdoor space can be seen reaching 49.99 C with an extremely wide difference with that of the indoor space only reaching 30.90 C. This difference reaches to its highest values from 12:00 to 16:00. Likewise, on 2nd of June, the highest calculated record of PMV is observed for the outdoor space reaching 3 while having a considerably wide distance from the indoor PMV values only reaching a maximum of 2.14.

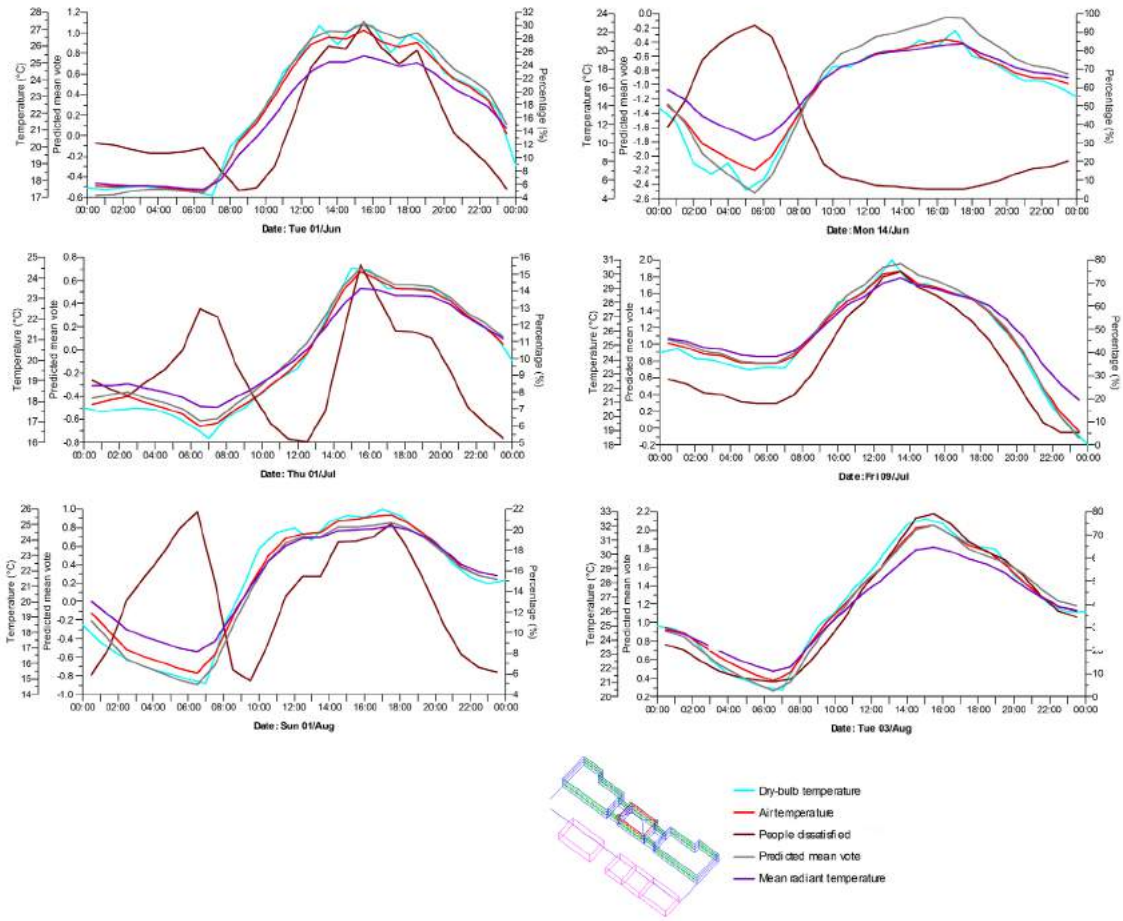

Figure 7. Variation of dry indoor air temperature, PMV, and PPD during particular days in the hot months of June, July and August.

To further debate, while due to the very long winter period in Canada, most people are very open to be exposed to solar radiation and enjoying the hot weather, the PMV values present thermally uncomfortable conditions in many days during the summer.

Furthermore, looking at the whole duration of thermal discomfort in the selected indoor and outdoor spaces, over the course of summer, the outdoor space can be thermally uncomfortable with PMV value above 1 for approximately 677 hours while this duration for the indoor space at the third level of building is 227. Moreover, the study analyzes the number of hours in summer when the level of people dissatisfaction is more than 70%. It accordingly shows that in the outdoor space, for 474 hours, PPD values go beyond 70% while the indoor space's people dissatisfaction can go above 70% for only 118 hours. With such analysis, it can be strongly debated that with the alteration of the design configuration, location and orientation of the selected urban building block, all spaces, particularly the outdoor space, can be substantially enhanced from the thermal comfort perspective.

2.2 Alteration of Adjacent Building Blocks' Height Using IES-VE

With the increasing urban densification in Toronto, it is likely that the Ryerson University campus, being located in Toronto downtown area, will face numerous construction developments of high-rise buildings in near future. Hence, the study looks at the possibilities of enhancing the current status through the impact of increasing the adjacent building blocks' height.

The study compares three different conditions for adjacent building blocks: a) height not increased b) height increased (3 times) c) height increased (6 times). The analysis clearly shows that the increase of adjacent building heights does not have a significant impact on the indoor temperature and PMV values during summer.

On the contrary, increasing the height of adjacent building blocks substantially impacts the Tmrt and PMV values within the outdoor space throughout the focused months. Furthermore, looking at the first days of June, July, and August, the influential role of adjacent buildings' height blocking the solar radiation and their impact on both temperature and PMV values can be seen (Figure 9).

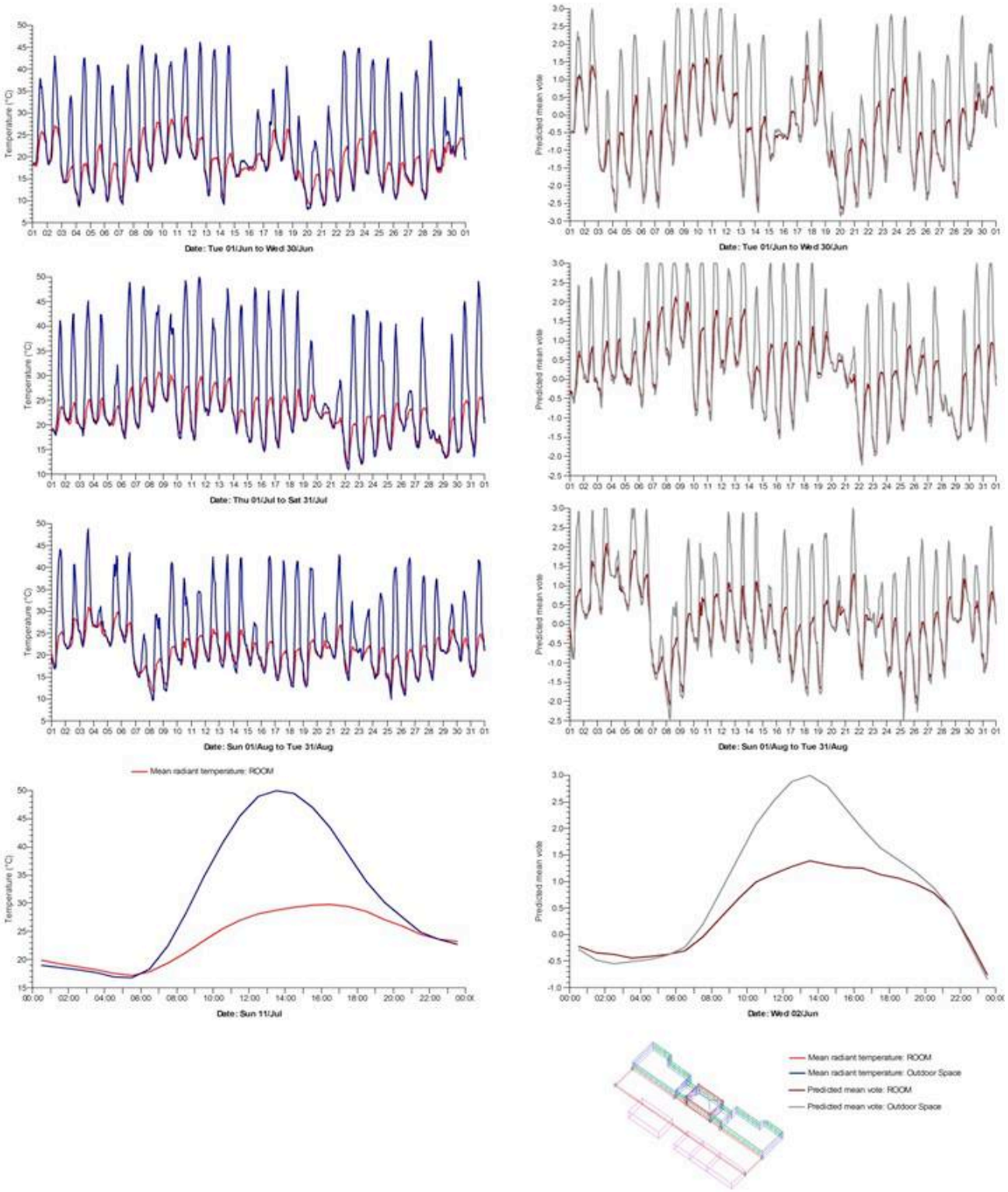

Figure 8. Variation of mean radiant temperature and PMV in the hot months of June, July and August.

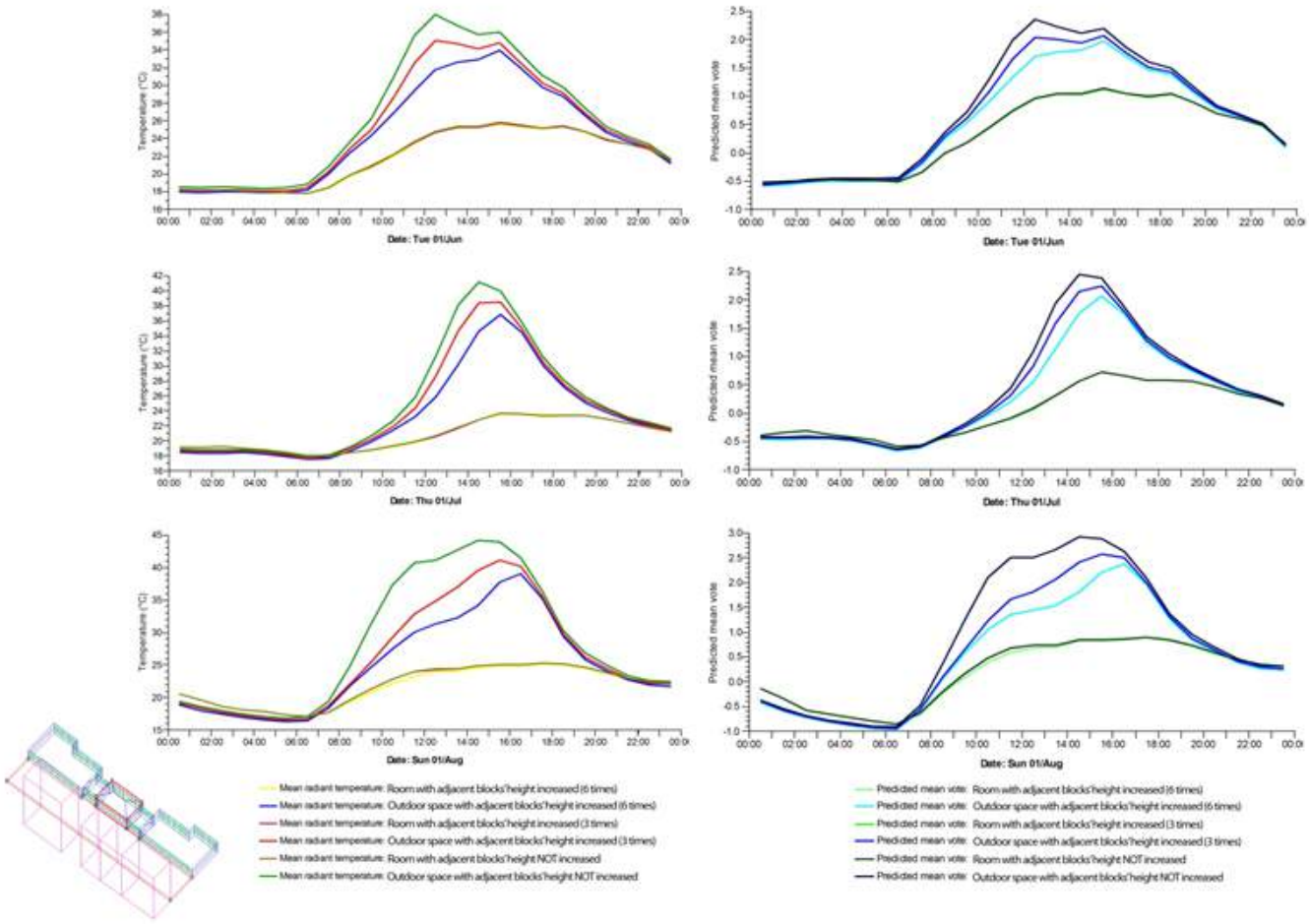

Figure 9. Variation of temperature and PMV values in three different building height conditions.

2.3 Alteration of Buildings' WWR Using IES-VE

In this phase, the study examines the possible impacts of increasing window to wall ratio (WWR) values on both outdoor and indoor thermal conditions. The study looks at three scenarios during the three hot months of June, July and August: a) WWR =20 b) WWR = 50 c) WWR = 80

The simulation results present that the increase of WWR does not have a meaningful impact on the PMV variation of outdoor space and accordingly, the comfort condition remains as the existing condition. Nevertheless, looking at both monthly and daily variations, it is proven that WWR alteration can influence the indoor PMV values. As a result, increasing the WWR values, leads to increase of solar gain and PMV values. Hence, during the days when PMV value is generally above the comfort condition (above 1), having an increased WWR is an unfavorable response to the indoor thermal comfort condition. In contract, during the days when the PMV value is below 1 representing cold and slightly cold conditions, increase of WWR can positively contribute to the indoor comfort.

2.4 Thermal Analysis Using ENVI-met

In this part, looking at study area B, the study investigates the spatial variations of mean radiant temperature in comparison with the levels of direct SW radiation at two critical times of the day (12:00 and 14:00) using ENVI-met. As displayed in Figure 10, the entire area receives relatively high level of direct solar radiation reaching 800 W/m2 and beyond. This can be considered one of the main reasons of observing high levels of thermal discomfort at this period of daytime. Nevertheless, despite these excessive solar radiations, at both 12:00 and 14:00, there are several spots in the site which receive considerably fewer radiations ranging from 200 to 400 W/m2 (referring to the light colored spots).

After comparing the spatial variations with the original aerial map of the selected urban area, it is found that these light coloured spots are exactly highlighted on the location of the existing trees and green areas of the site confirming the strong influence of greeneries, particularly tall and dense trees, towards blocking the sun and providing shade. From another viewpoint, looking at the variations of mean radiant temperature, it is inferred that the same zones which receive high level of PMV values (reaching 4 and above) are in fact

receiving higher mean radiant temperature values compared to their surrounding context. In the thermal discomfort zones as highlighted previously, mean radiant temperature reaches 61.85 to 65.85 °C and even exceeds this range while in other zones of the site, it drops to 33.85 °C and below. Likewise, the spatial variations of direct solar radiation and mean radiant temperature are in reasonable agreement as in general, the areas with high level of radiation embrace high level of mean radiant temperature and those with less radiation have less mean radiant temperature values.

2.5 CFD Analysis Using IES-VE

In this part, the study uses IES-VE simulation to evaluate microclimate conditions and to assess urban canopy layer (UCL) for further exploring the thermal analysis. Therefore, the IES-VE simulation assesses the variation of wind velocity in the selected area of the University of Malaya campus on a developed model from the online street map.

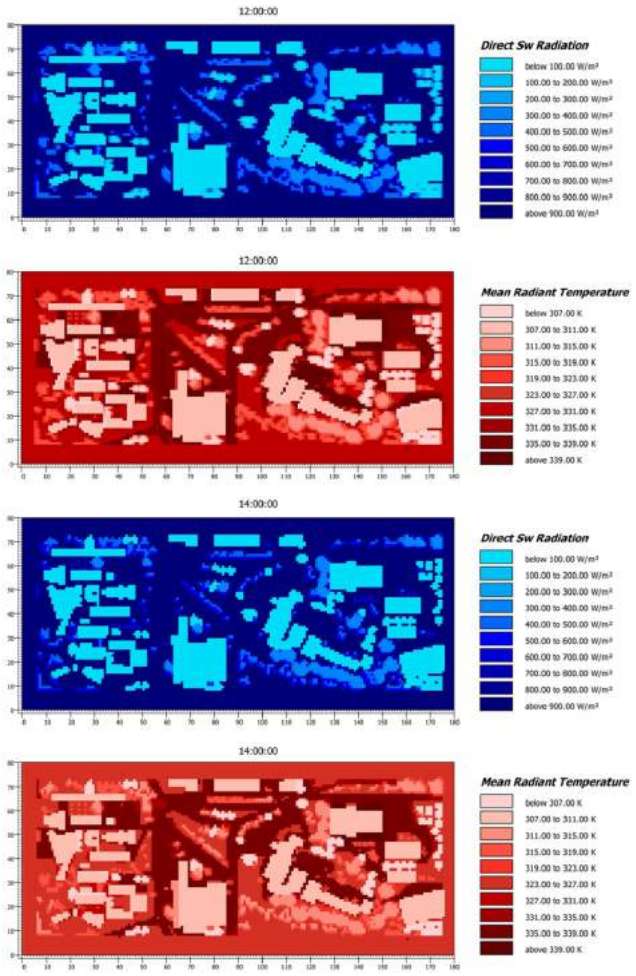

Figure 10. Comparison of the simulated spatial distributions of mean radiant temperature and direct solar radiation.

The study tested the condition of wind velocity in the developed IES-VE model through Microflo (CFD) tool from several directions for the external condition. The purpose of testing the model from different directions is due to the diversity of wind directions obtained from the field measurements which is also indicated by the measurement output that support the condition of unpredictable wind movement in Kuala Lumpur. Figure 11 shows the readings of wind speeds from four directions (0:N, 90:E, 180:S, 270:W). The results indicated that there is no consistency with wind movement which could be dropped to 0 m/s or exceeds 0.8m/s in the site. From the comparison of more than 10 locations, the wind velocity was significantly different when wind directions were various. It is found that taking into consideration several factors such as soft and hard landscape, trees location, shape of trees canopy, and buildings height are considerably important to maintain a desired level of wind velocity.

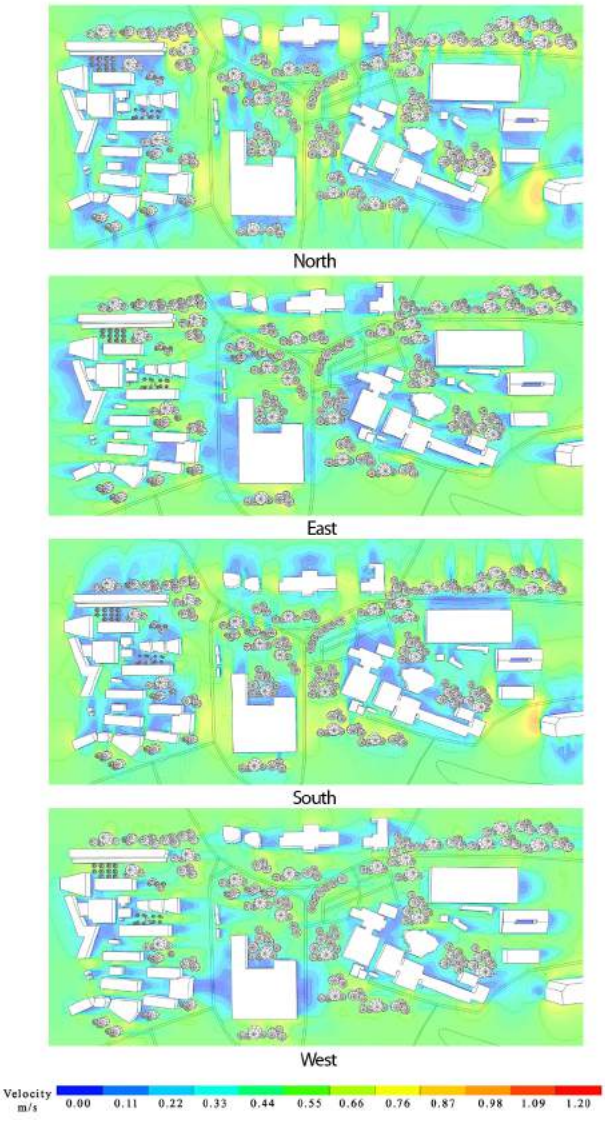

Figure 11. Simulated wind velocity in University of Malaya campus from 4 directions with speed of 1.1m/s.

3 DISCUSSION AND CONCLUSIONS

In recent years, utilization of computational modeling approaches has been a key focus of researchers to understand

the effective design strategies for optimizing the thermal performance of urban areas to achieve higher level of thermal comfort and mitigate the UHI impacts. This study proposes a multi-phase simulation approach using IES-VE and ENVI-met in order to indentify the most effective design configurations for substantially enhancing the thermal comfort condition of both outdoor and indoor spaces. The proposed approach is experimented and modeled, as part of effectiveness testing, at Ryerson University and University of Malaya campuses located in Toronto and Kuala Lumpur. It is believed that this multi-phase simulation approach would be highly promising and can achieve more meaningful output that can be effectively utilized in building industry and professional practice by architects and urban designers. Future studies will look at more complex and detailed computational approaches and attempt to add more phases of simulation to look at more practical aspects and the relationships between the tested variables.

REFERENCES

1. Berardi U. (2016) The outdoor microclimate benefits and energy saving resulting from green roofs retrofits, Energy and Buildings, 121, 217-229.
2. Berkovic, S., Yezioro, A., & Bitan, A. (2012). Study of thermal comfort in courtyards in a hot arid climate. Solar Energy, 86(5), 1173-1186.
3. Chatzidimitriou, A., & Yannas, S. (2016). Microclimate design for open spaces: Ranking urban design effects on pedestrian thermal comfort in summer. Sustainable Cities and Society, 26, 27-47.
4. ENVI-met (2016). "ENVI-met website" Online: http://www. envimet.com
5. Ghaffarianhoseini, A., Berardi, U., & Ghaffarianhoseini, A. (2015). Thermal performance characteristics of unshaded courtyards in hot and humid climates. Building and Environment, 87, 154-168.
6. IES-VE (2016). "IES-VE website" Online: https://www.iesve.com/
7. Kong, F., Sun, C., Liu, F., Yin, H., Jiang, F., Pu, Y., & Dronova, I. (2016). Energy saving potential of fragmented green spaces due to their temperature regulating ecosystem services in the summer. Applied Energy, 183, 1428-1440.
8. Lee, H., Mayer, H., & Chen, L. (2016). Contribution of trees and grasslands to the mitigation of human heat stress in a residential district of Freiburg, Southwest Germany. Landscape and Urban Planning, 148, 37-50.
9. Lin, B. S., & Lin, C. T. (2016). Preliminary study of the influence of the spatial arrangement of urban parks on local temperature reduction. Urban Forestry & Urban Greening, 20, 348-357.
10. Roth, M., & Lim, V. H. (2017). Evaluation of canopy-layer air and mean radiant temperature simulations by a microclimate model over a tropical residential neighbourhood. Building and Environment, 112, 177-189.
11. Taleghani, M., Sailor, D., & Ban-Weiss, G. A. (2016). Micrometeorological simulations to predict the impacts of heat mitigation strategies on pedestrian thermal comfort in a Los Angeles neighborhood. Environmental Research Letters, 11(2), 024003.
12. Wang, Y., Berardi, U., & Akbari, H. (2016). Comparing the effects of urban heat island mitigation strategies for Toronto, Canada. Energy and Buildings,114, 2-1

Computational method for variable objectives and context aware solar envelopes generation

Francesco De Luca and Hendrik Voll

Tallinn University of Technology
Tallinn, Estonia
{francesco.deluca, hendrik.voll}@ttu.ee

ABSTRACT

Daylight requirements are an important factor for the layout and image of cities. In Estonia complex requirements of direct solar access guarantee the right-to-light for existing and new housing buildings. Nowadays different environmental design software permits to calculate the quantity of direct sunlight hours for facades or windows and allows designers to generate solar envelopes. This is an efficient method to calculate the shape of the maximum buildable mass on a plot that allows the neighboring buildings to receive a required amount of direct sunlight. The existing method to generate solar envelopes presents a significant limitation when applied to the Estonian daylight standard. The present work discusses a method that consider specific amounts of direct solar access and take the context into account to improve the actual solar envelope generation method and available tools. The tests carried out in four different urban areas show that the proposed method is superior to the existing. It generates significantly larger size solar envelopes that fulfill the requirements with a small margin of error. The outcomes can be generalized to underline the importance to consider the requirements of specific facades when calculating solar envelopes in urban environments and the incidence of the context layout.

Authors Keywords

Urban design; Solar design; Direct solar access; Solar Envelope; Environmental analysis; Computational design.

ACM Classification Keywords

I.6 SIMULATION AND MODELING; J.5 ARTS AND HUMANITIES – Architecture; J.6 COMPUTER-AIDED ENGINEERING – Computer-Aided Design (CAD)

1 INTRODUCTION

Daylight is the most appreciated source of illumination for exteriors and interiors of buildings for human beings. Its balanced spectrum of colors ensures comfort of vision and enhances the circadian rhythm [11]. Daylight in buildings therefore strongly influences the physiological and psychological well-being of people.

Natural light penetrates the interiors of buildings in different forms: as direct solar radiation, as diffused by the sky and clouds, and as reflected by the surroundings. Direct solar radiation is the most appreciated and it is considered the most efficient source of natural light for its quantity, quality and distribution. The quantity is the intensity necessary to perform different tasks and to perceive the surroundings comfortably. The quality is inherent to the property to render colors properly to make the interiors more pleasant for the occupants [14]. The distribution is the capacity to light the interiors at a remarkable depth due to its intensity and to be uniformly diffused where it is more useful by proper floor, window, or facade layout.

Building and planning requirements set daylight standard to guarantee adequate quantity of natural light into residential premises. Direct solar access is regulated in Estonia by the standard "Daylight in dwellings and offices" [5]. It states that new buildings have to allow the neighboring premises to receive at least 50% of the direct sunlight hours of the precedent situation for each day from 22nd of April to 22nd of August. The present work develops an efficient method for the computation of the maximum buildable volumes to allow specific quantities of direct sunlight on neighboring facades as requested by the Estonian regulation (Figure 1).

The solar envelope constitutes an efficient method to determine the massing of new buildings that have to allow a specific amount of direct solar access on neighboring facades [8]. It is a method that, differently from others, e.g. the undifferentiated setbacks, takes the location, the plot's orientations and size, the distances from the surroundings, and the required time and period of the year during which direct sunlight has to be guaranteed into account [9-10].

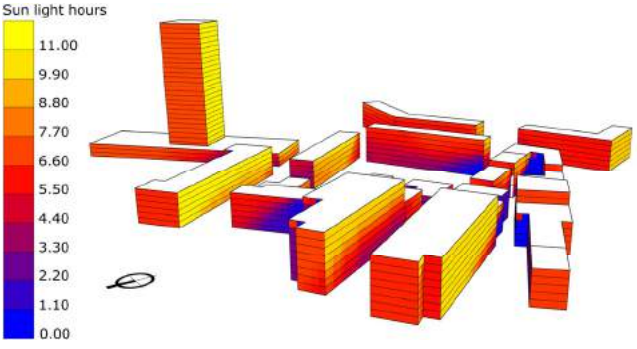

Figure 1. Analysis of daily minimum sunlight hours from 22nd of April to 22nd of August on buildings in the city center of Tallinn.

The solar envelope method as presented by Knowles has been further developed by Capeluto and Shaviv [3] who distinguish between a solar rights envelope and a solar collection envelope. The former is a direct result of Knowles' studies, it is the shape of the maximum volume on a given plot that guarantees direct sunlight on neighboring facades during specific hours and periods of the year. The latter is the shape derived by the minimum heights on a given plot at which the building's windows should be located to receive direct sunlight during specific hours and periods of the year without being obstructed by neighboring buildings.

2 EXISTING METHOD

The estimation of the size and shape of the solar envelope can be done on paper using the data about solar azimuth and altitude at the required time and days [1]. Nonetheless, with the calculations on paper it is possible to determine solar envelopes only for simple conditions, with a tedious process and getting imprecise results for more complex environments.

Computer tools to automatically generate solar envelopes have been developed for decades by now. Uen-Fang devised the software SolVelope for maximum volumes allowed on rectangular plots [16]. Juyal, Kensek, and Knowles proposed the tool SolCAD that takes into account irregular plots and different types of surrounding buildings [7]. Capeluto and Shaviv developed the automated system SustArc that includes the solar collection calculation [2].

Nowadays environmental design software and tools integrated into parametric design applications based on the existing method permit to generate solar envelopes [6-12-15]. The requested inputs vary depending on the software or tool. The most advanced applications use latitude of the location, area of the solar envelope, baseline of the surrounding facades, start and end hours of the day and period of the year during which direct solar access has to be guaranteed. The shape generated is an irregular polyhedron that defines the maximum envelope of the future building.

The existing method has a significant limitation in relation to the Estonian standard. It is the start and end hours input, that can be used to generate solar envelopes only for ordinances that require specific hours per day (e.g. from 10 am to 14 pm, at noon) and for single facades, but it is not adequate in case the requirement specifies the amount of hours every day, without specifying when during the day, and for different facades with different orientations. Each facade, and in an urban contexts even each window, gets a different amount of direct sunlight per day. To guarantee the required quantity to all the facades it is necessary to include in the calculation the real amount of sunlight hours received by each facade per day in the existing situation.

An additional limitation, related to the available environmental design tools, together with the start and end hours input, is not including the context in the calculations, even though it is an important factor for the generation of the correct shape of solar envelopes in urban environments.

3 PROPOSED METHOD

To overcome the discussed limitation the authors proposes a method to generate solar envelopes that takes the actual amount of direct solar access hours on each facade and portion of it into account. The proposed method, tested in different urban conditions, has proved to be significantly more efficient than the existing method in cases of complex right-to-light requirements like the Estonian daylight standard in urban environment. Moreover, the algorithm developed for the proposed method includes the context layout and surrounding buildings' mass in the calculations.

The method is developed using the visual programming environment of Grasshopper for Rhinoceros 3D and the environmental analysis suite Ladybug Tools [15]. The algorithm is implemented using standard Ladybug components and parametric design of a recursive process of sun vectors selection for the solar envelope generation.

The authors already developed an advanced method adequate for the Estonian regulation to generate solar envelopes using multi-objective optimization, based on actual amount of direct solar access and context layout [4]. This research takes advantage of the previous findings and develops a new deterministic method suitable to be implemented in tools to be used by architects and planners.

3.1 Urban areas with different density

The method described is applied to four urban areas with different density. The scope is to quantify the different effects, when generating solar envelopes, of specific requirements of direct solar access, of the surrounding context, and, if existing, of buildings to be demolished.

The location of the study is the city of Tallinn (Lat. 59°26'N Lon. 24°45'E). The area of Padriku Street is located in the low density suburb district of Pirita, situated in the north-east sector of the city developed mostly in the beginning of 2000s. The plot is surrounded only from two sides by a few four floor residential buildings (Figure 2).

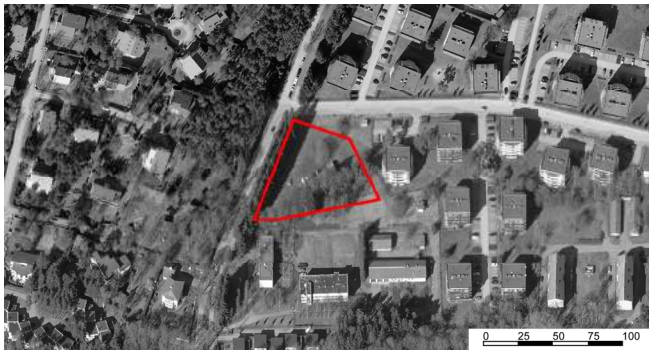

Figure 2. The plot in the low density area at Padriku Street.

The area of Tammsaare Street is located in the Soviet era housing district of Mustamäe built in the 60s and 70s. The plot under study is surrounded by five story buildings on three sides in a medium density neighborhood (Figure 3).

The areas of Kaupmehe Street, and Laikmaa Street are both located in the high density city center (Kesklinn district). The plot on the former street is surrounded from all the sides by close buildings built in different years in the second half of the 20th century and of diverse heights, from three to seven floors (Figure 4). The plot on the latter street is surrounded by different types of buildings on all sides, like five story mid-20th century residential buildings, a multi-story commercial center and an office complex with a tower of twenty-three floors both built in the beginning of 2000s. What is characteristic to this plot is the former building marked by the red area in Figure 5.

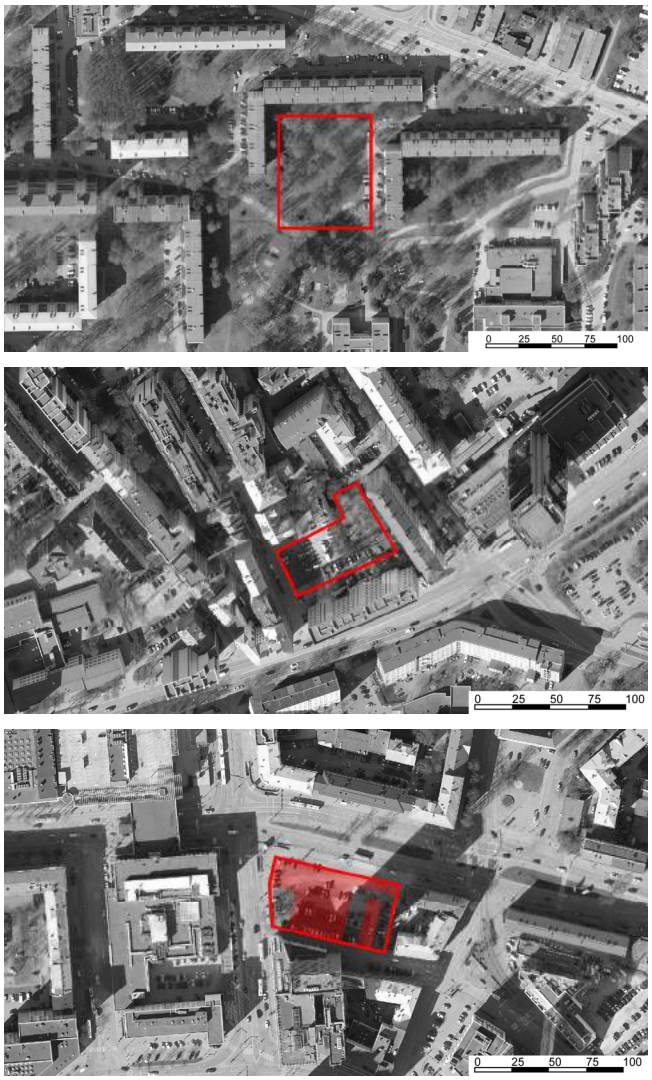

Figures 3, 4 and 5. (From top to bottom) The plot in the medium density area at Tammsaare Street. The plots in the high density areas at Kaupmehe Street and Laikmaa Street.

3.2 Geometric model set-up

The urban areas have been modeled with "shoe-box" polysurfaces representing the buildings. The facades facing the plots have been selected and for each one the heights of the lowest windows as target for the solar envelopes generation have been used. Since the lowest floor receives the least light, this selection guarantees the required quantity of direct solar access on the entire facade. Each façade's lowest floor has been subdivided into samples of 3 m by 3 m, each hosting a sensor node for the calculation of the quantity of direct sunlight hours. The lower edge of each sample has been used as shadow fence for the solar envelope generation [9]. The reason to not have just one single windows' height for all the facades has to do with achieving a higher accuracy of the solar envelope shape in complex and uneven urban environments (Figure 6).

3.3 Algorithm structure

The algorithm developed in Grasshopper makes use of off-the-shelf Ladybug components integrated by computation, selection and recursion tools realized by the authors. The standard components used are SunPath for the generation of the sun rays (sunVectors) of the period from 22nd of April to 22nd of August for every day from sunrise to sunset every 15 minutes (timeStep); Sunlight Hours Analysis for the calculation of the direct solar access hours on each facade's sample node; SolarEnvelope for the calculation of the maximum buildable shape and size on the selected plot. The sunVectors generated by the SunPath have been used in the Sunlight Hours Analysis component to get the pattern of the visible sun rays. A first part of the algorithm selects which sun rays are visible from the facade's sample and which are hidden by the surroundings. A second part selects the half of the sunVectors not obstructed by the context to determine those that are necessary by the Estonian daylight standard (50%). A recursive algorithm iterates the process for every facade's sample and the SolarEnvelope component generates the corresponding shape. A selection algorithm merges all the generated solar envelopes and a last algorithm creates the final shape on the plot.

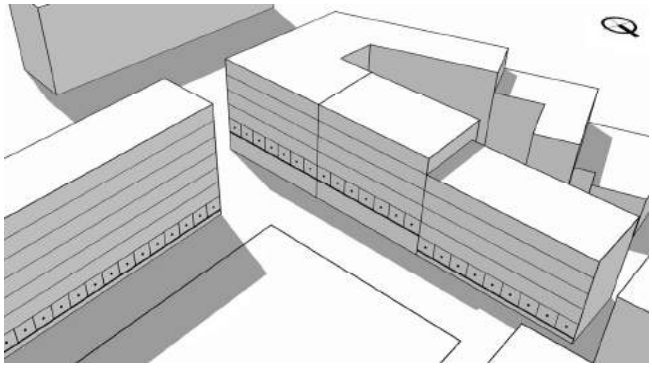

Figure 6. The facades' lowest floors at different heights divided in samples with the nodes for the direct solar access calculation. The sample's lower edge is the shadow fence of each solar envelope.

3.4 Context inclusion

By default the off-the-shelf SolarEnvelope component doesn't take into account the context in the calculations. The only inputs are the baselines of the facades to be not shaded and the sunVectors of the hours of the days in which direct sunlight has to be guaranteed. In the algorithm of the proposed method the Sunlight Hours Analysis component has been used to determine which sun rays are effectively visible by the facades' samples for the whole period using the output sunIsVisible. This is a single list of true/false values (1 and 0). The algorithm uses the pattern to cut-off all the obstructed sunVectors output of the SunPath (Figure 7). Consequently only the sun rays visible to the facades' samples have been used to calculate the solar envelope. Although the proposed method tackles mainly the hours input limitation of the existing method, the possibility to include the context, not present in the available tools, comes first in the algorithm structure and is presented as an outcome in itself in the results section.

3.5 Variable objectives

To include the possibility to select a direct solar access number of hours, as a minimum duration or as a ratio of the existing situation, i.e. the 50% requested by the Estonian daylight standard, a specific algorithm has been developed. It determines the quantity of sunlight hours (sunVectors) of every day of the period, and split accordingly the single list of the visible sunVectors for each facade's sample from the Sunlight Hours Analysis component. This way it is possible to compute the quantity of direct solar access hours for each facades' sample for every day and to identify the corresponding sunVectors. Consequently the tool permits to select, by ratio or quantity, a specific amount of visible sunVectors for each facades' sample every day. Then the half of the sunVectors with the highest solar altitude have been selected (Figure 7). The reason is that higher sun positions correspond to higher quantities of solar radiation hence they are more valuable and beneficial [13].

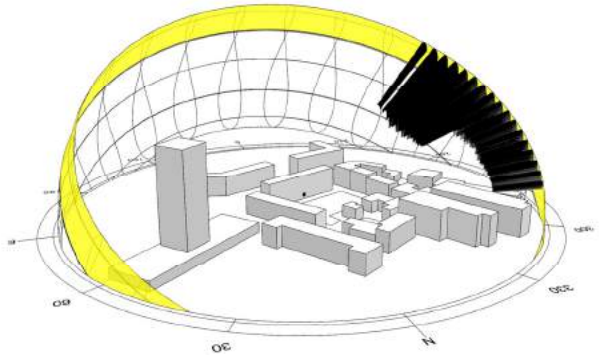

Figure 7. Annual sun path for the city of Tallinn. The yellow area represents all the sun positions from 22nd of April to 22nd of August. The lines are the sunVectors (15 min. step) visible to the selected facade's node (black dot). The longest lines are the 50% required by the Estonian standard with the highest solar altitude.

The selected sun rays have been used to calculate the solar envelope of each sample. This way the generated shape takes the Estonian daylight standard requirement and the context into account. The proposed method and tool can be used for any percentage different than 50% or exact quantity of required sunlight hours.

3.6 Recursion

For all the four cases in different urban areas the previously discussed algorithm used to generate solar envelopes that takes variable objectives or requirements and the context into account has been iterated for every sample of each facade through a recursion tool developed by the authors. The result is a list of different solar envelopes made of points that have the same X and Y coordinates but a different Z coordinate for every solar envelope.

The selection tool developed sorts the points with the lowest Z values, among those of all the solar envelopes, and at the end the final solar envelope Mesh is generated. This procedure guarantees that the resultant volume has the maximum size and shape and allows the requested amount of direct solar access hours on each sample every day during the required period of the year (Figure 8).

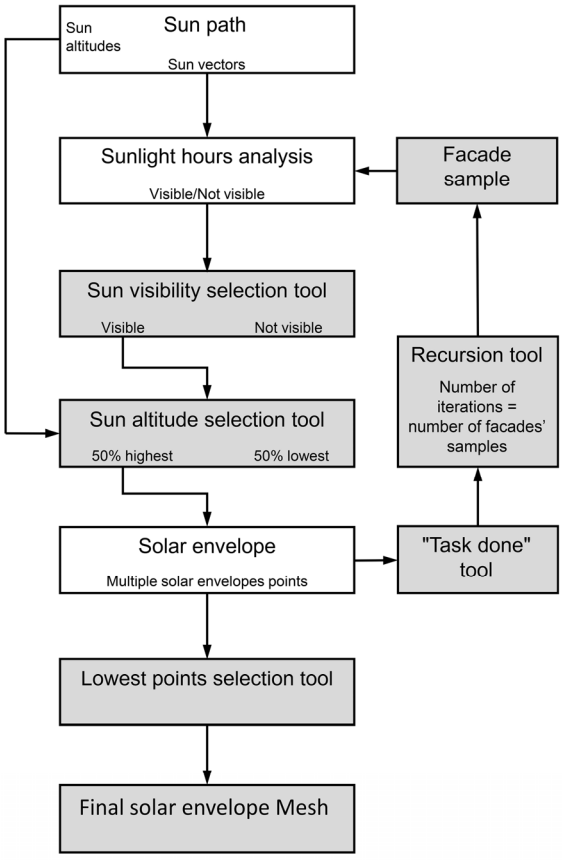

Figure 8. Flowchart of the algorithm. The tools developed by the authors in grey. Off-the-shelf components in white.

4 RESULTS

To compare the results, a solar envelope has been generated for each area with the existing tools (Figures 9, 10, 11 and 12). Its volume (m³) has been calculated and used as reference to compare the developed algorithm that includes only the context and the proposed method that includes the context and the Estonian daylight standard.

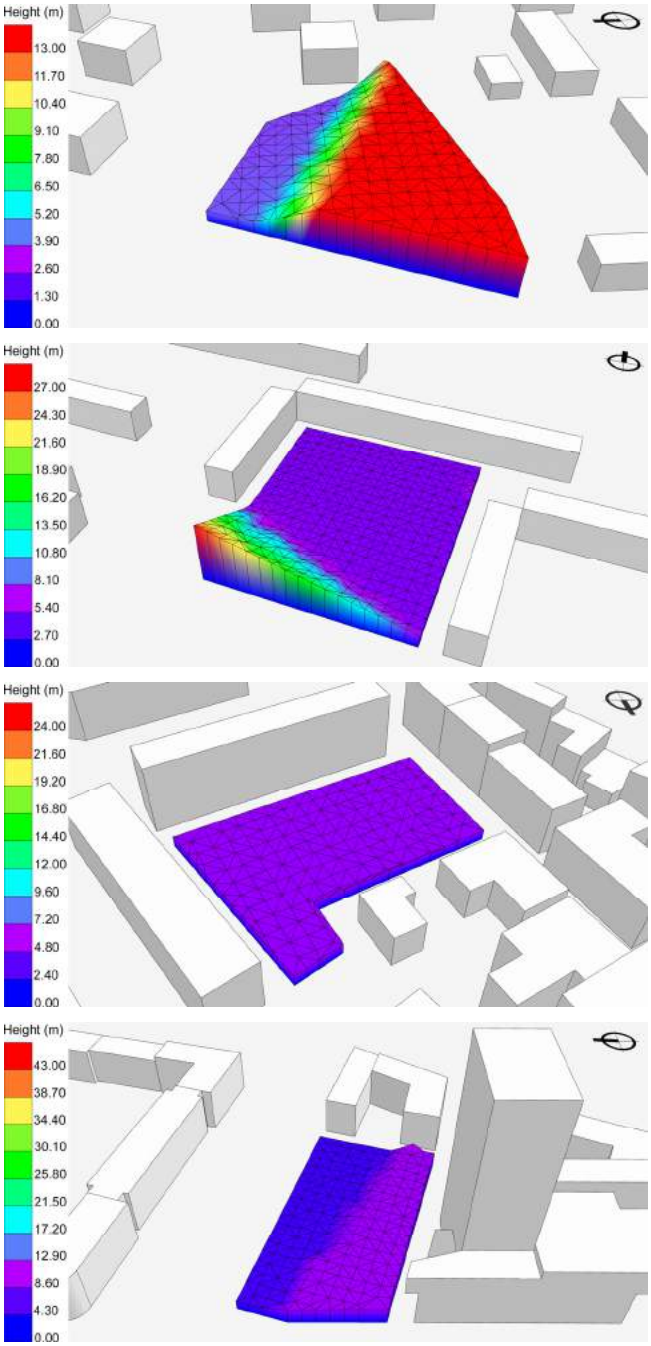

Figures 9, 10, 11 and 12. (From top to bottom) Solar envelope generated with the existing tools in the low density area, in the medium density area, in the high density area and in the high density area formerly occupied by a building.

Furthermore, to evaluate the solar envelopes generated with the proposed method new sunlight hours analysis on the surrounding facades have been performed and the performances have been compared.

4.1 Case 1 – Low density area

The plot at Padriku Street is located in the low density area of Pirita that is populated by single family houses and low residential buildings (Figure 2). The existing empty plot has an irregular shape and is surrounded by a few four story buildings that are a different distance away. The facades considered for the right-to-light analysis belong to buildings on two sides towards the north-east. The maximum height used for the solar envelope is 13 m, which is the maximum height of the surrounding buildings.

The results show that the solar envelopes generated with the existing tools (Figure 9) and with the developed algorithm that includes the context (Figure 13) have a very similar shape. Both use the maximum height for 2/3 of the plot and for the remaining part the height of the selected shadow fence (the samples' lower edge), with a slope in between. The size of the solar envelope that takes the context into account is 101% larger than the one of the existing tools.

The solar envelope built with the proposed method that takes the context and the Estonian standard into account almost matches the maximum allowed volume. It is an extrusion of 13 m of the entire plot and its size is 136% larger than that of the existing method (Figure 14).

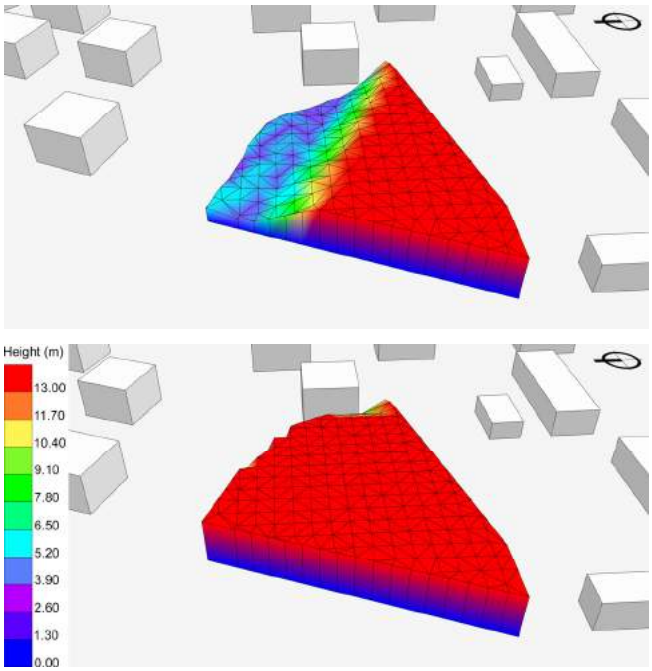

Figures 13 and 14. The solar envelope generated on the plot at Padriku Street with the proposed method that includes the context only (top), the full size solar envelope generated that includes the context and the daylight standard requirement included (bottom).

4.2 Case 2 – Medium density area

The rectangular plot at Tammsaare Street, located in a medium density neighborhood in the district of Mustamäe, is surrounded on two and half sides by three five story buildings at a distance of 8 m, towards north, east and west. The south side and half of the east side are clear. The three buildings' facades facing the plot have been considered for the solar envelope calculation. The area between the buildings is currently a public green area. The proposed plot has been located at the fire security distance between buildings as requested by city regulations (Figure 3).

The maximum solar envelope height for this plot is 28 m like the highest nine floor housing building in the area. The solar envelope generated with the existing tools has a low flat volume with a single peak at the maximum height at the open corner of the plot (Figure 10). The solar envelope generated with the developed algorithm that includes the context has a variable surface with the maximum height also at the open corner and a volume 145% larger of the one generated with the existing tools (Figure 15).

The maximum buildable shape generated with the proposed method that includes the context and the Estonian daylight requirement of 50% has a thicker block with more than the half of the plot's footprint extruded to the maximum allowed height. Sloping surfaces are located only in correspondence with the surrounding buildings' facades not to be overshadowed. Its volume is 415% larger than the one generated with the existing method (Figure 16).

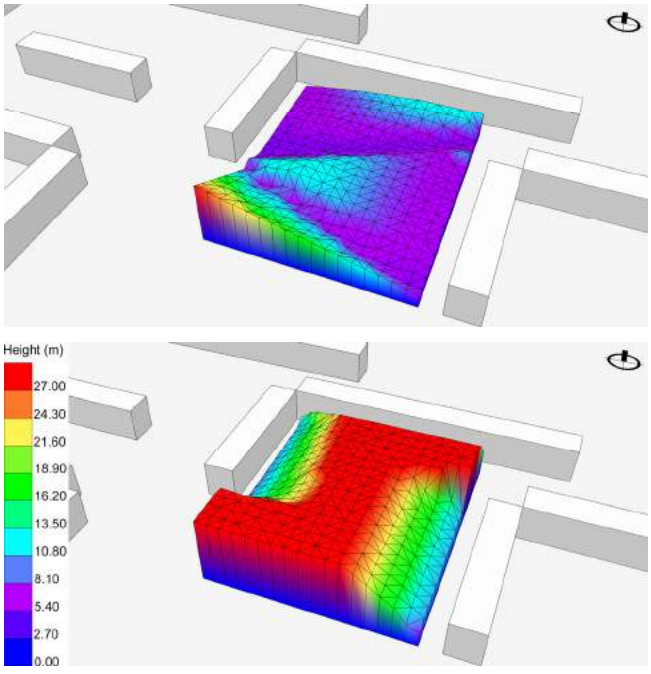

Figures 15 and 16. The solar envelope generated on the plot at Tammsaare Street with the proposed method that includes only the context (top), the solar envelope generated that includes the context and the Estonian daylight standard requirement (bottom).

4.3 Case 3 – High density area

The plot at Kaupmehe Street, located in a high density neighborhood in the city center, is L-shaped and is surrounded by buildings of different heights on all the six sides (Figure 4). The proposed plot, currently used as a parking, is at a distance of 8 m from the surrounding facades as requested by the fire security regulations. The maximum height set for the solar envelope on this plot is 25 m like the highest building in the area.

Due to the complexity of the surroundings and to the presence of buildings on all the sides of the plot the solar envelope generated with the existing tools has a thin flat volume of the same height like the surrounding facades' lowest floor windows (Figure 11). Since the existing tools don't consider the context, it cuts the solar envelope using the lowest solar altitudes sun vectors (dawn and sunset) for every facade's orientation.

The solar envelope generated with the developed algorithm that includes only the context is capped by a variable surface that takes the differences of the surrounding buildings' heights into account. Its size is 199% larger of the one generated with the existing tools (Figure 17). The solar envelope built with the proposed method that includes the context and the Estonian daylight requirement is a very articulated form with peaks along the central longitudinal axis of the plot and on the edge with larger distance from the facing building. Its size is 479% larger of the one generated with the existing method (Figure 18).

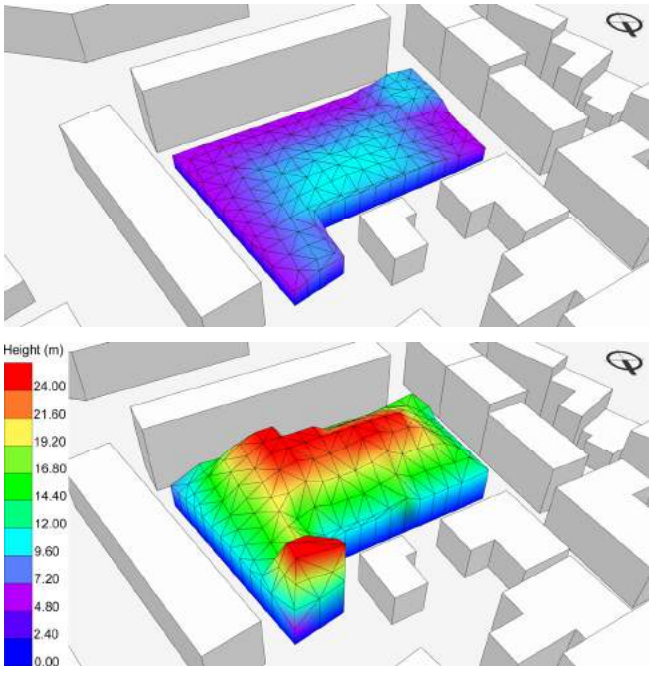

Figures 17 and 18. The solar envelope generated on the plot at Tammsaare Street with the proposed method that includes the context only (top), the solar envelopes generated that includes the context and the Estonian daylight standard requirement (bottom).

4.4 Case 4 – High density area with former building

The buildable rectangular plot at Laikmaa Street, currently utilized as a parking area, is in the high density commercial and financial district in the city center. On all the sides, it is surrounded by buildings at different distances and with very different heights from five to twenty-three floors. The facades considered for the solar envelope computation are on two sides, towards the north and towards the east.

The plot was formerly occupied by a building, the former Estonian Academy of Arts. It has been demolished to be replaced by the winning proposal in an international architectural competition, but was never built. Nonetheless, the former building has been considered for the generation of the solar envelope with the proposed method that takes the context and the Estonian daylight standard into account. The maximum height set for the solar envelope is 43 m, the one indicated in the brief of the competition.

The solar envelope calculated with the existing tools has a low volume with a slightly variable top surface, lower towards the facades to be not shaded (Figure 12). The solar envelope generated with the developed algorithm including the context has a 484% larger shape. It is characterized by a sloped surface descending towards the facades to be not shaded closer to the plot and by peaks 43 m high towards the more distant facades (Figure 19). The solar envelope generated with the proposed method including the context and the 50% requirement has a larger area at 43 m. Its size is 683% larger than that of the existing method (Figure 20).

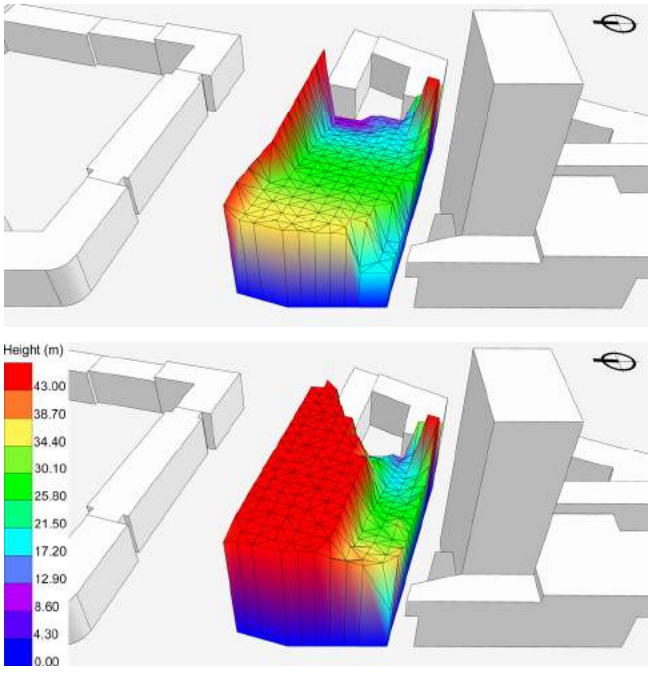

Figures 19 and 20. The solar envelope generated on the plot at Laikmaa Street with the proposed method that includes only the context (top), the solar envelope generated including the context, the former building and the Estonian daylight standard (bottom).

4.5 Summary of results

In the four cases the importance of considering the context is constantly increasing after case 1 in which the solar envelopes generated with the existing tools and the developed algorithm including the context are very similar. The solar envelope that includes the context is 1.49, 1.99 and 4.84 times larger in case 2, 3 and 4 respectively. The hike in case 4 is due to the very close tall office building. The evidence shows that the size of the solar envelope generated with the proposed method that includes the context and the direct solar access objective of 50% is even larger than that of the existing method and also increase constantly. It is 1.36, 4.15, 4.79 and 6.83 times larger in case 1, 2, 3 and 4 respectively. Case 4 is the biggest for the former presence of the building in the plot (Figure 21).

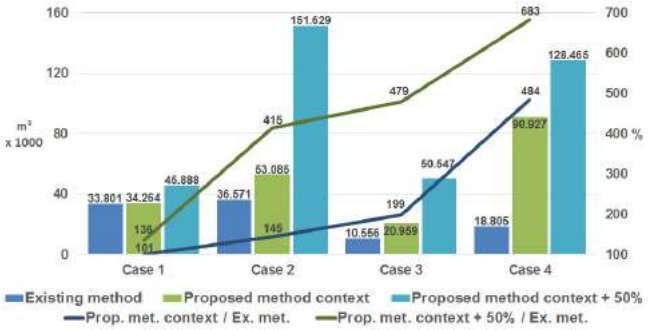

Figure 21. Solar envelope comparison for the four cases.

To evaluate the performances of the generated solar envelopes, new direct solar access hours calculations have been conducted on the surrounding facades (Table 1). The solar envelopes generated that take only the context into account allow direct sunlight with small average deviations from 100% increasing with the complexity of the surroundings. Nonetheless, more than half of the samples receive the same quantity as the empty plot, except case 3. The solar envelopes generated that take the context and the Estonian standard into account, have larger deviations but in most cases they allow more light than the required 50%. For the large quantity of calculations have been used medium accuracy settings (hour time-step and solar envelope grid subdivision). Higher accuracy settings tested have produced significant improvement of performances.

	Case 1	Case 2	Case 3	Case 4
Av. dev.	-2.7	-1.5	-4.2	-10.3
= 100%	63.6	79.1	46.5	57.1
Av. dev.	25.4	18.7	11.6	13.7
>50%	81.1	82.1	59.2	57.1

Table 1. Deviations (%) in comparison with existing conditions for the generated solar envelopes that include the context (rows 1 and 2), and that include the context and the specific objective of 50% max reduction of direct solar access (rows 3 and 4).

5 CONCLUSIONS

The present work presents a method for the generation of solar envelopes through computational design. The scope is to improve the existing method that doesn't permit to input specific quantity of direct solar access hours to be guaranteed on the surrounding facades, as required by the Estonian standard, and to improve the existing tools that don't consider the context in the calculations. Using actual environmental design software and the most advanced tools, the generated solar envelopes' size is underestimated and the shape unfit, above all in urban environments.

An algorithm has been developed with three main functions:

- It includes the context in the calculations by selecting only the sun rays (sun vectors) visible by each facade's sample for every day of the required period.
- Among the visible it selects a quantity of sun rays corresponding to the specific requirement. In this study the 50% of direct solar access duration has been used as requested by the Estonian daylight standard.
- It iterates the two previous functions for all the facades' subdivisions (samples) generating one solar envelope for each using the selected sun rays and finally merging them all.

The proposed method has been tested on four different urban environments, with increasing density and complexity. As the evidence of the results shows, the proposed method is significantly more efficient than the existing one in the case of the Estonian regulation. It permits to generate larger and manifold solar envelopes with a size difference and shape articulation augmenting with the increase of the density and complexity of the surrounding urban environment in comparison with the existing method. This research underlines, in brief, the importance to consider specific amounts of sunlight hours for each facade, when required, instead of the fixed start and end time, and the necessity for the available tools to be developed to include the context in the calculations.

The possibility to use more efficient methods and tools can give to architects and planners powerful ways to improve the design process, reducing time consuming trial-and-error procedures. The ability to create variable objectives and context aware solar envelopes, with size and manifold shape adequate to the complexity of the surrounding urban environment, can strongly contribute to shape sustainable, healthy and energy efficient urban environments.

The future work of this research is to investigate methods for the buildings' mass generation from solar envelopes and layout optimization for solar collection taking the typology of the future buildings into account.

ACKNOWLEDGMENTS

The research was supported by the Estonian Research Council, with personal research funding grant PUT-652.

REFERENCES

1. Brown, G. and Z., DeKay, M. *Sun, Wind and Light. Architectural Design Strategies.* Second edition, John Wiley & Sons, New York, NY, USA, 2001.
2. Capeluto, I. G. and Shaviv, E. Modeling the design of urban fabric with solar rights considerations. *Proc. IBPSA 1999*, Kyoto, Japan (1999), 1341-1347.
3. Capeluto, I. G. and Shaviv, E. On the Use of Solar Volume for Determining the Urban Fabric. *Solar Energy 70*, 3 (2001), 275-280.
4. De Luca, F. Solar Envelope Optimization Method for Complex Urban Environments. *Proc. CAADence in Architecture 2016*, Faculty of Architecture Budapest Univ. of Technology and Economics (2016), 223-229.
5. Estonian Centre for Standardization. *Daylight in Dwellings and Offices*. Standard EVS 894:2008/A2:2015, 2008.
6. Jakubiec, A. and Reinhart, C. F. DIVA 2.0 Integrating Daylight and Thermal Simulations Using Rhinoceros 3D, Daysim, and EnergyPlus. *Proc. Building Simulation 2011*, Sydney, Australia (2011), 2202-2209.
7. Juyal, M., Kensek, K. and Knowles, R. L. SolCAD: 3D Spatial Design Tool to Generate Solar Envelope. *Proc. ACADIA 2003 Crossroads of Digital Discourse*, Indianapolis, USA (2003), 411-419.
8. Knowles, R. L. *Sun Rhythm Form*. MIT Press, Cambridge, MA, USA, 1981.
9. Knowles, R. L. The solar envelope: its meaning for energy and buildings. *Energy and Buildings 35*,1 (2003), 15-25.
10. Knowles, R. L. *Energy and Form*. MIT Press, Cambridge, MA, USA, 1974.
11. Lockley, S. W. Circadian Rhythms: Influence of Light in Humans. *Chap. Encyclopedia of Neuroscience,* vol. 2, Academic Press, Cambridge, MA, USA, 2009, 971-988.
12. Marsh, A. Computer-optimized Shading Design. *Proc. IBPSA 2003*, Eindhoven, Netherlands (2003), 831-837.
13. Ratti, C. and Morello, E. SunScapes: Extending the 'Solar Envelopes' Concept Through 'Iso-Solar' Surfaces. *Proc. PLEA 2005*, Beirut, Lebanon (2005), 815-820.
14. Reinhart, C. F. *Daylighting Handbook I. Fundamentals. Designing with the Sun*. MIT Press, Cambridge, MA, USA, 2014.
15. Sadeghipour, M. and Pak, M. Ladybug: a parametric environmental plugin for grasshopper to help designers create an environmentally-conscious design. *Proc. IBPSA 2013*, Chambéry, France (2013), 3128-3135.
16. Uen-Fang, P, Y. *Computer Aided Solar Envelope Design*. ProQuest, Ann Arbor, MI, USA, 1992.

Simulation-based Sensitivity Analysis of Future Climate Scenario Impact on Residential Weatherization Initiatives in the US Midwest

Charvi Jagani, Ulrike Passe

Iowa State University
Ames, USA
{cjagani,upasse}@iastate.edu

ABSTRACT

The existing building stock in countries across the world is designed to shelter against the current typical climate conditions. It may not be prepared to counter the possible extreme climate conditions of the 21st century. Based on the projections for the typical climatic conditions in the future, this project is simulating the energy consumption of a neighborhood in the US Midwest that is scalable to a city. Traditional building energy simulation programs mostly take into consideration – the location, weather, construction materials, type of use and occupancy. They do not, however, effectively simulate group of buildings or a neighborhood altogether. We are using a Rhinoceros-based, urban modelling design tool called Urban Modeling Interface (umi) that is capable of simulating building energy while taking into consideration the surrounding urban environment. Using umi, our model simulates the energy consumption of built environment across a street section and thus accounts for factors such as floor area ratio, built density, and other urban morphology parameters that affect the individual building energy consumption. These simulations are performed for current and future typical meteorological conditions using the FTMY data sets developed by Patton in 2013. Weatherization is simulated and tested as a design strategy to overcome the increased energy demands in predicted future climate conditions. In this way, we are examining a design strategy on real world urban conditions and presenting an analysis of how we could maintain the current thermal comfort in future climates.

Author Keywords

Urban Building energy simulation; climate change; future typical meteorological year; weatherization; housing

ACM Classification Keywords

I.6.1 SIMULATION AND MODELING, I.6.6 SIMULATION OUTPUT ANALYSIS

1 INTRODUCTION

The global climate change affects the built environment and it is important that we build considering the anticipated future changes in the climate. There are several tools available to simulate building energy consumption, but most of them do not factor in the urban environment that the building occupy. Urban building energy modelling applies physical models of heat and mass flows in and around buildings to predict operational energy use as well as indoor and outdoor environmental conditions for groups of buildings [6]. Using one such urban building energy modeling platform - Urban Modelling Interface (umi), we are simulating energy consumption of an existing neighborhood and testing design strategies to combat climate change. Umi is a Rhinoceros-based design environment for architects and urban planners interested in modeling the environmental performance of neighborhoods and cities with respect to operational and embodied energy use, walkability and daylighting potential [23].

Des Moines, Iowa in the US is the location under study to simulate the impact of weatherization strategies on existing residential building stock. Des Moines is located at 41.6° N latitude. It has harsh winters and hot humid summers. For a standard house in the city, active energy systems are required almost throughout the year. The existing residential building stock in inner urban neighborhoods is often not well equipped for the climatic challenges with little insulation, older windows and leaky envelopes.

Weatherization includes a wide variety of energy efficiency measures that encompass the building envelope, its heating and cooling systems, its electrical system, and electricity consuming appliances. Weatherization benefits residents by reducing their energy bills over a long period. According to the United States Department of Energy (DOE), the average value of weatherization improvements is 2.2 times greater than the cost. [24] Some measures, such as increasing the efficiency of heating/cooling equipment, provide savings for 10-15 years, and other measures, such as insulating walls or roofs, providing savings for the lifetime of a house, i.e., 30 years or more [24]. However, weatherization involves up-front investment and potentially long-term financial payback, which may be unappealing or infeasible, particularly for low-income residents.

To address this issue, federally-funded weatherization programs have been created to increase adoption among low-income residents by subsidizing home improvements. For example, the DOE Weatherization Assistance Program (WAP) provides grants to states, territories, and some Indian tribes to improve the energy efficiency of the homes of low-

income families. These governments, in turn, contract with local governments and nonprofit agencies to provide qualified residents with state-of-the-art and cost-effective energy efficiency upgrades that improve their building's thermal performance. Since the program began in 1976, the DOE has helped improve the lives of more than 7 million families by reducing their energy bills [18]. Furthermore, these upgrades not only increase energy performance, but also address health concerns associated with poor indoor air quality [5].

The objective of this paper is to present an integrated modeling methodology that simulates the impact of weatherization in future climates using Future Typical Meteorological Year (FTMY) data sets developed by Patton [19]. This method evaluates typical meteorological year (TMY3) data recorded at Des Moines International Airport for total sky cover, dry-bulb temperature, dew-point temperature, relative humidity, absolute humidity, pressure, and wind speed for the period 2041 to 2070 [14]. These data sets use regional future climate data obtained from the North American Regional Climate Change Assessment Program (NARCCAP) and three emission scenarios (high, medium, low) [10]. Taking into consideration the present and future weather conditions, we have simulated the energy consumption for two typical rows of houses facing each other in the Des Moines East Bank neighborhood. The impact of weatherization with two strategies (reduced infiltration and increased insulation) is tested on these 29 houses under present and future climate conditions.

2 STUDY AREA

The Capitol East neighborhoods in Des Moines are used as pilot study area for the urban energy simulation. The Capitol East Neighborhoods were chosen as a test case for a pilot study, primarily because of its social and economic composition. In the 1990s Capitol East was one of the first neighborhoods in Des Moines to take part in the neighborhood revitalization program "to help enhance, stabilize and revitalize neighborhoods" throughout Des Moines [8]. The neighborhood plan has undergone significant redesign over the years in partnership with Iowa State University's Community and Regional Planning Department, and its second edition has recently been approved. This is an indication for a strong neighborhood association and buy-in by the local residents, which will be important for future development and implementation of modeling and decision support tools.

Capitol East is situated just east of the Iowa state capitol building, near downtown Des Moines. On the whole, it is a young and diverse neighborhood. However, it faces some economic challenges: its median income is less than half the Des Moines average, and there are more renter occupied properties than other neighborhoods in Des Moines. Capitol East has been targeted by Habitat for Humanity's "Rock the Block" program, which includes building ramps and door modifications, repairing roofs, porches, siding, windows, driveways and sidewalks, insulating, weatherstripping, painting, landscaping and other maintenance projects. The hybrid simulation model described in this paper has been developed as a decision support tool that will help city officials, planners, and residents to develop policies and programs that will enhance these efforts and increase weatherization adoption among Capitol East residents [5].

3 URBAN MODELLING INTERFACE (UMI)

Umi is a Rhinoceros based tool used to perform Urban Building Energy Modeling (UBEM). Davila and Reinhart have used umi for modeling Boston [22]. They classify umi as a "bottom up" UBEM that apply "engineering" analytical methods to represent each building individually in a model. They point out that "to understand spatiotemporal energy demand patterns due to buildings, different types of urban models have been proposed over time, which fall into two main categories: "top-down" or "bottom-up" models [4]. Traditional "top-down" building stock models link energy use to macroeconomic variables, such as population trends and economic activity. They serve the purpose of predicting near future energy use by extrapolating from the status quo" [22,4]. They are therefore limited when exploring new technologies or analyzing interventions where energy demands need to be characterized at the scale of the building. In our case, we are analyzing the effects of weatherization for each building in a neighborhood. Bottom up models can rely on a set of archetypical or actual sample buildings that represent a segment of the building stock [7]. A fundamental difference of these models compared to umi is that bottom up models treat all buildings of the same type as identical for statistical purposes. Umi, being architectural and urban design focused, is particularly interested in resolving differences in energy use of buildings due to local urban microclimatic conditions such as self-shading and urban heat island effects.

Umi uses the WINDOWS based NURBS modeler Rhinoceros [16] as its CAD modeling platform, EnergyPlus for thermal building - by - building simulations, Daysim for daylight simulations and custom Python scripts for walkability evaluations [7]. Umi generates EnergyPlus files for each building and runs annual simulations on each building in the study area. Multizone EnergyPlus models are generated in two steps. The building volume, as defined by the building envelope, is initially broken into different levels. Core and envelope zones are then auto-generated by umi using shoebox algorithm [22], with all envelope zones having a depth that corresponds to twice the floor-to-floor-height. All zones are assigned the same construction types, schedules and infiltration rates specified in the building's template. Umi currently reports HVAC energy use based on EnergyPlus ideal air loads system combined with user-defined coefficients of performance. During each individual building simulation, neighboring objects are modeled as shading objects. Energy simulation results can be mapped back into the Rhinoceros scene (Figure 3) and be combined

with aggregate analysis and visualizations of building performance.

4 WORKFLOW

Rhinoceros 3D (Rhino) and the Urban Modelling Interface (umi) plugin were used to create the digital model of the block and to simulate the energy performance of each house within the selected study area. Accuracy of the simulation output is dependent on the input data precision. The first phase of the simulation as shown in Figure 1, was the data collection process. The three major data input sources of the model are: Geographic Information System (GIS) files maintained by City of Des Moines, the Assessor's data and the weather files (TMY3 and FTMY).

Spatial information used to model the physical geometry such as building footprints, streets, sidewalks and lot boundaries was extracted from GIS maps that are maintained by the city of Des Moines [5]. The GIS data is in shape file (.shp) format, which is a vector data storage format for storing the location, shape, and attributes of geographic features [21]. To generate the base model of the East Bank neighborhood, the GIS shape file is imported to Rhino using GIS data-parsing plugin: Meerkat. In this way, a precise geographically located base-framework for simulation is set up. This workflow makes the energy simulation process easily scalable to city level and beyond. It is also deployable to any other location for which the GIS data is available. The information available from the Polk County Assessor's database is then used to refine the Rhino model at building scale. Once the physical model is generated, the weather data of the location under study becomes a critical aspect for energy model. Meteorological inputs for specific locations are required by the thermal models of the building energy simulation systems. Typical Meteorological Year (TMY3) obtained from the Department of Energy and Future Typical Meteorological Year (FTMY) obtained with the Patton methodology developed in 2013 is used for this purpose [19].

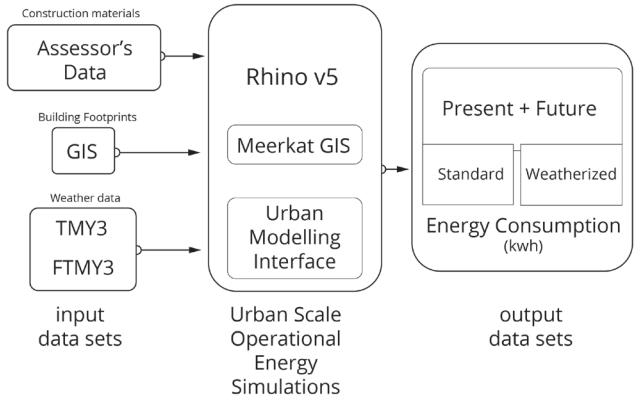

Figure 1. Work Flow

The curated data about building footprint, building forms, construction materials and weather conditions served as a basis for the Rhino model. The parametric Rhino model was then run through umi for the energy simulation process. The output datasets of umi are then used for analysis of the impacts of weatherization on future residential building energy consumption. (see section 4.2).

4.1 Datasets

Typical Meteorological Year (TMY3) and Future Typical Meteorological year (FTMY):

A detailed weather data is required for evaluating the climatic impact on buildings. Currently, energy performance predictions are based on climate data of the recent past, for example, the Typical Meteorological Year (TMY3). The TMY3 database provides designers and other users with a reasonably sized annual dataset consisting of hourly meteorological values that are intended to typify conditions at a specific location over a longer period of time, such as 30 years [14]. In order to simulate the future energy consumption of the residential building stock, Future Typical Meteorological (FTMY) data, as prepared by Patton is used in the energy model [19]. Projected changes in climate were combined with existing TMY3 data to create FTMY data sets. Four weather files were used to simulate energy scenarios for the urban model: the base file is the Des Moines International Airport TMY3 weather file. The next three are projected future climate files that are transformations of the base file that produce high, medium and low emission scenarios of Future Typical Meteorological Years (FTMY) for the middle of the 21st century (periods 2041–2070). Bhandari, Shrestha, and New [15] highlight the significance and accuracy that weather files have on building loads, therefore, the FTMY data were extracted to develop three regional climate models representing a low-change, moderate-change, and a high-change scenario. Future typical meteorological year datasets were created using the method described by Rabideau [20] and Patton [19], for each of the eight available climate model combinations under the North American Regional Climate Change Assessment Program (NARCCAP) [17]. For further detailed description on the FTMY construction, refer to [14].

Geographic Information System (GIS) Data:

The GIS shape files for the Capitol East Neighborhoods are obtained from City of Des Moines [9]. This serves as 2d line work base for 3d Rhino Model. Additionally, it helped in geo-locating the Assessor's database using the geoparcel id common to both GIS file and the assessor's database. Grasshopper, which is an algorithmic modelling tool was used as an interface between GIS data and Rhino model. Grasshopper using Meerkat GIS, extracts the relevant information about building footprints and heights from the GIS file. The 2d layer of building footprint was then extruded to the extent of the heights of each building. Building heights in the Rhino model is referenced from the GIS data maintained by the City of Des Moines.

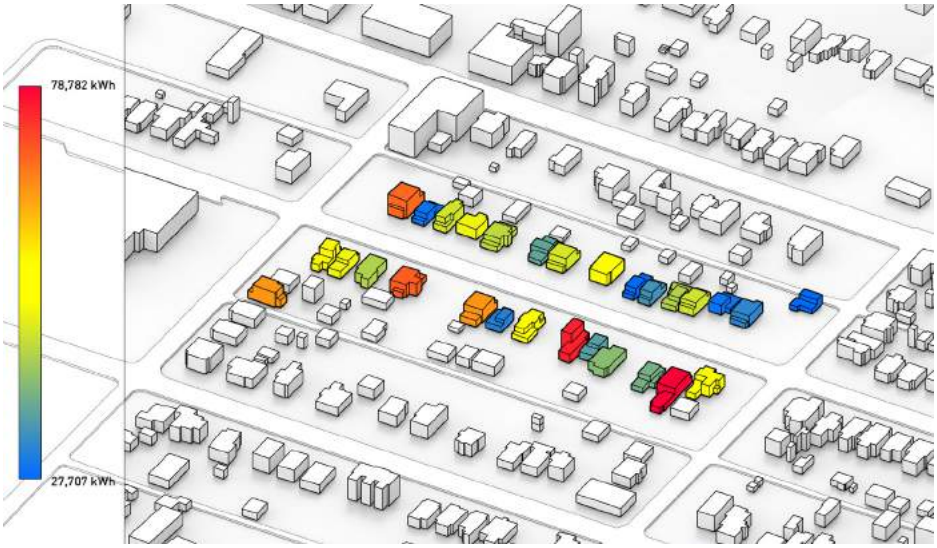

Figure 2. Umi model: energy consumption visualization of Capitol East neighborhood

Assessor's Data:

The Polk County assessor data provided another layer of information for the Rhino model. Each building's address, parcel number, number of building stories, date of construction, and number of separate residences contained within were extracted from the assessor's data [18]. Assessor's data also provided the information about the type of construction materials used and occupancy. All this information helped in generating the umi templates that were assigned to each house. An identification system for each house was derived from the parcel number of each lot and was used to cross-reference information between the Rhino-umi model and the Assessor's data [5]. To maintain privacy for the residents, the exact location of the block is not communicated in this paper. Roof elevations included within the GIS data were used to create 3d building models by extruding the building footprints. Model was then manually edited later using measurements from assessor's floorplans to more accurately reflect the true size of the house. Assessor's data also enabled taking into consideration the porch areas, since they would be the non-enclosed part of the building volume. Differentiating between the enclosed and open spaces of the buildings was an important step in producing more accurate results. Additionally, assessor's data provides information about the type of roofs on each building. In the 3D Rhino model the height of the buildings were reduced for the structures with sloped roof, which better represents the true volume of the building.

4.2 Urban Scale Operational Energy Simulation

Umi is the basis for the simulation of the 29 houses in Capitol East Neighborhoods. A visualization of the building energy consumption as it appears in Rhino - umi model for the area under study is shown in Figure 2.

The model prepared in Rhino from GIS and assessor's data is fed into umi. Umi's operational energy simulations uses the EnergyPlus-based 'shoeboxer' algorithm to automatize conversion of architectural massing models into thermal 'shoeboxes' which consists of a two zone thermal model for perimeter and core regions [22]. The UMI 'shoeboxer' algorithm breaks the building into volumetric "boxes" for energy simulation, so editing the forms to more accurately represent the true insulated volume of each house is necessary. This was made possible by breaking the houses into different volumes with different heights using the information extracted from assessor's data.

Building templates for umi are generated by referencing the GIS and assessor's data. A building template is created by combining a set of construction information to describe the materials properties and performance of an entire structure. In turn, the construction assemblies are a collection of materials with defined performance characteristics. Each house is assigned a building template, which reflects the construction type and condition of the house. This is translated into thermal performance and infiltration rate. All the houses in the area analyzed are residential and are of similar wood frame construction. Umi offers the ability to edit the material assembly of individual houses in the neighborhood, such that the potential impact of different weatherization strategies (e.g., re-caulking windows to decrease air infiltration; adding spray insulation in unfinished attics to prevent heat loss during the winter) can be tested [5]. A second template was then assigned to each house, increasing the thermal performance of the house's envelope and decreasing the infiltration rate of the attic to test the effects of weatherization.

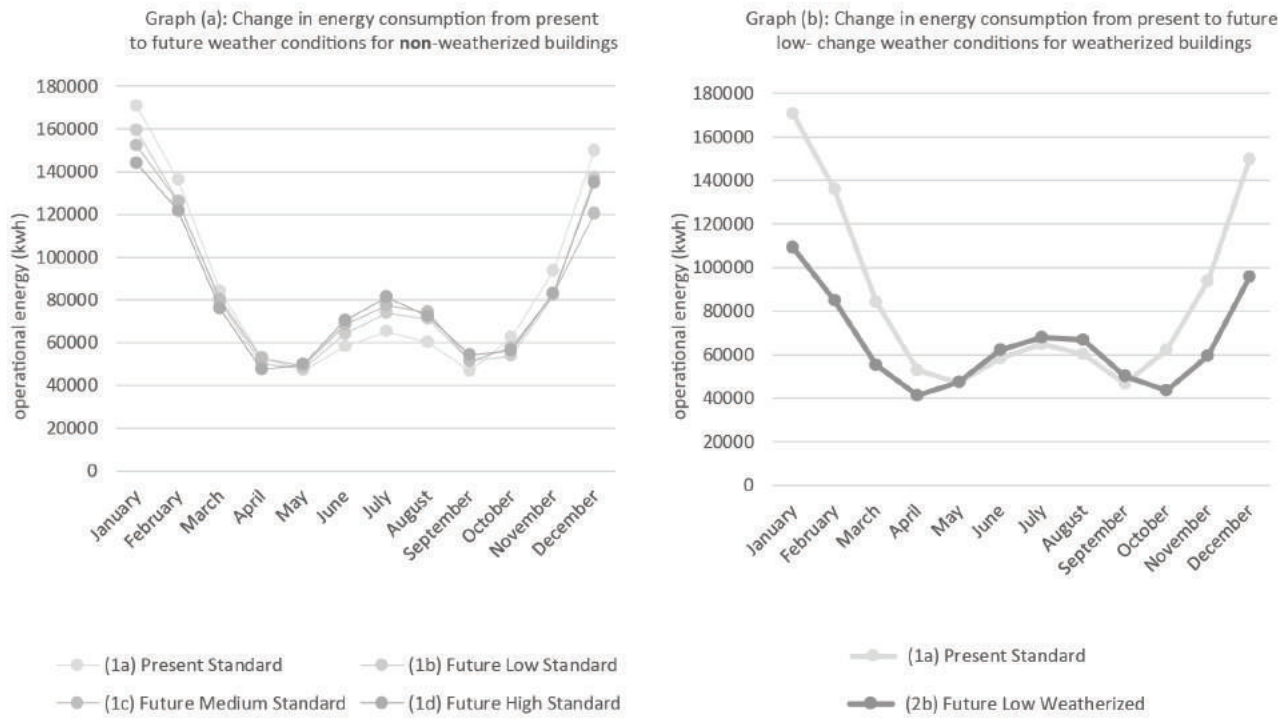

Figure 3. Simulated energy consumption data set output from umi model.

The energy consumption of the 29 houses is simulated under two scenarios. In scenario-1, the energy modelling is done for the actual construction at present. The air infiltration rate for scenario-1 is 0.75 ACH. In scenario-2, the houses are simulated under weatherized conditions. To simulate weatherization, the air infiltration rate is reduced from 0.75 ACH to 0.25 ACH. Additionally, the thickness of insulation of the roof is doubled as compared to the thickness assigned in standard scenario-1. This provides a basis to compare the energy consumption under both conditions and test the effectiveness of weatherization in terms of attic insulation and airtightness.

5 RESULTS: OUTPUT DATA SETS

The umi model generated through the data sets as previously explained is simulated in the Rhino environment. As shown in Figure 4, the data outputs are generated for two major scenarios – for actual constructions (scenario 1) and for weatherized constructions (scenario 2). Both these scenarios are simulated for all four weather files i.e. TMY3, FTMY low change, medium change and high change.

Firstly, the results compare the change in energy consumption from present to future climate conditions. Secondly, the results examine the effect of weatherization on future increases in building operational energy consumption.

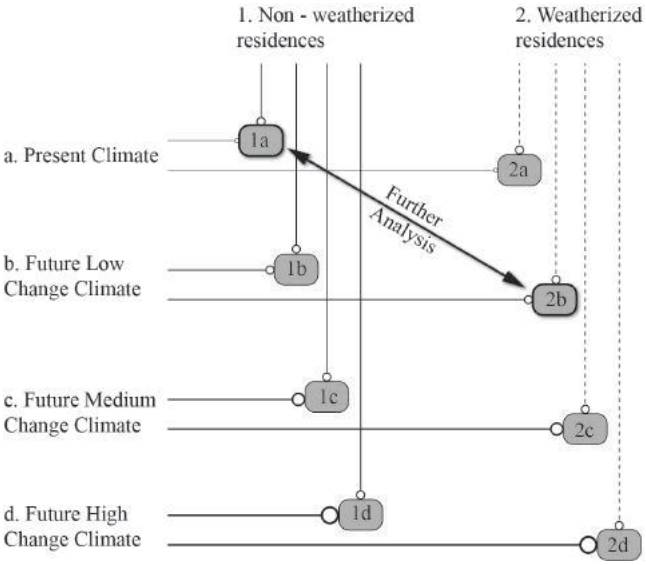

Figure 4. Scenarios for simulation for different climate files used on the standard and weatherized homes

The chosen scenarios allow to conduct a comparative analysis of the energy consumption between present and future weather conditions as show in graph a, Figure 3. The graph is a plot of aggregate monthly energy consumption of all 29 houses for present climate situation and for future scenarios.

As can be seen from the graph (a) of Figure 3, the energy loads in the summer months i.e. from May to September increase substantially in future; while, energy loads decrease in the future winter months i.e. from November to February. This shows that the cooling energy loads will increase in future. Patton's [19] research also highlights this fact and estimates an increase of 30 – 75 % in cooling energy consumption for cold locations like Des Moines. There is a 30% projected increase in cooling energy load as per our simulation for the Capitol East neighborhoods. To maintain the current understanding of thermal comfort, existing building stock needs to cope with the increasing temperatures. As a result, weatherization is tested as a strategy to maintain the current energy loads and thermal comfort levels.

The data sets presented in graph (b) of Figure 3, suggest that, just by weatherizing the attic, increasing energy consumption in the future summers can be prevented. Since the energy consumption in future winter months is expected to decrease, overall annual energy loads may go down as shown in the Figure 3. The difference (present standard, 1a – future low weatherized, 2b) between the two scenarios is 7440 kwh (Figure 5), which equates to $805 in savings per household at Iowa's energy rate of 10.82 cent/kwh [12]. The weatherization method as discussed in this paper does not bring down the energy bills to a larger extent, but at least helps maintain the current levels of energy loads.

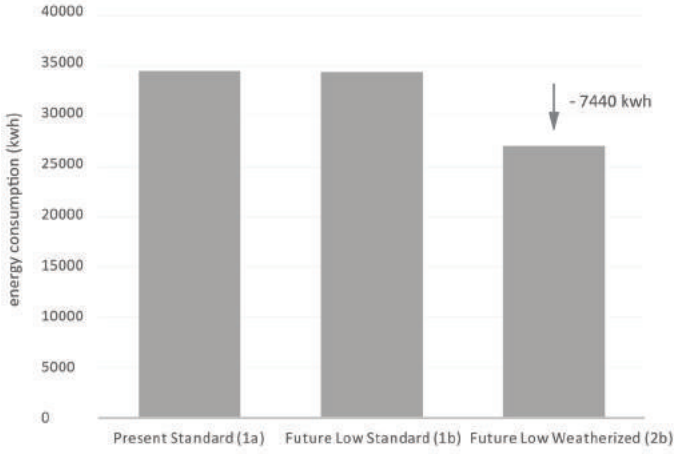

Figure 5. Average annual operational energy of a house in the study area.

6 DISCUSSION ON RESULTS

The aforementioned results indicate that the future climate calls for designing the built environment in Iowa and similar climate zones more for cooling condition and utilize weatherization strategies to combat cooling more so than heating. Weatherization of roof assemblies is one effective method of controlling interior thermal comfort. Modifications to the building envelope could potentially have a significant impact on energy savings, such as high albedo surfaces and cool roofing [10].

Also, thermal comfort is largely affected by relative humidity percentages in the atmosphere. Mann et al. have identified that a 1% increase in the climate saturate vapor pressure requires 0.5% in increased energy to counteract it [3]. To maintain current human thermal comfort standards in buildings of the future, managing humidity will be costlier (in terms of energy consumption) than managing temperature [14]. Consequently, cities like Des Moines that have hot and humid conditions during summer will face larger energy loads than places where humidity is moderate. This issue will have to be addressed with future research and more refined data collection in the neighborhood in order to evaluate strategies, which can cope with the future increase in relative humidity for inner - urban residential neighborhoods with older building stock.

7 CONCLUSION AND FUTURE WORK

The urban environment energy simulations conducted with Urban Modelling Interface and FTMY are indicative of a rise in cooling energy demand. This increase can be mitigated with weatherization – in our case doubling the roof insulation and reducing infiltration rates from 0.75 ACH to 0.25 ACH.

Vegetation and urban tree coverage can also be used as a mitigation strategy to offset the energy loads of built environments. Trees can lower surface and air temperatures by providing shading and through evapotranspiration. [26] Evapotranspiration, alone or in combination with shading, can help reduce peak summer temperatures by 2–9°F (1–5°C) [11,13]. The current model does not take into consideration the existing tree cover that requires information about tree height and canopy width. The umi plugin provides a layer in Rhino to add trees and other shading objects in a neighborhood. Trees and shading objects are represented as closed polysurfaces in Rhino. The data collection for this parameter is on-going and once the most accurate data is available, it will further inform the model for more accurate results. One of the challenges with simulating green cover is that it is dynamic and changes must faster than building infrastructure. This makes it difficult to quantify its effect on ambient surroundings.

Future work

Sustainable Design Lab at MIT have ventured into modelling urban heat island effect through their tool - Urban Weather Generator (UWG). It is a new urban design tool with urban heat island effect considerations and its implications for thermal comfort and energy [1]. According to the sensitivity analysis performed by UWG developers, urban heat island effect is most affected by site coverage ratio, façade to site

ratio, and sensible anthropogenic heat. Site coverage ratio and façade to site ratio can be obtained from umi model. UWG estimates the hourly urban canopy air temperature and humidity using weather data from a rural weather station. It takes a rural weather file and an input file, which describes the urban canyon under study. The output is a morphed weather file that captures urban heat island effect and is compatible with many building performance simulation programs [2]. The vegetation data and urban canopy information can be fed into UWG to develop a more accurate weather file that can improve the umi simulation process. Availability of the tree inventory data will prove critical in generating a morphed weather file. UWG can further provide testing of the effects of green roofing on urban heat island.

Overall, the workflow for our model is scalable to larger regions and applicable to other locations. The results of the simulation could prove to be instrumental in the decision-making process of the City in restoring the existing building stock and new construction. The preparedness of the urban dwellers for the climatic changes in upcoming decades will work towards the sustainable cities of future.

ACKNOWLEDGMENTS

The work presented in this paper was funded by the 2016 Iowa State University Presidential Initiative for Interdisciplinary Research (PIIR) into Data Driven Science. The authors are grateful for the support.

REFERENCES

1. A. Nakano , B. Bueno , L. Norford , C. Reinhart, Urban Weather Generator – A Novel Workflow for Integrating Urban Heat Island Effect within Urban Design Process. *Building Simulation* (2015)
2. B. Bruno, L. Norford, J. Hidalgo, and G. Pigeon, The Urban Weather Generator. *Journal of Building Performance Simulation 6*, no. 4 (2013) 269-81. doi:10.1080/19401493.2012.718797.
3. B. Mann, U. Passe, S. Rabideau, and E. Takle, Future Context for Thermal Comfort: Impact of a Changing Climate on Energy Demand and Human Thermal Comfort. *Proceedings of Windsor Conference* (2012)
4. C. Davila, C. Reinhart, J Bemis, Modeling Boston: A workflow for the generation of complete urban building energy demand models from existing urban geospatial datasets. *Energy* (2016) 237 – 50. doi:http://dx.doi.org/10.1016/j.energy.2016.10.057
5. C. Krejci, U. Passe, M. Dorneich, and Nathan Peters, A Hybrid Simulation Model for Urban Weatherization Programs. *Proceedings of WinterSim* (2016)
6. C. Reinhart, and C. Cerezo Davila, Urban Building Energy Modeling – A Review of a Nascent Field. *Building and Environment 97* (2016) 196-202. doi:10.1016/j.buildenv.2015.12.001.
7. C. Reinhart, T. Dogan, J. A. Jakubiec, T. Rakha, and A. Sang, Umi – An Urban Simulation Environment for Building Energy Use, Daylighting and Walkability. *Proceedings of Building Performance Simulation* (2013): 476 – 83.
8. Capitol East Neighborhood Charter Plan Update. Retrieved from: http://lib.dr.iastate.edu/cgi/viewcontent.cgi?article=1001&context=resilientneighborhoods_plans. As of 26 February, 2017.
9. City of Des Moines GIS data. Retrieved from: https://maps.dmgov.org/apps/mapcenter/GetDSMData.aspx. As of 1 May 2016.
10. Climate Protection Partnership Division in the U.S. EPA's Office of Atmospheric Programs, Reducing Urban Heat Islands: Compendium of Strategies, Climate Protection Partnership Division in the U.S. EPA's Office of Atmospheric Programs, 2013, Retrieved from http://www.epa.gov/heatisland/mitigation/coolroofs.htm As of 27 November, 2016
11. D. Kurn, S. Bretz, B. Huang, and H. Akbari. 1994. The Potential for Reducing Urban Air Temperatures and Energy Consumption through Vegetative Cooling (1994) (PDF) (31 pp, 1.76MB). *ACEEE Summer Study on Energy Efficiency in Buildings, American Council for an Energy Efficient Economy*.
12. Iowa Electricity Rates. Electricity Local. Retrieved from: http://www.electricitylocal.com/states/iowa/. As of 28 November, 2016.
13. J. Huang, H. Akbari, and H. Taha, The Wind-Shielding and Shading Effects of Trees on Residential Heating and Cooling Requirements. (1990*) ASHRAE Winter Meeting, American Society of Heating, Refrigerating and Air-Conditioning Engineers*. Atlanta, Georgia.
14. K. Kalvelage, U .Passe, S. Rabideau, and E. S. Takle, Changing Climate: The Effects on Energy Demand and Human Comfort. *Energy and Buildings 76* (2014) 373-80. doi:10.1016/j.enbuild.2014.03.009.
15. M. Bhandari, S. Shrestha, J. New, Evaluation of weather datasets for building energy simulation. *Energy and Buildings 49* (0) (2012) 109–118, doi: http://dx.doi.org/10/10.1016/j.enbuild.2012.01.033
16. McNeel, 2013, Rhinoceros version 5.0, Retrieved from: www.rhino3d.com/ As of 28 February 2017.
17. NARCCAP, National Center for Atmospheric Research Earth System Grid data portal. [Data file], The North American Regional Climate Change Assessment Program dataset, 2010, Retrieved from http://www.narccap.ucar.edu/data/data-tables.html.
18. Polk County Assessor website. 2015. Retrieved from: http://web.assess.co.polk.ia.us/cgi-bin/web/tt/infoqry.cgi?tt=home/index. As of 6 April, 2016.

19. S. Patton, Development of a future typical meteorological year with application to building energy use. *Master of Science Thesis*, Iowa State University, Ames, IA, 2013, http://lib.dr.iastate.edu/etd/13635 Paper 13635.

20. S. Rabideau, U. Passe, E. Takle, Exploring alternative to the "Typical Meteorological Year" for incorporating climate change into building design. Report CH12-CO49, *ASHRAE Transactions* 118 (1) (2012) 384–391.

21. Shapefiles. Retrieved from: https://doc.arcgis.com/en/arcgis-online/reference/shapefiles.htm. As of 1 December, 2016.

22. T. Dogan, and C. Reinhart. Automated Conversion of Architectural Massing Models into Thermal 'Shoebox' Models. *Proceedings of Building Performance Simulation* (2013) 3745 – 52.

23. Umi, Rhino based design environment. Retrieved from: http://www.urbanmodeling.net/. As of 27 November, 2016.

24. United States Department of Energy. 2016a. "What is Weatherization?" Retrieved from: http://energy.gov/eere/wipo/what-weatherization. As of 4 June, 2016.

25. United States Department of Energy. 2016b. "Weatherization Assistance Program." Retrieved from: http://energy.gov/eere/wipo/weatherization-assistance-program. As of 4 June, 2016.

26. Using Trees and Vegetation to Reduce Heat Islands https://www.epa.gov/heat-islands/using-trees-and-vegetation-reduce-heat-islands. As of 28 February, 2017.

Energy Performance of Residential Buildings at District Level from Data Perspective

Yuezhong Liu, Rudi Stouffs

Department of Architecture,
National University of
Singapore, Singapore
liuyuezhong@u.nus.edu,
stouffs@nus.edu.sg

ABSTRACT

Energy performance becomes more and more important during the urban planning/design process. There are two fundamental methods used to predict and analyze the residential building stock: top-down and bottom-up. However, both methods face the issues from data source and analysis method. While urban planners/designers manage to handle complicated design problems, the huge increase in data from sensors and simulations does not help to reduce the burden of designers. On the contrary, unfamiliar data sets can bring designers into a hopeless tangle. This research proposes a method using data mining techniques (k-means and S3VM) to address such issues and enhance the design process. The problem statement will be discussed both from design and data perspectives. A scenario analysis is proposed to evaluate the new methods to predict the electricity consumption of public housing in Singapore. The low difference proves the feasibility and possibility to apply the familiar and unfamiliar data concept into the design process in the future.

Author Keywords

Spearman correlation; K-means; S3VM; Energy performance; Top-down and Bottom-up.

ACM Classification Keywords

I.6.3 SIMULATION AND MODELING Applications; H.2.8. Database Applications (Data mining).

1 INTRODUCTION

More than 80% of Singapore's resident population lives in public residential buildings. These buildings are developed and managed by the Housing and Development Board (HDB), and are all under temporary leaseholds. Figure 1 shows the existing HDB locations with blue color. Based on the annual report from Energy Market Authority of Singapore [7], buildings (including residential and non-residential) consume about half of the total electricity use in Singapore. Therefore, it is essential to focus on energy reduction in the building sector via design or engineering technologies that can significantly improve the energy efficiency of buildings, while ensuring livability and sustainability. From the urban planner perspective, the evaluation of the performance of a building is trending upwards to play an important role during the design process. Hence how to deal with the data to evaluate the energy performance becomes more important to designers and researchers.

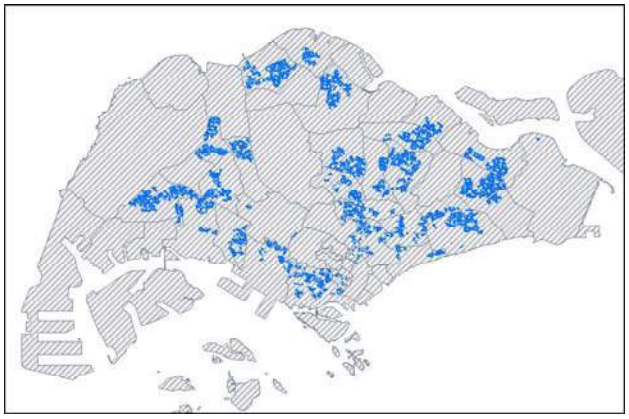

Figure 1. Existing HDB areas in Singapore.

This research will summarize the energy performance models from top-down and bottom-up approaches and propose a new method using Semi-Supervised Support Vector Machines (S3VMs) to deal with the familiar and unfamiliar data during the design process. A scenario analysis was carried out to discuss the possibility and feasibility for designers in the future.

2 LITERATURE REVIEW FOR RESIDENTIAL ENERGY PERFORMANCE AT DISTRICT LEVEL

This section only highlights the roadmap of methodologies and the underlying techniques available for residential building sector, which has already been given elsewhere [4, 21, 35, 37]. There are two fundamental methods used to predict and analyze the residential building stock energy performance: the top-down and bottom-up approaches [3]. Due to the limitations of the two fundamental methods, data mining technologies will be further reviewed from a semi-supervised learning perspective to check the possibility of solving these limitations.

SimAUD 2017 May 22-24 Toronto, Canada

2.1 Top-Down Method

Due to the energy crisis at the end of seventies, the top-down method was carried out to understand consumer behavior with changing supply and pricing for national energy planning [15, 17, 32]. Most top-down methods utilized historic aggregated energy information to regress the energy consumption of the building stock. Hence the top-down method relies on large statistical data and economic theory. Zhang used a regression model to examine the relationship between the annual energy consumption per household (UEC) and heating degree-days for China, Japan, Canada, and the United States [38]. He also found that the annual consumption of coal is decreasing while the consumption of electricity and gases still keeps growing since the 1990s. Ozturk et al. developed energy estimation equations based on a genetic algorithm (GA) for the residential-commercial sector and examined the effect of the design parameters on the energy input of the sector [30]. The input data contained gross domestic product (GDP), population, import, export, house production, cement production and basic house appliances consumption figures.

Swan and Ugursal concluded that the top-down method treats the residential energy consumption as an energy sink rather than individual end-uses [36]. They listed out the common variables for the top-down models, which include macroeconomic indicators (gross domestic product (GDP), employment rates, and price indices), climatic conditions, housing construction/demolition rates, and estimates of appliance ownership and number of units in the residential sector. Summerfield and Lowe developed two models: 1) the annual delivered energy, price, and temperature (ADEPT) model using multiple linear regression and 2) a seasonal temperature energy price (STEP) model using polynomial multiple regression to identify the trajectory of total delivered energy to UK households [35]. The National Energy Modeling System (NEMS) is developed and maintained by the Energy Information Administration (EIA) Office to provide projections of domestic energy-economy markets in the long term and perform policy analyses requested by decision-makers [8-10]. NEMS consists of one integrated module, four supply modules, two conversion modules, four demand modules, and two simulation modules. These modules enable NEMS to predict and analyze the energy and economy interactions (macroeconomic activity).

The top-down approach is used to provide long-term projections in the absence of energy supply and pricing shocks, and technological breakthroughs. Because of its lack of energy consumption of end-uses, such as quantifying the role of other factors and the effectiveness of specific policy measures, it is not suitable to identify key areas for improvements for the reduction of energy consumption [21, 35].

2.2 Bottom-Up Method

The bottom-up methods estimate residential energy consumption explicitly accounting for the end-uses (cooling load, heating load, electricity of appliances, water and etc.) for a specific group of buildings. From the previous review on modeling energy consumption of the residential sector [21, 35], the bottom-up methods commonly consist of two categories: the statistical method and the engineering method.

The bottom-up statistical method utilizes a regression technique and a variety of known indicator variables to attribute total measured energy consumption to individual end-uses [1, 6, 18, 20, 26]. The bottom-up engineering method measures energy consumption of the end-uses based on their variables or characteristics [11, 13, 16, 29]. Swan, Ugursal, and Beausoleil-Morrison have developed a national residential energy model of Canada using a detailed database of nearly 17,000 buildings [36]. The research result showed that each of these house records contain sufficient data to enable the accurate characterization of its energy performance through building performance simulation. Kavgic et al. further elaborated and compared the common bottom-up models from different countries for residential energy consumption. They pointed out that the most important shortcoming of all these current models is their lack of transparency and quantification of inherent uncertainties [21].

Hence, the current bottom-up methods lack publicly available detailed data and underlying reliable algorithms during inputs and outputs process [21].

2.3 Data Mining

Data mining appears as a recognizable research discipline in the early 1990s [31], which also is the core stage of the knowledge discovery process that is aimed at the extraction of interesting and implicit information from large data [12]. Data mining can be considered a superset of many different methods: statistical methods and machine learning [19]. Due to this sense, data mining could be categorized into 1) supervised learning (predictive), 2) unsupervised learning (descriptive), and 3) semi-supervised learning (predictive and descriptive). The goal of supervised learning is to learn a relationship between input and output data [22]. Unsupervised learning aims to find interesting structures in the data [14]. The target of semi-supervised learning is to enhance the accuracy of both predictive and descriptive processes [5]. Zhu and Goldberg pointed out that most semi-supervised learning strategies are based on extending either unsupervised or supervised learning to include additional information typical of the other learning paradigm [40]. The comprehensive fundamental methods and algorithms have been given elsewhere [5, 40]. They identified the popular methods such as expectation maximization with generative mixture models, self-training, co-training, transductive support vector machines, and graph-based methods. This research addresses the question

whether semi-supervised learning is meaningful to solve the large data problems during the urban planning process. Specifically, in comparison with a supervised algorithm that uses only labeled (familiar) data, can one hope to have a more accurate prediction by taking into account the unlabeled (unfamiliar) data points? In principle, the answer is "yes". However, there is an important prerequisite: that the distribution of examples, which the unlabeled data will help elucidate, is relevant for the classification problem.

3 RESEARCH METHODOLOGY

This research will address two design problems: 1) From a planner perspective, how many data will be enough to evaluate the energy performance from urban planners' perspective? From a data perspective, the question becomes how to reveal the sufficient key variables to predict energy consumption? 2) As an urban planner, how to deal with the large data from different disciplines? From a data perspective, the question becomes how to deal with labeled and unlabeled data?

There are five steps to answer the two problems:

1) Available data: the available data will include all the influence variables from different domain subjects.

2) Correlation (Spearman): this step will check the correlation index between the energy usage intensity and the other variables (population, weather, economic, etc.).

3) Clustering (K-means, k=3): from the correlation results from step 2, all the variables will be grouped into three categories: high impact, medium impact and low impact.

4) Semi-Supervised Support Vector Machines (S3VMs): the classification method will be carried out to predict the district energy consumption for HDB buildings.

5) Comparison: this step compares the results from step 4 to identify the accuracy of different variables. The variables will be dynamically categorized with reference to designers into two groups: familiar and unfamiliar.

The systemic diagram of the proposed method is shown in Figure 2.

3.1 First Step: Available Data

In order to make the proposed method more understandable, this research clarifies some terms from data mining and urban planning/design. Considering urban planning as a profession, with its background domain knowledge, the large dataset coming from the design process could be categorized into two groups: familiar and unfamiliar to the designer, commonly denoted with the terms labeled and unlabeled in data mining.

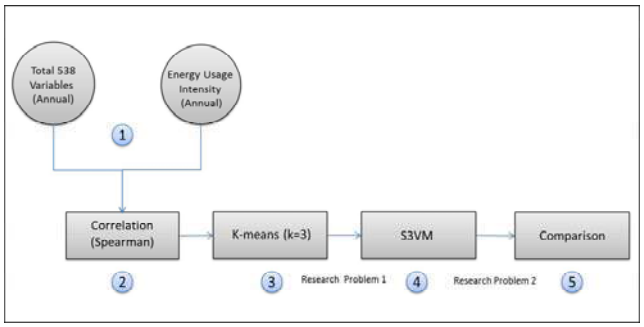

Figure 2. The five steps of the proposed systemic method.

Figure 3 summarizes the important variables with impact on energy consumption of the top-down and bottom-up methods from literature. These can be classified respectively as familiar and unfamiliar. However, due to the policy and privacy issues, not all of the variables are available in Singapore. This research collects the recent 10 years' annual data from various data sources. There are in total 538 variables from different knowledge domains. Table 1 shows the total annual electricity consumption by dwelling type. HDB buildings have a fixed internal design: 2-room (45.3 sqm), 3-room (65.4 sqm), 4-room (90.3) and 5-room (110.2 sqm). Given the design area and total energy consumption, the energy usage intensity (kwh/m2) can be considered as the base variable. The other variables will be calculated from the correlation value to the base variables.

3.2 Second Step: Spearman's Rank Correlation Coefficient

Spearman's rank correlation coefficient is represented as r_s for a sample statistic. It assesses how well the relationship between two variables can be described using a monotonic function. And it is appropriate when one or both variables are skewed or ordinal and is robust when extreme values are present [23]. For a correlation between variables x and y, the formula for calculating the sample Spearman's correlation coefficient is given by [27, 28]:

$$r_s = 1 - \frac{6*\sum_{n=1}^{n} d_i^2}{n*(n^2-1)} \quad (1)$$

where, d_i is the difference between the two ranks of each observation, and n is the number of observations.

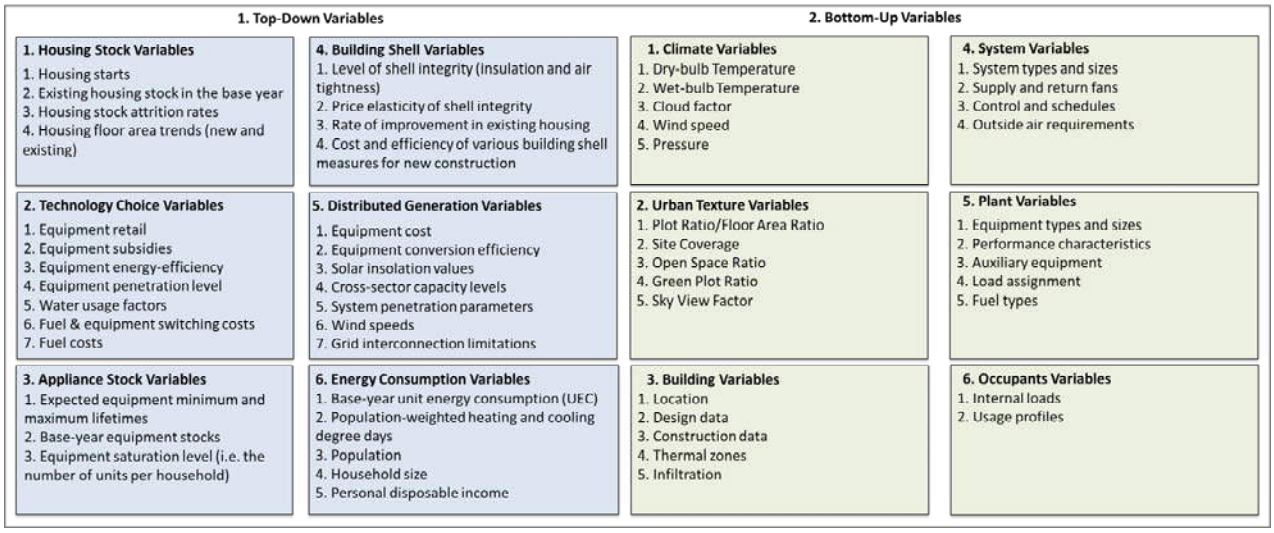

Figure 3. The important top-down and bottom-up variables.

3.3 Third Step: K-means Clustering

K-means [25] is one of the simplest unsupervised learning algorithms that solve the clustering problem. The procedure follows a simple and easy way to classify a given data set through a certain number of clusters (assume k clusters) fixed a priori. The goal of K-Means algorithm is to find the best division of n entities in k groups. Formally, it is to partition the n entities into k sets S_i, in order to minimize the within-cluster sum of squares (WCSS), which is defined as:

$$\sum_{j=1}^{k}\sum_{i=1}^{n}\left\|x_i^j - c_j\right\|^2 \quad (2)$$

where the term $\left\|x_i^j - c_j\right\|^2$ presents the distance between an entity point and the cluster's centroid.

The k-means algorithm is composed of the following steps [24]:

1. Define an initial set of k means m^1, …, m^k. A very common one is to assign random values for the centroids of all groups. In this research, k=3. Hence the clustering results will contain three groups: high impact, medium impact and low impact.

2. Assign each entity to the cluster that has the closest centroid. In order to find the cluster with the most similar centroid, the algorithm must calculate the distance between all the entities and each centroid.

3. Recalculate the values of the centroids. The values of the centroids' fields are updated, taken as the average of the values of the entities' attributes that are part of the cluster.

4. Repeat steps 2 and 3 iteratively until entities no longer change groups.

3.4 Fourth Step: Semi-Supervised Support Vector Machines

Semi-Supervised Support Vector Machines (S3VMs) are developed from Support Vector Machines (SVMs). SVMs rely on training data to generate a separating hyperplane that splits the given data into two different classes. SVMs are formulated into optimization problems in order to find a series of weights and a constant b, which together represent the separating plane. Such a decision boundary is defined as [2]:

$$f(x) = w^T x + b \quad (3)$$

where w^T is the parameter vector that specifies the orientation and scale of the decision boundary, and b is an offset parameter.

Base Variables	2005	2006	2007	2008	2009	2010	2011	2012	2013	2014	2015
Overall	6,092.5	6,109.1	6,163.7	6,094.0	6,430.8	6,636.0	6,482.7	6,629.5	6,754.9	6,924.4	7,220.9
Public Housing	3,777.4	3,746.9	3,767.3	3,724.0	3,902.3	4,011.0	3,911.6	3,970.1	4,038.8	4,125.7	4,284.2
1/2 -Room	78.4	70.9	72.0	71.9	76.6	81.2	85.0	90.5	97.9	108.3	120.7
3-Room	703.5	690.1	695.1	690.5	722.9	744.6	726.5	729.0	734.1	748.2	770.1
4-Room	1,498.3	1,486.1	1,490.0	1,475.3	1,548.5	1,596.6	1,564.4	1,597.9	1,633.0	1,675.8	1,748.8
5-Room and Executive	1,497.2	1,499.7	1,510.3	1,486.2	1,554.3	1,588.5	1,535.7	1,552.6	1,573.9	1,593.3	1,644.6

Table 1. Total Household Electricity Consumption by Dwelling Type, 2005 - 2015.

However, the traditional SVMs require the data to be labeled before classification analysis. Figure 4 shows the difference between SVMs and S3VMs. With only labeled data (a), the linear decision boundary that maximizes the distance to any labeled instance is shown in solid line. Its associated margin is shown in dashed lines. With additional unlabeled data (b), under the assumption that the classes are well-separated, the decision boundary seeks a gap in unlabeled data.

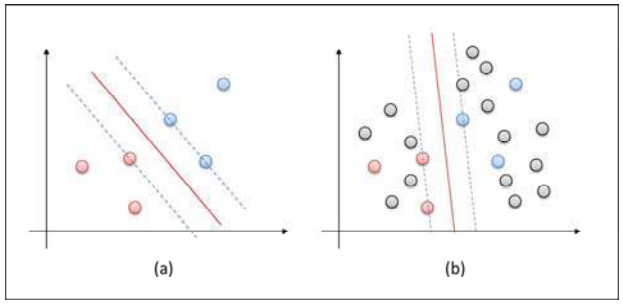

Figure 4. Difference between SVMs and S3VMs; a) SVM decision boundary, b) S3VM decision boundary.

3.5 Fifth Step: Comparison

This step will carry out a scenario analysis to integrate the results from the preview steps. The scenario analysis will be started from an urban planner's perspective. As the data is proposed as familiar and unfamiliar, the scenarios consider the urban planners divided into two groups: novices and experts. The difference between the results comes from the definition of familiar and unfamiliar data for designers. Figure 5 shows the workflow of the proposed scenario analysis.

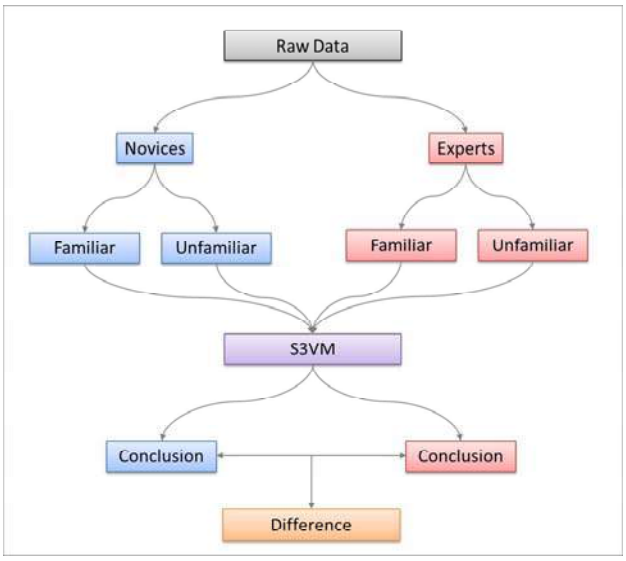

Figure 5. Scenario analysis for defining familiar and unfamiliar data by different planners.

4 RESULT AND DISCUSSION

A comparison between the actual electricity consumption of HDB buildings and the predicted consumption using the proposed method is made. Figure 6 shows the real HDBs' electricity consumption in 2015 obtained from the Energy Market Authority of Singapore [7]. The HDB buildings with postcodes starting with 820 were built in 2005, each with 19 4-room apartments (90~96 sqm) and 74 5-room apartments (110 sqm); the HDB buildings with postcodes starting with 163 were completed in 1975, each with 156 2-room apartments (38 sqm) and 12 3-room (76 sqm) apartments. The HDB buildings with postcodes starting with 080 were completed in 1975, each with 29 3-room apartments (76 sqm), 87 4-room (90~96 sqm) apartments and 29 5-room (110 sqm) apartments. The actual energy consumption will be compared to the result predicted by the S3VM method. Considering the results from the steps, the discussion will be categorized into two parts respected to the two design problems: result from k-means and result from S3VM.

District Area	Postcode	Units per Building	Total Electricity Consumption
	820643 820645 820646 820647 820848 820649 820651 820652	4-room: 19 5-room: 74	87,036.0 kWh/annum
	163002 163004 163006 163008	2-room: 156 3-room: 12	23,111.3 kWh/annum
	080009 080011 080012 080013 080016 080017 080018 080019	3-room: 29 4-room: 87 5-room: 29	98,834.4 kWh/annum

Figure 6. Energy consumption (in 2015) of three district level residential buildings from three locations in Singapore.

4.1 Result of k-means

Considering the final variables from Figure 3, the k-means clustering is applied to the correlation result of a total of 538 variables. The center values are 0.8756 (first clustering), 0.4481 (second clustering), and 0.0252 (third clustering). Figure 7 shows the high impact clustering (first row), medium clustering (second row) and low clustering (third row) with respect to energy consumption. The k-means result reveals that there are 36 variables in the high impact clustering: 1) professional, scientific, technical, administration and support activities, 2) percentage of population living in public flats, 3) real change in median monthly household income from work per household member, 4) real change in average monthly household income from work per household member, 5) air

temperature absolute extremes maximum, and 6) planning area energy consumption. Hence for the planners/designers who consider the long-term (annual) energy performance, the prior choice should analyze the data from the listed six aspects. Hence these variables should be considered as core knowledge for planners/designers. In other words, these are the familiar datasets for planners/designers. The medium impact clustering contains 42 variables: 1) wholesale and retail trade, 2) electricity tariff, 3) gross domestic product (GDP) deflator, 4) percentage of home-ownership flats, 5) real change in median monthly household income from work, 6) number of rainy days and 7) power suppliers in Singapore. The data of this clustering mainly comes from subjects of economy and meteorology. Due to the variety of the data and the limitation of the profession, the datasets of this clustering would be considered as unfamiliar datasets for planners/designers. The knowledge of this clustering could be the line of differentiation between novices and experts. Finally, the low impact clustering includes 460 variables, which mainly relate to electricity generation, building construction, unit's number of planning area, and part of weather data. It reveals that the variables of facilities will be more important than total population. These datasets will also be considered as unfamiliar data for planners/designers.

Figure 7. Variables clustering by k-means (number represents unique ID for each variable).

4.2 Result of S3VM

In order to improve the prediction results, there are two approaches: a) improve the data quality and b) improve the calculation algorithms. Hence the scenario analysis will make two assumptions: 1) The domain knowledge of novices is less than experts; 2) novices and experts both choose the S3VM as the base data analysis method. From the result of k-means, the high, medium and low clustering variables are used to calculate the electricity consumption of three locations by the S3VM method. The kernel function is based on the result of k-means. S3VM will classify all the available input data by planners as positive/negative variables. The sum of results from S3VM is considered as the bias for the simulation results of energy simulation (EnergyPlus). According to the three clustering variables, three input files for EnergyPlus are generated. Figure 8 shows the energy prediction difference with respect to the three clustering variables without considering bias value from S3VM.

Urban planners are distinguished between novices and experts. We draw two different scenarios: 1) Familiar and unfamiliar data. The novices are only familiar with the data from the high impact clustering and the experts are not only familiar with the knowledge from the high but also from the medium clustering. Hence if they all use same prediction method, the difference will be 4.88% for novices and 2.22% for experts (2.22% is based on the inputs including the high and medium variables together). 2) Semi-Supervised learning method. Both the novices and experts choose to use the S3VM method to add bias for the prediction result. The difference will be 3.10% for novices and 2.22% for experts. The bias of S3VM helps to reduce the difference from 4.88% to 3.1% for novices, which also proves the effectiveness of this proposed method.

Hence, we refer to the research problems in the methodology part: 1) how many data will be enough to evaluate the energy performance from an urban planner's perspective? This is an open question. With respect to the S3VM method, the data could be as much as possible. But the sufficient data should include all the high and medium impact variables shown in figure 7. 2) How should urban planners deal with the large data from different disciplines? This research proposes to distinguish the familiar and unfamiliar concept for designers' domain knowledge. The semi-supervised learning methods have the ability to deal with the labeled and unlabeled data. S3VM will be one solution to deal with the energy performance data.

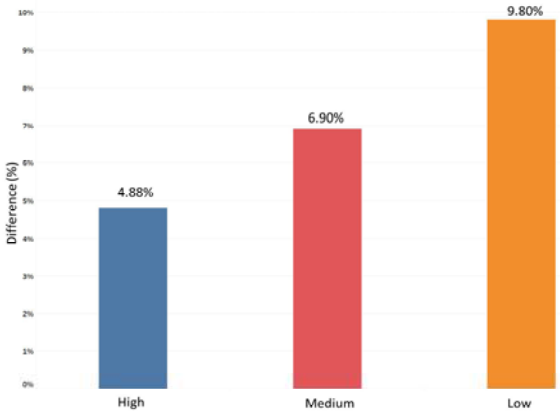

Figure 8. Energy difference between three clustering.

5 CONCLUSION

This paper highlighted the data process problems for energy performance during the urban planning. The two fundamental questions from data source and analysis method are raised and answered by applying data mining technologies. The results show the Semi-supervised learning methods have the ability to deal with the design data from different disciplines.

This paper also expands on the problem statement and gives a brief overview of the literature review on sufficient energy performance variables. The k-means clustering results suggest the sufficient variables: 1) professional, scientific, technical, administration and support activities, 2) percentage of population living in public flats, 3) real change in median monthly household income from work per household member, 4) real change in average monthly household income from work per household member, 5) air temperature absolute extremes maximum and 6) planning area energy consume. Two scenarios distinguishing between novice and expert designers are described. The result of S3VM shows the feasibility and possibility to apply the familiar and unfamiliar concept to the analysis stage of the urban planning/design process.

However there remain some limitations to this study, namely the robustness experiment of the S3VM method has not been tested with respect to other design data. The sufficient variables also depend on building types and countries. But the familiar and unfamiliar concept could be expanded in the design research field. In the future, the proposed method will be further developed to become readily usable as an urban planning/design support tool within research, education and, possibly, practice.

ACKNOWLEDGMENTS

The authors would like to acknowledge National Environment Agency (NEA) and Singapore Department of Statistics (DOS) for supporting the essential data.

REFERENCES

1. Aydinalp-Koksal, Merih, and V. Ismet Ugursal. 2008. "Comparison of Neural Network, Conditional Demand Analysis, and Engineering Approaches for Modeling End-Use Energy Consumption in the Residential Sector." *Applied Energy* 85(4): 271–96.
2. Bennett, Kristin P, and Ayhan Demiriz. 1999. "Semi-Supervised Support Vector Machines." *Advances in Neural Information Processing Systems*: 368–74.
3. Böhringer, Christoph, and Thomas F Rutherford. 2008. "Combining Bottom-up and Top-Down." *Energy Economics* 30(2): 574–96.
4. Böhringer, Christoph, and Thomos F. Rutherford. 2009. "Integrated Assessment of Energy Policies: Decomposing Top-down and Bottom-Up." *Journal of Economic Dynamics and Control* 33(9): 1648–61.
5. Chapelle, Olivier, Bernhard Scholkopf, and Alexander Zien. 2006. *Semi-Supervised Learning*. Cambridge, MA: MIT Press.
6. Douthitt, Robin A. 1989. "An Economic Analysis of the Demand for Residential Space Heating Fuel in Canada." *Energy* 14(4): 187–97.
7. EMA. 2015. "Energy Market Authority : Operation Statistics." http://www.ema.gov.sg/reports/id:72/\ninternal-pdf://989/id72.html.
8. Energy Information Administration. 2009. 581 *The National Energy Modeling System : An Over View 2009*. www.eia.doe.gov/oiaf/aeo/overview/.
9. Energy Information Administration. 2013. *Residential Demand Module of the National Energy Modeling System: Model Documentation 2013*. US. http://www.eia.gov/forecasts/aeo/nems/documentation/residential/pdf/m067(2013).pdf.
10. Energy Information Administration. 2014. *Integrating Module of the National Energy Modeling System : Model Documentation 2014*. US. https://www.eia.gov/forecasts/aeo/nems/documentation/integrating/pdf/m057(2014).pdf.
11. Farahbakhsh, H, V I Ugursal, and A S Fung. 1998. "A Residential End-Use Energy Consumption Model for Canada." *INTERNATIONAL JOURNAL OF ENERGY RESEARCH* 19(22): 1133–43.
12. Fayyad, Usama, Gregory Piatetsky-Shapiro, Padhraic Smyth, and Ramasamy Uthurusamy. 1996. *Advances in Knowledge Discovery and Data Mining*. Menlo Park, CA: American Association for Artificial Intelligence.
13. Firth, S. K., K. J. Lomas, and A. J. Wright. 2010. "Targeting Household Energy-Efficiency Measures Using Sensitivity Analysis." *Building Research & Information* 38(1): 25–41.
14. Ghahramani, Zoubin. 2004. "Unsupervised Learning BT - Advanced Lectures on Machine Learning." *Advanced Lectures on Machine Learning* 3176(Chapter 5): 72–112.
15. Haas, Reinhard, and Lee Schipper. 1998. "Residential Energy Demand in OECD-Countries and the Role of Irreversible Efficiency Improvements." *Energy Economics* 20(4): 421–42.
16. Hens, H., G. Verbeeck, and B. Verdonck. 2001. "Impact of Energy Efficiency Measures on the CO2 Emissions in the Residential Sector, a Large Scale Analysis." *Energy and Buildings* 33(3): 275–81.
17. Hirst, E., and J. Carney. 1979. "The ORNL Residential Energy-Use Model: Structure and Results." *Land Economics* 55(3): 319–33.
18. Hsiao, Cheng, C. Mountain, and Kathleen Ho Illman. 1995. "A Bayesian Integration of End-Use Metering and

Conditional-Demand Analysis." *Journal of Business & Economic Statistics* 13(3): 315–26.

19. Jackson, Joyce. 2002. "Data Mining: A Conceptual Overview." *Communications of the Association for Information Systems* 8: 267–296.
20. Kalogirou, Soteris a. 2006. "Artificial Neural Networks in Energy Applications in Buildings." *International Journal of Low-Carbon Technologies* 1(3): 201–16.
21. Kavgic, M. et al. 2010. "A Review of Bottom-up Building Stock Models for Energy Consumption in the Residential Sector." *Building and Environment* 45(7): 1683–97.
22. Kotsiantis, Sotiris B. 2007. "Supervised Machine Learning: A Review of Classification Techniques." *Informatica* 31: 249–68.
23. Lehman, Ann, and Norm O Rourke. 2005. Analysis *JMP for Basic Univariate and Multivariate Statistics A Step-by-Step Guide*. Cary, NC: SAS Press.
24. MacKay, D J C. 2003. "An Example Inference Task: Clustering." *Information Theory, Inference and Learning Algorithms*: 640.
25. Macqueen, J. 1967. "Some Methods for Classification and Analysis of Multivariate Observations." *Proceedings of the Fifth Berkeley Symposium on Mathematical Statistics and Probability* 1(233): 281–97.
26. Mihalakakou, G., M. Santamouris, and A. Tsangrassoulis. 2002. "On the Energy Consumption in Residential Buildings." *Energy and Buildings* 34(7): 727–36.
27. Mukaka, M. M. 2012. "Statistics Corner: A Guide to Appropriate Use of Correlation Coefficient in Medical Research." *Malawi Medical Journal* 24(3): 69–71.
28. Myers, Jerome L., and Arnold D Well. 2003. *Research Design and Statistical Analysis*. New York: Routledge.
29. Natarajan, Sukumar, and Geoffrey J. Levermore. 2007. "Predicting Future UK Housing Stock and Carbon Emissions." *Energy Policy* 35(11): 5719–27.
30. Ozturk, Harun Kemal, Olcay Ersel Canyurt, Arif Hepbasli, and Zafer Utlu. 2004. "Residential-Commercial Energy Input Estimation Based on Genetic Algorithm (GA) Approaches: An Application of Turkey." *Energy and Buildings* 36(2): 175–83.
31. Piateski, Gregory, and Frawley William. 1991. *Knowledge Discovery in Databases*. Cambridge, MA: MIT Press.
32. Saha, G P, and J Stephenson. 1980. "A Model of Residential Energy Use in New Zealand." *Energy* 5(2): 167–75.
33. Snäkin, J. P. 2000. "An Engineering Model for Heating Energy and Emission Assessment. The Case of North Karelia, Finland." *Applied Energy* 67(4): 353–81.
34. Summerfield, A J, and R J Lowe. 2010. "Two Models for Benchmarking UK Domestic Delivered Energy." *Building research and information* 38(1): 12–24.
35. Swan, Lukas G., and V. Ismet Ugursal. 2009. "Modeling of End-Use Energy Consumption in the Residential Sector: A Review of Modeling Techniques." *Renewable and Sustainable Energy Reviews* 13(8): 1819–35.
36. Swan, Lukas, Ismet Ugursal, and Ian Beausoleil-Morrison. 2009. "A Database of House Descriptions Representative of the Canadian Housing Stock for Coupling to Building Energy Performance Simulation." *Journal of Building Performance Simulation* 2(2): 75–84.
37. Tuladhar, Sugandha D. et al. 2009. "A Top-down Bottom-up Modeling Approach to Climate Change Policy Analysis." *Energy Economics* 31(SUPPL. 2): S223–34.
38. Zhang, Qingyuan. 2004. "Residential Energy Consumption in China and Its Comparison with Japan, Canada, and USA." *Energy and Buildings* 36(12): 1217–25.
39. Zhou, Zhi Hua, and Ming Li. 2010. "Semi-Supervised Learning by Disagreement." *Knowledge and Information Systems* 24(3): 415–39.
40. Zhu, Xiaojin and Goldberg, A.B. 2009. "Introduction to Semi-Supervised Learning." *Morgan-Claypool*.

On Holistic Urban Energy Modelling and Optimization

Ralph Evins

Energy Systems and Sustainable Cities group,
University of Victoria, BC, Canada
revins@uvic.ca

ABSTRACT

New developments are needed in computational systems to facilitate truly 'holistic' urban energy modelling and optimization. This applies to the understanding of how to model holistically, which is poorly understood on a theoretical level, and the practicalities of how to achieve this, both computationally and in terms of collaborative model development.

This paper first summarises the development of the Holistic Urban Energy Simulation platform (HUES), covering the platform philosophy (multi-model ecologies), core modelling areas, an example application, and benefits and limitations. Barriers to greater holistic integration are discussed from theoretical and practical perspectives.

Future directions are posited for making modelling and optimization more holistic: appropriate modularity, better ways of linking computational modules (easier modularisation, a software bus, GUI-based reprogramming, semi-automated model configuration), use of statistical emulators (meta-models), and multi-method modelling. Conclusions are given related to theoretical and practical measures that could improve the holistic modelling and optimization of urban energy-related issues.

Author Keywords

Holistic; Modelling; Optimization; Building Energy; Urban Energy; Systems.

ACM Classification Keywords

I.6 SIMULATION AND MODELING.

1 INTRODUCTION

There is clearly a desire to perform 'holistic' modelling, design and optimization, in order to better capture the interactions that characterise problems in the urban energy realm; multiple attempts are reviewed in [1]. The driving motive is to find synergies that would not otherwise be available if analysed or optimized separately. Various areas in which buildings interact with each other and with the wider context are summarised below.

'Holistic' can be defined as the concept that

"...the parts of something are intimately interconnected and explicable only by reference to the whole." [2]

This captures many of the issues surrounding urban energy use, thus explaining its popular use as a buzzword in both commercial and research contexts. However, it is important to examine the implications of this from a modelling and optimization perspective, in order to be clear that approaches which are described as holistic are really so. A comprehensive, assessable definition of 'holistic' in urban energy is beyond the scope of this paper, but could include spanning more than one of the following 'dimensions':

- Demand, supply, networks & hubs (see §2.1)
- Time-scales (microseconds to years)
- Spatial scales (rooms to cities or countries)
- Energy streams (heat, electricity, cooling etc.)
- Other systems (transport, city planning etc.)
- Other contexts (financial, social etc.)

Buildings in urban areas affect each other directly via over-shading and sheltering. There is also a growing trend for buildings to be linked together into urban energy systems that share energy, for example using district heating or electrical microgrids. The design of future energy systems (centralised generation, distribution grids, district heating networks etc.) is inexorably linked to the buildings they supply through daily and annual demand and supply profiles, potential for load shifting and storage. This is true from the local scale (specific buildings, district networks) to much larger scales (aggregations into districts, city expansions, national grids). There are also other domains (electric vehicle deployment, urban transportation, urban planning) that both influence buildings (e.g. urban density) and are influenced by them (e.g. renewable energy supplies).

There is an ongoing move towards the use of computational optimization in building and urban energy [3], and this exacerbates many problems that are faced in holistic modelling. Progress has been made by applying standard optimizers (for example genetic algorithms) in an out-of-the-box manner to typical problems regarding building and urban design. However, there are limits to these approaches that can only be overcome by coupling optimization and modelling more closely. The most obvious way in which optimization can be holistic in scope is to embed holistic models within optimization processes. However, it is not necessarily effective or even possible to apply a simple optimizer to a complex problem.

It is sometimes not appropriate to use the same optimizer for all parts of an optimization problem. For example, MILP solvers have issues with many binary variables (such as discrete design choices), whilst meta-heuristic algorithms perform poorly at operational optimization. This can be overcome by splitting the problem into multiple levels. For example, the upper level (using a meta-heuristic) can determine building properties and system capacities, which are passed to a lower level (using MILP) that determines the operation [4]; further constraints, for example a check on grid capacity violations, can also be included in the upper level. The needs of holistic optimization processes

must also be accounted for when considering holistic modelling.

This paper first examines a previous effort in developing a platform for holistic urban energy simulation (HUES) and its application to integrated UES modelling. Barriers to the wider use of integrated modelling are proposed, then possible future directions are suggested that could aid in holistic modelling and optimization. Finally conclusions are drawn regarding theoretical and practical improvements that might be accomplished.

2 THE HOLISTIC URBAN ENERGY SIMULATION PLATFORM (HUES)

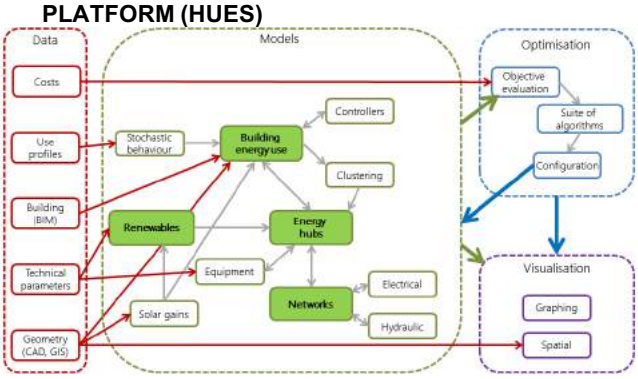

Figure 1. An overview of interactions between core modelling areas explored using the HUES platform (from [6]).

The HUES platform[i] contains many modules across a range of domains (see Figure 1); an introduction was presented in [5] and is summarised here. The *repository* contains *modules* of code and data that are navigated with the aid of a *semantic wiki* that details the *functionality* and *interconnectivity* of modules. Users submit modules via the wiki interface; repository updates are automatically reflected in the wiki. *Collections* of multiple modules and data together can be used to provide specific combinations that offer a particular functionality, for example as used for a publication. The means of interconnecting modules is bespoke; a script is developed to pass information and execution commands for any particular pathway that is required. The implementation environment is also specific to the module (e.g. EnergyPlus for energy modelling), with linking scripts in Python or occasionally MatLab for legacy reasons. The provision of a general infrastructure for module deployment aids expandability and adaptability, thus allowing complex systems to be modelled by incrementally adding relatively simple components.

The platform was developed with two aims in mind: to make it easier to integrate new modelling efforts, and to make it easier to integrate disparate models to better achieve holistic modelling. Whilst initially focussed on the simulation of urban energy systems, the platform provides an example of how interactions can be effectively modelled across the range of issues affecting urban energy use. Further applications are given in [6].

[i] See https://hues-platform.github.io/ and other links given in the electronic version of this paper.

The core concept behind the platform is that of a multi-model ecology (MME), as developed by Bollinger et al. in [7]. Rather than developing a single unmanageably complex code-base that cannot change and adapt to new problems, MMEs provide an *ecology* in which many modules interact and grow together to meet new challenges. The HUES MME is based on a code repository together with a semantic wiki that describes the modules, datasets and relationships between them.

2.1 Core module groups

Core modules of HUES are grouped around four topics critical to holistic modelling of urban energy systems.

Demand. Many building energy models exist, but they typically pre-date the need to model multiple buildings simultaneously. Core factors in modelling buildings as components of wider systems include:

- variability between buildings (concurrency of loads is critical to predicting the magnitude of peaks)
- thermal and electrical network connections
- geo-dependant modelling.

Supply. Buildings and urban areas have great potential for the generation of renewable energy. However, the temporal and spatial distribution of this availability must be modelled together with many other factors (e.g. over-shading and grid capacity for PV).

Networks. Connecting buildings together, either electrically or thermally, allows fluctuations in demands and supplies to be balanced locally, giving more efficient use and reducing impacts on the wider electrical grid. Key issues include:

- optimizing network connectivity and layout [8]
- assessing electrical grid capacity [9].

Hubs. So that energy flows are balanced across networks, operational optimization is needed; design optimization should account for these operational issues. Energy hubs [10] provide a process for achieving this.

2.2 Example application

An excellent example of the cross-domain use of the HUES platform concerns the optimization of an urban energy system in conjunction with building demands, district heating networks and electrical grid constraints [11]. Separate modules in the platform were combined to evaluate each of these areas:

- A set of EnergyPlus models evaluated building loads.
- Non-linear powerflow was assessed using MatPower.
- Linearised powerflow was included in the optimization.
- District heating layout optimization was included.
- An energy hub model optimized the whole problem.

It was established that omitting any of these areas leads to significantly sub-optimal solutions. For example, assessing electrical grid limitations together with system design and operation allows 37% lower costs for a given carbon emissions level, or 25% lower emissions for a given cost. The work analysed the best means of linearizing powerflow calculations, which relied on the interoperability between the detailed and simplified model implementations.

An integrated platform greatly assisted in the reuse of these modules to answer different research questions [8,9] and to apply them to new applications, e.g. electric vehicles [12]. It will also aid in the transfer of models and data to other users in the same research group; the easy sharing of such models is also expected to increase their reuse by other researchers.

2.3 Benefits and limitations

HUES currently consists of 27 computational modules from 15 contributors, as well as 13 datasets, a technology database, 11 scripts and 12 code snippets. It has proven effective at facilitating the integration and reuse of models (see above). Another example is a study on the effects of district size on optimal energy hub configuration considering demand variability. It has also aided cooperation amongst researchers, with initial contributions from many project partners, and subsequent expansion to other institutions and countries.

The interoperability of modules is currently limited to the use of bespoke scripts to link them; this is being addressed in 'Layer 2' modules that form coherent sets together with data sources and linking scripts. Modules interact as specified locally, with no means of determining all variables that could be exposed; this could be partially addressed by more rigorous use of the data specification. Users are currently required to install all necessary programs themselves, preventing 'one-click execution'; this could be overcome using a custom virtual machine.

3 BARRIERS TO HOLISTIC MODELLING

Below are a number of barriers that may impede more holistic modelling. They are generalisations of problems encountered with HUES, but also broadly apply to other platforms that encourage integrated modelling (e.g. Grasshopper, TRNSYS, CitySim, Modelica).

Lack of interconnectivity. Currently there are still far too few ways of getting programs to talk to each other, and methods that exist are often time-consuming, error-prone and limited in scope (e.g. manipulation of text input files).

Going backwards is hard. It may be necessary to deconstruct existing programs into smaller computational elements in order to recombine their parts in more holistic ways, which is psychologically challenging.

Computational inefficiency. Introducing interfaces between modules inevitably causes barriers to communication, which may become serious bottlenecks, particularly if the links are quick hacks. These could be overcome by clever coding, but this takes a lot of effort.

Exploding complexity. The more you can do, the harder it is to do anything (and the harder it is to know what to do). Platforms with vast potential functionality become very hard to use (Modelica currently falls into this category). Users may also become paralyzed by choice; greater guidance is needed from the theoretical side to understand what should be modelled for a particular purpose.

Parochial platforms. Many modellers are tied to a favourite platform, either psychologically, due to steep learning curves or language limitations, or commercial necessities.

4 NEW DIRECTIONS IN HOLISTIC MODELLING

Based on the examination of holistic modelling and optimization approaches discussed, and the barriers identified, some possible future directions are presented below, summarised in Figure 2; these form a long-term plan for the development of the HUES platform.

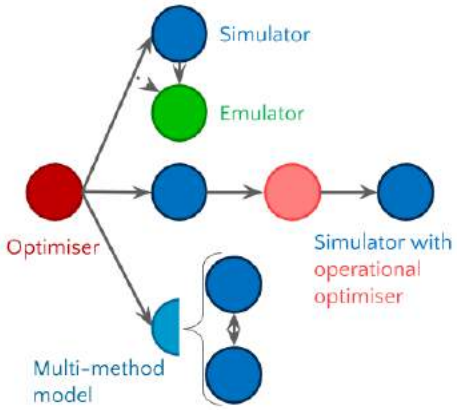

Figure 2. A possible configuration of a more holistic modelling and optimization framework.

4.1 Appropriate levels of modularity

The idea that a concept should be made *as simple as possible but no simpler* (often attributed to Einstein) is at the heart of the multi-model ecology way of thinking. Whilst care needs to be taken regarding the decomposability of systems through rigorous analysis at the higher level, modularisation will improve the ease with which model elements can be combined in new ways.

A first step in achieving more modularity in modelling is in being able to make any computational element into a self-contained module such that it can be configured, executed and interrogated from an external environment. This could apply to the whole element or to sub-elements.

4.2 Easier ways of linking modules

If modularity is pursued, it will become necessary to link ever more diverse modules. There is an inherent dichotomy between the need to regiment the interconnections between diverse computational modules (e.g. through enforcement of syntax) and the desire for a flexible set of modules to be combined in unforeseen ways. Below are some possible ways to address this (in increasing order of difficulty).

A software bus. A form of service--oriented architecture designed to facilitate the interconnection of diverse interchangeable components, this would aid integration and reconfiguration of models but also distributed development and deployment in the cloud.

GUI-based reprogramming. As well as using a GUI to connect specific data flows between modules (as in Grasshopper, TRN-SYS etc.), we need a graphical means of controlling the entire computational process. This would enable the flow of information and dependence between modules to be reconfigured much more rapidly.

Semi-automated reconfiguration. A self--organising system of models, where new 'paths' emerge based on the problems and priorities posed by users, experimenting and adapting to new problem instances and types.

4.3 Model emulation

Computational time is still a barrier to integration for many domains, for example CFD. Emulators (statistical models based on Gaussian processes or other approaches) to could be fitted model outputs, allowing slower modules to be replaced with fast approximations. For example, a meta-model can be used to predict wind flows around buildings for use in an energy simulation [13].

More advanced uses of emulation (which is a form of machine learning, currently a hot topic across many domains) could include emulating controller behaviour, emulating optimization results for lower-level optimization problems, or moving to emulated results in an optimization process as a model becomes well-fitted.

4.4 Multi-method modelling

The inclusion of other modelling paradigms such as agent-based modelling, systems dynamics or discrete event modelling could facilitate modelling that is more inclusive of different types of behaviour. For example, energy hub models embedded within agents could model system operation together with market dynamics. Combining multiple models with multiple optimizers (meta-heuristics, MILP etc.) will also facilitate multi-level optimization.

Another possibility is to include pre-existing models from one domain in another area, for example embedding of controller models in simulation models. Operational optimization using the energy hub approach does not accurately capture the behaviour of real controllers due to imperfect information (e.g. weather and use forecasts). The inclusion of controllers directly within simulations would overcome this, by co-simulating a control algorithm within a building or system model (e.g. using Modelica).

5 CONCLUSIONS

Much has been achieved in holistic modelling and optimization regarding urban energy, but much remains to be done. The platforms that currently exist may lure us into believing that many things are possible, but it may be worth considering their limitations before we over-commit.

Theoretical considerations in holistic modelling could strengthen the impact of work in this field, which is sometimes lacking in analytic rigour: it's too easy to point an algorithm or modelling approach at a new problem and hope for the best. This particularly applies to holistic optimization, where many poorly conceived or ill-posed problems receive attention. Stronger links should be made to concepts from systems theory regarding complexity and emergence. Can this be assessed *a priori*? How can we determine the degree of decomposability of a set of black-box systems? Can we perform an analysis of the results of an optimization and learn from this effectively?

There are practical considerations to address concerning easy-to-use integration platforms, computationally efficient module-based computation and better use of the immense potential of machine-learning. Better ways of avoiding 'model-death' (all those dusty files lost on hard-drives), effectively collaborating (via model and data sharing) and publishing (the elusive 'executable paper') may be serendipitous outcomes of this. Progress may require significantly different methods, revolutionary rather than evolutionary in approach.

REFERENCES

1. Allegrini, J, et al. 2015. A review of modelling approaches and tools for the simulation of district-scale energy systems. Renewable and Sustainable Energy Reviews, 52, 1391-1404.
2. Oxford Dictionaries online. https://en.oxforddictionaries.com/definition/holistic.
3. Evins, R. 2013. A review of computational optimisation methods applied to sustainable building design. Renewable and Sustainable Energy Reviews, 22, 230-245.
4. Evins, R. 2015. Multi-level optimization of building design, energy system sizing and operation. Energy, 90 Part 2, 1775-1789.
5. Bollinger, L, Evins, R. 2015. HUES: A Holistic Urban Energy Simulation platform for effective model integration. CISBAT conference, Lausanne, Switzerland.
6. Evins, R, Orehounig, K, Dorer, V. 2015. Integrated urban energy modelling approaches to support the Swiss Energy Strategy 2050. CISBAT conference, Lausanne, Switzerland.
7. Bollinger, L. A. et al. 2015. Multimodel Ecologies: Cultivating Model Ecosystems in Industrial Ecology. Journal of Industrial Ecology, 19, 252–263.
8. Morvaj, B, Evins, R, and Carmeliet, J. 2015. The impact of low energy buildings on the optimal design of distributed energy system and networks. Building Simulation, Hyderabad, India.
9. Morvaj, B, Evins, R, Carmeliet, J. 2016. Optimization framework for distributed energy systems with integrated electrical grid constraints. Applied Energy, 171, 296-313.
10. Evins, R, et al. 2014. New formulations of the 'energy hub' model to address operational constraints. Energy, 73, 387-398.
11. Morvaj, B. Holistic optimisation of distributed multi energy systems for sustainable urban areas. PhD thesis. *Forthcoming.*
12. Morvaj, B, et al. 2016. Integrating Multi-Domain Distributed Energy Systems with Electric Vehicle PQ Flexibility: Optimal Design and Operation Scheduling for Sustainable Low-Voltage Distribution Grids. Sustainable Energy, Grids and Networks, 8, 51–61
13. Evins, R, Allegrini, J, Moonen, P. 2014. Emulating site-specific wind flow information for use in building energy simulations. Building Simulation and Optimisation conference, London, UK

Modeling Energy for Urban Form Archetypes

Jonathan Salter, Ronald Kellett, Cynthia Girling and Fausto Inomata

University of British Columbia
Vancouver, Canada
{jsalter, rkellett, cgirling}@sala.ubc.ca, fausto.inomata@gmail.com

ABSTRACT
Increasingly, municipalities are planning for climate change at urban scales. Techniques for modeling the energy and emissions consequences of planning options are crucial to do this well, however, it can be difficult to simulate alternative energy and emissions options in smaller municipalities, with limited data. This paper describes an approach for simulating the energy use and greenhouse gas emissions of alternative policy scenarios. We use 3D archetypes that represent patterns of urban form common to many municipalities as the basis for modeling. Our process will translate these archetypes to parametric rules in Esri's CityEngine to facilitate rapid iteration of scenario variables. The broader purpose of this research is to inform planners and urban designers about the effectiveness of energy and emissions strategies in diverse, heterogeneous urban form patterns.

Author Keywords
Urban form; building energy; energy simulation; parametric modeling; CityEngine

ACM Classification Keywords
I.6.0 SIMULATION AND MODELING

1 INTRODUCTION

Increasingly, communities of all sizes are planning for emissions reductions at the municipal scale [1]. Therefore, understanding the interactions of urban form and energy for different patterns of development are critically important. In recent years, researchers and practitioners have come to better understand the importance of interactions between urban form, energy and emissions [2,3,6]. Most of these studies, however, have been conducted in large, more densely populated urban centres, and questions remain about the relationships between urban form, energy consumption and emissions across communities of different scales and compositions.

Large cities tend to have more, and higher quality, data with which to investigate climate change impacts and alternative energy and emission strategies. With fewer resources, smaller municipalities do not have the same opportunities to evaluate strategies for addressing energy demand and energy supply options in their communities. The research discussed in this paper, part of a larger Pacific Institute for Climate Solutions-funded project, aims to provide policy-relevant guidance on energy and emissions to communities across the province of British Columbia, Canada.

This paper presents ongoing research to develop an approach that draws upon urban form archetypes and parametric modeling of key spatial and aspatial variables to simulate the energy use and emissions consequences of alternative policy options. It draws upon and scales-up a common building archetypes modeling approach [1,10] to develop urban form archetypes derived from geospatial analysis. The approach uses MIT's Urban Modeling Interface (UMI) [1,5] to model energy and emissions in those archetypes. Finally, future work will convert archetypes into parametric rule sets in Esri's CityEngine, so that both archetypes and policy scenarios can be rapidly and iteratively modified to determine what options are energy- and cost-effective in different settings and climates.

2 METHODOLOGY

Figure 1 illustrates our methodology. Our approach began with a geospatial analysis of BC communities and subsequent development of archetypal patches of urban form (Figure 1, box a). The methodology then developed an energy modeling component (Figure 1, box b) using MIT's UMI to simulate energy end use for the archetypes of urban form. Future work will be focused on converting the archetypes to parametric rules in Esri's CityEngine, so they can be tailored to local land use policies (Figure 1, box c). Rapid iteration of alternative scenarios will enable us to test which energy reduction strategies suit different communities and urban form types. The sections that follow will discuss each of these methodological components in more detail.

2.1 Geospatial Analyses

Two primary questions motivated our geospatial analyses: in which patterns do most people in BC live, and in which patterns does most population growth concentrate? To conduct this analysis we used Census Canada Dissemination Area (DA) data for all of BC.

From this larger BC-wide analysis, we selected six municipalities with open or accessible data to conduct a more detailed land use and parcel-level analysis. Additional criteria were developed to ensure a broad cross-section of communities, including city population, growth rates, geography and climate. The six communities selected were Saanich, Vancouver, Surrey, Kelowna, Prince

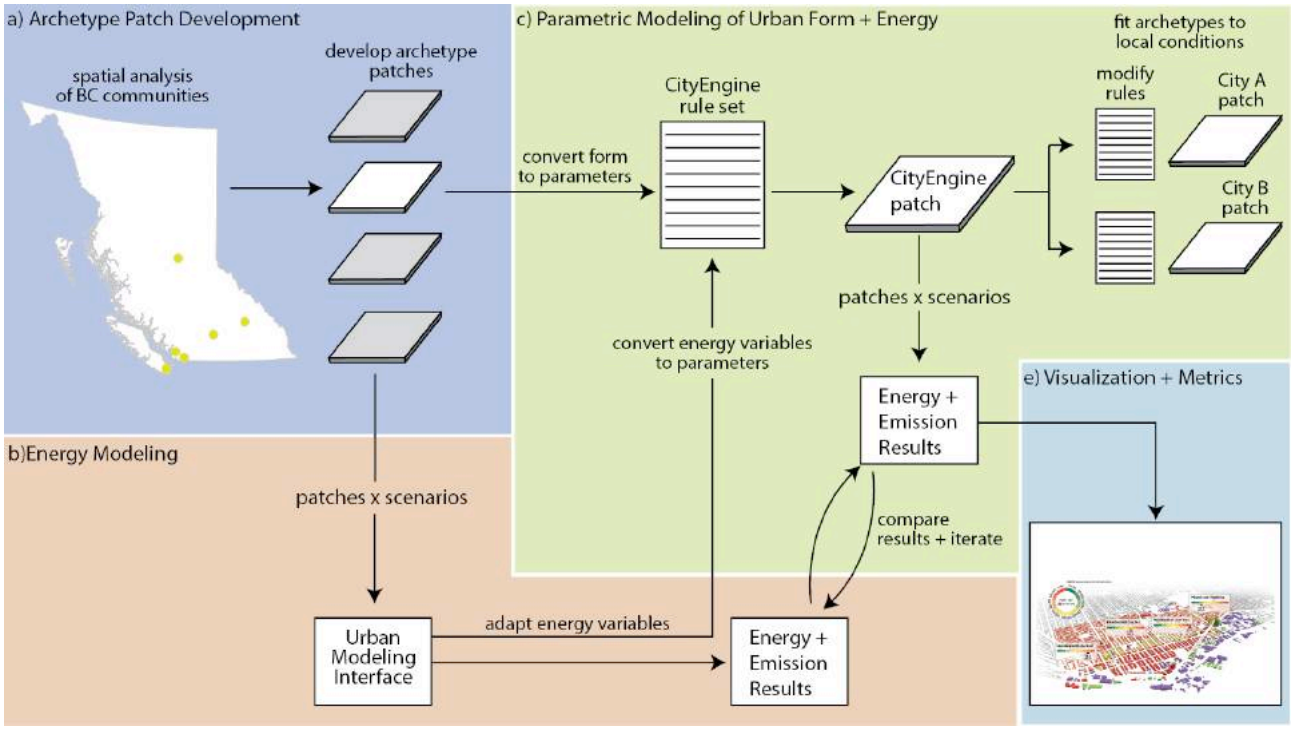

Figure 1. A diagram of the methodology and workflow discussed in this paper.

George and Revelstoke. Our archetypes are based on urban development patterns revealed in these six cities.

For each of the six cities we examined the land use composition of each census DA, then categorized DAs by a combination of population density and the proportion of land uses. From this analysis we identified nine archetypes that represent distinct urban form characteristics in BC municipalities. Table 1 presents the characteristics of these nine archetypes.

The predominance of archetypes with population densities below 35 pph is indicative of population densities and urban form in BC communities outside of the City of Vancouver, where 2/3 of British Columbians live at population densities below 35 pph. New growth in centres such as Saanich, Kelowna and Prince George also tend to be concentrated at these lower population densities.

Each archetype is based on median values for urban form metrics within a given density category, including: lot size, lot density, lot coverage, building footprint ratio, and street intersection density (see Figure 2).

Additional archetype design constraints included a 400m square configuration, to address walkability [8], and the need for each 400m patch to be surrounded by roads, so that they can be assembled to create 'super archetypes' that replicate larger neighbourhood and city patterns. Figure 2

20-35 pph	**loops and lollipops street pattern** 100% single family
20-35 pph	**loops and lollipops street pattern** >50% single family, <10% commercial
20-35 pph	**gridded street pattern** 100% single family
20-35 pph	**gridded street pattern** >50% single family, >15% multifamily, <10% commercial
0-35 pph	**Street pattern not applicable** >50% single storey commercial
40-65 pph	**loops and lollipops street pattern** >50% single family, >10% civic/institutional, >10% commercial
60-75 pph	**gridded street pattern** >50% single family, >10% multifamily, >10% commercial and mixed use
85-120 pph	**gridded street pattern** >50% multifamily, >10% commercial
210-250 pph	**gridded street pattern** >75% multifamily and mixed use, 0% single family

Table 1. Population density and land use characteristics in nine urban form archetypes.

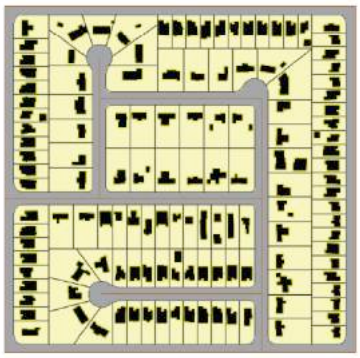

	20-35 pph single family median values	archetype values
lot density	8.39	8.25
lot size	722.20	800
coverage	192.49	194.52
footprint ratio	0.25	0.22
3-way inters.density	0.36	0.31
4-way inters.density	0.09	0.06

Figure 2. A low density single-family archetype example, showing archetype metrics compared to the DA median values for all DAs in a category.

illustrates the 20-35 pph single family, 'loops and lollipops' archetype. In order to conduct energy simulation on these archetypes, however, we needed 3D building models and associated data. For this we used our lab's existing database of building cases (www.elementsdb.ca) which has been developed and populated with real-world examples over the last decade. Each building case in the database has a 3D model and associated energy-relevant information such as building age, window-to-wall ratio, conditioned floor area, etc. The result is a 3D archetype with representative measured buildings (see 3D archetype example, Figure 3).

2.2 Energy Modeling

Traditionally, community-scale energy modeling has been performed using building archetypes – simple accounting models based on spreadsheet energy use values for known buildings similar to buildings in a study area [1,10]. Using this approach, it is possible to model building energy data over large areas with relatively irresolute data [5, 10].

More recently, researchers have been working to develop approaches that incorporate 3D building simulation to allow energy modeling that is more sensitive to exploration of alternative strategies, for example allowing for the simulation of different window-to-wall ratios, or the effects of building siting on solar gain. Two examples of this work are the SimStadt project at Hochschule für Technik Stuttgart [4] and MIT's UMI [1,5].

For this research project, we are using MIT's UMI to simulate energy demand for our archetype patches. UMI acquires 2D spatial data and 3D building data from Rhino. Energy-relevant information for each building is described in a building template file. This information, along with a local weather file for the study location are then passed to the US Department of Energy's EnergyPlus simulation engine to calculate energy end use. Figure 3 shows an example result for a simulation of the 20-35 pph, single family loops-and-lollipops archetype described in Figure 2. This example shows energy end use for the archetype populated with single-family homes constructed according to the current BC Building Code for the lower mainland zone, using Vancouver weather station data.

Based upon an analysis of applicable municipal and provincial policies, we are developing portfolios of energy reduction strategies to test against the nine urban form archetypes in different regions of BC (i.e. under different climate conditions). These portfolios will focus on both existing building stock (retrofitting and equipment changes) and new building stock (infill and new development). Using the UMI modeling approach, these portfolios of strategies can be incorporated into the 2D plan of archetypes, the 3D design of building models, and the materials and systems technologies of building template files.

2.3 Parametric Modeling

Recent developments in design, modeling and geospatial software have focused on parametric approaches which facilitate rapid iteration through alteration of model variables [9]. Relevant to our current research, parametric

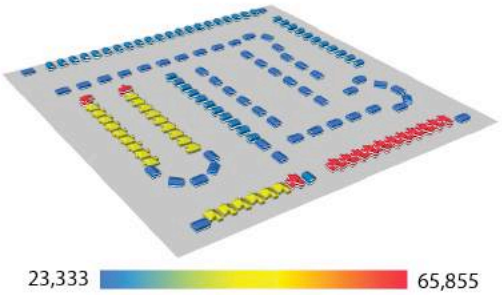

	# of Homes	Total Energy	Lighting	Equipment	Heating	Cooling	DHW
	32	24,264	2,027	2,455	13,065	388	6,328
	14	52,096	5,736	6,946	19,472	2,035	17,906
	24	36,558	3,829	4,637	14,752	1,386	11,954
	44	27,123	2,432	2,945	13,192	961	7,593
	18	23,413	2,027	2,455	12,208	395	6,328
Totals	**132**	**3,998,016**	**380,604**	**460,841**	**1,844,931**	**123,559**	**1,188,082**

Figure 3. An example UMI energy simulation for a low density, single-family archetype under Vancouver climate conditions. All energy numbers are in kW/h.

approaches will allow us to alter 2D features of our archetypes such as parcel sizes or building setbacks, and 3D features of our buildings, such as number of storeys or building orientation. This will enable us to fit our archetypes to different local conditions such as adjusting parcel sizes and road right-of-way widths to comply with municipal planning policies.

Additionally, these parametric approaches present the opportunity to incorporate energy variables and building performance algorithms directly into parametric rule files. This will facilitate the dynamic generation of both urban form *and* relevant energy metrics for rapid iteration of alternative energy and emissions scenarios.

Figure 4. An example conversion of an elementsdb building model (left) to parametric rules in CityEngine (right).

Through an NSERC Engage Plus, we are currently working with researchers from Esri Canada to convert our urban form archetypes into CityEngine parametric rule sets. As Figure 1 indicates, future work will focus on incorporating building energy performance metrics into those rule sets to explore alternative energy scenarios. Figure 4 shows the results of early work in this process, converting existing elementsdb models into CityEngine rules. A simple early prototype of energy use intensity based on building volume has been developed as a proof of concept, however, significant work remains.

3 DISCUSSION

This paper has described ongoing research to develop an approach for modeling energy at the neighbourhood scale across communities of different scales and different urban form characteristics. The goal of this research is to provide energy and emissions planning guidance to municipalities across BC. Associated research is developing portfolios of strategies to evaluate against the urban form archetypes described in this paper. Prototyping with UMI has demonstrated that this evaluation is possible using the described methodology. More significant challenges remain, however, in adapting the urban form archetypes and associated energy variables to parametric rules in Esri's CityEngine. However, the parametric approach presents significant advantages in both tailoring the archetypes to local conditions, and allowing for more rapid scenario iteration. The current application is focused on energy, however, the longer-term goal is to integrate energy metrics with other sustainability indicators to provide more comprehensive guidance to decision-makers [cf. 7, 8].

ACKNOWLEDGMENTS

We would like to thank our research partners at UBC and Esri Canada. We would also like to acknowledge funding for this research provided by the Pacific Institute for Climate Solutions, the National Science and Engineering Council, and Esri Canada.

REFERENCES

1. Cerezo Davila, C., Reinhart, C., & Bemis, J. Modeling Boston: a workflow for the generation of complete urban building energy demand models from existing urban geospatial datasets. *Technical Paper*, Boston Planning and Development Agency, 28 pp.
2. Futcher, J.A., & Mills, G. The role of urban form as an energy management parameter. *Energy Policy* 53 (2013), 218-228.
3. Kellett, R., Christen, A., Coops, N., van der Laan, M., Crawford, B., Tooke, R., Olchovski, I. A systems approach to carbon cycling and emissions modeling at an urban neighborhood scale. *Landscape and Urban Planning* 45,2 (2011), 6057-6069.
4. Nouvel, R., Brassel, K.H., Bruse, M., Duminil, E., Coors, V., Eicker, U., & Robinson, D. SIMSSTADT, a new workflow-driven urban energy simulation platform for CityGML. In Proceedings of the CISBAT Conference (2015), Lausanne, Switzerland.
5. Reinhart, C.F., & Cerezo Davila, C. Urban building energy modeling – a review of a nascent field. *Building and Environment* 97 (2016), 196-202.
6. Rode, P., Keim, C., Robazza, G., Viejo, P., & Schofield, J. Cities and energy: urban morphology and residential heat-energy demand. *Environment and Planning B: Planning and Design* 41 (2014), 138-162.
7. Rueda, S., de Cáceres, R. Cuchí, A. & Brau, L. El *Urbanismo Ecológico: Su Applicación En El Diseño De Un Ecobarrio En Figueres*. BCNecologia, Barcelona, Spain.
8. Salat, S. *Cities and Forms: On Sustainable Urbanism*. Urban Morphology Laboratory, Trieste, Italy. (2011).
9. Schaller, J., Ertac, O., Freller, S., Mattos, C., & Rajcevic, Z. Geodesign apps and 3D modelling with CityEngine for the city of tomorrow. *in. Proceedings of Digital Landscape Architecture* (2015), Anhalt, DE, 59-70.
10. Senbel, M., van der Laan, M., Kellett, R., Girling, C., & Stuart, J. Can a form-based code help reduce municipal greenhouse gas emissions in small towns? The case of Revelstoke, British Columbia. *Canadian Journal of Urban Research*, 22, 1 (2013), 72-92.

Presenting Author Biographies

Aly Abdelalim

Aly Abdelalim is currently a Ph.D. candidate in Environmental Engineering program at Carleton University (CU). He is within one year of completion of his PhD. He is also a team member in HBI (Human Building Interaction) Laboratory. Mr. Abdelalim is leading an industry-funded project in collaboration with the School of Architecture: The Digital Campus project. Mr. Abdelalim PhD research focused on developing a multi-scale approach to exploiting measured and modelled building performance data to improve campus operations, which could yield greater insights about opportunities for operational improvements and retrofits. Before joining CU, Aly worked as a teaching assistant at the British University in Egypt. He acquired his Bachelor from ASU (Ain Shams University) and Master's degree in Architectural Engineering & Environmental Design from AAST (Arab Academy for Science and Technology) from Egypt. Moreover, he participated in the supervision of multiple dissertations with topics related to sustainability & built environment for senior undergraduate students in the dissertation module at The British University in Egypt (BUE).

Ajla Aksamija

Ajla Aksamija, PhD, LEED AP BD+C, CDT is a faculty member at the Department of Architecture, University of Massachusetts Amherst. Her research expertise includes building science and sustainability, emerging building technologies, digital design and representations, and information modeling. She directed Perkins+Will's Building Technology Laboratory ("Tech Lab"), one of the first practice-driven research laboratories focusing on advanced building technologies, high-performance buildings, computational design, and building facades. She has worked on developing building analysis and modeling applications, implementation of novel materials in architectural design, and development of computational models. She also has extensive professional experience working on complex building types, including healthcare facilities, research laboratories, academic and school buildings, commercial and mixed-use buildings. Dr. Aksamija has contributed to several books and has published over sixty research articles and invited papers. She is the author of two books, Sustainable Facades: Design Methods for High-Performance Building Envelopes (John Wiley & Sons, 2013) and Integrating Innovation in Architecture: Design, Methods and Technology for Progressive Practice and Research (John Wiley & Sons, 2016). She has presented at various national and international conferences, and is a frequent speaker at industry-based, scientific and academic conferences. She is the founder and editor of the Perkins+Will Research Journal.

Pantea Alambeigi

Pantea is an architect with diverse experience in various areas of design. She is currently a PhD candidate at RMIT University, Australia and a key participant in the Australian Research Council Linkage Project: The Sound of Space, led by Professor Jane Burry. Her area of special interest is bridging acoustic science and design in practice, and integrating sound performance analysis in the early stages of the design process. Her research focus is on the human perception of speech privacy and how architects can shape the space in response to the behavior of sound. She completed her Bachelor in Architecture at the University of Tehran and moved to the United States for her Masters degree at North Carolina State University during which she became interested in light and sound application in design. She spent years practicing architecture and developing her digital skills in residential, commercial and educational projects. She has also taught multiple architectural courses and studios since 2010 and published papers in journals and conferences.

Emad Al-Qattan

Emad Al-Qattan is a Ph.D. student at the college of architecture at Texas A&M University, Texas, The United States of America. His research interests include parametric modeling, computational BIM, physical computing, and tangible user-interfaces. He holds a Bachelor of Architecture from the College of Engineering and Petroleum at Kuwait University; and a Master of Science in Digital Technologies from the Taubman College of Architecture and Urban Planning at The University of Michigan. Al-Qattan's current research proposes a method to establish parametric relationships in computational models through tangible interaction. The work involves linking digitally fabricated architectural elements with virtual environments to create an intuitive interface for designers to setup and manipulate digital constraints. His work, developing hybrid systems, has been published in several Computer Aided Design conferences; and his academic achievements have been recognized by leading national and international honor societies; including Tau Sigma Delta, Phi Kappa Phi, and Golden Key International Honor Society.

Fawaz Alshehri

Fawaz graduated from GMIT with a BSc in Architectural Technology in 2013. He continued his education in UCD and graduated from the MArchSc in Sustainable Building Design & Performance from Architecture school achieving second class honours grade 1. His master's thesis investigate of passive cooling strategies applied to housing in hot dry regions. The purpose of this study was to investigate the potential for energy savings and improved indoor thermal comfort, through the use of various passive cooling strategies when applied to a new house design. The study included a series of dynamic simulations to evaluate the indoor thermal comfort. After graduation he worked as a BIM technical at IN2 Engineering Design Partnership Ireland, taking part in projects related with BIM, Thermal Analysis, Airflow Simulation and Building modeling and energy efficiency. He was involved with the design team for design Trinity School of Business, the project value was €40m. Fawaz commenced his PhD at UCD in January 2016 within the UCD Energy Institute. His research interests include indoor environment quality, Building Information Modeling (BIM) and Building Simulation tools. His current research project focuses on BIM for Thermal Comfort Analysis in Commercial Buildings.

María Lovísa Ámundadóttir

Maria graduated in 2016 with a PhD in Civil and Environmental Engineering from EPFL, the Swiss Federal Institute of Technology in Lausanne, Switzerland, that she conducted at the LIPID lab. Before joining EPFL, she obtained a MSc in Computational Science and Engineering from ETH Zurich and a BSc in Industrial Engineering from the University of Iceland. Maria's research explores the evolution of nonvisual light effects over time with respect to changes in intensity, spectral composition and duration of light exposure using mathematical models. This work has led to the development of simulation-based techniques that can inform designers about the effect of lighting on human health and wellbeing in real-life settings.

Umberto Berardi

Dr. Berardi is an Associate Professor at Ryerson University, in Toronto (Ontario, Canada). His main research interests and contributions are related to the study of building systems that incorporate new materials for improved performance. In the first years of his career, Dr. Berardi often worked on natural materials for acoustic applications and on sustainable design through natural materials. Recently, he has been focusing on integrating innovative materials, or nanotechnologies into building systems. He has mainly focused on organic PCMs, such as paraffin and bio-PCM, and on granular and monolithic aerogel. Dr. Berardi has a body of funded research comprising over $1M in government and private sector sponsored research. In the last two years, he has been awarded an NSERC Discovery Grant; Early Research Award from the MRI - Ontario; Building Excellence Research and Education Grants from the BC Housing - Homeowner Protection Office; a Ryerson University Innovation Equipment grant; Ryerson Dean's Research Fund for Tools and for Undergraduate Research Experience. Dr. Berardi has an extensive publication record for his career stage, including over 70 peer-reviewed journals, 60 international conference papers, and 3 books.

Justin Berquist

Justin Berquist is extremely interested in mechanical systems in buildings. He worked in the mechanical trades for Optimum Mechanical Solutions during the summers of his undergraduate degree at Queen's University. Upon completing his Bachelors of Science in Mechanical Engineering in 2014, he worked in the field as a mechanical designer for Goodkey, Weedmark, and Associates Ltd. In September of 2015 he resumed his education, beginning graduate studies. He is currently completing the Master of Applied Science in Mechanical Engineering program at Carleton University, where he is focused on the efficiency of mechanical systems. His graduate research has been spent developing a model-based fault detection and diagnostics system in order to gain insight on inefficient design strategies to influence future design choices. As part of his program requirements he completed a full time internship with Autodesk in Toronto, during which he worked on the project "An Investigation of Generative Design for Heating, Ventilation, and Air-Conditioning".

Parantap Bhatt

Parantap is a young designer, educator and researcher located in Toronto. With exposure in multidisciplinary fields like Architecture, Interiors, Art and Computation; he has explored several design domains and collaborative processes. His personal interests focus on intersections between architecture & technology that spread across different scales and disciplines. He is currently investigating an on-going research on the use of augmented reality tools and data driven techniques to tackle design problems. He holds a professional Architectural design degree with distinction, conferred from CEPT University and has also received a Masters of Architecture degree from the the Emergent Technologies and Design programme at Architectural Association in London, UK. Parantap's professional experience includes experiments and execution of design at various scales including buildings, spaces, products and installations in countries like UK, Canada, India & Germany. His work involves applications of generative algorithms, embedded systems, advanced digital fabrication, biomimetic approaches, evolutionary processes for multi-criteria optimisation and performance oriented design. He is currently heading a digital design studio at the Faculty of design, OCAD University and has been invited for lectures and workshops at various institutes around the globe.

Vishu Bhooshan

Vishu currently works as a senior designer at Zaha Hadid Architects as part of the Computation and Design (ZH CODE) research group at London. He has been part of the office since 2013. He completed his bachelor degree from Pune, India (2010) and his Master's degree at the Architectural Association, Design Research Lab (2013). He previously worked as an architect in India at B.S Bhooshan & Associates, Mysore & Mind Space Architects, Bangalore, India. His research focuses on topology optimisation, development of tools using statistical learning methods to predict structural and material optimization results in the early design pipeline and development of computational design tools using the current 3D printing fabrication methodology as a constraint. He has taught and presented/published work at various workshops, professional conferences and symposiums including ACADIA 2014, simAUD 2015, SCS SIMULATION 2015, AAG 2014, 16, IASS 2016, AAVS Global Summit 2015, Design Computing Community DCC London 2016 and at various institutes in India including Anthropology Survey of India, India Institute of Architects at Mysore and College of Engineering at Trivandrum.

Peter von Buelow

Peter von Buelow is Professor at the University of Michigan in Ann Arbor where he teaches in the area of structures at Taubman College of Architecture and Urban Planning. His area of research deals with the use of evolutionary computation for the exploration and optimization of architectural systems. Working at the University of Michigan, von Buelow has developed the ParaGen method to explore a wide range of problems based on visual as well as quantitative performance criteria. ParaGen combines parametric design and evolutionary computation for the exploration and optimization of architectural systems based on integrated criteria. The method has been used to search well performing solutions of a variety of architectural forms as well as towers, bridges, domes, frames and plate structures. Professor von Buelow holds a doctorate in Engineering from the Institute for Lightweight Structures and Conceptual Design (ILEK) at the University of Stuttgart (director Werner Sobek). He also carries degrees in both Civil Engineering, and Architecture from the University of Tennessee. He has worked professionally in both architecture and engineering offices in Germany and the US including: RFR-Stuttgart, Greiner Engineering and SL-Rasch. He also spent a year at IL in Stuttgart (under Frei Otto) as a Fulbright Scholar.

Tudor Cosmatu

Tudor Cosmatu is currently a researcher at the TUDelft working on the Double Face 2.0 research project. His main focus lies within the realm of architectural design where he addresses constraints given by material performances, as well as constraints from the sphere of additive manufacturing and robotic additive manufacturing. He has practiced and gained experience in the field of brand architecture and temporary structures, enabling him to use his knowledge in the field of computational design by addressing complex issues at the intersection of art, design, architecture, and engineering. He has been involved in organizing and tutoring numerous international computational design and digital fabrication workshops, as a co-founder of AL_TU and T_A_I, in Qingdao, Lodz, Munich, Moscow, Bucharest and Iasi.

Camilo Cruz

Camilo Cruz is a full time PhD researcher at the Melbourne School of Design (University of Melbourne), where he also serves as sessional tutor and studio leader at March level. His research focuses on investigating and developing evolutionary approaches to design using digital systems. With experience ranging from academia to professional practice, Camilo has served as full time lecturer at the Faculty of Architecture and Urbanism of the Universidad de Chile, associate at Office of Adrian Phiffer and Normal, in Toronto, Canada, visual artist at The Flat Side of Design, also in Toronto, and as a design manager at Eliash Arquitectura y Urbanismo, a small architecture firm based in Santiago (Chile), which mainly concentrates on institutional, educational and urban design projects around South America. Camilo received his Master of Urban Design from the University of Toronto (2011) and his bachelor and professional degrees in Architecture from Pontificia Universidad Catolica de Chile in 2006.

Kartikeya Date

Kartikeya Date is an architect and researcher from Mumbai, India. He did his doctoral work at University of California at Berkeley and is currently a researcher at the Technion, Israel Institute of Technology in Haifa. Before beginning graduate school, Kartikeya worked as an architect in Mumbai, where he also completed his undergraduate professional Bachelor of Architecture Degree. His research interests include the areas of Design Theories and Methods, Computing in Architectural Design, New Media in Architectural Design and Education. His current work is concerned with how computational methods reconfigure the design process and enable new concerns to be addressed. In his teaching he has been interested in two related questions. First, how might computing and computational thinking be introduced as a part of foundation courses in the architectural curriculum? Second, how might the field of computing in architecture be better integrated with fields of modern architectural history and theory? Kartikeya aims to be an academic researcher and teacher in the discipline of architecture.

Francesco De Luca

Francesco De Luca (Architect, PhD) is Scientific Researcher at the Department of Civil Engineering and Architecture of Tallinn University of Technology (TTÜ). His research is situated at the intersection of building performance analysis, computational design and architectural design and planning. He is author of the book Behind the scene - Avant-garde Techniques in Contemporary Design (Birkhäuser), of various papers published in journals including Analysis of the Insolation Criteria for nearly-Zero Energy Buildings in Estonia (ASHRAE - Science and Technology for the Built Environment), Horizontal or Vertical? Windows' Layout Selection for Shading Devices Optimization (Management of Environmental Quality - An international Journal) and in conference proceedings including Emergent, Adaptive and Responsive Urban Landscapes Design Strategies (EFLA 2011) and Solar Envelope Optimization Method for Complex Urban Environments (CAADence in Architecture 2016). He has been Lecturer at the Faculty of Architecture "L. Quaroni" of the University Sapienza of Rome where he taught CAAD, modeling and prototyping from 2001 to 2006, and Visiting Associate Professor at the Faculty of Landscape Architecture of TTÜ where he taught architectural and urban design by computational methodologies from 2010 to 2014. He has been tutor of many workshops including Computational Environmental and Energy Design at TTÜ in 2016.

Elif Erdine

Elif Erdine is an architect, designer, and researcher. She is a tutor ad researcher at the Architectural Association (AA) School of Architecture, Emergent Technologies and Design Graduate Programme. She is an Associate Lecturer at the MArchD Applied Design in Architecture ARB/RIBA Part 2, Faculty of Technology, Design and Environment, Oxford Brookes University. She is the Programme Director of AA DLAB Visiting School and AA Istanbul Visiting School. She has worked for Zaha Hadid Architects during 2006 - 2010. She received her B.Arch. degree from Istanbul Technical University in 2003 (High Honors), and M.Arch. degree from the AA Design Research Lab (AA DRL) in 2006 (Project Distinction). Her projects have been printed widely in international and national architecture publications. Her research interests include the role of the individual building within complex urban systems, and the exploration of various flows in the urban environment as design drivers, and biomimicry. She has presented her research in eCAADe, CAAD Futures, SimAUD, and ACADIA, among others.

Ralph Evins

Dr Ralph Evins leads the Energy Systems and Sustainable Cities research group at the University of Victoria, where he is a Tenure-Track Assistant Professor. His research interests focus on computational problem-solving methods across the domains of buildings and energy systems. This spans improvements to simulations, using optimization approaches to explore the space of possible designs, and cutting-edge machine intelligence techniques. This is inspired by the principles of systems thinking regarding holistic analysis and interconnectivity. He is also interested in the process of software development in an academic context. Dr Evins holds a Masters degree from Imperial College London, and completed an Engineering Doctorate with the University of Bristol entitled "Multi-objective optimisation as an aid to design space exploration for low-carbon buildings". During this time he worked as a research engineer for Buro Happold Ltd in London, applying his research to commercial projects. He is a Chartered Engineer in the UK with the Chartered Institution of Building Services Engineers. He has published 15 peer reviewed journal articles and 29 peer reviewed conference papers. He retains an affiliation with the Urban Energy Systems laboratory at Empa, and continues to actively develop the Holistic Urban Energy Simulation platform.

Gustav Fagerström

Gustav Fagerström is a registered architect and Digital Practice Leader with Walter P Moore New York where he leads the computational modeling for structural and façade engineering. Specializing in design computation, automation and Building Information Modeling he has developed his knowledge in all project phases from concept to construction. His work focuses on the areas of intersection of architecture, engineering and computer science and deals with the optimization and automation of design processes by means of novel techniques in computational modeling, analysis and programming. He has practiced with Urban Future Organization and with Kohn Pedersen Fox Associates in the UK, with UNStudio in the Netherlands and with BuroHappold Engineering in the US, gaining global project experience. Work of his has been exhibited and published in Europe, the Americas and Asia, and presented at Autodesk University, the Venice Architecture Biennale, CAADRIA, ACADIA, FABRICATE and the SmartGeometry conference. Frequently engaging with academia he has held positions at London Metropolitan University and VirginiaTech, and is presently faculty at Pratt Institute and a studio consultant at PennDesign. He has sat on design juries, given workshops and lectures at Columbia University, Yale University, the Architectural Association, UCL Bartlett, Chalmers University, the Royal Institute of Technology and the Royal Academy of Fine Arts in Stockholm.

Mathias Fuchs

Mathias currently works as a senior researcher at Zaha Hadid Architects as part of the Computation and Design (ZH CODE) research group at London. He has been part of the office since 2016. He has a PhD in Pure Mathematics and background in medical statistics and Bioinformatics as well as in freelance statistical consultancy. Before joining the office, he has held academical and industry-funded research positions: He worked as a Graduate at Universite de la Provence Aix-Marseille II, obtained a scholarship from Graduiertenkolleg Gruppen und Geometrie at the Mathematical Institute of Georg-August University Göttingen, held a visiting professorhip at the Institute for Pure and Applied mathematics, Göttingen, as well as postgraduate research positions at the Institute for Bioinformatics, at the Medical School of Georg August University Göttingen, and the Institut für medizinische Informationsverarbeitung, Biometrie und Epidemiologie at the Medical School of Ludwig Maximilian University of Munich.

Daniel Hackett

Daniel Hackett is a Senior Engineer and Associate at RWDI, and leads their Building Science engineering team in the company's UK office. Having studied Aerospace Engineering at Southampton University, he now specialises in assessing the aerodynamics of buildings, with particular regard to the impact this can have on pedestrians and vehicles in the built environment. Daniel has provided design advice and guidance for numerous high profile developments throughout the UK and around the world, including: the Queen Elizabeth Olympic Park in London, the proposed tall building clusters in the City of London, Vauxhall, and the Docklands (London), the Waterfront Masterplan (Liverpool), the St James Development (Edinburgh), Al Wakrah Stadium (Doha), King Abdulaziz Centre for World Culture (Dhahran) the Hofdatorg Masterplan (Reykjavik), and KL Eco City (Kuala Lumpur). He has also conducted assessments for helicopter safety (related to building-induced turbulence) for hospitals in the UK and Ireland, and sailing quality assessments at the West Ferry Printworks and Fulham Football Club sites in London. Daniel is an active member of the UK Wind Engineering Society and an organizer for the society's Young Members Group.

Navid Hatefnia

Navid got his MArch in 2008 from Iran/Sbu. After working few years as a lead architect and project manager, his team awarded a number of national and international architectural competitions. His interests in sustainability led him to research and develop software and methods in environmental field. By using computational programming and applying scientific methods, his goal is to have a better understanding of new challenges in architecture. Several challenges and methods are published and presented in related conferences and journals to share these ideas and processes. In the past few years his measure focus was to challenge the big data which can be gathered from different aspects of environment and present new analytical methods to evaluate thermal and visual comfort in terms of outdoor thermal comfort and glare issue respectively in an accurate and fast integrated process. He is now following his interests as a PhD student at Technical University of Munich (TUM).

Ramon van der Heijden

Ramon is currently a computational design specialist at Front Inc. in New York and Hong Kong. His work in Research and development, Building Information Modelling and Building Data Management has allowed him to develop a deep understanding of the technology that drives innovation in construction data management and design. Specializing in the generation of large, data rich building models has enabled him to author the Elefront add-in for Grasshopper. Ramon has taught computational design at Eindhoven University of Technology, and Construction Communication and Architectural Design at The University of Hong Hong. He has also hosted seminars on Elefront at Chinese University Hong Kong, The University of Hong Kong and for the AA Visiting School, Hong Kong. His work at Front includes Morpheus Hotel City of Dreams - Macau, BAM South tower - Brooklyn, Gabon Conference Center - Gabon, King Abdullah Financial District Geo-Science Centre - Riyadh, Barclays Center - Brooklyn

Cheli Hershcovich

Cheli Hershcovich is a bachelor and an MSc student at the faculty of architecture and town planning at the Technion, Israel Institute of Technology. She has a strong interest in parametric architecture, biomimetics, natural and vernacular systems and their growth patterns. She was chosen as a part of an excellence program to start early her master and so she is studying for both degrees in parallel. Her bachelor thesis focuses on the Bedouin villages in Israel, where she examines their inner logic in order to produce a growth simulation. This simulation will serve as a base for future village planning. Her master thesis focuses on complex geometry facades. Using CFD simulations she examines the potential of complex geometry to create a microclimate by changing the airflow on a building façade.

Omar Hesham

Omar Hesham is pursuing a PhD in Electrical and Computer Engineering at Carleton University's Advanced Real-time Simulation lab, where he researches topics in agent-based simulation and visualization. After an MSc in Systems Science (2012) during which he worked on mesh-free soft tissue tearing dynamics, he now focuses on crowd pathing and emergent task intelligence. Omar's undergraduate background in multimedia and design helped him lead an effort to overhaul the lab's Discrete Event System Specification (DEVS) development pipeline with a particular attention to user experience and interface design. His pedagogical interests have seen him design and teach new syllabuses, from high school enrichment programs to senior undergraduate studies in interactive procedural media. In his spare time, Omar enjoys running and developing content for Koldora, a Creative-Commons-licensed educational video channel that illustrates concepts in computer graphics research and computational geometry while catering to the visual learner in all of us.

Xiaoran Huang

Xiaoran Huang is a PhD. candidate at the University of Melbourne. He holds a BSc degree in urban planning. From 2013 - 2014, he worked and studied in the Bio-Digital Lab in the Bartlett School of Architecture; he received a master degree in Architecture from UCL with distinction in 2014. As an architectural practitioner, he used to work in Gensler, MAD Architects and Landscape Architecture Cooperation of China and has been actively involved in many projects in Beijing, Inner Mongolia and Shanghai. His interests lie in parametric design and digital simulation for both architectural and urban scales. His research is currently focusing on how to informing design process via agent-based modelling and its implementation for enhancing precinct walkability.

Charvi Jagani

Charvi Jagani is an Architecture and Urban Design graduate student at Iowa State University. Jagani currently works as a research assistant with Prof. Ulrike Passe, Director of Center of Building Energy Research at Iowa State University (ISU). She is funded by ISU Presidential Initiative for Interdisciplinary Research (PIIR) in data driven sciences for ISU sustainable cities project. As a part of this project, she does research work on urban building energy modeling and simulation. She has tested and used modeling and simulation tools like Urban Modeling Interface, Urban Weather Generator, Envimet, and Sefaira. Jagani has a background in Information Technology from India with a focus on Geographic Information System. While working as an Intern at Indian Space Research Organization (Ahmedabad, India) she has developed web GIS applications like Urban Growth Spatial Analyses tool and Indian Vegetation Monitoring System. Jagani is interested in innovative and sustainable architectural design; and urban design informed by data driven sciences.

Alexandros Kallegias

Alexandros Kallegias graduated from the Architecture School of the University of Patras in Greece and completed his postgraduate studies at the Architectural Association Design Research LAB (AADRL) in London, UK. He is the Head of the AA Summer DLAB and directs the AA Visiting School in different cities in Greece where he teaches as Studio Master. He is also a key member of the AA Istanbul Visiting School in Turkey. His research has been published in peer reviewed reports and international publications. He gives lectures in the UK, Greece and abroad while he has been invited in juries like the Archiprix 2015 in Ankara. He is an Associate Lecturer at the School of Architecture at Oxford Brookes University, and he has previously taught at the School of Architecture of Liverpool University. He is a Senior Architect at Zaha Hadid Architects, acting as BIM Coordinator for different projects in different countries.

Juchan Kim

Juchan Kim is a Master of Advanced Studies in Architecture student at University of British Columbia, Canada. He is currently working as a graduate research assistant at Elementslab at UBC collaborating with researchers who investigate the energy performance of various urban forms across British Columbia. He holds his bachelor's degree in Construction Engineering and intends to combine his experience with building science. His interests are passive house, sustainable design and construction. He devotes his time to voluntary projects using rammed earth for sustainable housing in Thailand and Kenya. He is a certified Passive House Consultant from the Passive House Institute Germany.

Marie de Klijn-Chevalerias

Marie de Klijn-Chevalerias is pursuing her Professional Doctorate in Engineering (PDEng) in Smart Energy Buildings and Cities under the supervision of Prof. Jan Hensen and ir. Roel Loonen at the Eindhoven University of Technology. Her PDEng project focuses on smarter utilization of thermal mass in high-performance buildings. Marie started out as a student of architecture in Clermont Ferrand (France), where she obtained her bachelor degree. She moved into the field of sustainable building by getting her master's degree in Energy-efficient and Environmental Building Design from Lund University (Sweden). Her master thesis was on the use of life cycle cost analysis in the early design phase and was done at Rau architects in Amsterdam. Marie's interests within the field of sustainable building are broad but are now mainly focused on how building performance simulation can be used to truly support design decisions. She is currently completing her company assignment on this topic at Arup, Amsterdam.

Jingyang Liu Leo

Jingyang Liu Leo is a computational designer and senior personnel in the Sabin Design Lab at Cornell University. He is currently a Master of Science student in a new collaborative research degree program, Matter Design Computation, which combines architectural research with study in the areas of material computation, adaptive architecture and digital fabrication. As the program's first enrolled student, Jingyang (Leo) Liu, M.Arch II '15 will complete his thesis in 2018. He is also a teaching associate for Sabin's option studio in digital ceramics. With education in both architecture and mathematics, Jingyang Liu treats computation as a generative and synthetic system to integrate construction tools, material performance, and biological principles into the design process.

Yuezhong Liu

Yuezhong Liu is a PhD candidate in Department of Architecture at National University of Singapore. His dissertation analyzes how to utilize data technologies and performance simulation to support urban design process. His primary research interests include 1) urban design and data science: how can urban design be actively informed and guided in terms of energy performance by applying data technologies? 2) the relationship between urban textural variables and energy performance: how to leverage the design process on energy-related urban performance aspects? and 3) data availability for performance simulation tools, How to utilize data technologies to complement the missing inputs of the simulation tools? He is engaged in performance simulation and design support tools research, and recently developed series of micro-scale typical meteorological weather (TMY) files based on urban textural settings for building energy simulation in Singapore. Current research efforts include the development of a decision-making tool for evaluating energy performance during urban design process by semi-supervised learning algorithms.

Wolfgang E. Lorenz

Wolfgang E. Lorenz, born in Vienna in 1972, studied Architecture at the TU Wien in Vienna, Austria. His diploma thesis on "Fractals and Fractal Architecture" was compiled under the supervision and in cooperation with the department of computer aided planning and architecture, where he has been employed since March 2004. The main focus of his research work lies on the examination and elaboration of the concept of applying fractal geometry to architecture, in which field he received his Ph. D. degree in Architecture for his thesis on "Analysis of Fractal Architecture using the Box-Counting Method" (TU Wien, 2014). In teaching, he is actively involved in algorithmic design studios teaching students how to generate form by programming. He is also the editor of a number of books that are based on the results of such studios, such as "prefabs - para siempre!" (2017), "flying bricks" (2015) and "brickster style" (2014).

Liat Margolis

Liat Margolis is Associate Professor of Landscape Architecture at the University of Toronto and Director of the Green Roof Innovation Testing (GRIT) Laboratory http://grit.daniels.utoronto.ca, an interdisciplinary research initiative that brings together the fields of Landscape Architecture, Urban Ecology, and Civil Engineering to study the environmental performance of green infrastructure. GRIT Lab was awarded the 2013 American Society of Landscape Architects Excellence Award in Research and has received support from the City of Toronto Environment and Energy Division, NSERC, Ontario Centres of Excellence, Mitacs, Connaught Fund, Landscape Architecture Canada Foundation, RCI Foundation, and from over a dozen industry partners. Professor Margolis is a book review editor forLandscape Journal and scientific committee member of Sustainable Canada Dialogues, an initiative that mobilizes over sixty Canadian scholars to advance climate change mitigation in Canada. She is also member of the City of Toronto Green Streets Technical Review Committee and Pollinators Advisory Group. She received a Bachelor of Fine Arts in Industrial Design from the Rhode Island School of Design and a Masters of Landscape Architecture from the Harvard Graduate School of Design.

Sarah Mokhtar

Sarah Mokhtar is a practicing architect and researcher exploring topics merging between architecture, technology, and sustainability. She just completed a Master of Science in Adaptive Architecture and Computation at the Bartlett School of Architecture (UCL) with distinction, where she explored morphogenetic programming, machine learning, optimization algorithms, physical computing, and other technologies for architecture. Material computation, a rising domain of interest in adaptive architecture, framed the focus of her work and culminated with her thesis 'Material-Based Actuation of Facades: An Adaptive Performative Approach', which was awarded the UCL Turner prize: an annual award for one outstanding thesis. Trained and qualified as an architect engineer, she earned her professional BSc with highest honours in 2014 from the American University in Cairo (AUC) and worked on the design of various local and international projects from their conception to schematic design taking initiatives to merge between computation, building information modelling and sustainability. In line with the professional path, she maintained her academic involvement through working as a research and teaching assistant at the Bartlett, UCL and the AUC respectively, and conducting workshops in the fields of building performance simulation and shape memory alloys in architecture for undergraduates and master's students.

Nicole Phelan

As a Design Researcher on WeWork's Product Research team, Nicole develops strategies and insights through the application of various quantitative and machine learning techniques. Her research is particularly focused on the design of workspaces and has covered topics such as meeting room usage, adaptive programming of office space, and the physical components of an office that make it successful. Prior to joining WeWork, Nicole spent five years collecting and analyzing data on how ADP employees use their workspaces to drive Corporate Real Estate decisions and ensure optimal conditions for employee productivity. Realizing the competitive advantage to data-driven strategies and decisions, Nicole pursued her MBA from Rutgers University with concentrations in both Analytics and Information Management, and Supply Chain Management. When she's not working or hanging out with her dog Loki, she can be found in an ambulance as a volunteer EMT for the Weehawken Volunteer First Aid Squad in New Jersey.

Navid Pourmousavian

Navid Pourmousavian (MSc, LEED AP BD+C) is currently a building scientist and energy modeler at Internat Energy Solutions Canada(IESC). He is a recent graduate of Building Engineering program at Concordia University, with also a bachelor degree in mechanical engineering from Tehran Polytechnic. As a member of Concordia Center for Zero Energy Building Studies (CZEBS), his research was focusing on building performance simulation as a design tool to facilitate decision-making in the design of high-performance buildings as well as net-zero energy buildings and to help the project teams to adopt the integrated design process. He was the Engineering project lead for the Montreal Solar Decathlon team (TeamMTL) during his master program at Concordia university. Navid has more than three years of energy modeling experience working at EnergyHouse Co. and MontrealZero and currently at IESC where he is involving in the audit and energy modeling of residential and commercial buildings. He also has teaching experience in different energy modeling tools.

Siobhan Rockcastle

Siobhan is a researcher exploring topics at the intersection of architectural design, human perception, environmental dynamics, and building performance. She is in the final stages of her PhD at at the LIPID Lab of EPFL, the Swiss Federal Institute of Technology in Lausanne, Switzerland. Siobhan earned her professional BArch from Cornell University in 2008 and her SMArchS degree in Building Technology from MIT in 2011. Siobhan has held teaching positions at Cornell and Northeastern, where she taught courses on architectural design, daylight performance, and environmental systems. Her professional work experience includes positions at KVA matX, Snøhetta, Epiphyte Lab, and Gensler. She currently consults on daylight design integration and environmental performance for a number of architectural and urban-scale projects in Switzerland and the US. Siobhan's research proposes new metrics that predict the impacts of daylight and spatial composition on perception and emotion in architecture.

Jonathan Salter

Jon is a postdoctoral fellow in the School of Architecture and Landscape Architecture (SALA) at the University of British Columbia. He works in the elementslab (www.elementslab.ca) with Professors Ronald Kellett and Cynthia Girling on tools for urban design and planning. Jon completed his PhD in 2015 on public engagement in community-scale energy planning. His research interests focus on decision-support tools (primarily simulation and visualization) and engagement processes for sustainability planning. During his PhD, he managed the design and installation of the BC Hydro Decision Theatre in the Centre for Interactive Research on Sustainability at UBC. Jon is currently working on a Pacific Institute for Climate Solutions (PICS) funded project that is simulating the interactions between urban form, and energy and emissions under the effects of different policy interventions. The end goal of this PICS research is to provide policy-relevant recommendations to municipal governments and practitioners about effective approaches for meeting climate action targets.

Davide Schaumann

Davide Schaumann is an Architect and Ph.D. Candidate in the Faculty of Architecture and Town Planning at the Technion – Israel Institute of Technology. He holds BA and MSc degrees in Architecture from the Politecnico di Milano in Italy, and has worked for emerging architectural firms in Italy, Spain, Canada and Israel. Schaumann's research explores the mutual relations between a physical setting, the people who inhabit it, and the activities they engage in, to devise methods for designing settings that better meet people's needs through the use of Computer Aided Design and Building Information Modeling tools. In particular, Schaumann's research involves: human behavior simulation in built environments; knowledge representation for architectural design; development and application of ethnographic data collection methods to correlate user activities with the built environments in which they are performed; and use of video game engines and virtual reality tools to support evaluation and communication in architectural design.

Jim Stoddart

Jim Stoddart is an Associate Research Scientist and Designer at The Living, an Autodesk Studio—a research and design practice within Autodesk Research. His projects and research focus on novel applications of technology to applied design problems, including the use of new materials, incorporation of biological ecosystems and artificial intelligence, development of custom digital fabrication workflows, and exploration of new visualization technologies. Jim graduated from the Columbia University Graduate School of Architecture, Planning, and Preservation with a Masters of Architecture in 2014 and received his Bachelor of Science in Architecture from the Georgia Institute of Technology's College of Design in 2008. His work has been exhibited in the Chicago Architecture Biennial, the World Leadership Forum in Davos, the Museum of Modern Art (MoMA), MoMA PS1, and the Palais de Tokyo in Paris. Jim lives and works in New York City.

Todor Stojanovski

I graduated architecture at Ss. Cyril and Methodius University, Skopje, Macedonia and have MSc in built environment from KTH Royal Institute of Technology, Stockholm, Sweden. I was a PhD candidate in the division for Traffic and Logistics at KTH Royal Institute of Technology where I researched about TOD (Transit-Oriented Development) as a PhD candidate from 2009-2014. Since 2015 I am research assistant at the division for Urban and Regional Studies, KTH Royal Institute of Technology. My research is about multimodal transportation and urban form. My professional interests include: cities and public transportation, urban morphology and travel behaviour; urban and traffic planning, sustainability and future cities.

Rudi Stouffs

Rudi Stouffs is Associate Professor in the Department of Architecture at the National University of Singapore, and Guest Associate Professor at the Chair of Design Informatics, Faculty of Architecture, Delft University of Technology. He holds an MS in architectural engineering from the Vrije Universiteit Brussel, an MS in computational design, and a PhD in architecture from Carnegie Mellon University. He has held previous appointments at the School of Architecture at Carnegie Mellon University, the Chair for Architecture and CAAD at ETH Zurich, and the Chair of Design Informatics at TU Delft. His research interests include computational issues of description, modelling, and representation for design, mainly in the areas of shape recognition and generation, and building/city information modelling and analysis. He is a co-principal investigator in the Future Cities Laboratory Phase 2 (Singapore-ETH Centre) and a member of the NUS Centre of Excellence in BIM Integration, and he leads the Design, Technology and Sustainability Research and Teaching Group at NUS Department of Architecture. He teaches design studio, BIM and building simulation to BArch students and supervises MArch and PhD students.

Alan Tai

Alan Tai is an architect with specialized expertise in computational design and processes. He received the Bachelor of Science degree in Electrical Engineering from National Taiwan University, the Master of Architecture degree from University of Pennsylvania and the Master of Science degree in Design and Computation from MIT. He currently works as a Façade Consultant with Front, focusing on the design and fabrication of innovative facade systems. His work at Front includes Barclays Center, Gabon Conference Center, and BAM South Tower. He is the co-developer of Elefront add-on for Grasshopper, which enables a seamless work flow from the implementation of building information modeling to the automation of fabrication-ready documentation. He has taught computational design workshop at MIT and Tamkang University, and has been a visiting critic at UPenn, MIT and Pratt Institute.

Martin Tamke

Martin Tamke is Associate Professor at the Centre for Information Technology and Architecture (CITA) in Copenhagen. He is pursuing design led research in the interface and implications of computational design and its materialization. He joined the newly founded research centre CITA in 2006 and shaped its design based research practice. Projects on new design and fabrication tools for wood and composite production led to a research method centered on demonstrators, which explore an architectural practice engaged with bespoke materials and behaviour. This practice is enabled by design modelling strategies, which incorporate feedback from environment and process. His current work is characterised by strong links to computer science, with a focus on Machine Learning and Point Clouds, engineering, with a focus on simulation and ultralight hybrid structures, and material science, with a focus on bespoke cnc knit. Martin initiated and conducted a large amount of funded research projects in the emerging field of digital production in building industry and architectural computation. The research connects academic and industrial partners from architecture and engineering, computer and material science and the crafts. Currently he is involved in the Danish funded 4 year Complex Modelling research project and the adapt-r and InnoChain PhD research networks.

Milou Teeling

Milou Teeling was part of the TU Delft faculty and research team during 2016. In addition to her position as a lecturer at the Chair of Design Informatics, she also contributed to several ongoing research projects into computational optimization, including PULSE. Her pedagogical approach in the design studios combined digital processes with material methods of fabrication in search of concepts that are both informative and innovative. Also in her current position as an architect at Herzog de Meuron, she specializes in digital technologies, particularly focusing on the typological analysis and computational optimization of architectural configurations and structural details. In addition she is also co-managing the building information modeling process of a large public building. Milou Teeling' previous research involves the exploration of architectural form in relation to program, typology, systems, structure and environment. Her Master Thesis involved the environmental optimization of mass housing typologies through standardized façade systems depended on complex computational models that enhanced the architectural intelligence of the type. In 2014 Teeling graduated cum laude from Princeton University with a Masters Degree in Architecture. She also holds a Bachelor of Arts in Architecture with honors and a Bachelor of Business Administration in Real Estate from the University of San Diego.

Zachary Trattner

Zachary Trattner is an architect, designer, and urban planner whose works span various scales including furniture, buildings, and cities. He received his Bachelor of Architectural Sciences from Ryerson University in Toronto, Canada, and subsequently worked for several years as an architectural designer at BBB Architects. During this period Zachary focused mostly on sports and entertainment architecture, including a year spent working on the transformation of Madison Square Garden in New York City. Afterwards, Zachary attended the Institute for Advanced Architecture of Catalonia in Barcelona, Spain where he received his Masters of Advanced Architecture. During his studies there, Zachary pursued interests beyond traditional notions of architecture, incorporating urban data analytics and programming into his skillset. Since then, his work has explored the belief that patterns of human mobility in cities have the consequence of shaping our urban environments, and that advanced computational tools can inform the urban planning process. He currently works as an urban and architectural mobility consultant at Mobility in Chain New York. Zachary also provides freelance architectural services, including traditional design work, as well as developing custom architectural tools.

Michela Turrin

Michela Turrin is a Tenure Track Assistant Professor at Delft University of Technology. She leads several granted research projects with practice and industry; co-leads the Computation & Performance Research Program and is member of the Faculty Research Council. Her main expertise is computational design and optimization to support the exploration of design alternatives and integrate multi-disciplinary design criteria in the early phase of architectural design. Her current projects include optimization methods to support design exploration, both for complex buildings (toward collaborative design) and for interdisciplinary design of small scale building components (toward fabrication). In 2012, she was Marie Curie Fellow at Beijing University of Technology. She worked at Green World Solutions Ltd in Beijing. She taught in international events, among which the IFoU Summer School 2012 in Beijing and Winter School 2013 in Hong Kong. In 2014-2016 she was Excellent Oversea Instructor at South China University of Technology and awarded a grant by the Key State Laboratory of Subtropical Building Science; focusing on computational optimization for complex projects, i.e sport buildings. In 2012-2015 she was senior lecturer at Yasar University.

Lorenzo Villaggi

Lorenzo Villaggi is an Associate Research Scientist and Designer at The Living, an Autodesk Studio—a research and design practice within Autodesk Research. His projects and research focus on generative design, new materials and novel forms of visualization. More recently he has been exploring methods of quantifying spatial experience and its applicability to generative workflows for space planning. Lorenzo graduated from the Columbia University Graduate School of Architecture, Planning and Preservation with a Masters of Architecture in 2015 where he has taught a graduate seminar and received his Bachelor of Architecture from the Politecnico di Milano in 2012. Additionally, Lorenzo co-founded and co-edits: (pronounced “colon”), a collective workshop on architectural practices and ideas based in New York City, currently resident at the GSAPP incubator space. His work has been exhibited in internationally renowned venues including the Chicago Biennial, the Milan Design Week, the MoMA and the New Museum

Thomas Wortmann

Thomas is a PhD candidate and studio instructor in SUTD’s Architecture and Sustainable Design pillar. In 2013, he graduated from MIT with a Master of Science in Design and Computation, after having worked for several years as a project architect for the Dutch architectural practice of NOX, known for its pioneering use of digital design tools. In 2015, Thomas was responsible for designing and automatically generating cut sheets and assembly instructions for over 10.000 individual panels for the “Future of Us” grid shell in Singapore. Since 2014, he has taught design studios and parametric design courses at various universities and other institutions in Singapore. His research interest is the integration of computers into the architectural design process, with a focus on visual and interactive model-based optimization tools. He has authored numerous papers on topics such as benchmarking black-box optimization methods, multivariate visualization and shape grammar implementation. Thomas is the lead developer of Opossum, an award-winning model-based optimization tool for Grasshopper, which is available for free on food4rhino.com.

Ding Yang

Ding Yang is currently a joint Ph.D. Candidate in the Department of Architectural Engineering & Technology at TUD (Delft University of Technology) and in the Department of Architecture at SCUT (South China University of Technology). He received his B.Arch and M.Arch from SCUT, and worked in Sun Yimin Studio of SCUT from 2009, mainly focusing on the computational design of sports and recreational buildings. His recent research, in collaboration with Arup in Amsterdam and ESTECO in Italy, aims at developing a performance-based design approach for the conceptual design of indoor sports buildings. The proposed approach is able to improve multiple building performances, including daylight, thermal, energy and structural performances; and support the trade-off decision-making by utilizing multi-objective and multi-disciplinary design exploration and optimization techniques. To support this approach, he, with the help of ESTECO team, developed a computational design exploration system that integrates parametric modelling software with process integration and optimization software.

Zheng Yang

Zheng Yang is a postdoctoral fellow in the Department of Civil & Environmental Engineering at Stanford. Zheng is interested in dynamics, informatics and sustainability of built environments and urban systems. His current research explores the coupled dynamics of urban systems, and develops open-source energy benchmarking platforms to evaluate building energy performance at city scale. At Stanford Urban Informatics Lab, he is the research project manager working closely with City of Palo Alto to investigate how a deeper understanding of coupled urban dynamics and energy benchmarking could provide insights that lead to paradigm shifts in how design and manage cities more effectively. His objective is to quickly ingest overwhelming data and accurately translate into easily understood visualization tied to energy efficiency policy and program recommendations. Prior to joining Stanford, Zheng received his PhD in Civil Engineering with the specialization on Informatics for Intelligent Built Environment from University of Southern California.His past research was on the built environment energy efficiency from the perspective of enhanced interactions between occupants and building systems through advanced sensing, computation and algorithms.

Arta Yazdanseta

Arta Yazdanseta is a LEED certified architect, educator, and consultant. She is currently a Doctor of Design Candidate at the Harvard Graduate School of Design (GSD). She is a research assistant at the Harvard Center for Green Buildings and Cities where she is investigating the thermal impact of green walls on building energy performance. Her research explores the intersection between design, building science, and plant biophysical ecology and emphasizes coupling building energy performance with vertical vegetative surfaces through design. Arta received her Masters of Design in Energy and Environment from the GSD and her professional architectural degree from the Pratt Institute. She has worked with well-known design firms such as SHoP Architects and hMa. She founded her architectural design studio, LINX Architecture, in 2008 while serving as a visiting instructor at the Pratt Institute. Arta's team was the first prize winner of the 2012 IBPSA Student Competition Award in Chambery, France, and her master's thesis, Radiative Cooling Roof Systems, was a winner of the Harvard Sustainability Grant. She is a recipient of the Circle Award Fellowship and was an AIA Women's Architectural Auxiliary Eleanor Allwork Scholar. Her work has been displayed at the New York Chapter of the AIA and has been published in Metropolis magazine.

Ji Zhang

Dr ZHANG Ji is a Research Fellow at the Centre for Sustainable Asian Cities in the School of Design and Environment (SDE) and the Solar Energy Research Institute of Singapore (SERIS), National University of Singapore. Trained as architect and urban designer, Dr ZHANG Ji's research focuses on exploring urban sustainability from both a social-psychological and a spatial-environmental perspectives. His more recent research focuses on the multifaceted relationship between urban density, urban form and environmental performance, with a particular emphasis on the implications of building typology and urban morphology as performance optimization strategies in the early stage of urban planning and architectural design.

Yingyi Zhang

Yingyi Zhang is a Ph.D. candidate of School of Architecture, Victoria University of Wellington, New Zealand. She studied in timber-structure architecture, space syntax, and urban renewal design in Mainland China and Taiwan and got her master degree in Engineering Science in 2015. Now she is looking into testing Form-Based Code's technical and implemental capabilities in urban renewal design of high-density cities with a wide range of parametric approaches. She has published high impact articles and presented her works in international conferences. She is a member of the Digital Architecture Research Alliance (DARA), a student member of New Zealand Institute of Architecture (NZIA), a member of Wellington Photographic Society (WPS), and an active contributor of Design and Architecture Academy Link (DEAALI).

Organizing Committee

Symposium Chair

Michela Turrin, Assistant Professor, Faculty of Architecture and the Built Environment
Delft University of Technology

Program Chair

Brady Peters, Assistant Professor, Daniels School of Architecture, Landscape, and Design
University of Toronto

Scientific Committee Chairs

William O'Brien, Associate Professor, Human-Building Interaction Lab
Carleton University

Rudi Stouffs, Associate Professor, Faculty of Architecture
National University of Singapore

Timur Dogan, Assistant Professor, College of Architecture, Art, and Planning
Cornell University

International Scientific Committee

Aly Abdelalim
Carleton University

Alpha Yacob Arsano
MIT / Transsolar

Arianna Astolfi
Politecnico di Torino

Ramtin Attar
Autodesk

Shady Attia
Université de Liège

Martin Bechthold
Harvard GSD

José Nuno Beirão
Technical University of Lisbon

Justin Berquist
Carleton University

Denis Bourgeois
Universite Laval

Johannes Braumann
Association for Robots in Architecture

Peter von Buelow
University of Michigan

International Reviewing Committee (continued)

Angelos Chronis
Foster & Partners

Salmaan Craig
Harvard GSD

Jason Crow
Louisiana State University

Ryan Danks
RWDI

Daniel Davis
CASE

Christian Derix
Woods Bagot

Timur Dogan
Cornell University

Bing Dong
University of Texas at San Antonio

Stylianos Dritsas
Singapore University of Technology and Design

Tomás Méndez *Echenagucia*
ETH Zurich

Forest Flager
Stanford

Luis Fraguada
IAAC

Tomohiro Fukuda
Osaka University

Rhys Goldstein
Autodesk

Yasha Grobman
Technion, Israel Institute of Technology

Burak Gunay
Carleton University

Sean Hanna
UCL Bartlett

Timo Hartmann
University of Twente

Yeonsook Heo
University of Cambridge

Christina Hopfe
Loughborough University

Maarten Hornikx
Eindhoven University of Technology

Patrick Janssen
National University of Singapore

Nathaniel Jones
MIT

Azam Khan
Autodesk

Arto Kiviniemi
University of Liverpool

Reinhard Koenig
ETH Zurich

Branko Kolarevic
University of Calgary

Odysseas Kontovourkis
University of Cyprus

Lukáš Kurilla
ETZ Zurich

Katherine Liapi
University of Patras, Greece

Thorsten Loemker
Zayed University

Roel Loonen
TU/e

Iain MacDonald
National Research Council of Canada

Bob Martens
Vienna University of Technology

Kirk Martini
University of Virginia

Matan Mayer
Harvard GSD

Mark Meagher
University of Sheffield

Wendy Meguro
University of Hawaii

Annalisa Meyboom
University of British Columbia

International Reviewing Committee (continued)

Clayton Miller
ETH Zurich

Vahndi Minah
Arup

Erin Morrow
Arup

Volker Mueller
Bentley Systems

Mojtaba Navvab
University of Michigan

Lira Nikolovska
Autodesk

Les Norford
MIT

Nicholas Novelli
RPI

Shinya Okuda
National University of Singapore

Konstantinos-
Alketas Oungrinis
Technical University of Crete

Ye (Daniel) Park
Cornell University

Chengzi Peng
University of Sheffield

Stephen Ray
SOM

Dagmar Reinhardt
University of Sydney

Siobhan Rockcastle
EPFL

Davide Schaumann
Technion, Israel Institute of Technology

Yair Schwartz
UCL Bartlett

Gennaro Senatore
UCL Bartlett

Asbjorn Sondergaard
Aarhus University

José Pedro Sousa
University of Porto (FAUP)

Benjamin Spaeth
Cardiff University

Rudi Stouffs
National University of Singapore

Georg Suter
Vienna University of Technology

Paulo Tabares-Velasco
Colorado School of Mines

Martin Tenpierik
Delft University of Technology

Walid Tizani
University of Nottingham

Irmak Turan
MIT

Michela Turrin
Delft University of Technology

Brian Tysoe
MCW

Bryan Urban
Fraunhofer USA

Diederik Veenendaal
ETH Zurich

Robert Woodbury
Simon Fraser University

Gabriel Wurzer
Vienna University of Technology

Claudia Yamu
University of Groningen

Bin Yan
Harvard GSD

Sponsors

Sponsored by

In cooperation with

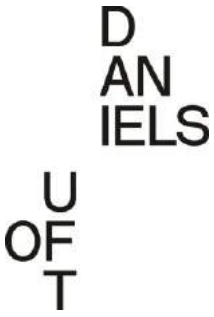

Cover Image Credits

A Performance Based Computational Method for Assembly Design of Reciprocal Architectural Systems with 2D Elements

Omid Oliyan Torghabehi, Peter von Buelow
University of Michigan
Alireza Seyedahmadian
Quarra Stone Company

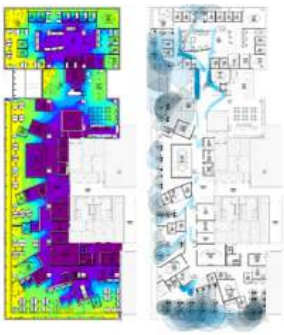

Project Discover: An Application of Generative Design for Architectural Space Planning

Danil Nagy, Damon Lau, John Locke, Jim Stoddart, Lorenzo Villaggi, Ray Wang, Dale Zhao and David Benjamin
The Living, an Autodesk Studio

PULSE: Integrated Parametric Modeling for a Shading System From Daylight Optimization to Additive Manufacturing

Milou Teeling, Michela Turrin and Paul de Ruiter
Delft University of Technology

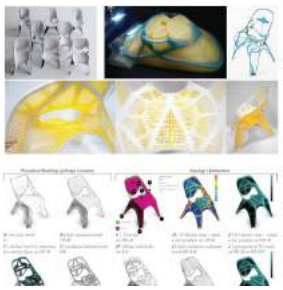

3D-Printing, Topology Optimization and Statistical Learning: A Case Study

Vishu Bhooshan, Mathias Fuchs and Shajay Bhooshan
Zaha Hadid Architects, Computation & Design Research Group

Integrating Technical Performances Within Design Exploration. The Case of an Innovative Trombe Wall.

Tudor Cosmatu, Yvonne Wattez, Michela Turrin and Martin Tenpierik
TU Delft, Faculty of Architecture and the Built Environment,

Simulation in Complex Modelling

Mette Ramsgaard Thomsen, Martin Tamke, Paul Nicholas, Anders Holden Deleuran, Phil Ayres
CITA, Royal Academy of Fine Arts, School of Architecture
Riccardo La Magna, Christoph Gengnagel
Department for Design and Structural Engineering / UdK

Augmented Assembly for Tessellated Structures

Parantap Bhatt, Nicolo Bencini, Spyros Efthymiou and Antoniya Stoitsova
AA Emtech

Context-sensitive Personal Space for Dense Crowd Simulation

Omar Hesham and Gabriel Wainer
Carleton University (Dept. of Systems and Computer Engineering)

A Case Study on the Relationship between Urban Morphology and Traffic Noise Distribution in High-density Urban Context

Ji Zhang,
National University of Singapore
Stephen Siu Yu Lau, Chye Kiang Heng, Siu-Kit Lau and Hongzhan Lai
National University of Singapore

Author Index

Y

Z

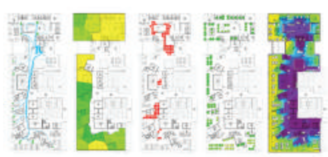

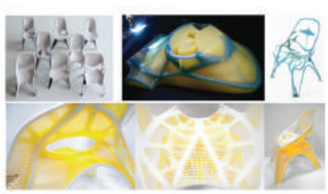

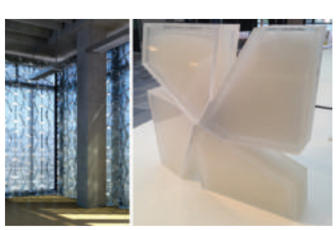

Symposium on Simulation for Architecture and Urban Design 2017

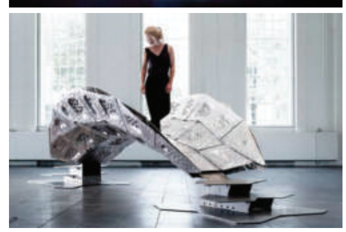

ISBN 978-1-365-88878-6